https://ntrs.nasa.gov/search.jsp?R=20160006309 2019-08-31T02:55:48+00:00Z

NASA/TM—2016–218971

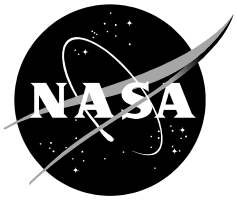

T-Cap Pull-Off and Bending Behavior for Stitched Structure

Andrew E. Lovejoy
Langley Research Center, Hampton, Virginia

Frank A. Leone, Jr.
Langley Research Center, Hampton, Virginia

April 2016

NASA STI Program ... in Profile

Since its founding, NASA has been dedicated to the advancement of aeronautics and space science. The NASA scientific and technical information (STI) program plays a key part in helping NASA maintain this important role.

The NASA STI program operates under the auspices of the Agency Chief Information Officer. It collects, organizes, provides for archiving, and disseminates NASA's STI. The NASA STI program provides access to the NTRS Registered and its public interface, the NASA Technical Reports Server, thus providing one of the largest collections of aeronautical and space science STI in the world. Results are published in both non-NASA channels and by NASA in the NASA STI Report Series, which includes the following report types:

- TECHNICAL PUBLICATION. Reports of completed research or a major significant phase of research that present the results of NASA Programs and include extensive data or theoretical analysis. Includes compilations of significant scientific and technical data and information deemed to be of continuing reference value. NASA counterpart of peer-reviewed formal professional papers but has less stringent limitations on manuscript length and extent of graphic presentations.

- TECHNICAL MEMORANDUM. Scientific and technical findings that are preliminary or of specialized interest, e.g., quick release reports, working papers, and bibliographies that contain minimal annotation. Does not contain extensive analysis.

- CONTRACTOR REPORT. Scientific and technical findings by NASA-sponsored contractors and grantees.

- CONFERENCE PUBLICATION. Collected papers from scientific and technical conferences, symposia, seminars, or other meetings sponsored or co-sponsored by NASA.

- SPECIAL PUBLICATION. Scientific, technical, or historical information from NASA programs, projects, and missions, often concerned with subjects having substantial public interest.

- TECHNICAL TRANSLATION. English-language translations of foreign scientific and technical material pertinent to NASA's mission.

Specialized services also include organizing and publishing research results, distributing specialized research announcements and feeds, providing information desk and personal search support, and enabling data exchange services.

For more information about the NASA STI program, see the following:

- Access the NASA STI program home page at http://www.sti.nasa.gov

- E-mail your question to help@sti.nasa.gov

- Phone the NASA STI Information Desk at 757-864-9658

- Write to:
  NASA STI Information Desk
  Mail Stop 148
  NASA Langley Research Center
  Hampton, VA 23681-2199

NASA/TM—2016–218971

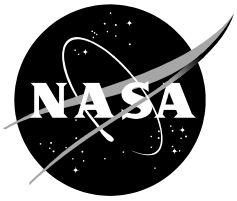

T-Cap Pull-Off and Bending Behavior for Stitched Structure

Andrew E. Lovejoy
Langley Research Center, Hampton, Virginia

Frank A. Leone, Jr.
Langley Research Center, Hampton, Virginia

National Aeronautics and
Space Administration

Langley Research Center
Hampton, VA 23681

April 2016

The use of trademarks or names of manufacturers in this report is for accurate reporting and does not constitute an official endorsement, either expressed or implied, of such products or manufacturers by the National Aeronautics and Space Administration.

Available from:

NASA STI Program / Mail Stop 148
NASA Langley Research Center
Hampton, VA 23681-2199
Fax: 757-864-6500

Abstract

The Pultruded Rod Stitched Efficient Unitized Structure (PRSEUS) is a structural concept that was developed by The Boeing Company to address the complex structural design aspects associated with a pressurized hybrid wing body aircraft configuration. An important design feature required for assembly is the integrally stitched T-cap, which provides connectivity of the corner (orthogonal) joint between adjacent panels. A series of tests were conducted on T-cap test articles, with and without a rod stiffener penetrating the T-cap web, under tension (pull-off) and bending loads. Three designs were tested, including the baseline design used in large-scale test articles. The baseline had only the manufacturing stitch row adjacent to the fillet at the base of the T-cap web. Two new designs added stitching rows to the T-cap web at either 0.5- or 1.0-inch spacing along the height of the web. Testing was conducted at NASA Langley Research Center to determine the behavior of the T-cap region resulting from the applied loading. Results show that stitching arrests the initial delamination failures so that the maximum strength capability exceeds the load at which the initial delaminations develop. However, it was seen that the added web stitching had very little effect on the initial delamination failure load, but actually decreased the initial delamination failure load for tension loading of test articles without a stiffener passing through the web. Additionally, the added web stitching only increased the maximum load capability by between 1% and 12.5%. The presence of the stiffener, however, did increase the initial and maximum loads for both tension and bending loading as compared to the stringerless baseline design. Based on the results of the few samples tested, the additional stitching in the T-cap web showed little advantage over the baseline design in terms of structural failure at the T-cap web/skin junction for the current test articles.

Table of Contents

List of Tables

List of Figures

Introduction

The Pultruded Rod Stitched Efficient Unitized Structure (PRSEUS)[1] is a structural concept that was developed by The Boeing Company (Boeing) to address the complex structural design aspects associated with a pressurized hybrid wing body (HWB) aircraft configuration as shown in Figure 1. The HWB has long been a focus of the NASA Environmentally Responsible Aviation (ERA) Project, with structures development primarily addressing the pressurized, non-circular fuselage portion of the HWB. PRSEUS is an integral structural concept whereby skins, frames, stringers and tear straps are all stitched together, then infused and cured in an out-of-autoclave process. Skins, flanges, and webs are composed of layers of carbon material that are knitted into multi-ply stacks. A single stack has the thickness of 0.052 in. and comprises seven plies with stacking sequence [+45, −45, 0, 90, 0, −45, +45] and percentages of the 0, 45 and 90-degree fibers equal to 44.9, 42.9, and 12.2, respectively. The PRSEUS concept is shown in Figure 2 as it has been applied to pressurized HWB fuselage structure. The concept has evolved out of stitching technology development from several NASA-Boeing and AFRL-Boeing programs starting in the 1990's.[2-5] The key to the PRSEUS concept is the pre-cured, pultruded rod that is contained within the stringer wrap plies and that passes through the frames, providing an uninterrupted load path through the acreage in the stringer direction. At the same time, the full-depth frame stiffener is also continuous, except for the keyhole through which the stringer passes, providing an uninterrupted load path in the direction perpendicular to the stringer. These efficient structural stiffening members provide the majority of the panel stiffness, permitting the use of minimum skin thickness for many applications.

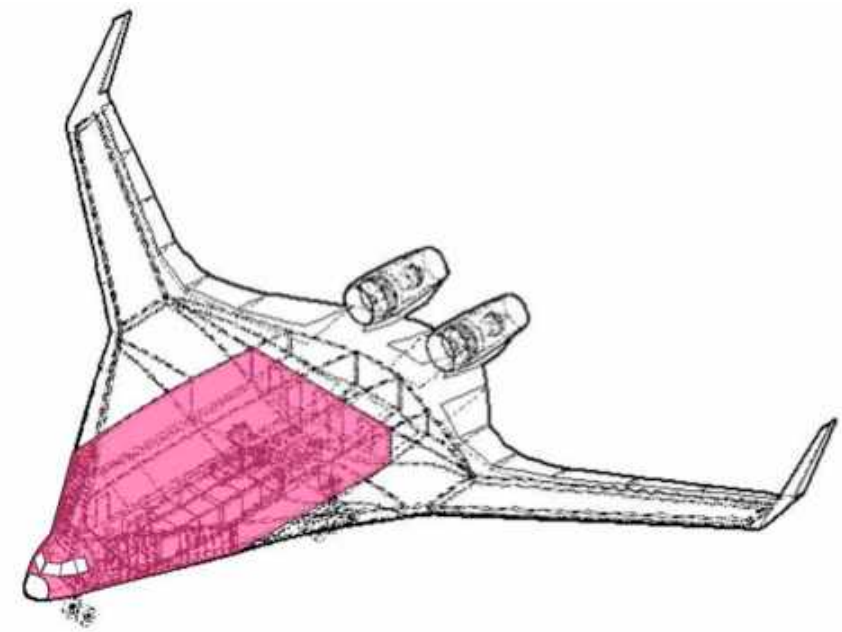

Figure 1. Typical pressurized portion of a HWB aircraft concept.

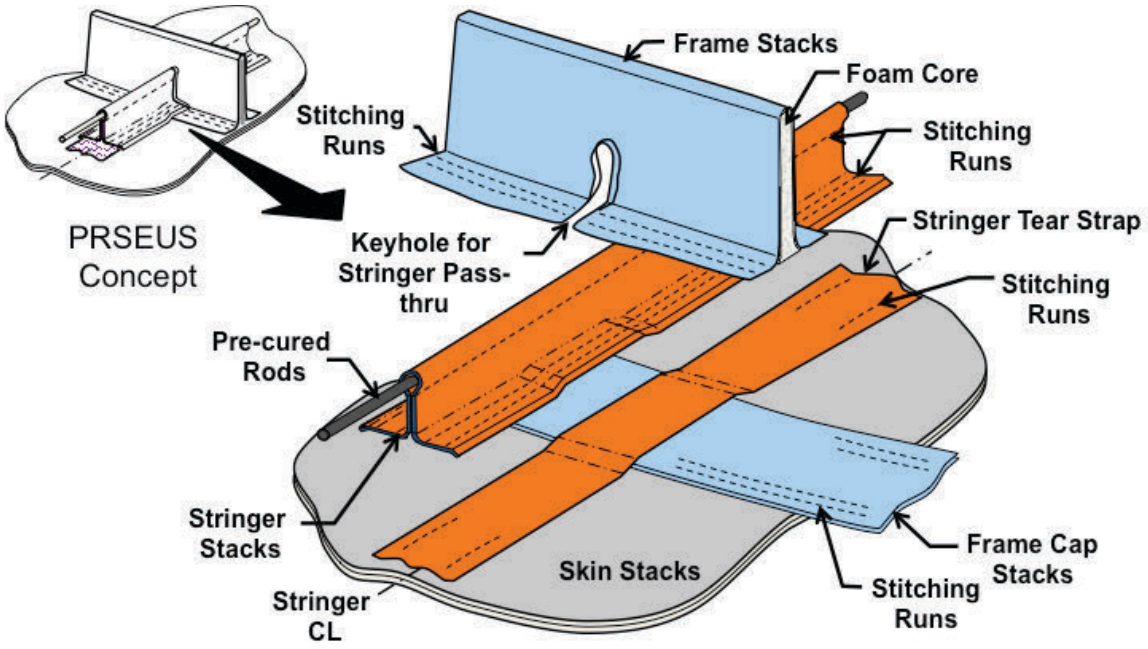

Figure 2. Typical PRSEUS concept.

Throughout ERA, the building block approach has been used to design, analyze, build, and test HWB PRSEUS structural components leading to an 80% scale center portion of the HWB as shown in Figure 3 (identified as the Multi-Bay Pressure Box (MBB) in the lower right portion of the figure). The MBB began testing in the NASA Langley Research Center (LaRC) Combined Loads Test System (COLTS) Facility[6, 7] in April 2015, and was subjected to a series of load conditions. A photograph of the test article between the platens in the COLTS Facility and a graphical representation of the COLTS arrangement are shown in Figure 4. The platens were rotated to apply mechanical loads to the test article. Five loading condition combinations were applied to the pristine MBB in a series of experiments, first up to design limit load (DLL) and then up to design ultimate load (DUL) levels for each condition. These loading conditions were 1) an internal pressure load alone; 2) a load simulating a 2.5-g wing up-bending condition which subjects the crown panel to compressive loads; 3) a -1-g wing down-bending condition which subjects the crown panel to tensile loads; 4) a combination of pressure and -1-g wing down-bending; and 5) a combination of pressure and 2.5-g wing up-bending. Details of the MBB testing, load conditions, and results are presented in References 8-10.

An important design feature of the MBB is the integrally stitched T-cap, shown in Figure 5 as the magnified portion of the panel, which provides connectivity of the corner joint between orthogonal panels and enables determinant assembly. The integrally stitched T-cap was introduced in the composite semi-span test article that was tested at LaRC as part of the Advanced Subsonic Technology (AST) Wing Program.[11-13] In Figure 5, the test specimen harvest pattern for various test articles is shown, with the T-cap harvest area identified by the red highlighting and the T1 and T2 labels. The stringer and frame locations and labels are also shown. The T-cap is a blade configuration with a web attached to the adjacent panel, and with flanges integrated into the skin region of the panel as shown in Figure 6. The stacks that comprise the web are those that wrap at its base to make up the outer and inner flanges. Inner refers to the pressurized side (pressurized portion interior), and outer refers to the unpressurized side (exterior) of the T-cap web. Filler material, referred to as the noodle, was inserted into the cavity created by the flange wrap radii and the skin stacks. The baseline T-cap has stitches at the locations indicated by the dashed light green lines in Figure 6. When incorporated into the final structure, the integral T-cap web height is trimmed according to the

fastener pattern to reduce weight. A close-up view showing the effect of trimming on the integral T-cap joining the MBB crown to the upper bulkhead is shown in Figure 7, with the integral T-cap being incorporated into the crown panel. T-caps were first integrated and tested for PRSEUS panels in the Pressure Cube, which is highlighted in Figure 3 with the MBB, where the highlighted region indicates the only PRSEUS test articles that have the integral T-caps. The Pressure Cube was loaded under only pressure load and was tested at the COLTS Facility.[14, 15] While being loaded under pressure, the T-caps are both pulled in tension and bent about the base. During testing of the Pressure Cube, areas of delamination were detected in the region of the T-cap base and radii (web/skin interface).[16] In order to better characterize the performance of the T-cap, a series of bending and tension tests were conducted on several designs of the T-cap. This paper presents and summarizes the test results for the T-cap tension and bending tests.

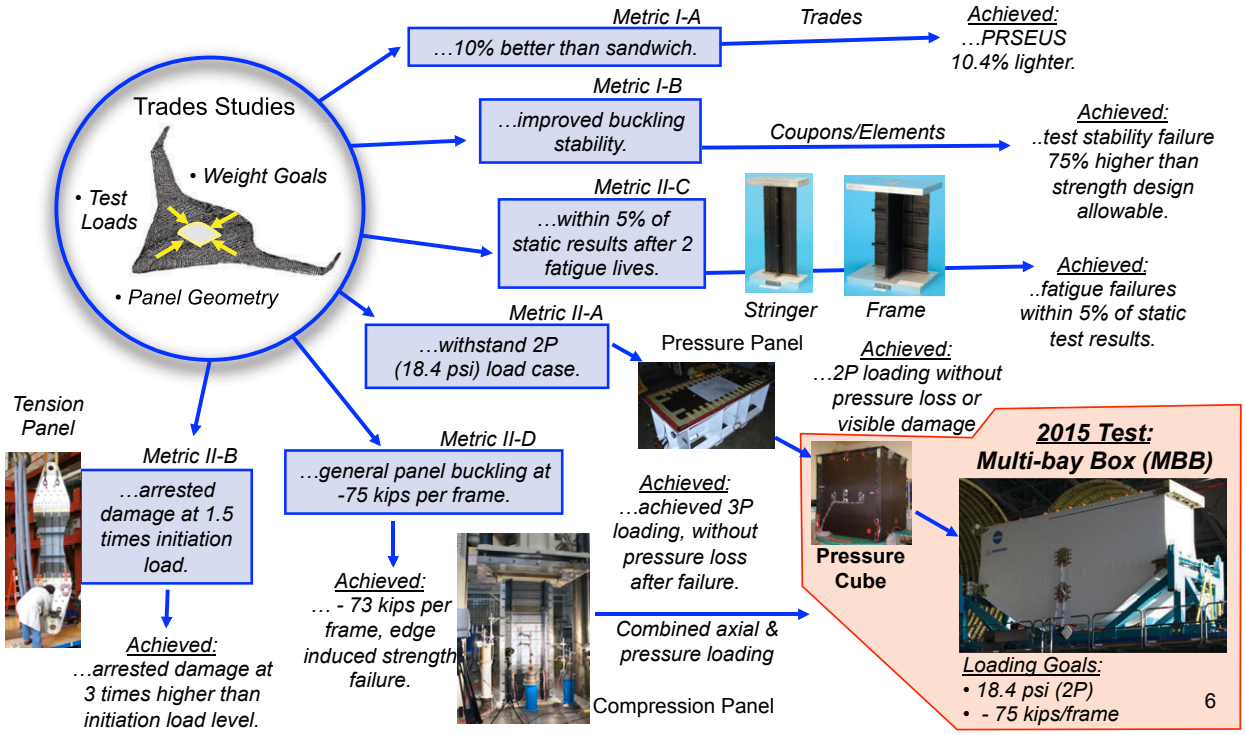

Figure 3. HWB structural development building-block approach.

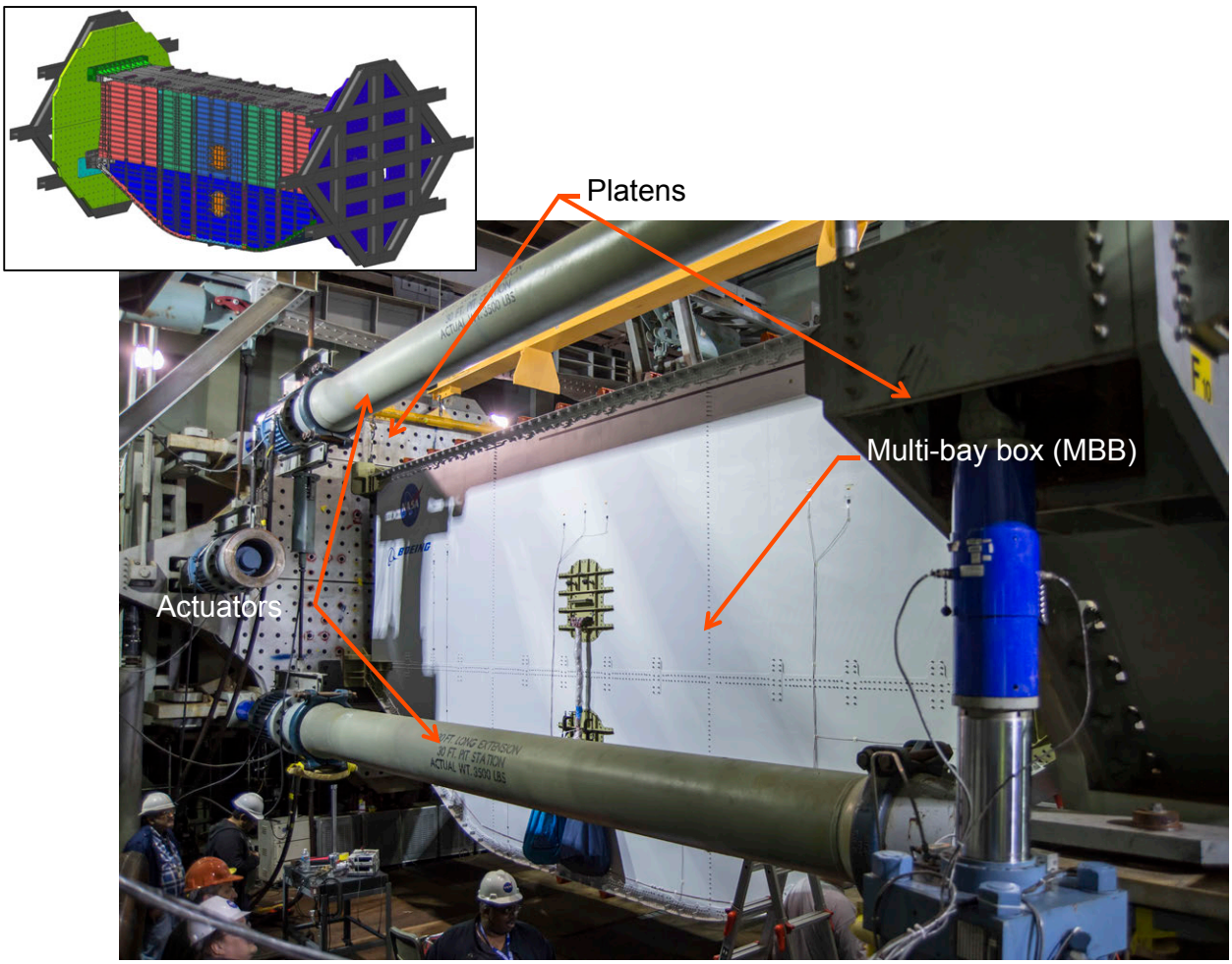

Figure 4. Photograph of the Multi-bay pressure box in the COLTS test chamber and graphical representation (inset).

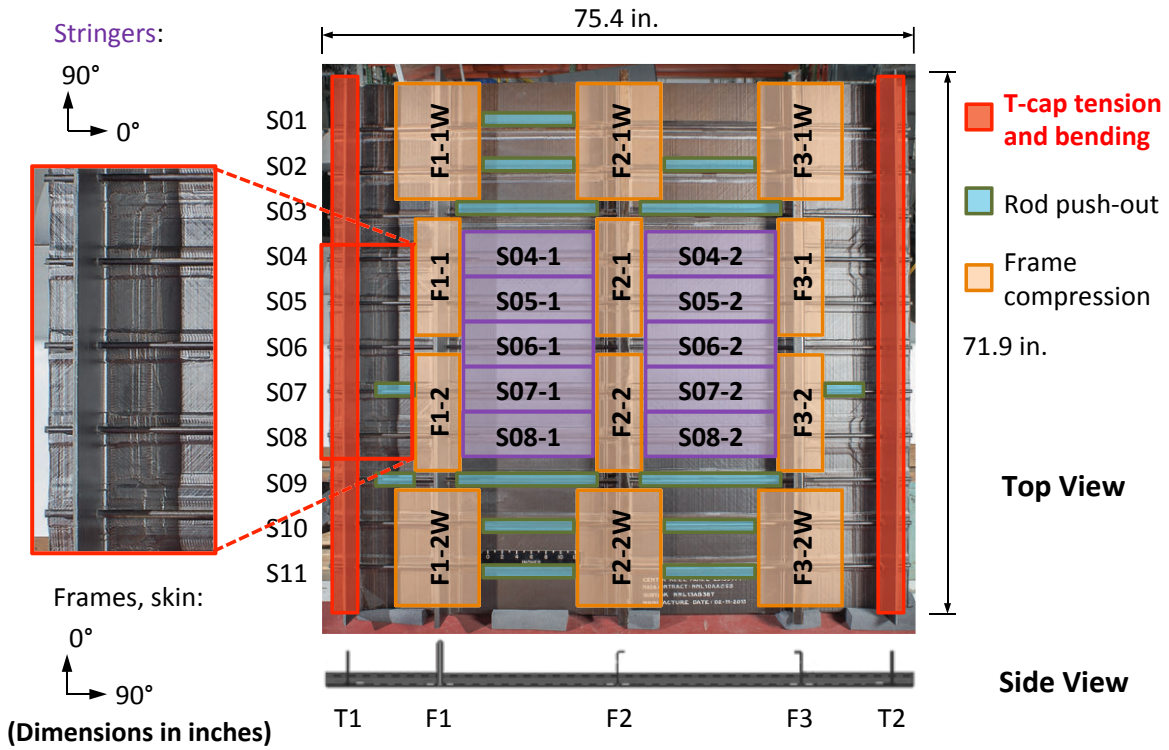

Figure 5. Alternate center keel panel with integral T-caps.

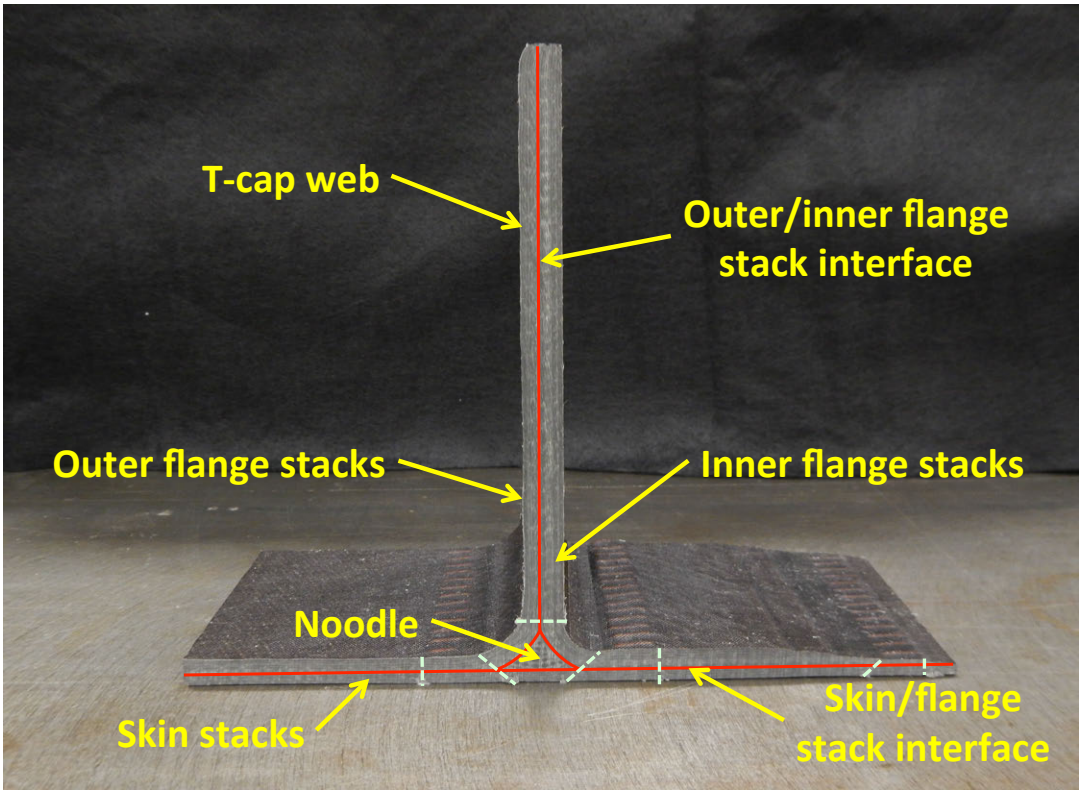

Figure 6. T-cap configuration showing test article cross-section, with light green dashed lines indicating typical manufacturing stitch locations.

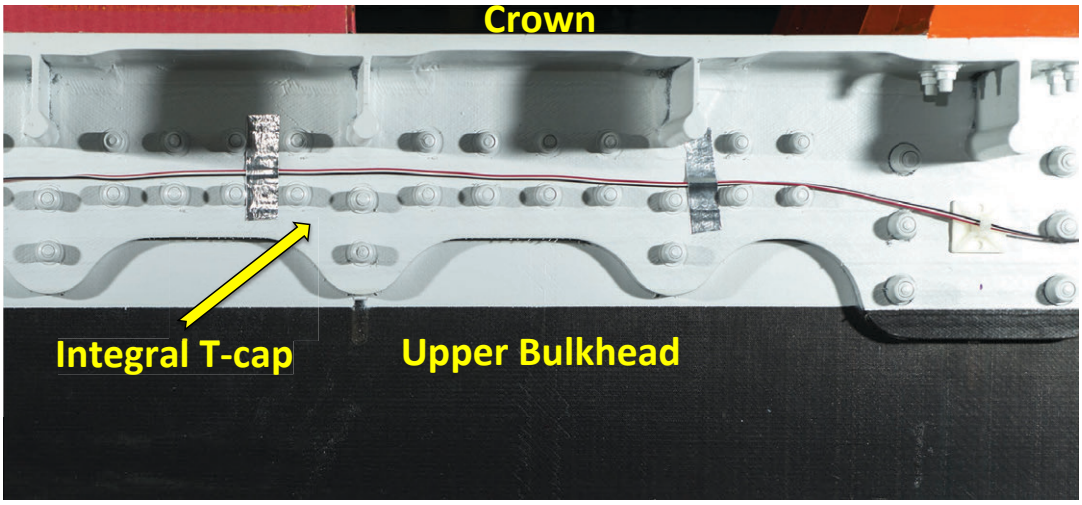

Figure 7. Close-up of crown integral T-cap on MBB.

The objectives of the T-cap testing were as follows:

- Determine the failure loads for various T-cap configurations and designs under only tension or bending load.
  - Identify load at initial failure.
  - Identify residual strength (maximum sustained load).
  - Characterize the failure modes associated with the failure loads identified in conjunction with this objective.
- Provide analysis validation data.

Test Article Description

The T-cap test articles were cut from the alternate keel (Figure 5) that was manufactured for the MBB as a risk-reduction article, as it would supply material in case the MBB needed repair involving a structural patch.[17] Since no such repair was required, the alternate keel became the source for a number of component test articles. In addition to the T-cap specimens that are the focus of this report, test articles cut from the alternate keel included stringer compression (including a new wrap), frame compression (including a two new solid frame designs), and stringer push-out (including ones with adhesive between the wrap and rod), all of which are discussed in other reports.[18, 19]

The alternate keel included three different T-cap designs for subcomponent testing. The baseline T-cap has only one stitch row at the base of the T-cap web located at the top of the fillet, and is the design that was used in the MBB. The two additional designs added stitching rows to the T-cap web at either 0.5- or 1.0-inch spacing along the height of the web to determine if there were advantages to additional web stitching. Web stitching patterns are shown in Figures 8a-8c, with stitch line locations indicated by the arrows. For each of these web stitch patterns, there are two configurations of specimens included, namely one without a stringer and one that has a stringer penetrating the T-cap web through a keyhole. The overall T-cap testing matrix is shown in Table 1. Specimens are of the same general dimensions for both the tension and bending tests, with typical test article cross-section and dimensions shown in Figure 9. However, due to slight variability in manufacturing, and in variations in cutting the test articles, test article designations and their as-measured dimensions are provided in Table 2, with groups of like specimens shown with unshaded or shaded row groupings. In the table, location refers to the T-cap and stringer location from which the test article was cut (see Figure 5).

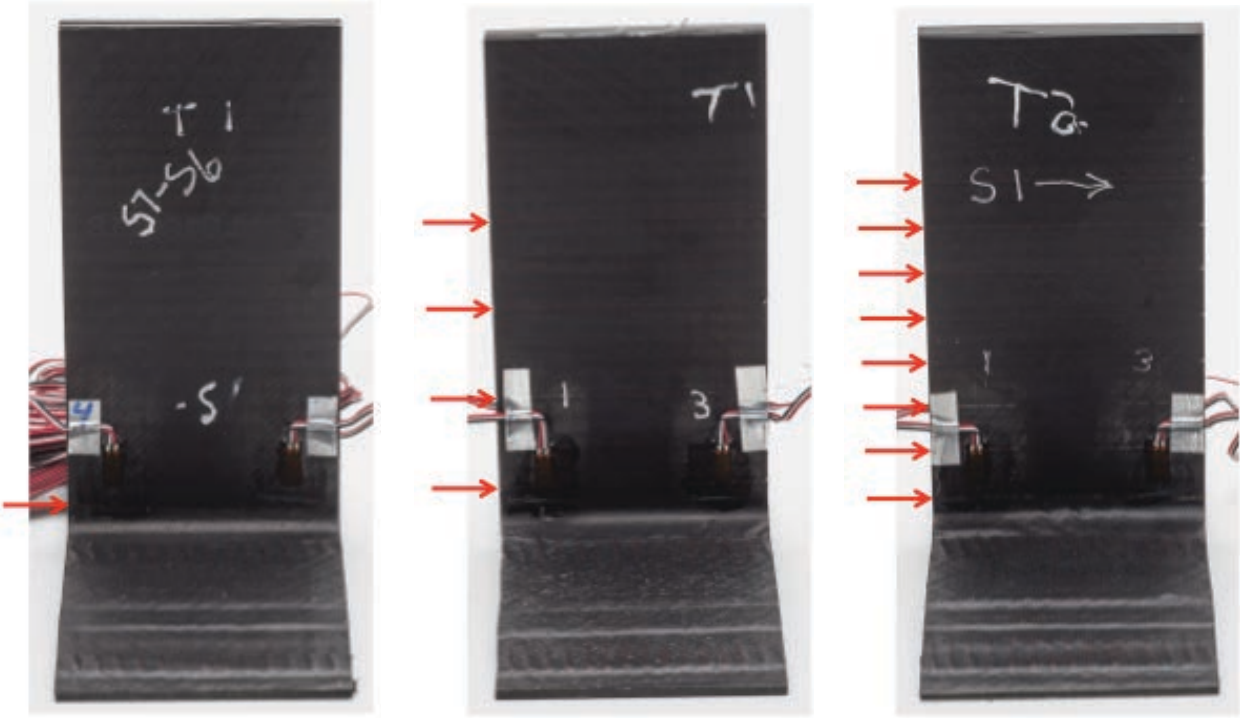

a) Baseline, radius only b) 1-inch spacing c) ½-inch spacing

Figure 8. T-cap web stitching patterns, all with row of stitching at top of fillet region adjacent to flanges. Arrows indicate locations of web stitch lines.

Table 1: Summary T-cap testing matrix.

Test	Web Stitching	With Stringer	No Stringer
Bending	None (baseline)	3	2
	0.5 inch spacing	3	3
	1.0 inch spacing	3	3
Tension	None (baseline)	3	2
	0.5 inch spacing	3	3
	1.0 inch spacing	3	3

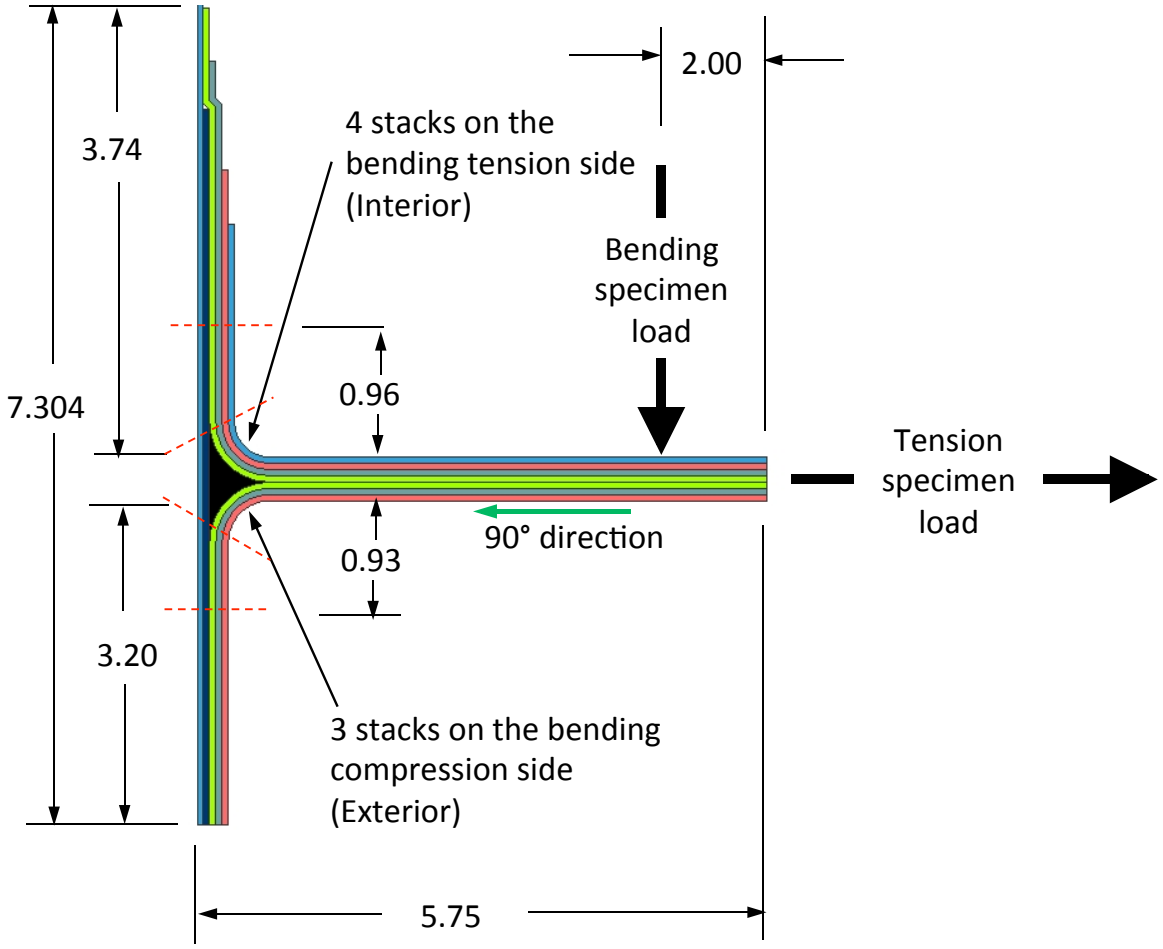

Figure 9. T-caps test article cross-section sketch. The stack 0-degree direction is perpendicular to the cross-section, and the specimens are nominally 2.9 inches wide. (Dimensions in inches)

Table 2: Detailed T-cap testing matrix. (Dimensions in inches)

							Stringer Edge Distance (Measured on overhang Side)							
Test Article ID	**Description**	**Location**	**Web Width - Top**	**Web Thickness - Top (L/R)**	**Web Width - Bottom**	**Web Thickness - Bottom (L/R)**	**L of bulb**	**R of bulb**	**Stringer Dia. (calculated)**	**Stringer Dia. (measured)**	**Center Distance**	**Actual Center Dist.**	**Center Dist. Diff.**	**Gages 1 & 3 Side**
BNS1	Bending, no web stitching, with stringer	T1, S7	2.8855	0.3685/0.3635	2.9090	0.3630/0.3695	1.7380	1.2145	0.5235	0.4845	1.4545	1.4568	-0.0023	Interior
BNS2	Bending, no web stitching, with stringer	T2, S5	2.8790	0.3665/0.3610	2.8880	0.3580/0.3600	1.6390	1.1345	0.5045	0.4890	1.4440	1.3790	0.0650	Interior
BNS3	Bending, no web stitching, with stringer	T2, S6	2.9085	0.3695/0.3615	2.9100	0.3695/0.3610	1.7130	1.2210	0.4920	0.4905	1.4550	1.4663	-0.0113	Interior
BNN1	Bending, no web stitching, no stringer	T1, S6-S7	2.8620	0.3670/0.3650	2.8640	0.3575/0.3680	N/A	N/A	N/A	N/A	N/A	N/A	N/A	Exterior
BNN2	Bending, no web stitching, no stringer	T2, S6-S7	2.9225	0.3685/0.3585	2.9210	0.3660/0.3645	N/A	N/A	N/A	N/A	N/A	N/A	N/A	Interior
B5S1	Bending, 0.5 inch web stitching, with stringer	T1, S9	2.8870	0.3600/0.3645	2.8785	0.3765/0.3730	1.6535	1.1190	0.5345	0.5370	1.4393	1.3875	0.0518	Interior
B5S2	Bending, 0.5 inch web stitching, with stringer	T2, S1	2.8860	0.3680/0.3605	2.9110	0.3760/0.3765	1.6890	1.2070	0.4820	0.4755	1.4555	1.4448	0.0108	Interior
B5S3	Bending, 0.5 inch web stitching, with stringer	T2, S2	2.9115	0.3545/0.3665	2.9275	0.3655/0.3735	1.7175	1.2465	0.4710	0.4750	1.4638	1.4840	-0.0202	Interior
B5N1	Bending, 0.5 inch web stitching, no stringer	T1, S11-S12	2.8565	0.3660/0.3685	2.8105	0.3685/0.3690	N/A	N/A	N/A	N/A	N/A	N/A	N/A	Interior
B5N2	Bending, 0.5 inch web stitching, no stringer	T2, S1-	2.9220	0.3565/0.3605	2.9070	0.3715/0.3810	N/A	N/A	N/A	N/A	N/A	N/A	N/A	Interior
B5N3	Bending, 0.5 inch web stitching, no stringer	T2, S2-S3	2.9310	0.3655/0.3710	2.9000	0.3665/0.3685	N/A	N/A	N/A	N/A	N/A	N/A	N/A	Interior
B1S1	Bending, 1.0 inch web stitching, with stringer	T1, S3	2.8685	0.3580/0.3690	2.9190	0.3620/0.3720	1.7030	1.2035	0.4995	0.4905	1.4595	1.4488	0.0108	Interior
B1S2	Bending, 1.0 inch web stitching, with stringer	T2, S10	2.9000	0.3655/0.3600	2.9055	0.3645/0.3585	1.6775	1.1830	0.4945	0.4915	1.4528	1.4288	0.0240	Interior
B1S3	Bending, 1.0 inch web stitching, with stringer	T2, S11	2.8735	0.3595/0.3685	2.9030	0.3660/0.3710	1.6880	1.2335	0.4545	0.4760	1.4515	1.4715	-0.0200	Interior
B1N1	Bending, 1.0 inch web stitching, no stringer	T1, S1-	2.9035	0.3595/0.3640	2.8810	0.3705/0.3665	N/A	N/A	N/A	N/A	N/A	N/A	N/A	Interior
B1N2	Bending, 1.0 inch web stitching, no stringer	T2, S9-S10	2.9185	0.3605/0.3610	2.9105	0.3620/0.3590	N/A	N/A	N/A	N/A	N/A	N/A	N/A	Exterior
B1N3	Bending, 1.0 inch web stitching, no stringer	T2, S10-S11	2.8775	0.3600/0.3630	2.8965	0.3690/0.3695	N/A	N/A	N/A	N/A	N/A	N/A	N/A	Interior
TNS1	Tension, no web stitching, with stringer	T1, S5	2.9205	0.3540/0.3580	2.9220	0.3765/0.3765	1.6935	1.2255	0.4680	0.4715	1.4610	1.4613	-0.0002	Interior
TNS2	Tension, no web stitching, with stringer	T1, S6	2.8840	0.3600/0.3720	2.9120	0.3790/0.3750	1.7300	1.2530	0.4770	0.4615	1.4560	1.4838	-0.0277	Interior
TNS3	Tension, no web stitching, with stringer	T2, S7	2.8715	0.3640/0.3575	2.9160	0.3715/0.3600	1.7365	1.2620	0.4745	0.4715	1.4580	1.4978	-0.0398	Interior
TNN1	Tension, no web stitching, no stringer	T1, S5-S6	2.8935	0.3705/0.3660	2.9065	0.3830/0.3825	N/A	N/A	N/A	N/A	N/A	N/A	N/A	Interior
TNN2	Tension, no web stitching, no stringer	T2, S5-S6	2.8880	0.3640/0.3640	2.8980	0.3760/0.3715	N/A	N/A	N/A	N/A	N/A	N/A	N/A	Exterior
T5S1	Tension, 0.5 inch web stitching, with stringer	T2, S3	2.8735	0.3715/0.3640	2.9250	0.3745/0.3655	1.6915	1.1765	0.5150	0.5125	1.4625	1.4328	0.0297	Interior
T5S2	Tension, 0.5 inch web stitching, with stringer	T1, S10	2.8945	0.3540/0.3670	2.8915	0.3730/0.3720	1.6635	1.1625	0.5010	0.4900	1.4458	1.4075	0.0382	Interior
T5S3	Tension, 0.5 inch web stitching, with stringer	T1, S11	2.8700	0.3640/0.3650	2.8845	0.3770/0.3865	1.6495	1.2070	0.4425	0.4705	1.4423	1.4423	0.0000	Interior
T5N1	Tension, 0.5 inch web stitching, no stringer	T1, S11+	2.8895	0.3615/0.3675	2.8870	0.3775/0.3785	N/A	N/A	N/A	N/A	N/A	N/A	N/A	Interior
T5N2	Tension, 0.5 inch web stitching, no stringer	T1, S9-S10	2.8715	0.3700/0.3690	2.8730	0.3740/0.3770	N/A	N/A	N/A	N/A	N/A	N/A	N/A	Exterior
T5N3	Tension, 0.5 inch web stitching, no stringer	T2, S1-S2	2.9025	0.3710/0.3675	2.9115	0.3745/0.3705	N/A	N/A	N/A	N/A	N/A	N/A	N/A	Interior
T1S1	Tension, 1.0 inch web stitching, with stringer	T1, S1	2.9065	0.3650/0.3630	2.8945	0.3715/0.3785	1.7220	1.2395	0.4825	0.4815	1.4473	1.4803	-0.0330	Interior
T1S2	Tension, 1.0 inch web stitching, with stringer	T1, S2	2.8740	0.3665/0.3600	2.8960	0.3680/0.3730	1.6795	1.2140	0.4655	0.4660	1.4480	1.4470	0.0010	Interior
T1S3	Tension, 1.0 inch web stitching, with stringer	T2, S9	2.8915	0.3600/0.3685	2.8940	0.3690/0.3685	1.7650	1.2525	0.5125	0.4995	1.4470	1.5023	-0.0552	Interior
T1N1	Tension, 1.0 inch web stitching, no stringer	T1, S1-S2	2.9220	0.3690/0.3720	2.9095	0.3750/0.3650	N/A	N/A	N/A	N/A	N/A	N/A	N/A	Interior
T1N2	Tension, 1.0 inch web stitching, no stringer	T1, S2-S3	2.8640	0.3685/0.3695	2.8910	0.3685/0.3630	N/A	N/A	N/A	N/A	N/A	N/A	N/A	Exterior
T1N3	Tension, 1.0 inch web stitching, no stringer	T2, S11+	2.9275	0.3660/0.3600	2.8995	0.3725/0.3695	N/A	N/A	N/A	N/A	N/A	N/A	N/A	Interior

* S#-S## indicates located between stringers # and ##, and S#+ or S#- indicates located between stringer # and the edge of the panel.

Test Setup

The tension and bending T-cap testing was conducted in two load frames located in the Materials Research Laboratory (MRL) at NASA LaRC. The following two sections outline the setup for the tension and bending tests, respectively.

T-cap Tension Test Setup

Tension testing of the T-caps was conducted in the 50-kip capacity load frame shown in Figure 10. The locations of the cameras used for digital image correlation (DIC), a linear variable displacement transducer (LVDT), and other instrumentation features, are shown in the figure and are described in the Instrumentation section. The test article was bolted to a base plate fitting that was held by the hydraulic grip mounted to the load cell at the base of the load frame, as shown in Figure 11. The web of the test article was held by an upper hydraulic grip that is kept from sliding on the test article by the presence of a diamond knurl pattern on the surface of the grip wedges. Grip hydraulic pressure was set between 1000 and 1200 psi. The upper grip was located such that two inches of the T-cap web was within the grip wedges, which exposed a height of the T-cap web of 3.75 inches as measured from the exterior skin surface. Two bolts and a clamp plate are used to affix the test article to the base plate through both the inner and outer skin/flange regions. Also seen in Figure 11 are shims inserted at the inner skin/flange location to account for the stack drops, with shimming required for all test articles at this location. For the test articles having a stiffener, there were also shims used on the outer skin portion. Details of the base plate fitting and clamp plates are provided in Appendix A, along with the drill template that was used for drilling tension and bending test articles to match the fixture components.

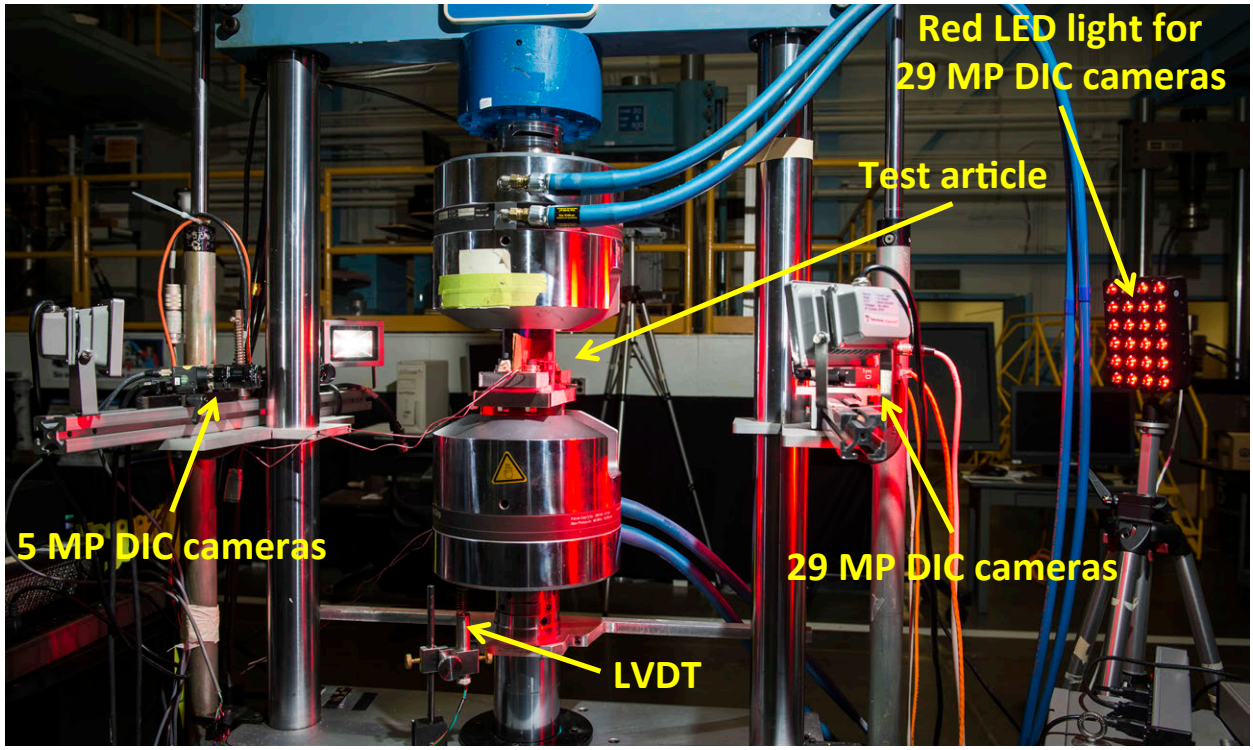

Figure 10. T-cap tension testing load frame with 50-kip load capacity.

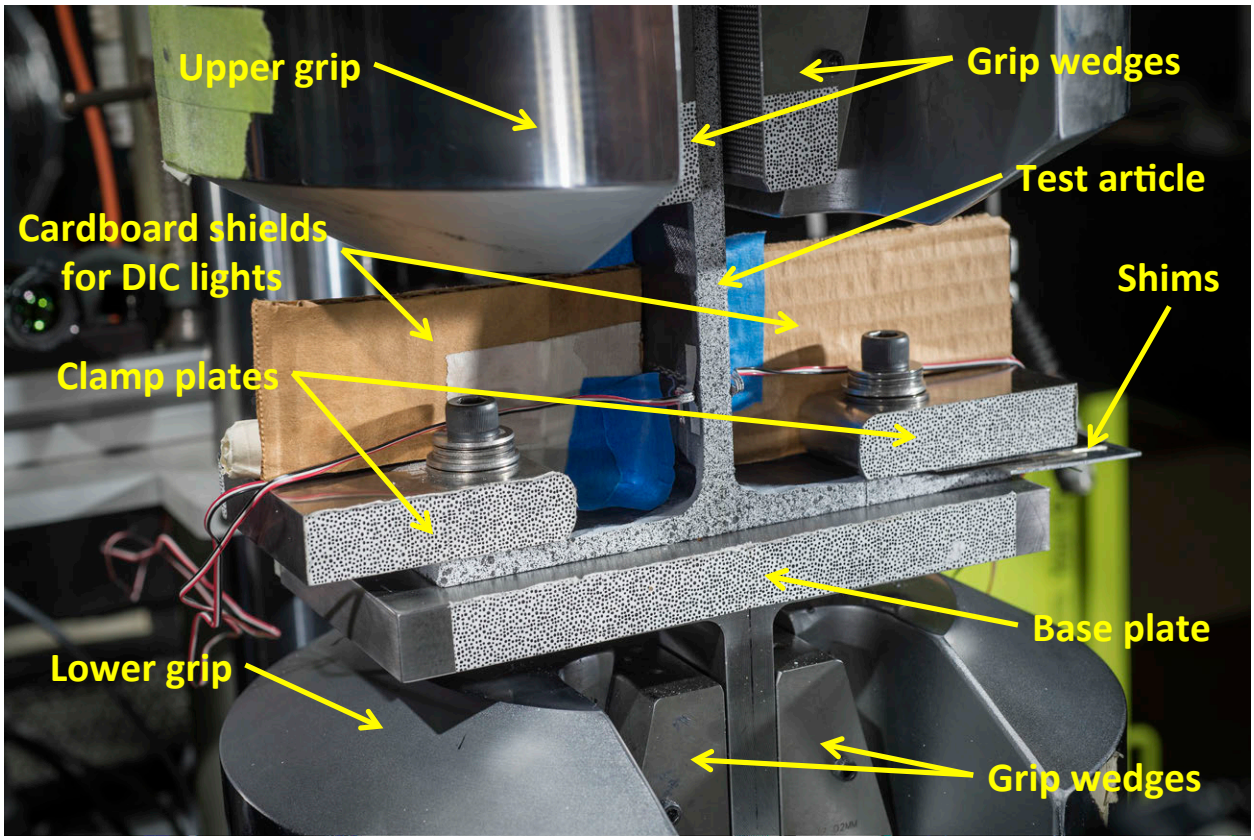

Figure 11. Close-up of stringerless T-cap test article mounted in tension load frame. (View from 29MP VIC system side)

T-cap Bending Test Setup

Bending testing of the T-caps was conducted in a 2.5-kip capacity load frame as shown in Figure 12. The test article was bolted to an assembly attached to bolting slots located at the base of the load frame. The clamp plates from the tension tests were used for the bending tests. Similarly, the test article was shimmed on the inner skin/flange region for all test articles, and on the outer skin/flange region for the test articles having stringers. A close-up of a test article mounted in the load frame is shown in Figure 13. The pusher that applies the line load to induce bending is attached using a threaded rod, connecting it to the load cell that is mounted on the upper portion of the load frame. As shown in Figure 9, the bending line load was applied at a distance of 3.75 inches from the skin outer mold line. Details of the bending test fixture components are provided in Appendix B.

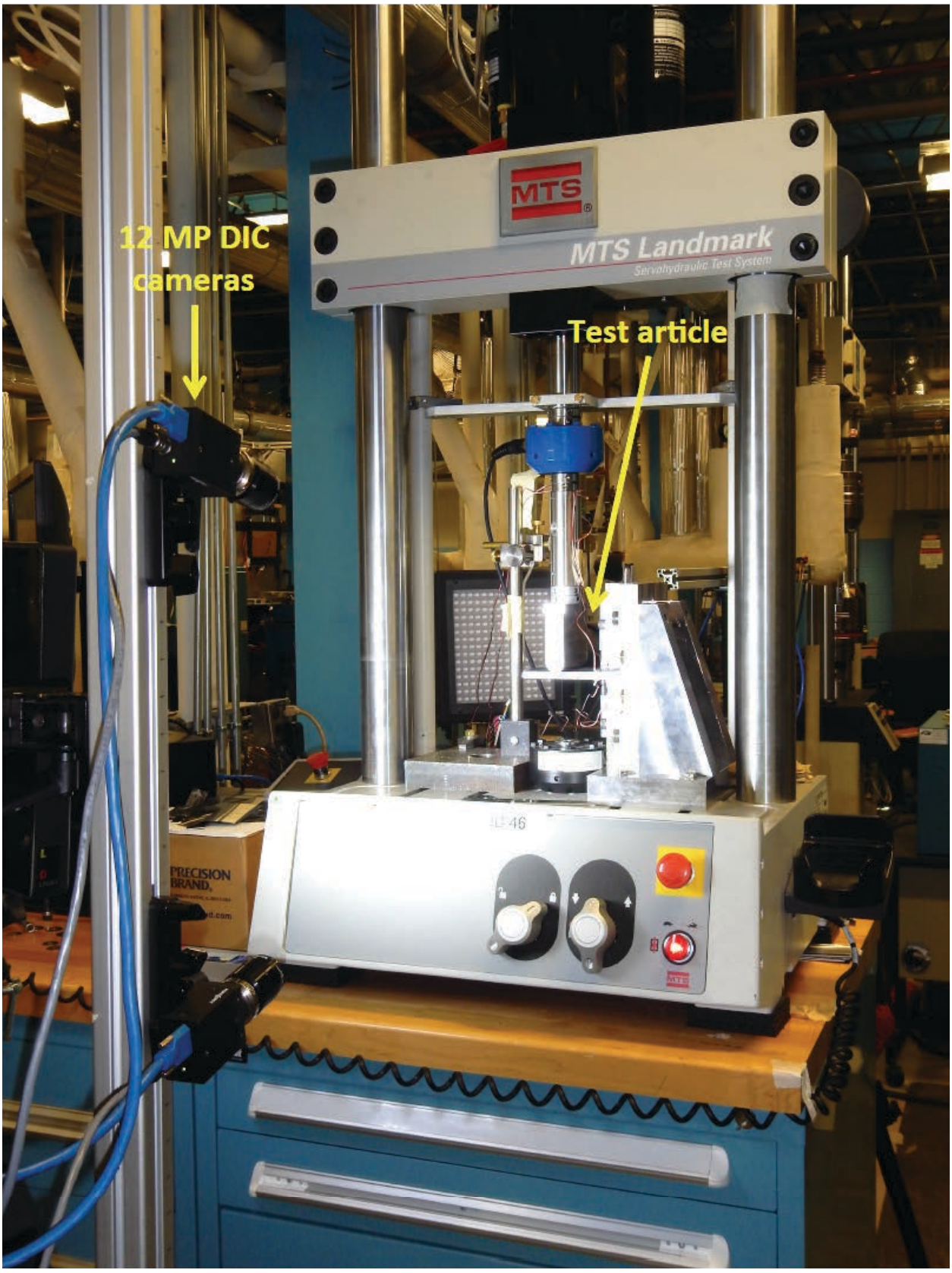

Figure 12. T-cap tension testing load frame with 2.5-kip load capacity. (View from front)

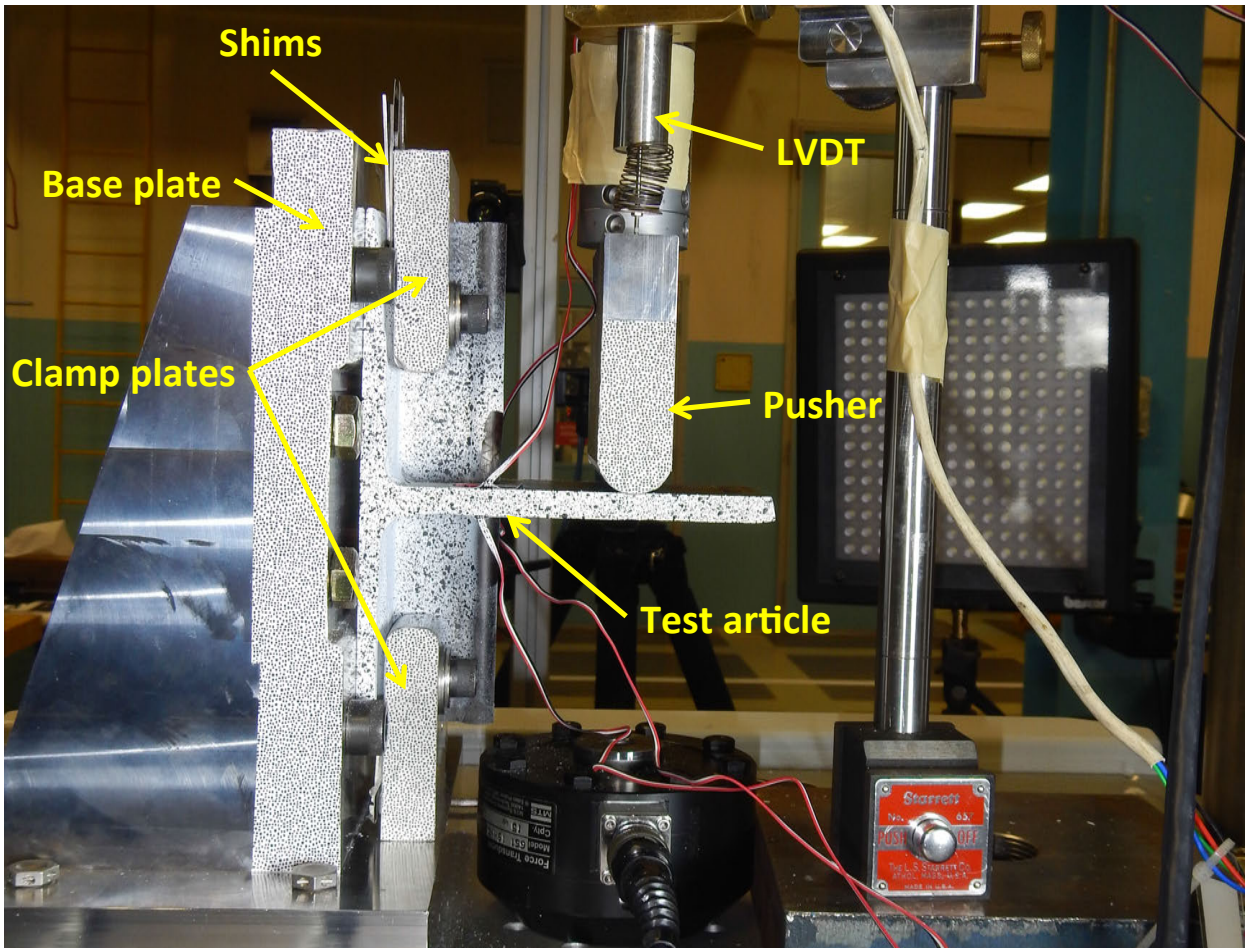

Figure 13. Close-up of stringerless T-cap test article mounted in bending load frame. (View from back)

Test Conditions and Summary

The tests were performed at ambient room temperature in the high bay of the MRL. The load frames applied load under displacement control, and each test article was loaded until final failure occurred as determined by the test engineer. Initial failure is defined as the initiation of delaminations, while final failure was defined as having reached the maximum load attainable for the specimen. Test article response was measured and recorded using standard instrumentation and DIC techniques.

Each of the 34 test articles identified in Table 2 was loaded in a single load sequence. Uniform displacement was monotonically applied until failure occurred, with the resulting load being measured by the load cell. The anticipated failure mechanism was expected to be delamination and separation in the radius region of the t-cap web/flange interface or below the web within the noodle region adjacent to the skin stack. Stitches were expected to arrest the delaminations until stitch failure allowed the failures to grow. Details of the failure growth are discussed for each type of test article in the Test Data and Discussion section.

The stroke rates used for the testing depended on the presence of a stringer and on load type (tension or bending). Table 3 shows the loading rates used for each test article. The stroke rate for the tension test articles was kept constant throughout each test. However, the stroke rate for the bending tests was increased after several delamination failures were observed, and after the behavior became reasonably stable, in order to shorten the length of the tests. Tension tests typically took about 8-10 minutes for the stringerless test articles, and 18-20 minutes for

the stringer test articles. Bending tests typically took about 18-20 minutes for the stringerless test articles, and 12-17 minutes for the stringer test articles.

Table 3: Stroke rates for T-cap testing.

Tension Test Articles		Bending Test Articles			
	Initial		Initial	Accelerated	
ID	Rate (in/min)	ID	Rate (in/min)	Rate (in/min)	@ stroke (in)
TNS1	0.01	BNS1	0.04	N/A	N/A
TNS2	0.01	BNS2	0.04	0.08	0.4
TNS3	0.01	BNS3	0.05	0.1	0.4
TNN1	0.02	BNN1	0.025	N/A	N/A
TNN2	0.02	BNN2	0.05	0.1	0.5
T5S1	0.01	B5S1	0.04	0.08	0.4
T5S2	0.01	B5S2	0.05	0.1	0.4
T5S3	0.01	B5S3	0.05	0.1	0.4
T5N1	0.02	B5N1	0.05	0.1	0.5
T5N2	0.02	B5N2	0.05	0.1	0.52
T5N3	0.02	B5N3	0.05	0.1	0.45
T1S1	0.01	B1S1	0.04	0.08	0.425
T1S2	0.01	B1S2	0.05	0.1	0.42
T1S3	0.01	B1S3	0.05	0.1	0.45
T1N1	0.02	B1N1	0.05	0.1	0.4
T1N2	0.02	B1N2	0.05	0.1	0.5
T1N3	0.02	B1N3	0.05	0.1	0.5

For the tension tests, the test articles were drilled to match the base plate using a drill template. The test articles were positioned so that the web of the integral T-cap was co-planar with and centered above the tang of the base plate, However, due to tolerances in drilling the mounting holes in the test specimen and in aligning the test article with the drill plate, it was not possible to guarantee that this alignment was attained. Therefore, strains were measured during the gripping of the T-cap web by the upper grip in order to characterize the induced bending and twist that resulted from any misalignment. Strains were measured during loading from this initial strain state such that the strains measured during the test included both the initial prestrain due to misalignment and the applied load. For the bending tests, the test articles were drilled to match the base plate so that the T-cap web plane was perpendicular to the plane of the pusher, and the pusher attained line contact simultaneously along the width of the web. However, again due to drilling and alignment tolerances, this was not always the case. Any twist that may have been introduced due to misalignment was immediately apparent upon the introduction of the load, and the strains through the test were a measure of the total strain that included strains introduced by both misalignment and the applied load.

Instrumentation

Each test article had responses measured and recorded using standard instrumentation and digital image correlation techniques. Displacements of the actuated components were recorded using an LVDT, and load frame stroke was also recorded. Strain gages were used to monitor load symmetry. DIC was used to monitor the response, displacement and strains of both of the

test article cross-section surfaces and adjacent test fixtures. Additional details of the instrumentation is provided in the following sections.

Conventional Instrumentation

The strain gage pattern is shown in Figure 14, and consists of two back-to-back pairs of strain gages. Gages 1 and 3 are on the same surface of the test article, and gages 2 and 4 are back-to-back to gages 1 and 3, respectively. Typically, gages 1 and 3 were located on the interior surface of the T-cap web, with gages 2 and 4 located on the exterior surface of the T-cap web (see Figure 9). However, several of the test articles had gages 1 and 3 installed on the exterior surface of the T-cap web. Table 2 indicates the surface on which the gages 1 and 3 were installed for the various test articles. CEA-06-250UN-350 strain gages were used, and had 10-ft. lead wires. The gages were used to monitor gross response of the web during loading, as mentioned previously, to monitor if bending was being applied during clamping of the test article web by the grips during the tension tests, and to monitor if twisting was being applied to the web during initial contact of the pusher during the bending tests.

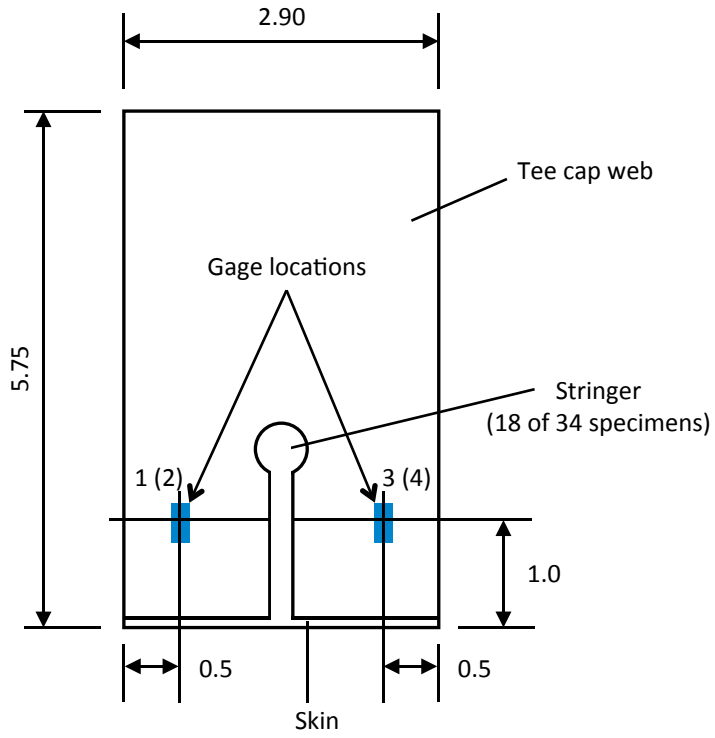

Figure 14. T-cap strain gage pattern for all test articles.

Displacements were recorded using an LVDT for the actuated grip and the pusher for the tension and bending tests, respectively. Locations of the LVDTs can be seen in Figures 10 and 13 for the tension and bending tests, respectively. Load frame stroke was also recorded during loading for direct comparison to the LVDTs. During the tests, response was monitored by plots of load vs. stroke, load vs. LVDT displacement, and strains vs. stroke.

Digital Image Correlation

DIC was used to monitor the response of the T-cap cross-sections and the adjacent fixture components. The DIC setup for the tension and bending test articles were not the same. For the tension tests, different camera arrangements were used to view the opposite sides of the test article. One side used a single set of Allied Vision Technologies Prosilica GT6600 (29 MP) cameras.[20] These 29 MP cameras provided a single field of view that encompassed the entire T-cap cross-section and the adjacent fixture, and viewed the test article with the interior portion of the skin on the right side of the image. The other side of the test article was viewed using two sets of Point Grey Flea3 FL3-GE-50S5M-C (5 MP) cameras.[21] One set provided a global view of the T-cap cross-section and the adjacent fixture, and one set provided a view that was localized on the noodle region at the T-cap web/flange interface. The global and local 5 MP cameras viewed the test article with the interior portion of the skin on the left side of the image. Figure 15 shows the approximate area of the test article covered by the local DIC, which was a field of view approximately 1.5 inches high and 2.0 inches wide. For the bending tests, an identical camera arrangement was used to view both sides of the test article. The camera setup used a set of Point Grey Grasshopper3 GS3-U3-120S6M-C (12 MP) cameras.[21] Each set of cameras provided a single field of view that encompassed the entire T-cap cross-section and the adjacent fixture.

White light sources were used for the DIC, with the exception of the area covered by the GT6600 cameras for which red light sources were used. In the case of the tension tests, it was necessary to mask regions not filled by the test article to avoid interference from opposing lighting sources. This was accomplished using cardboard as seen in Figure 11. DIC was performed using the Correlated Solutions VIC3D software.[22] Real-time data were displayed during the test to monitor strains and displacements. Load was recorded by each DIC system and correlated with the image numbers.

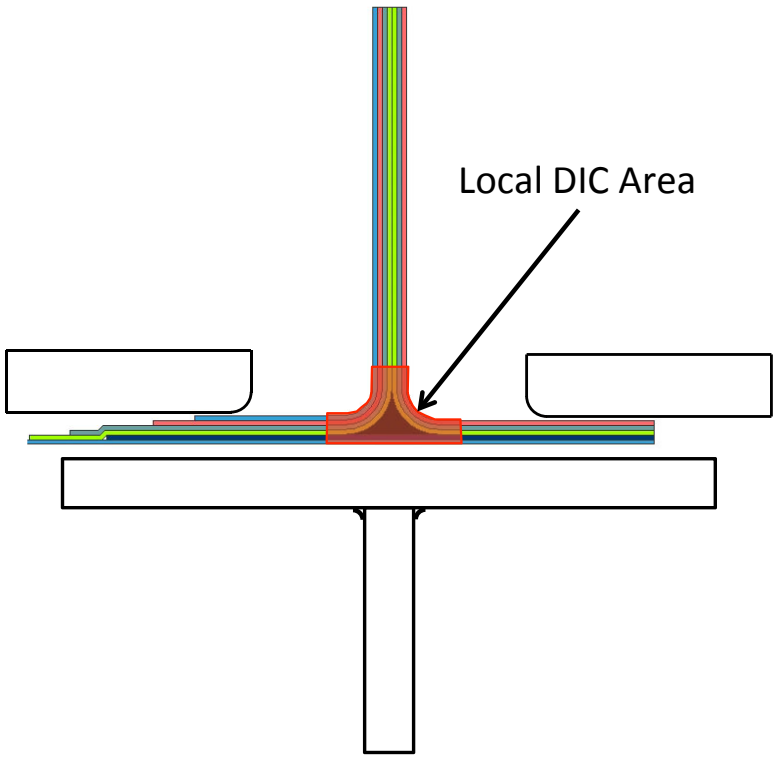

Figure 15. Tension test DIC region coverage area surfaces and local DIC area.

Test Data and Discussion

Raw test data for the 34 test articles are presented in Appendix C. Data presented in the appendix include xy-plots of load vs. stroke and load vs. strain, contour plots of strains at various loads for selected test articles (one of each type), and images of the failures that occurred for the selected test articles for which strain contours were provided. This section summarizes and discusses the test data presented in the appendix.

There are several pieces of information pertaining to the previously stated objective of determining the failure loads for the various T-cap configurations under only tension or bending load. First is to identify the initial failure load and the associated mode, and second is to identify the maximum load and the failure mode that is associated with the maximum load. Between these failure loads, it is desired to describe and discuss the progression of the damage growth. Failure loads were obtained by looking at the load vs. strain and load vs. stroke plots in Appendix C. For example, see Figure 16, which is the load vs. strain plot for the TNS1 test article. First, it is noticed that at zero load, there is nonzero strain measured by the four strain gages. As previously mentioned, it was very difficult to ensure that the web of the T-cap was planar with and centered over the base plate tang. The nonzero strains represent the presence of bending induced on the test article while the T-cap web was being gripped by the upper grip wedges. Additionally, an induced torsion of the T-cap web is indicated by the back to back strain gage pairs on either side of the web, gages 1 and 3 on one side and 2 and 4 on the other, not measuring the same strain values. In this case, the side of the specimen with gages 3 and 4 back to back is exhibiting slightly more bending than the other side This indicates that the gages 3 and 4 side is farther off the plane of the base plate tang than the gages 1 and 2 side. Second, the plot is used to identify the initial failure load. In Figure 16, there is a discontinuity in the strain gage plot for gage 2 at just over 2000 lbs. However, this response is localized since there is no corresponding change in plots for the remaining strain gages, and DIC did not indicate the formation of a delamination crack, so this response is considered not to be initial failure. The first load at which all four gages show a change in response is at 2599 lbs, and this value is chosen as the initial failure load since it results in a delamination that spans the entire width of the test article. As seen in the load vs. stroke plot presented in Figure 17 for the TNS1 test article, there is no appreciable load drop associated with this event, but it is clearly indicated in the strain gage data. The maximum load is obtained from the load vs. stroke plot as indicated in Figure 17, and is 7287 lbs. While the load vs. strain and load vs. stroke plots were sufficient to clearly determine the initial and maximum failure loads for the TNS1 test article, there were test articles when this was not the case. For those test articles, the DIC strain contour plots were used as the primary means to identify the initial delamination failure since the DIC data indicated the presence of failures on the cross-section surfaces that resulted in very small or not clearly observable changes the conventional data plots.

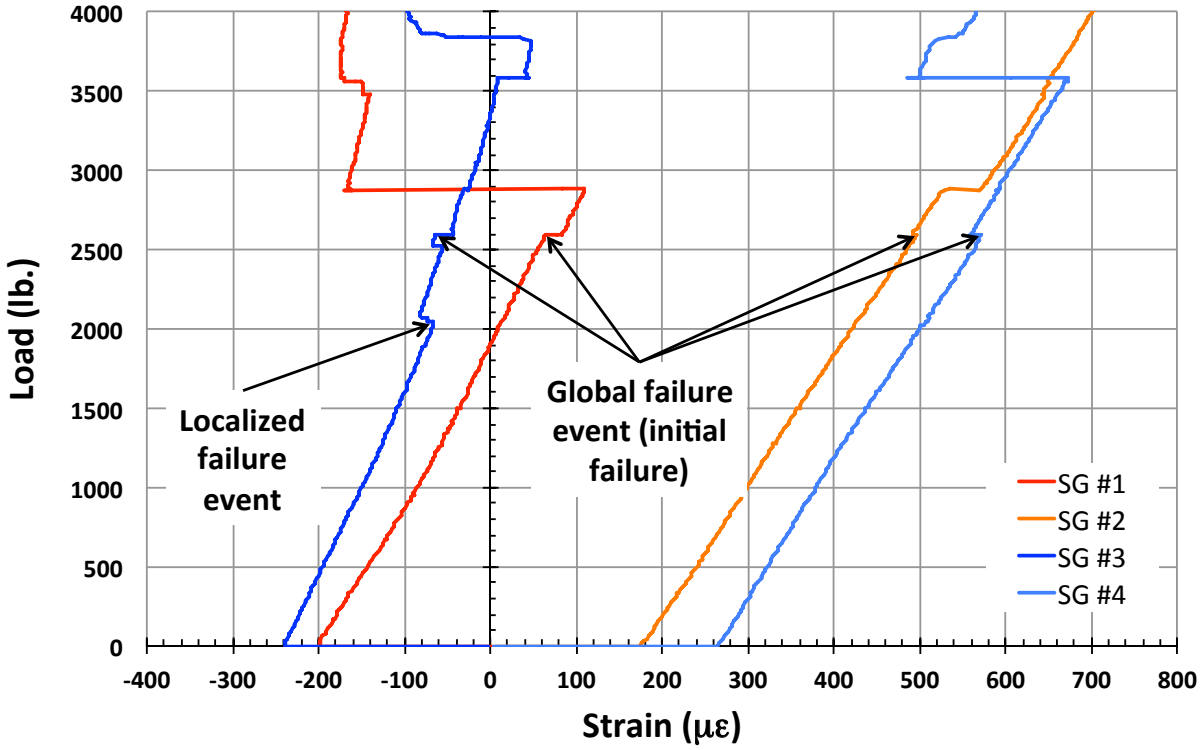

Figure 16. TNS1 load vs. strain, initial loading.

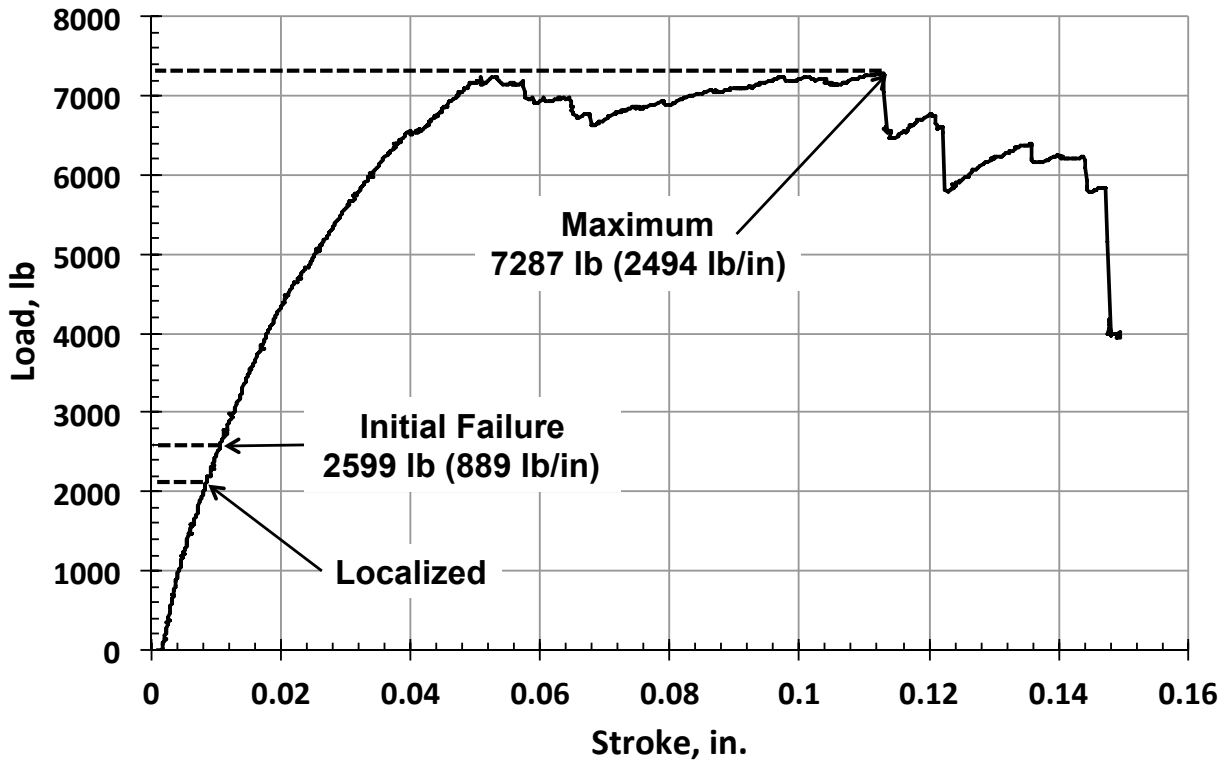

Figure 17. TNS1 load vs. stroke.

Initial failure and maximum achieved running loads are compiled and summarized in Tables 4 and 5 for the tension-only and bending-only tests, respectively. These results are graphed for ease of comparison in Figures 18 and 19 for the tension-only and bending-only T-cap tests, respectively. In these figures, the test articles are identified and grouped according to configuration and design. Also in the figures, the stitching designated for each group refers to additional stitching in the T-cap web, where the original PRSEUS baseline only has stitching normally associated with the PRSEUS construction with no additional stitches in the web. In the plots of Figures 18 and 19, the initial failure load is identified by the darker solid portion of the bar, while the partially transparent lighter extension of the bar identifies the maximum valued attained. Also included in the plots is the average value for each of the specimen configurations within each design, and is located on the right side of each grouping in a lighter color variation from the test articles. The black dashed lines in each grouping with or without stiffeners also identifies the average baseline initial failure load, while the grey dashed line identifies the average baseline maximum load.

Table 4: Tension T-cap test initial failure and maximum attained running loads, Nx (lb/in).

Test Article	Initial Failure	Maximum	Initial Failure Ave.	Maximum Ave.
TNN1	787	914		
TNN2	781	914	784	914
T5N1	688	1118		
T5N2	711	943		
T5N3	710	964	703	1009
T1N1	743	858		
T1N2	684	862		
T1N3	743	1052	723	924
TNS1	889	2494		
TNS2	872	2415		
TNS3	971	2922	911	2610
T5S1	888	2535		
T5S2	753	3014		
T5S3	1069	3256	903	2935
T1S1	1214	2558		
T1S2	748	2602		
T1S3	768	2992	910	2717

Table 5: Bending T-cap test initial failure and maximum attained running moments, Mx (in-lb/in).

Test Article	Initial Failure	Maximum	Initial Failure Ave.	Maximum Ave.
BNN1	479	670		
BNN2	414	837	447	753
B5N1	436	666		
B5N2	436	892		
B5N3	454	767	442	775
B1N1	514	909		
B1N2	447	797		
B1N3	377	781	446	829
BNS1	666	1802		
BNS2	1021	1739		
BNS3	787	1623	825	1721
B5S1	916	1849		
B5S2	1325	1831		
B5S3	1089	1766	1110	1815
B1S1	758	1656		
B1S2	1097	1940		
B1S3	1518	1908	1124	1834

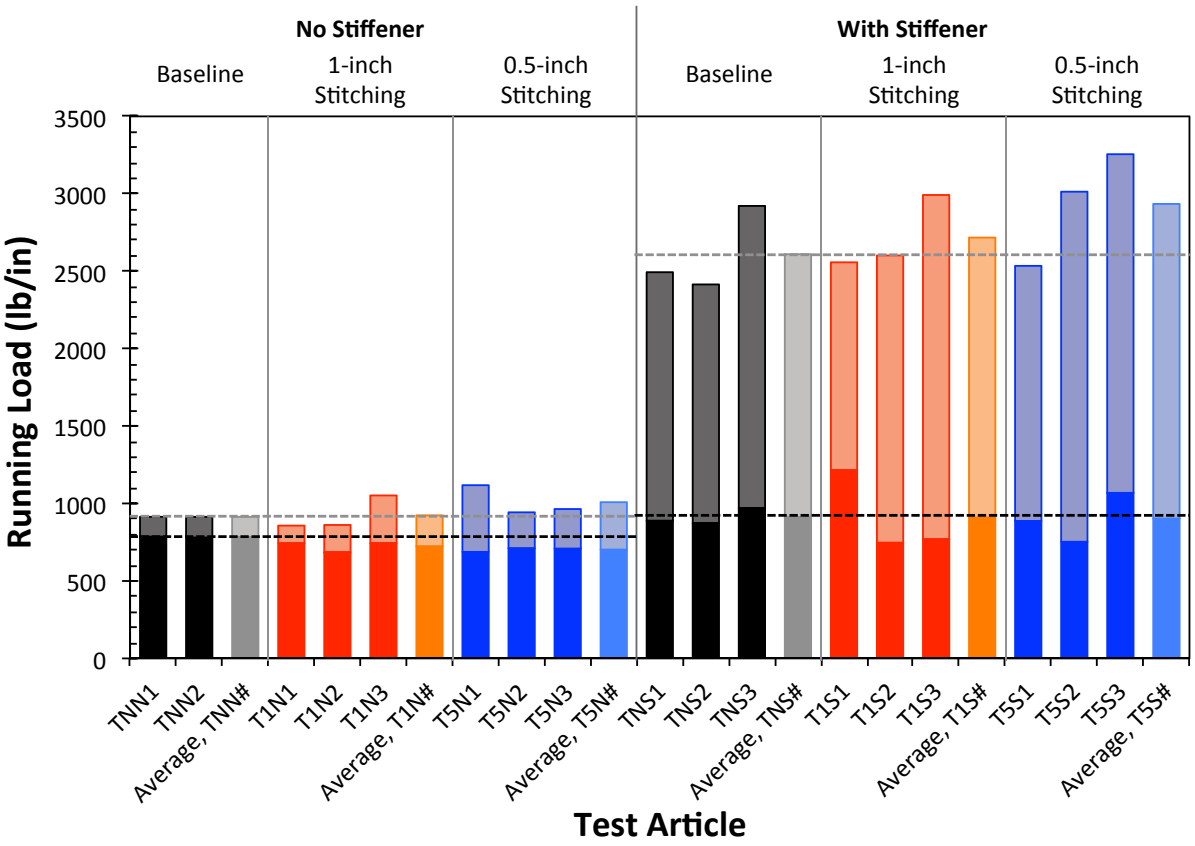

Figure 18. Running load, N_x, for tension test T-cap specimens.

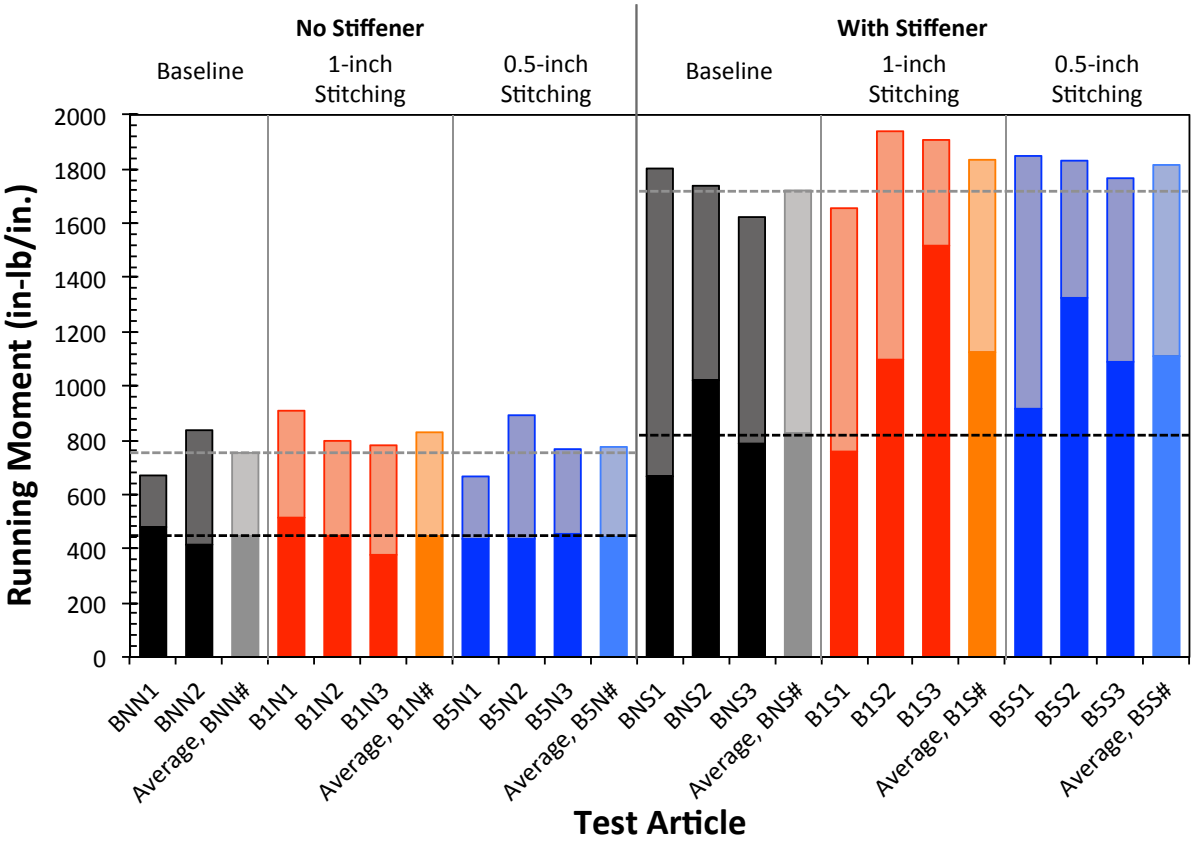

Figure 19. Running moment, M_x, for tension test T-cap specimens.

Examination of Figures 18 and 19 provides some interesting results concerning the effects of the additional stitching and the presence of the stiffener in the new integral T-cap designs. The data from Figures 18 and 19 are tabulated in Table 6 in the form of normalized average initial failure and average maximum loads. The normalizing load is the corresponding average load for the baseline configuration without web stitching, with or without the stiffener present. Notice that the initial failure load for tension only is adversely affected by the additional T-cap web stitching. The average initial failure load decreases by 7.7% and 10.3% for the designs with 1-inch and 0.5-inch stitch spacing in the T-cap web, respectively, for test articles without a stiffener. Failures initially occur as delamination in the vicinity of the noodle region at the base of the T-cap web. As the displacement was applied to the test article, the load continued to increase and then drop as additional delamination regions were created. Delaminations grew to the stitching in the web and/or the flange regions and were arrested by the stitching. There were load drops associated with failures of the stitches, which typically resulted in some of the largest load drops. For the test articles with a stiffener present, the initial failure load decreases by 0.1% and 0.8% for the designs with 1-inch and 0.5-inch stitch spacing in the T-cap web, respectively, which is not a significant deviation. However, as seen in Table 4, the initial failure loads for the test articles with stiffeners were significantly higher than those without a stiffener, about 16% higher than the baseline test article without the stiffener. Initial failures for the stiffener test articles occur as delaminations in the vicinity of the noodle at the intersection of the T-cap web and flanges, as was seen in the stiffenerless test articles. However, early in the loading there were small audible pops that were likely associated with the keyhole/stiffener junction as no evidence of delaminations was observed. As loading continued, in addition to the delaminations that continued to form, failures were also observed in the web of the stiffener indicating that load was being passed through the stiffener to the skin/flange region away from the T-cap web.

Table 6: Normalized average initial failure and average maximum loads.

Tension Test Articles			
Configuration		Normalized Initial Failure Load	Normalized Maximum Load
Stiffener	Web Stitch Spacing		
No	None (baseline)	1.000	1.000
	1.0	0.923	1.011
	0.5	0.897	1.103
Yes	None (baseline)	1.000	1.000
	1.0	0.999	1.041
	0.5	0.992	1.124

Bending Test Articles			
Configuration		Normalized Initial Failure Load	Normalized Maximum Load
Stiffener	Web Stitch Spacing		
No	None (baseline)	1.000	1.000
	1.0	0.998	1.101
	0.5	0.989	1.029
Yes	None (baseline)	1.000	1.000
	1.0	1.363	1.066
	0.5	1.346	1.055

For test articles with no stiffener, the maximum attained load increases by 1.1% and 10.3% for the designs with 1-inch and 0.5-inch stitch spacing in the T-cap web, respectively. However, the maximum load is not significantly higher than the initial failure load for these test articles. Additionally, the maximum load occurs after multiple load drops, and after significant damage has accumulated. For test articles with the stiffener present, the maximum attained load increases by 4.1% and 12.4% for the designs with 1-inch and 0.5-inch stitch spacing in the T-cap web, respectively. Also note that the maximum load for these test articles is significantly larger than the initial failure load, on the order of 2.5 to 3 times larger. After the initial failure occurs, the load typically continues to increase with small variations until a near maximum load was attained prior to noticeable load drop. The maximum load for these test articles typically occurs later in the test, but is usually not significantly larger than the load obtained at the end of the initial rise of the load versus displacement curve that is prior to the first significant load drop (see Figure 17). The continued load increase, and the significant increase in maximum load compared to the initial failure load, may be a result of a mechanical connection that is formed by the stringer and the keyhole in the T-cap through which the stringer passes. This connection permits the T-cap web to transfer load into the stringer, which then passes load into the surrounding skin, rather than all the load having to pass through the base of the T-cap web as is the case for the stringerless test articles. This is borne out by the delaminations at the base of the stringer web as shown in Figure 20, which clearly indicates a load path through the stringer and into the skin region. Lastly, because of the presence of the keyhole that separates the base of the web on either side of a stringer, delaminations in the base of the stringer don't necessarily occur at the same load on either side of the stringer as this separation arrests the delamination due to the discontinuity. When a stringer is not present, the delamination is free to grow across the complete width of the test article and thus the DIC identified the origination of the delamination at nearly the same load on both sides. This phenomenon applies to both the tension and bending tests. Note that the presence of the stiffener increased the initial and maximum tension failure loads by about 16% and 200%, respectively, compared to the stiffenerless baseline test article. This increase can likely be attributed to the web pulling up on

the stringer during loading through the mechanical connection of the keyhole enveloping the stringer, which provided load distribution away from the fillet region of the web and flange interface. This type of behavior would not be seen for tension loading if the stiffener were a blade configuration, for example, so this load redistribution is dependent on the design of the stringer.

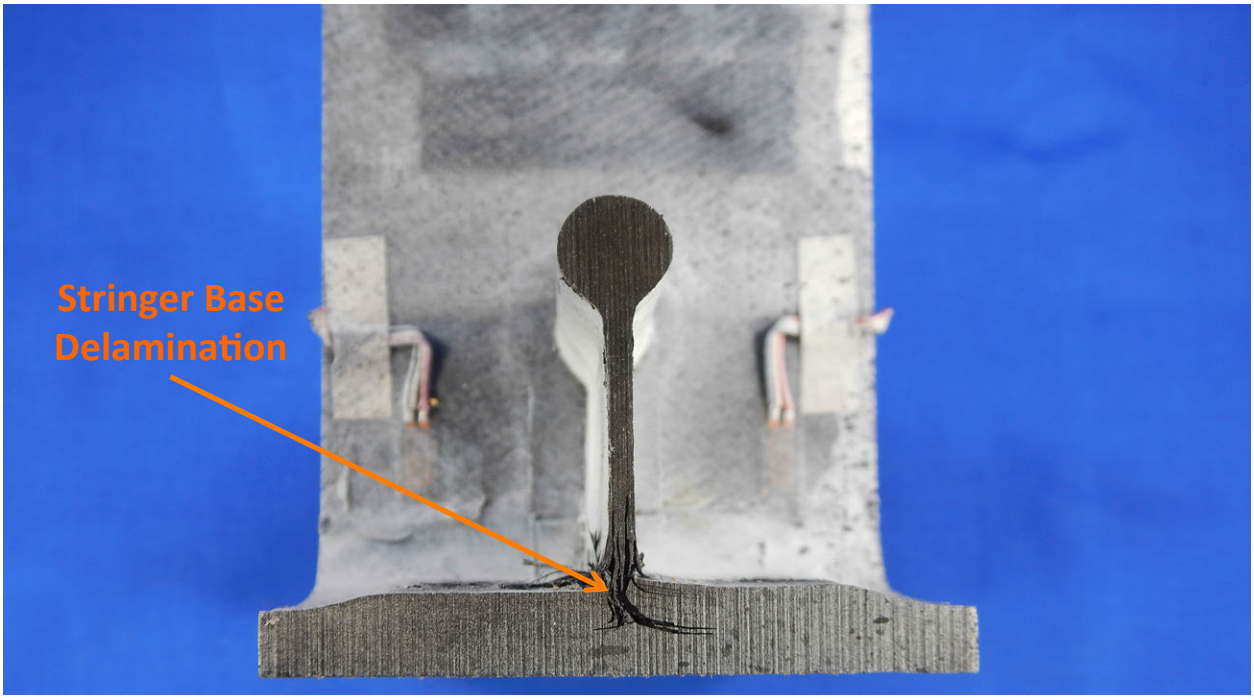

Figure 20. Delaminations at the stringer base observed in test article TNS1.

For the bending test articles, Figures 18 and 19 and Table 6 indicate that the initial failure load for bending is relatively unaffected by the additional T-cap web stitching for test articles without a stiffener. The average initial failure bending moment errors for these test articles were less than 2.0%. Initial failures developed as a delamination at the noodle region of the web and flange intersection on the tension, interior, side of the web. The maximum bending moment occurs prior to the final bending moment drop, and was the result of crippling of the outer plies on the compression, exterior, side of the web. Crippling occurred for all test articles in the vicinity of the stitch row at the top of the fillet region, which is the stitch row associated with normal assembly of the PRSEUS structure. For test articles with a stiffener present, the initial failure bending moment increased by 36.3% and 34.6% for the designs with 1-inch and 0.5-inch stitch spacing in the T-cap web, respectively. This is a significant increase over the test articles without the additional stitching. Initial failures developed in the same manner as those without the stiffener and occurred in the interior (tension side) radius near the noodle. The maximum bending moment was reached just prior to crippling failure on the compression side of the web at the height of the stiffener, which is higher up the web than the crippling observed in the test articles without the stiffener. Figures 21 and 22 show the crippling failure on for the representative test articles with and without a stringer, respectively. The maximum attained load increased with increased stitching in the T-cap web. For test articles without a stiffener, the maximum attained load increases by 10.1% and 2.9% for the designs with 1-inch and 0.5-inch stitch spacing in the T-cap web, respectively. For test articles with a stiffener present, the maximum attained load increases by 6.6% and 5.5% for the designs with 1-inch and 0.5-inch stitch spacing in the T-cap web, respectively. It is likely that bearing of the T-cap web on the top of the stringer resulted in the higher bending moment at initial failure as the load was carried in the stringer rather than in bending of the web. This is also likely the cause of the relocation of

the crippling area that developed at maximum load. Note that the presence of the stiffener increased the initial and maximum bending failure loads by about 85-150% and 129-142%, respectively, compared to the stiffenerless baseline test article. This significant increase can likely be attributed to the web bearing on the stringer during loading, which provided load distribution away from the fillet region of the web and flange interface. This type of behavior is likely to occur regardless of the stringer design.

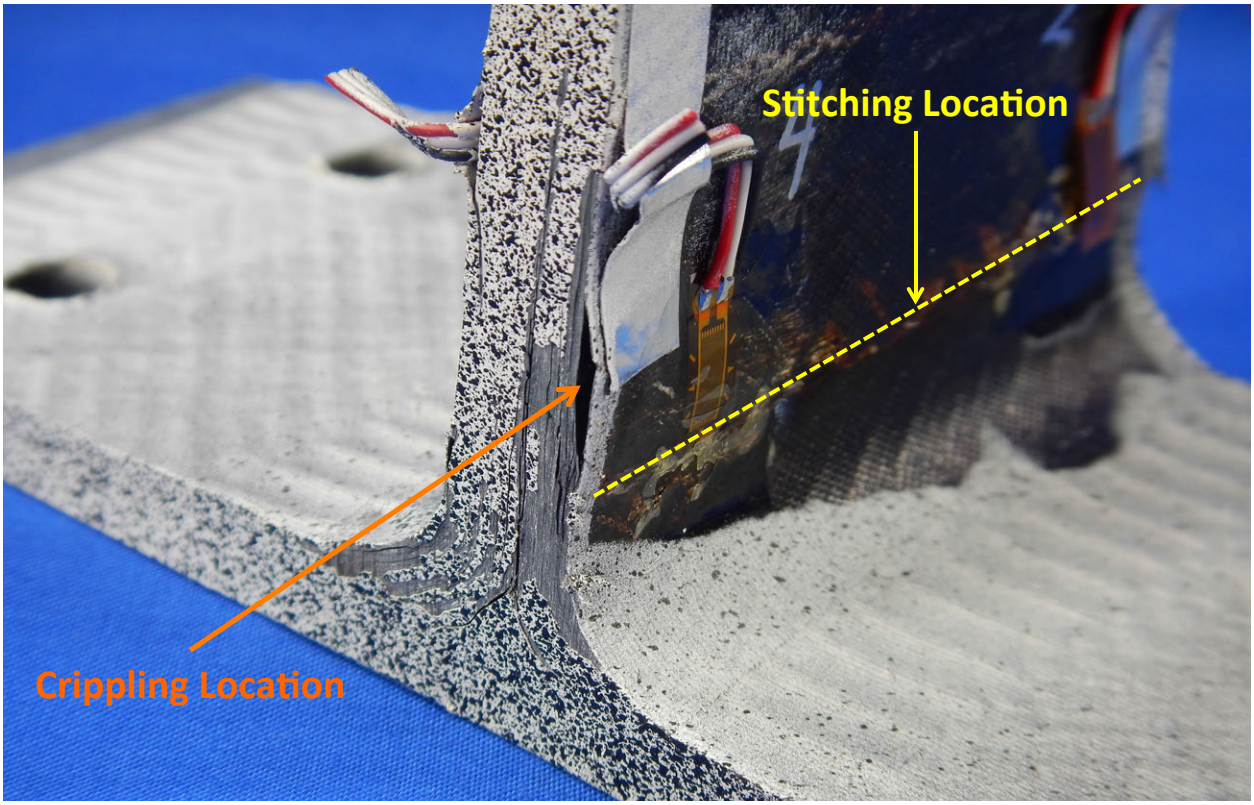

Figure 21. Crippling resulting from maximum load observed in test article B1N1.

Lastly, one of the objectives of the testing was to provide data for analysis validation. While time did not permit analysis validation to be performed and presented in this paper, a discussion of the type of data available in Appendix C is provided herein to give some insight into possible validation techniques. As previously mentioned, the data in the appendix only include strain contour plots for one of each type of test article design, however, contour data are archived for all test articles. An initial examination of the data shows that a plot of maximum principal strain is a good indicator that a delamination has developed, and may also be a good indicator that the delamination is about to develop. Maximum principal strain plots before and after the initial delamination failure for test article TNN1, as recorded by the 5 MP local DIC system, are shown in Figures 23 and 24. In Figure 23, there are a couple of possible regions that indicate where the initiation may occur at a maximum principal strain level of approximately 0.004 in/in, with the most likely one being the slightly larger region of light orange as indicated on the figure. Small areas at the edge of the DIC processing area that are at the strain scale limits are spurious values that may ocassionally occur due to various factors in the image processing, such as the presence of stitch fiber tufts or some other imperfection.

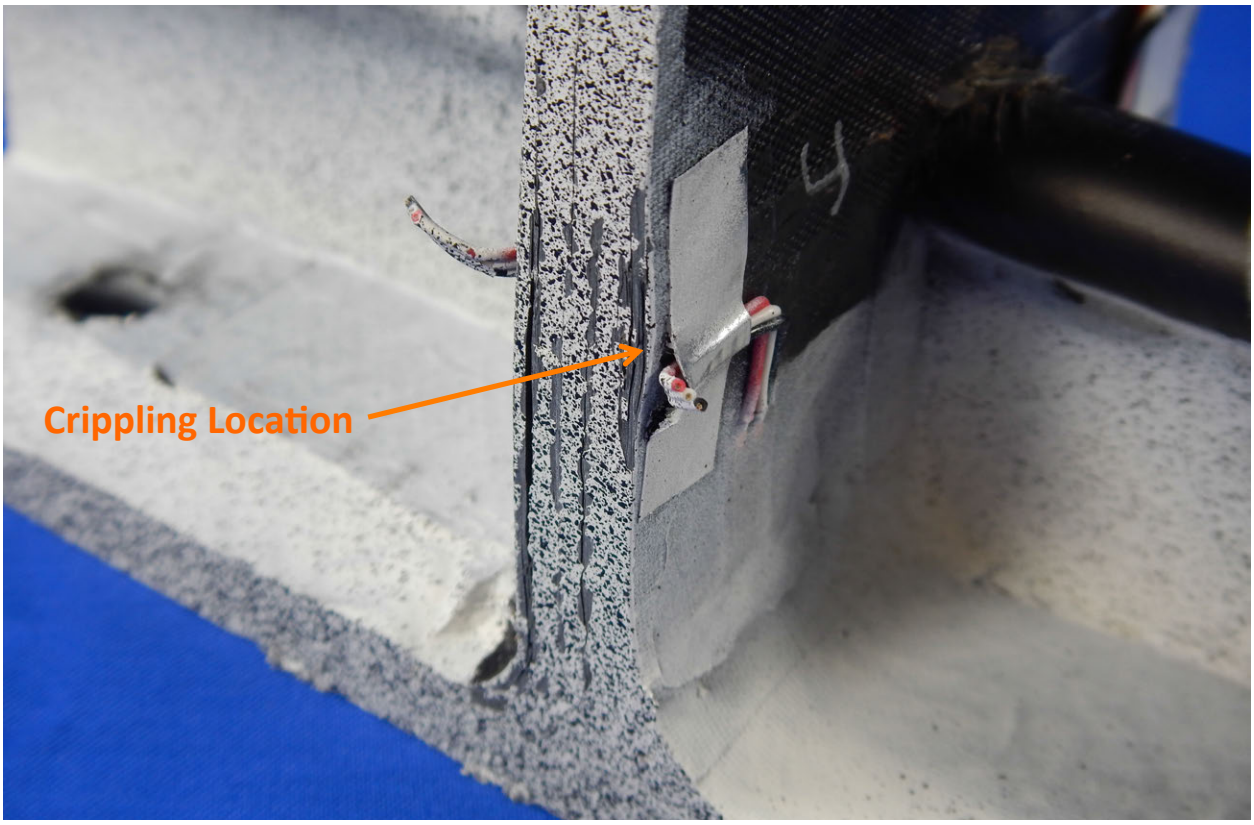

Figure 22. Delaminations at the stringer base observed in test article BNS1.

Figure 24 shows that the initial delamination failure did actually occur and pass through the region indicated on Figure 23 as the most likely failure location. While reported as a maximum principal strain in Figure 24, in the vicinity around the delamination crack, these are actually fictitious strain values, as it is really a measure of the gap separation rather than an actual strain measure within the material itself. A close-up image of the TNN1 delamination is shown in Figure 25. The dashed yellow line in the figure shows the approximate location of the delamination crack, which is difficult to see with the eye, but was easily detected by DIC. While the delamination passed the stitch line at the top of the web base radii, as seen in Figure 24, it was observed that the stitching did prevent significant further delamination growth until the failure of the stitching that occurred at the maximum load. It should also be noted that while for TNN1, the initial delamination occurred at the major failure surface that developed at the maximum load, this was not always the case. Additionally, the major failure surface was uniformly located at the interfaces of the inner and outer flange stacks with each other, the noodle region and the skin stacks, which are identified by the red lines in Figure 6.

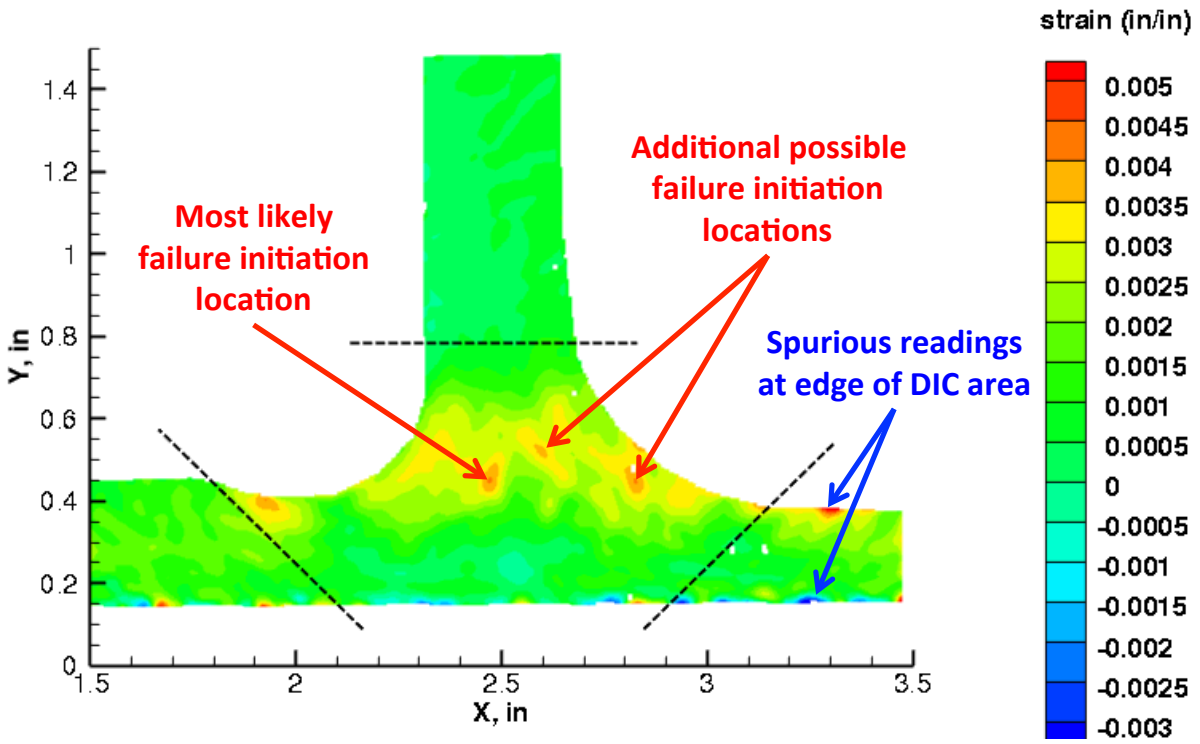

Figure 23. Maximum principal strain in test article TNN1 from 5 MP local DIC system just prior to initial delamination failure.

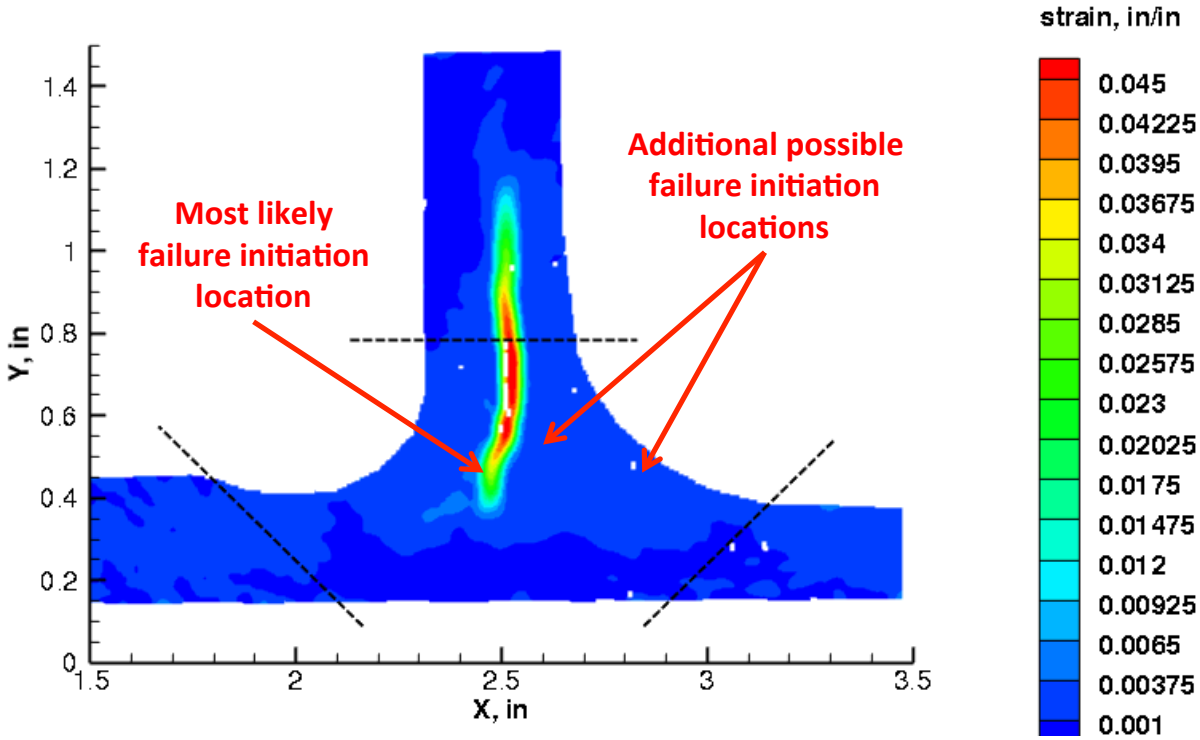

Figure 24. Maximum principal strain in test article TNN1 from 5 MP local DIC system just after initial delamination failure.

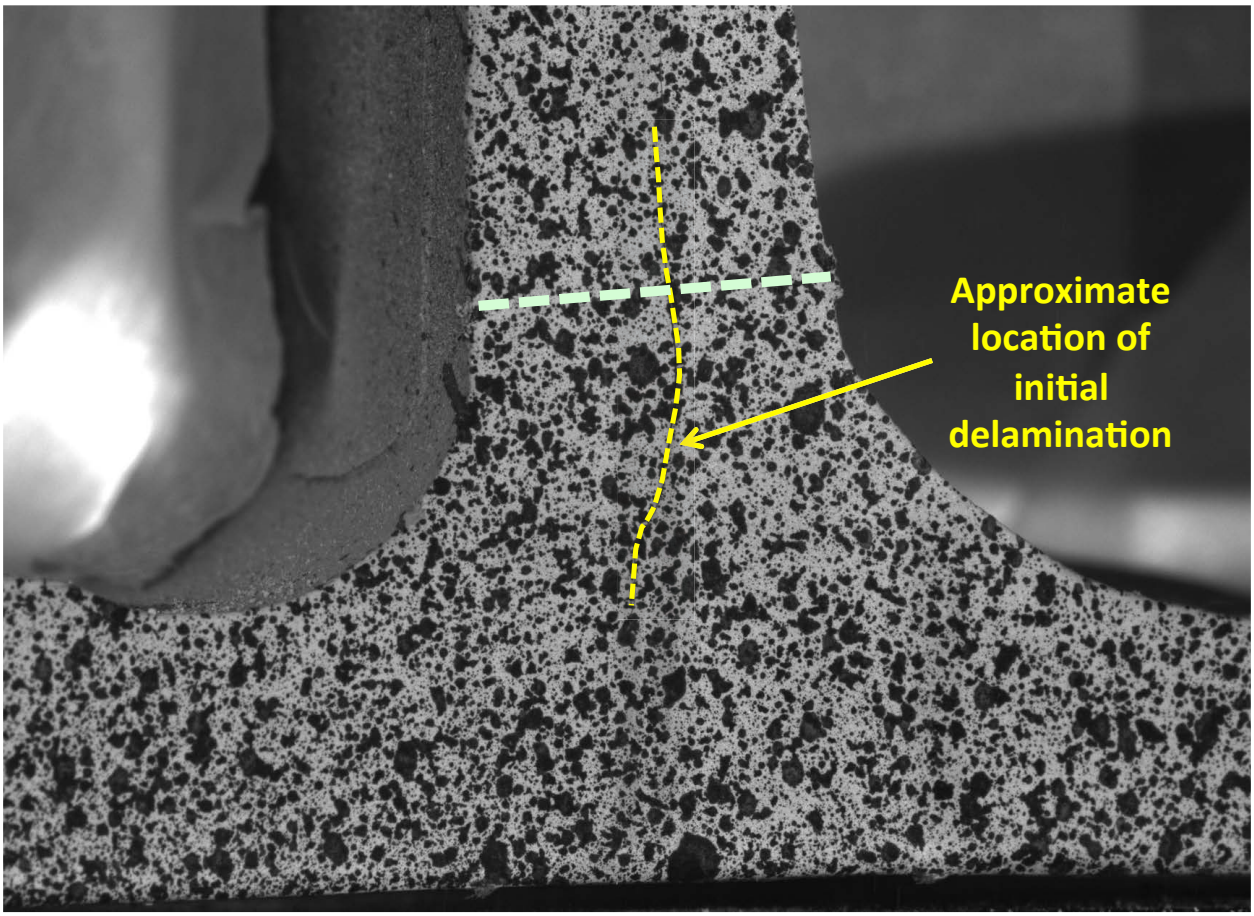

Figure 25. Image of initial delamination failure location in test article TNN1 from 5 MP local DIC system.

Conclusions

A series of tests were conducted on a variety of T-cap integral caps similar to what was used for assembly of the PRSEUS MBB. These test articles were cut from an alternate keel, and included specimens with and without a stiffener passing through the web. Additionally, three designs were tested, including the original design that had no additional stitching along the length of the web, one that had additional stitching at 1-inch increments, and one that had additional stitching at 0.5-inch increments. Specimens were tested in either tension-only or bending-only loading. There were three specimens for each configuration, design combination, and load condition, with the exception of those specimens without a stringer and without additional stitching.

Test data were presented and discussed, leading to a number of observations, which are as follows:

- Presence of the additional web stitching:
  - Decreased the initial failure load for tension only tests for test articles without a stiffener. There was no significant difference in the initial failure loads for the tension only test articles with a stiffener present, with only a slight reduction in initial failure load observed.
  - Increased the maximum tension load attained for all test articles, however, those without a stiffener and with 1-inch stitch spacing exhibited minimal improvement.

    - Showed no significant difference on the initial failure bending moment for bending only tests for test articles without a stiffener. However, there was a significant increase in the initial failure bending moment for test articles with a stiffener present.
    - Stitching increased the maximum bending moment attained for all test articles.
- The presence of the stiffener:
    - Increased the initial and maximum tension failure loads compared to the stiffenerless baseline test article. This increase can likely be attributed to the web pulling up on the stringer during loading through a mechanical connection, which provided load distribution away from the fillet region of the web and flange interface, a type of behavior that would not be seen if the stiffener were a blade configuration, for example, so this type of load redistribution is dependent upon the design of the stringer.
    - Increased the initial and maximum bending failure loads significantly, compared to the stiffenerless baseline test article. This increase can likely be attributed to the web bearing on the stringer during loading, which provided load distribution away from the fillet region of the web and flange interface. This type of behavior is likely to occur regardless of the stringer design.
- Initial delaminations occurred anywhere within the web thickness, and did not always coincide with an interface of the flange stacks, noodle or skin stacks.
- The major delamination surfaces associated with the maximum load were located along the interfaces of the stack groupings and noodle region, although many delaminations were present throughout the thickness of the web.

Based on these observations, combined with the small sample size for each configuration, it is not clear that additional stitching along the height of the T-cap web is beneficial. Consider that the completed testing was conducted under tension-only or bending-only load, while in service these T-caps are expected to experience a combination of tension and bending load due to the presence of internal pressure. Tension and bending loads appear to have opposing effects on the response, so combined loading may have a net zero effect on the response. Additionally, since design will likely be driven by the initial failure load, the testing documented herein shows that the original design is slightly superior to the two designs with additional stitching along the height of the web because loads for the baseline design are higher than or similar to the new designs. Stitching did show some benefit in maximum load, so for damage tolerance purposes, it may be desirable to include the additional stitching and take the minimal hit on initial failure loads. Lastly, there may be other damage tolerance reasons to include the additional stitching, but if it is desirable to maximize the initial failure load, it would be advisable to have the first row of stitching in the web as far from the fillet stitch as possible.

Acknowledgements

The authors would like to acknowledge the contributions of Diane Griffin and George Cowley for setting-up and performing the tension and bending T-cap tests, respectively. The authors would also like to acknowledge Nathaniel Gardner, Michael McNeill and David Dawicke for setting-up and performing the optical measurements, and collecting and analyzing the data.

References

[1]Velicki, A., "Damage Arresting Composites for Shaped Vehicles, Phase I Final Report," NASA CR-2009-215932, September 2009.

[2]Velicki, A., and Hansen, D., "Novel Blended Wing Body Structural Concepts," NRA-03-LaRC-02 Maturation for Advanced Aerodynamic and Structures Technologies for Subsonic Transport Aircraft: Phase I Final Report, July 13, 2004.

[3]Hoffman, K., Air Vehicle Technology Integration Program (AVTIP), Delivery Order 0059: Multi-role Bomber Structural Analysis, AFRL-VA-WP-TR-2006-3067, May 2006, Final Report for 14 December 2004 – 08 May 2006, AFRL-VA-WP-TR-2006-3067.

[4]Karal, M., "AST Composite Wing Study – Executive Summary," NASA/CR-2001-210650, Prepared for NASA, Langley Research Center under Contract NAS1-20546, March 2001.

[5]Velicki, A. and Thrash, P. J., "Advanced Structural Concept Development Using Stitched Composites," 49th AIAA/ASME/ASCE/SHS/ASC Structures, Structural Dynamics, and Materials Conference, April 7-10, 2008, Schaumburg, Illinois, AIAA Paper 2008-2329.

[6]Lovejoy, A. E., "PRSEUS Pressure Cube Test Data and Response," NASA/TM-2013-217795, May 2013.

[7]Yovanov, N., Lovejoy, A., Baraja, J., and Gould, K., "Design, Analysis and Testing of a PRSEUS Pressure Cube to Investigate Assembly Joints," 2012 Airworthiness & Sustainment Conference, April 2-5, 2012, Baltimore, Maryland.

[8]Jegley, D. C., Rouse, M., Przekop, A., and Lovejoy, A. E., "Testing of a Stitched Composite Large-Scale Multi-Bay Pressure Box," AIAA Paper 2016-2175, 57th AIAA/ASCE/AHS/ASC Structures, Structural Dynamics, and Materials Conference, San Diego, California, January 3-8, 2016.

[9]Przekop, A., Jegley, D. C., Lovejoy, A. E., Rouse, M., and Wu, H. T., "Testing and Analysis of a Composite Non-Cylindrical Aircraft Fuselage Structure, Part I: Ultimate Design Loads," AIAA Paper 2016-2176, 57th AIAA/ASCE/AHS/ASC Structures, Structural Dynamics, and Materials Conference, San Diego, California, January 3-8, 2016.

[10]Przekop, A., Jegley, D. C., Lovejoy, A. E., Rouse, M., and Wu, H. T., "Testing and Analysis of a Composite Non-Cylindrical Aircraft Fuselage Structure, Part II: Severe Damage," AIAA Paper 2016-2177, 57th AIAA/ASCE/AHS/ASC Structures, Structural Dynamics, and Materials Conference, San Diego, California, January 4-8, 2016.

[11]Rouse, M., "Methodologies for Combined Loads Tests Using a Multi-Actuator Test Machine," presented at the Society for Experimental Mechanics meeting, June 2013.

[12]Rouse, M., and Jegley, D., "Preparation for Testing a Multi-Bay Box Subjected to Combined Loads," presented at the Society for Experimental Mechanics meeting, June 2015.

[13]Ayale, Andrew and Thrash, Patrick, "AST Composite Wing Program: Semi-Span Wing Fabrication Tests and Supporting Technology," Final Report for NASA Contract NASl-20546, 2000, Long Beach, CA.

[14]Moon, D. and Velicki, A., "AST Composite Wing Program: Full-Scale Stitched/Resin Film Infused Wing Design, Fabrication and Structural Verification," Final Report for NASA Contract NASl-20546, 2000, Long Beach, CA.

[15]Jegley, D. C., Bush, H. G., and Lovejoy, A. E., "Structural Response and Failure of a Full-Scale Stitched Graphite-Epoxy Wing," *Journal of Aircraft*, Vol. 40, No. 6, November-December 2003, pp. 1192-1199.

[16]Johnston, P. H., "Ultrasonic Nondestructive Evaluation of PRSEUS Pressure Cube Article in Support of Load Test to Failure," NASA/TM-2013-217799, May, 2013.

[17]Velicki, A., Hoffman, K., Linton, K., Thrash, P., Pickell, R., and Turley, R., "Fabrication of Lower Section and Upper Forward Bulkhead Panels of the Multi-Bay Box and Panel Preparation," NASA/CR-2015-218981, NASA Langley Research Center, Hampton, VA, November, 2015

[18]Leone, F. A., Jegley, D.C., "Compressive Testing of PRSEUS Frame and Stringer Alternate Configurations," NASA/TM-2015-218974, NASA Langley Research Center, Hampton, VA, November, 2015.

[19]Leone, F. A., "Pultruded Rod/Overwrap Testing for Various PRSEUS Stringer Configurations," NASA/TM-2015-218975, NASA Langley Research Center, Hampton, VA, November, 2015.

[20]https://www.alliedvision.com.

[21]http://www.ptgrey.com.

[22]http://www.correlatedsolutions.com.

Appendix A – Tension Test Fixture Drawings

Slot Nut (Rev. 2)

Quantity = 8

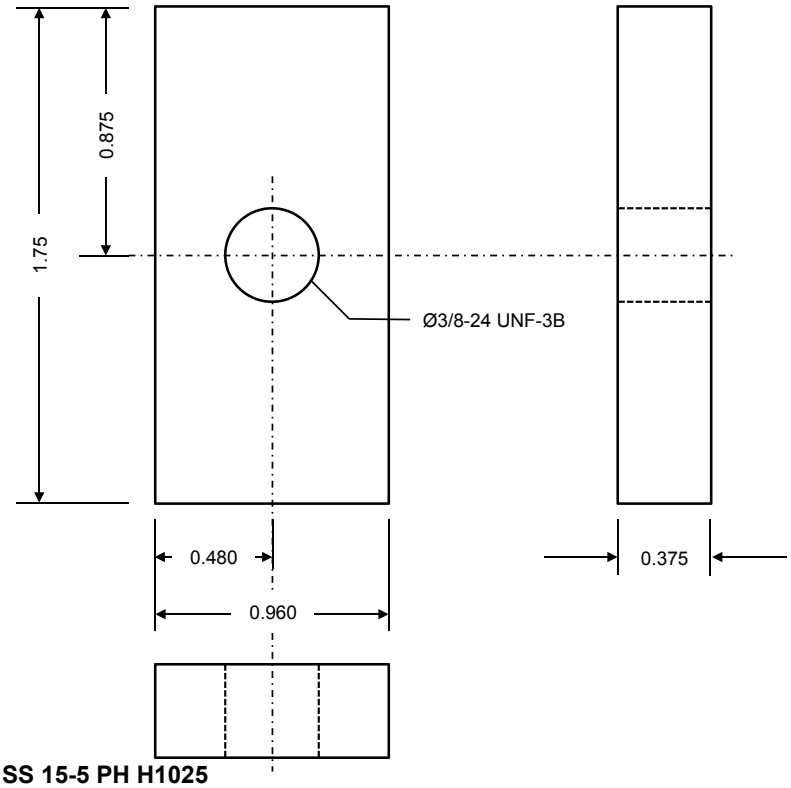

All units in inches
Not to scale
Material: AMS 5659, SS 15-5 PH H1025

Tolerances:
X.XX = ±0.01
X.XXX = ±0.005

Tension Base Fitting (Rev. 2)

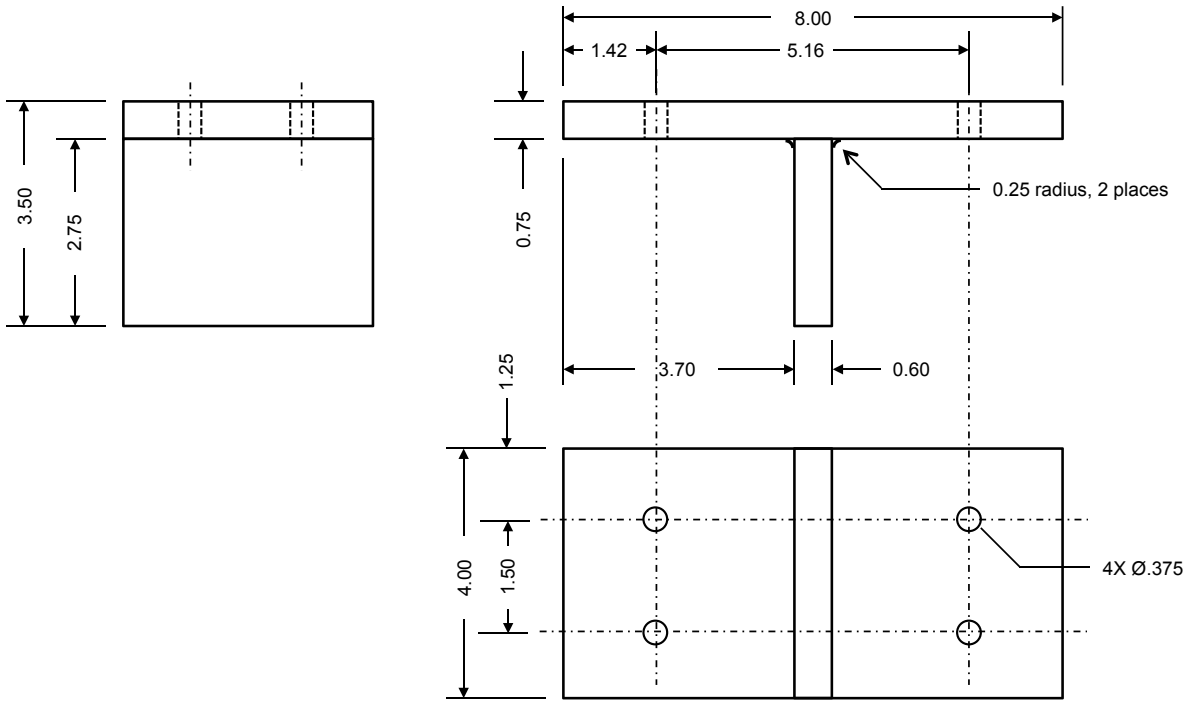

All units in inches
Dimensions not to scale
Material: AMS 5659, SS 15-5 PH H1025

Tolerances:
X.XX = ±0.01
X.XXX = ±0.005

Specimen Drill Plate

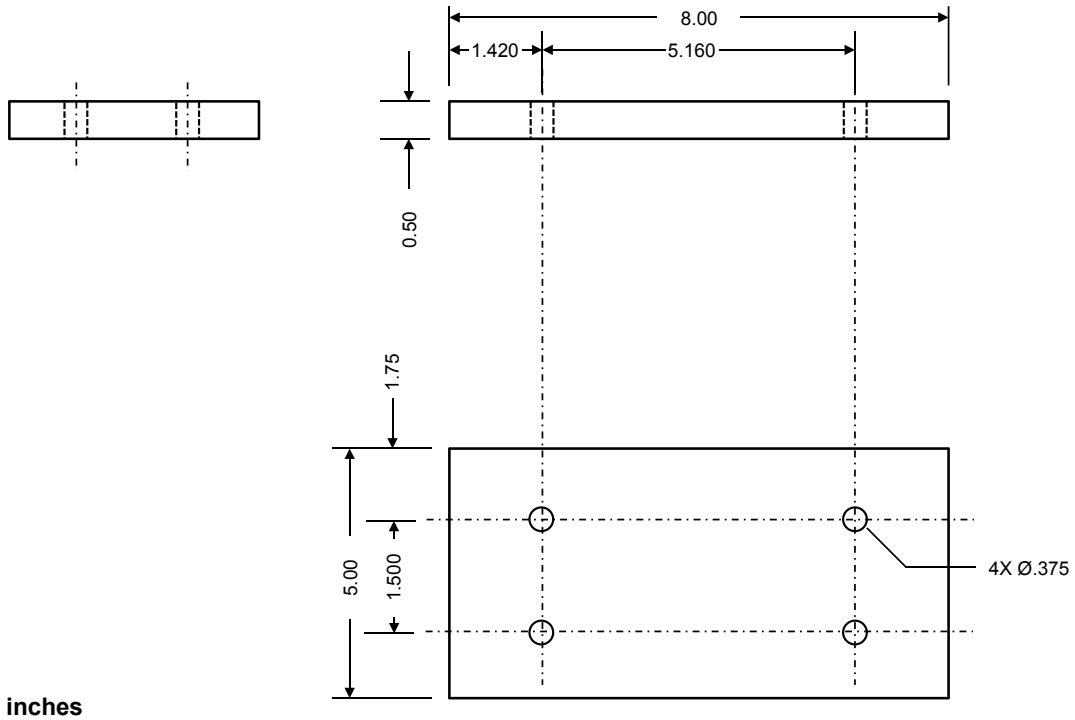

All units in inches
Dimensions not to scale
Material: steel

<u>Tolerances:</u>
X.XX = ±0.01
X.XXX = ±0.005

Appendix B – Bending Test Fixture Drawings

Tee Cap – Specimen Plate

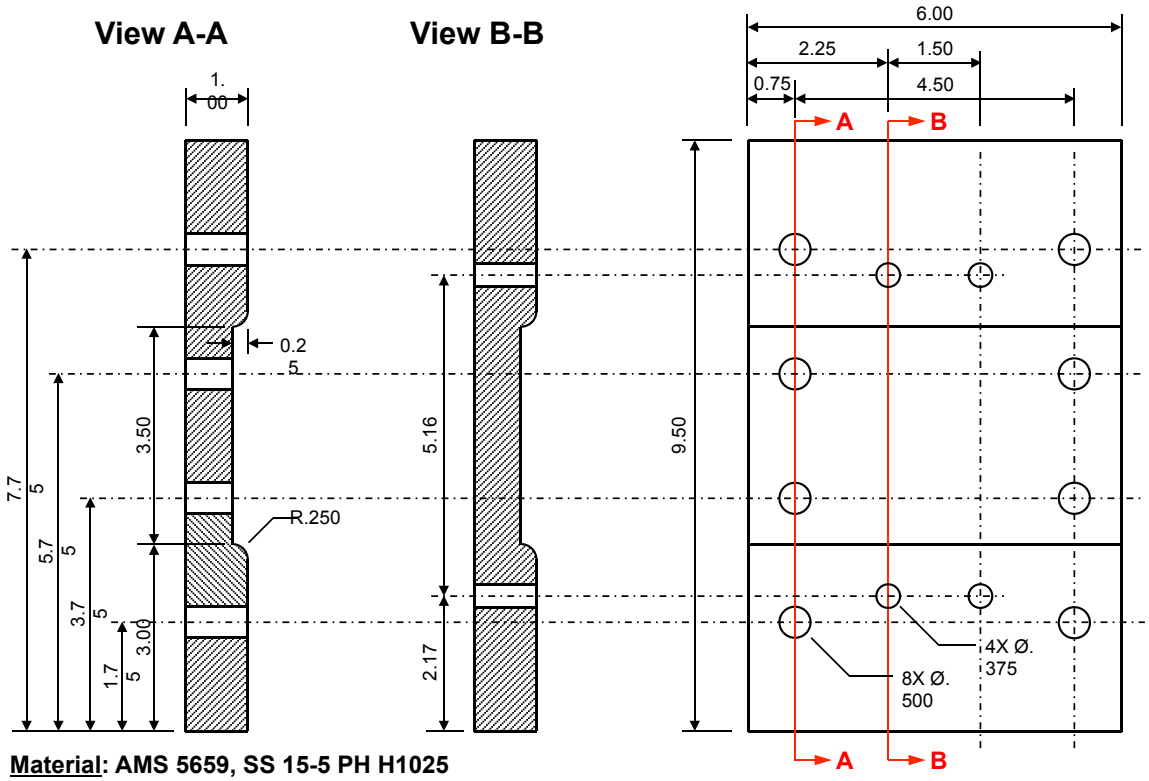

Material: AMS 5659, SS 15-5 PH H1025
All units in inches
Drawings not to scale

Tee Cap – Brace (Quantity: 2)

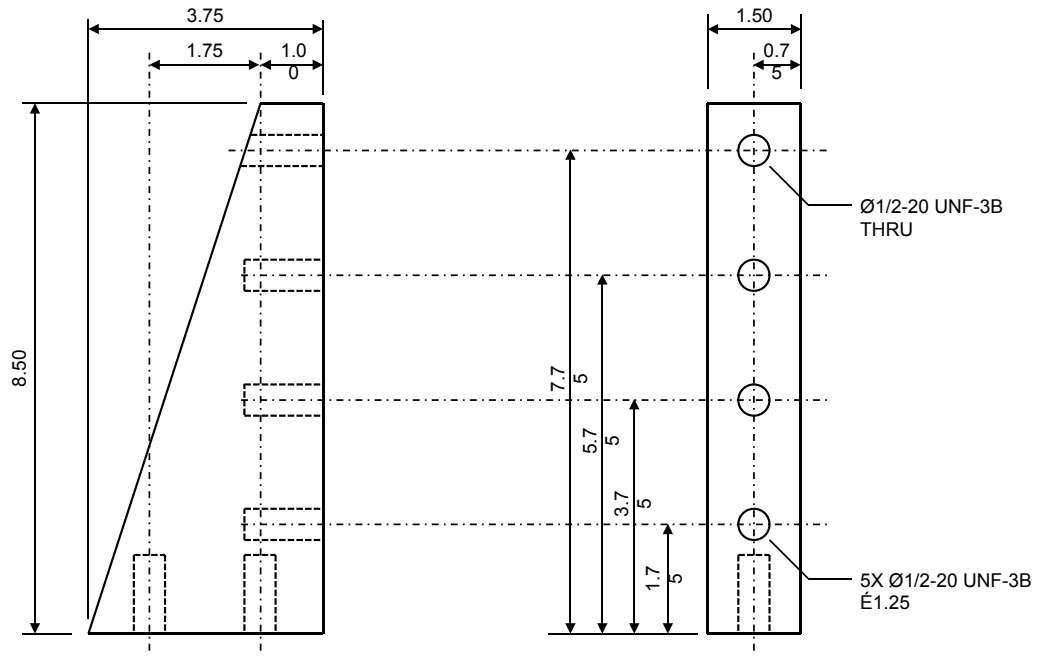

Material: AMS 5659, SS 15-5 PH H1025
All units in inches
Drawings not to scale

Tee Cap – Base Plate

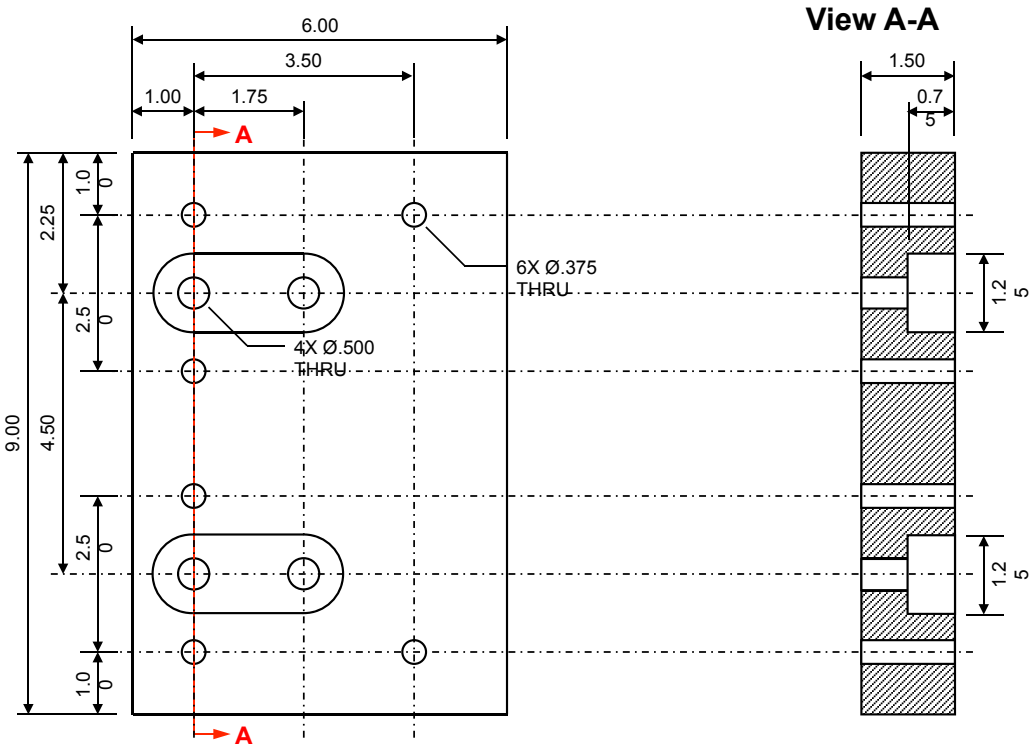

Material: AMS 5659, SS 15-5 PH H1025
All units in inches
Drawings not to scale

Tee Cap – Inside Clamp Plate

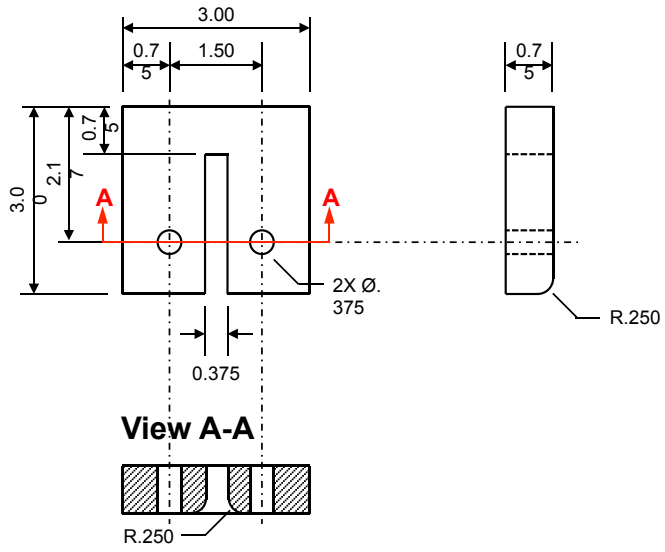

Material: AMS 5659, SS 15-5 PH H1025
All units in inches
Drawings not to scale

Tee Cap – Outside Clamp Plate

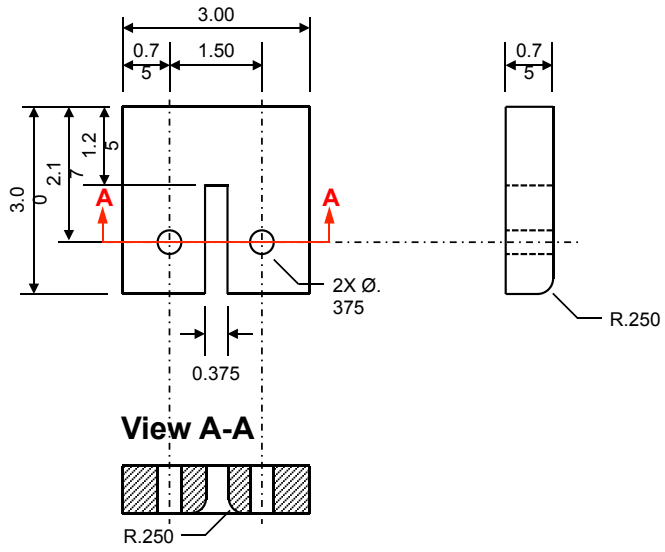

Material: AMS 5659, SS 15-5 PH H1025
All units in inches
Drawings not to scale

Tee Cap – Indenter

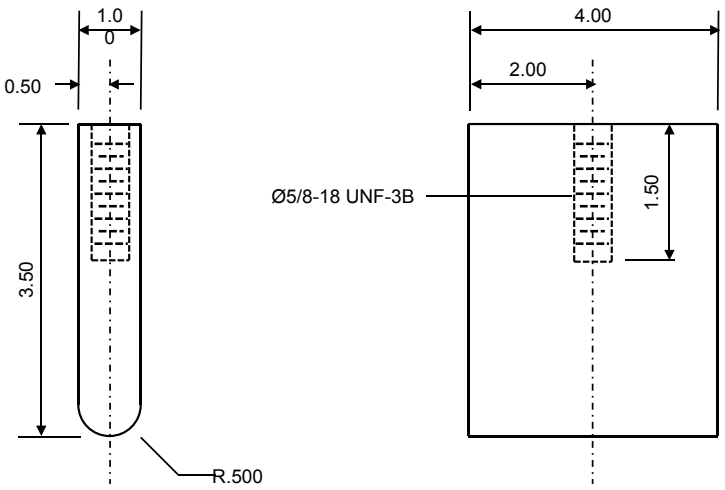

<u>Material</u>: AMS 5659, SS 15-5 PH H1025
All units in inches
Drawings not to scale

Assembly

Side View

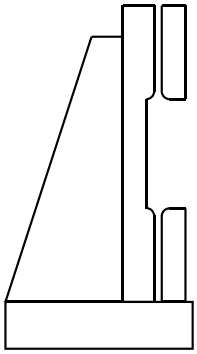

Rear View

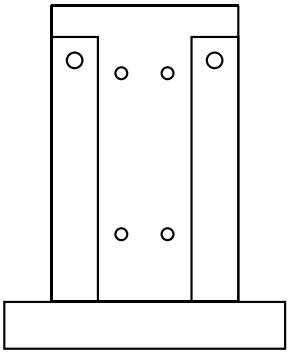

Top View

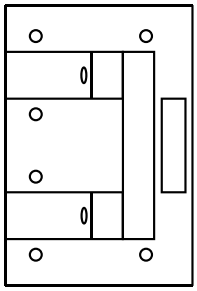

Drawings not to scale

Appendix C: Raw Test Data

This appendix presents the raw test data for the 34 test articles. First, tension test results are presented, followed by the bending test results. Presented data includes xy-plots of load vs. stroke and load vs. strain for all test articles. Contour plots of strains before and after initial failure are presented for select test articles. In these strain contour plots, approximate stitch locations for the typical assembly stitching that is present in all designs are indicated by black dashed lines. Also presented for select test articles are pictures of the visible damage after the initial failure and after the maximum applied load. Tables C1 and C2 provide the load applied by the load frame for the initial failure and the maximum load for each of the test articles, as well as averages of these loads for each type of test article type. Test articles that are highlighted in the tables are the ones for which the contour plots and pictures are included. DIC data required for contour plots, as well as the raw images, have been archived for all test articles for future use as needed.

Table C1: Tension T-cap test initial failure and maximum attained test frame loads (lb).

Test Article	Initial Failure	Maximum	Initial Failure Ave.	Maximum Ave.
TNS1	2599	7287		
TNS2	2538	7032		
TNS3	2831	8520	2656	7613
TNN1	2286	2657		
TNN2	2263	2649	2275	2653
T1S1	3514	7403		
T1S2	2165	7536		
T1S3	2224	8660	2634	7866
T1N1	2161	2495		
T1N2	1978	2491		
T1N3	2153	3051	2097	2679
T5S1	2597	7414		
T5S2	2178	8714		
T5S3	3084	9391	2620	8506
T5N1	1986	3229		
T5N2	2042	2710		
T5N3	2066	2808	2031	2916

Table C2: Bending T-cap test initial failure and maximum attained test frame loads (lb).

Test Article	Initial Failure	Maximum	Initial Failure Ave.	Maximum Ave.
BNS1	517	1398		
BNS2	786	1339		
BNS3	611	1260	638	1332
BNN1	366	512		
BNN2	323	652	344	582
B1S1	590	1289		
B1S2	850	1503		
B1S3	1175	1477	872	1423
B1N1	395	698		
B1N2	347	619		
B1N3	291	603	344	640
B5S1	703	1419		
B5S2	1029	1422		
B5S3	850	1379	861	1407
B5N1	327	499		
B5N2	338	691		
B5N3	351	593	339	595

Tension Tests

TNS1

This section presents the test data for the TNS1 test article, and includes strain plots and failure images.

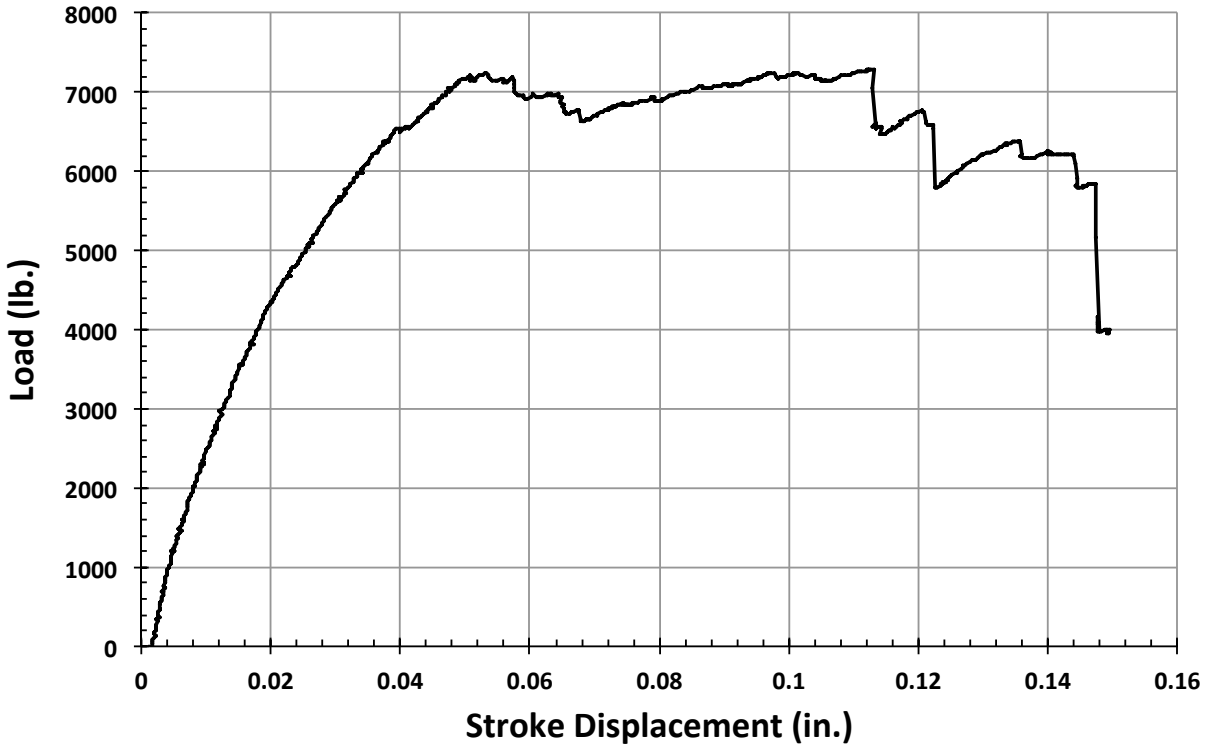

Figure C1. TNS1 load vs. stroke.

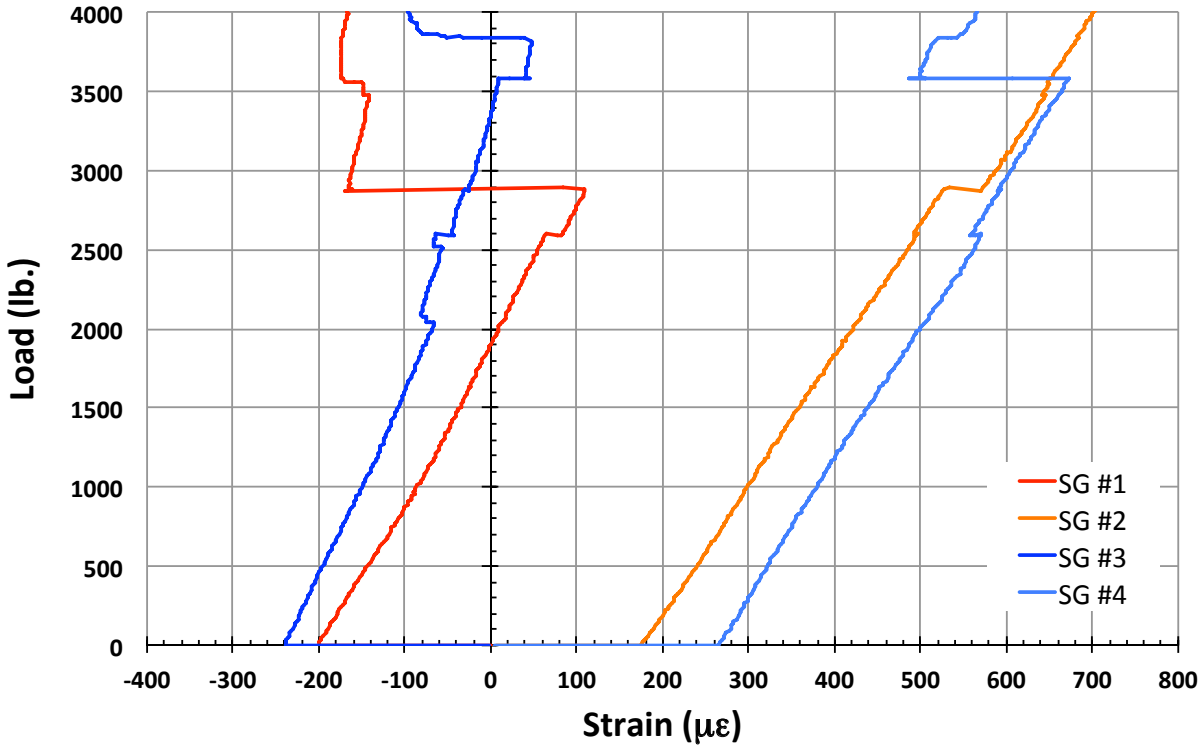

Figure C2. TNS1 load vs. strain, initial loading.

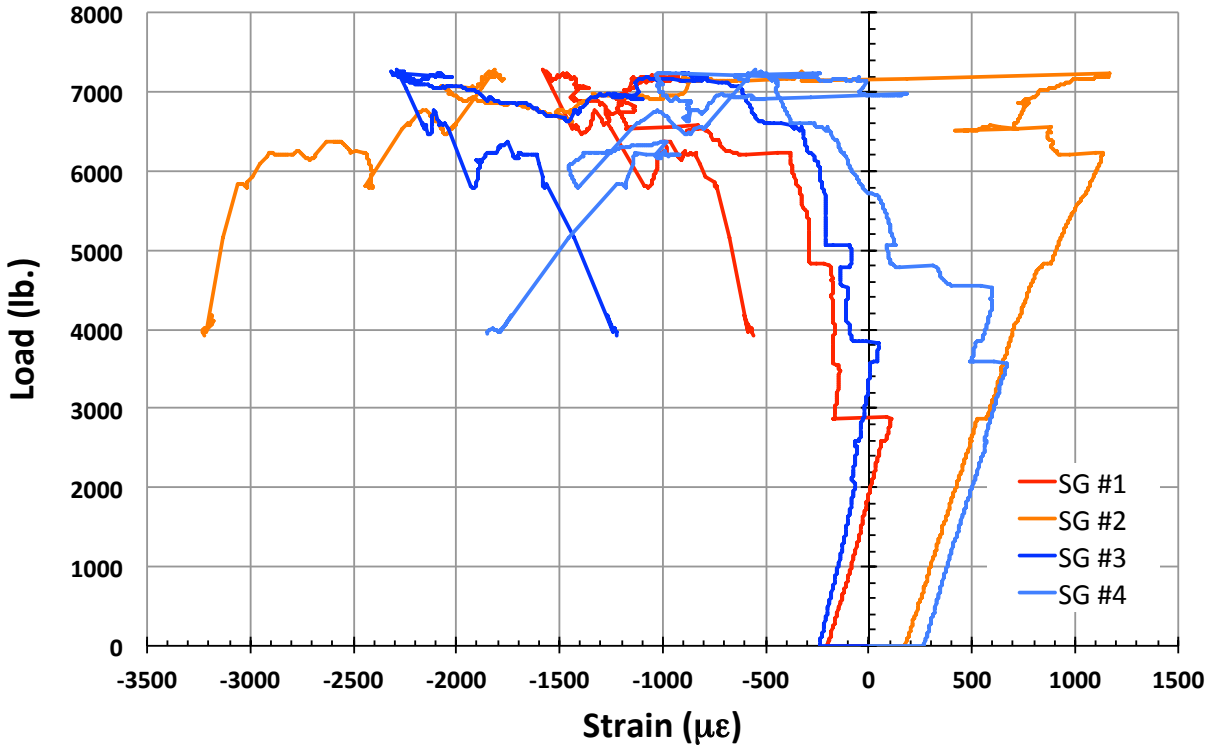

Figure C3. TNS1 load vs. strain.

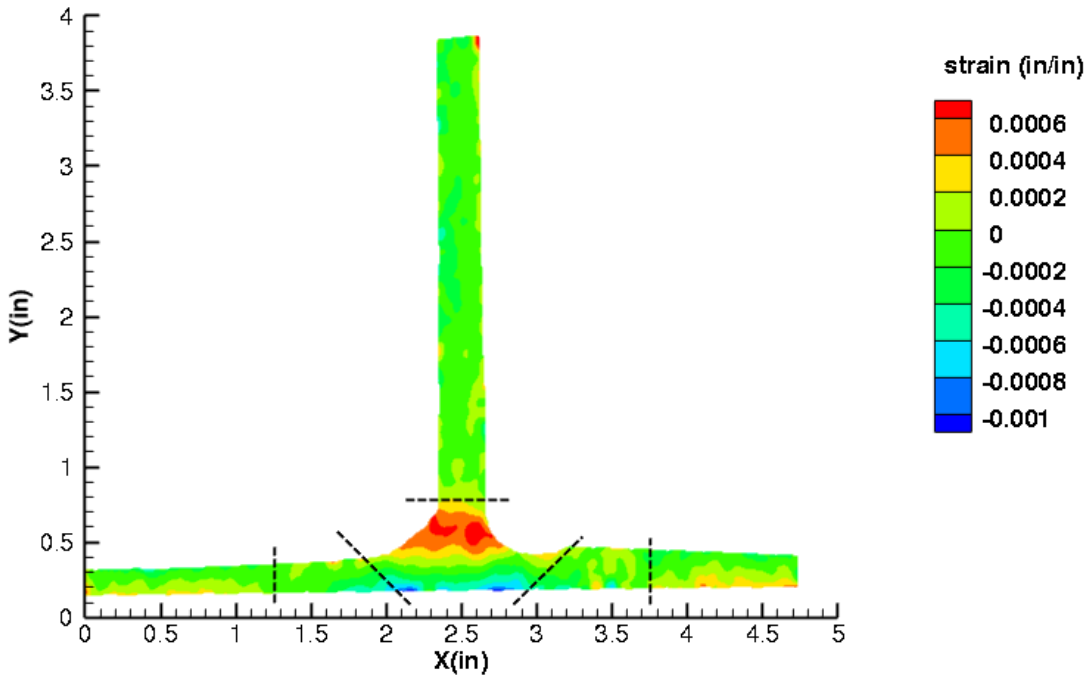

Figure C4. TNS1 strain contours for ε_{xx} at 2599 lb. load, prior to initial failure, 29MP VIC data.

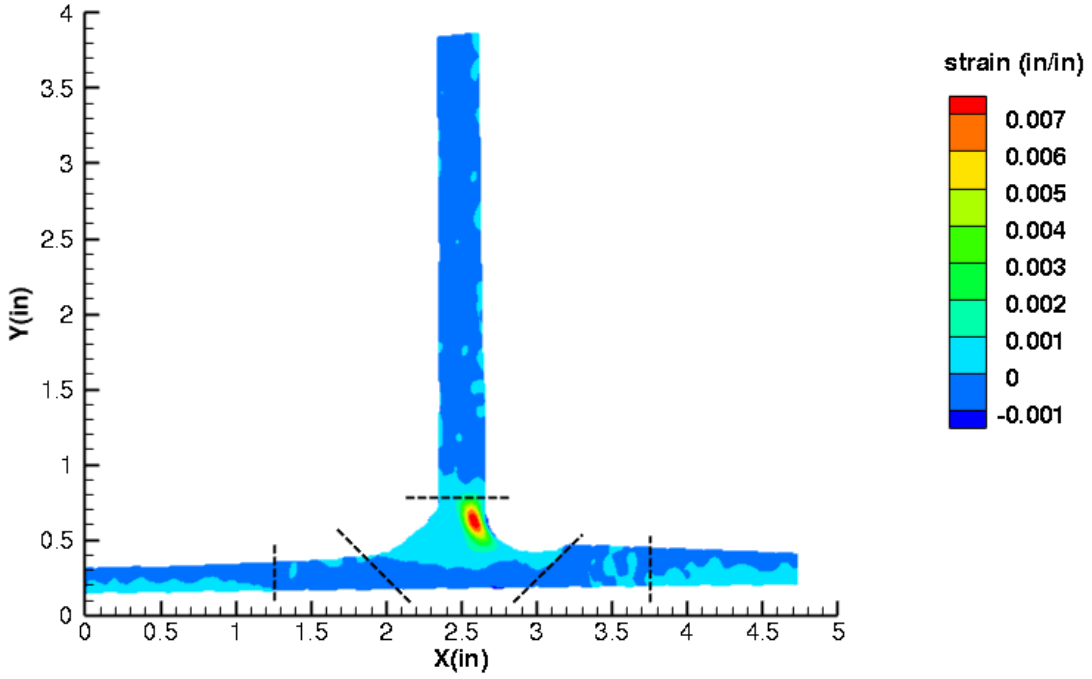

Figure C5. TNS1 strain contours for ε_{xx} at 2593 lb. load, just after initial failure, 29MP VIC data.

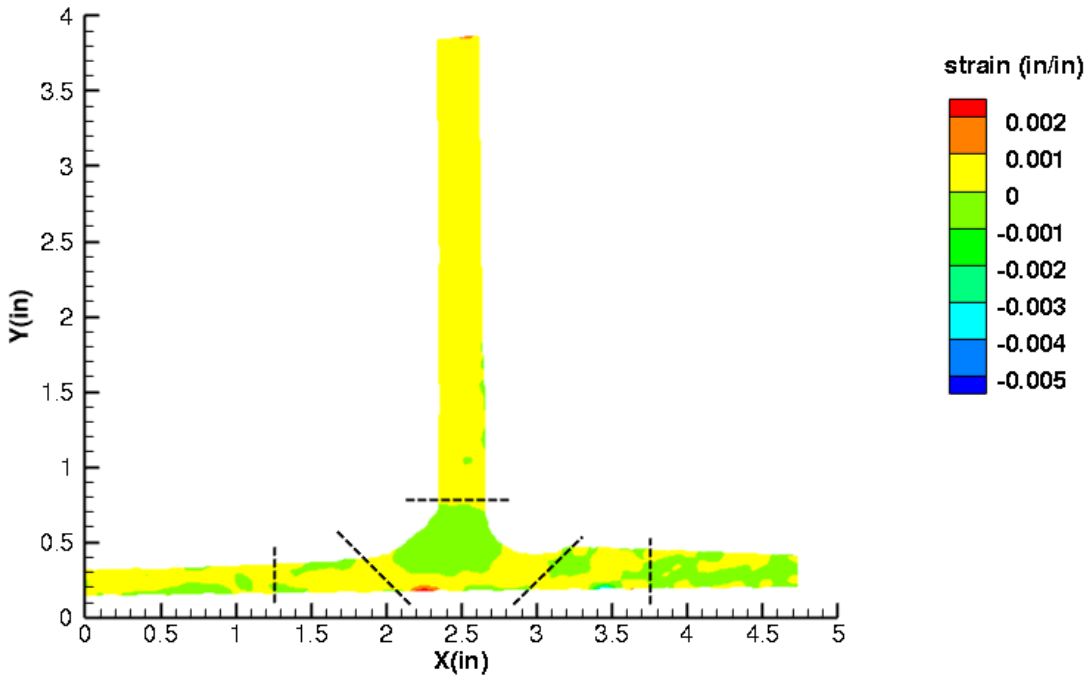

Figure C6. TNS1 strain contours for ε_{yy} at 2599 lb. load, prior to initial failure, 29MP VIC data.

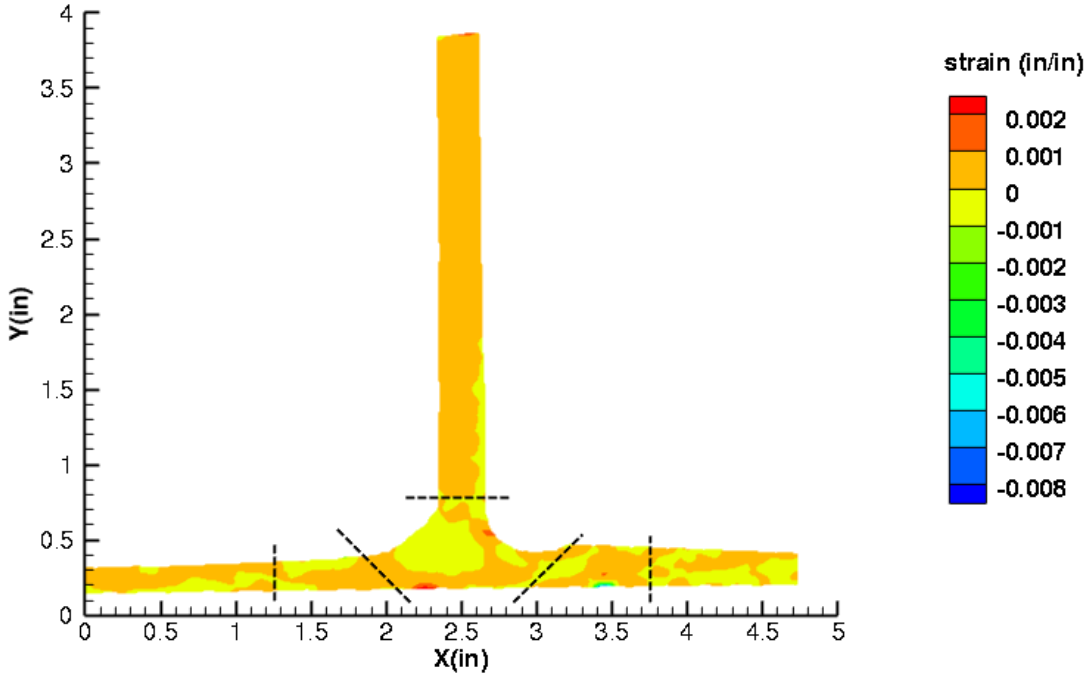

Figure C7. TNS1 strain contours for ε_{yy} at 2593 lb. load, just after initial failure, 29MP VIC data.

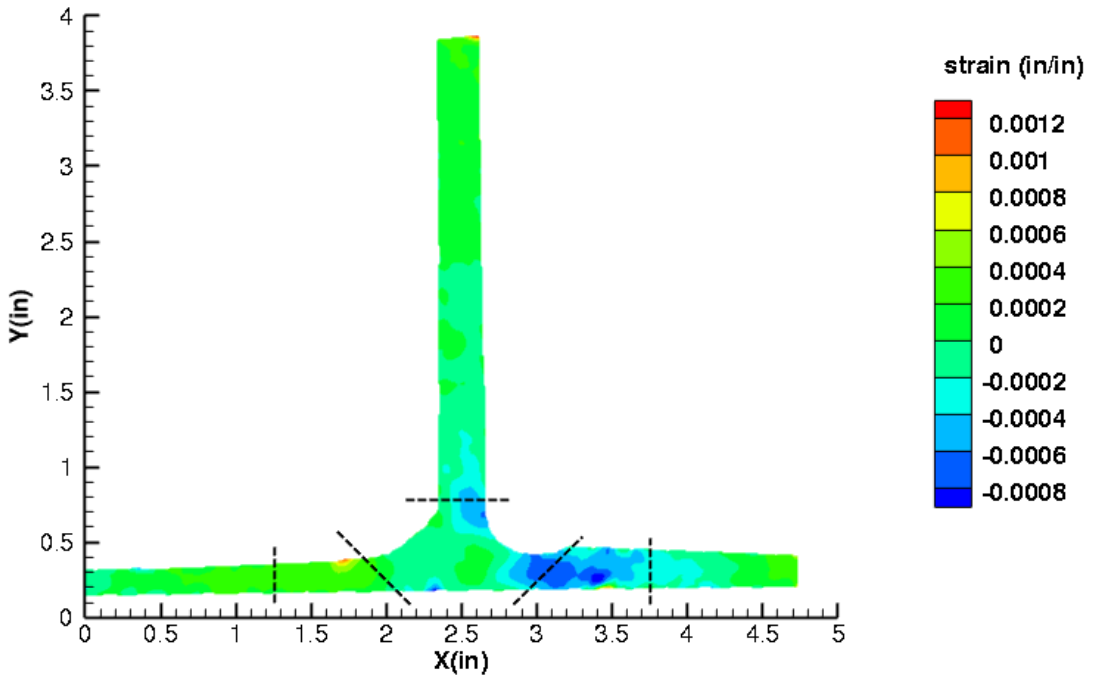

Figure C8. TNS1 strain contours for ε_{xy} at 2599 lb. load, prior to initial failure, 29MP VIC data.

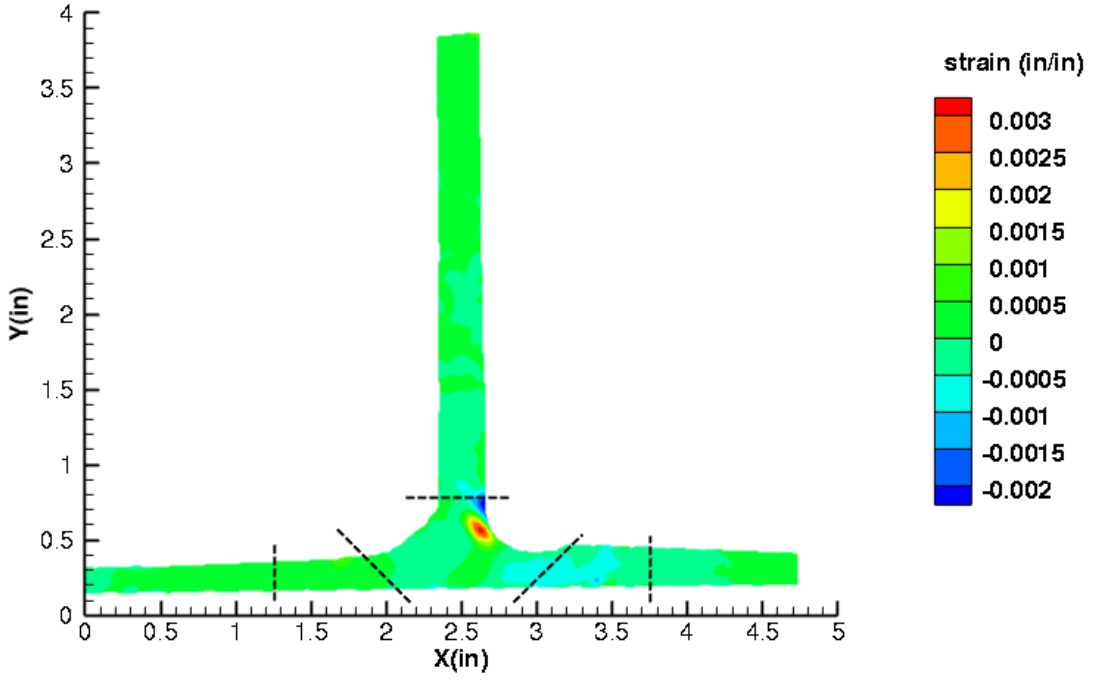

Figure C9. TNS1 strain contours for ε_{xy} at 2593 lb. load, just after initial failure, 29MP VIC data.

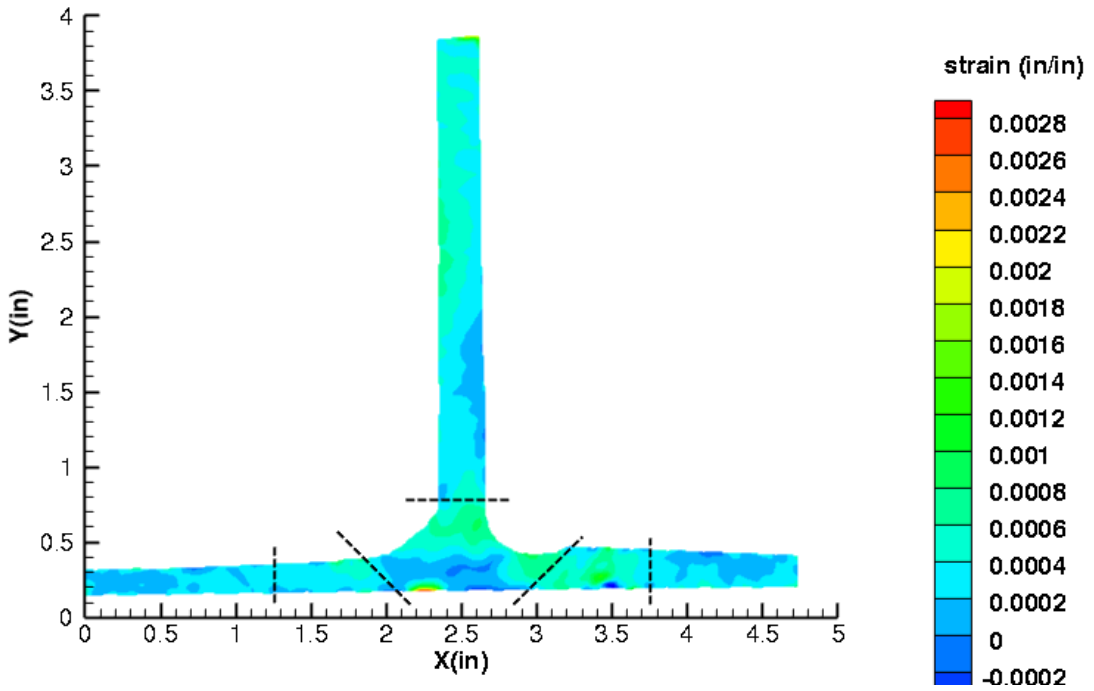

Figure C10. TNS1 strain contours for maximum principal strain at 2599 lb. load, prior to initial failure, 29MP VIC data.

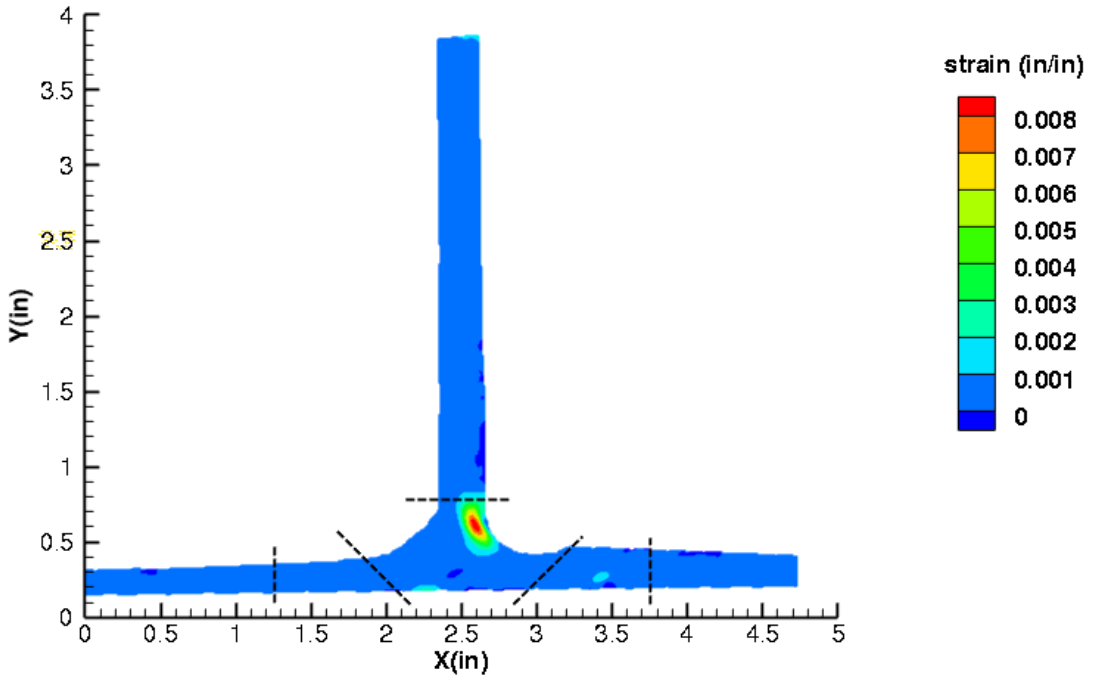

Figure C11. TNS1 strain contours for maximum principal strain at 2593 lb. load, just after initial failure, 29MP VIC data.

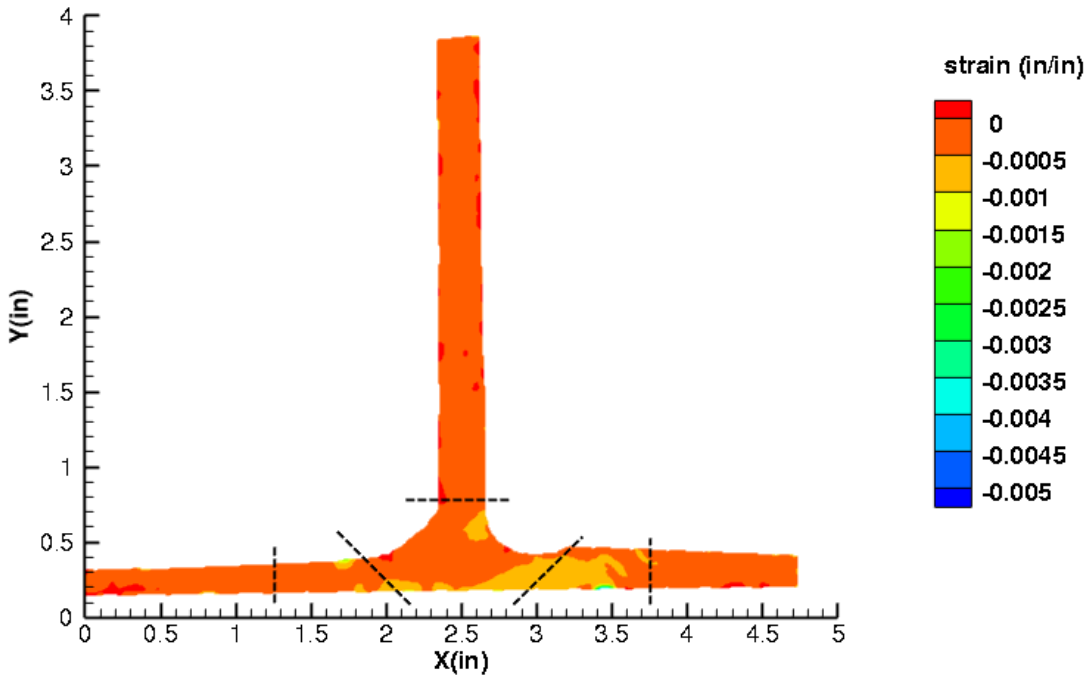

Figure C12. TNS1 strain contours for minimum principal strain at 2599 lb. load, prior to initial failure, 29MP VIC data.

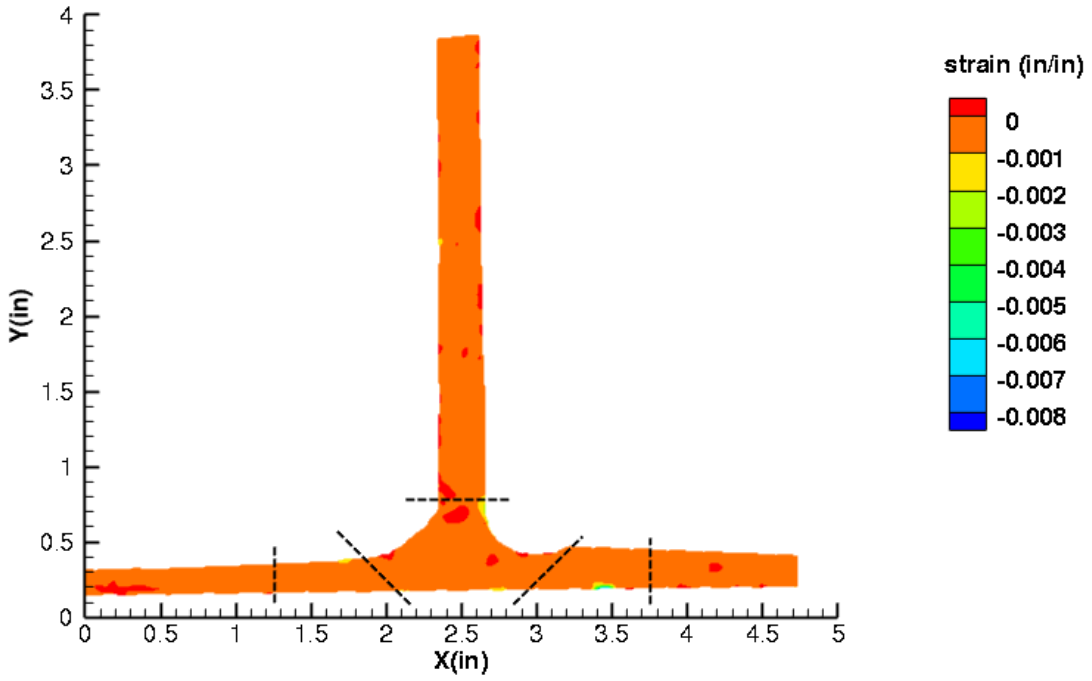

Figure C13. TNS1 strain contours for minimum principal strain at 2593 lb. load, just after initial failure, 29MP VIC data.

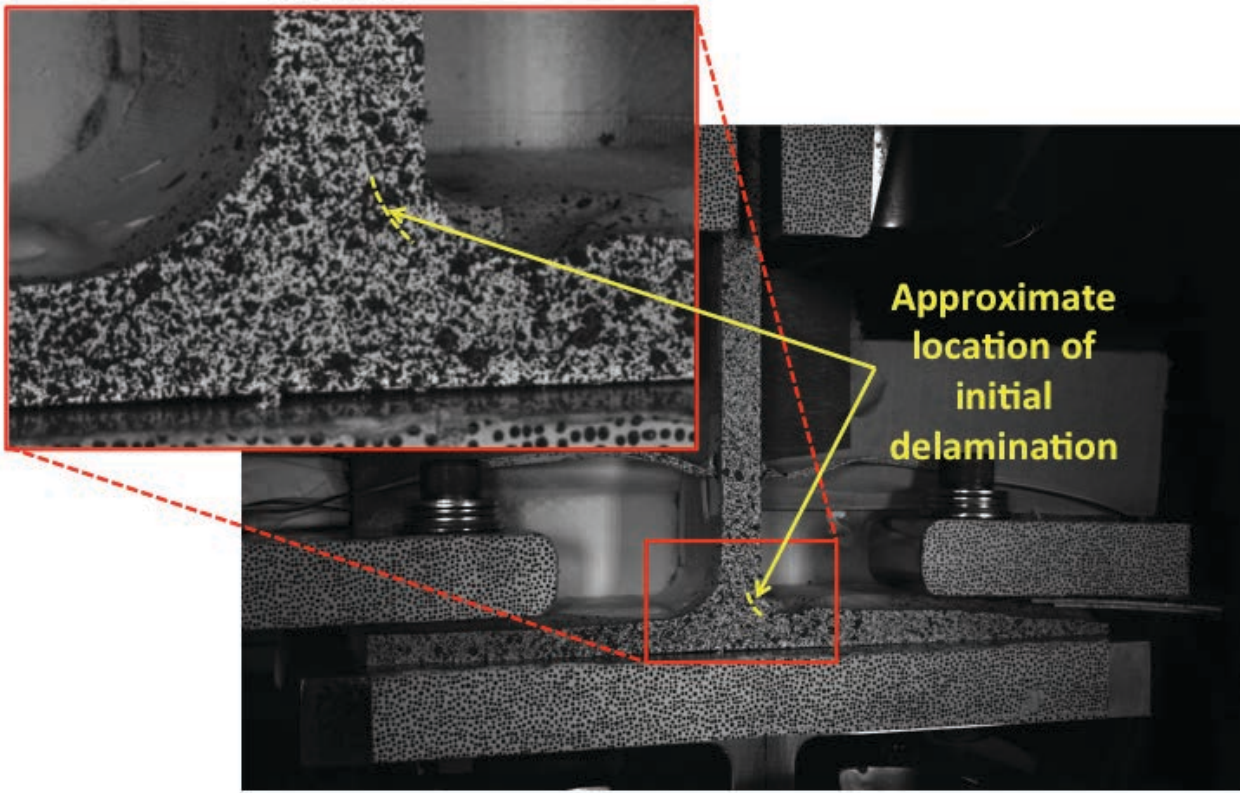

Figure C14. TNS1 image just after initial failure, 29MP VIC data.

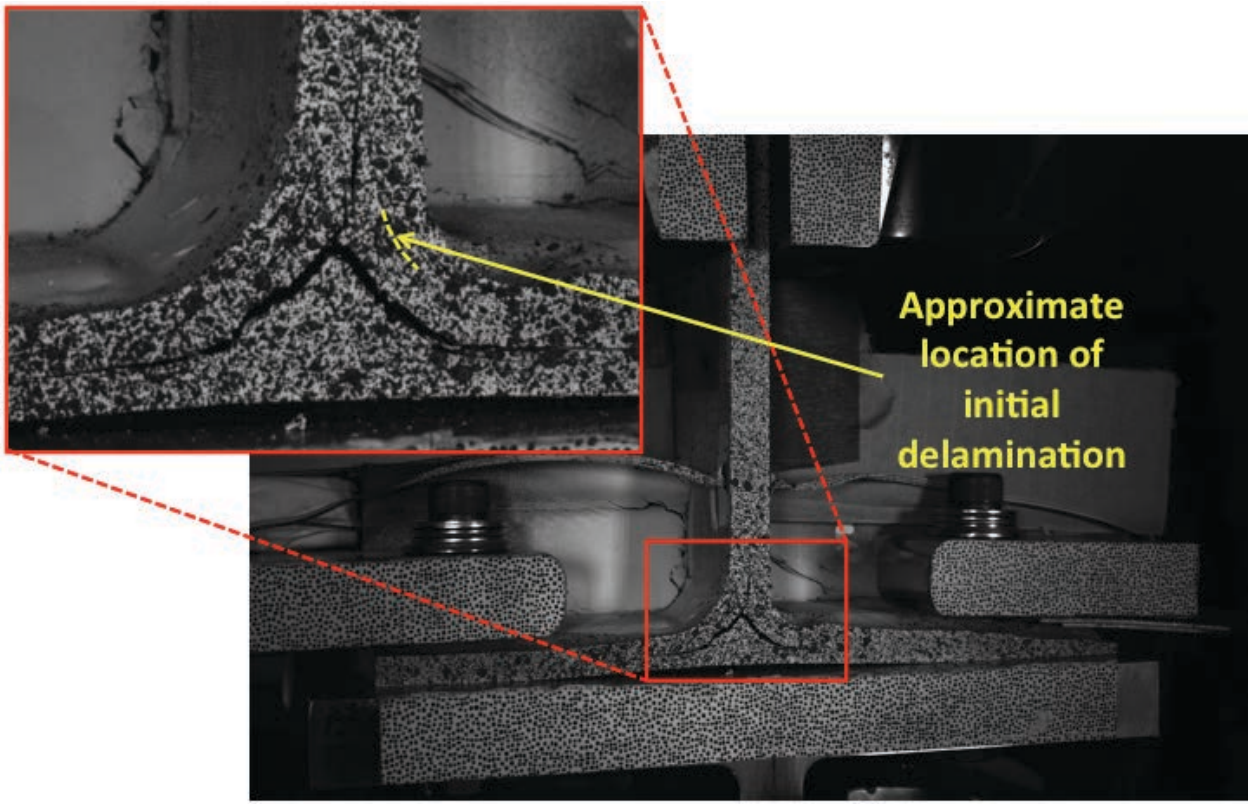

Figure C15. TNS1 image just after maximum load, 29MP VIC data.

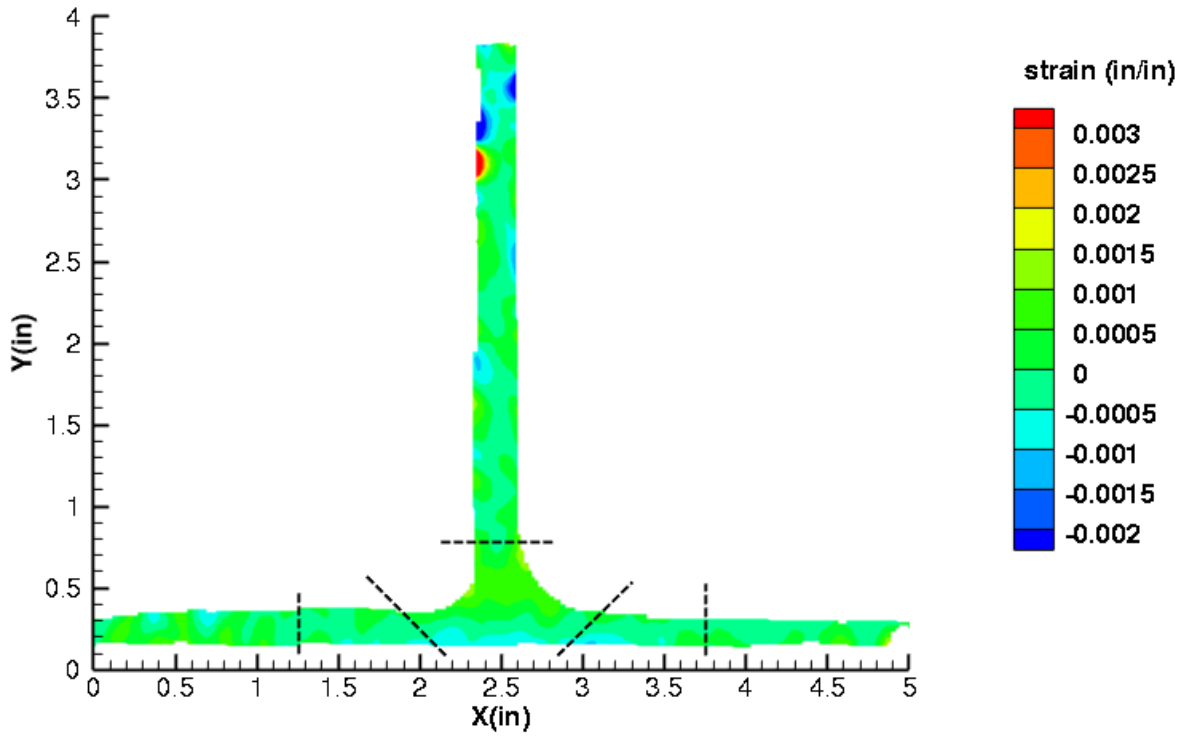

Figure C16. TNS1 strain contours for ε_{xx} at 3533 lb. load, prior to initial failure, 5MP VIC data.

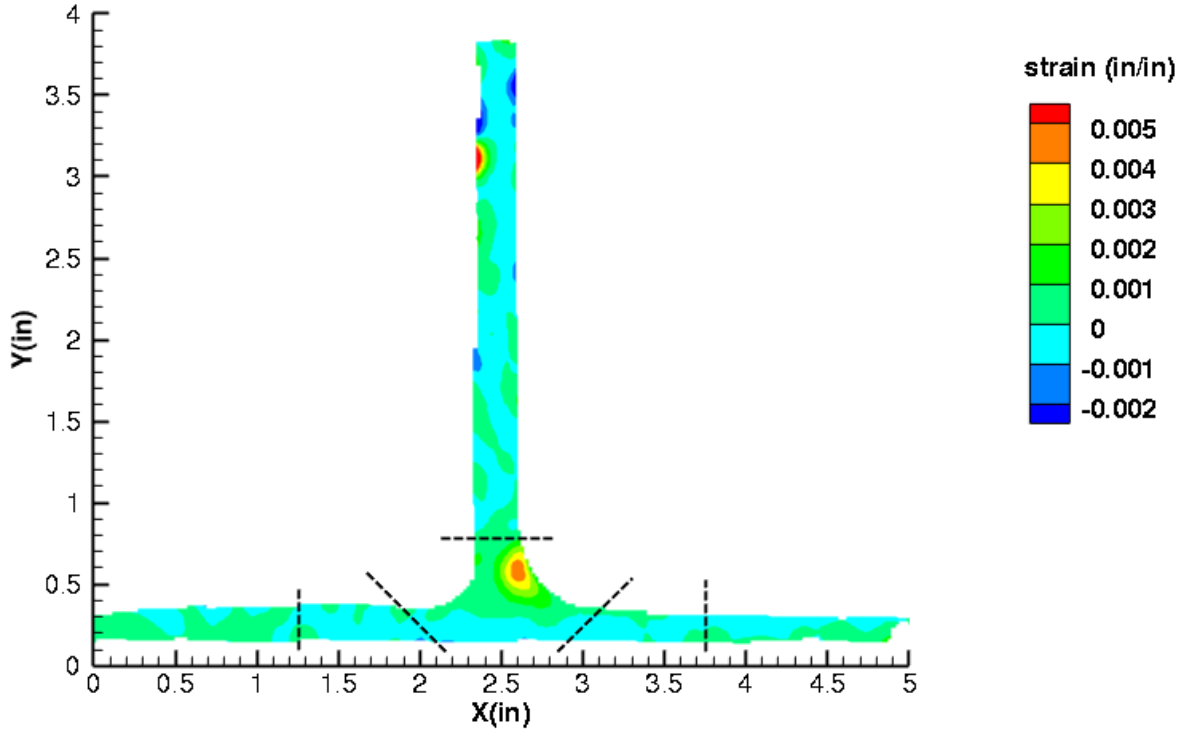

Figure C17. TNS1 strain contours for ε_{xx} at 3548 lb. load, just after initial failure, 5MP VIC data.

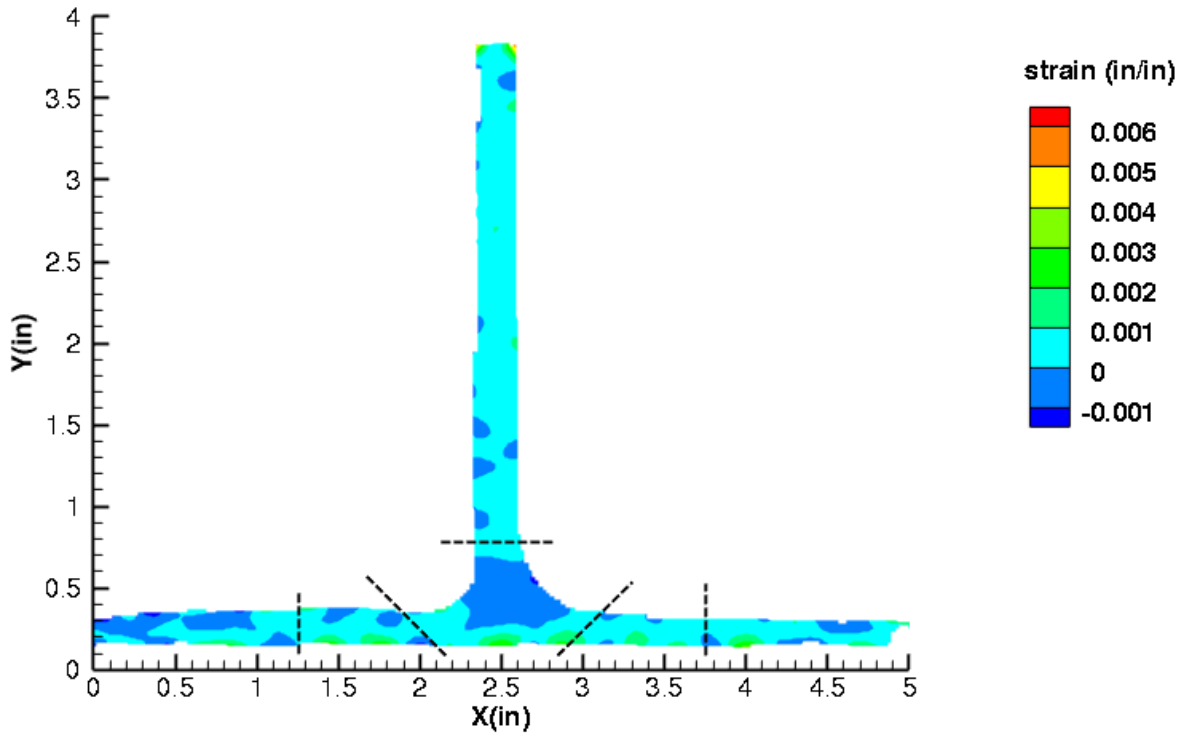

Figure C18. TNS1 strain contours for ε_{yy} at 3533 lb. load, prior to initial failure, 5MP VIC data.

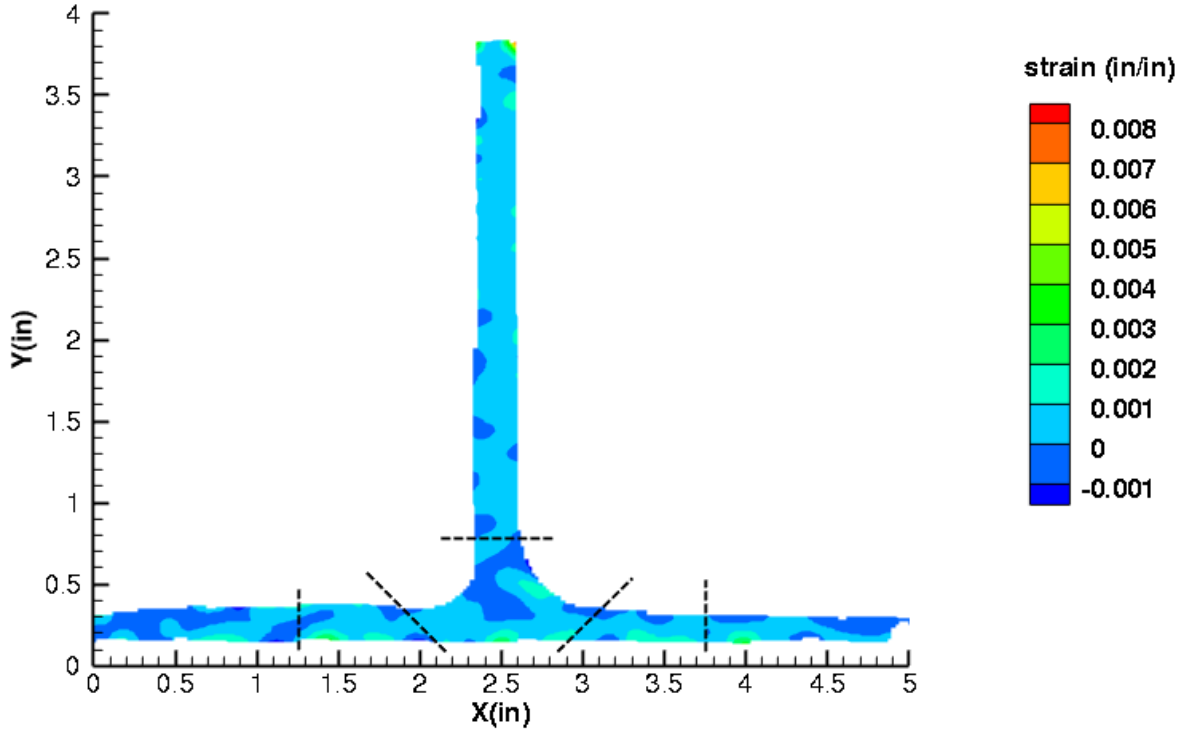

Figure C19. TNS1 strain contours for ε_{yy} at 3548 lb. load, just after initial failure, 5MP VIC data.

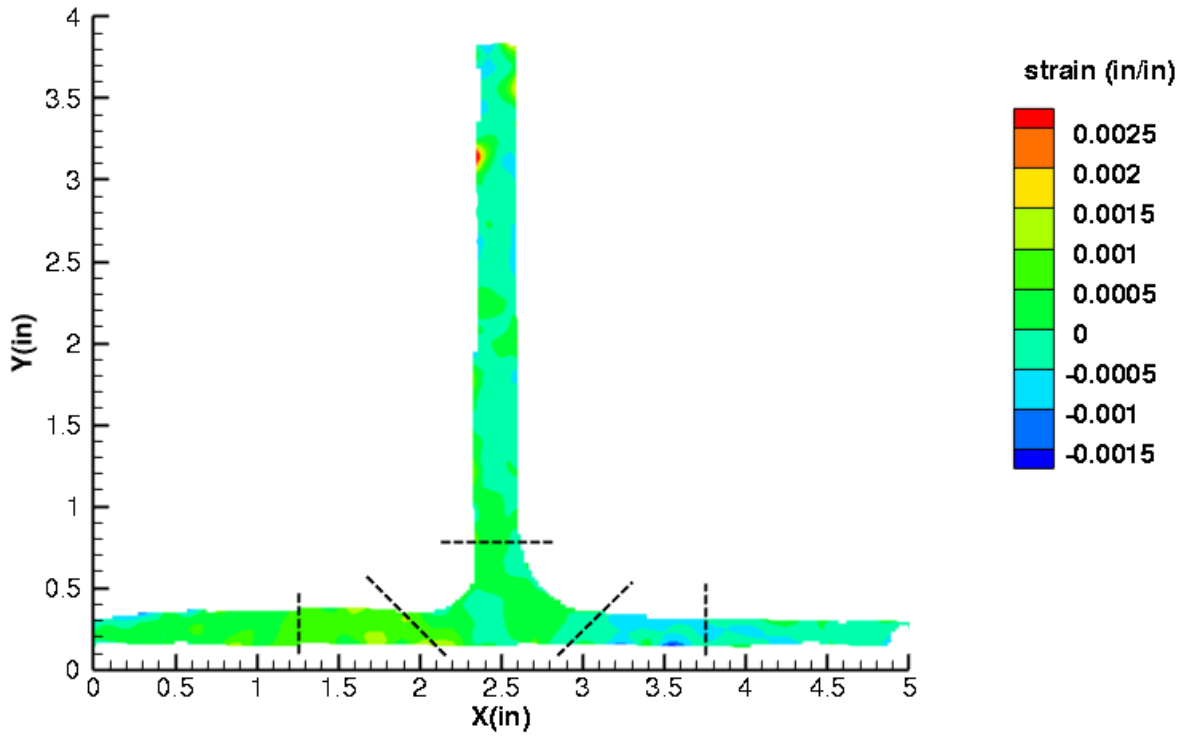

Figure C20. TNS1 strain contours for ε_{xy} at 3533 lb. load, prior to initial failure, 5MP VIC data.

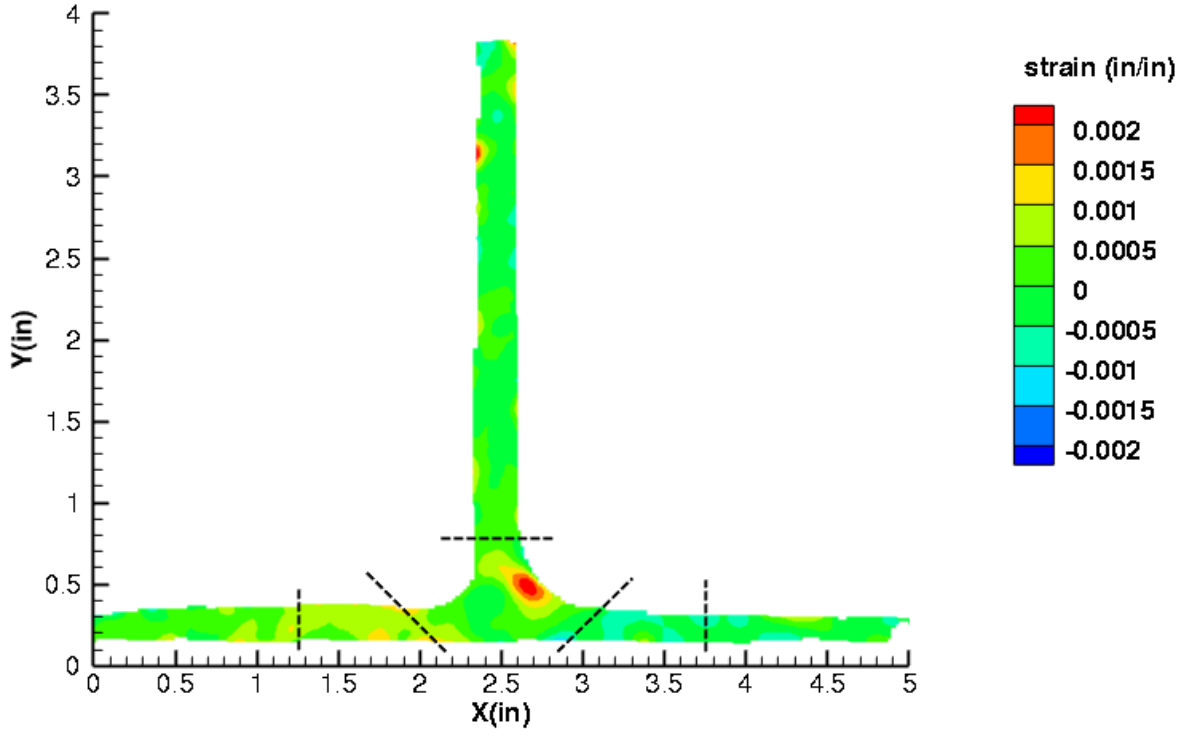

Figure C21. TNS1 strain contours for ε_{xy} at 3548 lb. load, just after initial failure, 5MP VIC data.

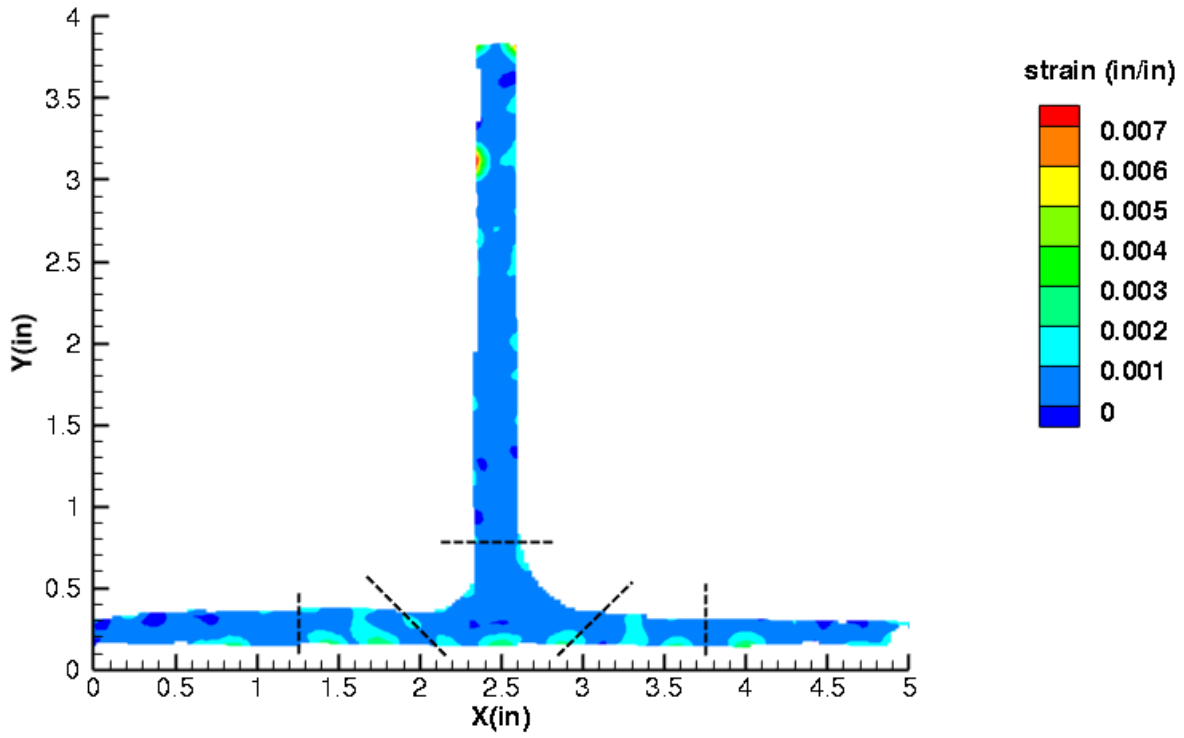

Figure C22. TNS1 strain contours for maximum principal strain at 3533 lb. load, prior to initial failure, 5MP VIC data.

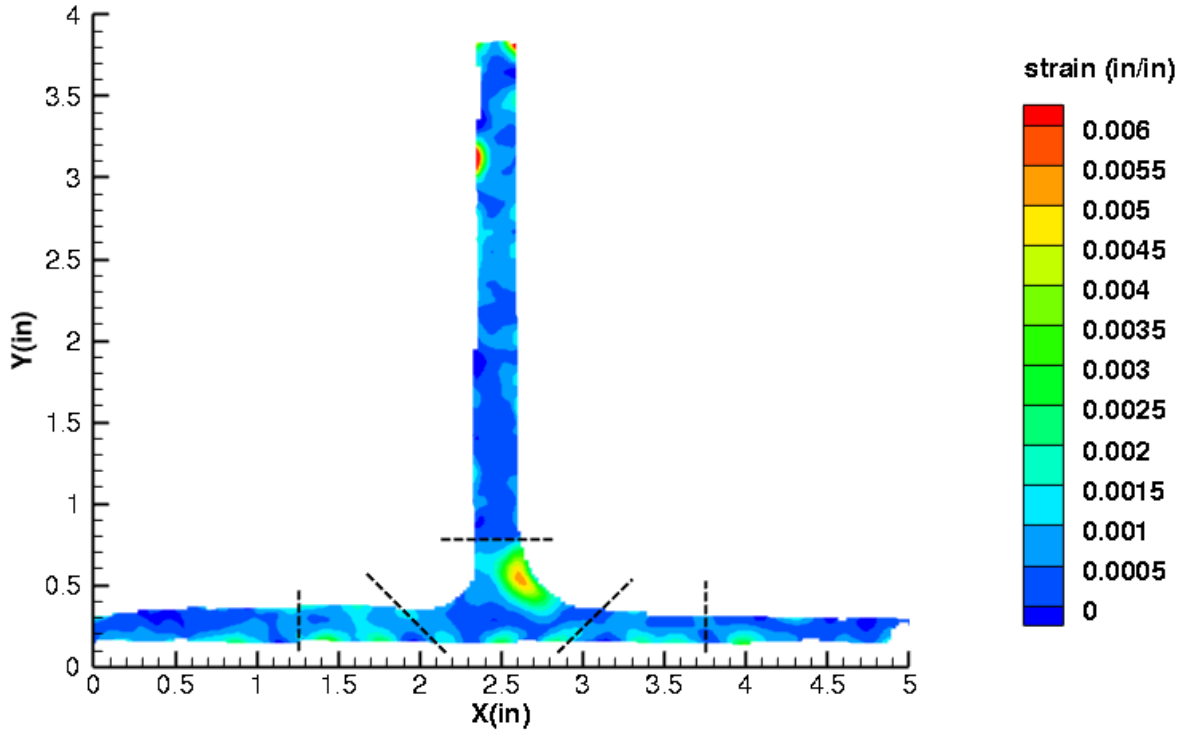

Figure C23. TNS1 strain contours for maximum principal strain at 3548 lb. load, just after initial failure, 5MP VIC data.

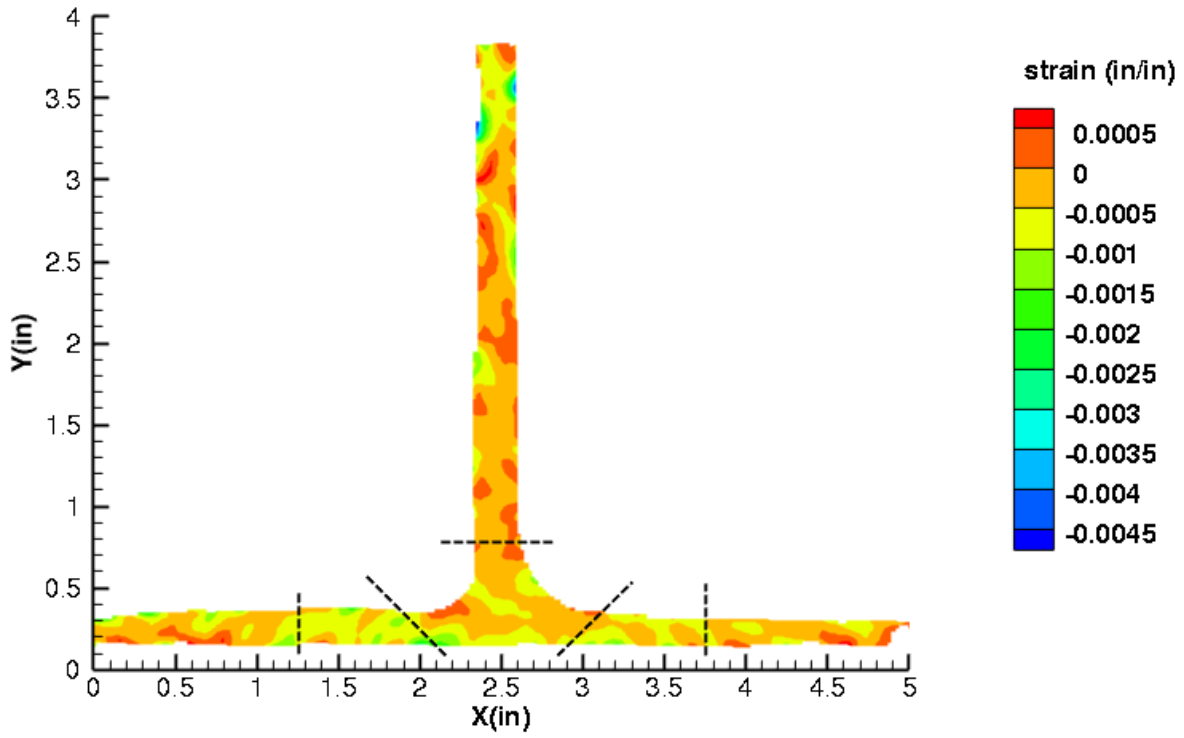

Figure C24. TNS1 strain contours for minimum principal strain at 3533 lb. load, prior to initial failure, 5MP VIC data.

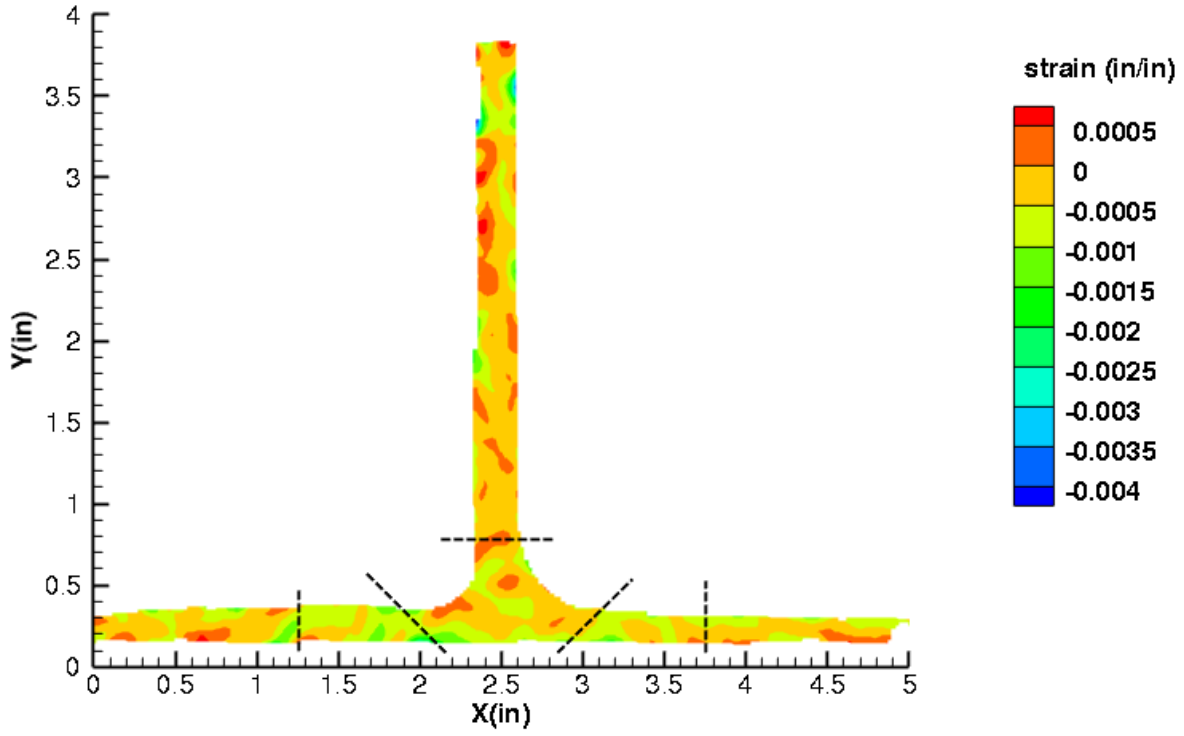

Figure C25. TNS1 strain contours for minimum principal strain at 3548 lb. load, just after initial failure, 5MP VIC data.

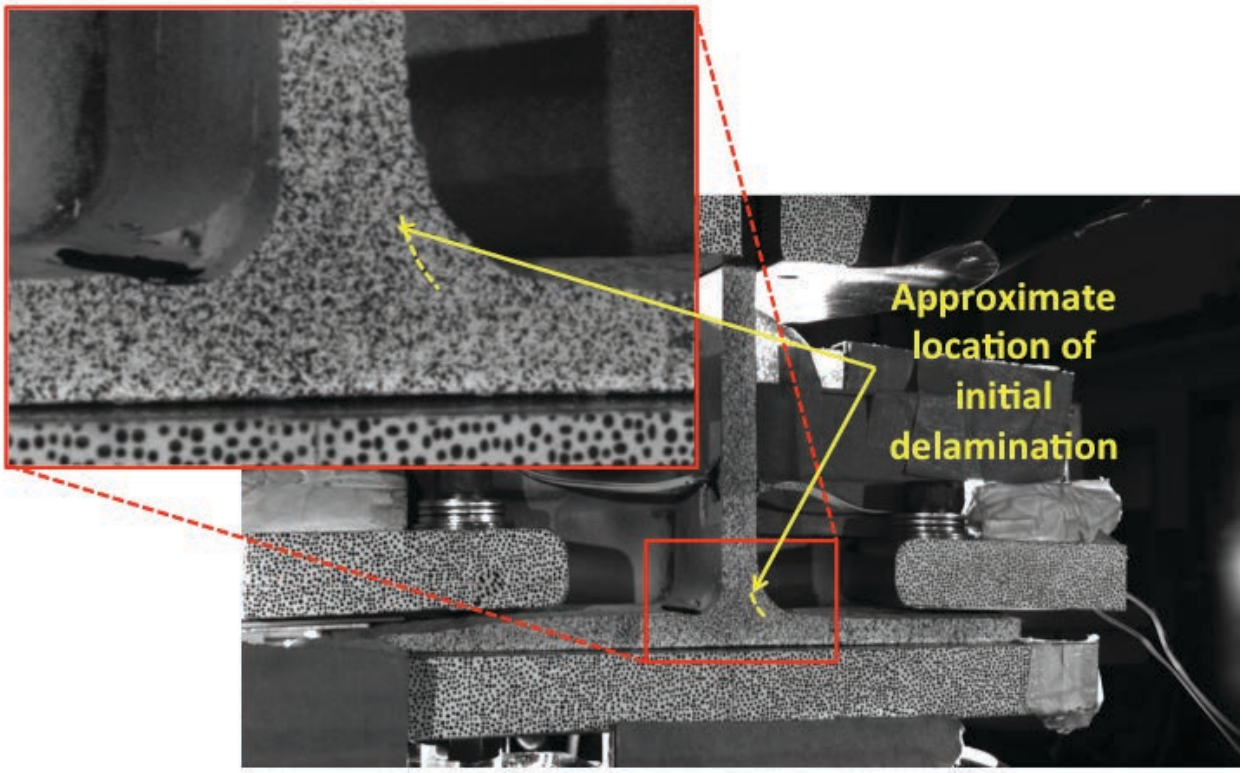

Figure C26. TNS1 image just after initial failure, 5MP VIC data.

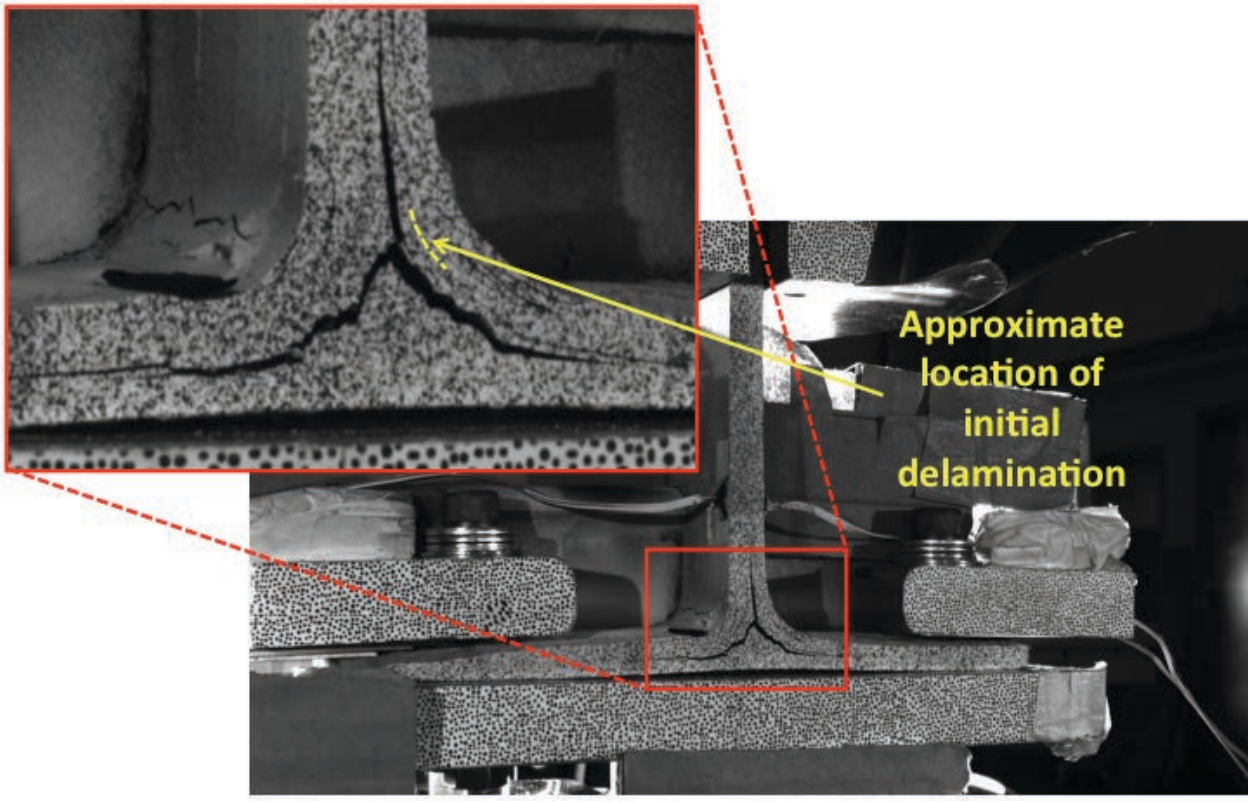

Figure C27. TNS1 image just after maximum load, 5MP VIC data.

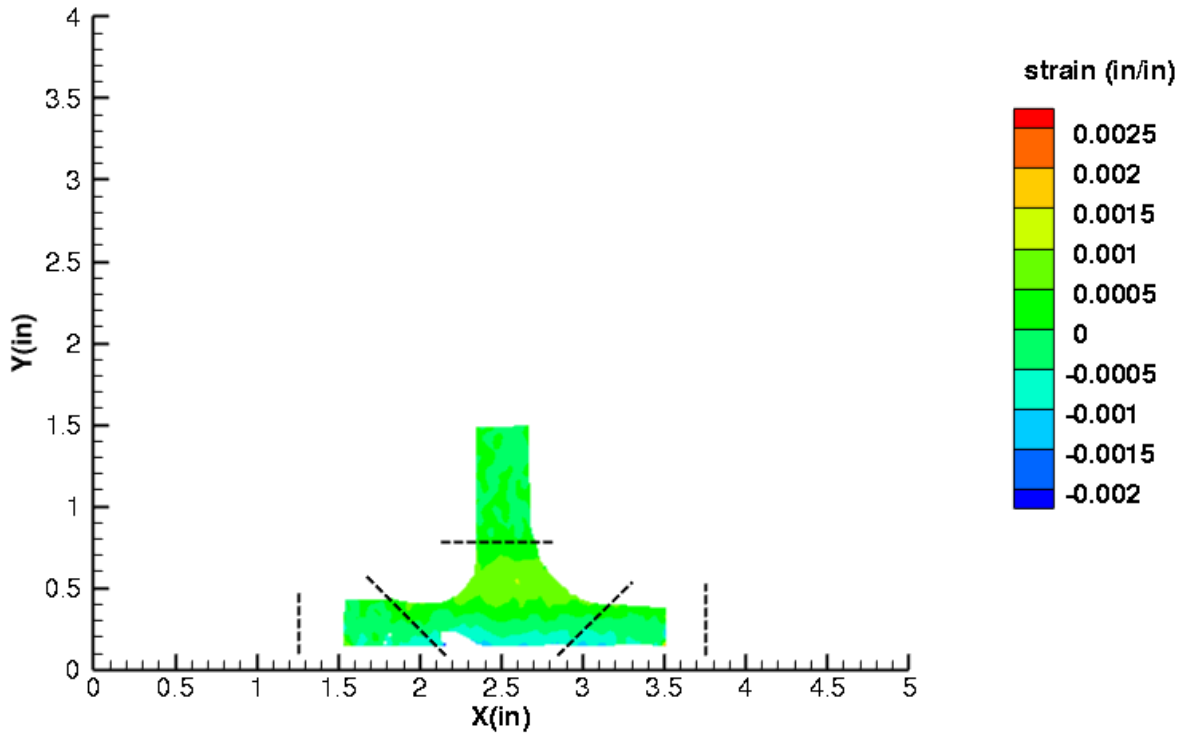

Figure C28. TNS1 strain contours for ε_{xx} at 3533 lb. load, prior to initial failure, local 5MP VIC data.

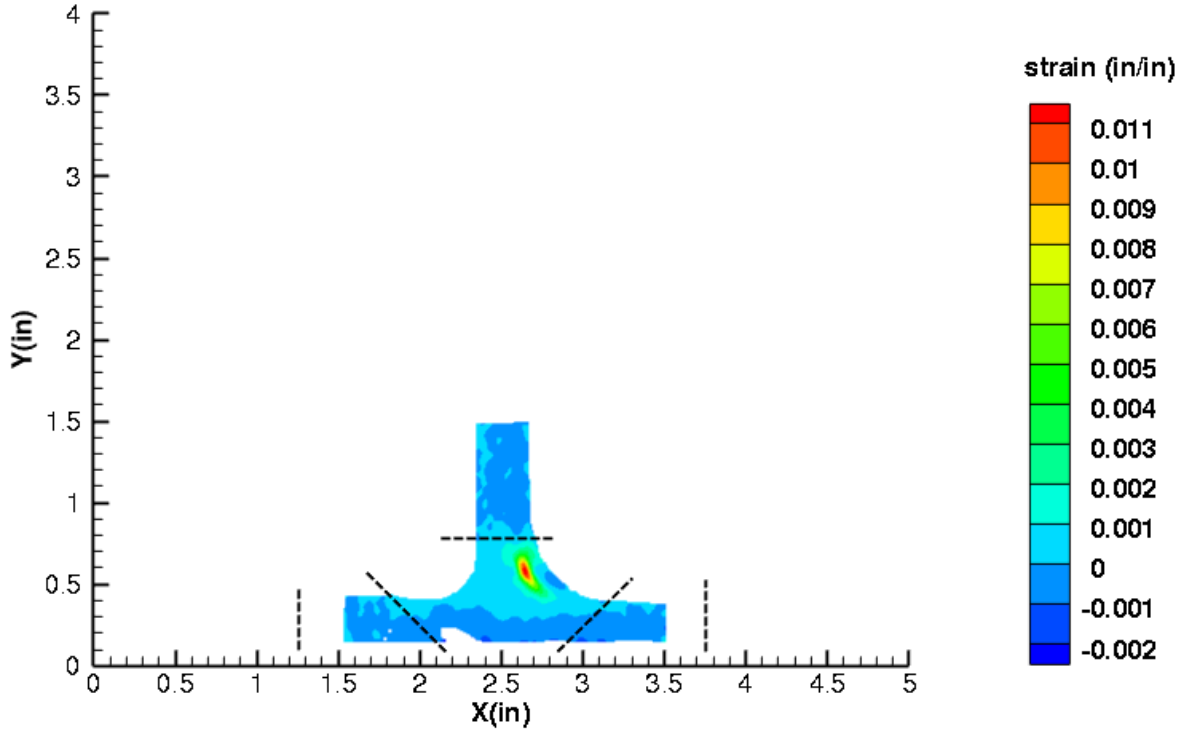

Figure C29. TNS1 strain contours for ε_{xx} at 3548 lb. load, just after initial failure, local 5MP VIC data.

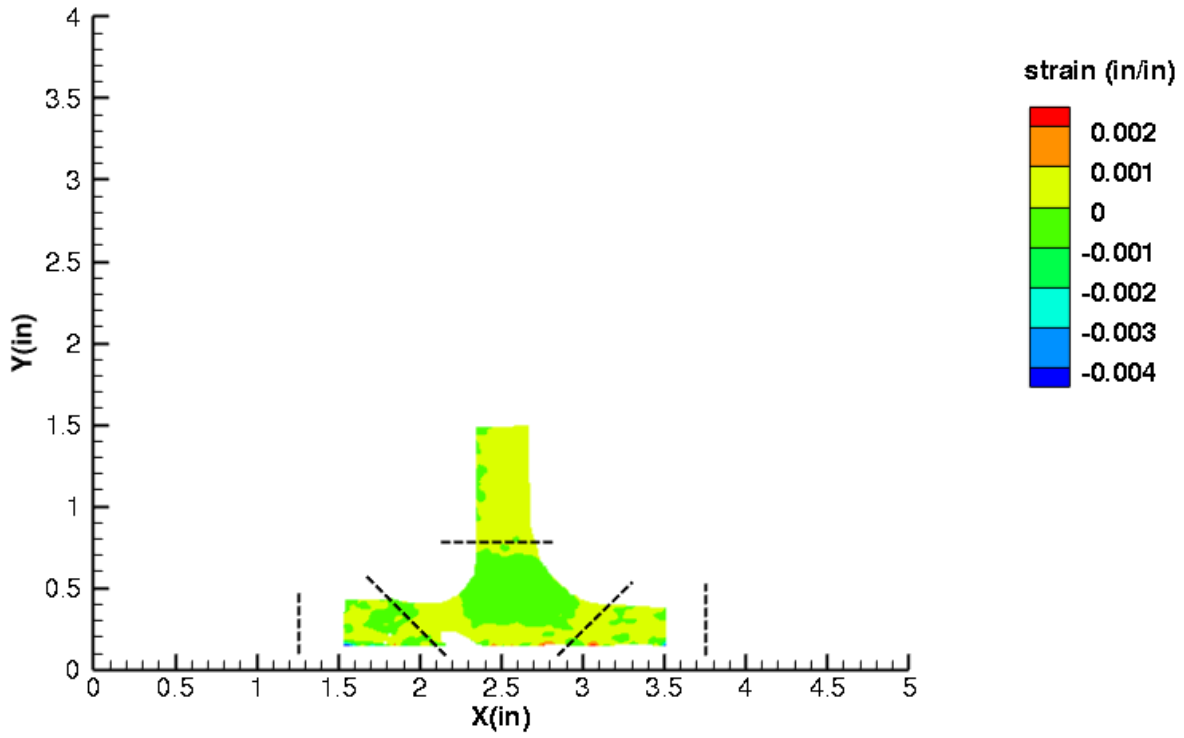

Figure C30. TNS1 strain contours for ε_{yy} at 3533 lb. load, prior to initial failure, local 5MP VIC data.

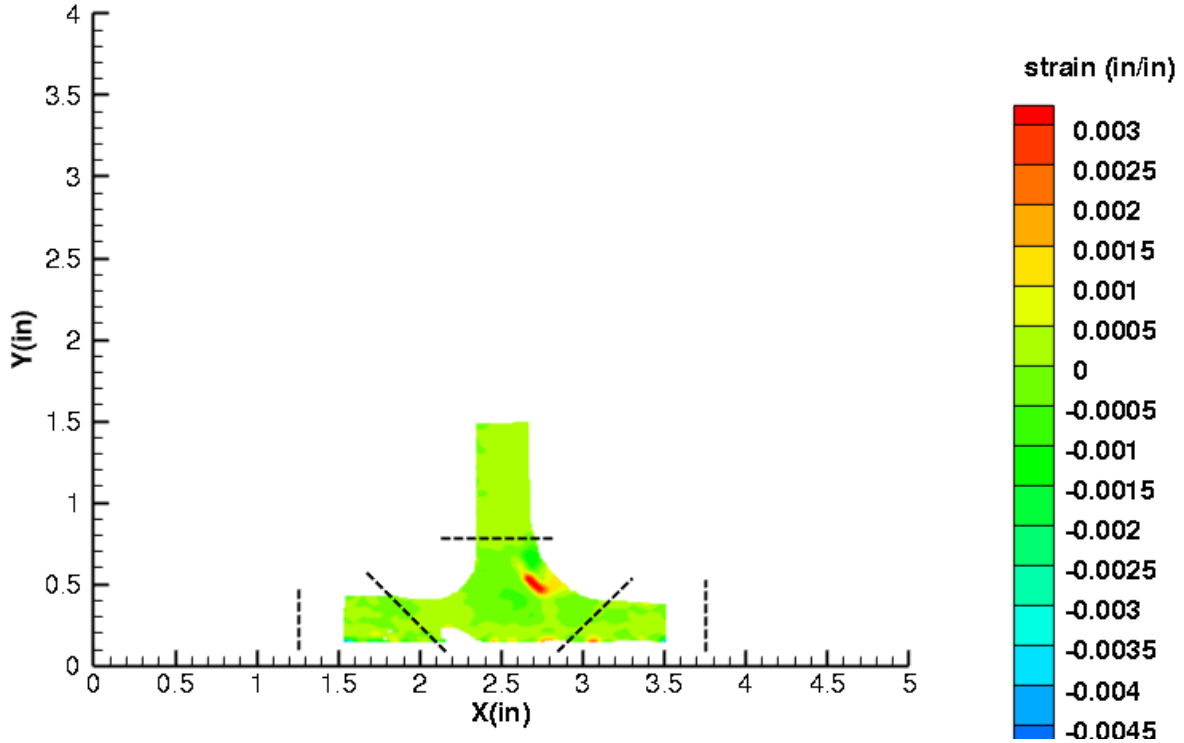

Figure C31. TNS1 strain contours for ε_{yy} at 3548 lb. load, just after initial failure, local 5MP VIC data.

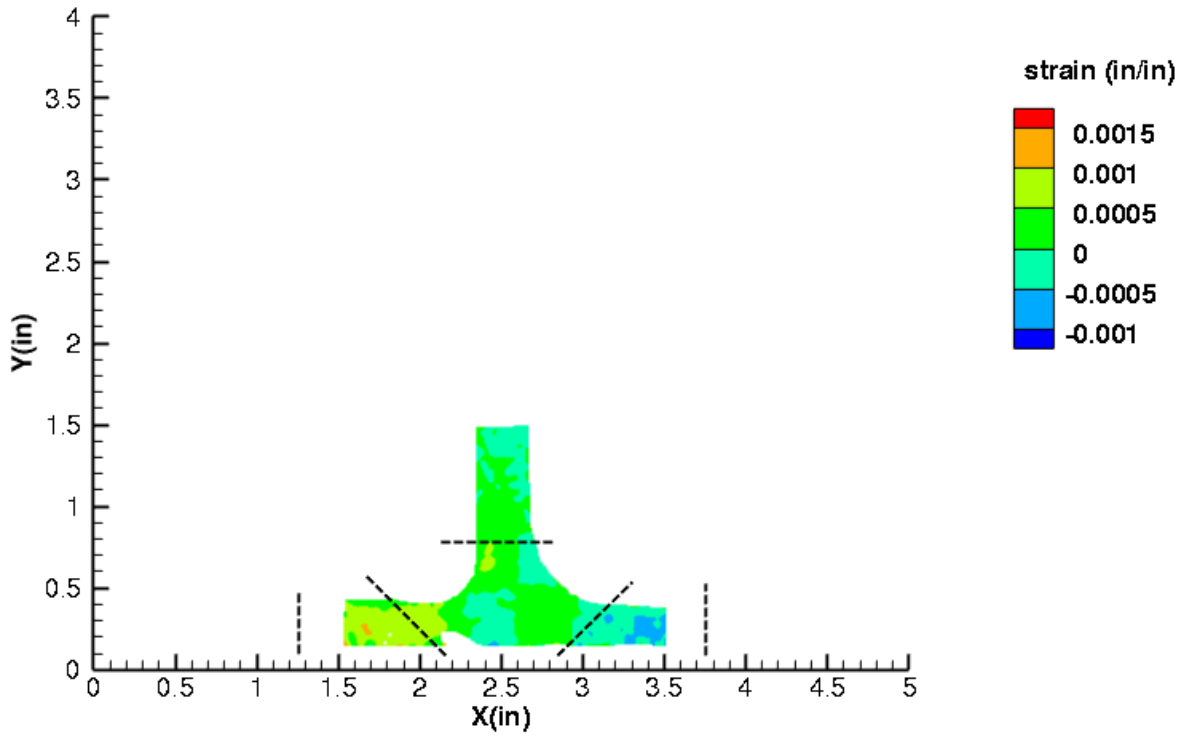

Figure C32. TNS1 strain contours for ε_{xy} at 3533 lb. load, prior to initial failure, local 5MP VIC data.

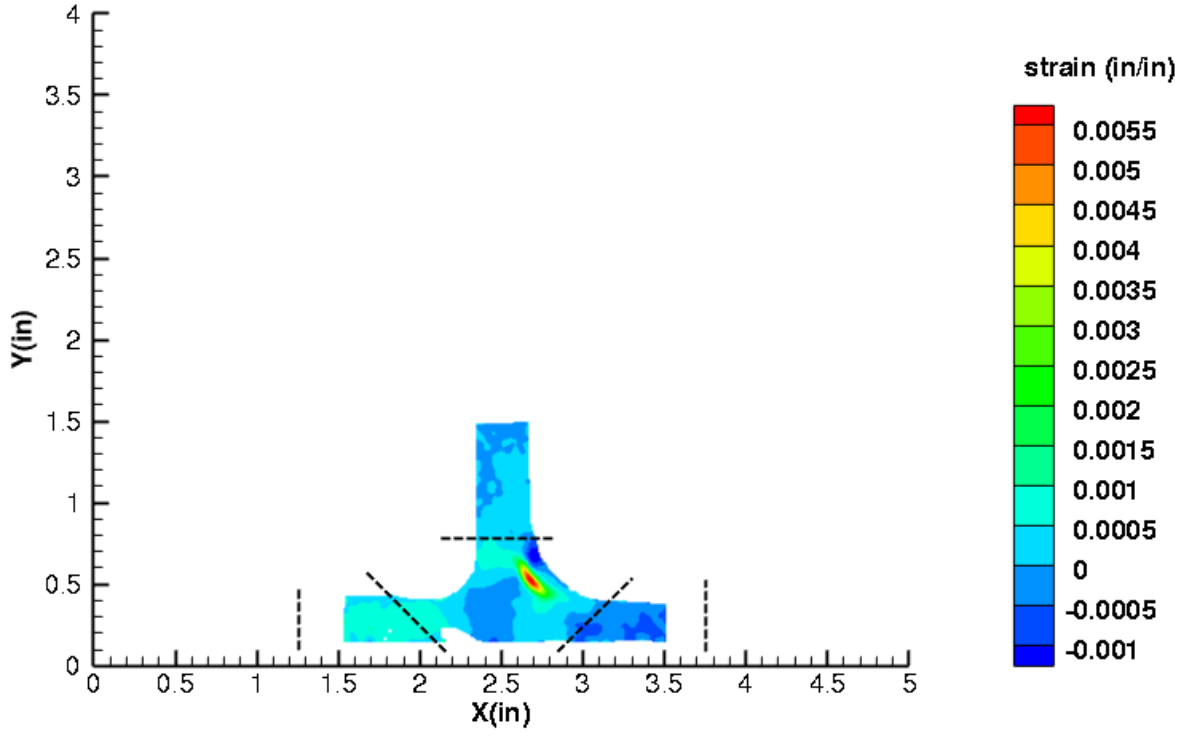

Figure C33. TNS1 strain contours for ε_{xy} at 3548 lb. load, just after initial failure, local 5MP VIC data.

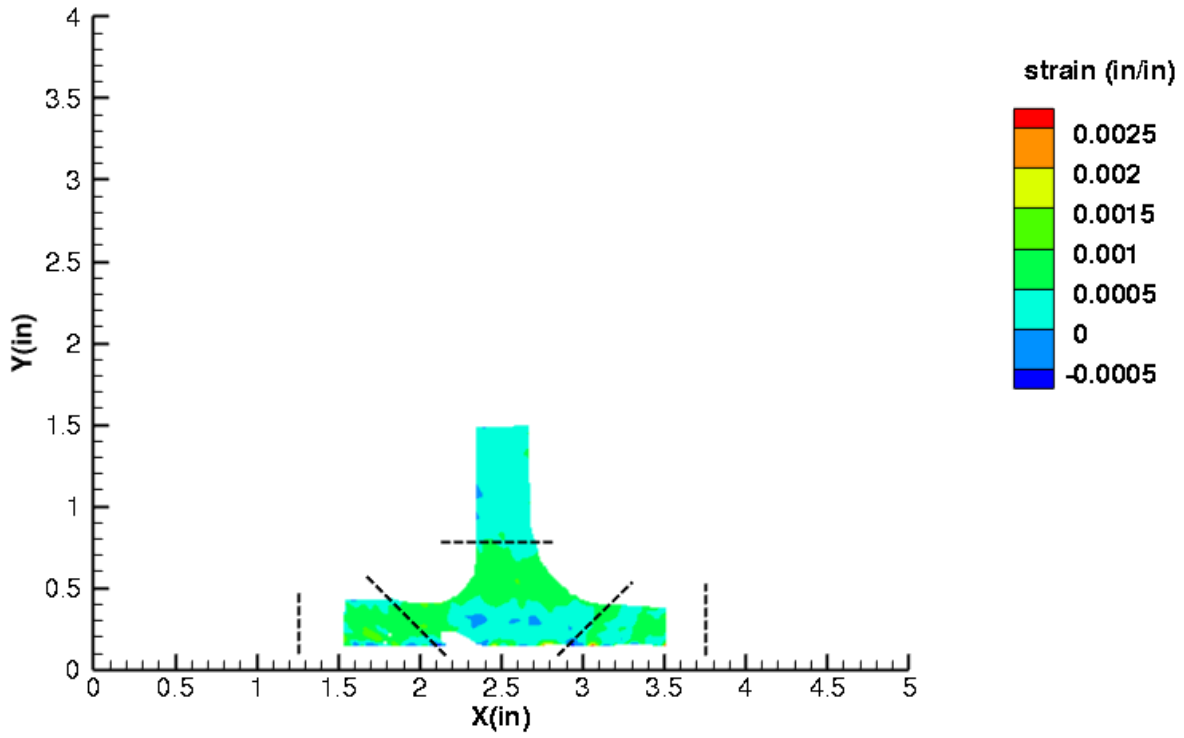

Figure C34. TNS1 strain contours for maximum principal strain at 3533 lb. load, prior to initial failure, local 5MP VIC data.

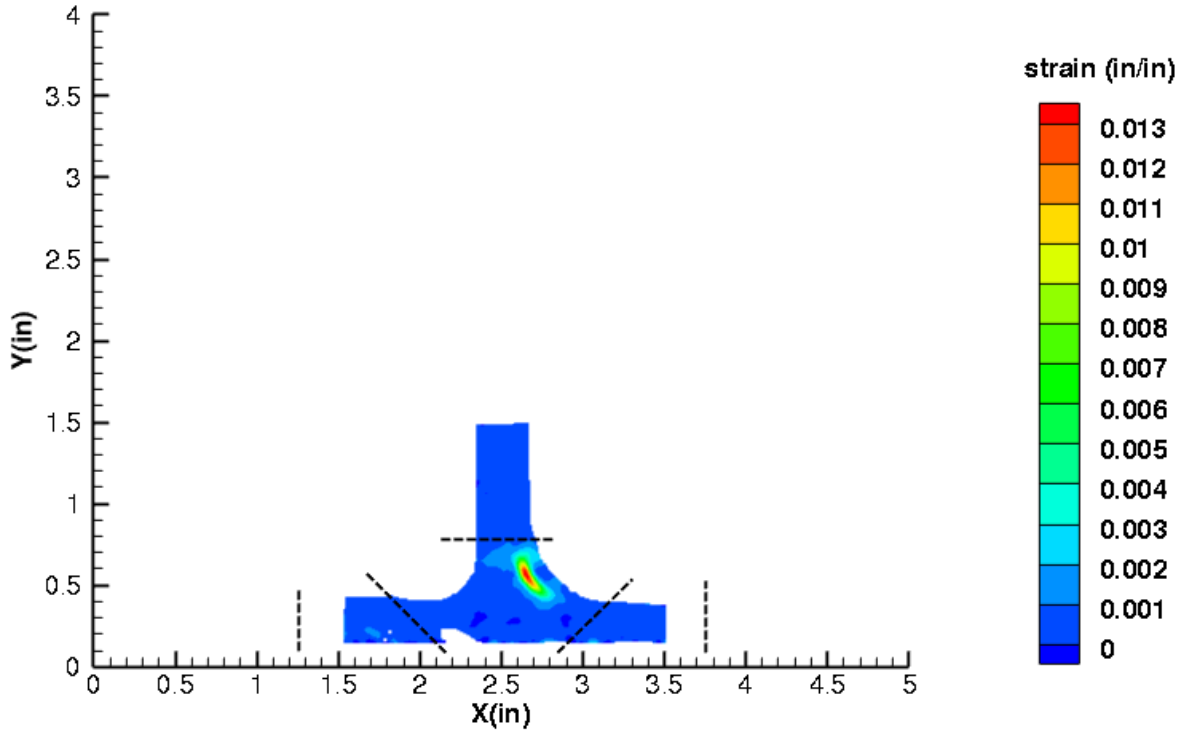

Figure C35. TNS1 strain contours for maximum principal strain at 3548 lb. load, just after initial failure, local 5MP VIC data.

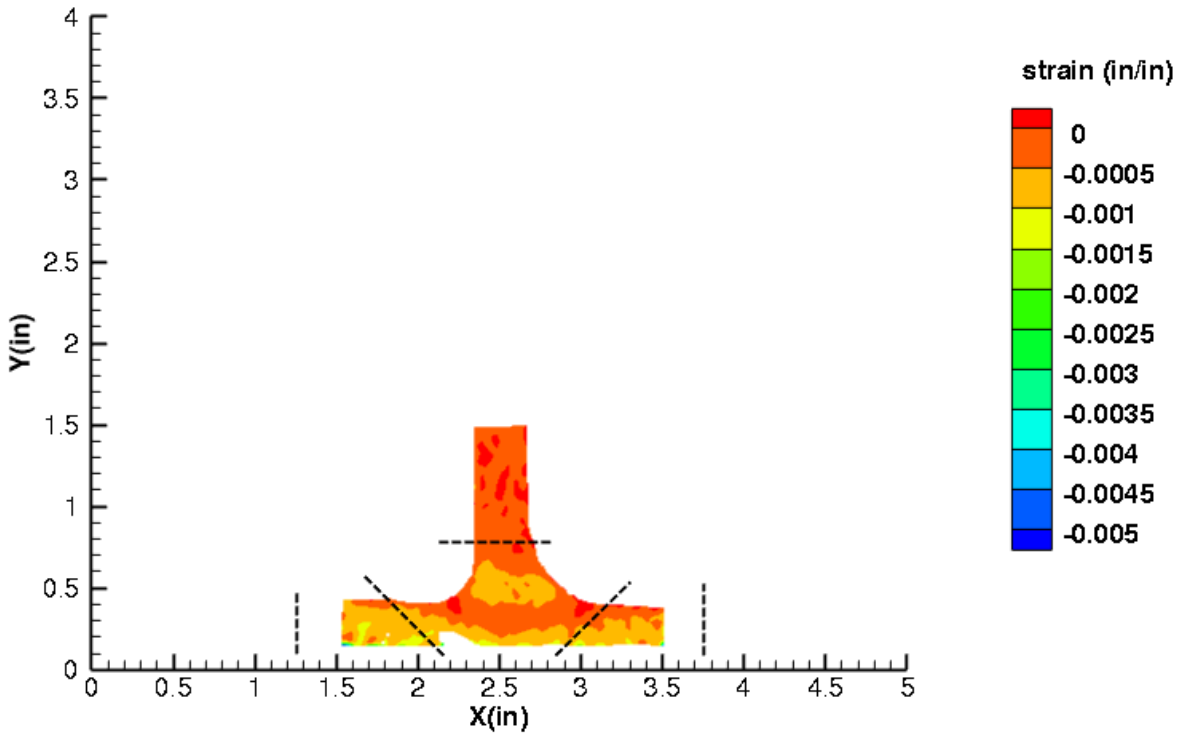

Figure C36. TNS1 strain contours for minimum principal strain at 3533 lb. load, prior to initial failure, local 5MP VIC data.

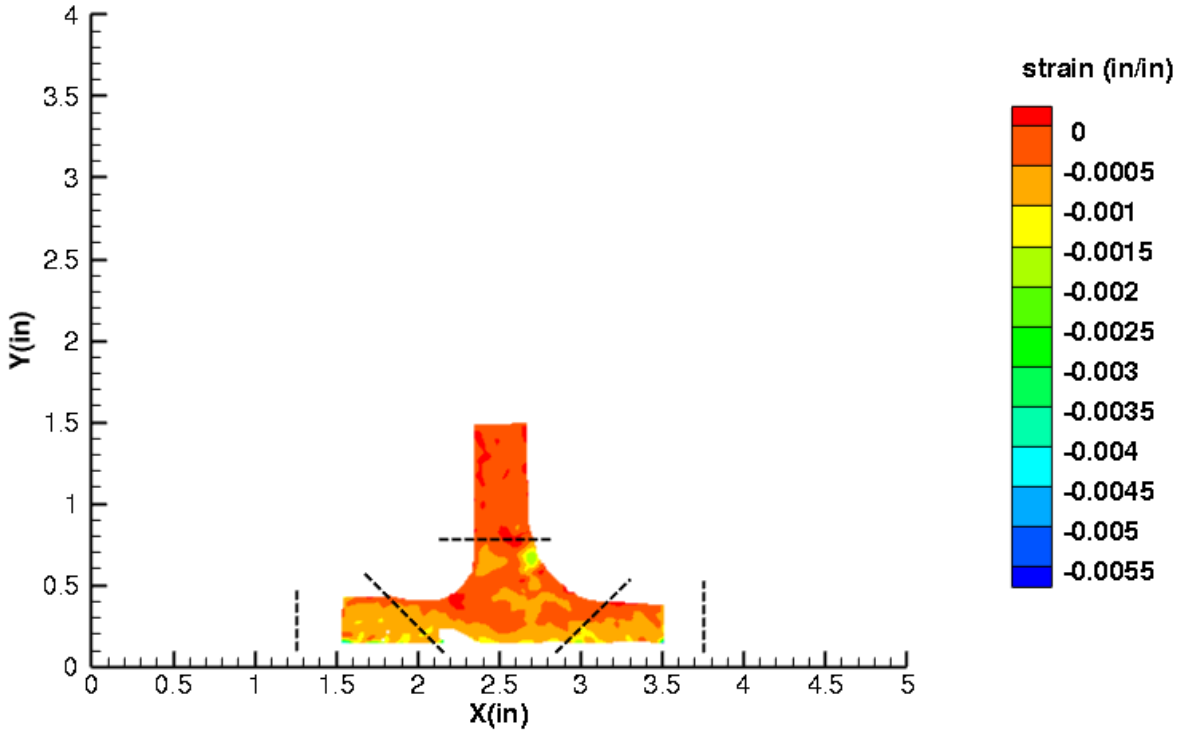

Figure C37. TNS1 strain contours for minimum principal strain at 3548 lb. load, just after initial failure, local 5MP VIC data.

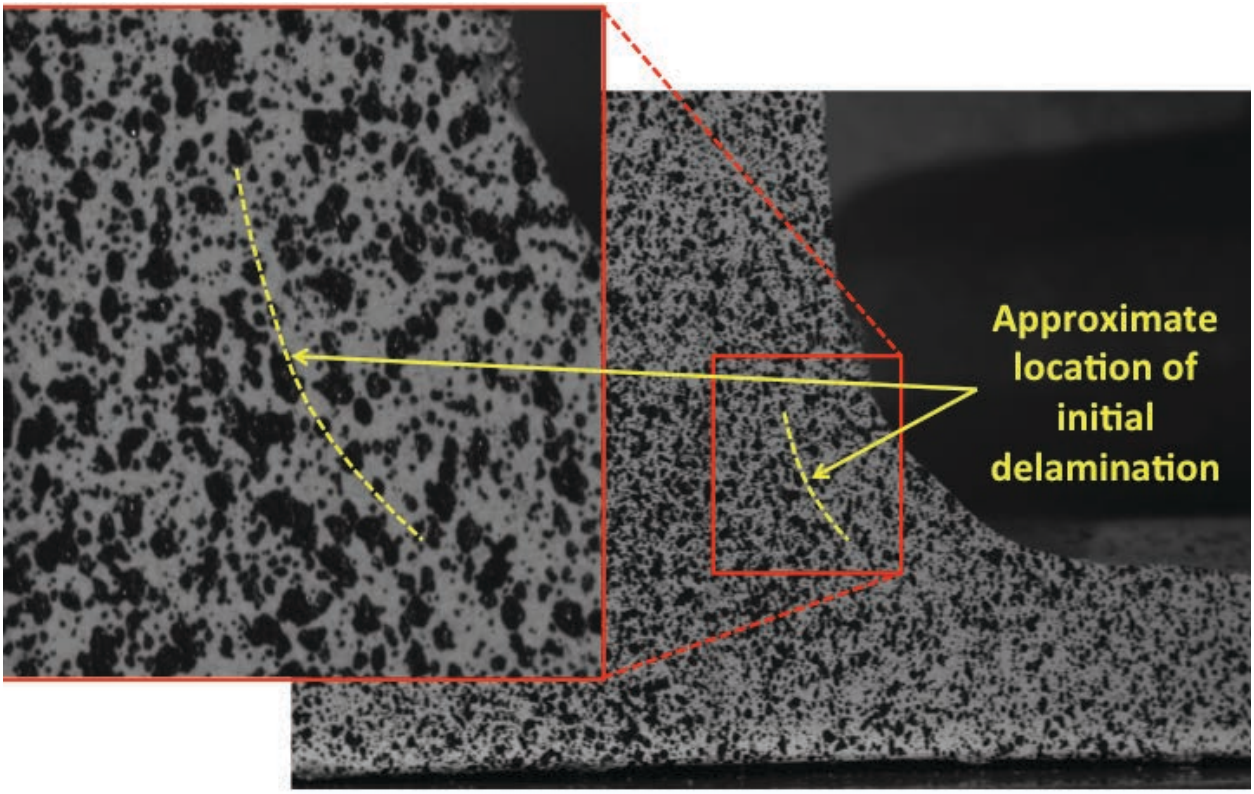

Figure C38. TNS1 image just after initial failure, local 5MP VIC data.

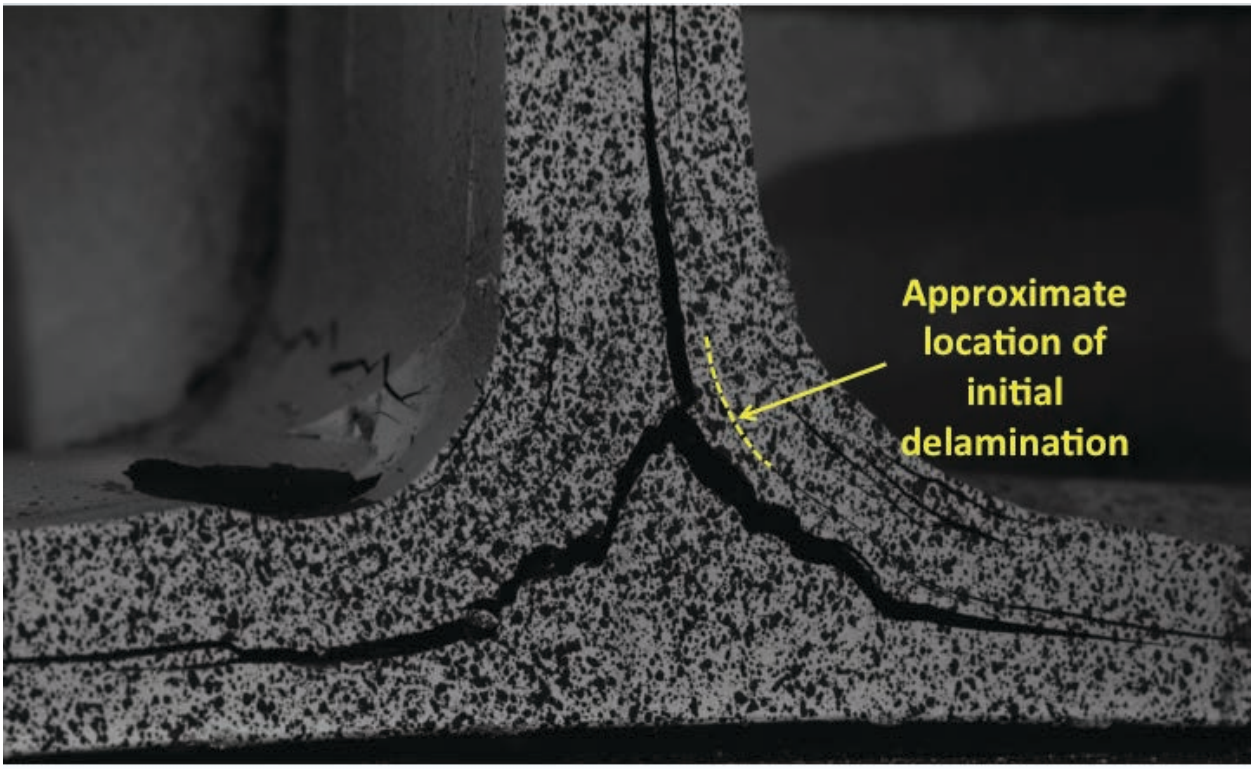

Figure C39. TNS1 image just after maximum load, local 5MP VIC data.

TNS2

This section presents the test data for the TNS2 test article.

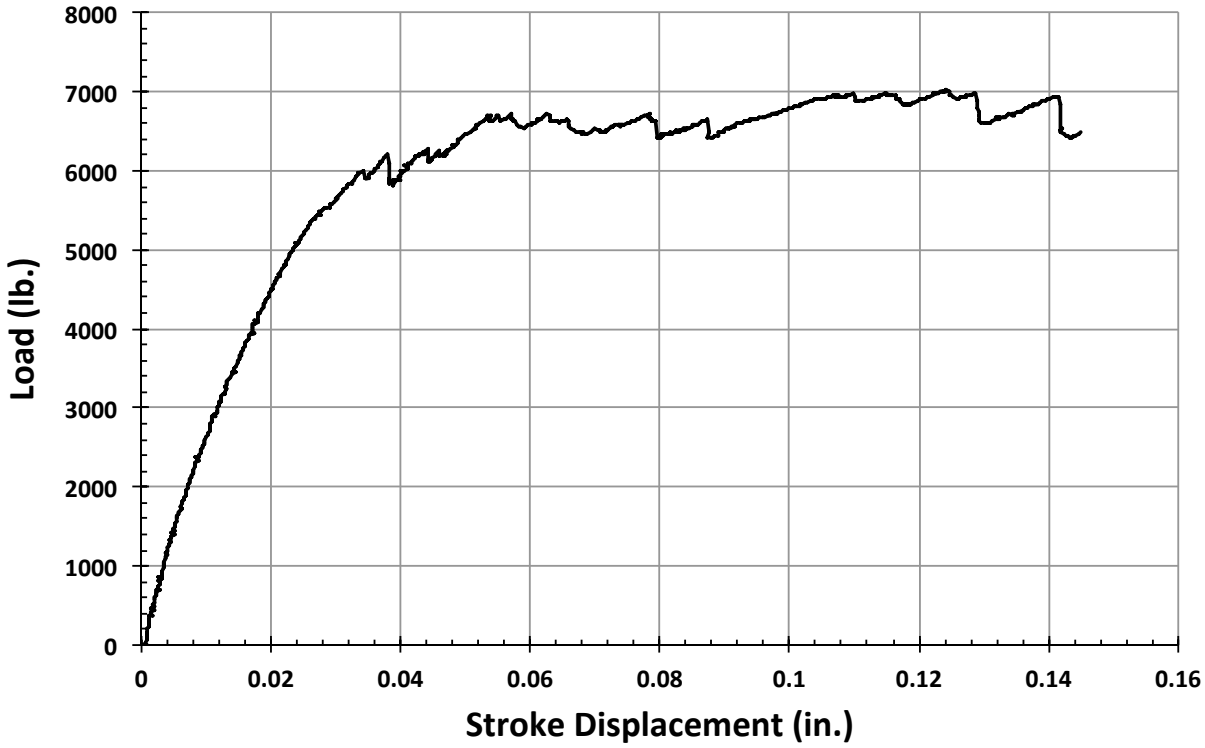

Figure C40. TNS2 load vs. stroke.

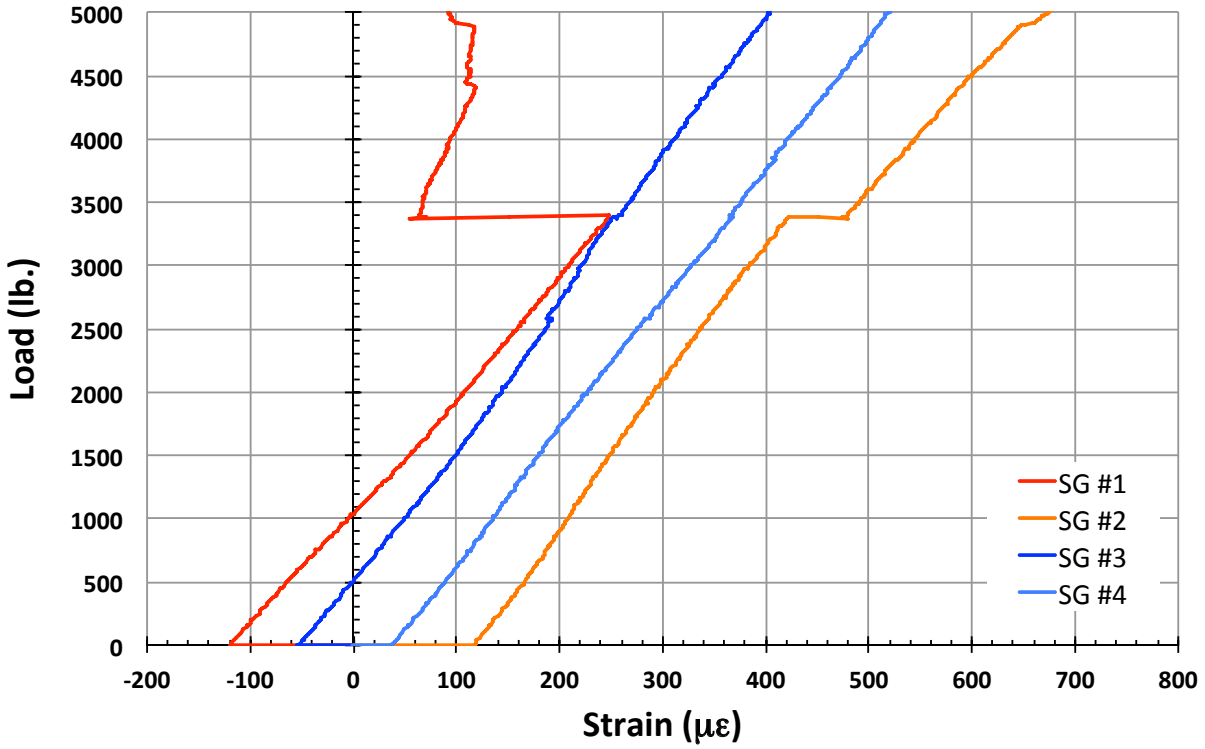

Figure C41. TNS2 load vs. strain, initial loading.

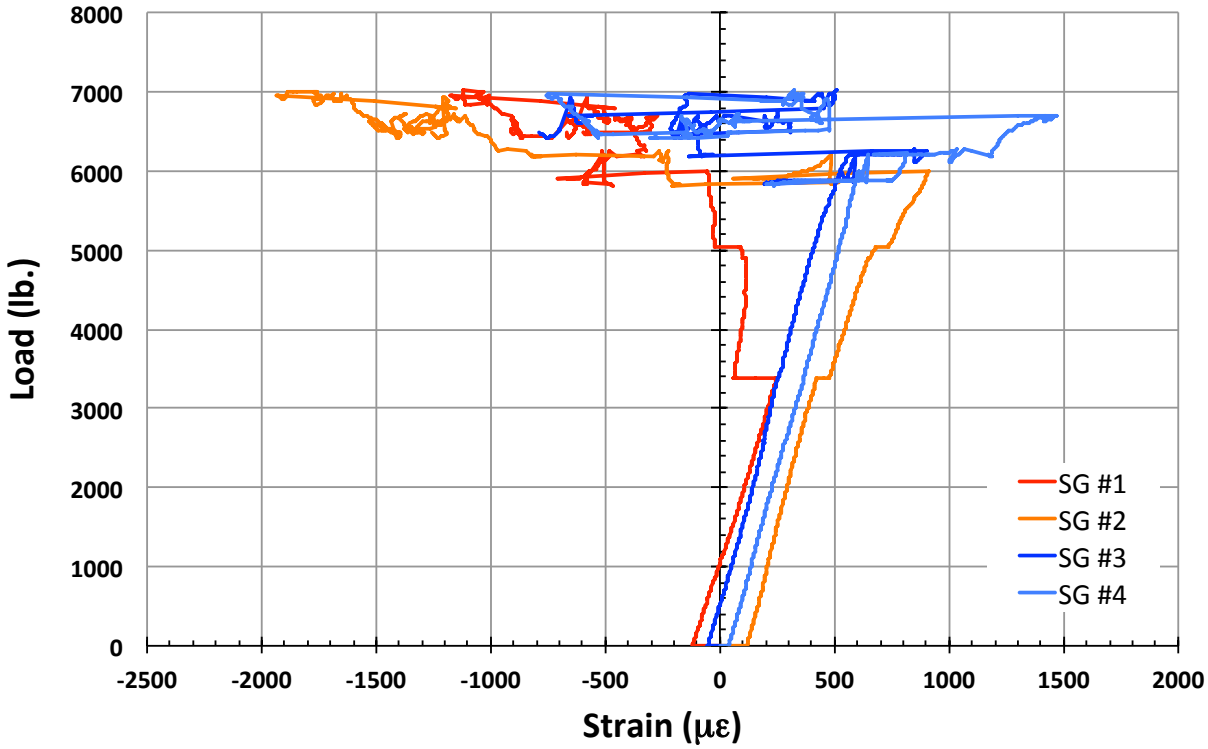

Figure C42. TNS2 load vs. strain.

TNS3

This section presents the test data for the TNS3 test article.

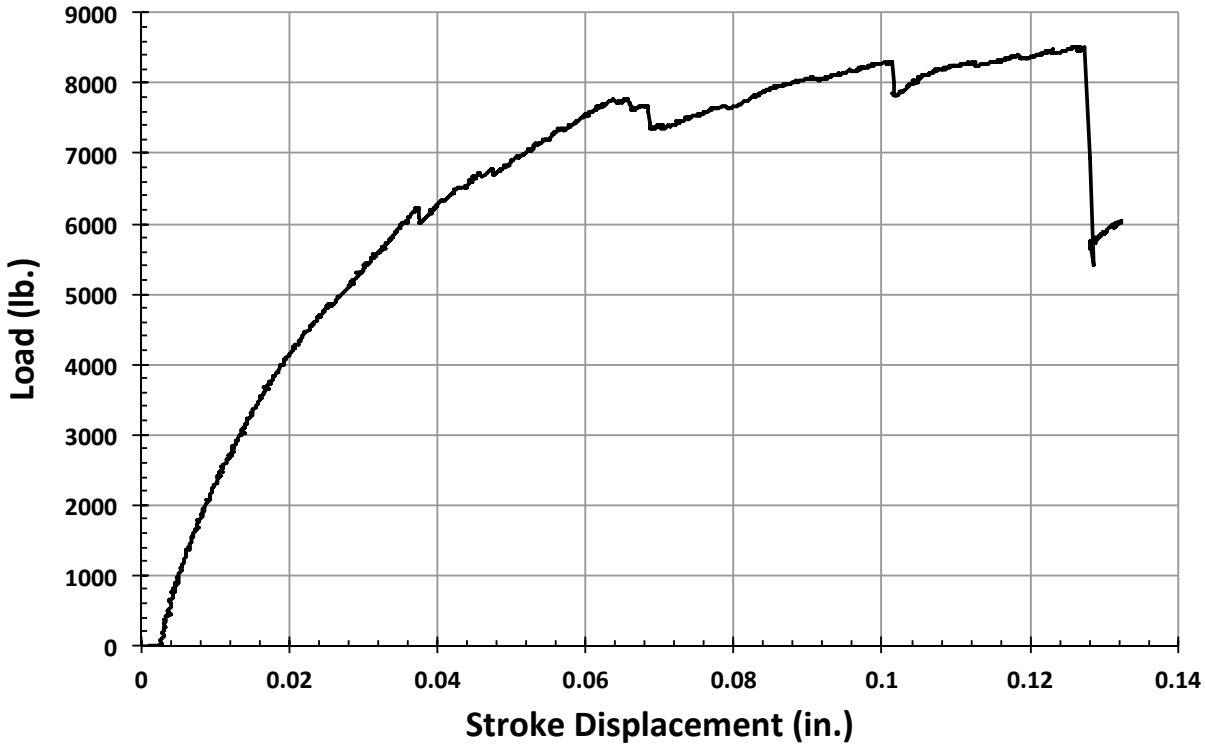

Figure C43. TNS3 load vs. stroke.

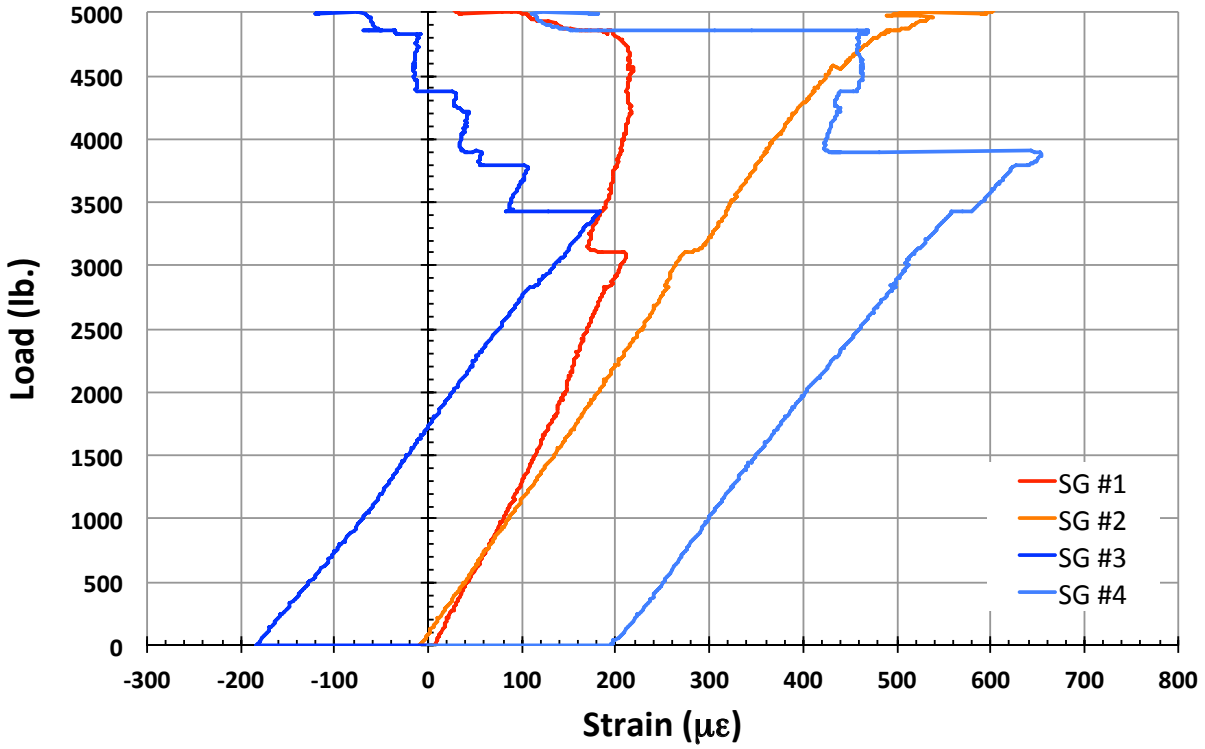

Figure C44. TNS3 load vs. strain, initial loading.

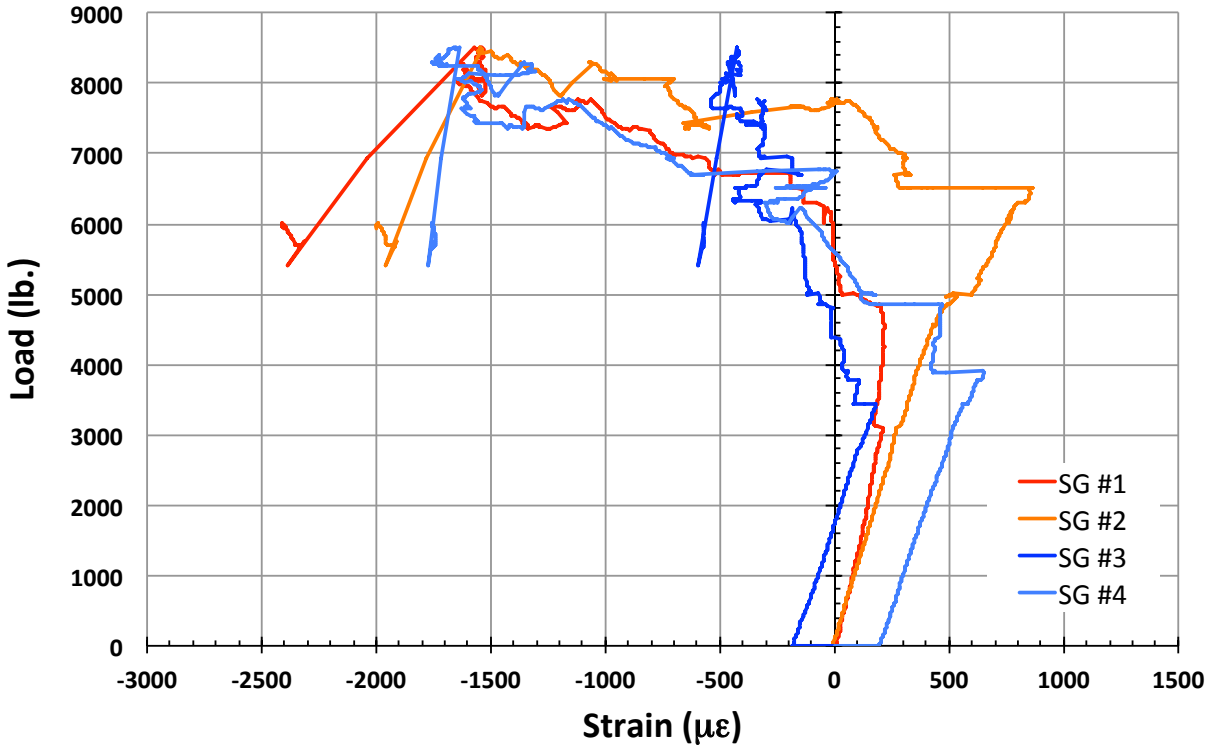

Figure C45. TNS3 load vs. strain.

TNN1

This section presents the test data for the TNN1 test article, and includes strain plots and failure images.

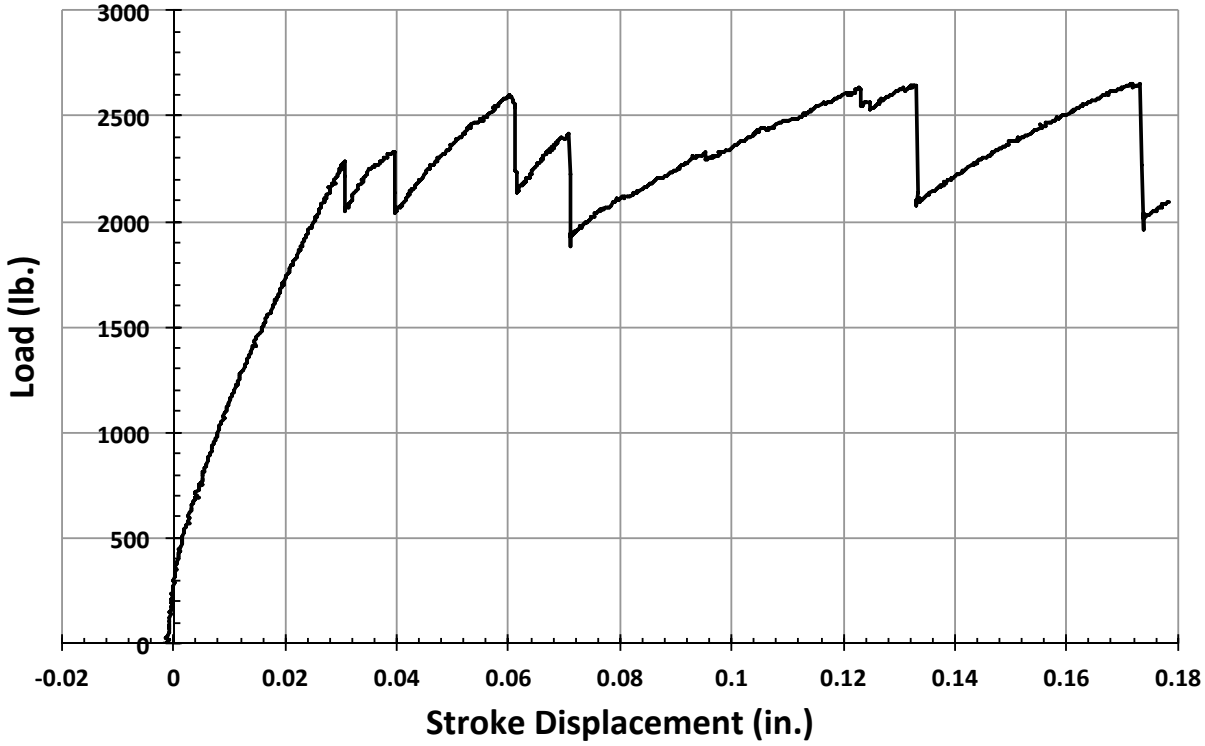

Figure C46. TNN1 load vs. stroke.

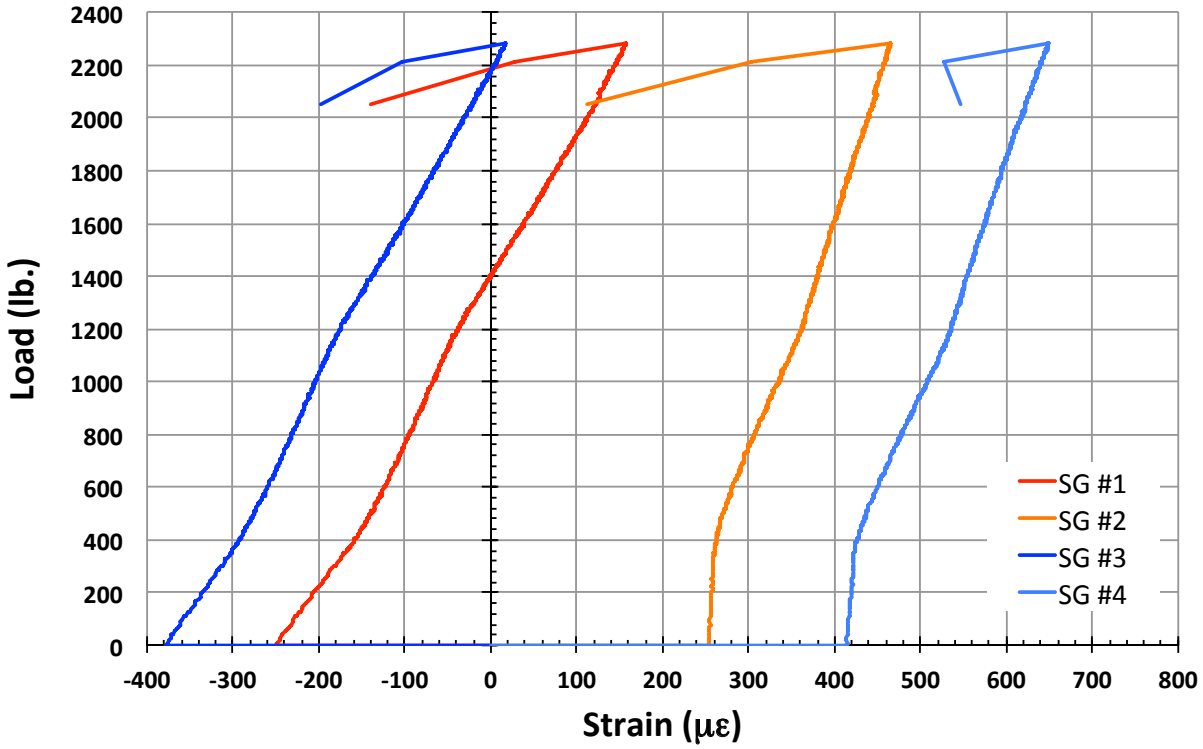

Figure C47. TNN1 load vs. strain, initial loading.

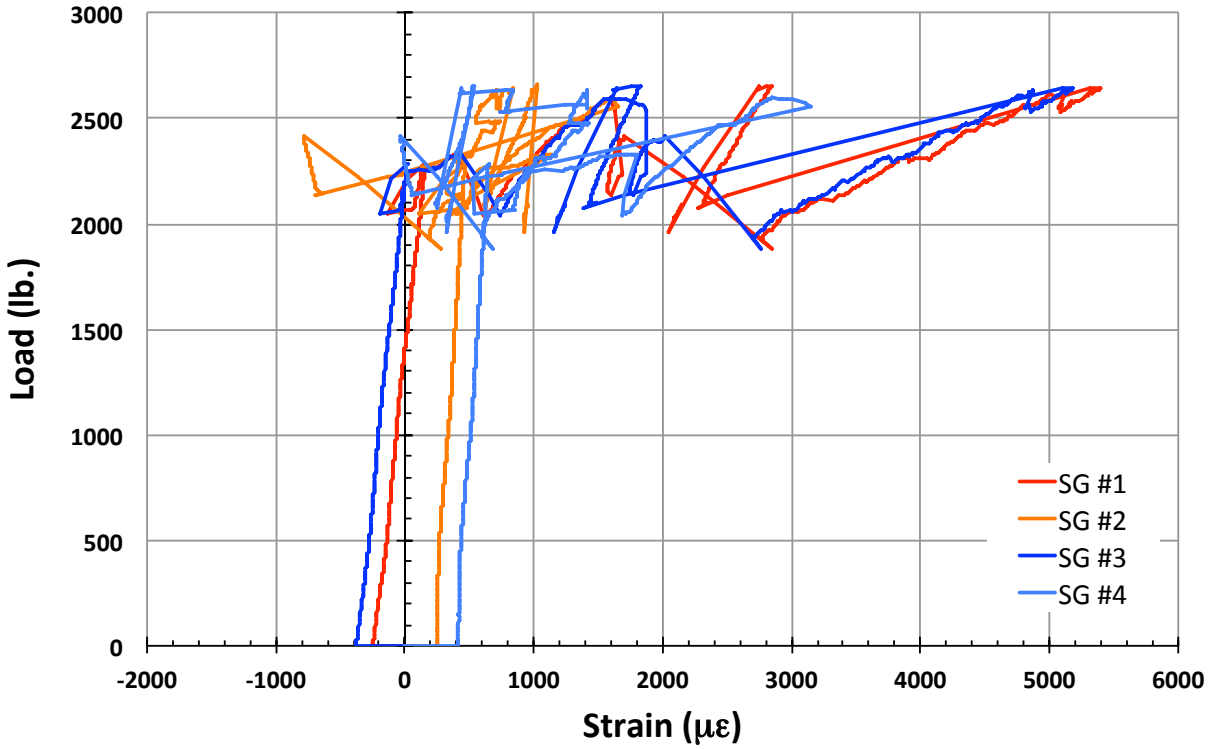

Figure C48. TNN1 load vs. strain.

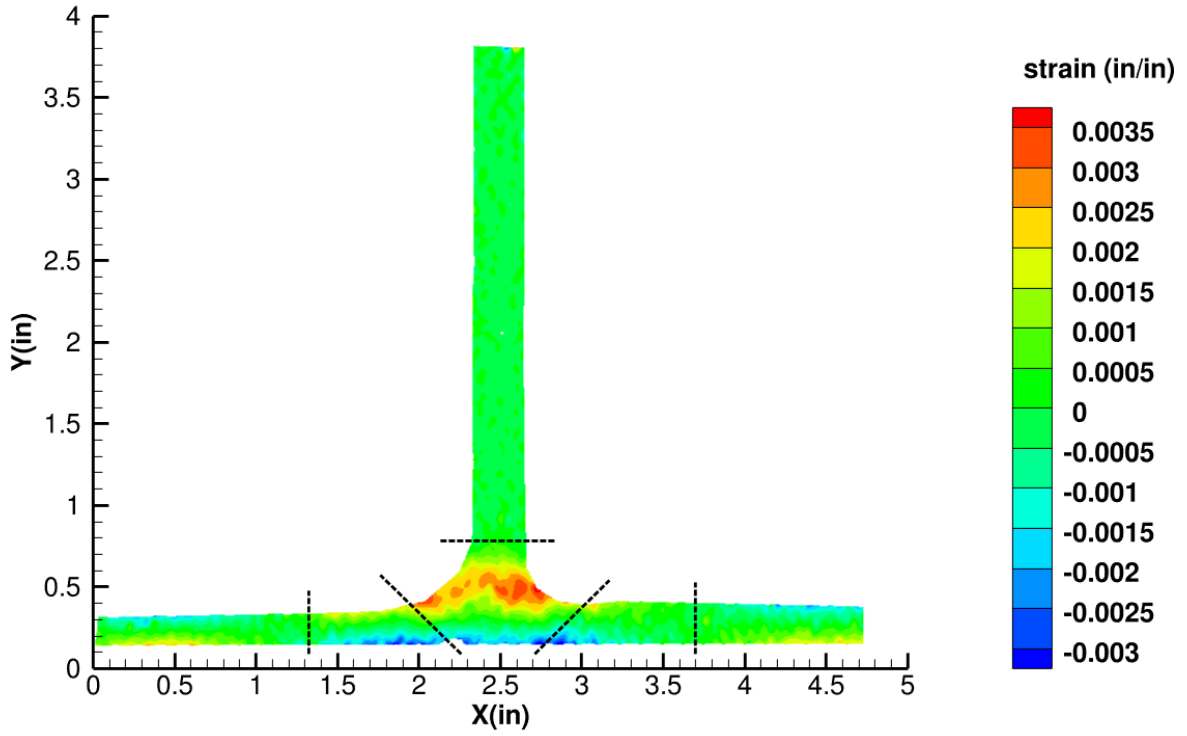

Figure C49. TNN1 strain contours for ε_{xx} at 2286 lb. load, prior to initial failure, 29MP VIC data.

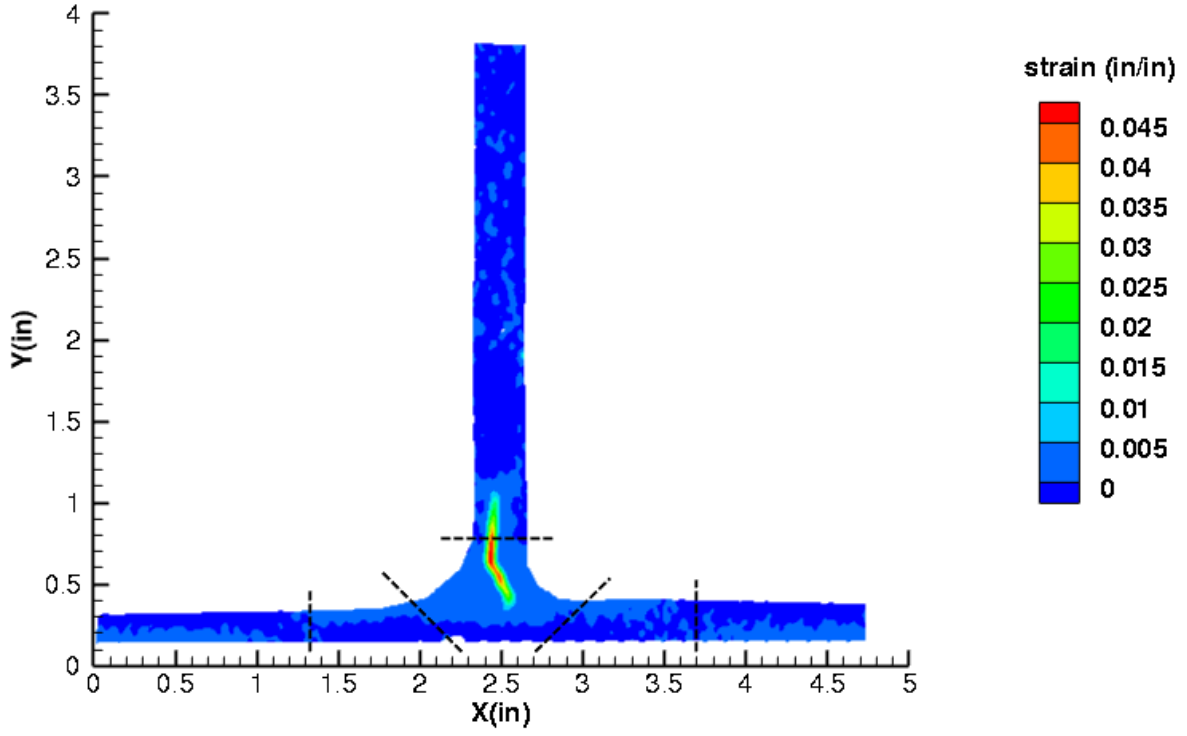

Figure C50. TNN1 strain contours for ε_{xx} at 2216 lb. load, just after initial failure, 29MP VIC data.

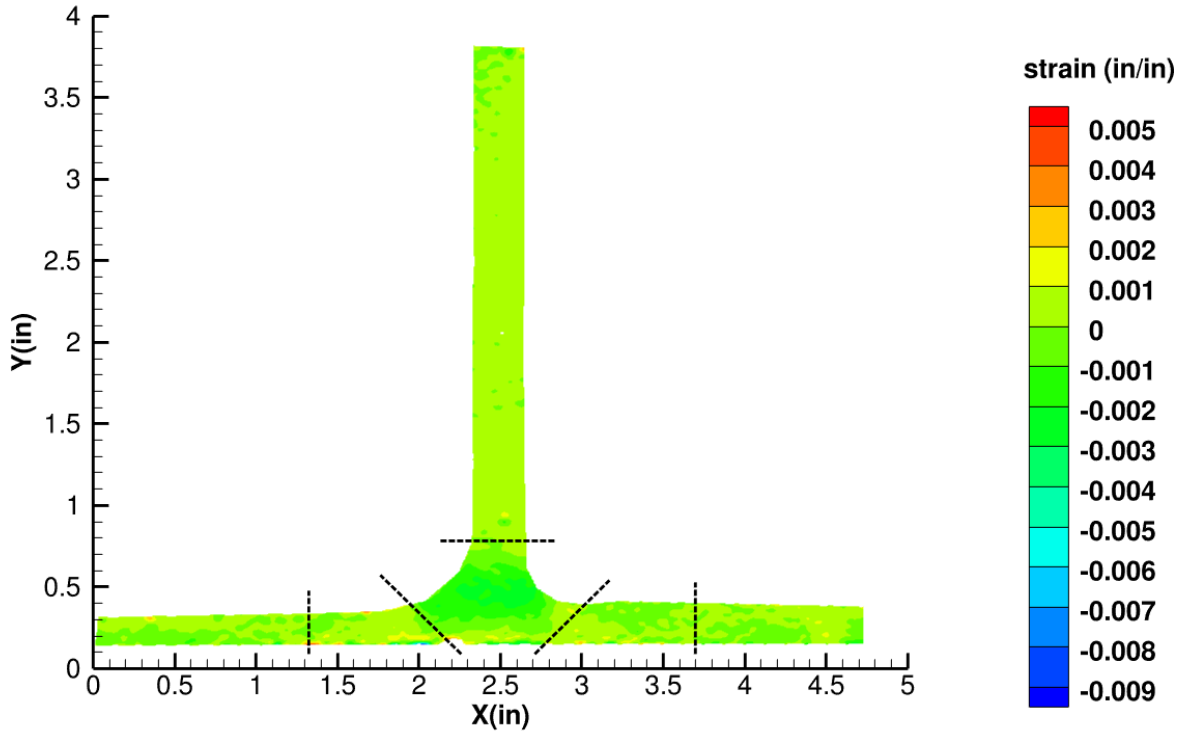

Figure C51. TNN1 strain contours for ε_{yy} at 2286 lb. load, prior to initial failure, 29MP VIC data.

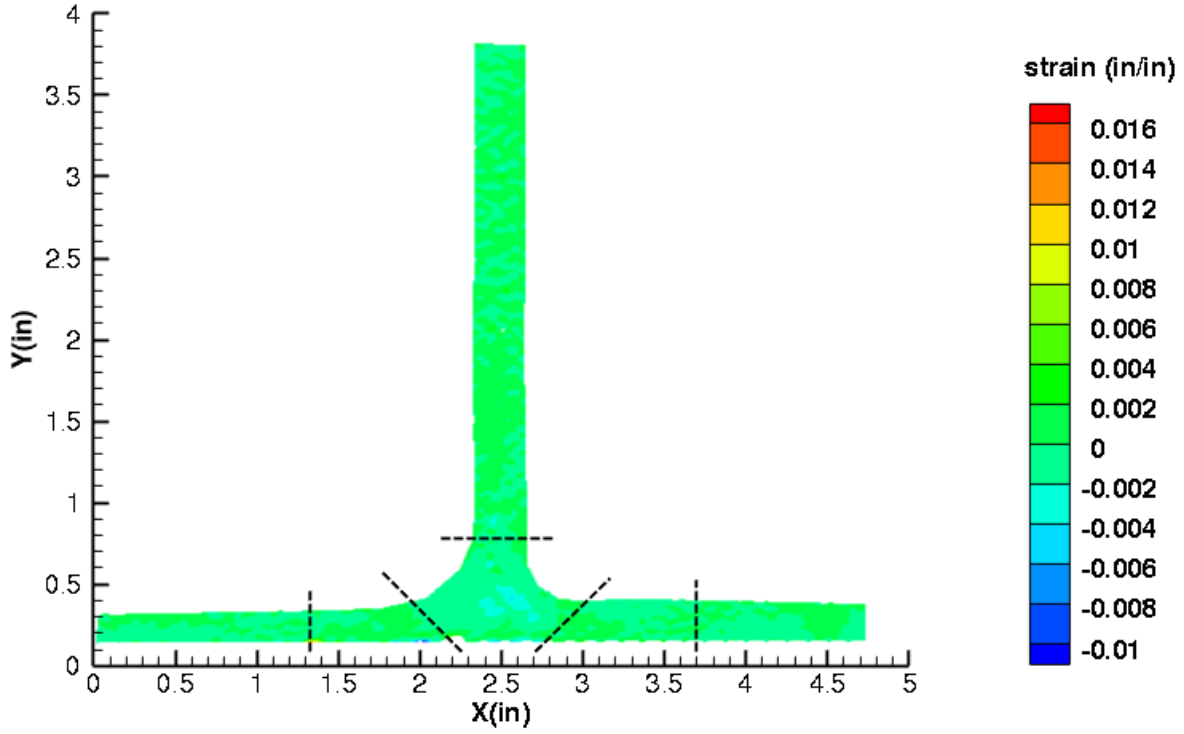

Figure C52. TNN1 strain contours for ε_{yy} at 2216 lb. load, just after initial failure, 29MP VIC data.

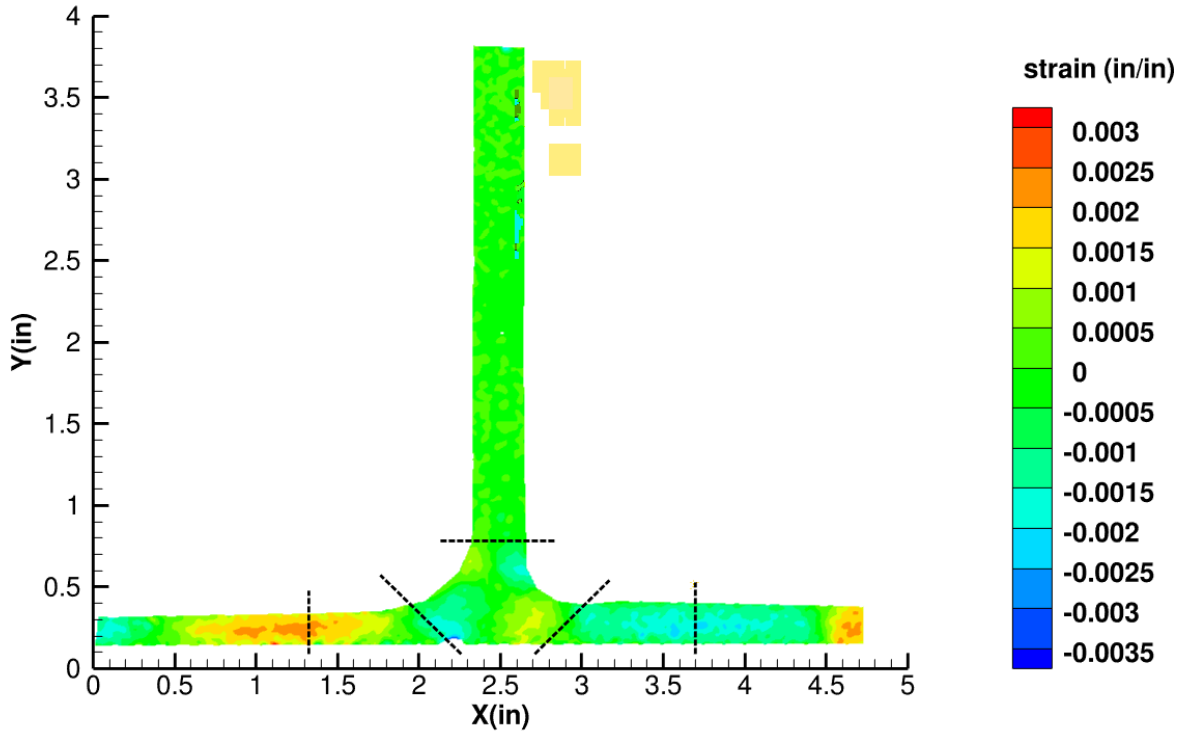

Figure C53. TNN1 strain contours for ε_{xy} at 2286 lb. load, prior to initial failure, 29MP VIC data.

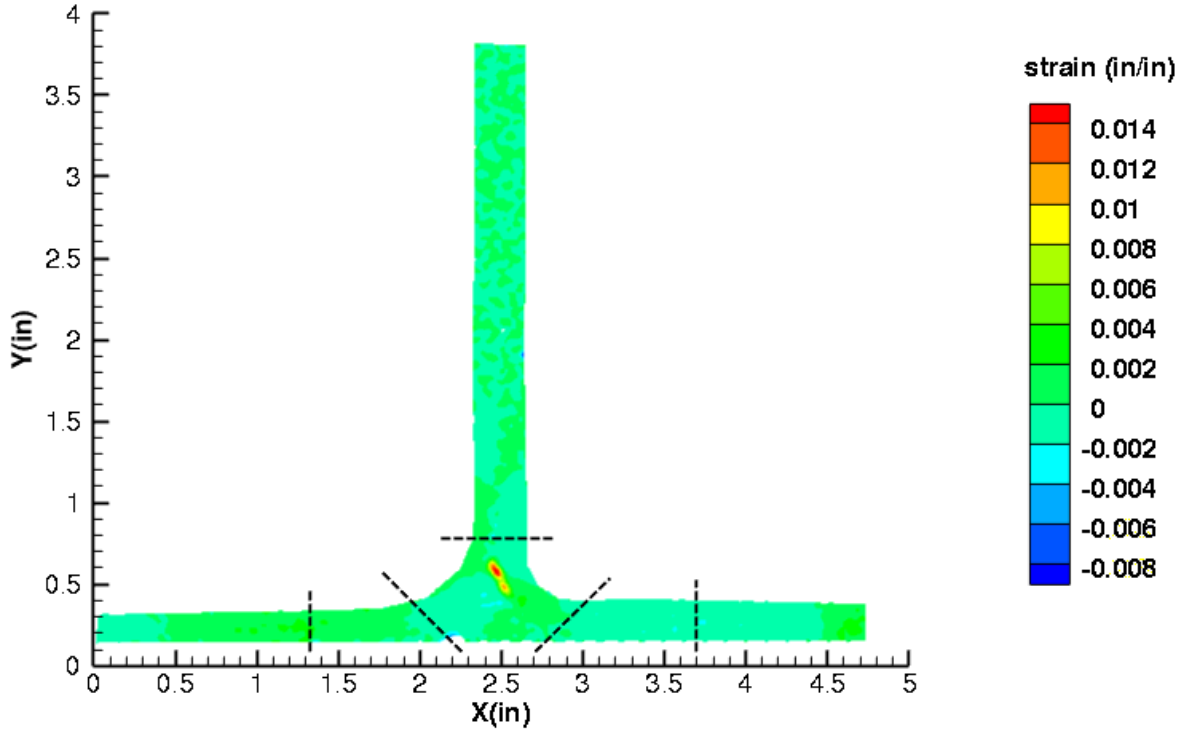

Figure C54. TNN1 strain contours for ε_{xy} at 2216 lb. load, just after initial failure, 29MP VIC data.

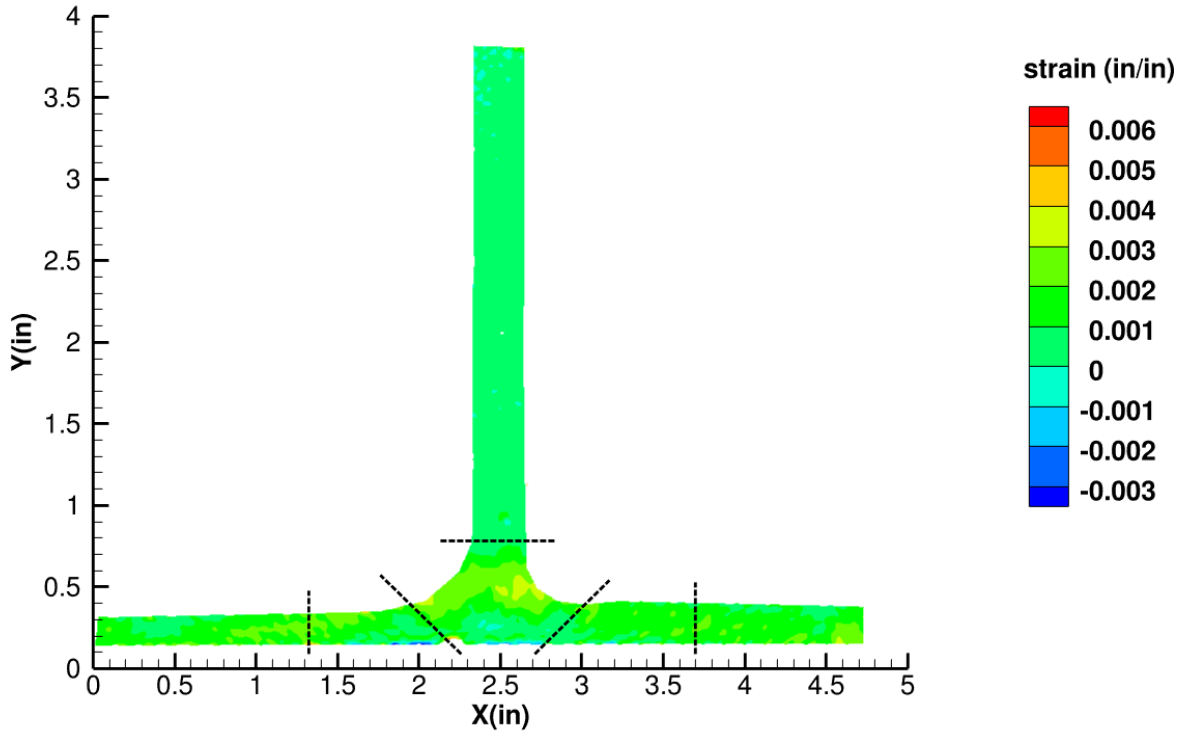

Figure C55. TNN1 strain contours for maximum principal strain at 2286 lb. load, prior to initial failure, 29MP VIC data.

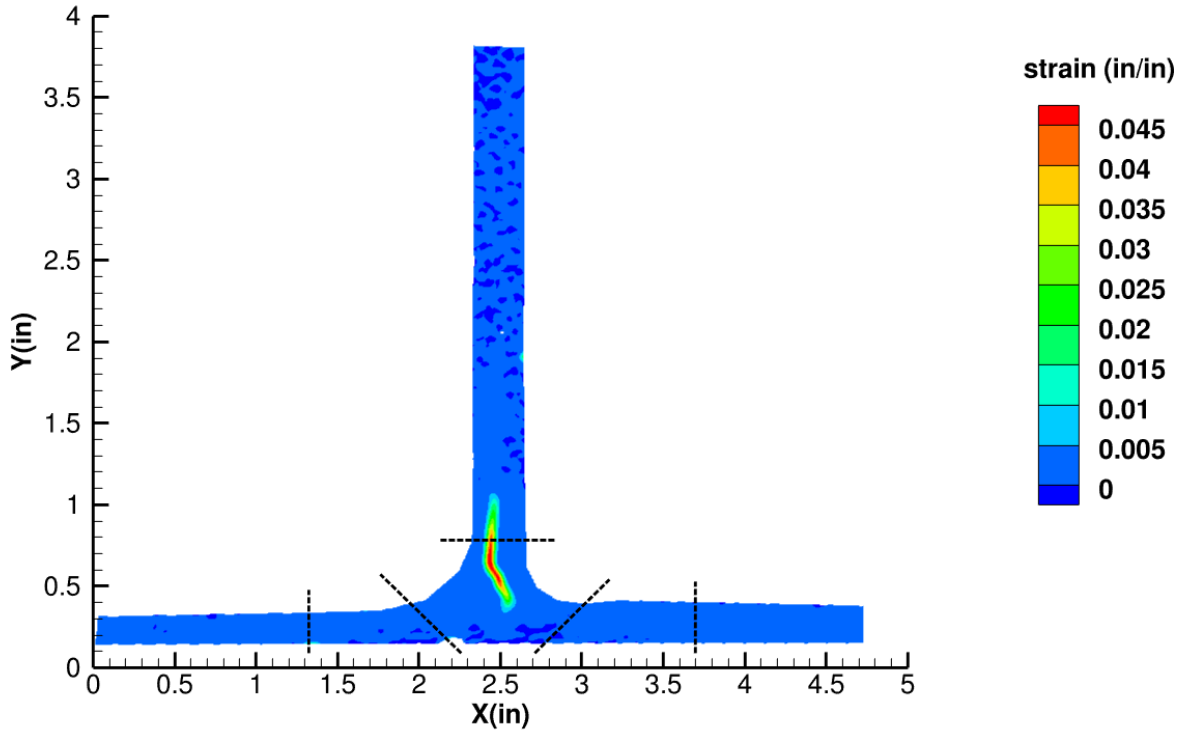

Figure C56. TNN1 strain contours for maximum principal strain at 2216 lb. load, just after initial failure, 29MP VIC data.

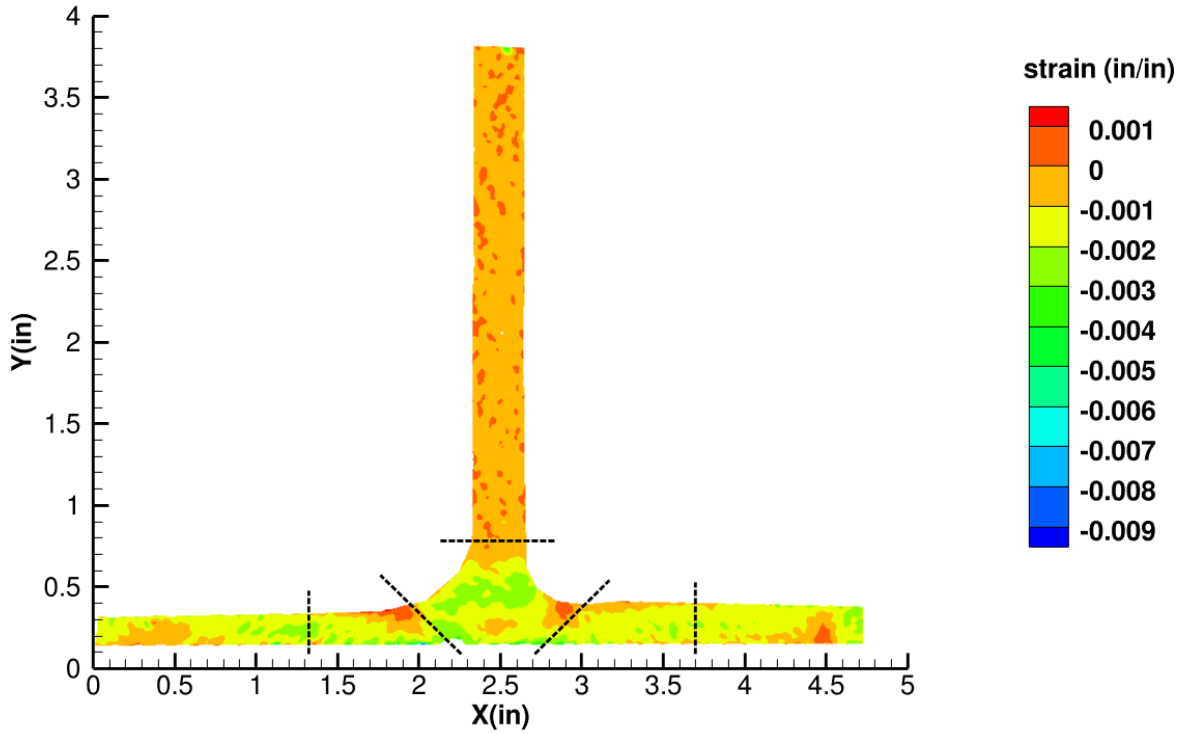

Figure C57. TNN1 strain contours for minimum principal strain at 2286 lb. load, prior to initial failure, 29MP VIC data.

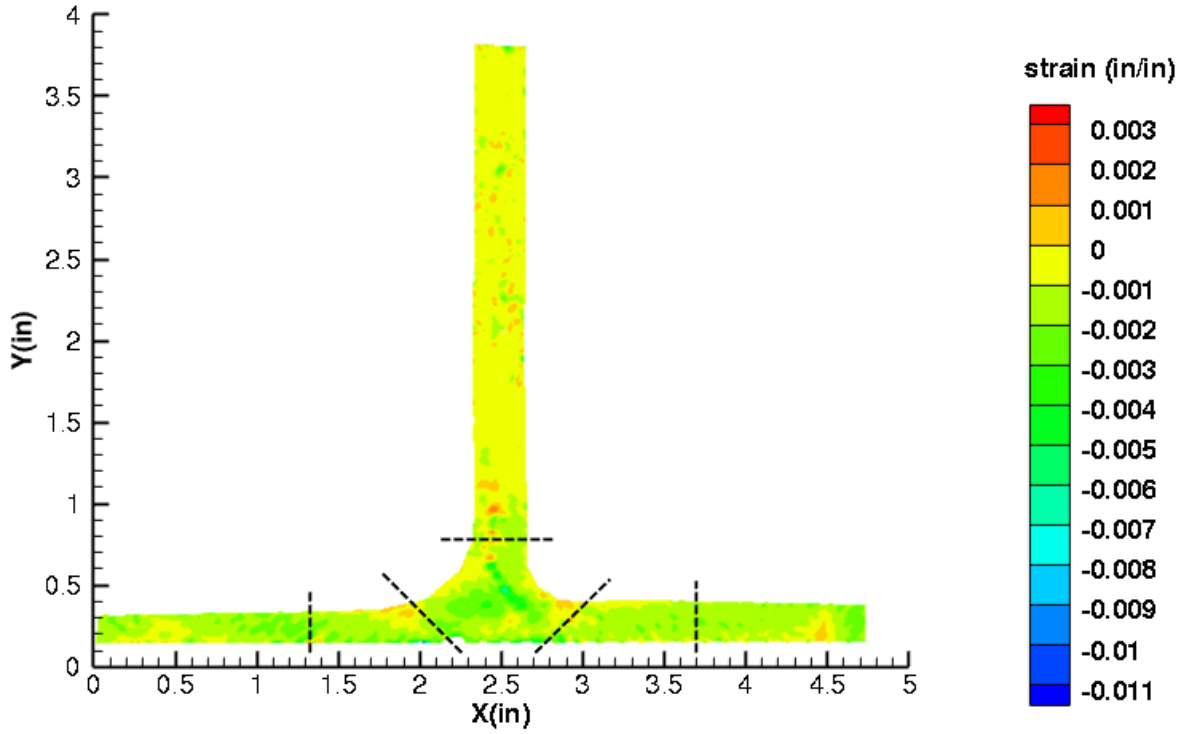

Figure C58. TNN1 strain contours for minimum principal strain at 2216 lb. load, just after initial failure, 29MP VIC data.

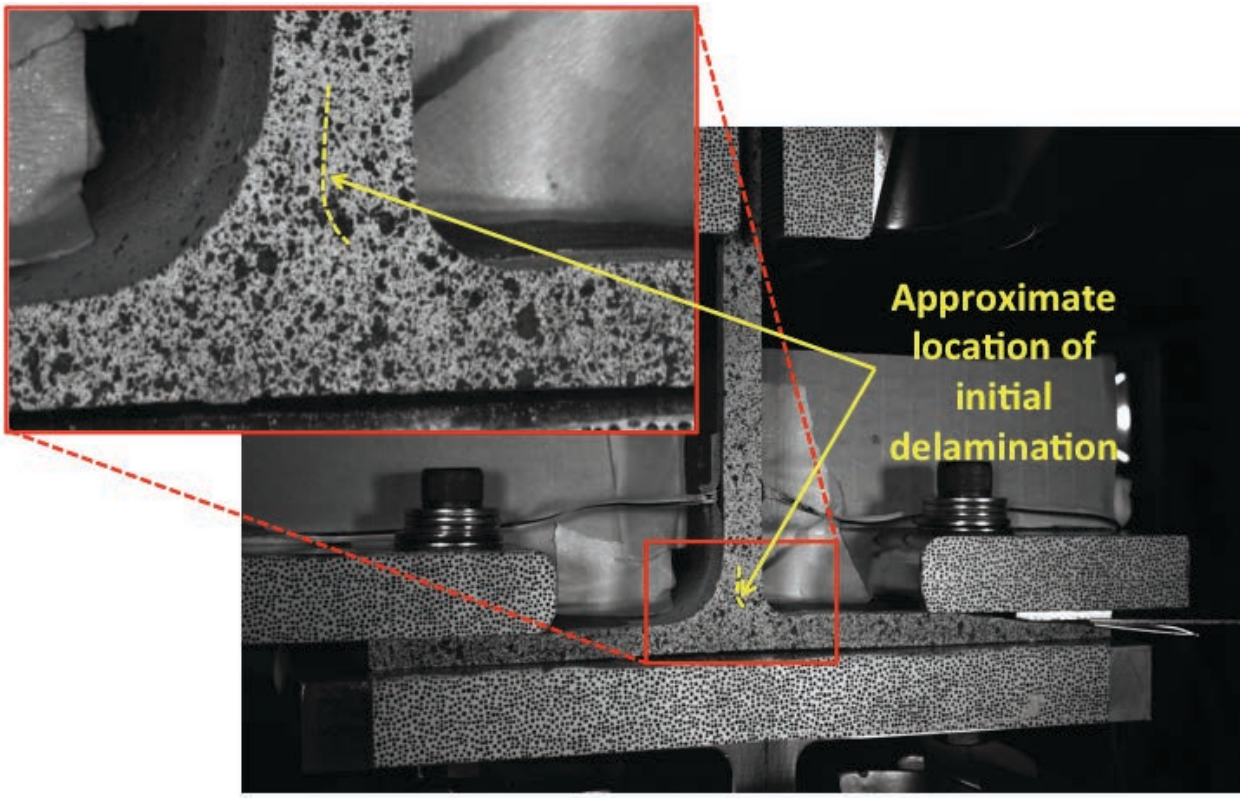

Figure C59. TNN1 image just after initial failure, 29MP VIC data.

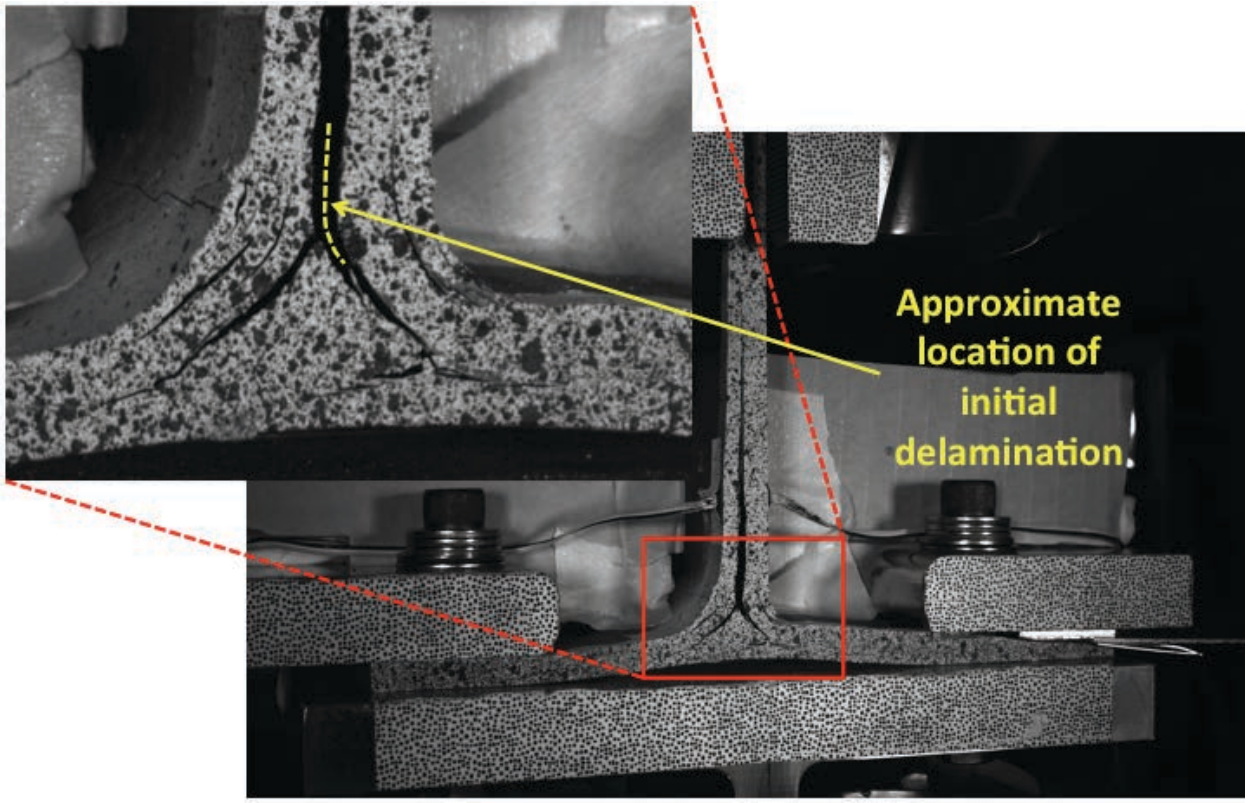

Figure C60. TNN1 image just after maximum load, 29MP VIC data.

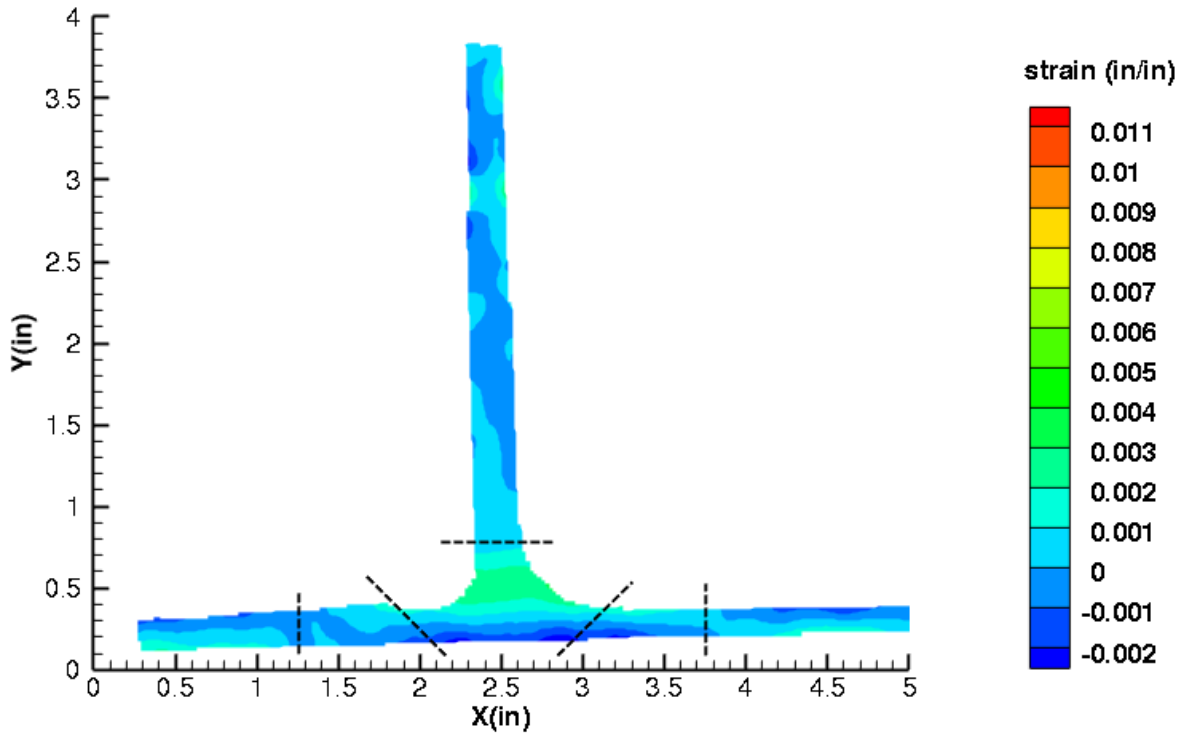

Figure C61. TNN1 strain contours for ε_{xx} at 2286 lb. load, prior to initial failure, 5MP VIC data.

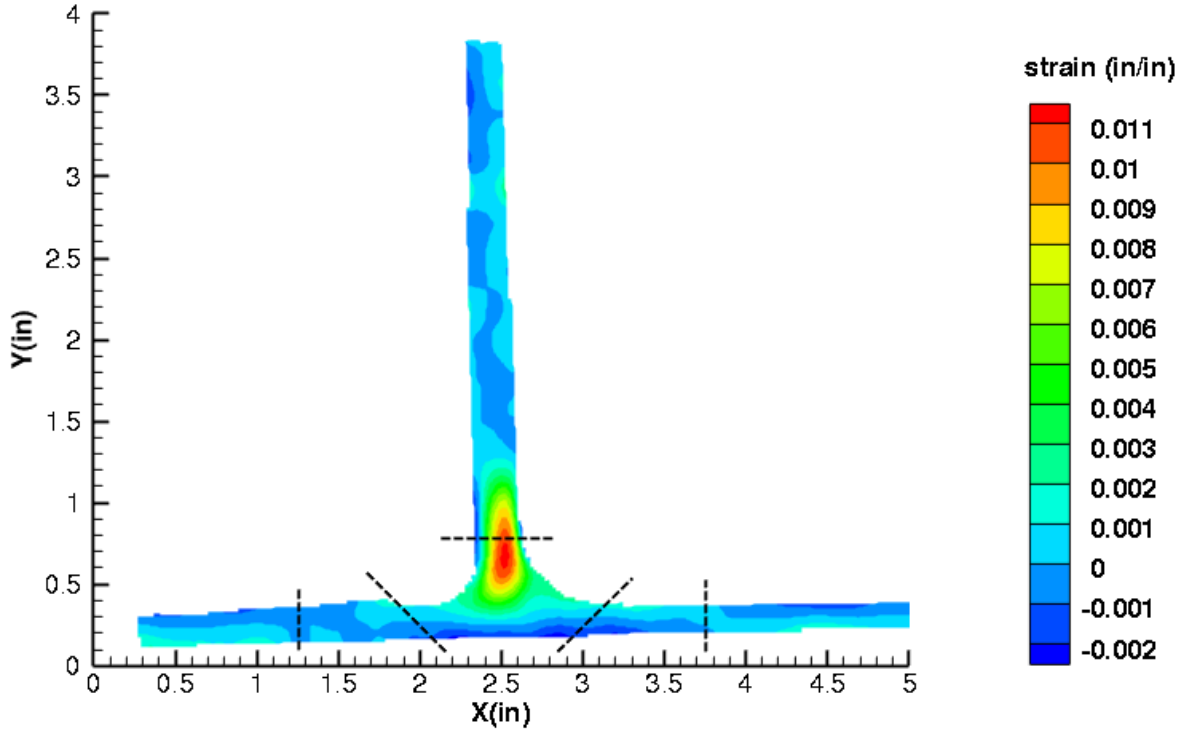

Figure C62. TNN1 strain contours for ε_{xx} at 2216 lb. load, just after initial failure, 5MP VIC data.

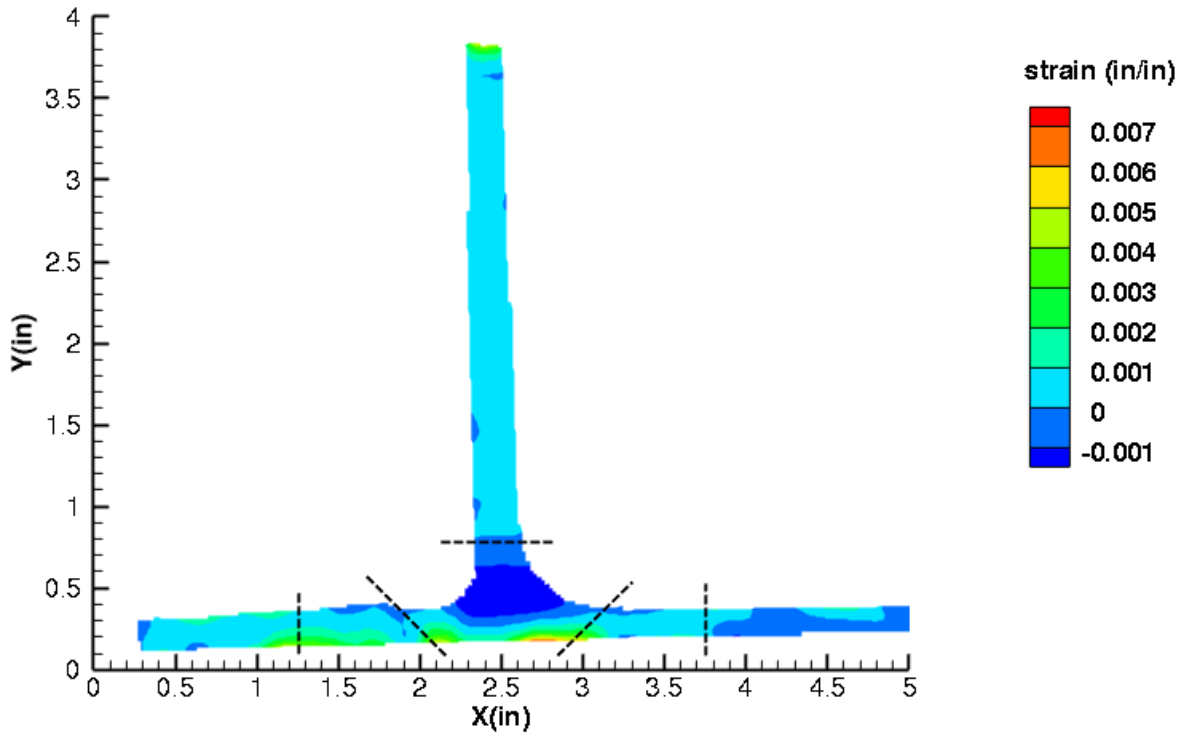

Figure C63. TNN1 strain contours for ε_{yy} at 2286 lb. load, prior to initial failure, 5MP VIC data.

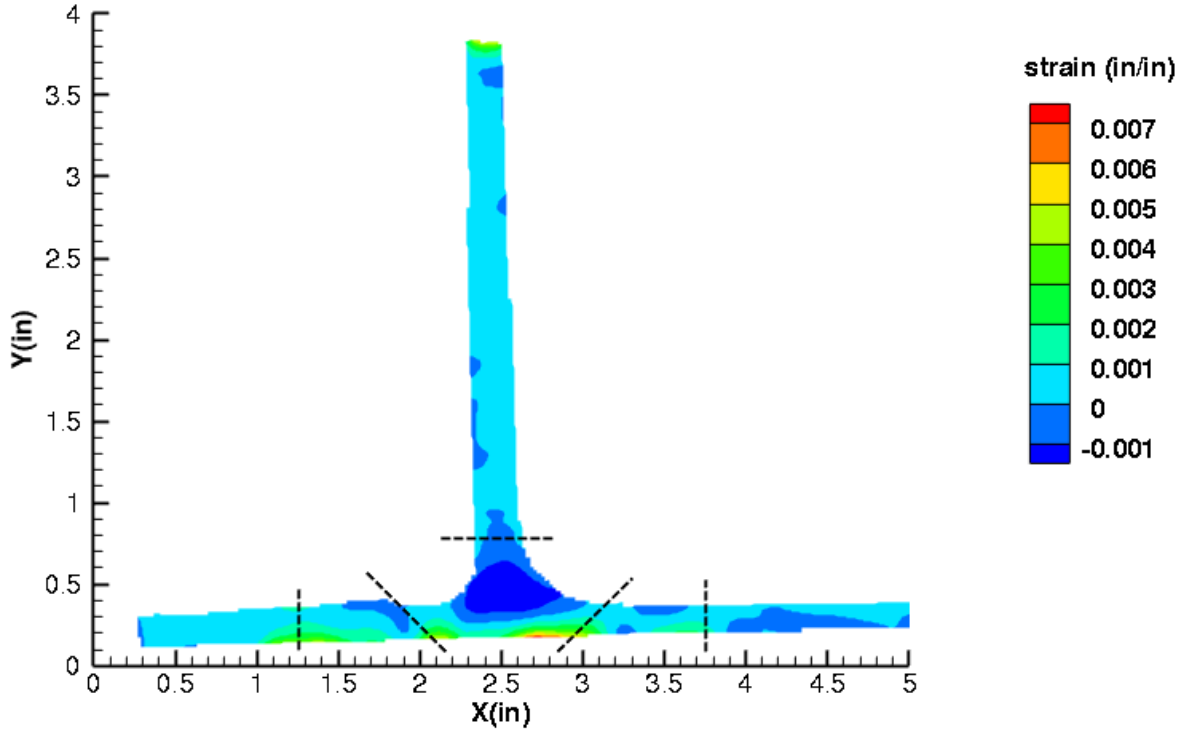

Figure C64. TNN1 strain contours for ε_{yy} at 2216 lb. load, just after initial failure, 5MP VIC data.

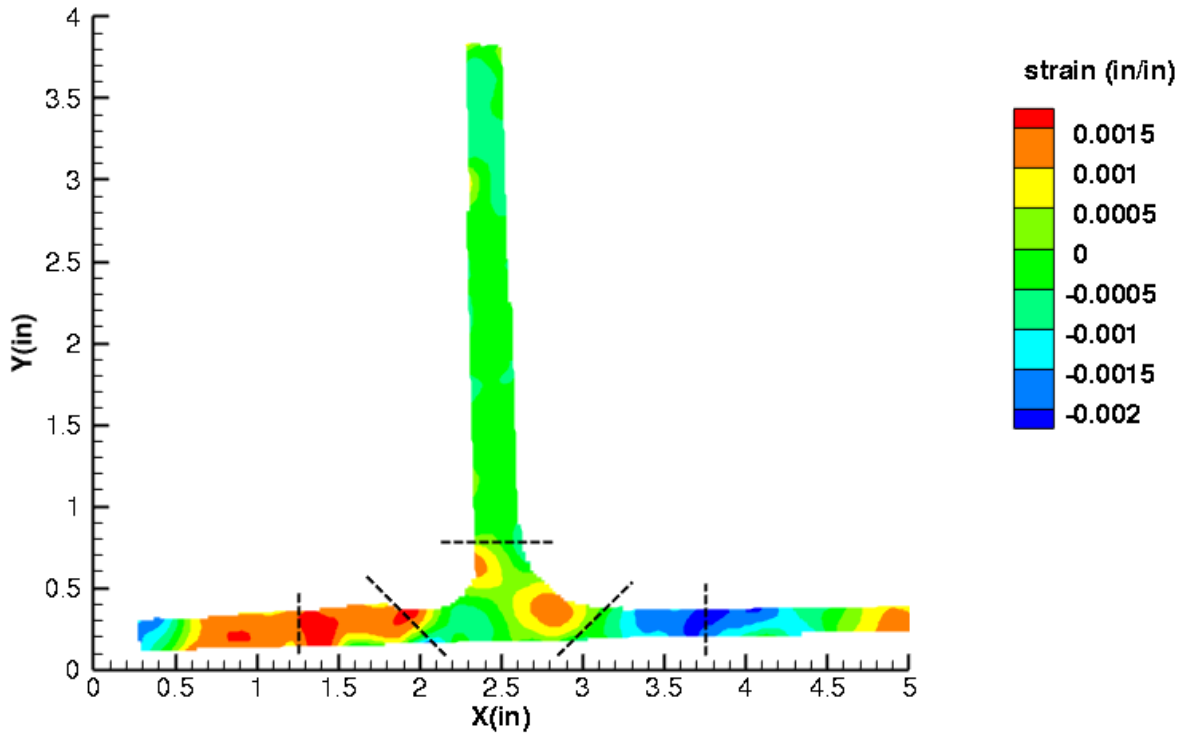

Figure C65. TNN1 strain contours for ε_{xy} at 2286 lb. load, prior to initial failure, 5MP VIC data.

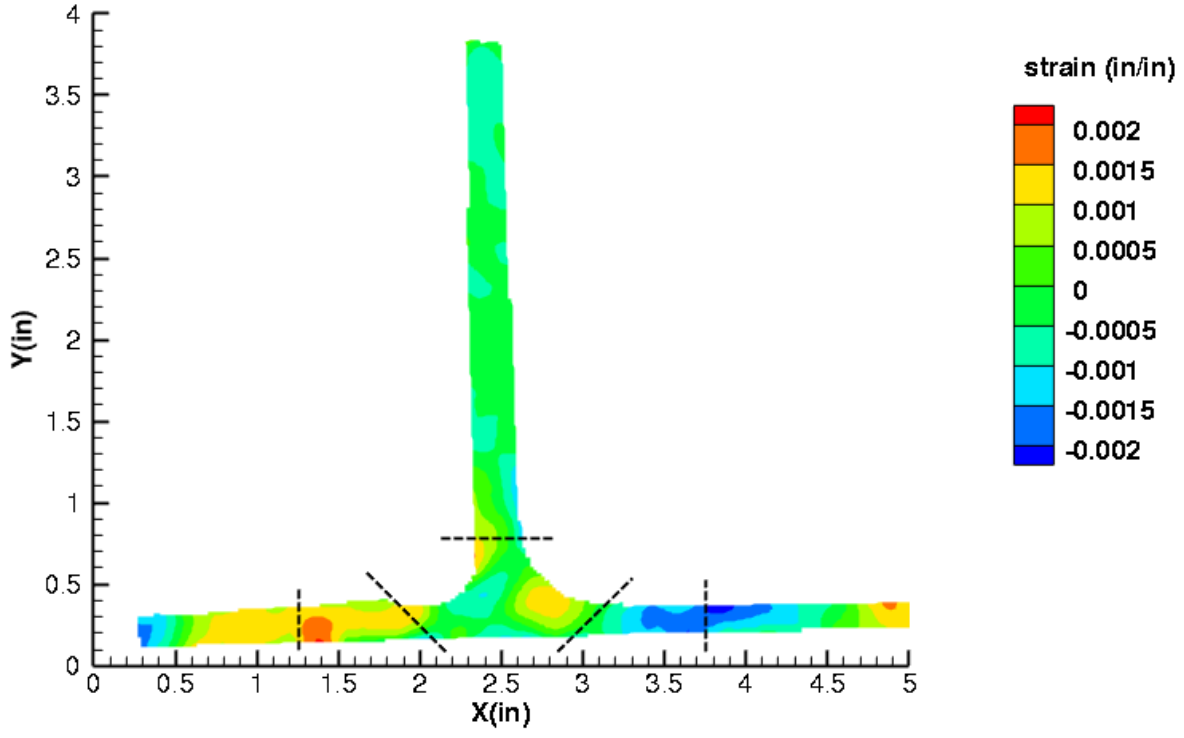

Figure C66. TNN1 strain contours for ε_{xy} at 2216 lb. load, just after initial failure, 5MP VIC data.

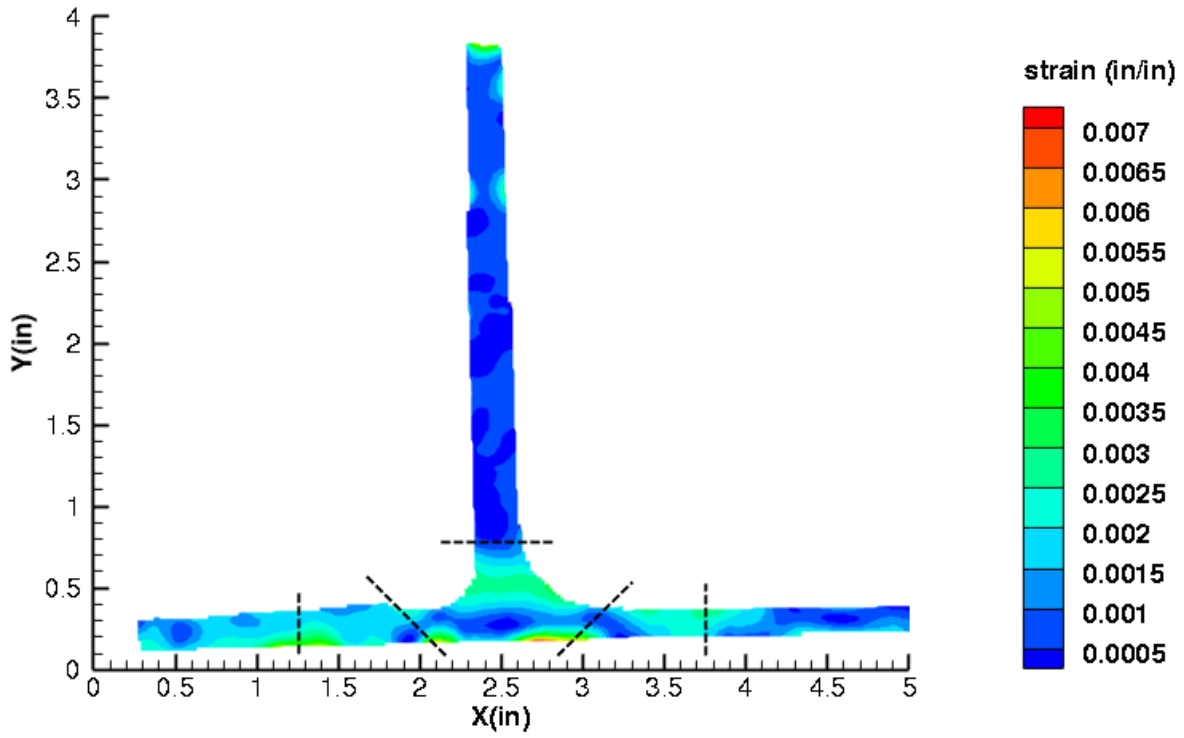

Figure C67. TNN1 strain contours for maximum principal strain at 2286 lb. load, prior to initial failure, 5MP VIC data.

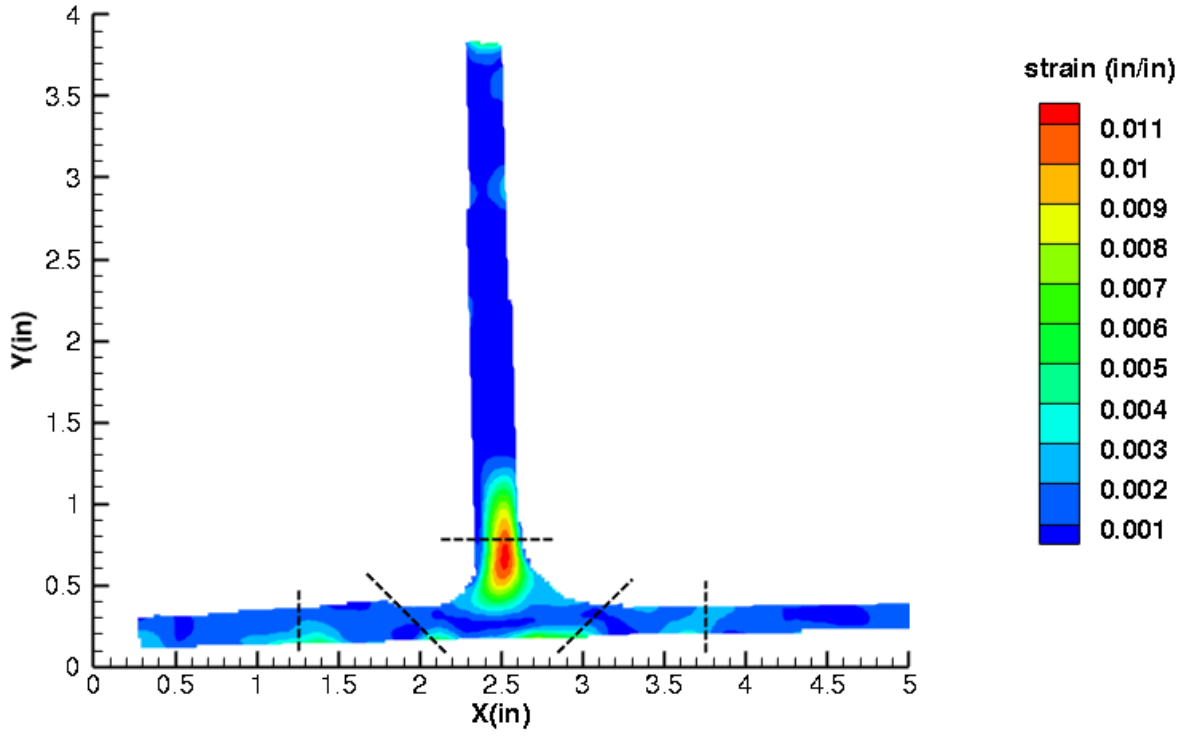

Figure C68. TNN1 strain contours for maximum principal strain at 2216 lb. load, just after initial failure, 5MP VIC data.

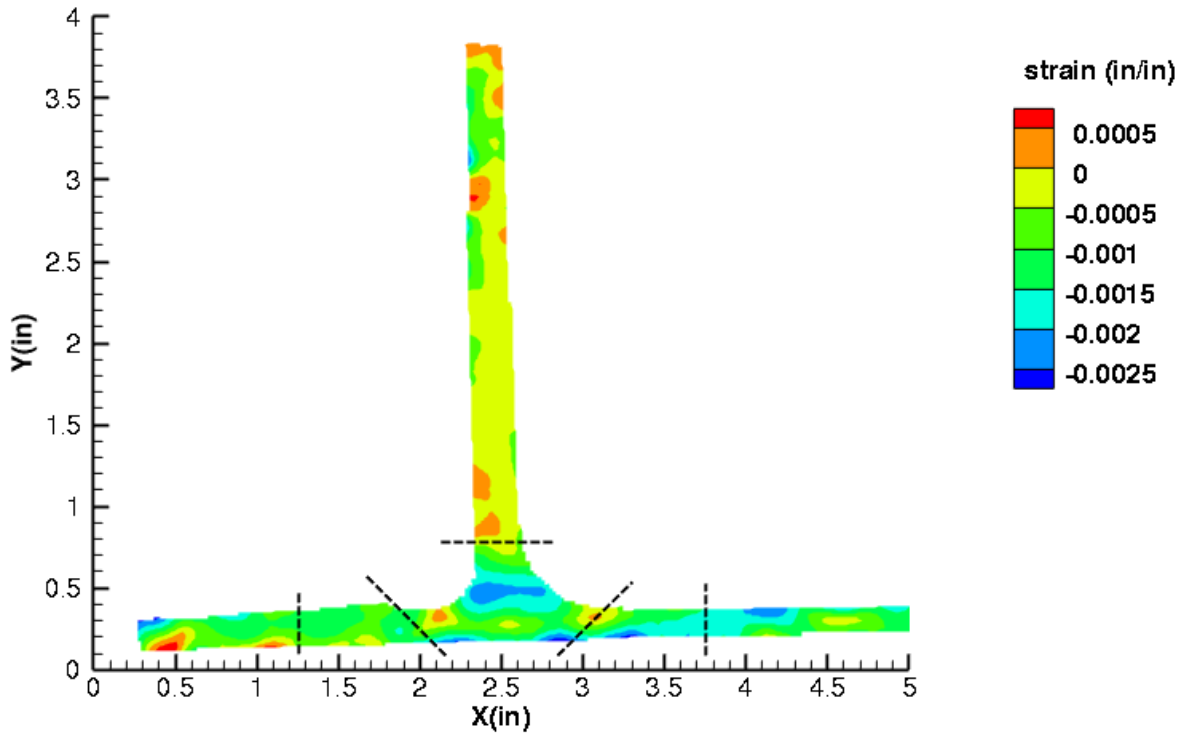

Figure C69. TNN1 strain contours for minimum principal strain at 2286 lb. load, prior to initial failure, 5MP VIC data.

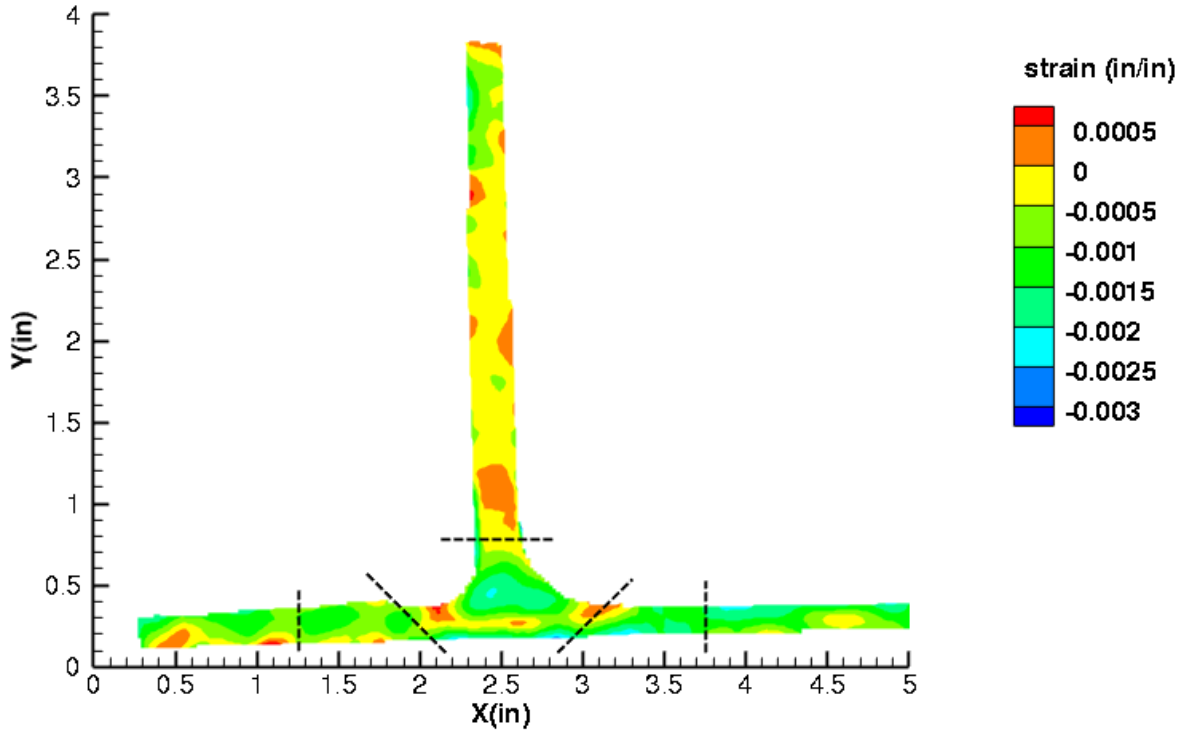

Figure C70. TNN1 strain contours for minimum principal strain at 2216 lb. load, just after initial failure, 5MP VIC data.

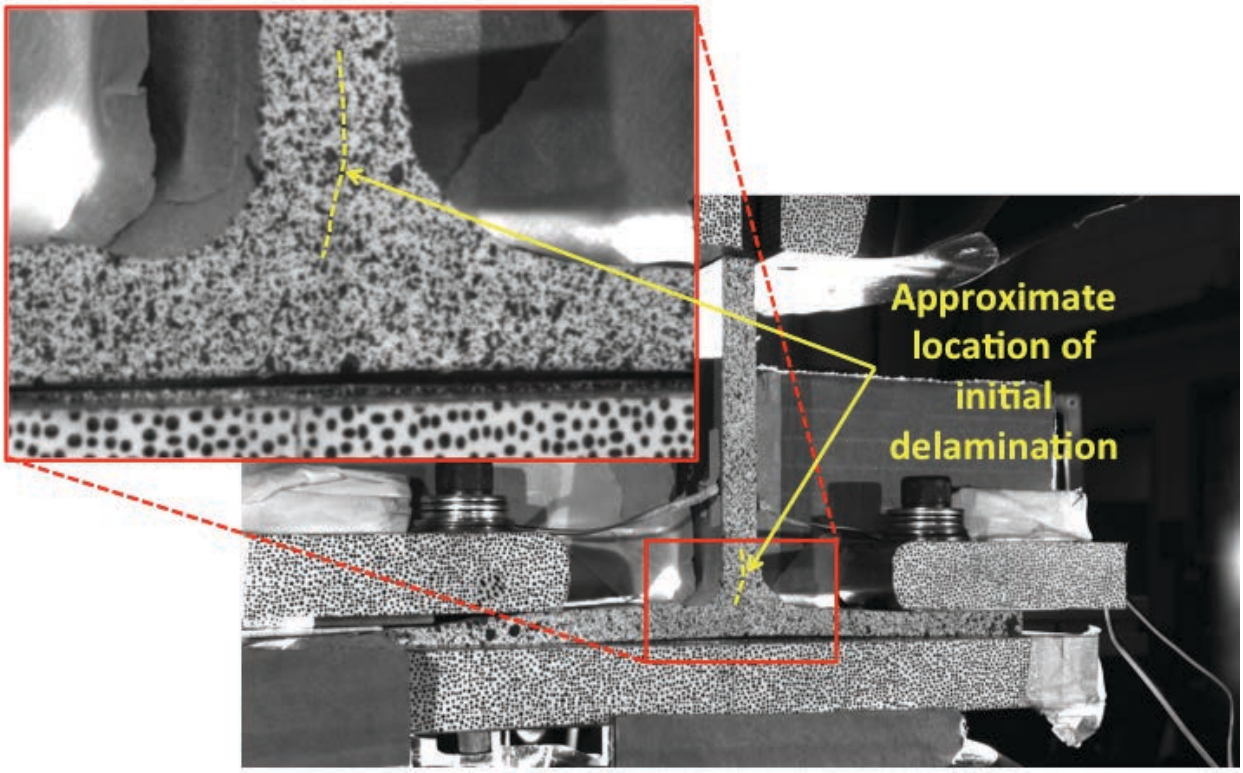

Figure C71. TNN1 image just after initial failure, 5MP VIC data.

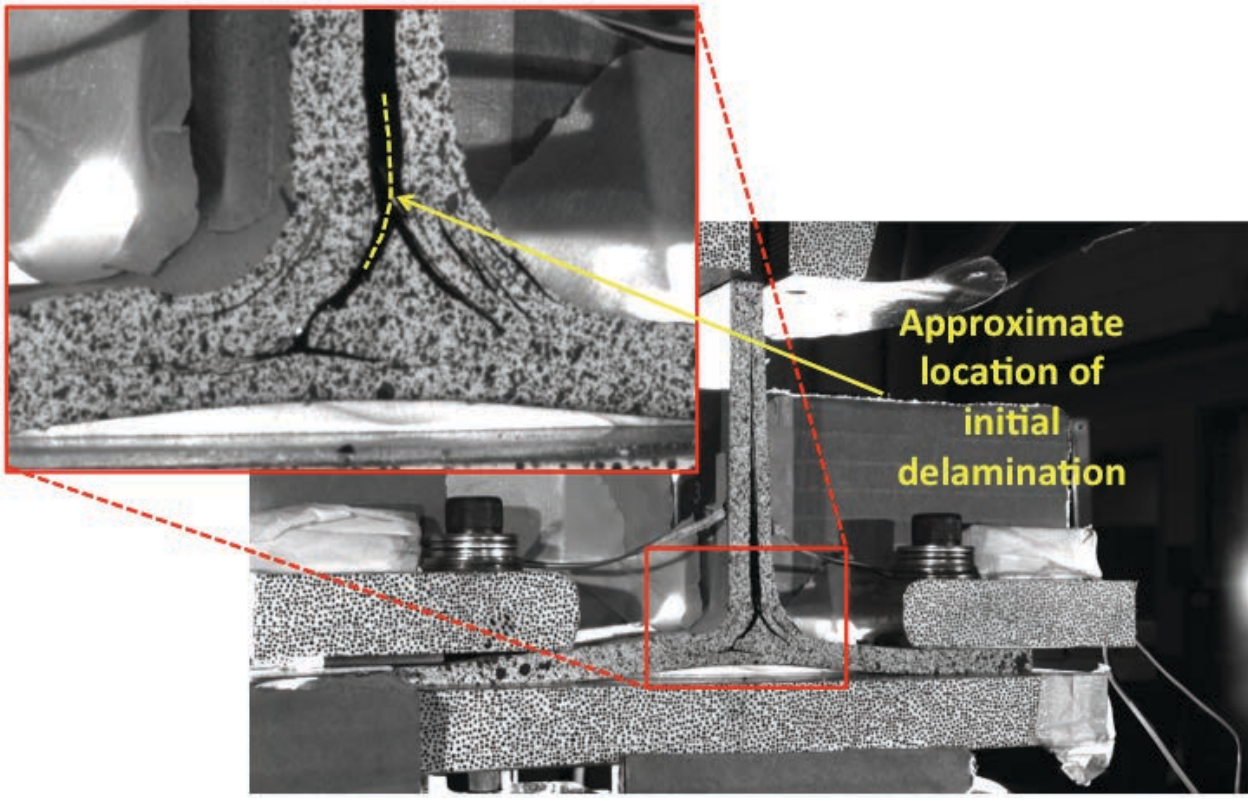

Figure C72. TNN1 image just after maximum load, 5MP VIC data.

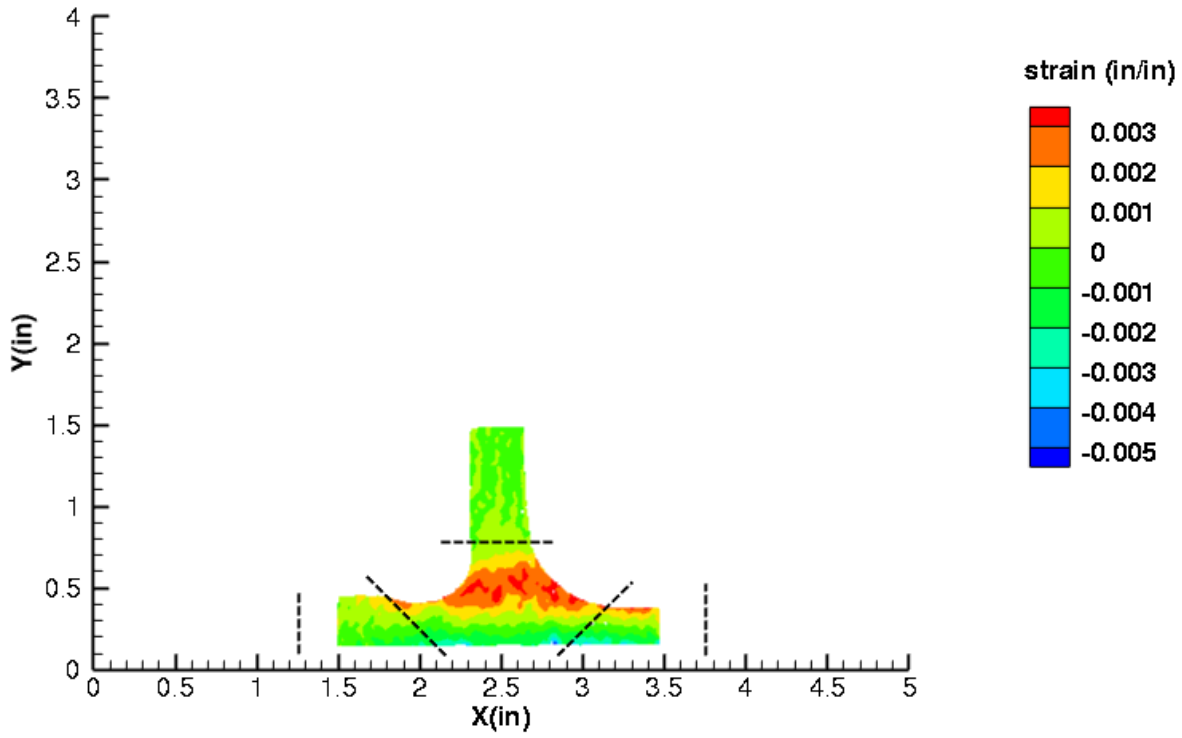

Figure C73. TNN1 strain contours for ε_{xx} at 2286 lb. load, prior to initial failure, local 5MP VIC data.

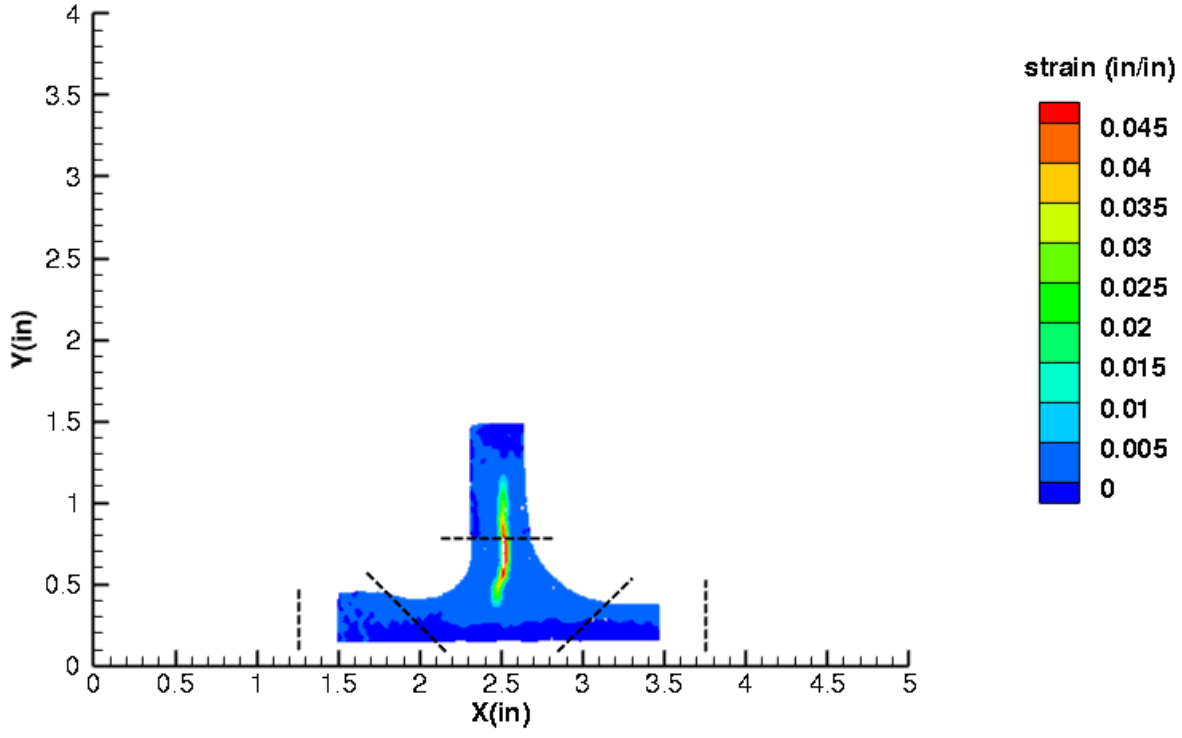

Figure C74. TNN1 strain contours for ε_{xx} at 2216 lb. load, just after initial failure, local 5MP VIC data.

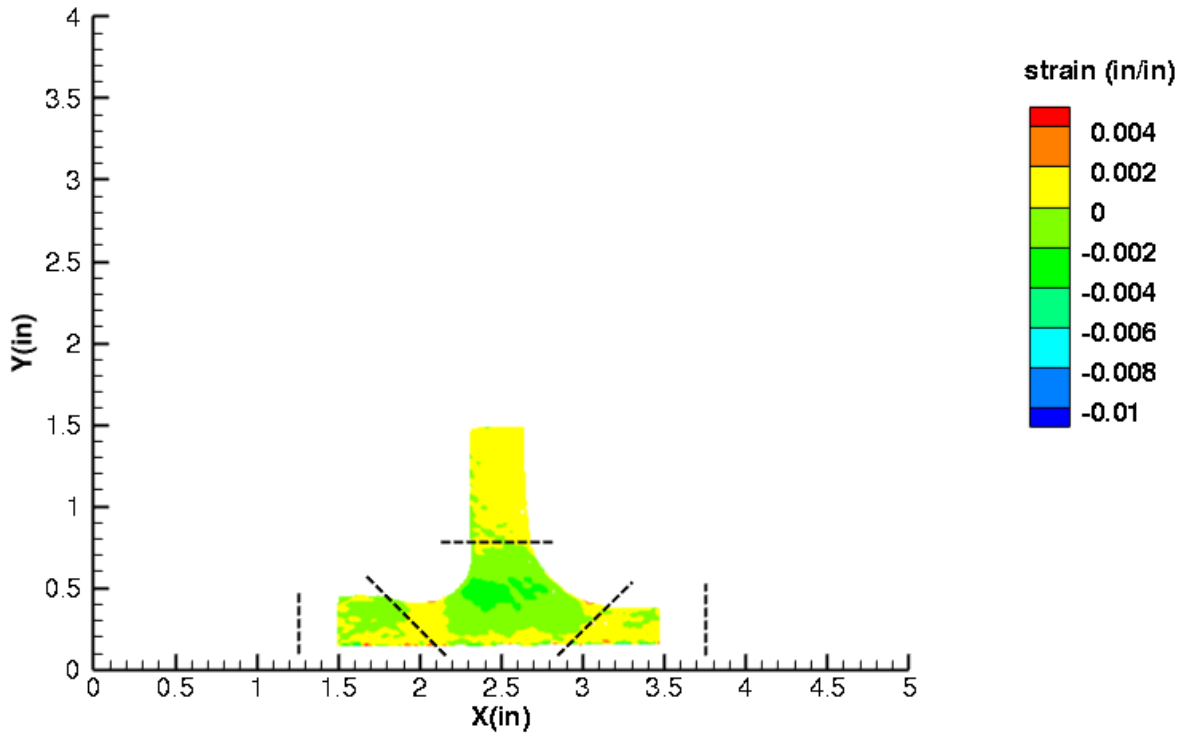

Figure C75. TNN1 strain contours for ε_{yy} at 2286 lb. load, prior to initial failure, local 5MP VIC data.

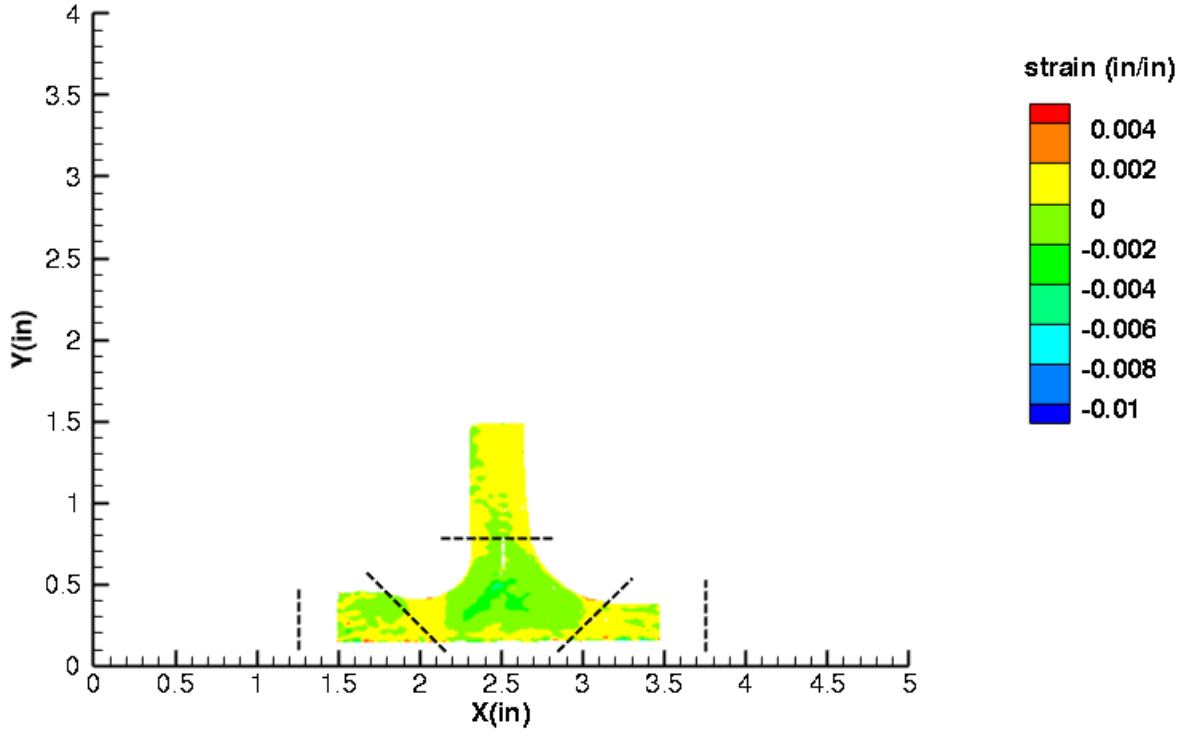

Figure C76. TNN1 strain contours for ε_{yy} at 2216 lb. load, just after initial failure, local 5MP VIC data.

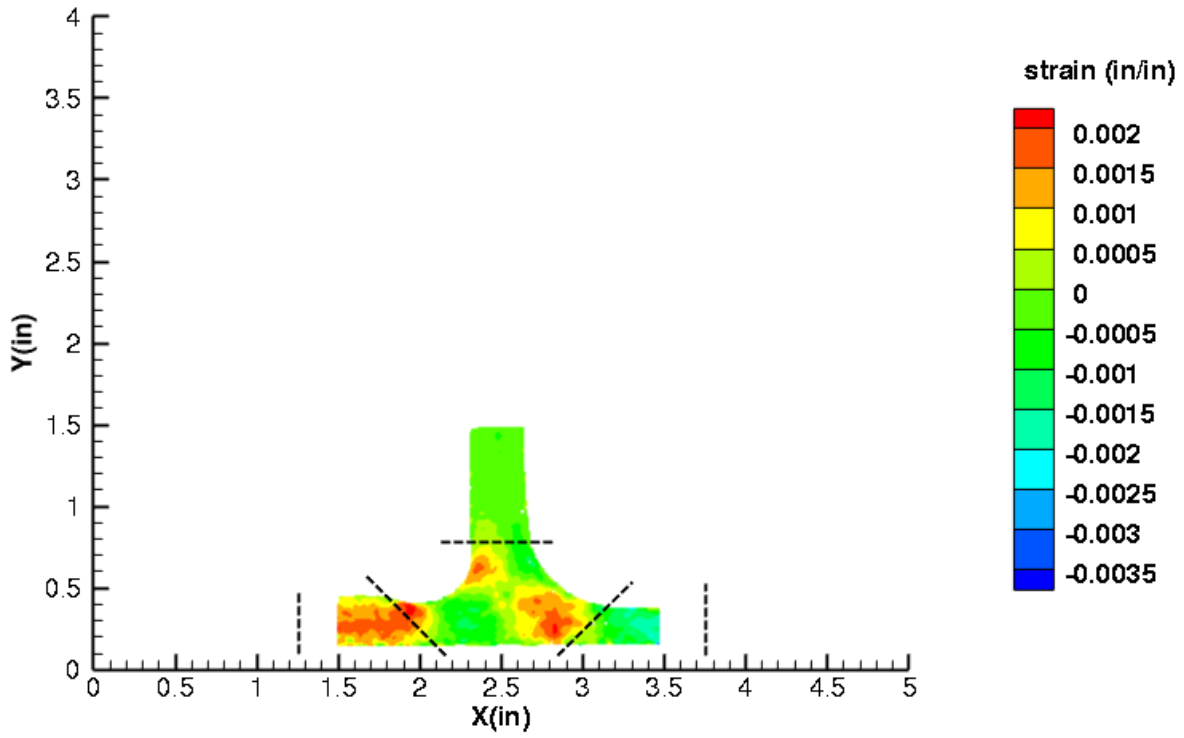

Figure C77. TNN1 strain contours for ε_{xy} at 2286 lb. load, prior to initial failure, local 5MP VIC data.

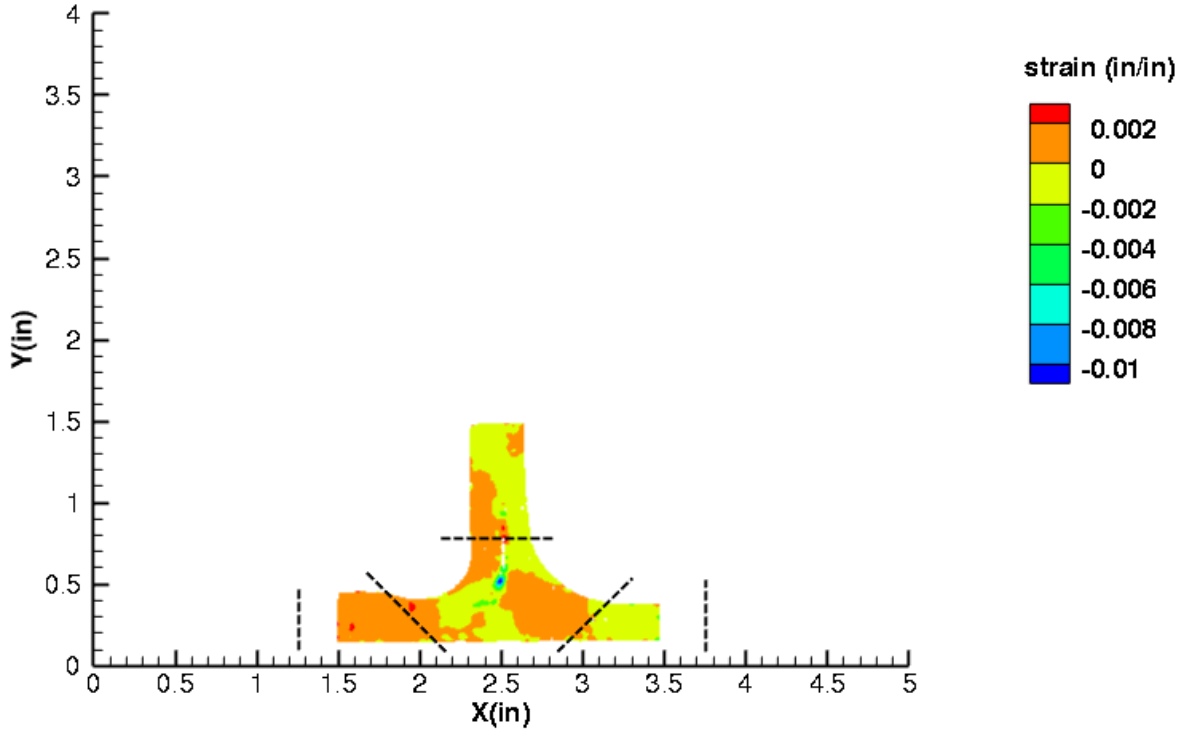

Figure C78. TNN1 strain contours for ε_{xy} at 2216 lb. load, just after initial failure, local 5MP VIC data.

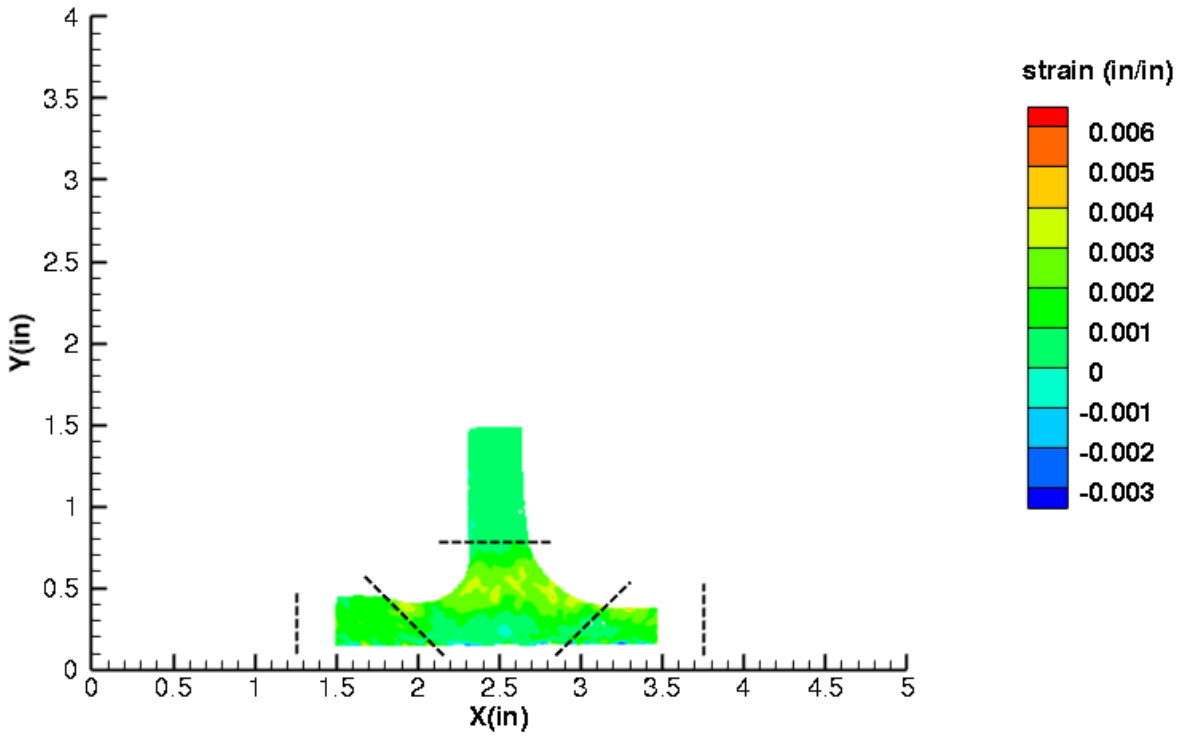

Figure C79. TNN1 strain contours for maximum principal strain at 2286 lb. load, prior to initial failure, local 5MP VIC data.

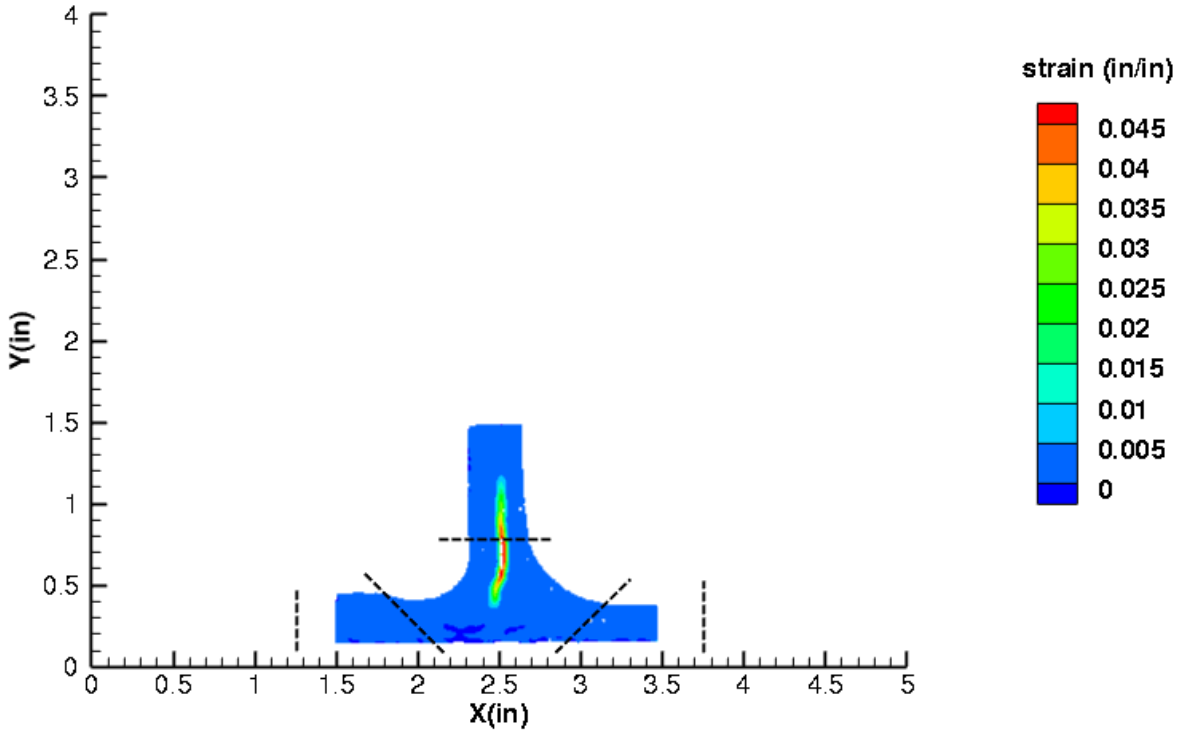

Figure C80. TNN1 strain contours for maximum principal strain at 2216 lb. load, just after initial failure, local 5MP VIC data.

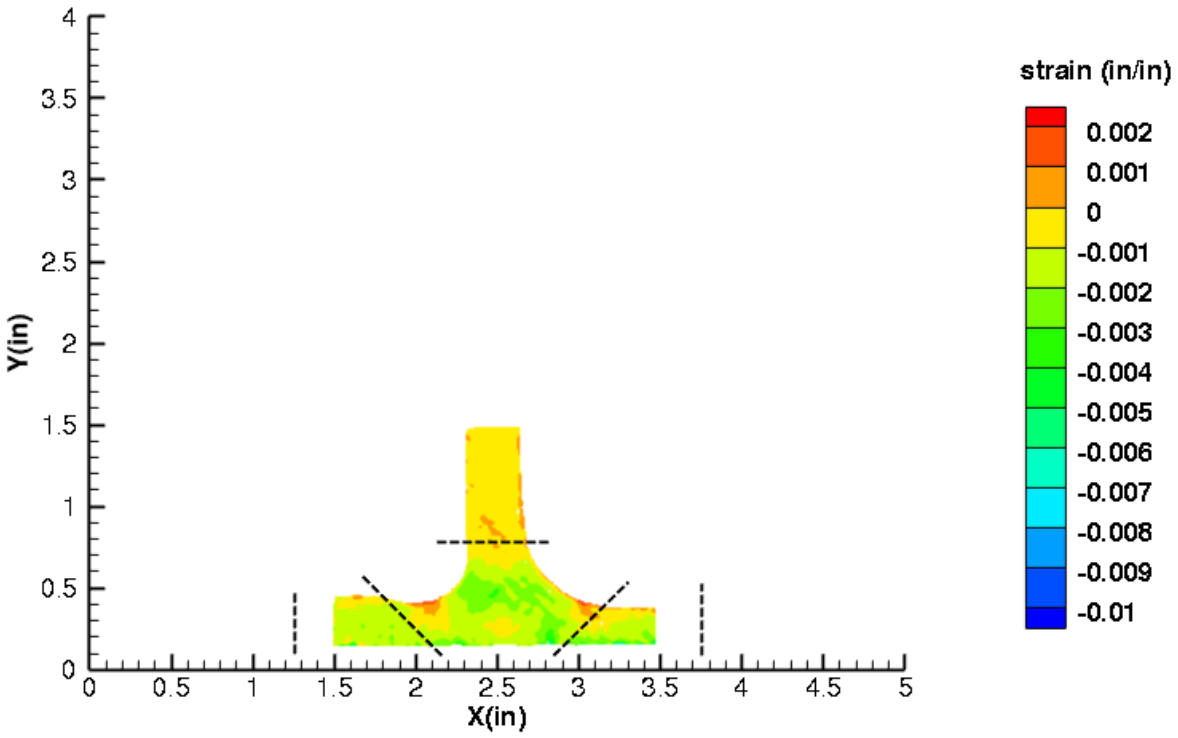

Figure C81. TNN1 strain contours for minimum principal strain at 2286 lb. load, prior to initial failure, local 5MP VIC data.

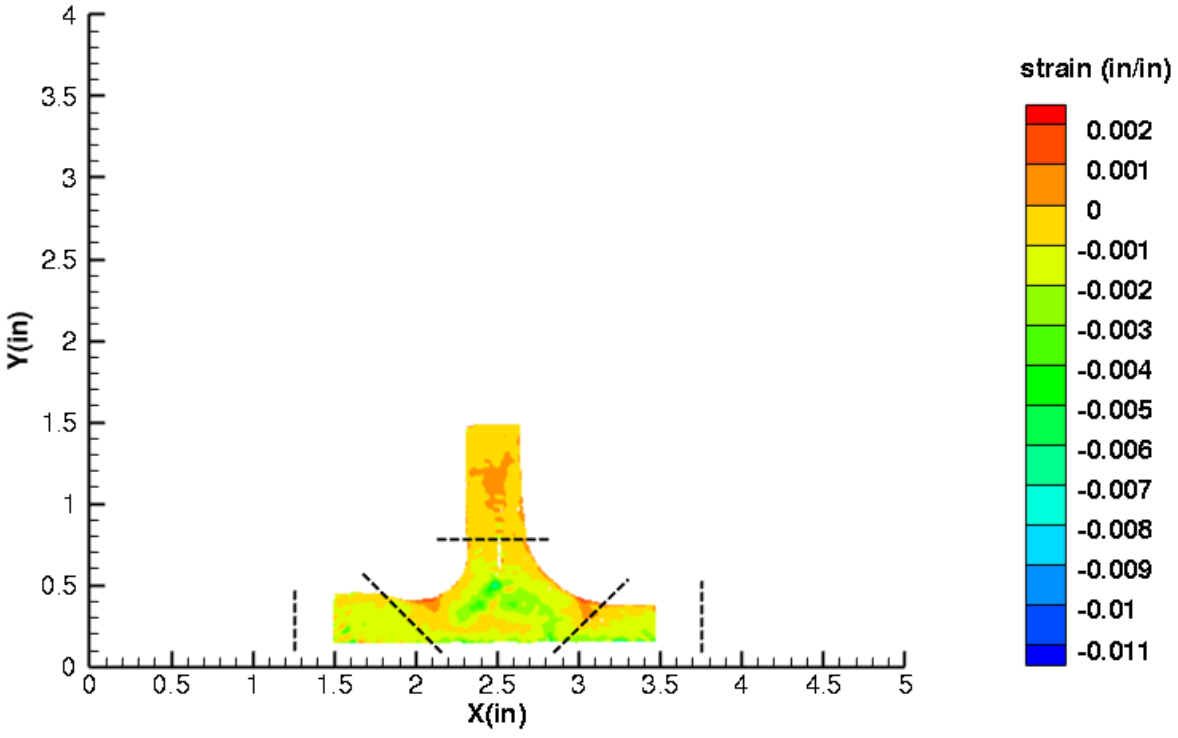

Figure C82. TNN1 strain contours for minimum principal strain at 2216 lb. load, just after initial failure, local 5MP VIC data.

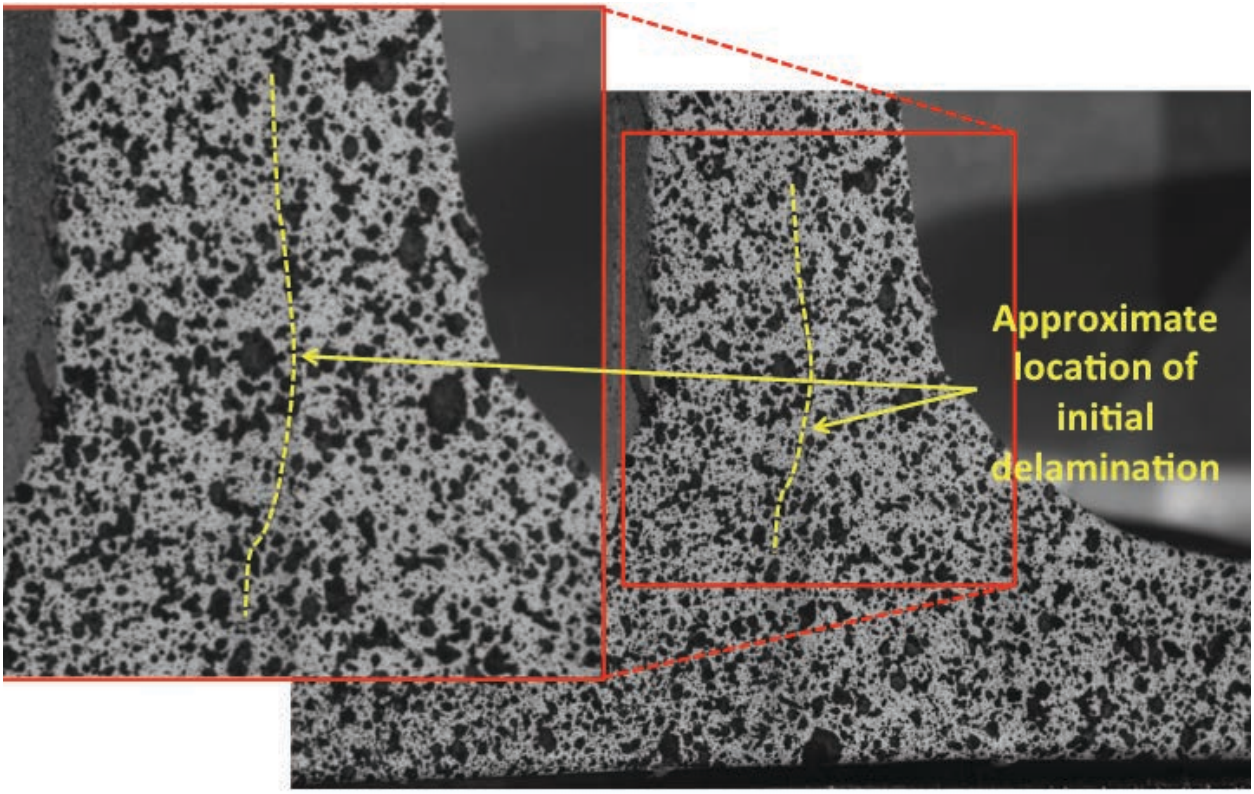

Figure C83. TNN1 image just after initial failure, local 5MP VIC data.

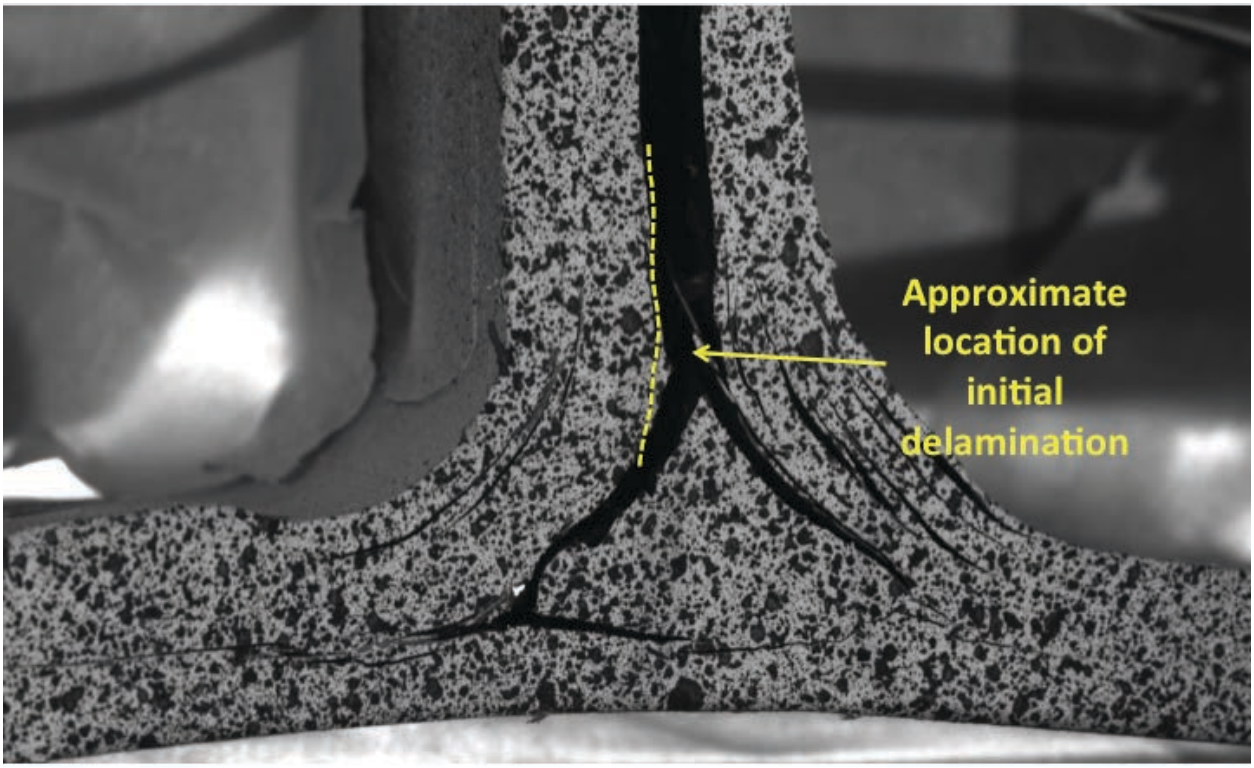

Figure C84. TNN1 image just after maximum load, local 5MP VIC data.

TNN2

This section presents the test data for the TNN2 test article.

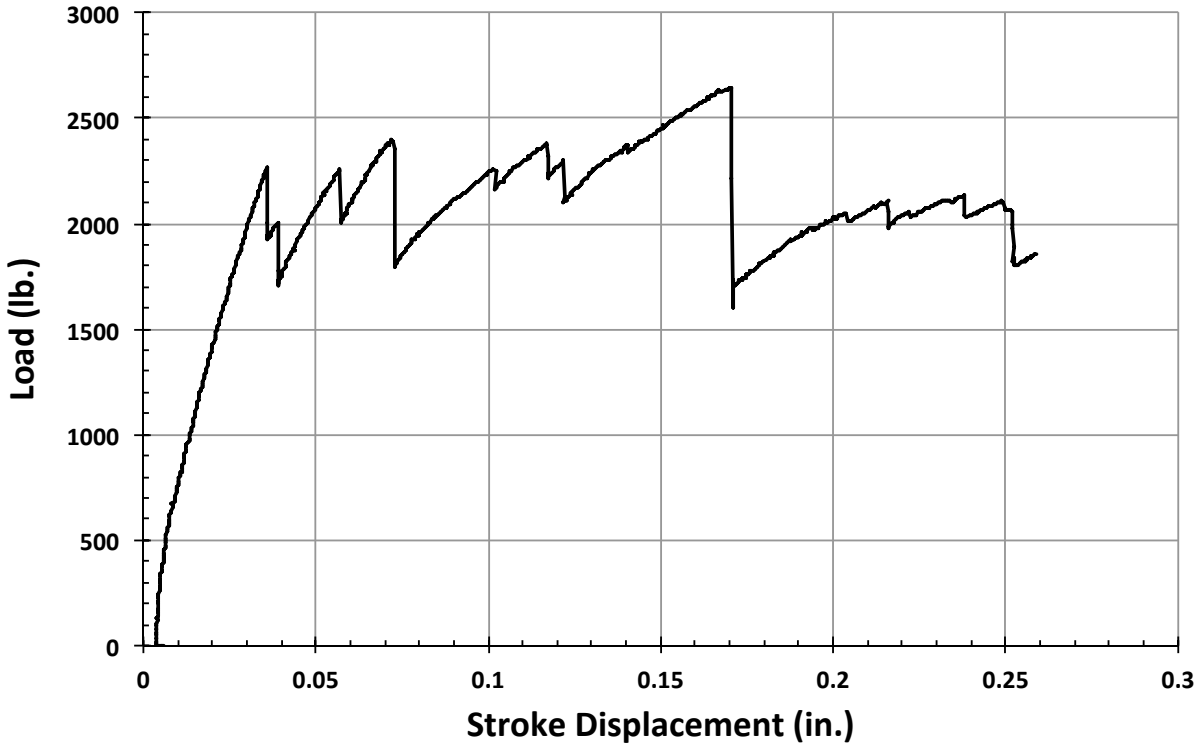

Figure C85. TNN2 load vs. stroke.

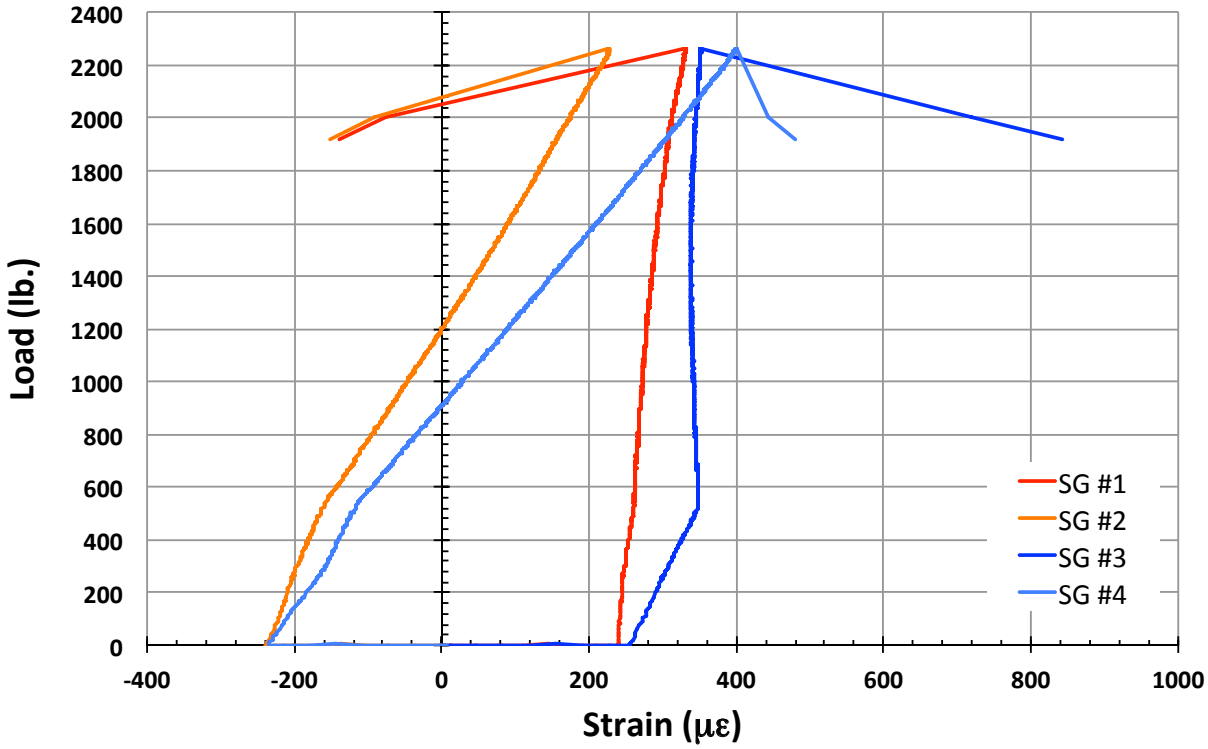

Figure C86. TNN2 load vs. strain, initial loading.

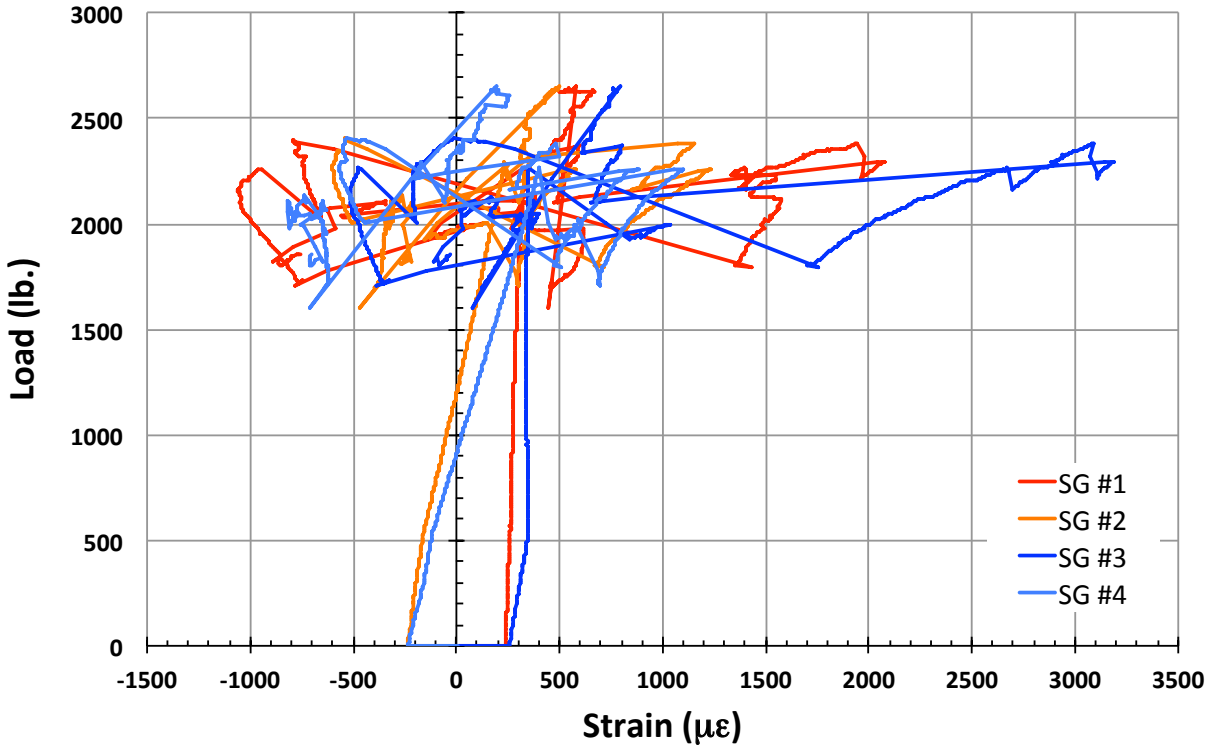

Figure C87. TNN2 load vs. strain.

T1S1

This section presents the test data for the T1S1 test article, and includes strain plots and failure images.

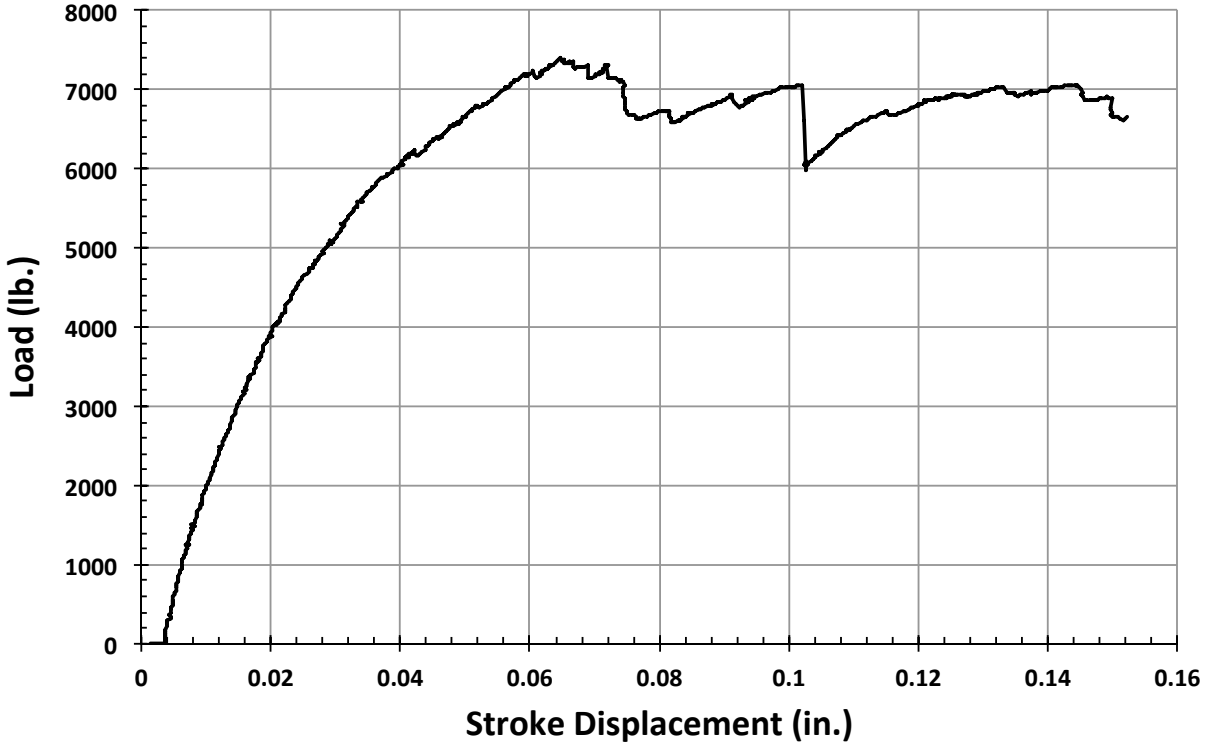

Figure C88. T1S1 load vs. stroke.

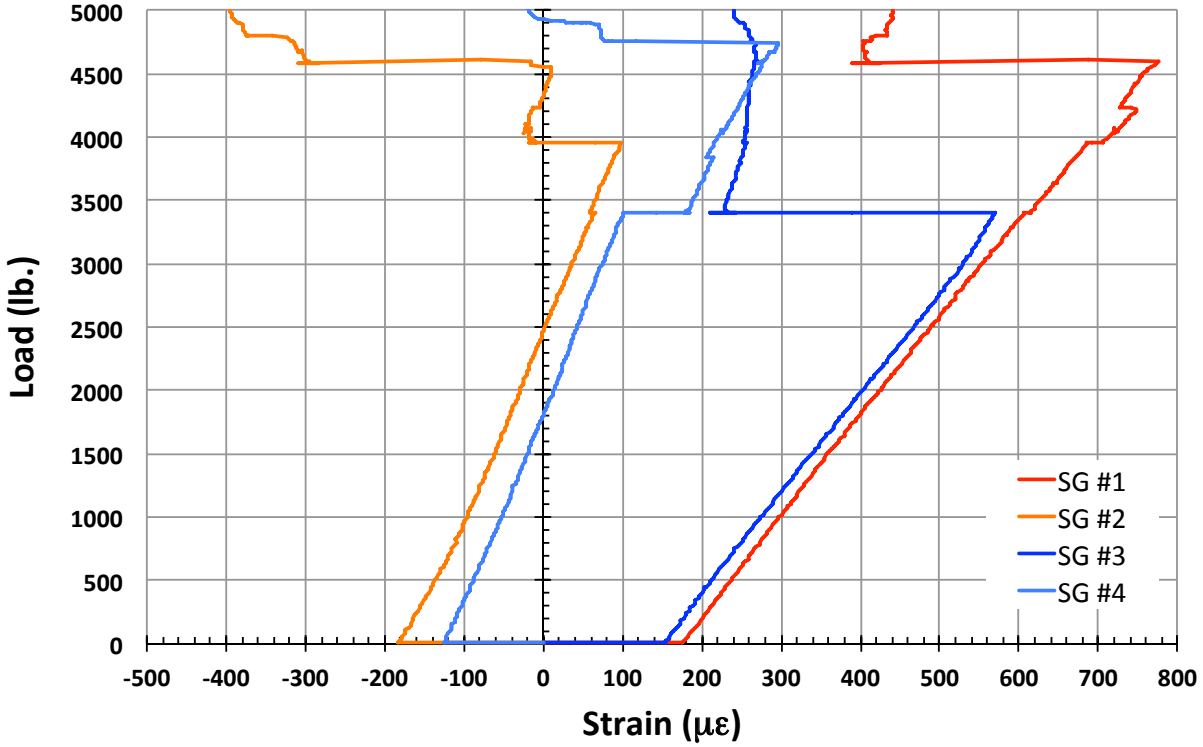

Figure C89. T1S1 load vs. strain, initial loading.

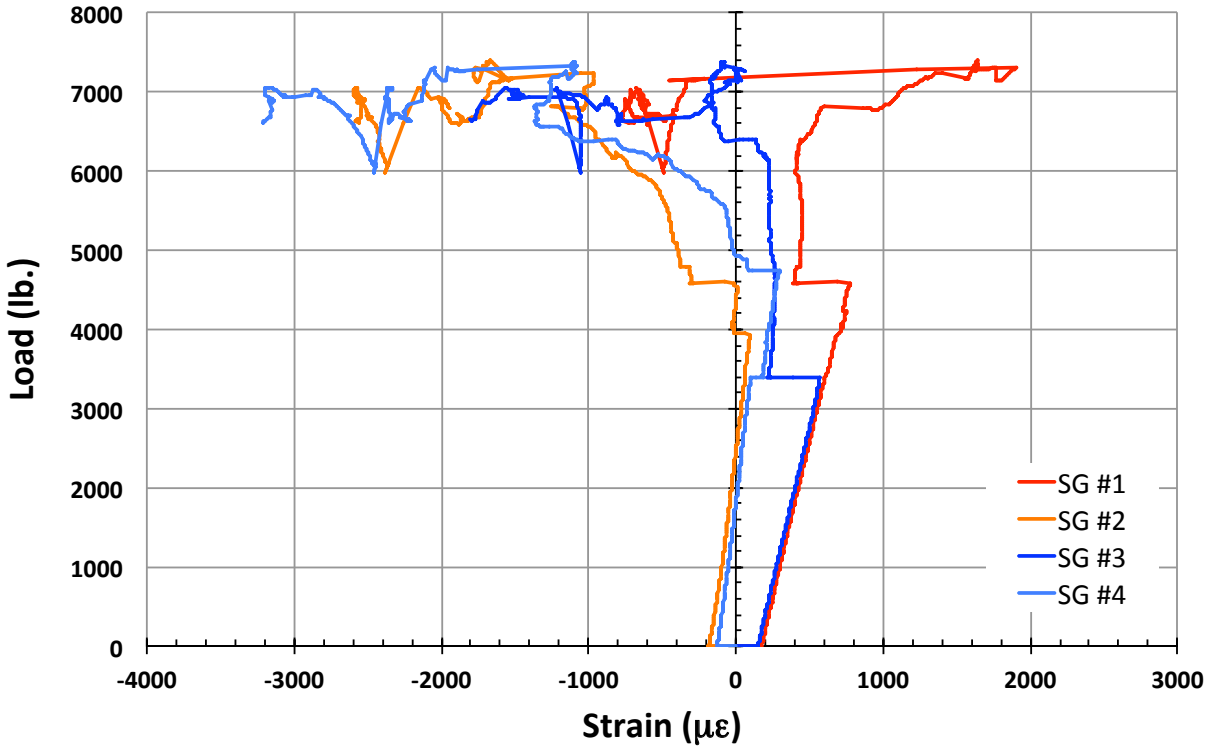

Figure C90. T1S1 load vs. strain.

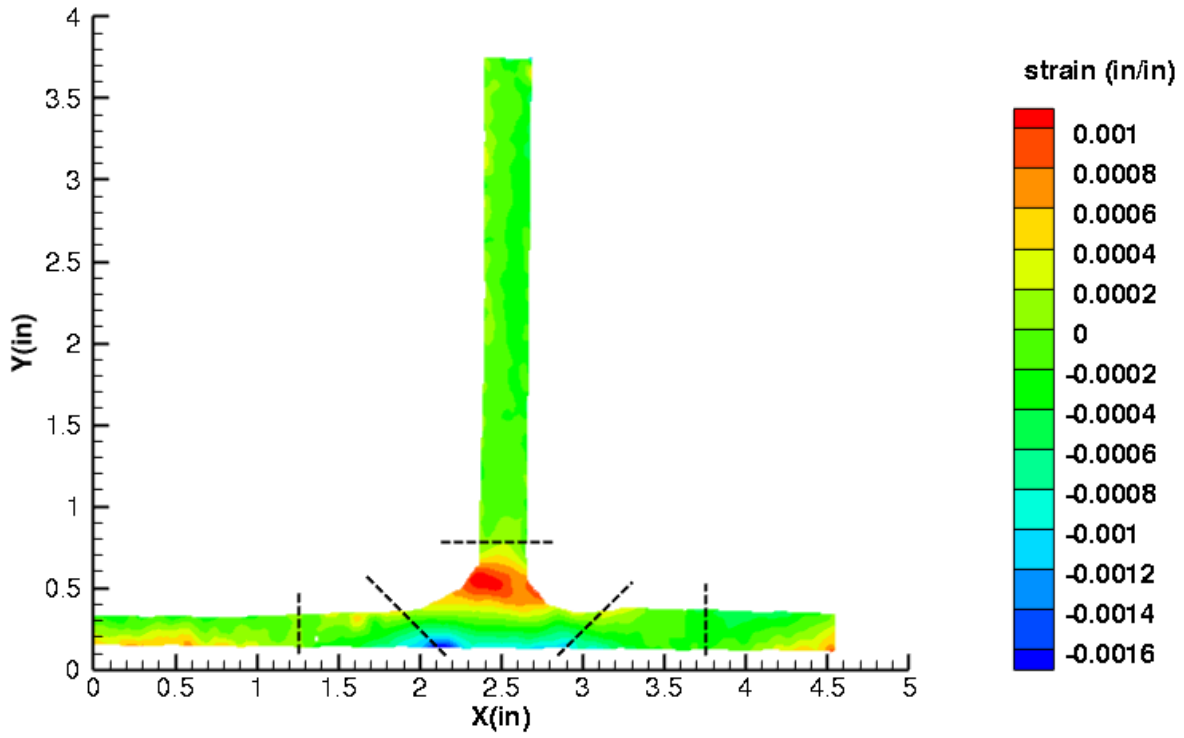

Figure C91. T1S1 strain contours for ε_{xx} at 3981 lb. load, prior to initial failure, 29MP VIC data.

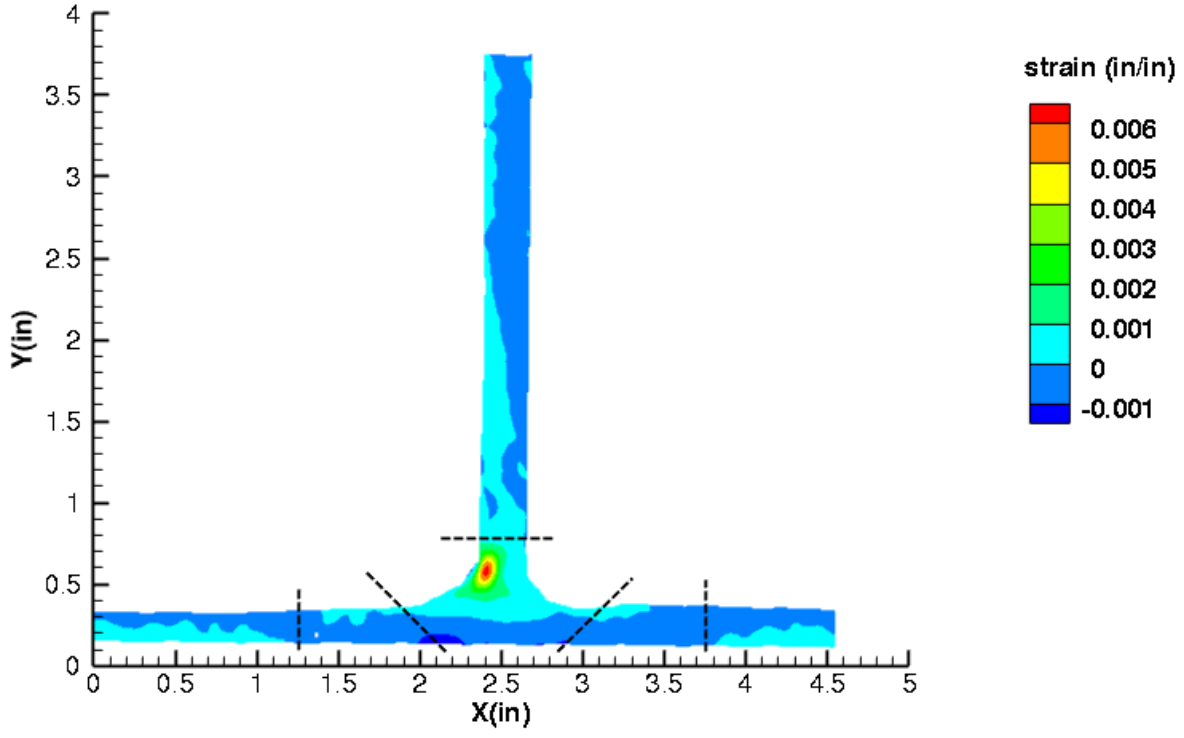

Figure C92. T1S1 strain contours for ε_{xx} at 3981 lb. load, just after initial failure, 29MP VIC data.

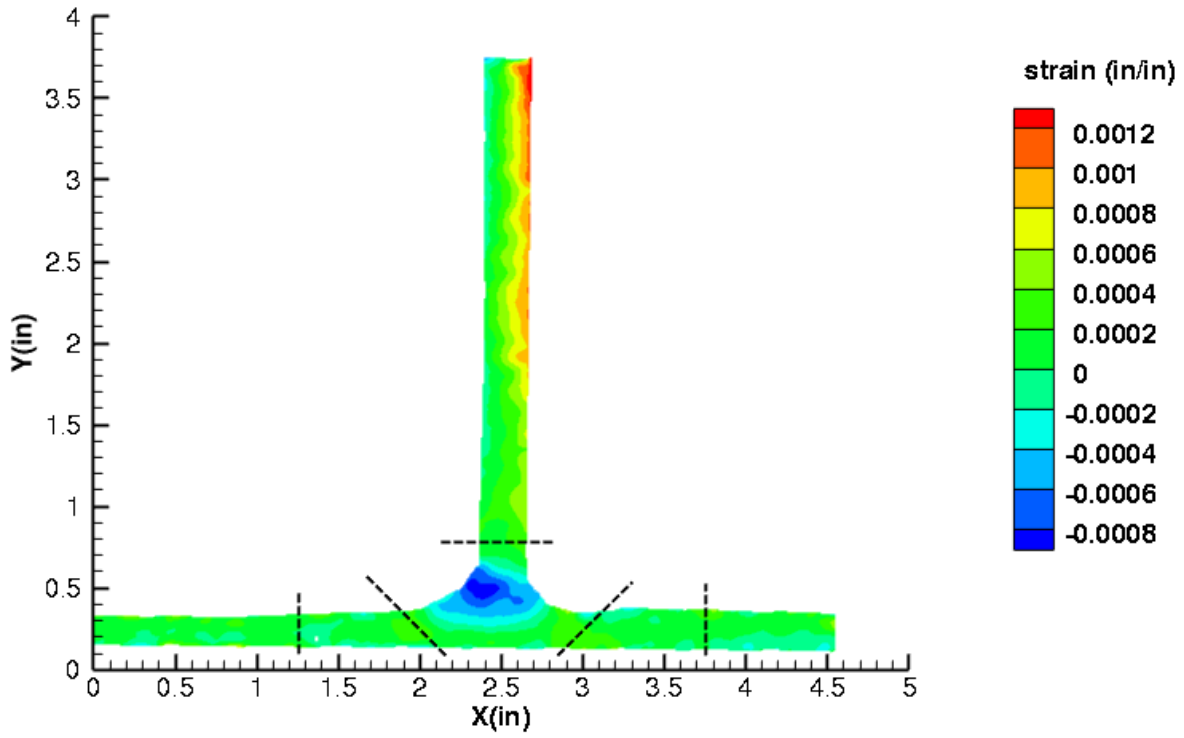

Figure C93. T1S1 strain contours for ε_{yy} at 3981 lb. load, prior to initial failure, 29MP VIC data.

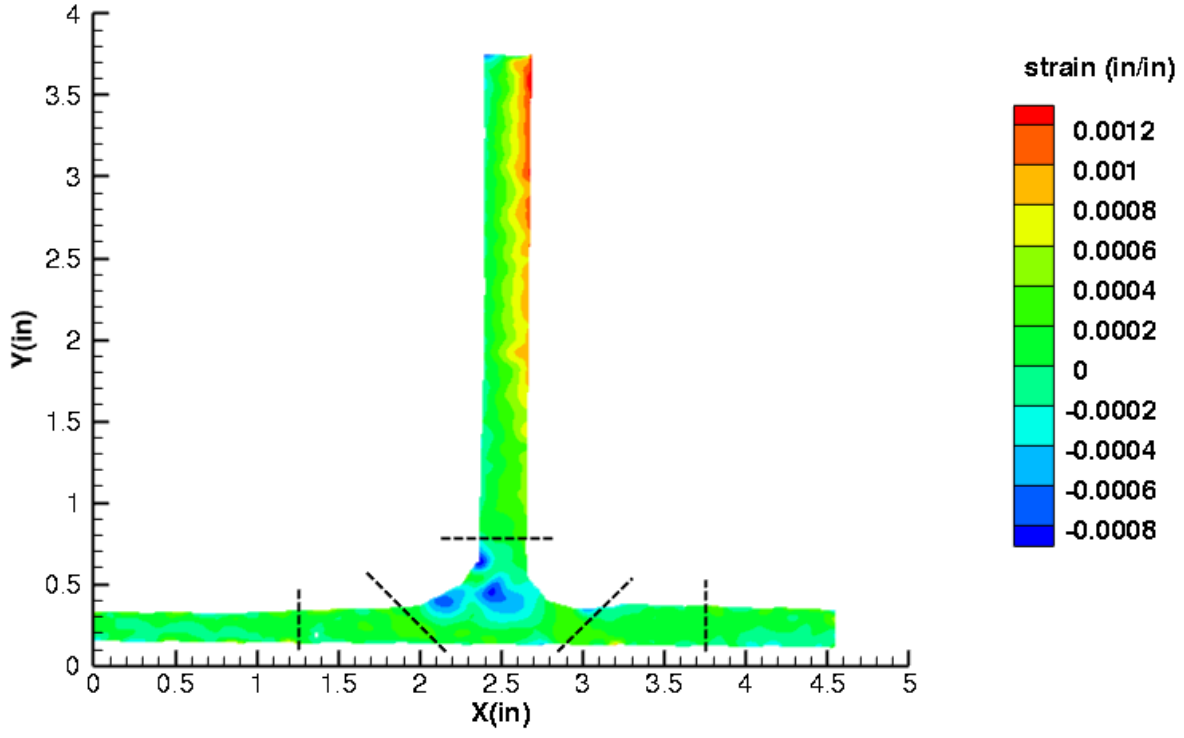

Figure C94. T1S1 strain contours for ε_{yy} at 3981 lb. load, just after initial failure, 29MP VIC data.

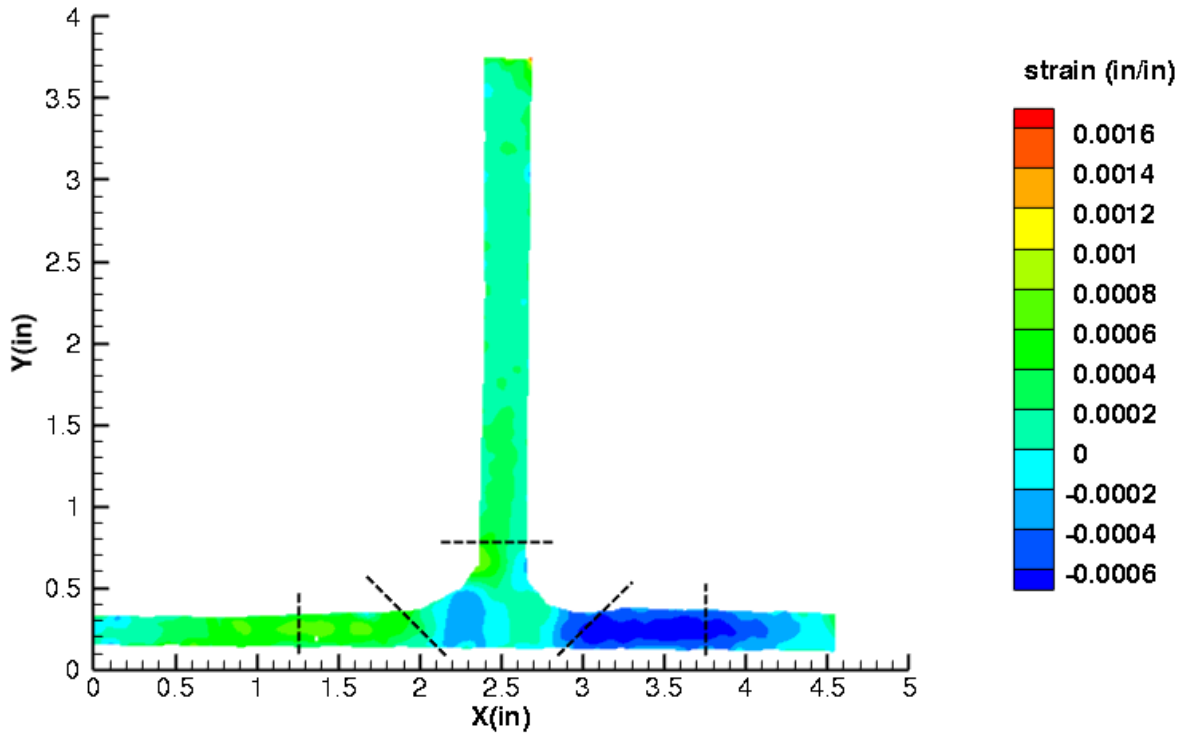

Figure C95. T1S1 strain contours for ε_{xy} at 3981 lb. load, prior to initial failure, 29MP VIC data.

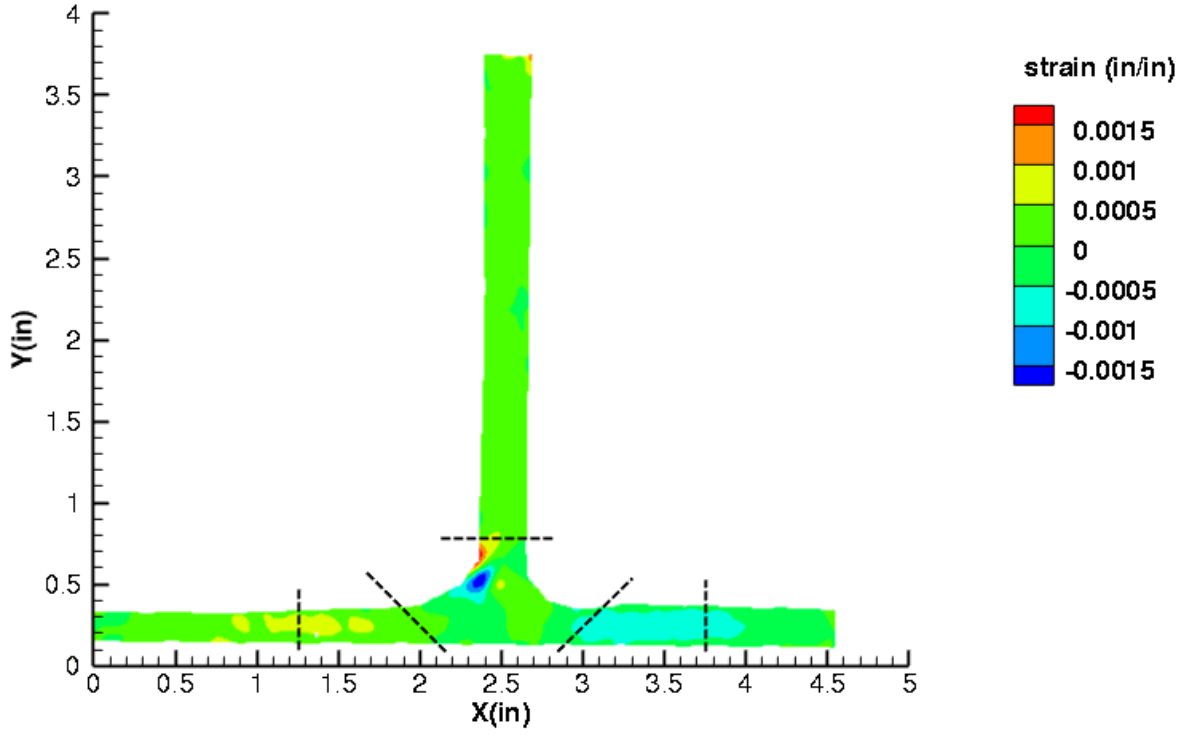

Figure C96. T1S1 strain contours for ε_{xy} at 3981 lb. load, just after initial failure, 29MP VIC data.

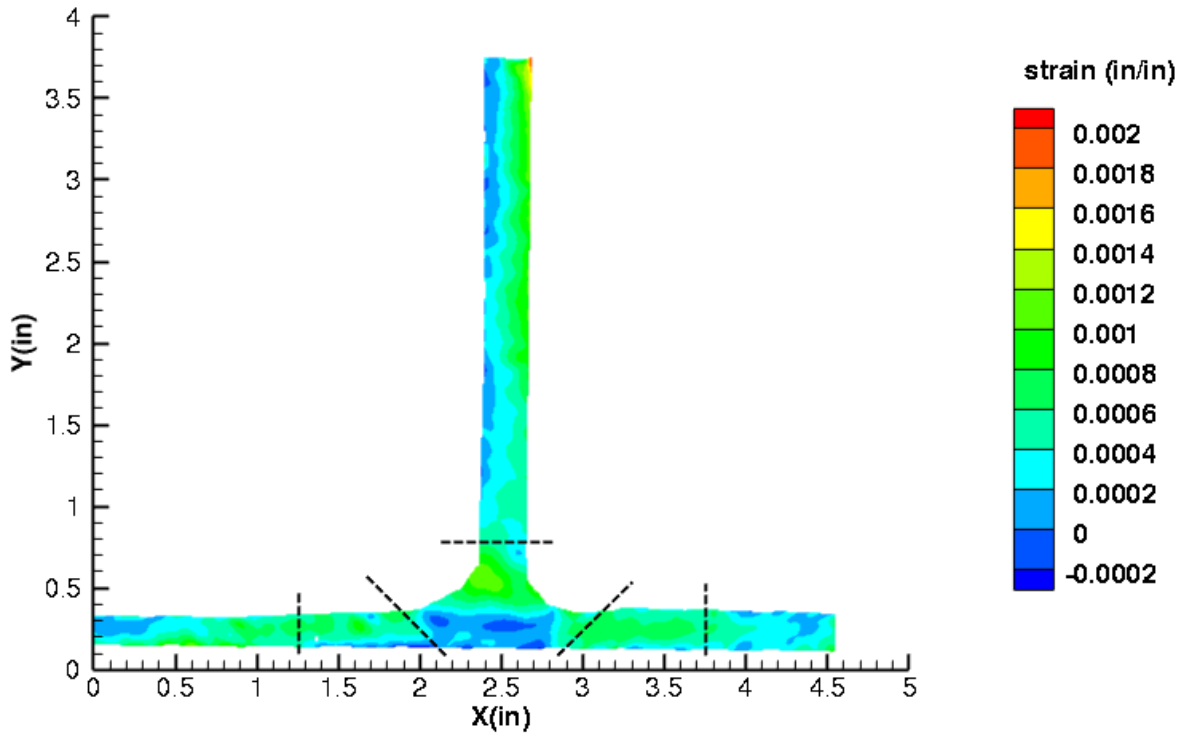

Figure C97. T1S1 strain contours for maximum principal strain at 3981 lb. load, prior to initial failure, 29MP VIC data.

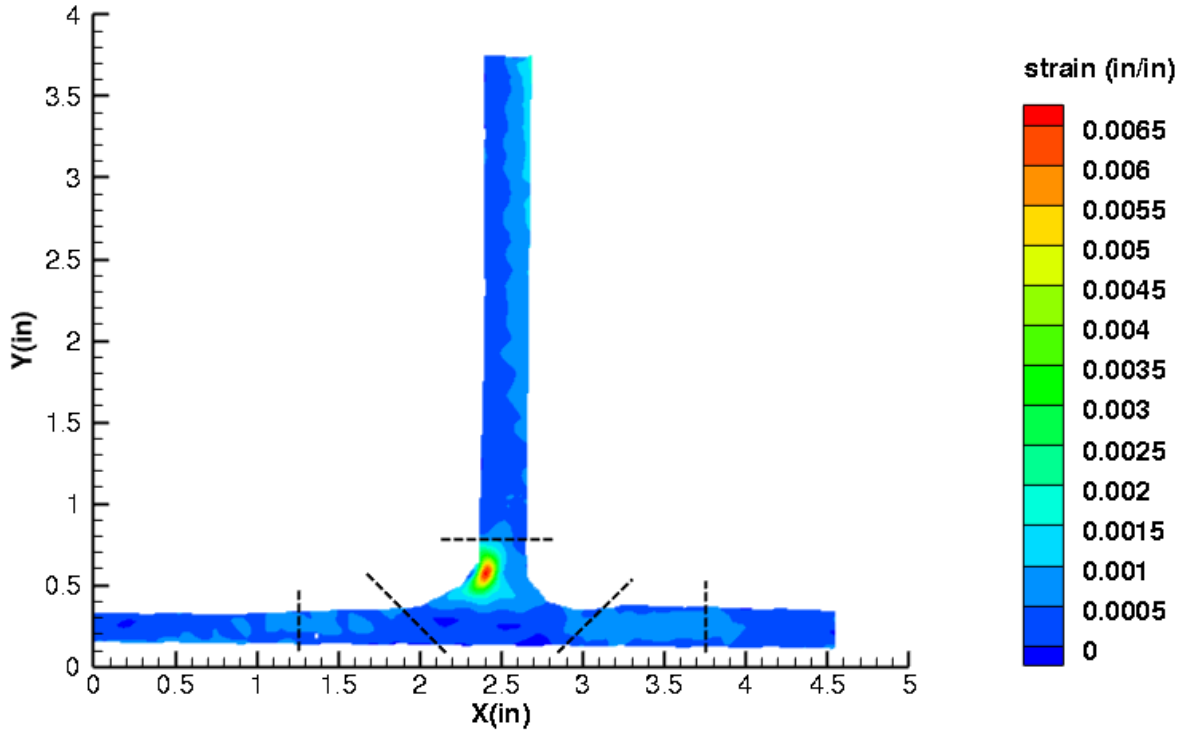

Figure C98. T1S1 strain contours for maximum principal strain at 3981 lb. load, just after initial failure, 29MP VIC data.

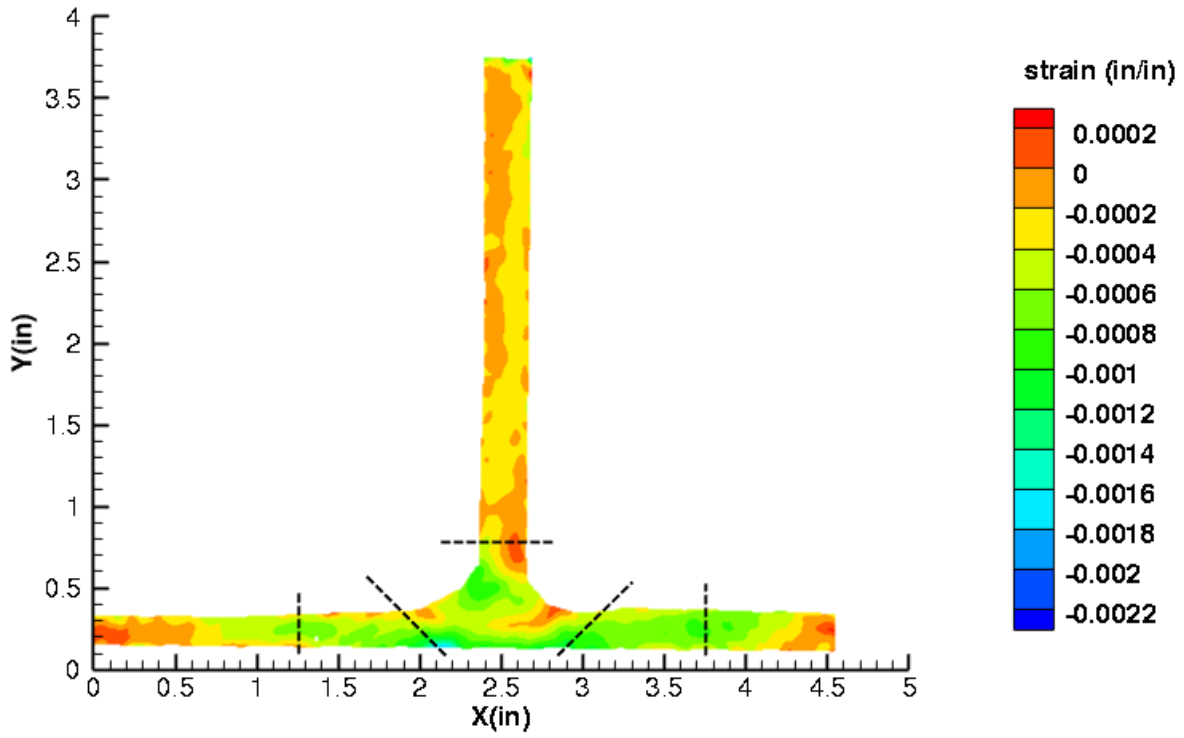

Figure C99. T1S1 strain contours for minimum principal strain at 3981 lb. load, prior to initial failure, 29MP VIC data.

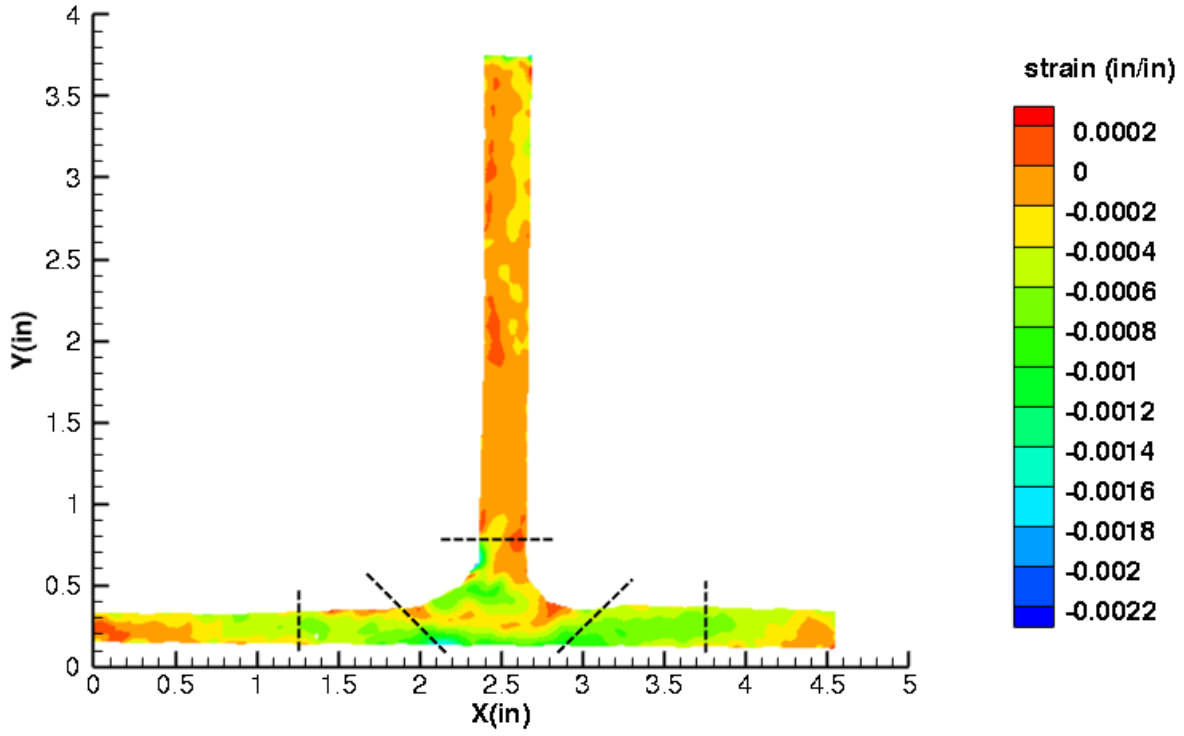

Figure C100. T1S1 strain contours for minimum principal strain at 3981 lb. load, just after initial failure, 29MP VIC data.

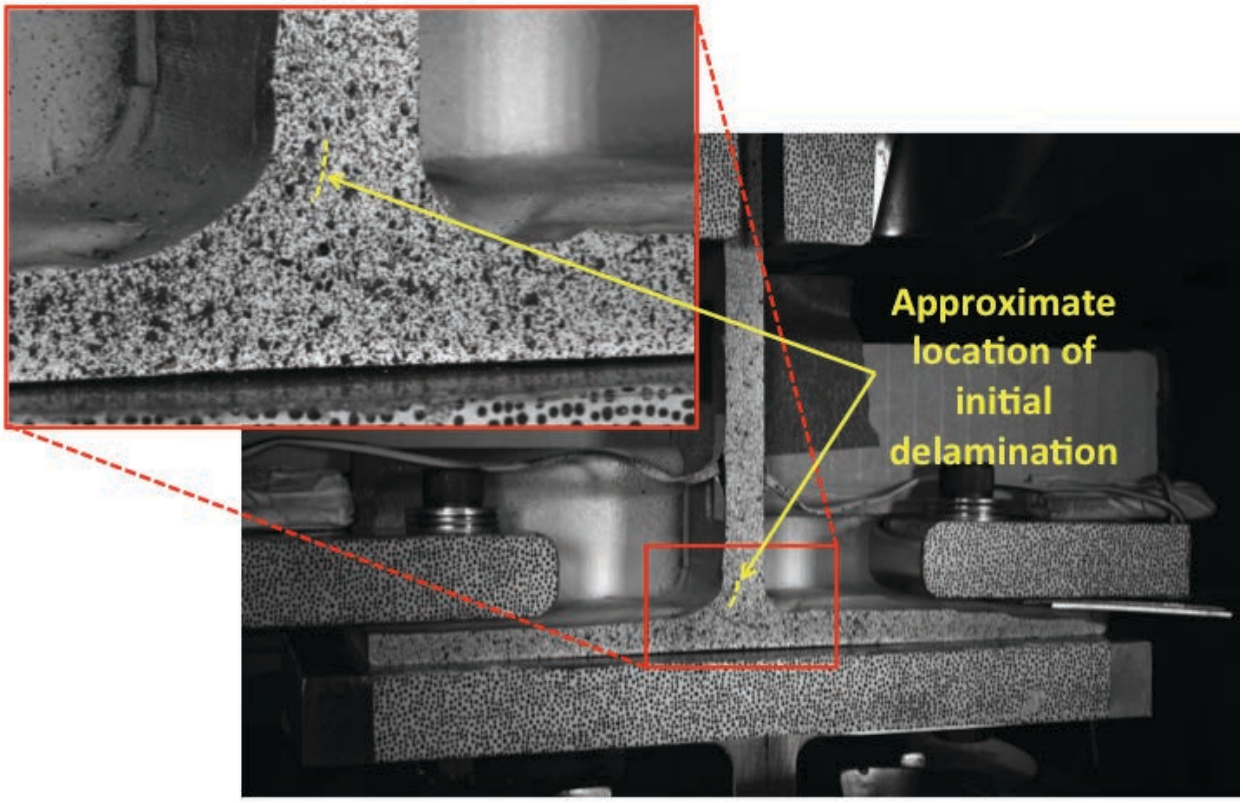

Figure C101. T1S1 image just after initial failure, 29MP VIC data.

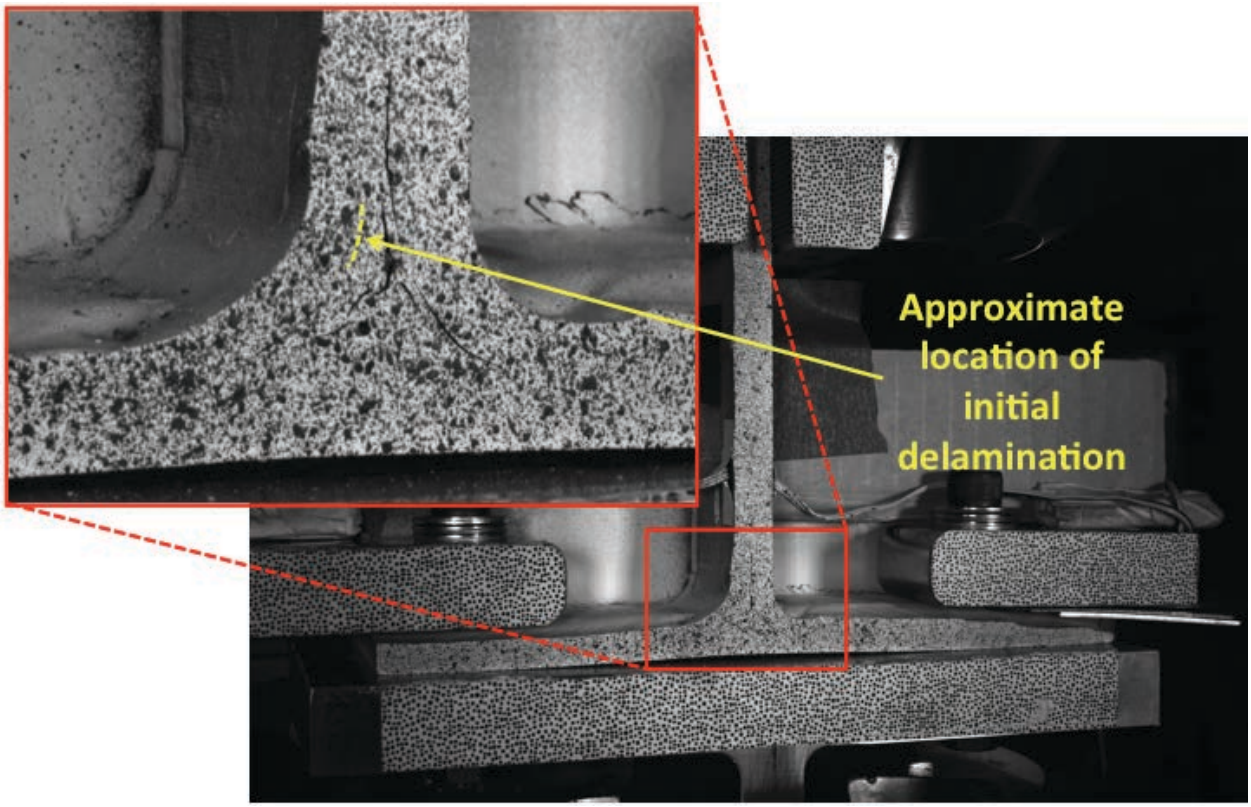

Figure C102. T1S1 image just after maximum load, 29MP VIC data.

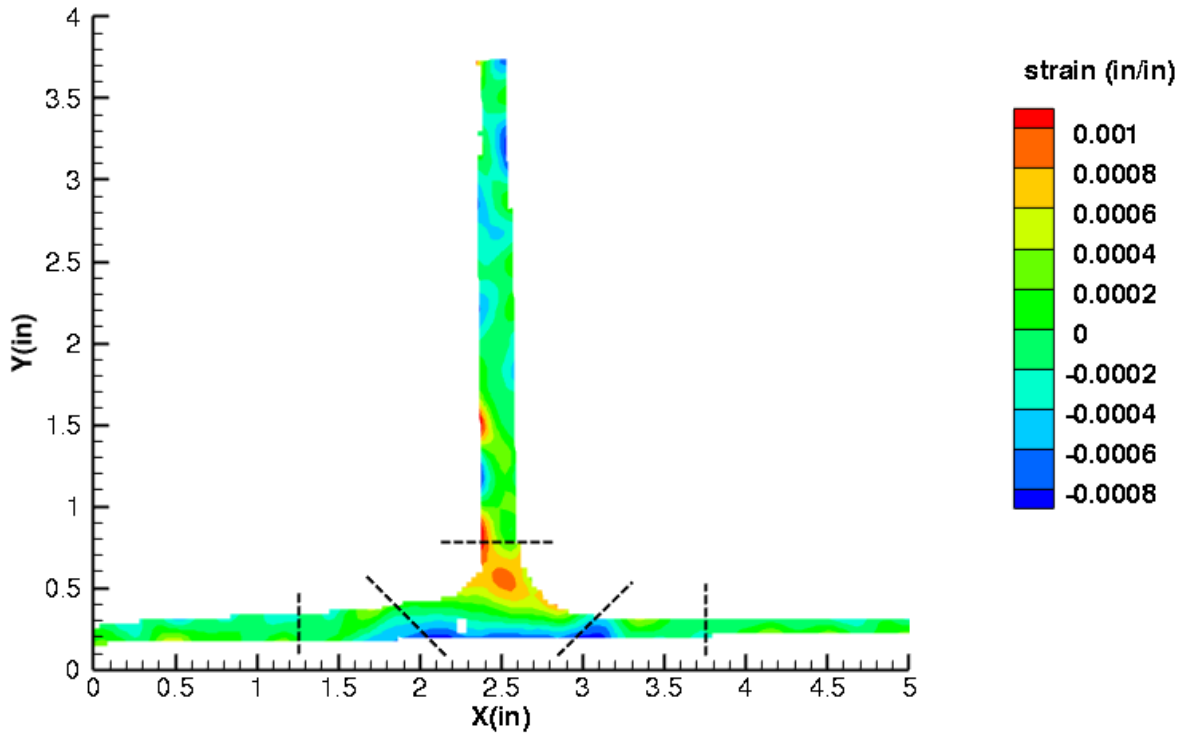

Figure C103. T1S1 strain contours for ε_{xx} at 3514 lb. load, prior to initial failure, 5MP VIC data.

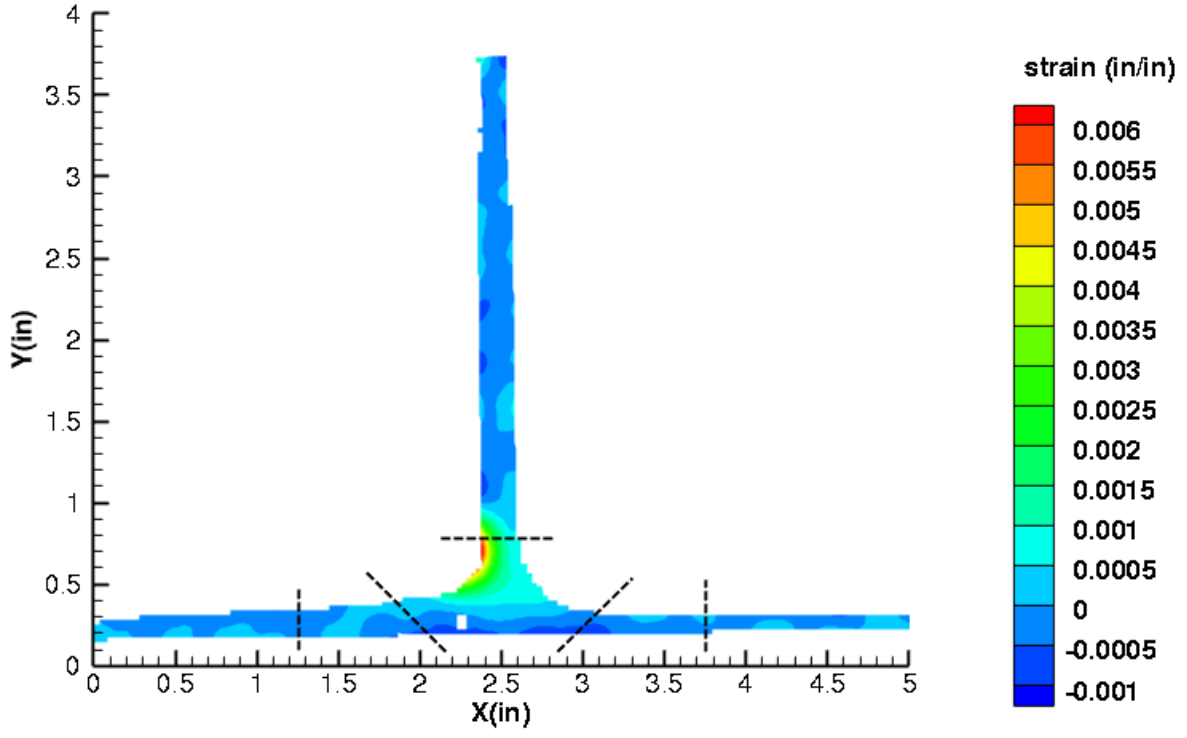

Figure C104. T1S1 strain contours for ε_{xx} at 3431 lb. load, just after initial failure, 5MP VIC data.

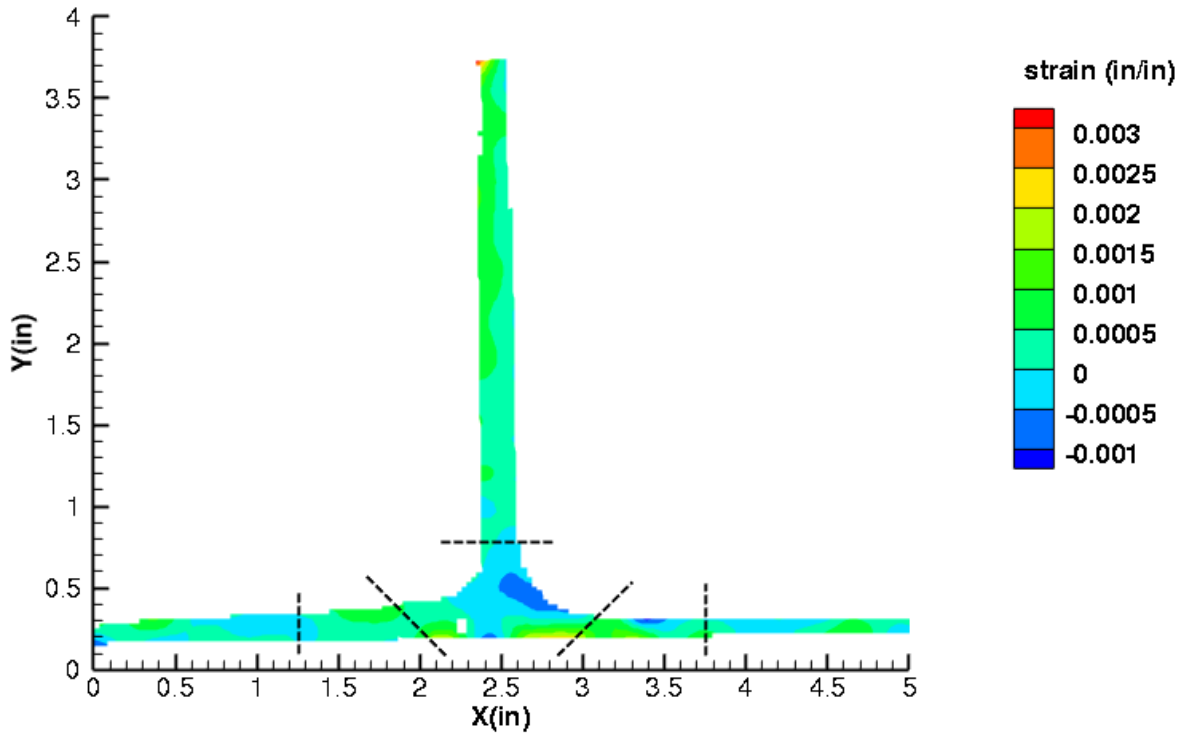

Figure C105. T1S1 strain contours for ε_{yy} at 3514 lb. load, prior to initial failure, 5MP VIC data.

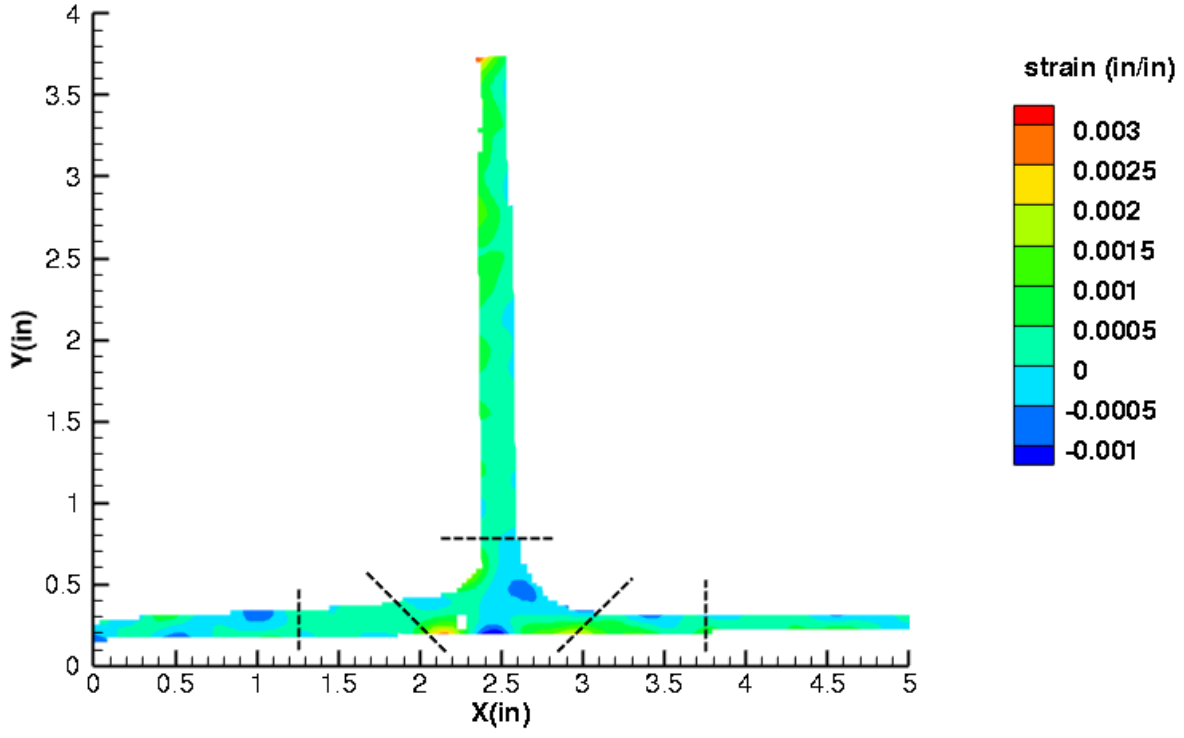

Figure C106. T1S1 strain contours for ε_{yy} at 3431 lb. load, just after initial failure, 5MP VIC data.

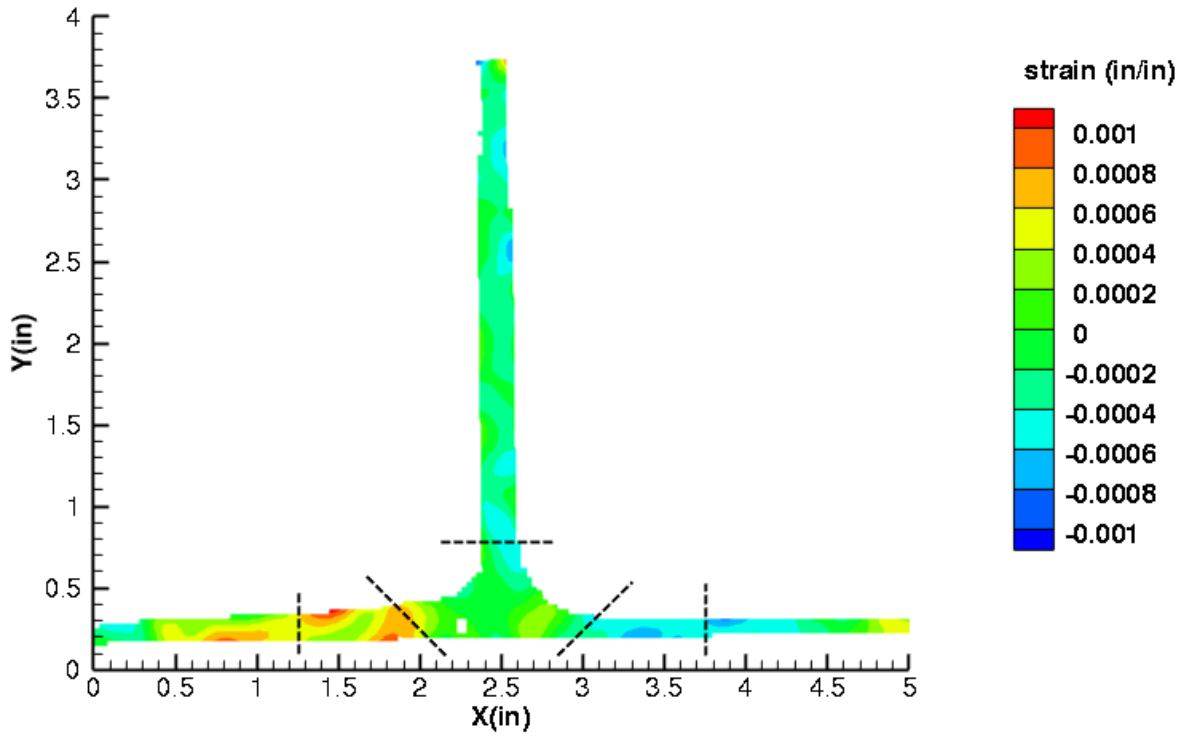

Figure C107. T1S1 strain contours for ε_{xy} at 3514 lb. load, prior to initial failure, 5MP VIC data.

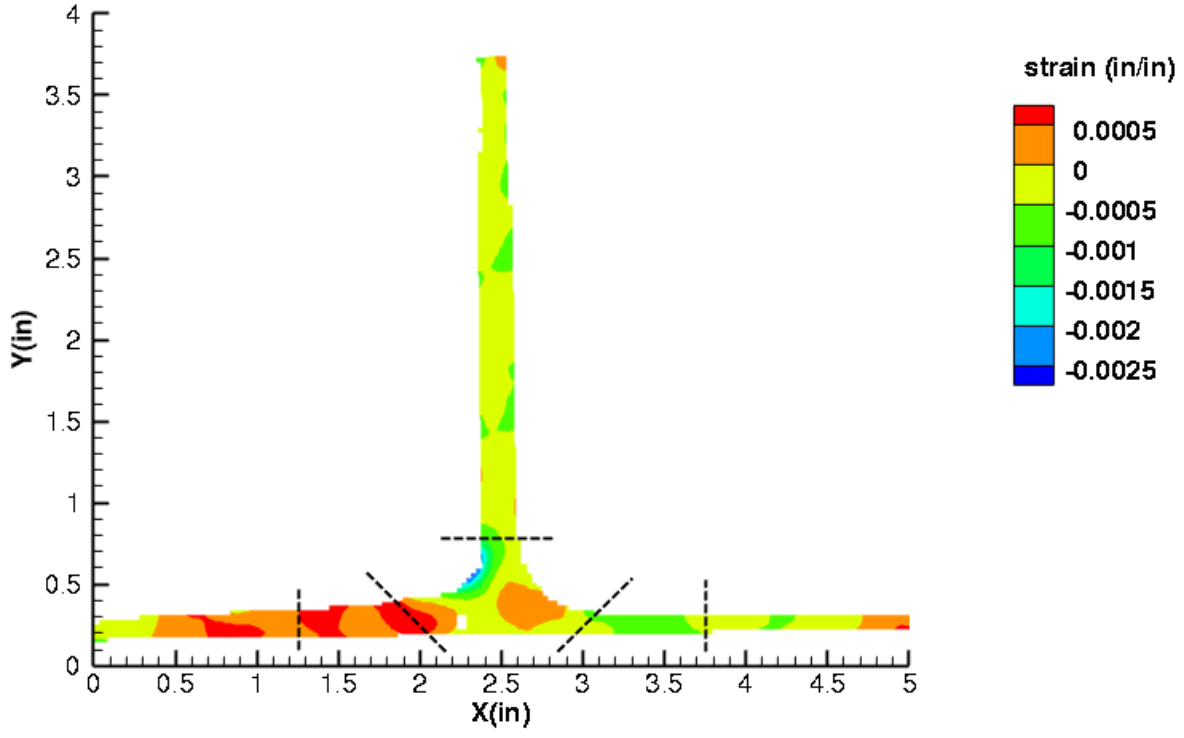

Figure C108. T1S1 strain contours for ε_{xy} at 3431 lb. load, just after initial failure, 5MP VIC data.

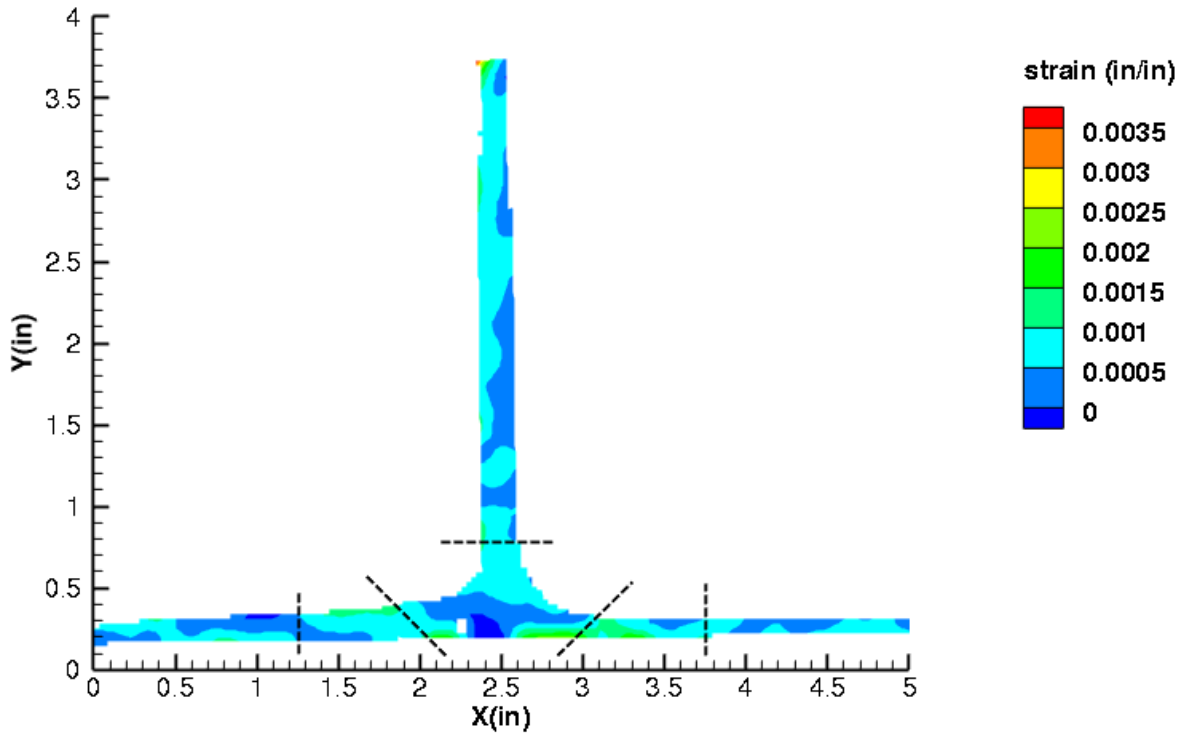

Figure C109. T1S1 strain contours for maximum principal strain at 3514 lb. load, prior to initial failure, 5MP VIC data.

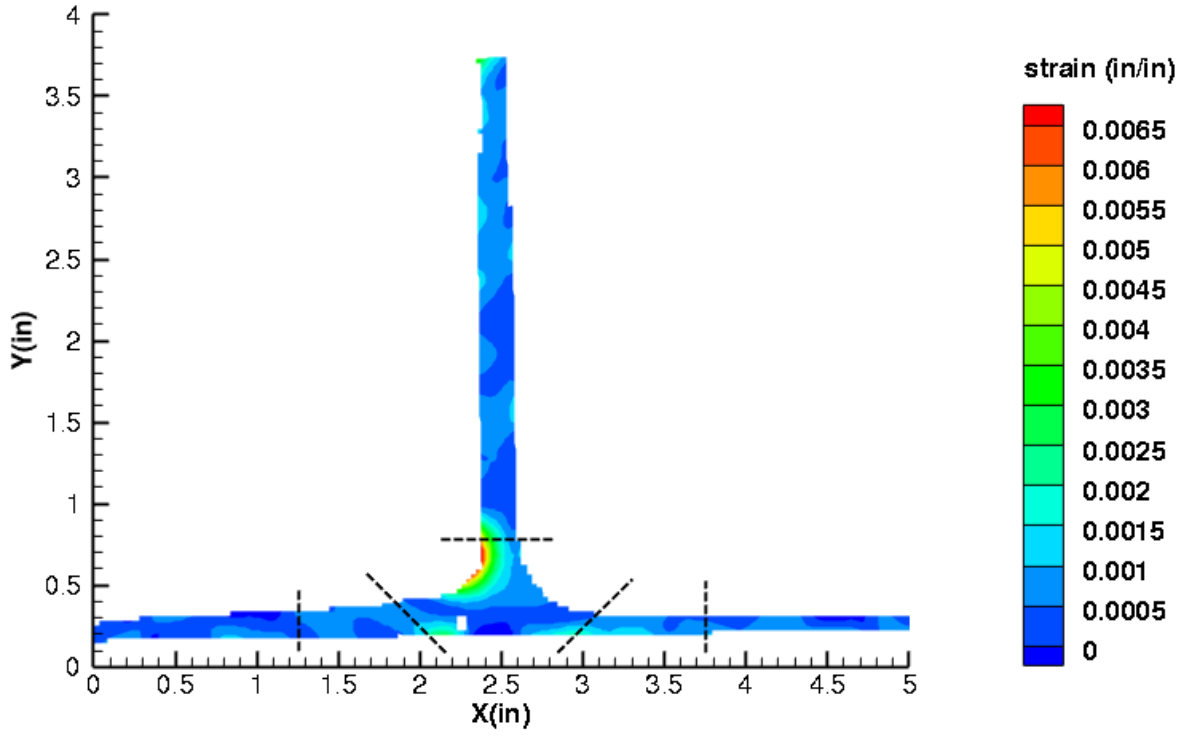

Figure C110. T1S1 strain contours for maximum principal strain at 3431 lb. load, just after initial failure, 5MP VIC data.

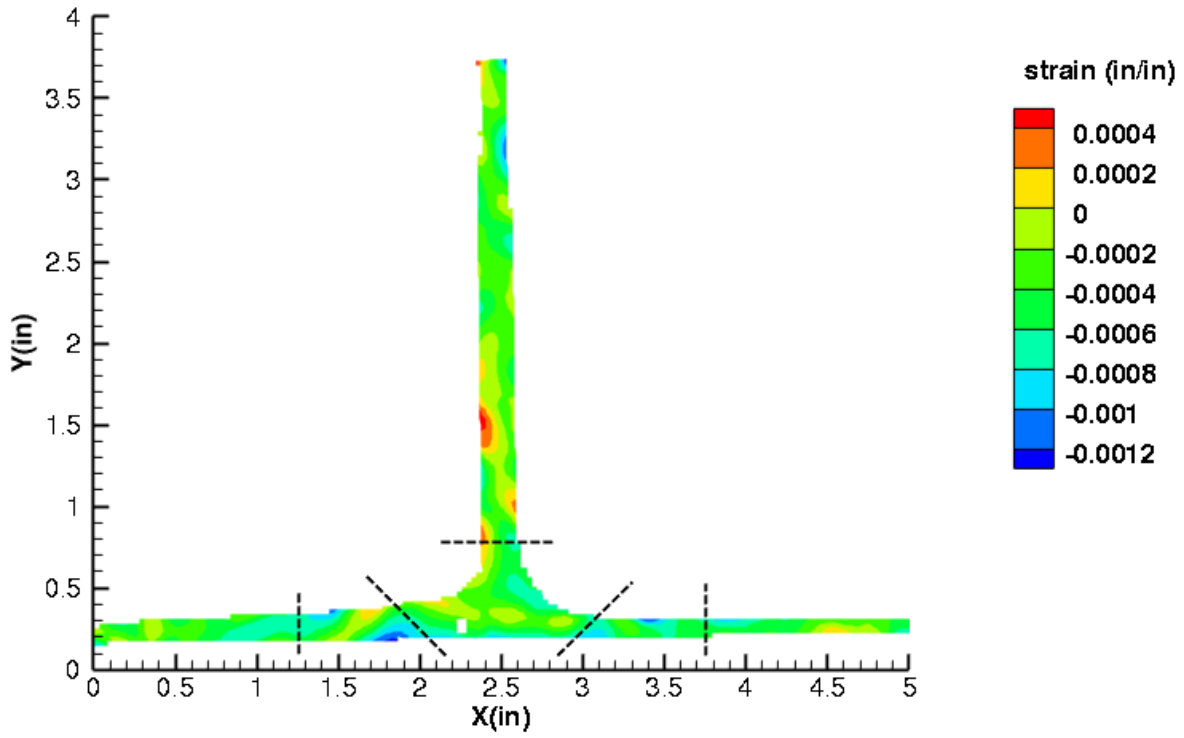

Figure C111. T1S1 strain contours for minimum principal strain at 3514 lb. load, prior to initial failure, 5MP VIC data.

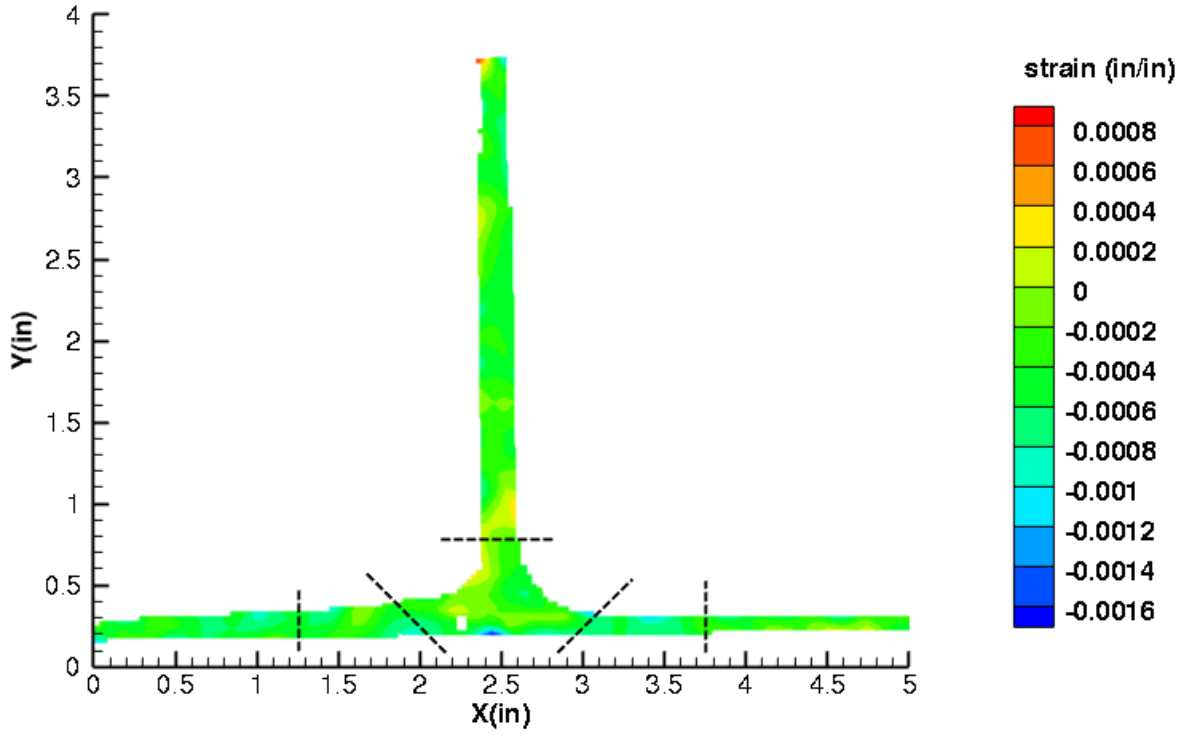

Figure C112. T1S1 strain contours for minimum principal strain at 3431 lb. load, just after initial failure, 5MP VIC data.

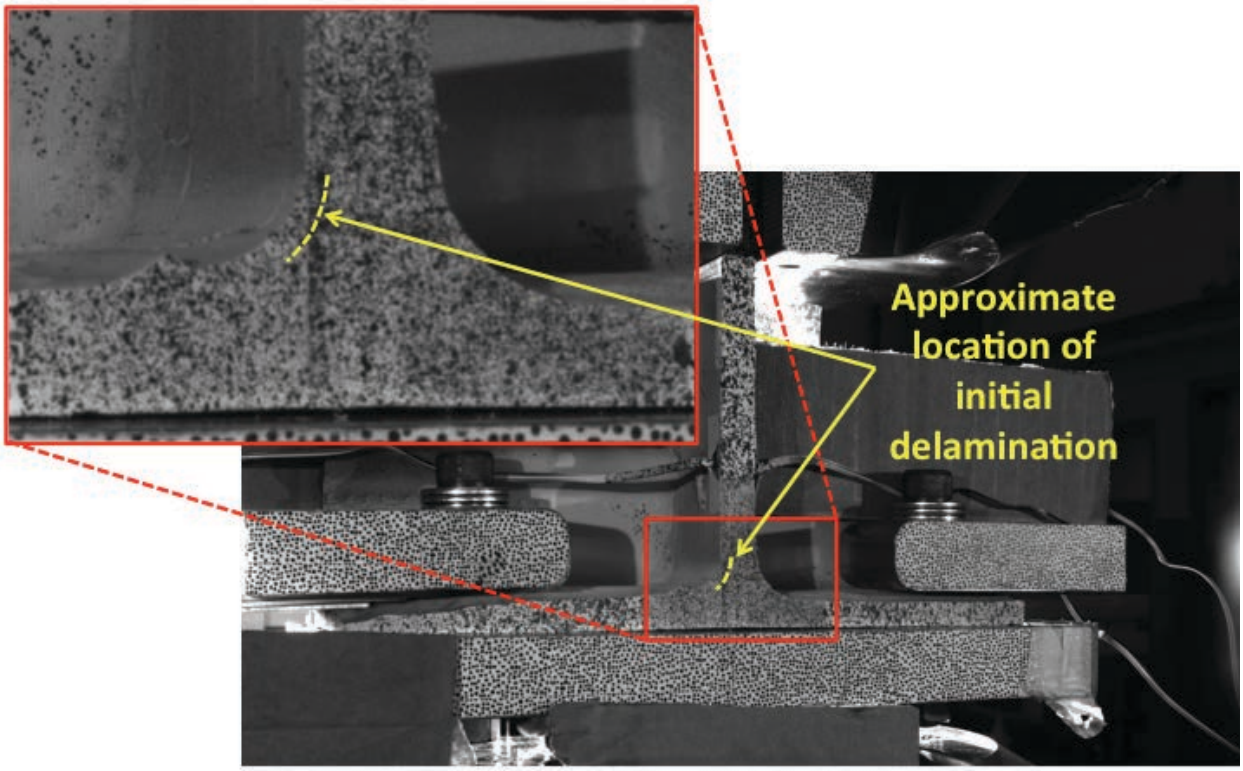

Figure C113. T1S1 image just after initial failure, 5MP VIC data.

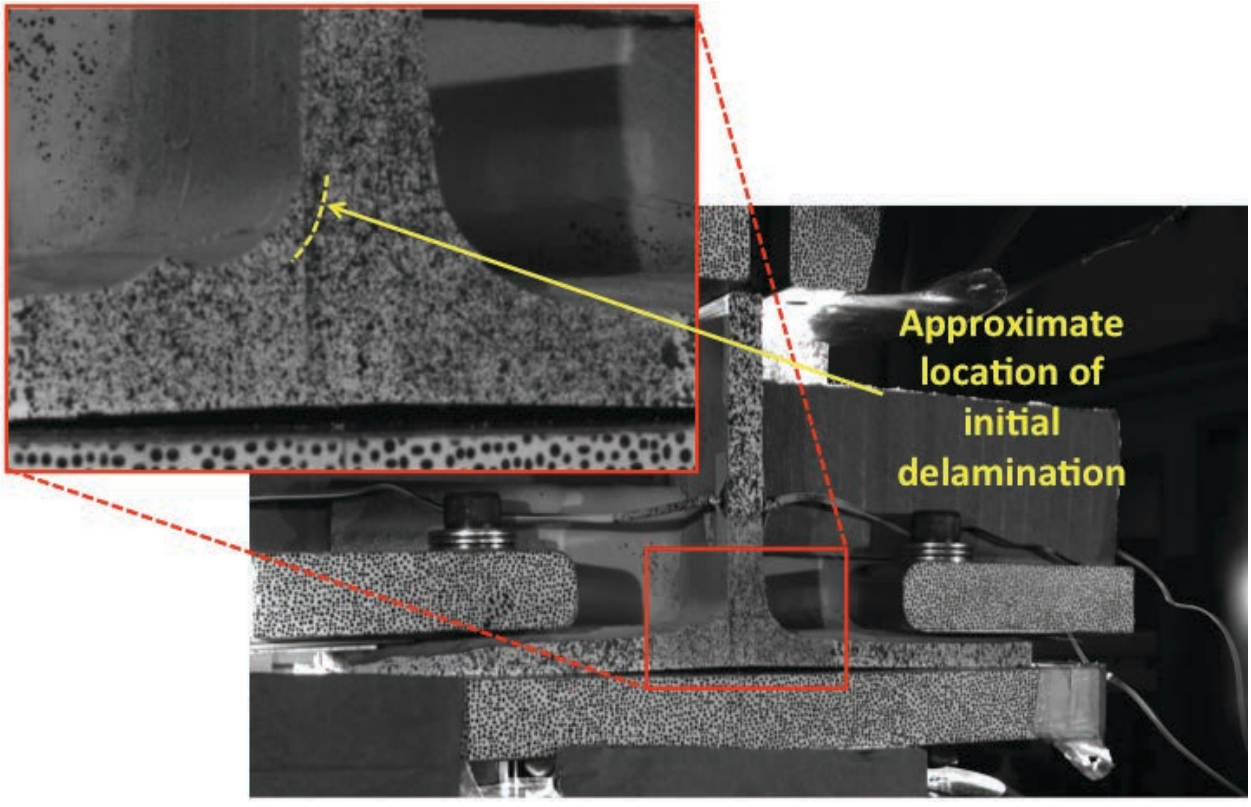

Figure C114. T1S1 image just after maximum load, 5MP VIC data.

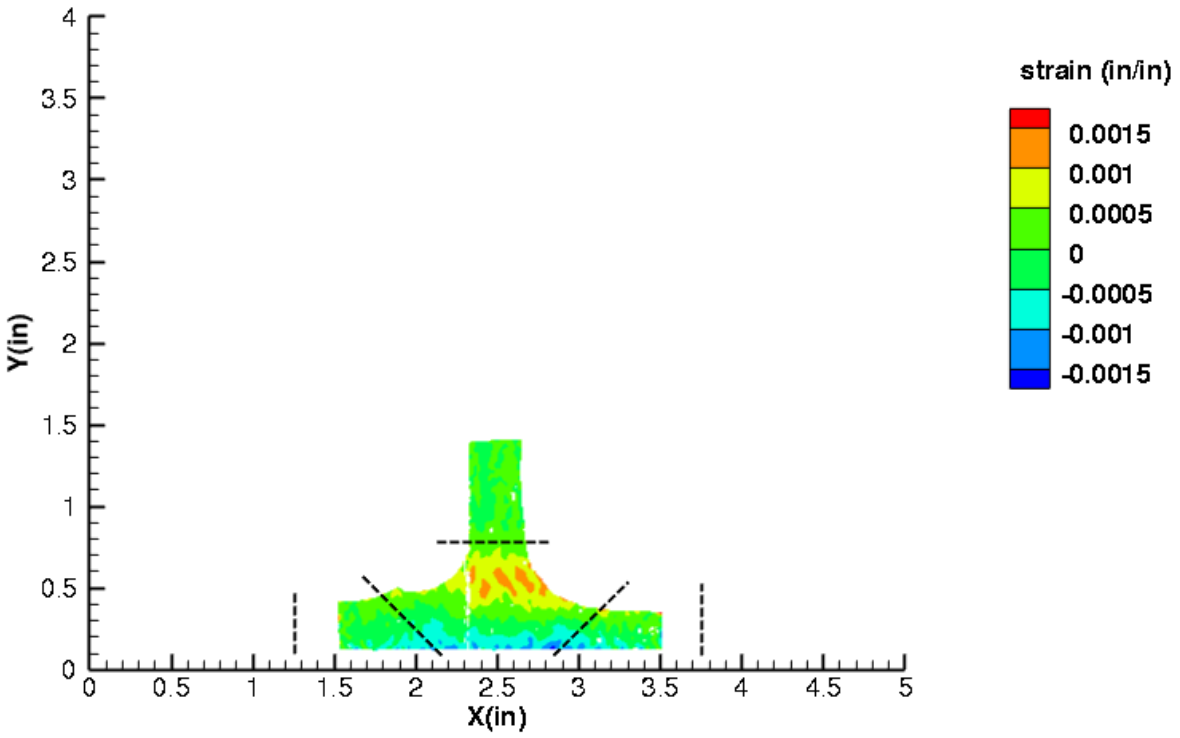

Figure C115. T1S1 strain contours for ε_{xx} at 3514 lb. load, prior to initial failure, local 5MP VIC data.

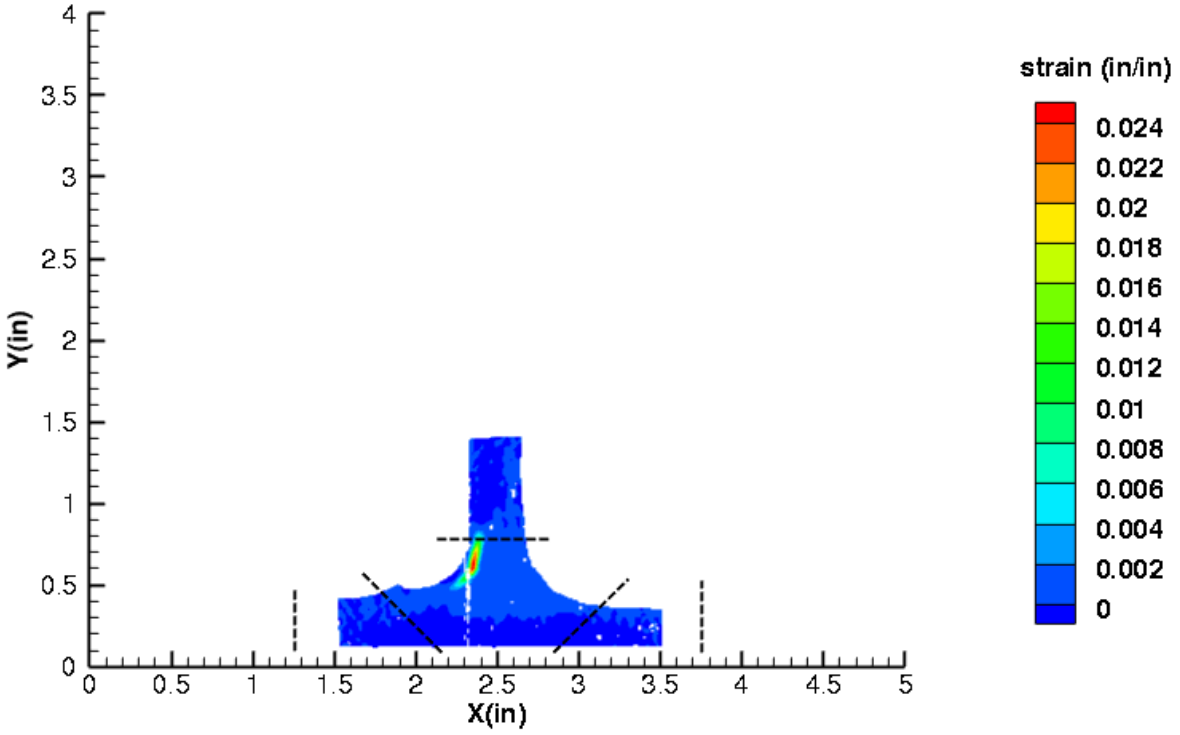

Figure C116. T1S1 strain contours for ε_{xx} at 3431 lb. load, just after initial failure, local 5MP VIC data.

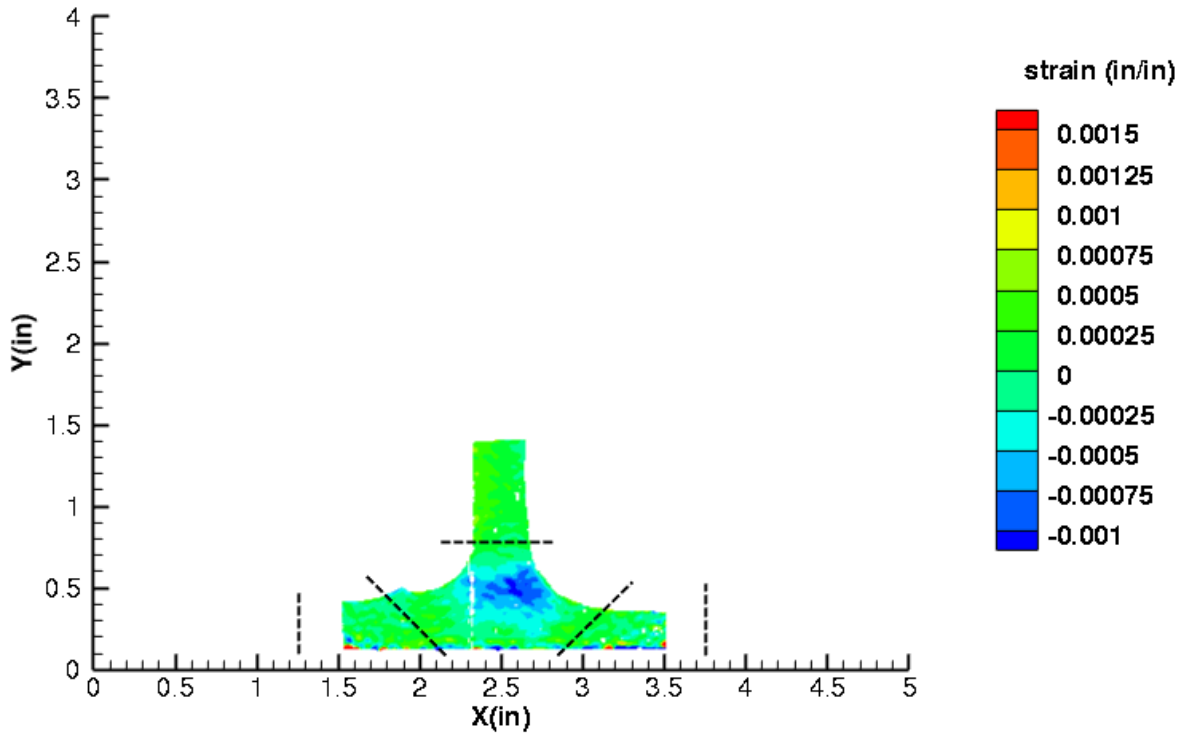

Figure C117. T1S1 strain contours for ε_{yy} at 3514 lb. load, prior to initial failure, local 5MP VIC data.

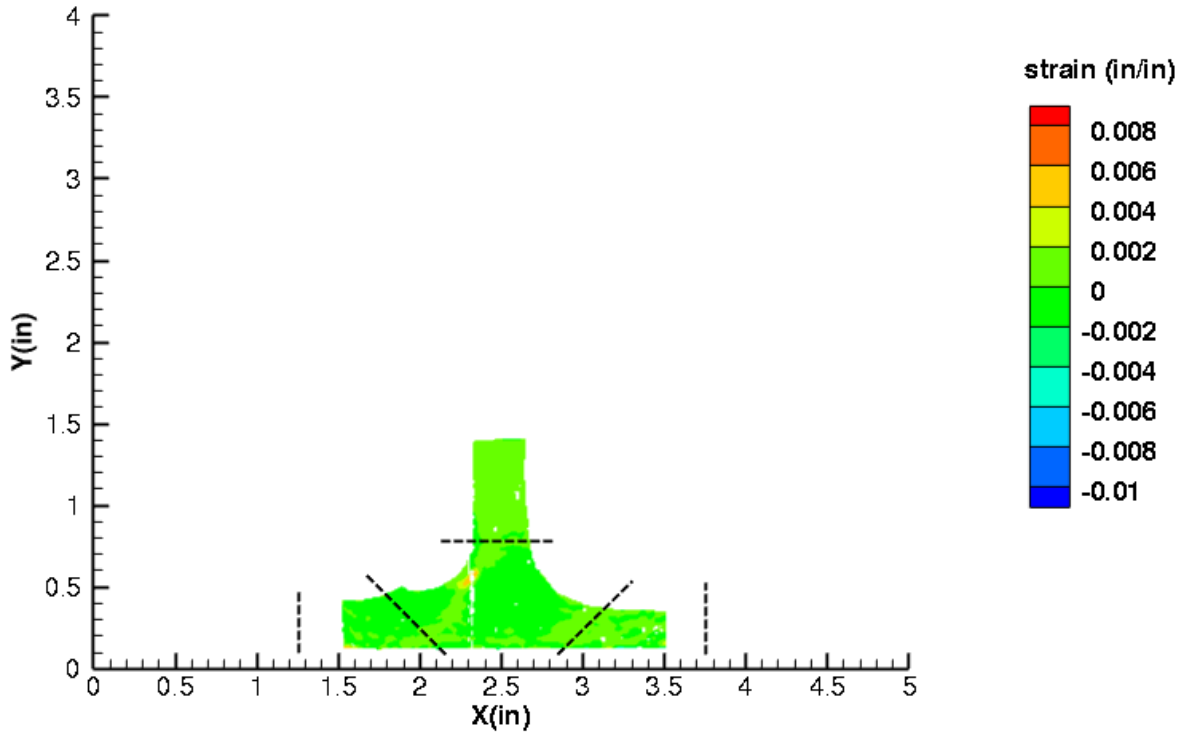

Figure C118. T1S1 strain contours for ε_{yy} at 3431 lb. load, just after initial failure, local 5MP VIC data.

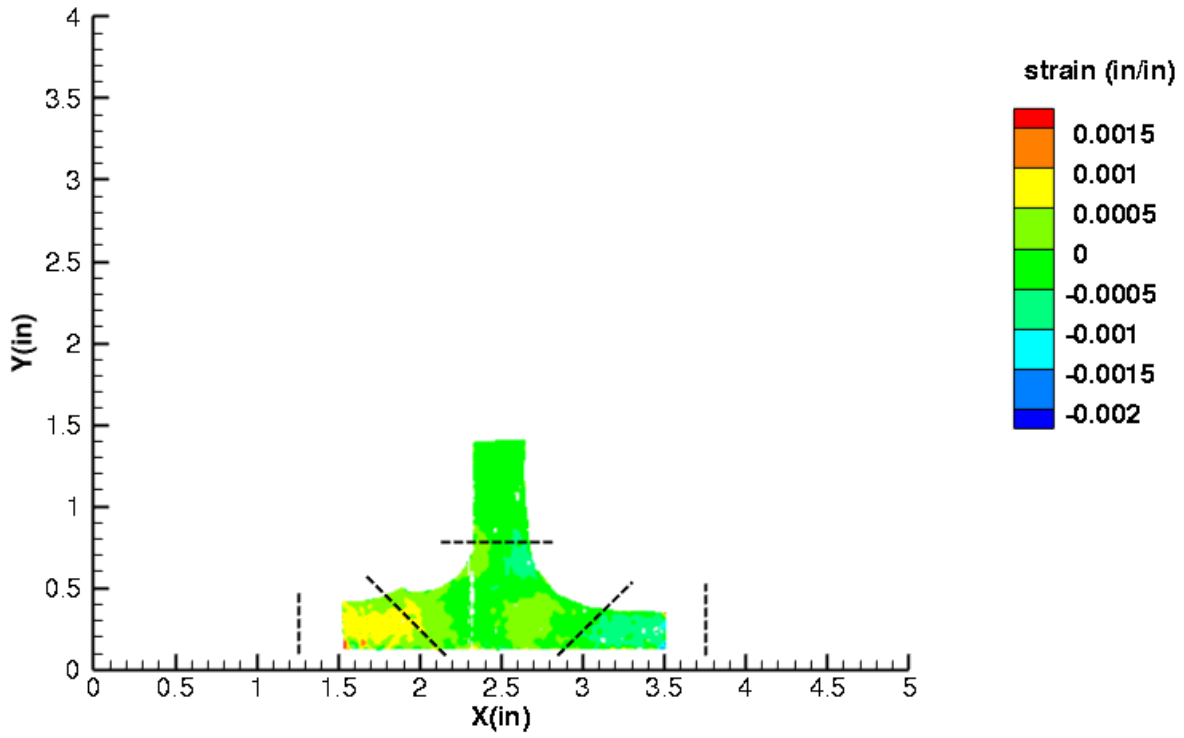

Figure C119. T1S1 strain contours for ε_{xy} at 3514 lb. load, prior to initial failure, local 5MP VIC data.

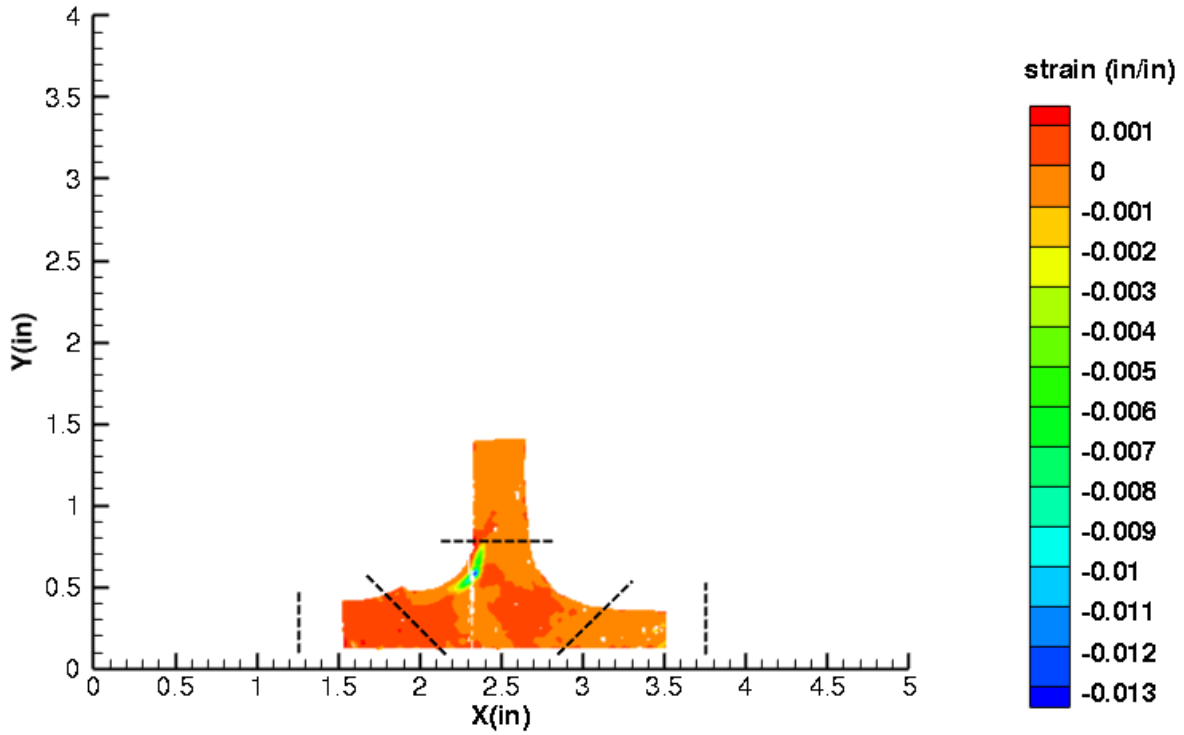

Figure C120. T1S1 strain contours for ε_{xy} at 3431 lb. load, just after initial failure, local 5MP VIC data.

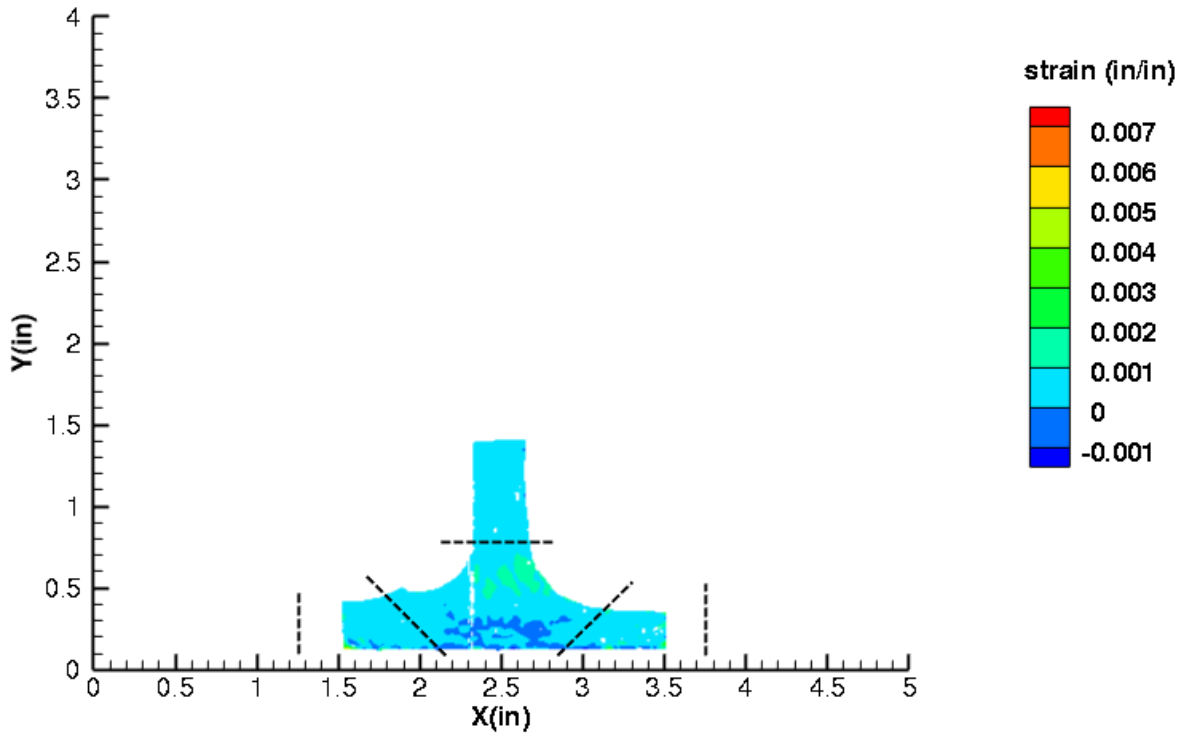

Figure C121. T1S1 strain contours for maximum principal strain at 3514 lb. load, prior to initial failure, local 5MP VIC data.

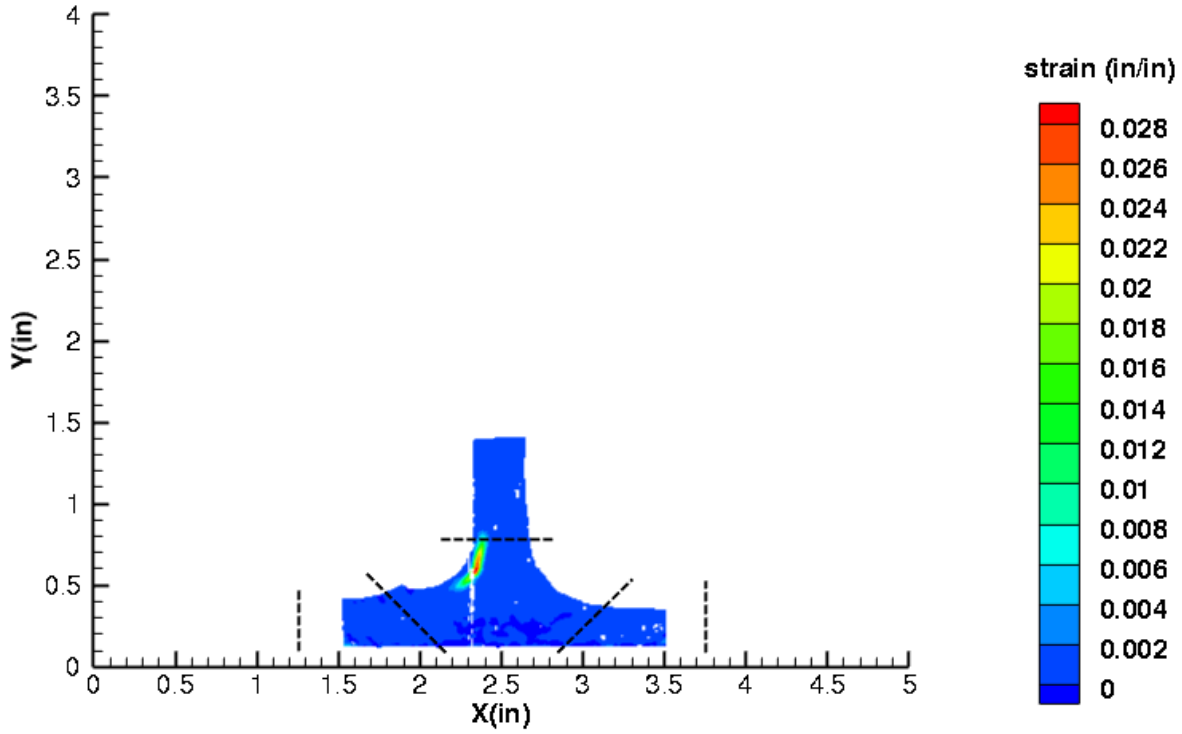

Figure C122. T1S1 strain contours for maximum principal strain at 3431 lb. load, just after initial failure, local 5MP VIC data.

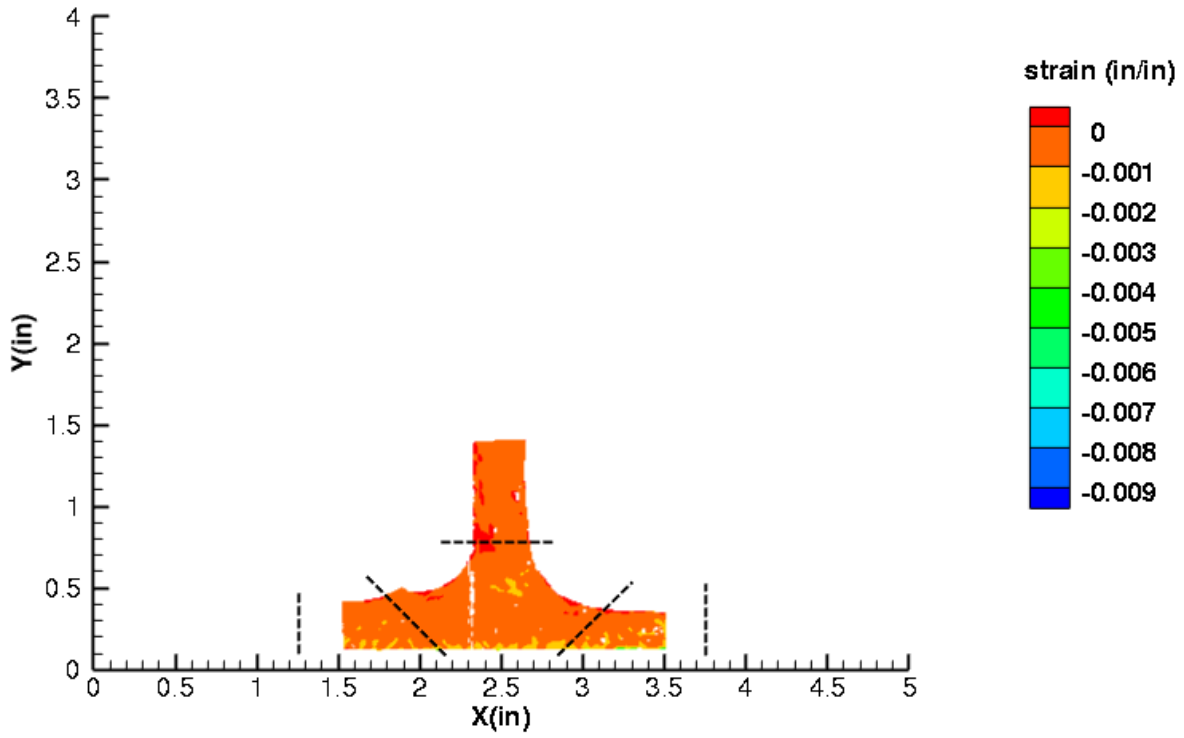

Figure C123. T1S1 strain contours for minimum principal strain at 3514 lb. load, prior to initial failure, local 5MP VIC data.

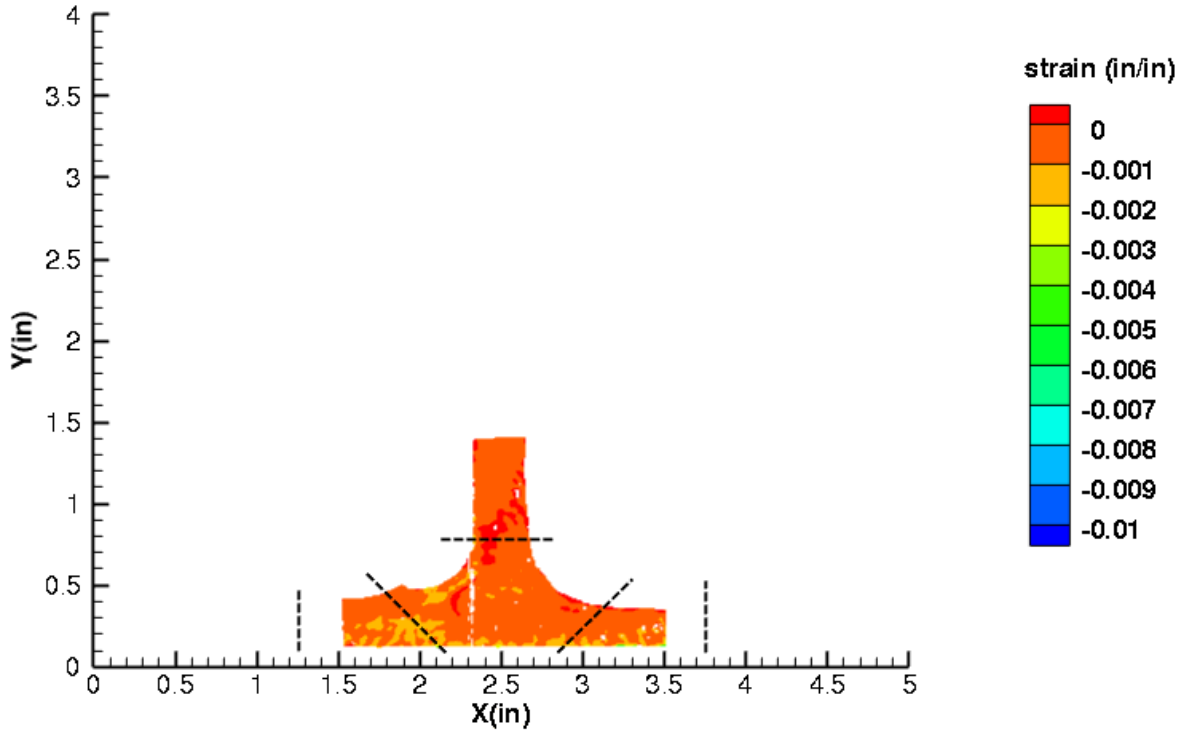

Figure C124. T1S1 strain contours for minimum principal strain at 3431 lb. load, just after initial failure, local 5MP VIC data.

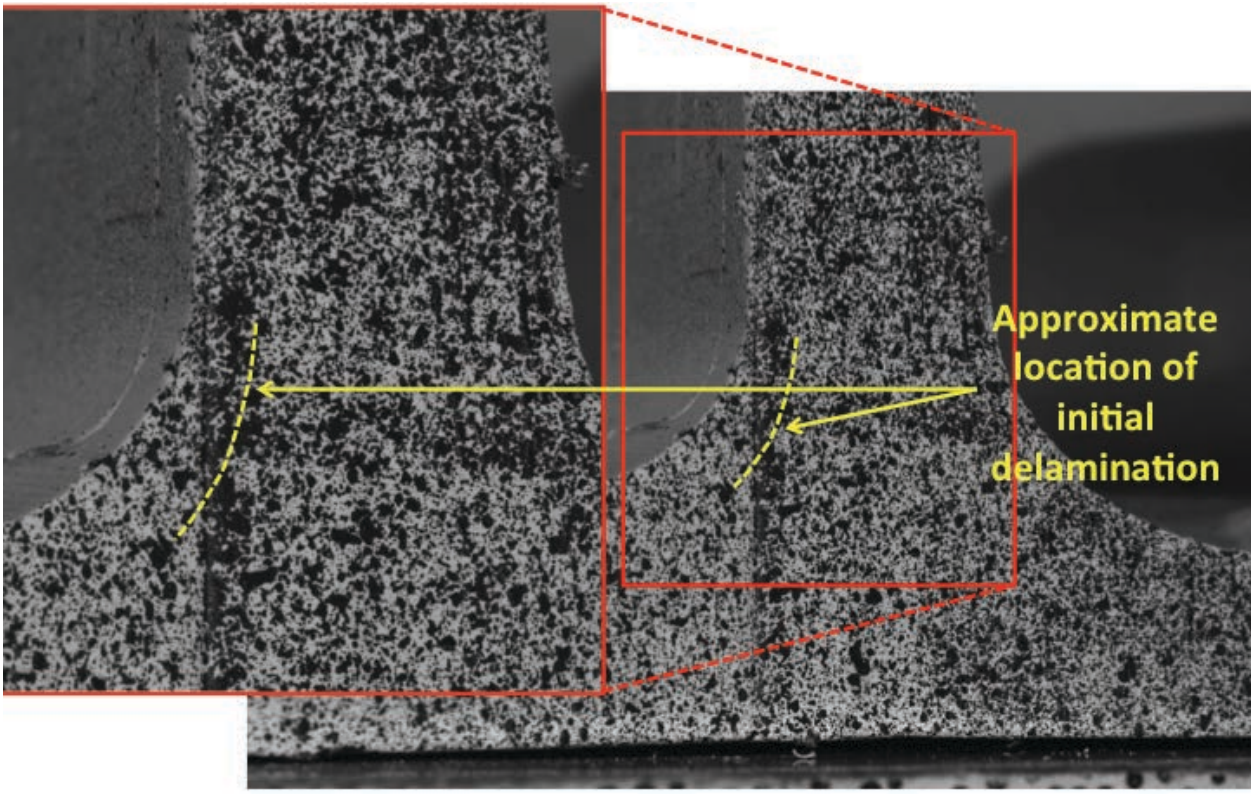

Figure C125. T1S1 image just after initial failure, local 5MP VIC data.

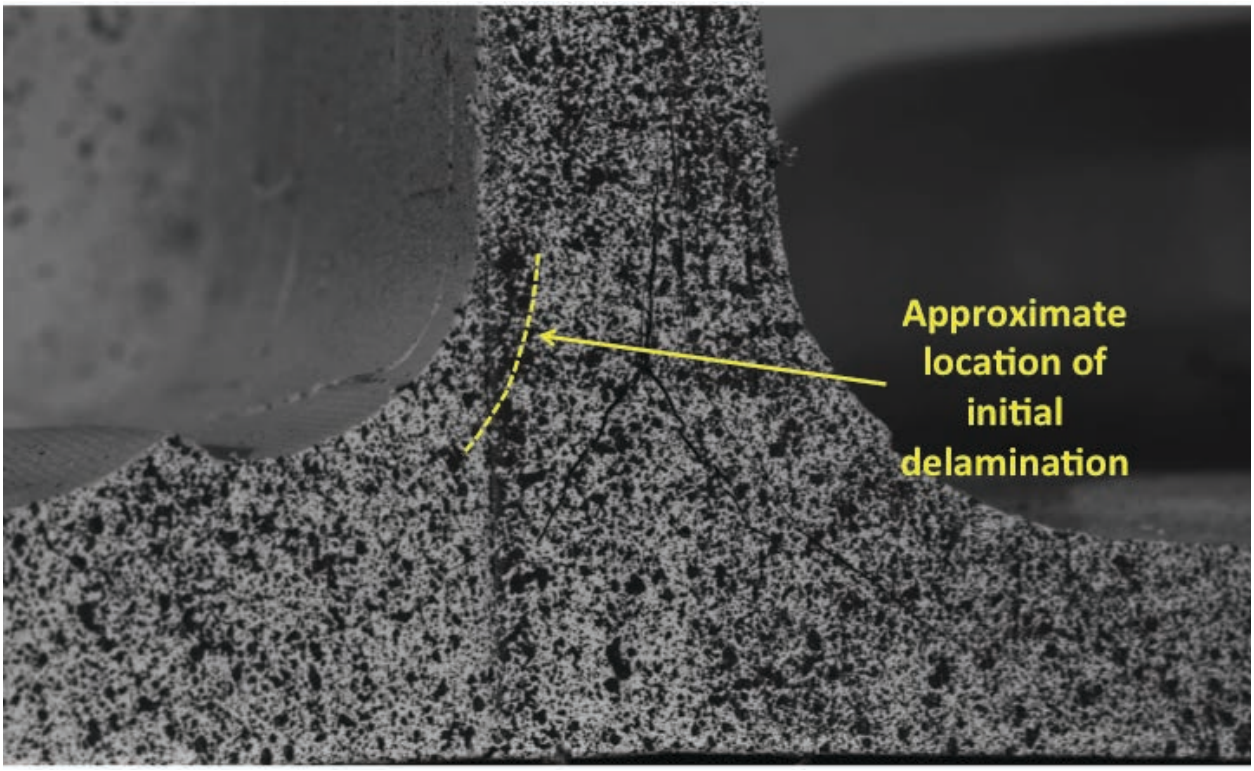

Figure C126. T1S1 image just after maximum load, local 5MP VIC data.

T1S2

This section presents the test data for the T1S2 test article.

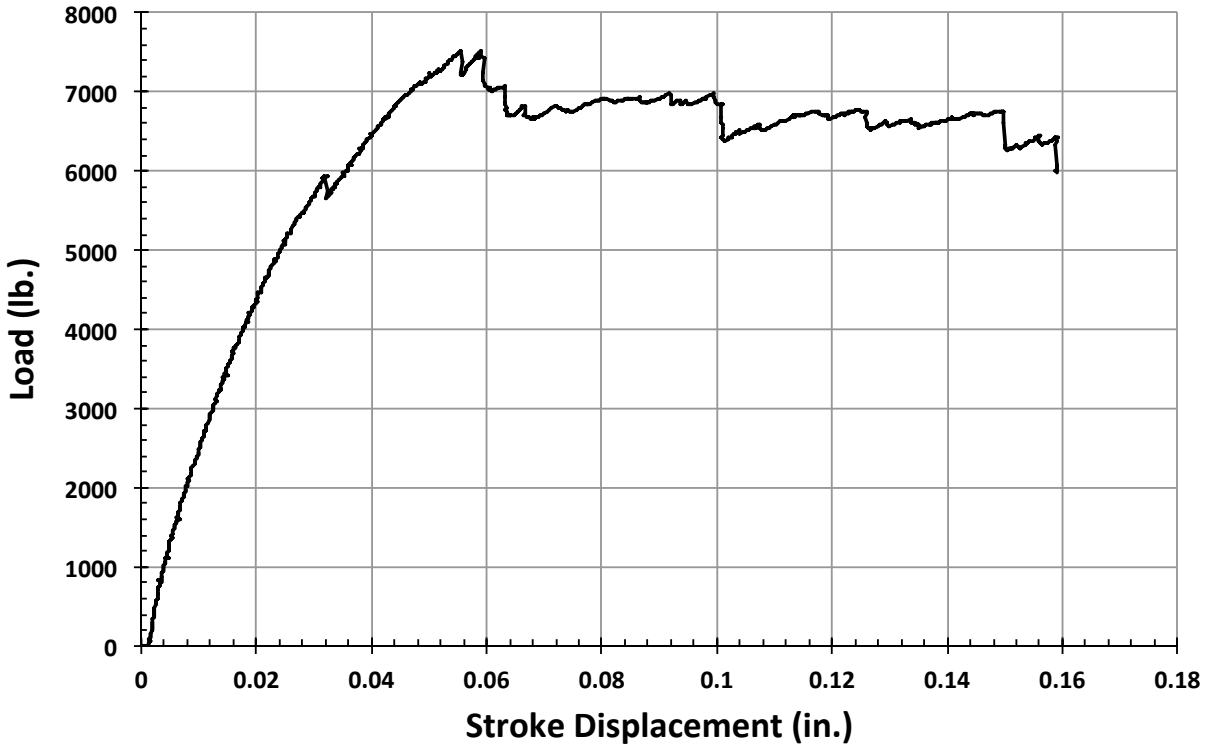

Figure C127. T1S2 load vs. stroke.

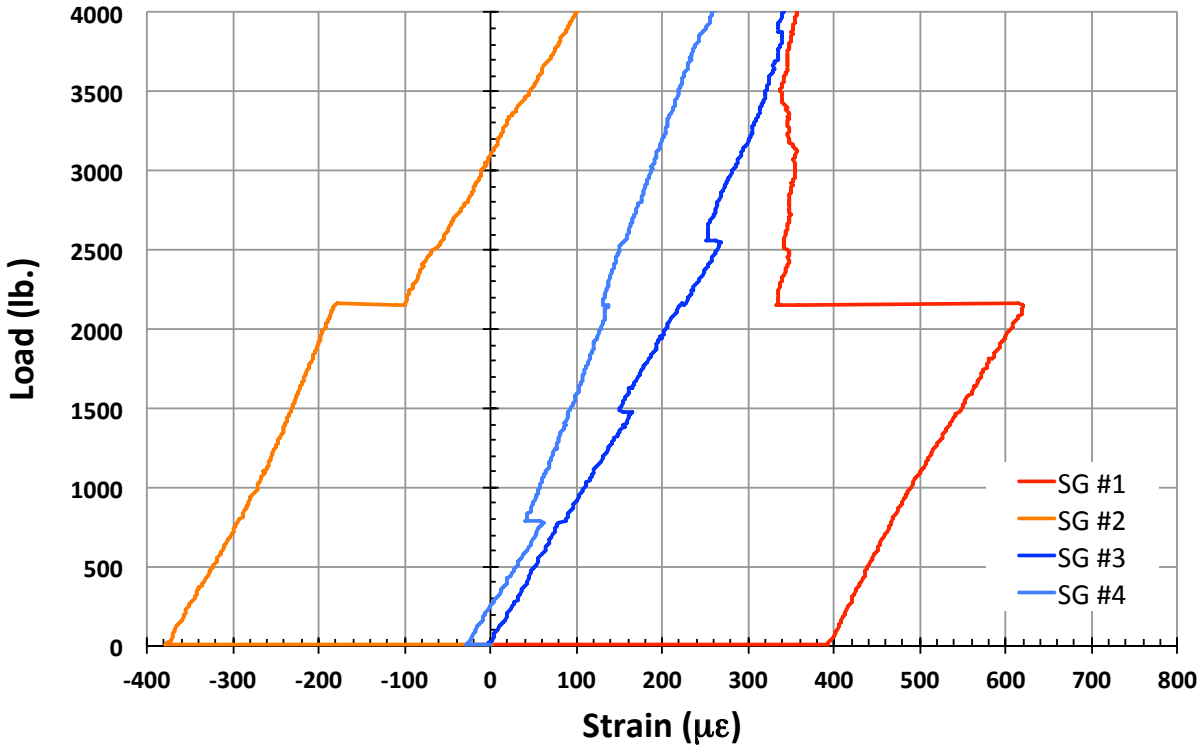

Figure C128. T1S2 load vs. strain, initial loading.

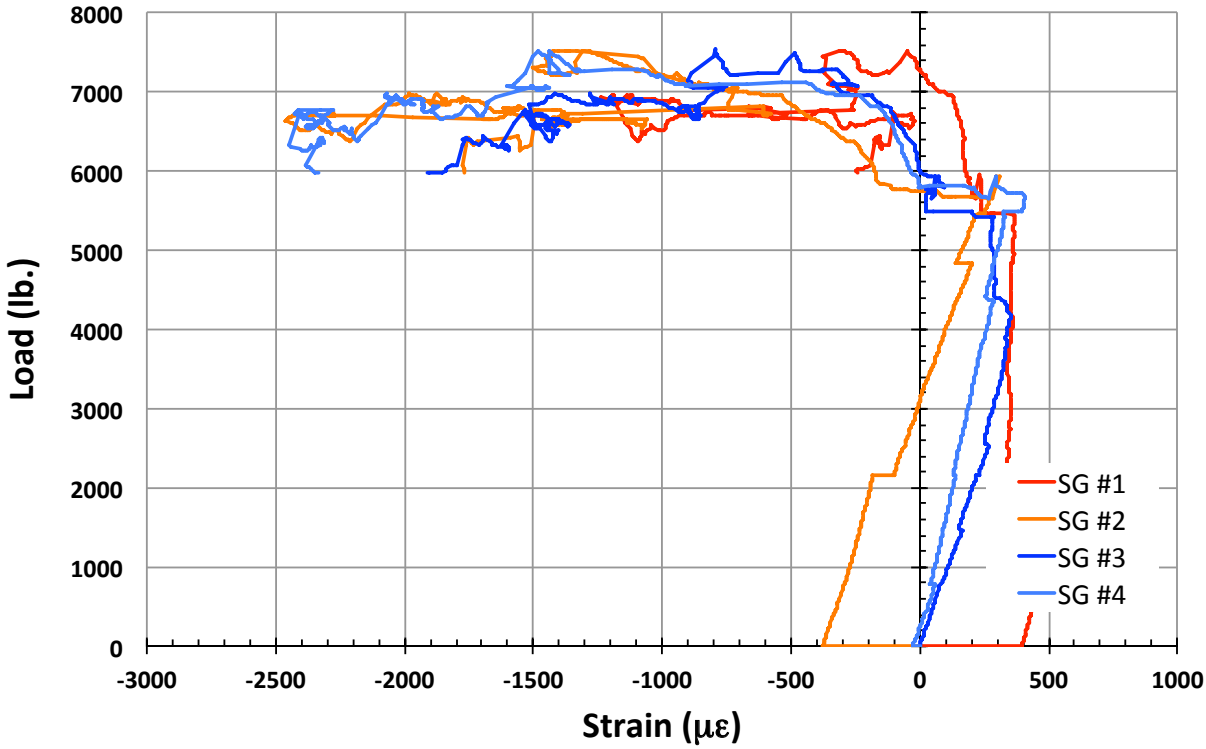

Figure C129. T1S2 load vs. strain.

T1S3

This section presents the test data for the T1S3 test article.

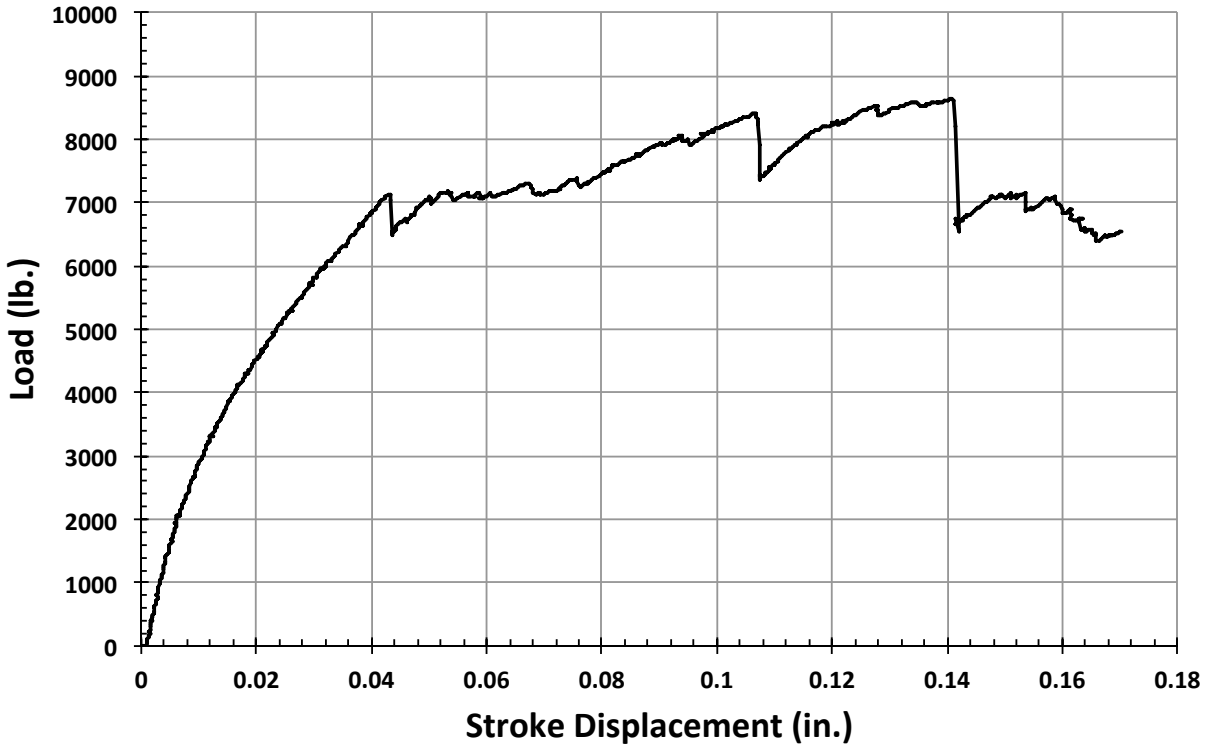

Figure C130. T1S3 load vs. stroke.

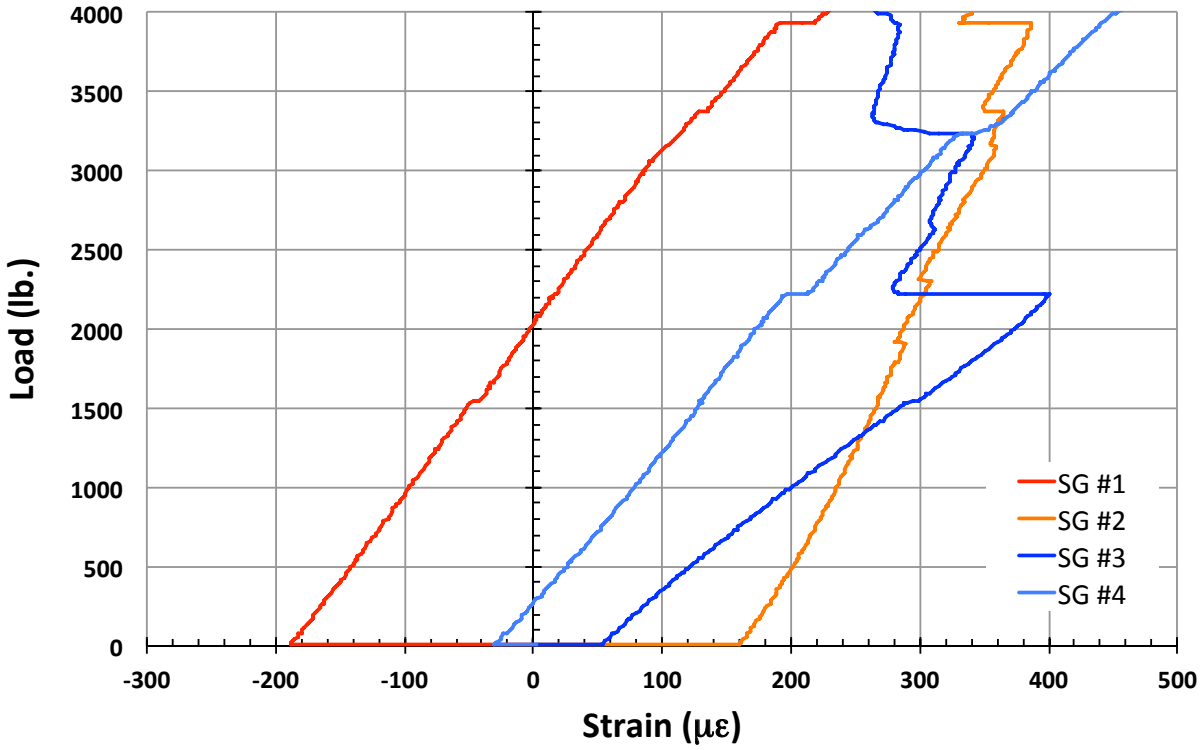

Figure C131. T1S3 load vs. strain, initial loading.

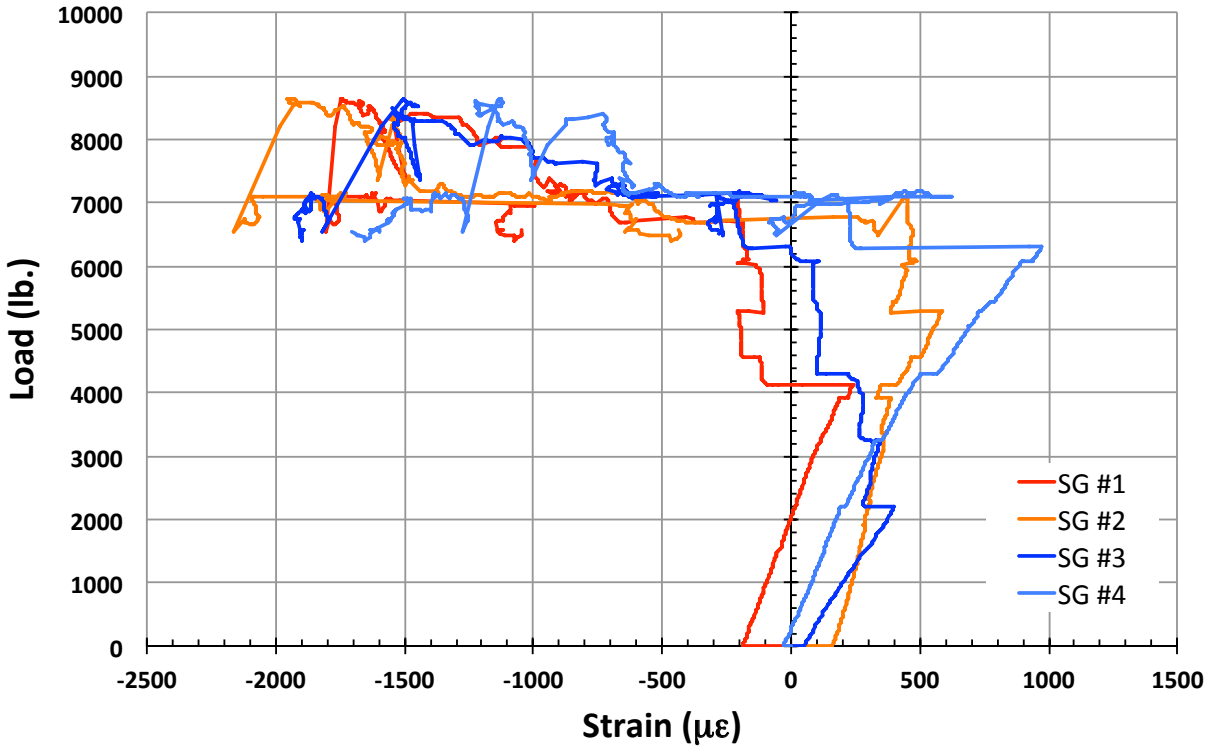

Figure C132. T1S3 load vs. strain.

T1N1

This section presents the test data for the T1N1 test article.

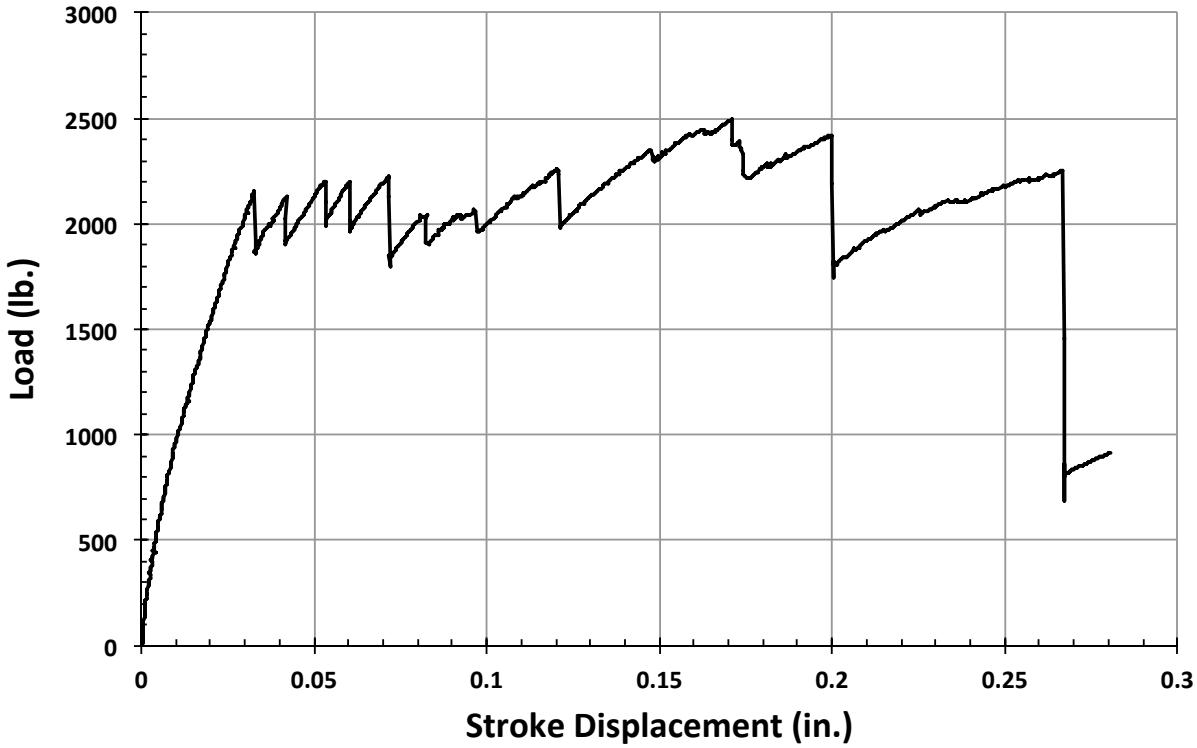

Figure C133. T1N1 load vs. stroke.

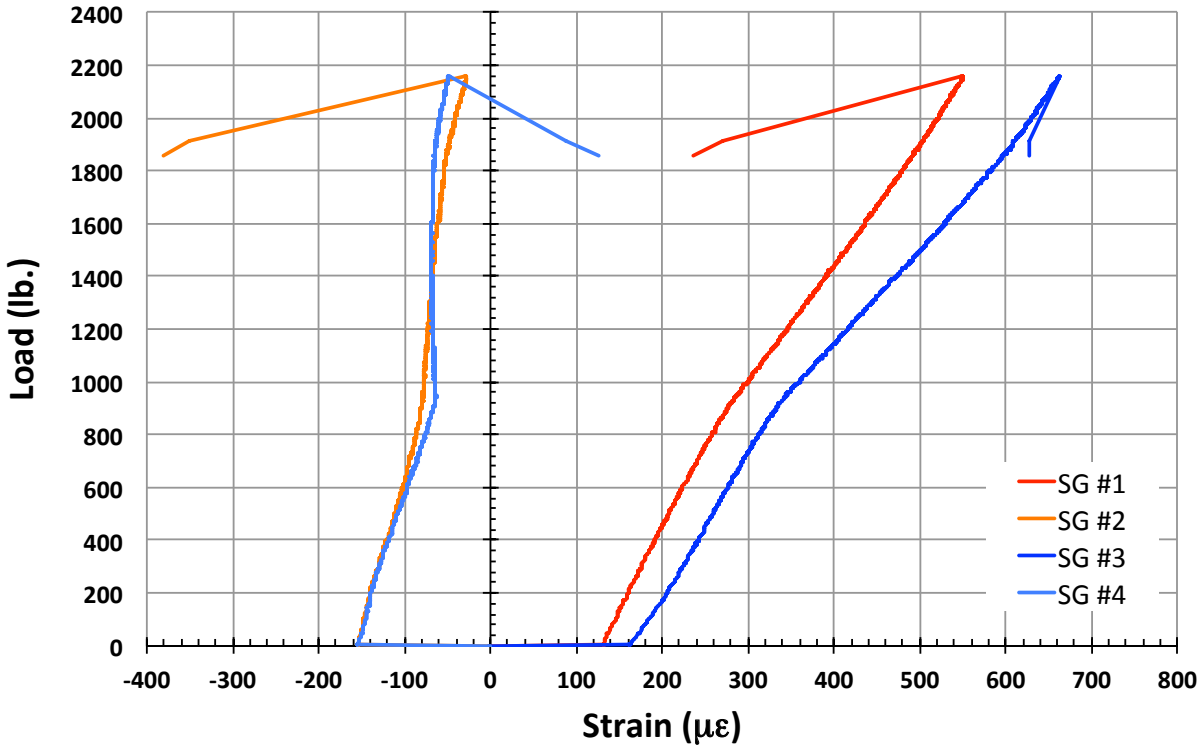

Figure C134. T1N1 load vs. strain, initial loading.

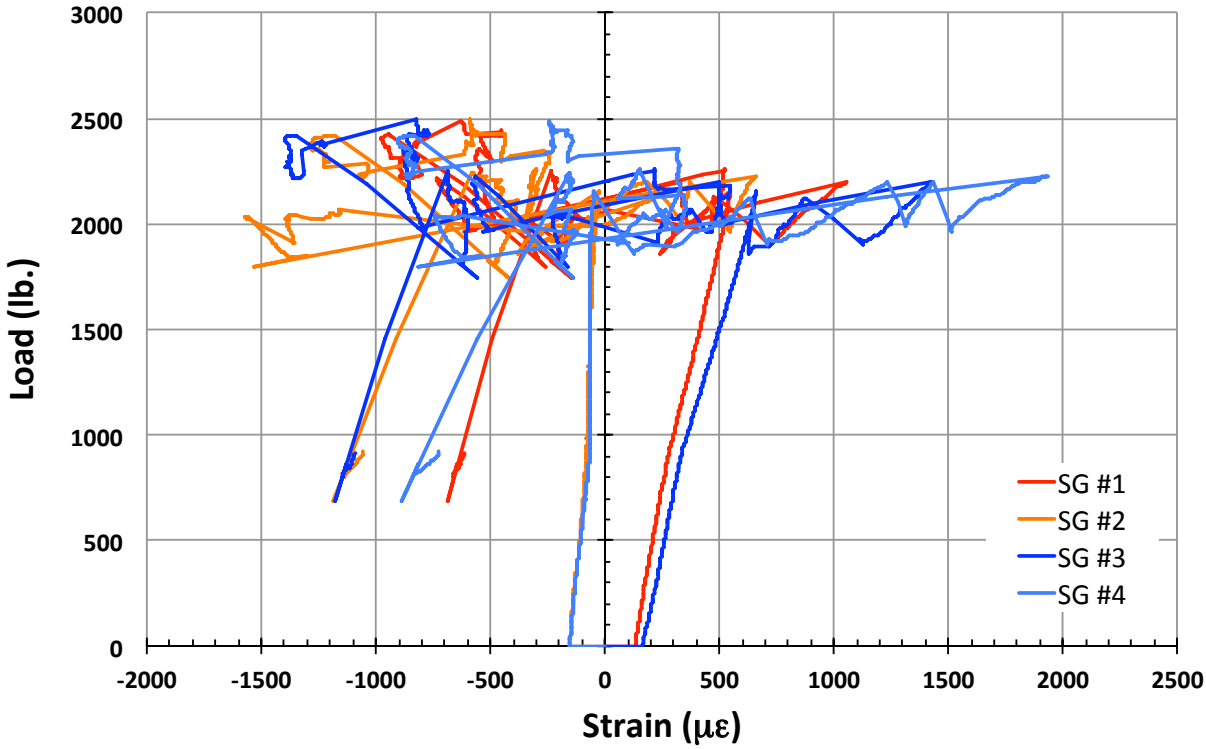

Figure C135. T1N1 load vs. strain.

T1N2

This section presents the test data for the T1N2 test article, and includes strain plots and failure images.

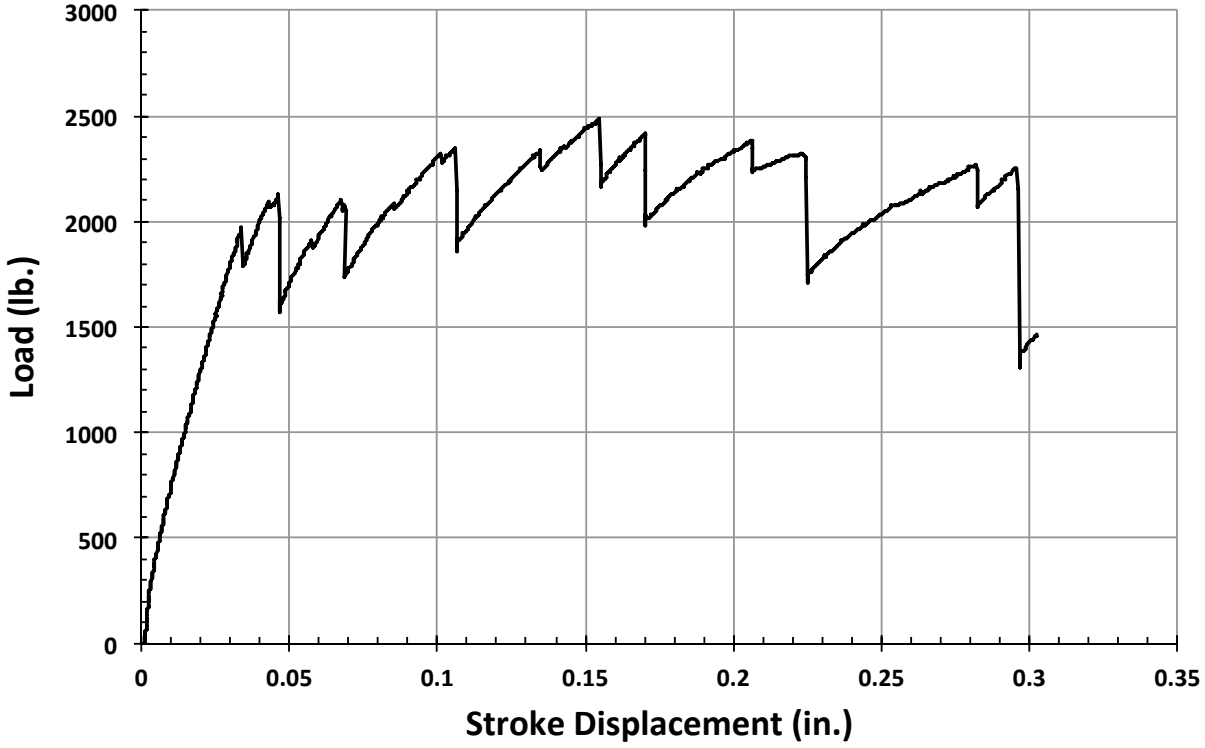

Figure C136. T1N2 load vs. stroke.

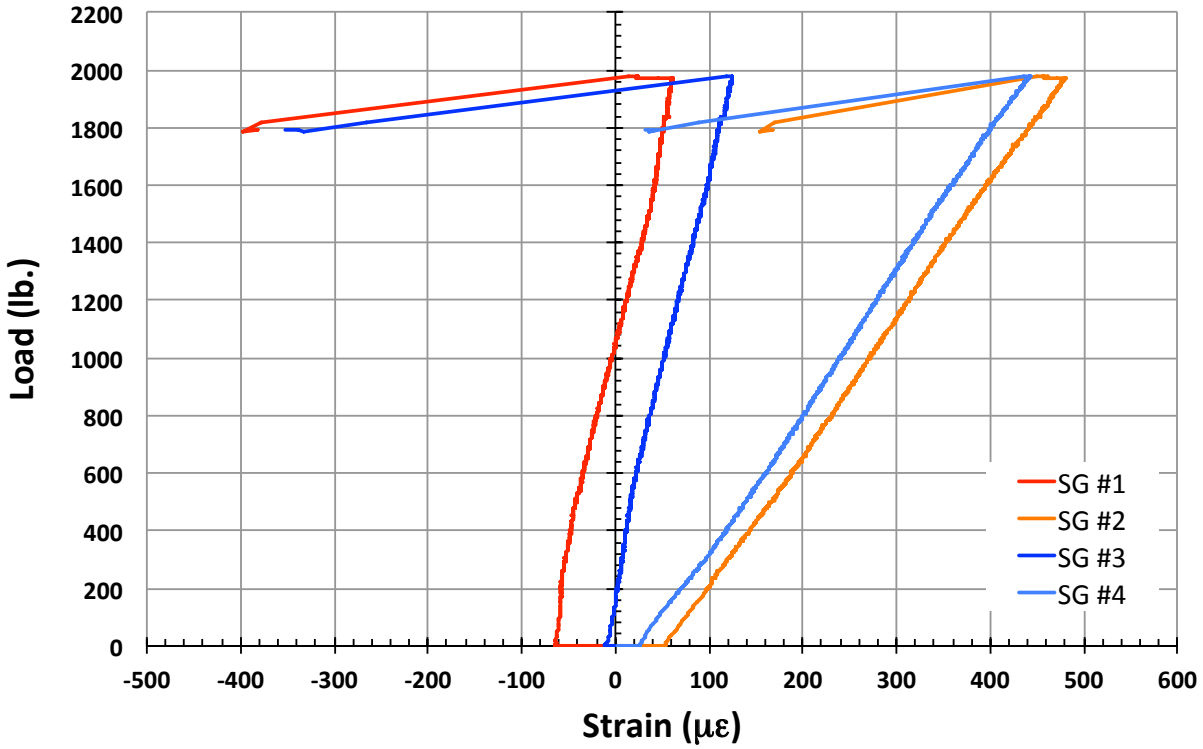

Figure C137. T1N2 load vs. strain, initial loading.

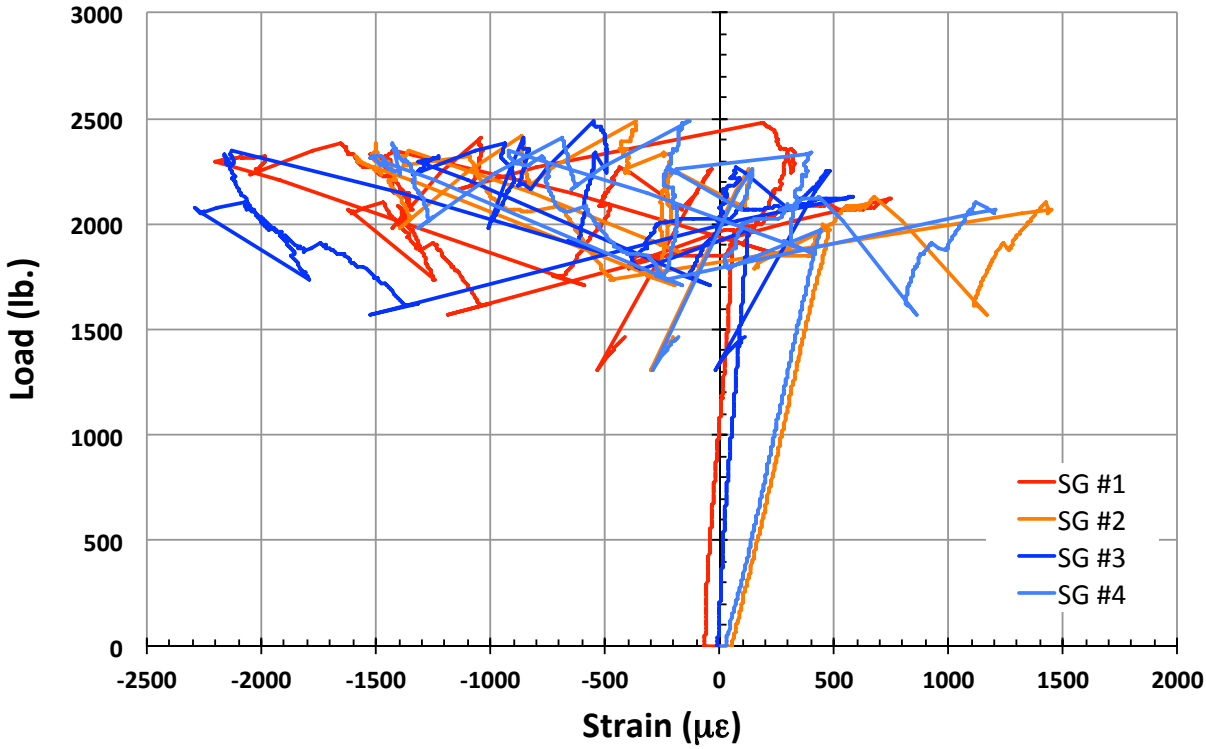

Figure C138. T1N2 load vs. strain.

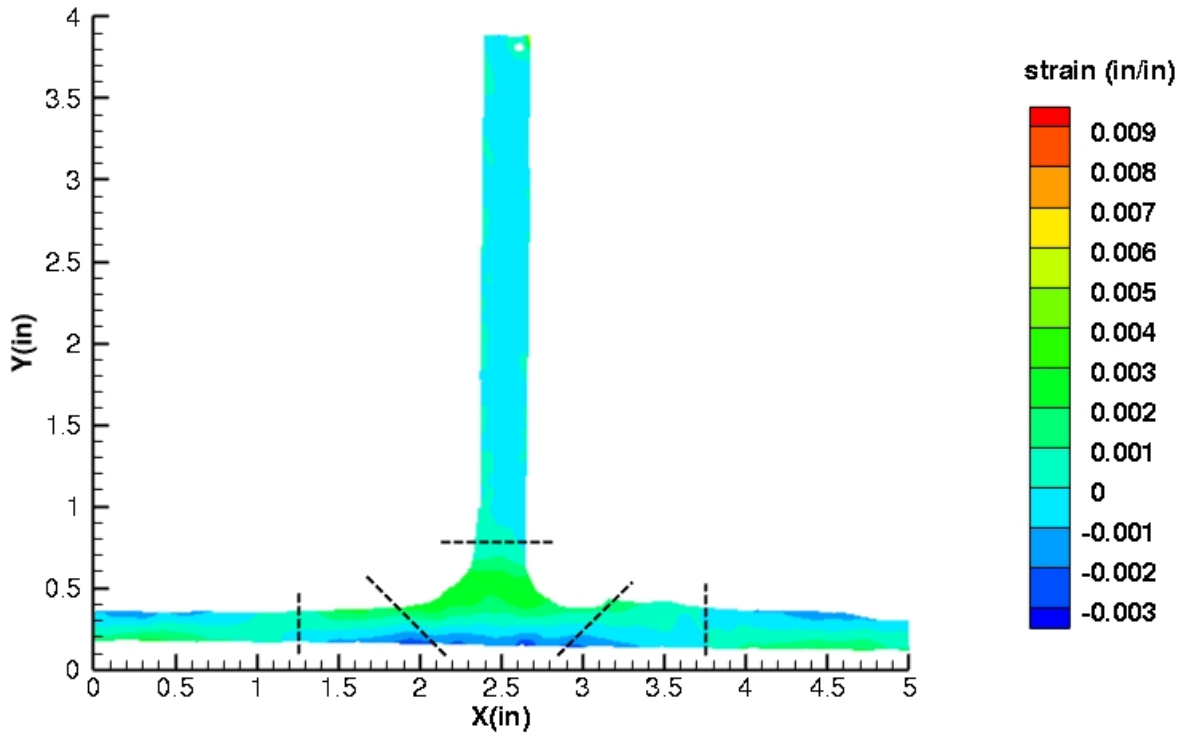

Figure C139. T1N2 strain contours for ε_{xx} at 1978 lb. load, prior to initial failure, 29MP VIC data.

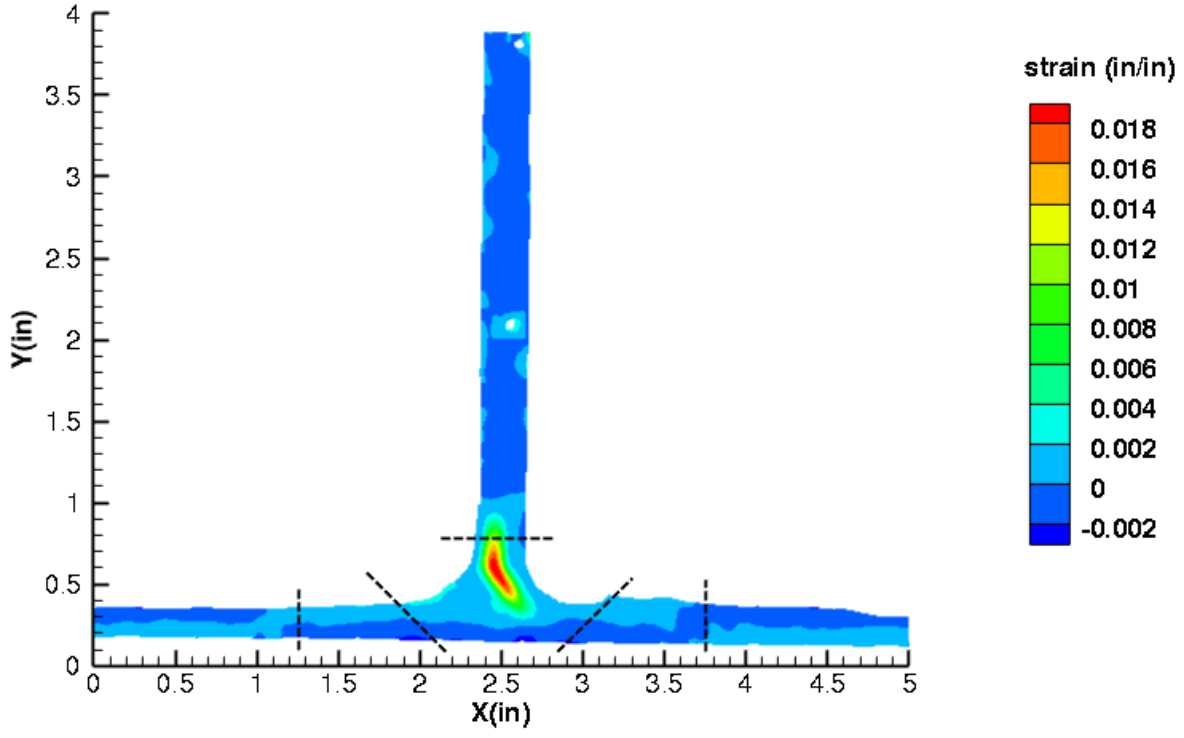

Figure C140. T1N2 strain contours for ε_{xx} at 1808 lb. load, just after initial failure, 29MP VIC data.

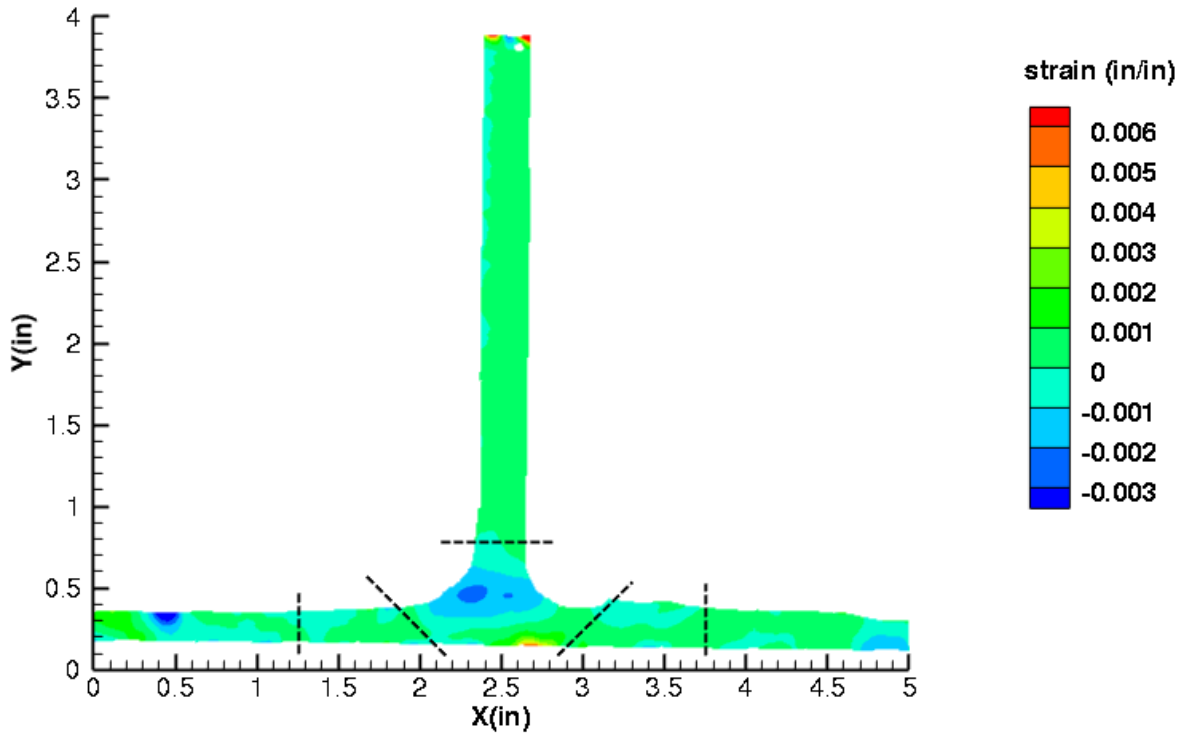

Figure C141. T1N2 strain contours for ε_{yy} at 1978 lb. load, prior to initial failure, 29MP VIC data.

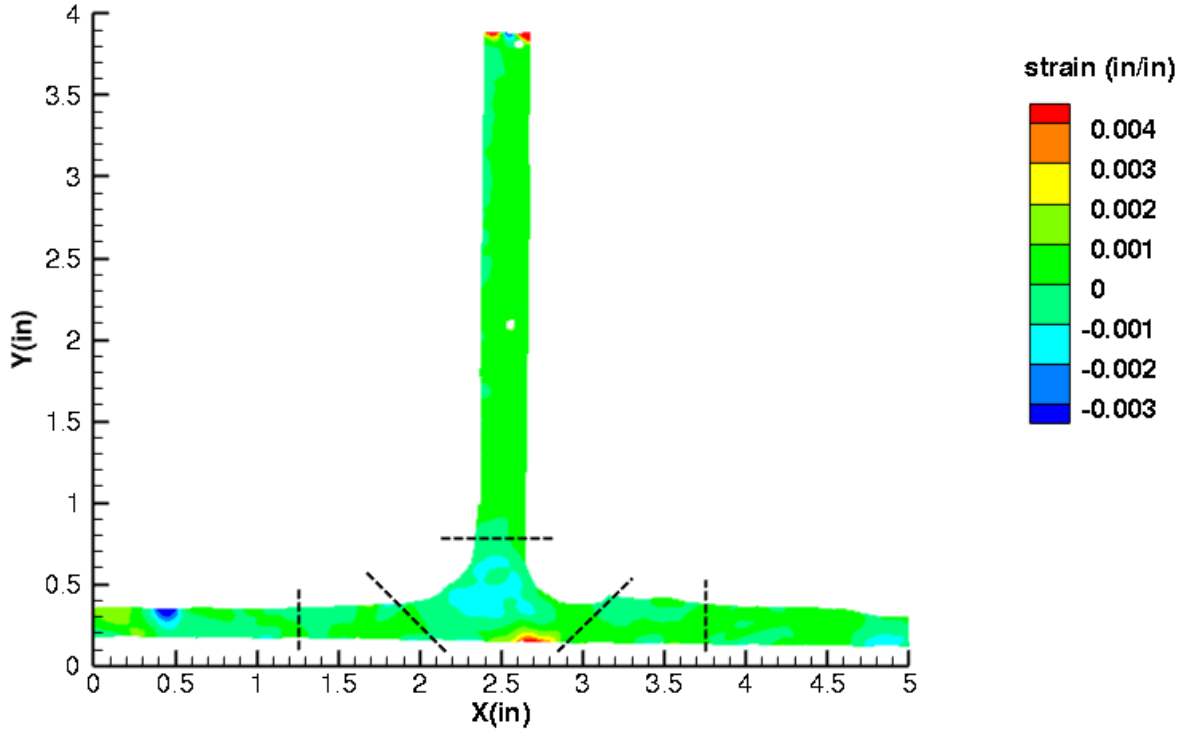

Figure C142. T1N2 strain contours for ε_{yy} at 1808 lb. load, just after initial failure, 29MP VIC data.

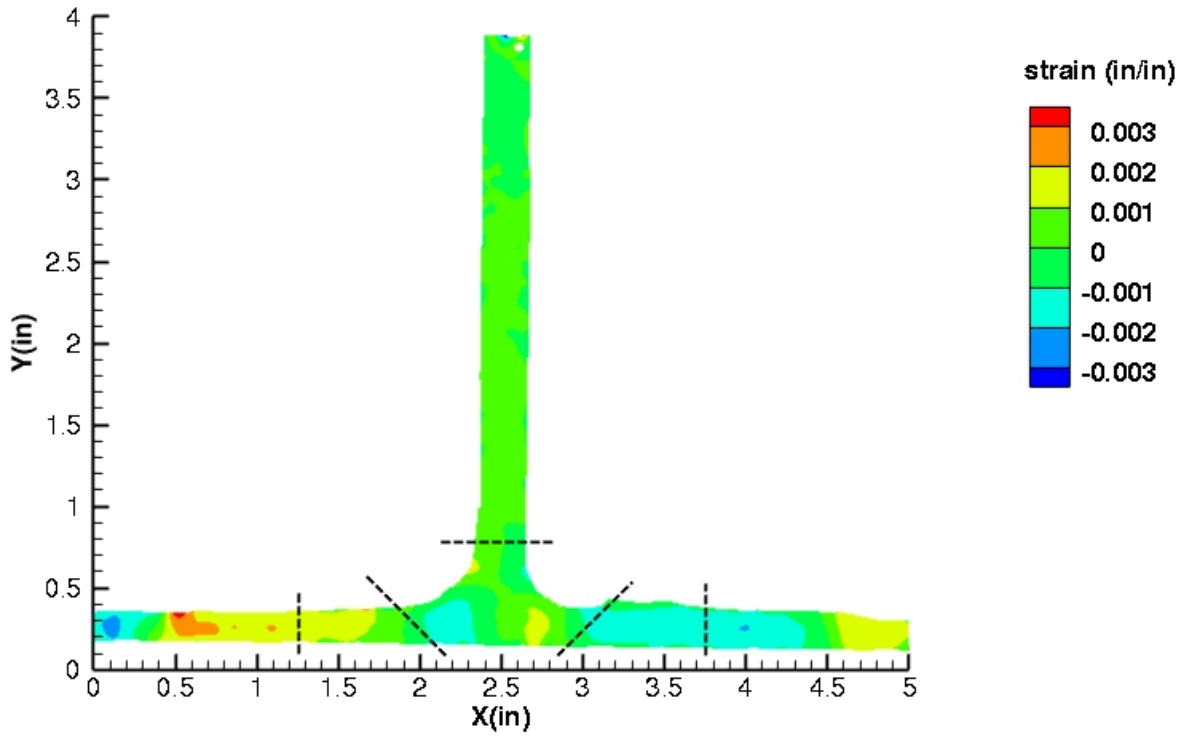

Figure C143. T1N2 strain contours for ε_{xy} at 1978 lb. load, prior to initial failure, 29MP VIC data.

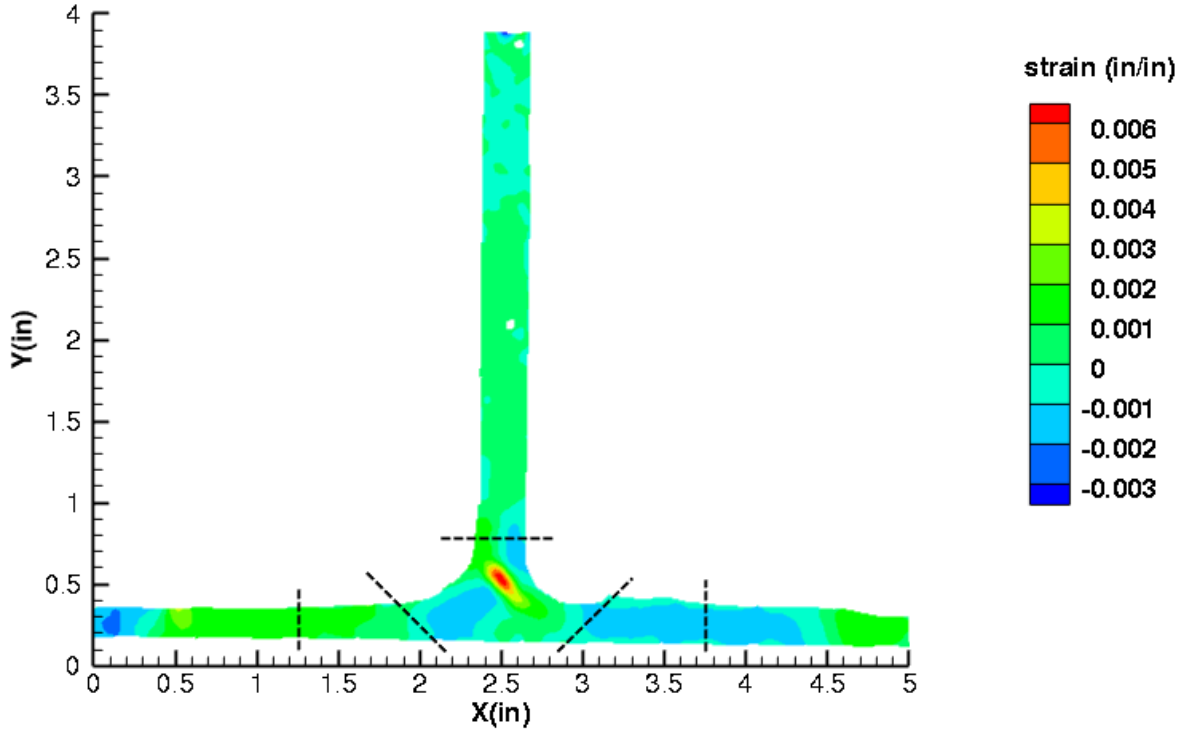

Figure C144. T1N2 strain contours for ε_{xy} at 1808 lb. load, just after initial failure, 29MP VIC data.

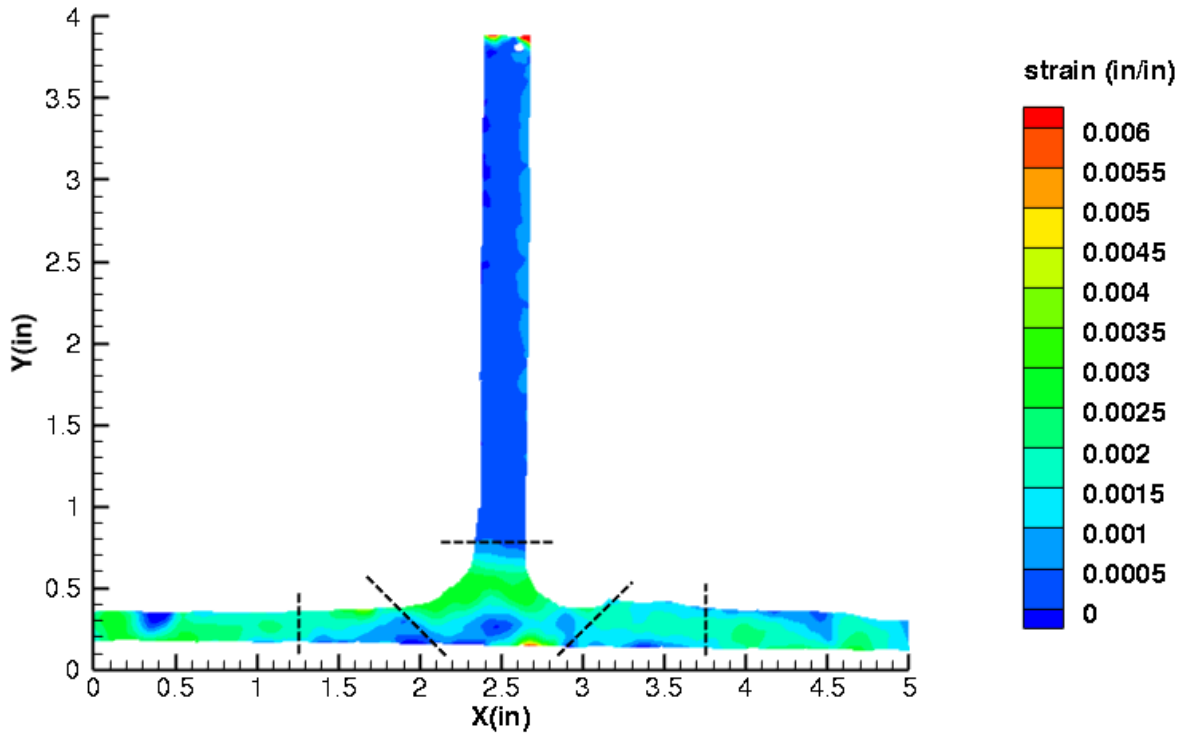

Figure C145. T1N2 strain contours for maximum principal strain at 1978 lb. load, prior to initial failure, 29MP VIC data.

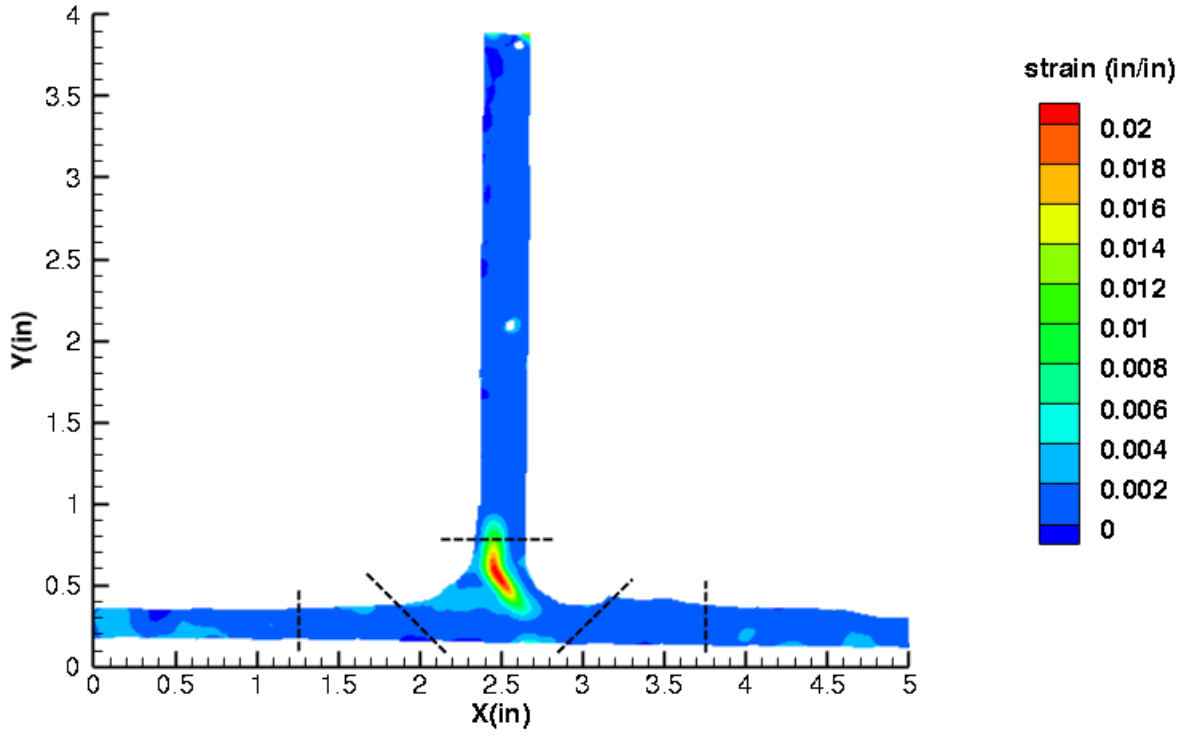

Figure C146. T1N2 strain contours for maximum principal strain at 1808 lb. load, just after initial failure, 29MP VIC data.

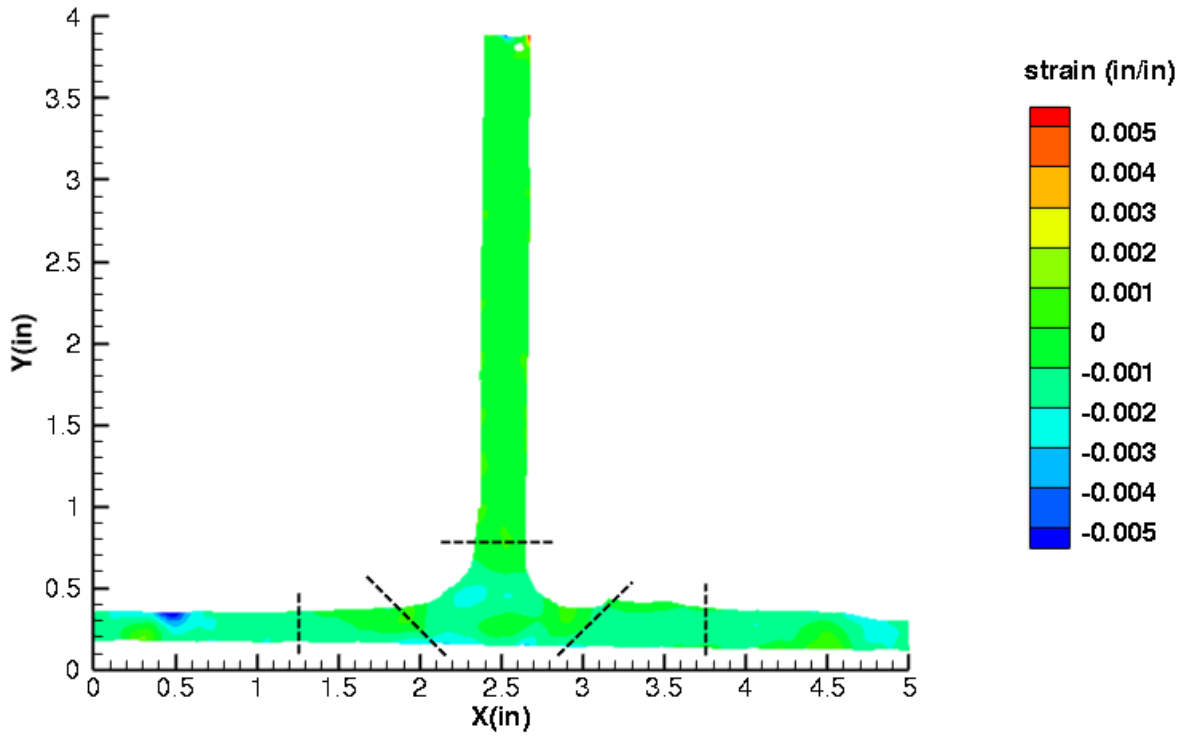

Figure C147. T1N2 strain contours for minimum principal strain at 1978 lb. load, prior to initial failure, 29MP VIC data.

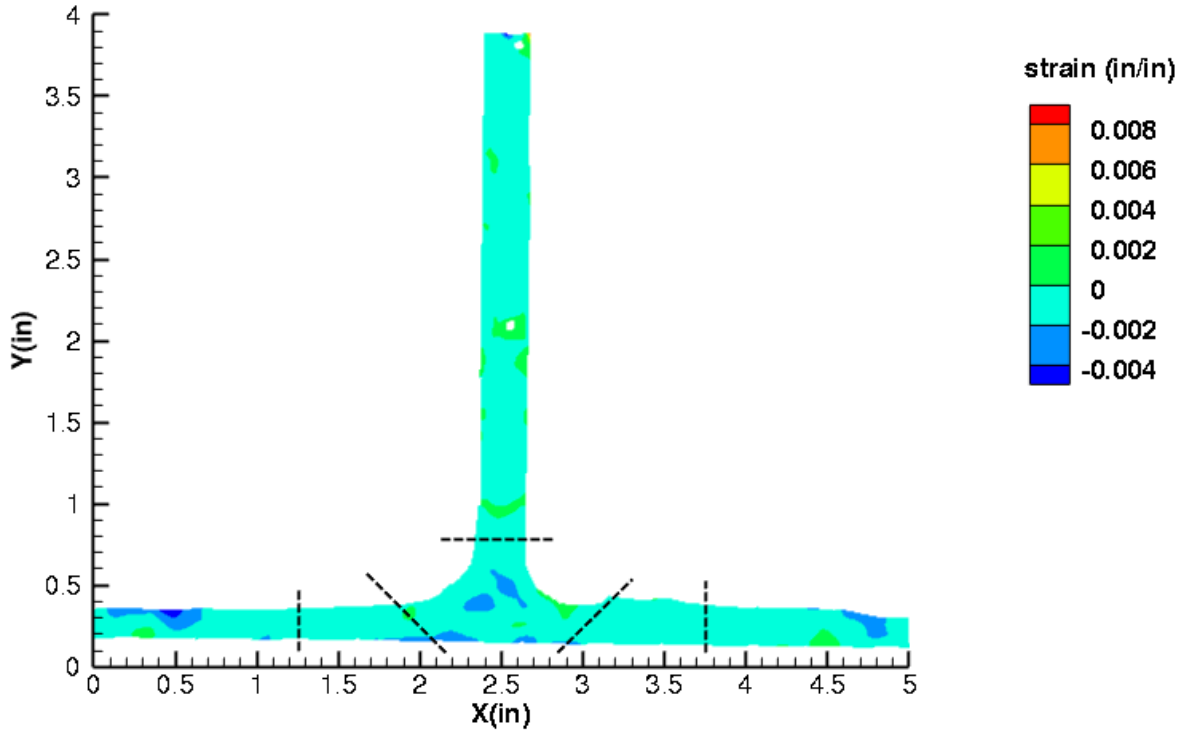

Figure C148. T1N2 strain contours for minimum principal strain at 1808 lb. load, just after initial failure, 29MP VIC data.

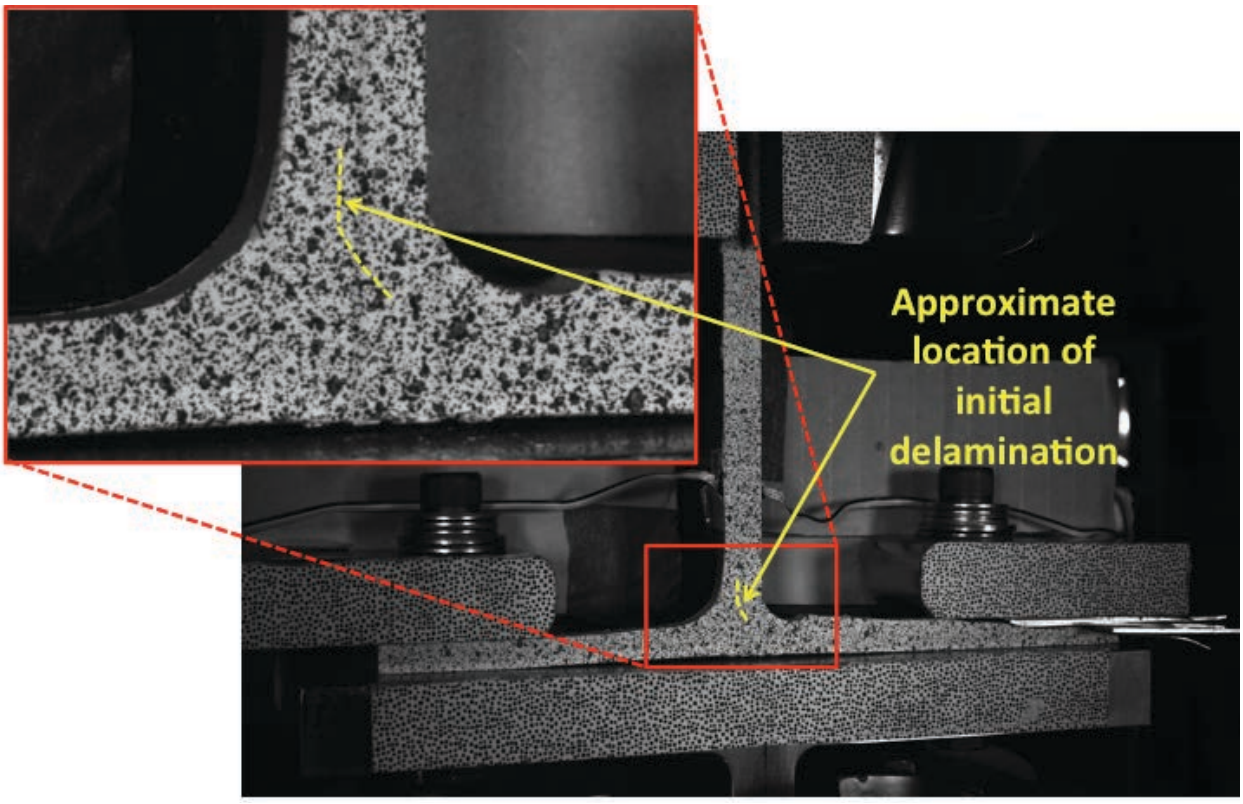

Figure C149. T1N2 image just after initial failure, 29MP VIC data.

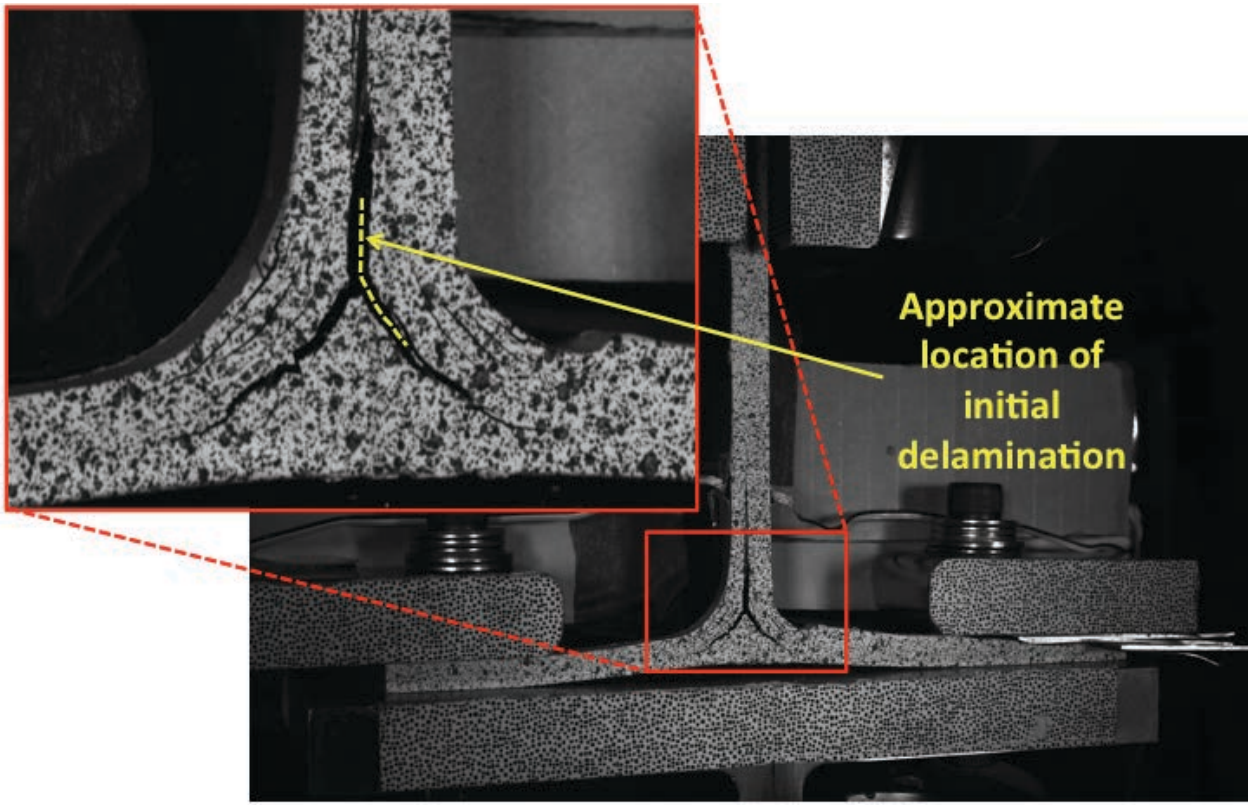

Figure C150. T1N2 image just after maximum load, 29MP VIC data.

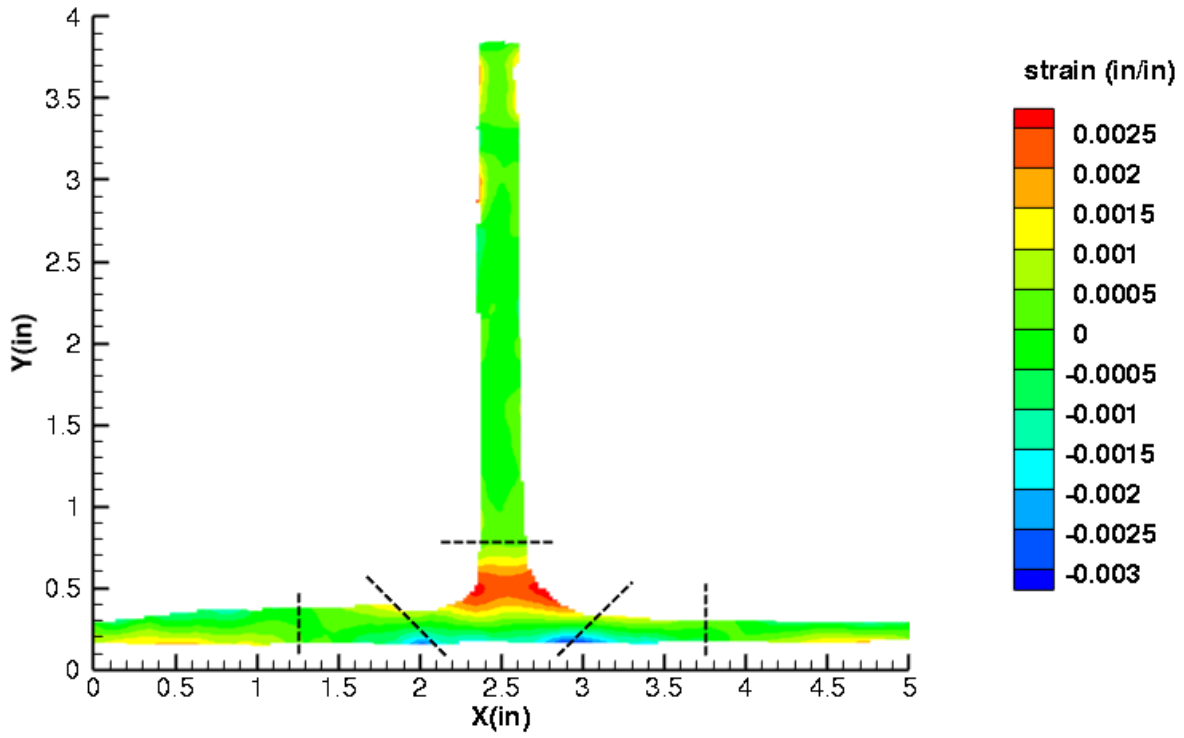

Figure C151. T1N2 strain contours for ε_{xx} at 1978 lb. load, prior to initial failure, 5MP VIC data.

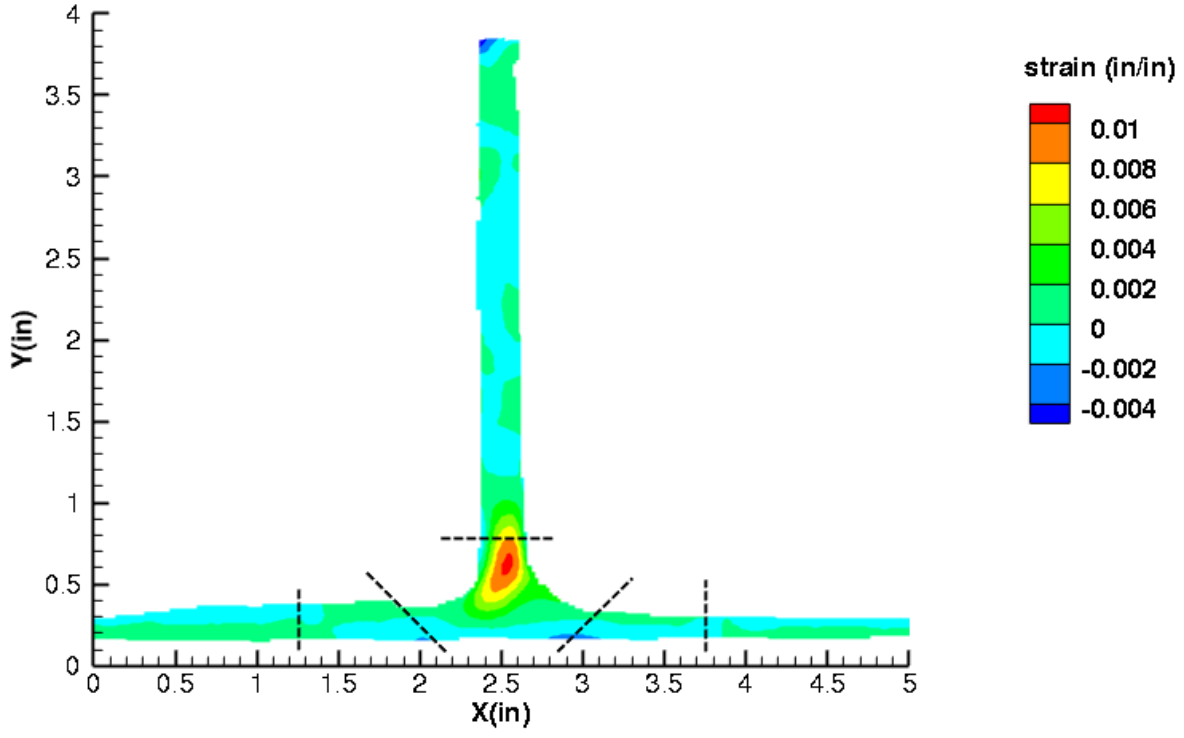

Figure C152. T1N2 strain contours for ε_{xx} at 1808 lb. load, just after initial failure, 5MP VIC data.

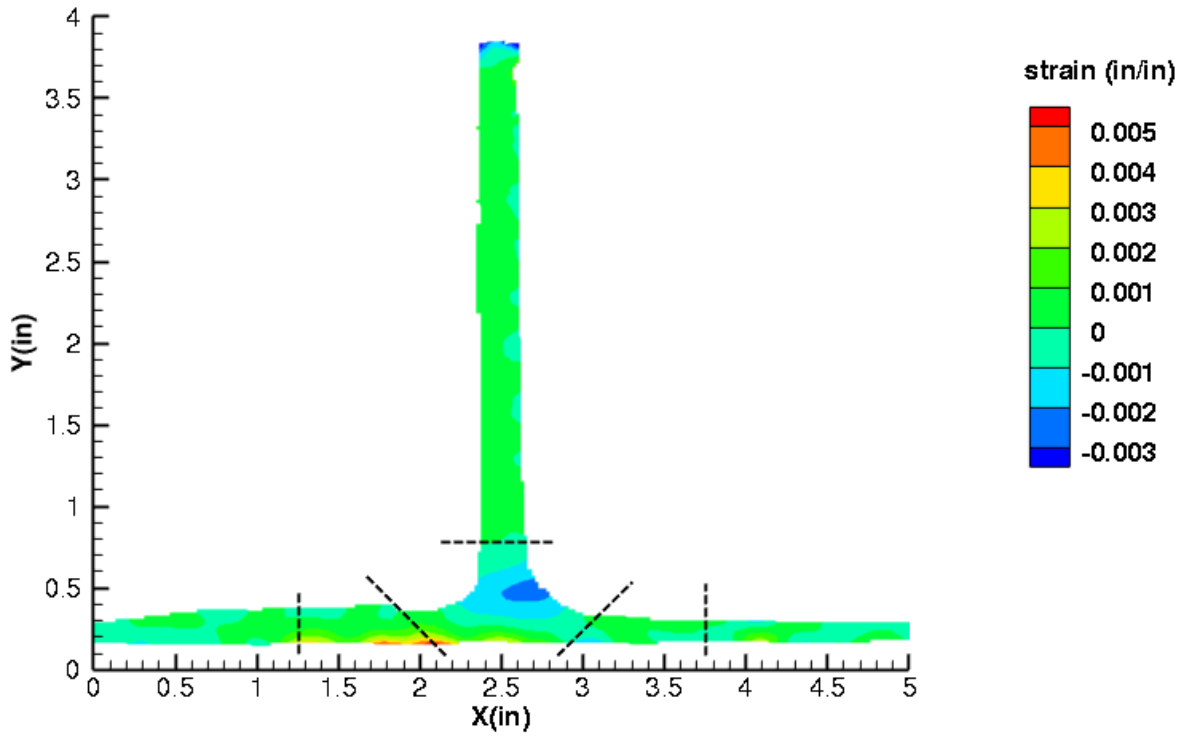

Figure C153. T1N2 strain contours for ε_{yy} at 1978 lb. load, prior to initial failure, 5MP VIC data.

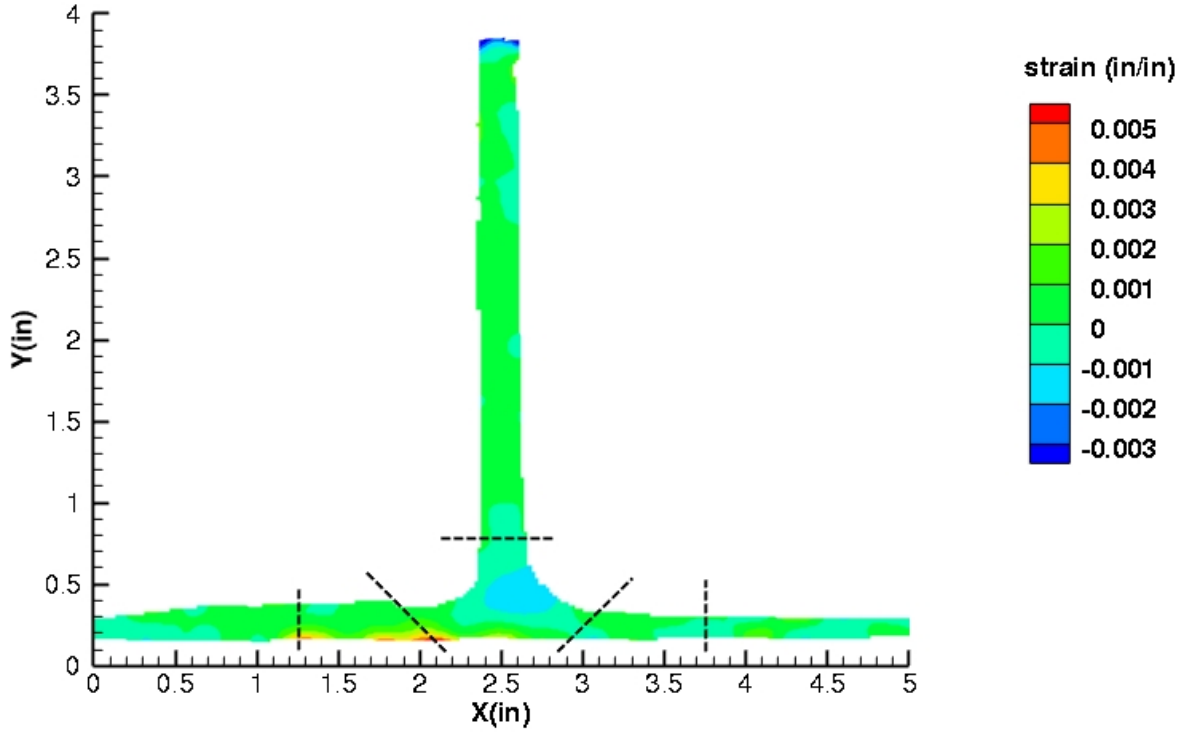

Figure C154. T1N2 strain contours for ε_{yy} at 1808 lb. load, just after initial failure, 5MP VIC data.

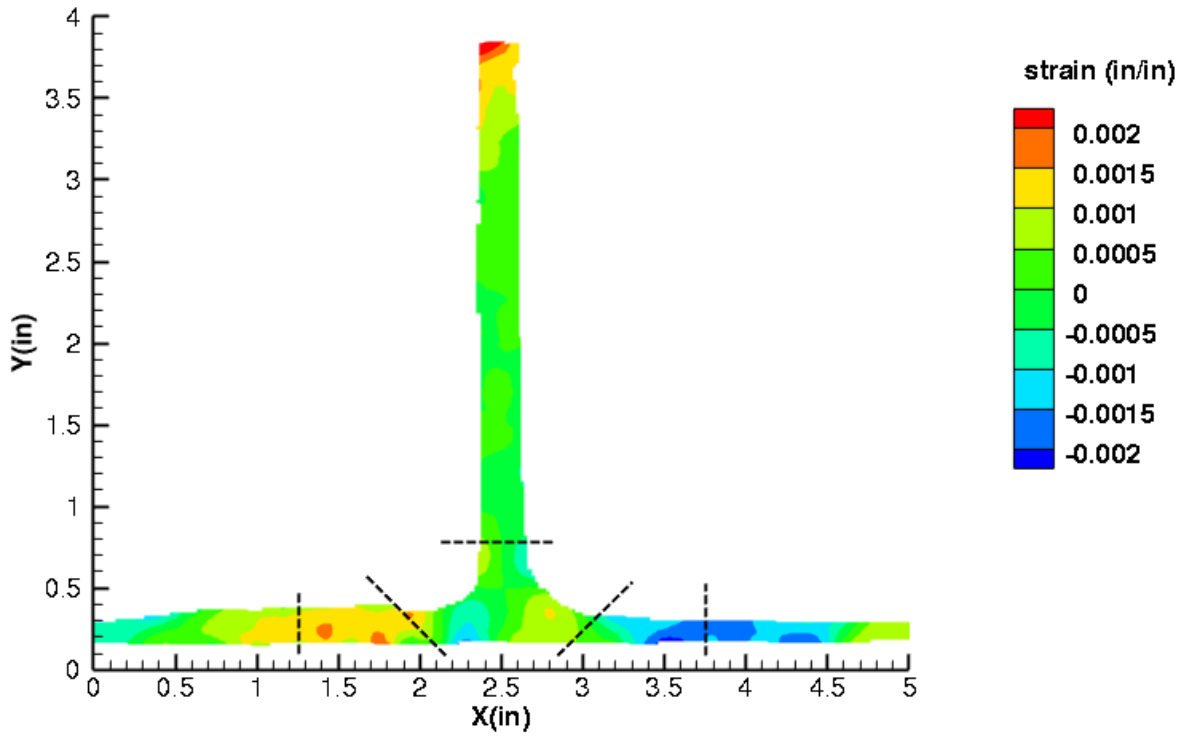

Figure C155. T1N2 strain contours for ε_{xy} at 1978 lb. load, prior to initial failure, 5MP VIC data.

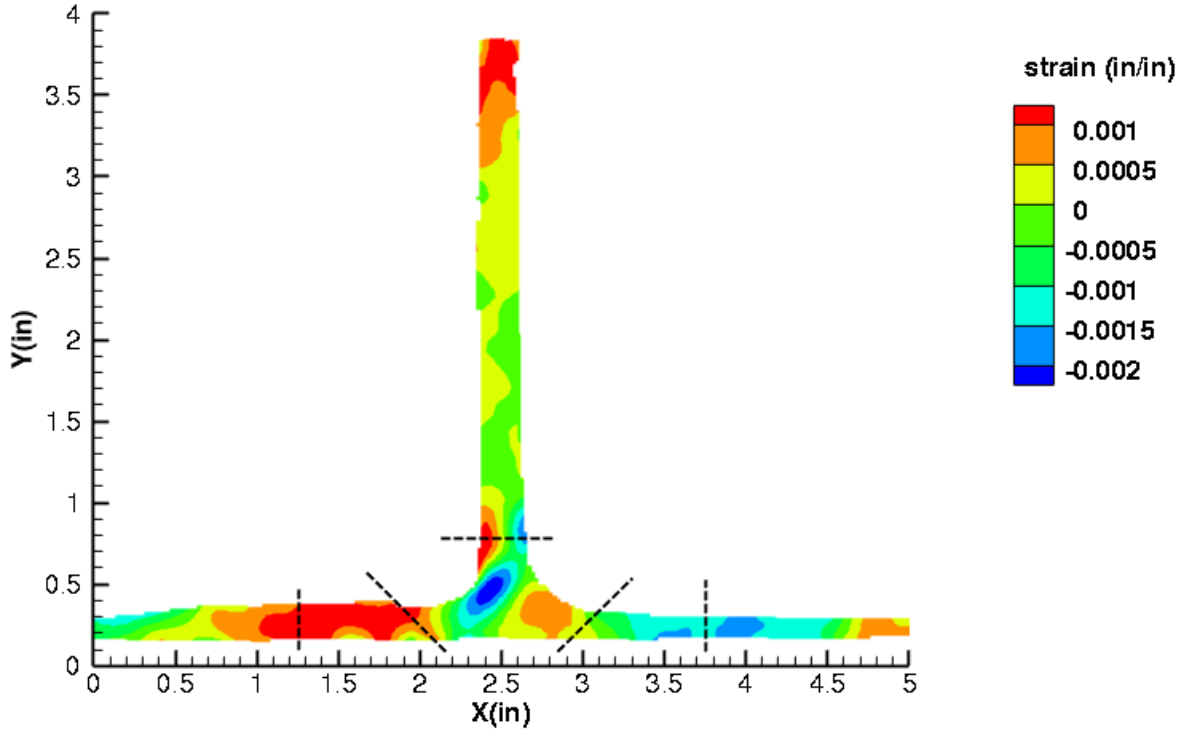

Figure C156. T1N2 strain contours for ε_{xy} at 1808 lb. load, just after initial failure, 5MP VIC data.

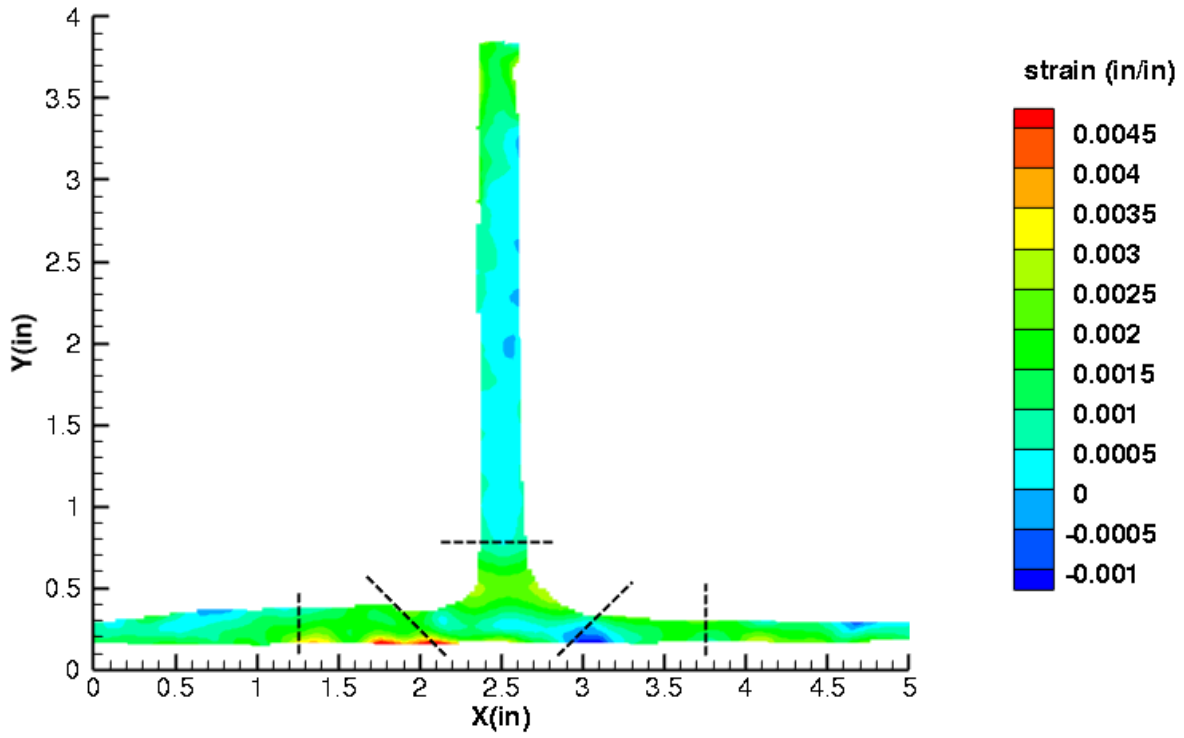

Figure C157. T1N2 strain contours for maximum principal strain at 1978 lb. load, prior to initial failure, 5MP VIC data.

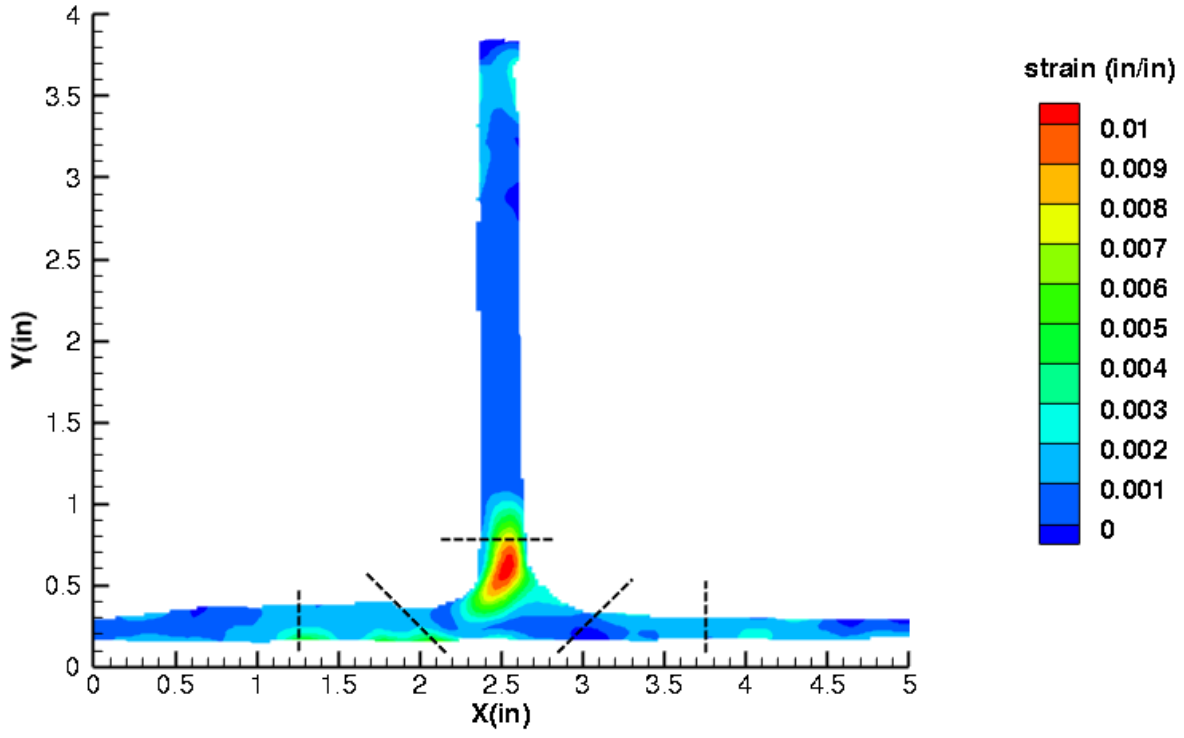

Figure C158. T1N2 strain contours for maximum principal strain at 1808 lb. load, just after initial failure, 5MP VIC data.

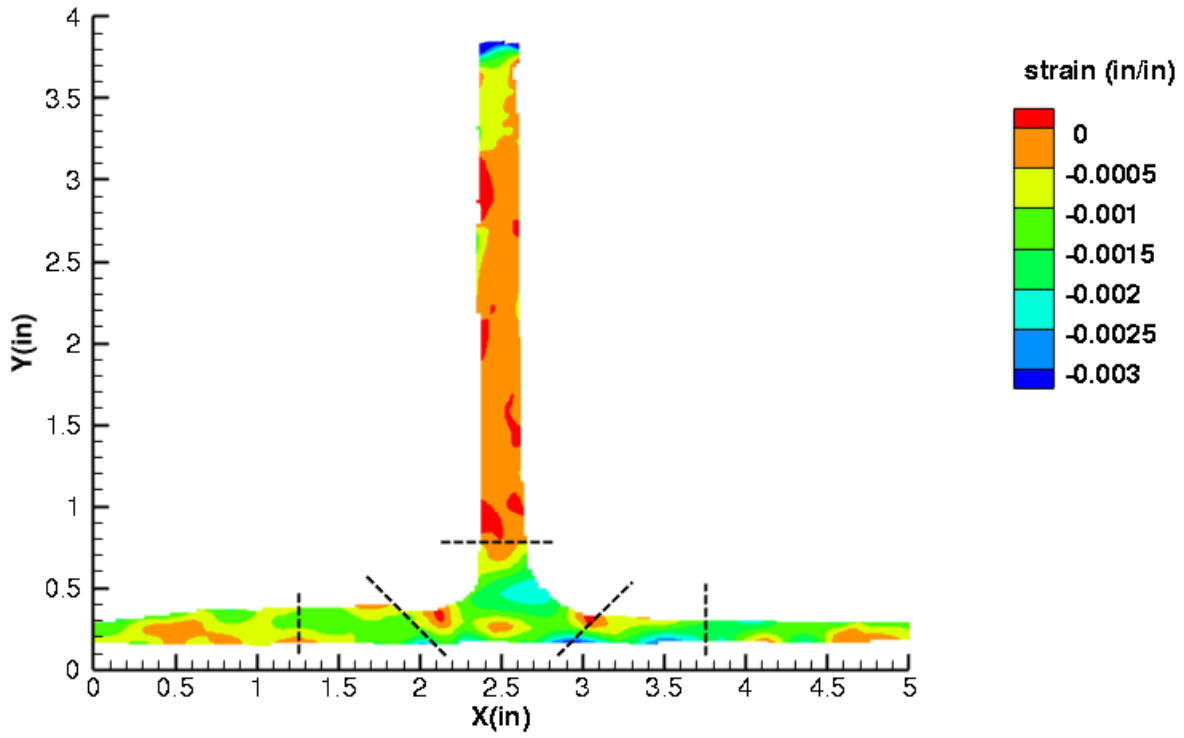

Figure C159. T1N2 strain contours for minimum principal strain at 1978 lb. load, prior to initial failure, 5MP VIC data.

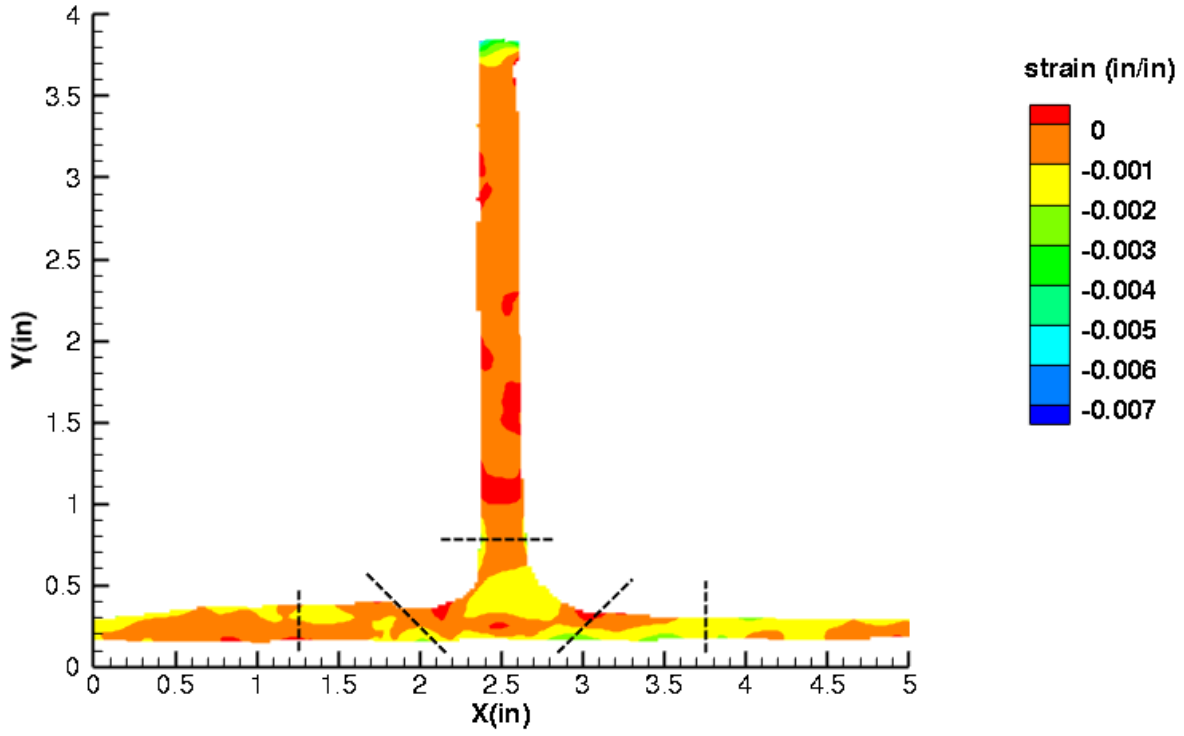

Figure C160. T1N2 strain contours for minimum principal strain at 1808 lb. load, just after initial failure, 5MP VIC data.

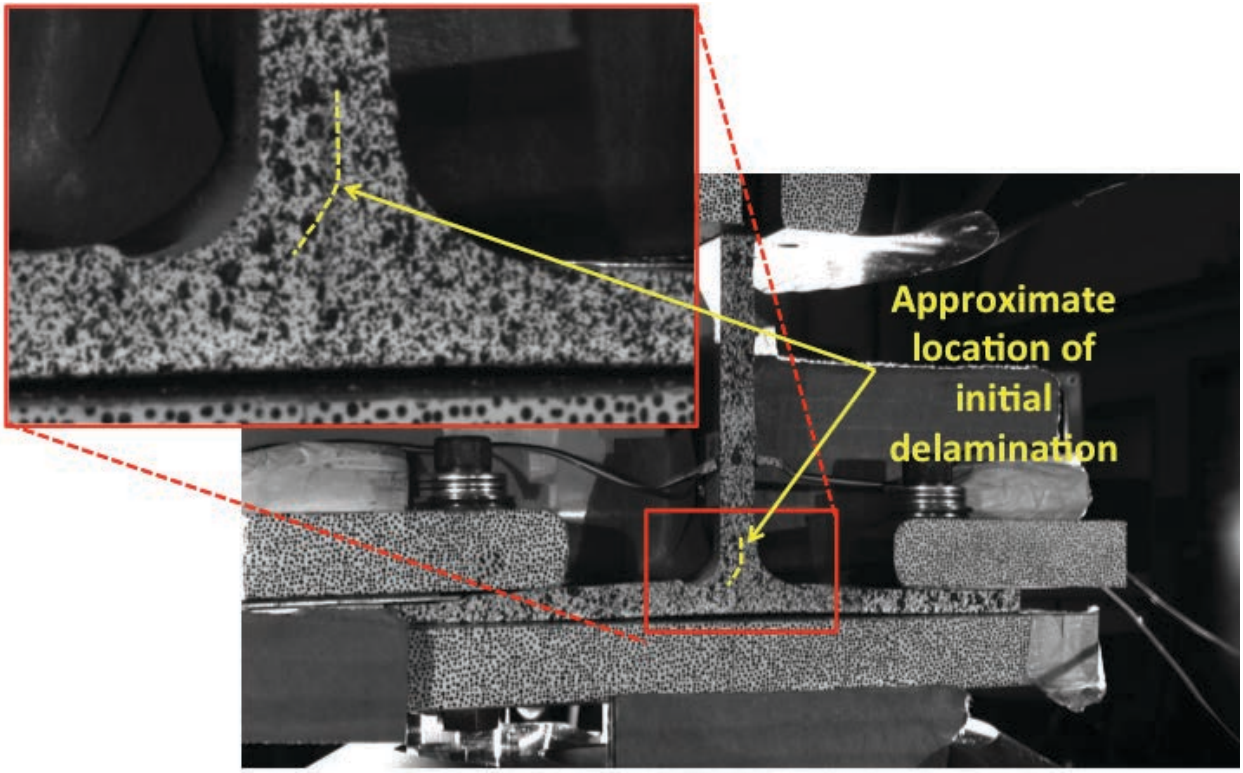

Figure C161. T1N2 image just after initial failure, 5MP VIC data.

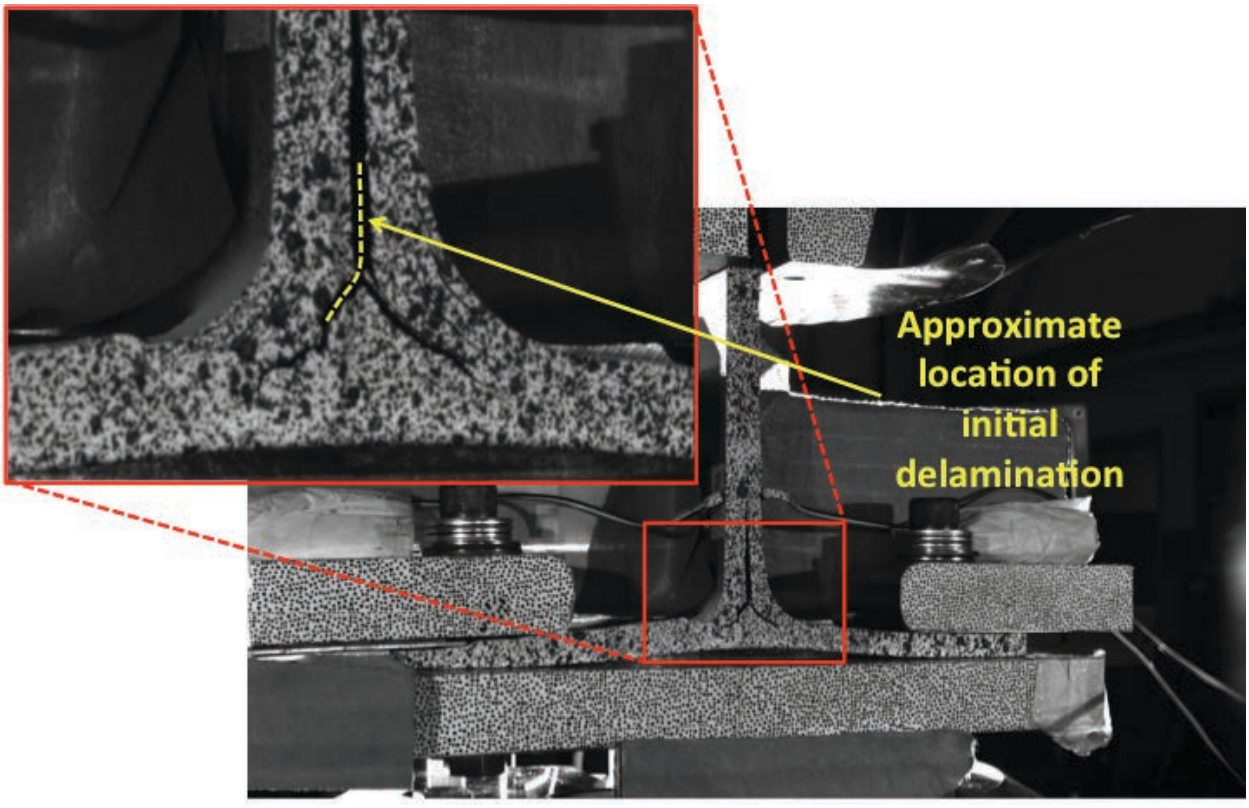

Figure C162. T1N2 image just after maximum load, 5MP VIC data.

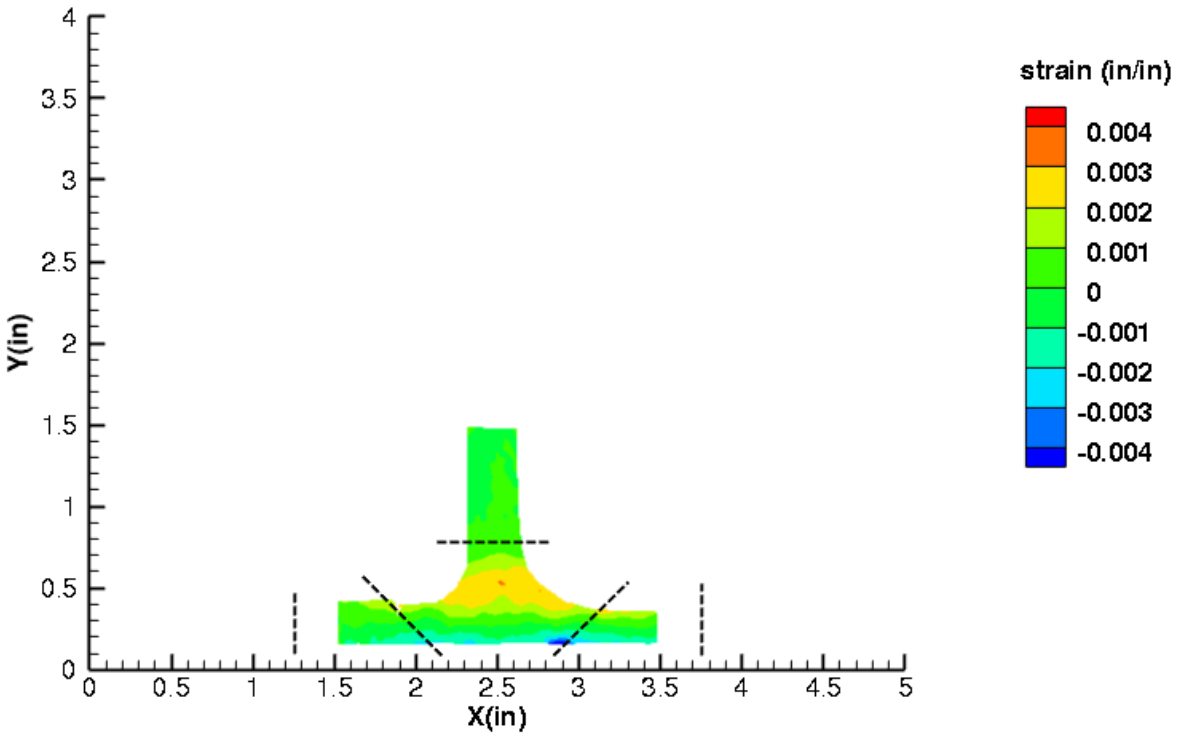

Figure C163. T1N2 strain contours for ε_{xx} at 1978 lb. load, prior to initial failure, local 5MP VIC data.

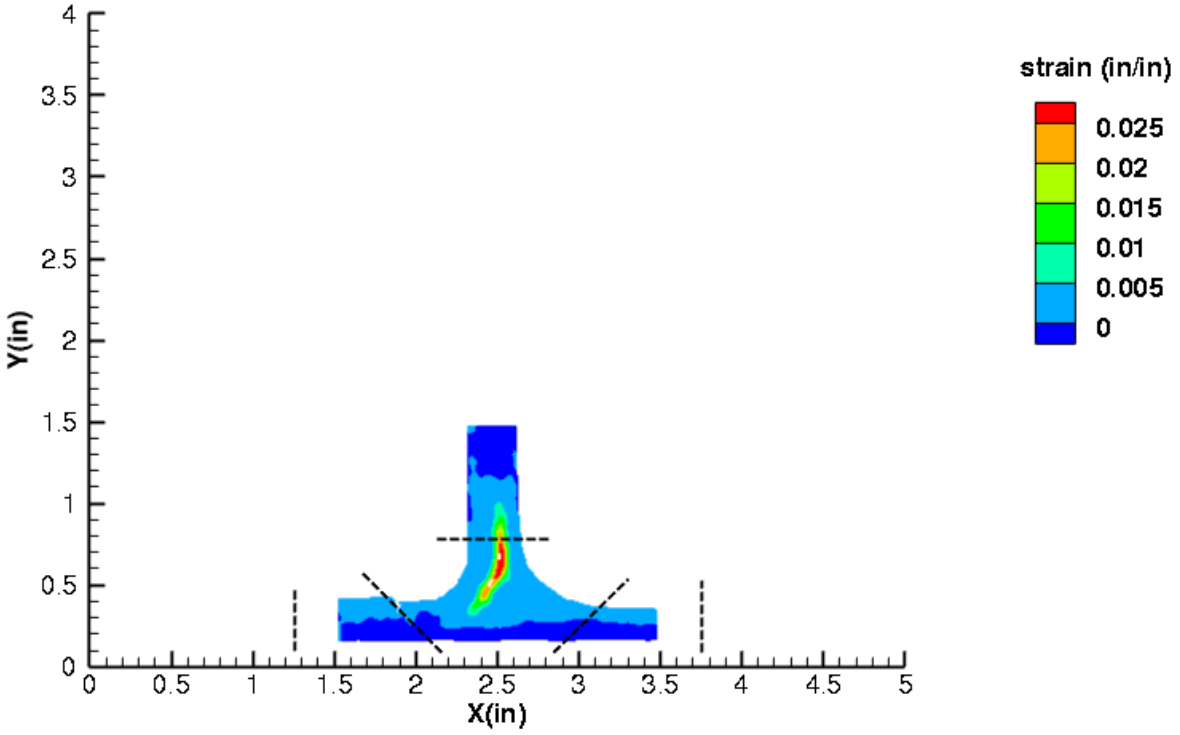

Figure C164. T1N2 strain contours for ε_{xx} at 1808 lb. load, just after initial failure, local 5MP VIC data.

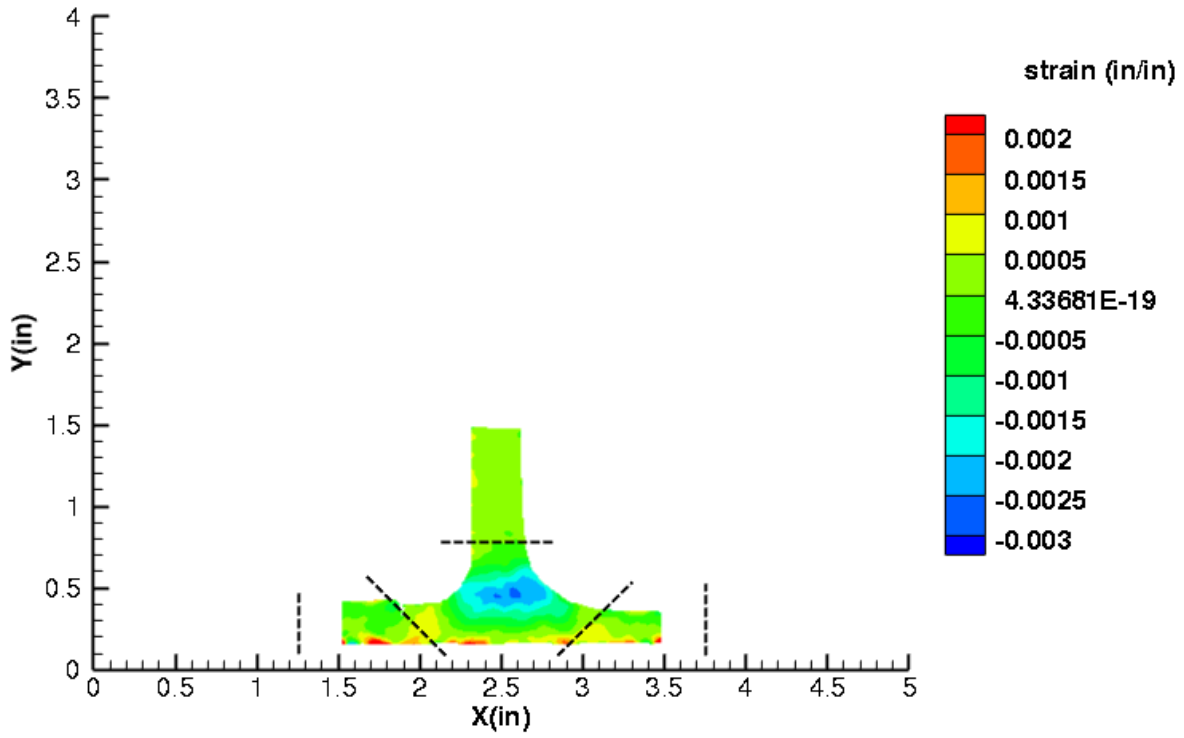

Figure C165. T1N2 strain contours for ε_{yy} at 1978 lb. load, prior to initial failure, local 5MP VIC data.

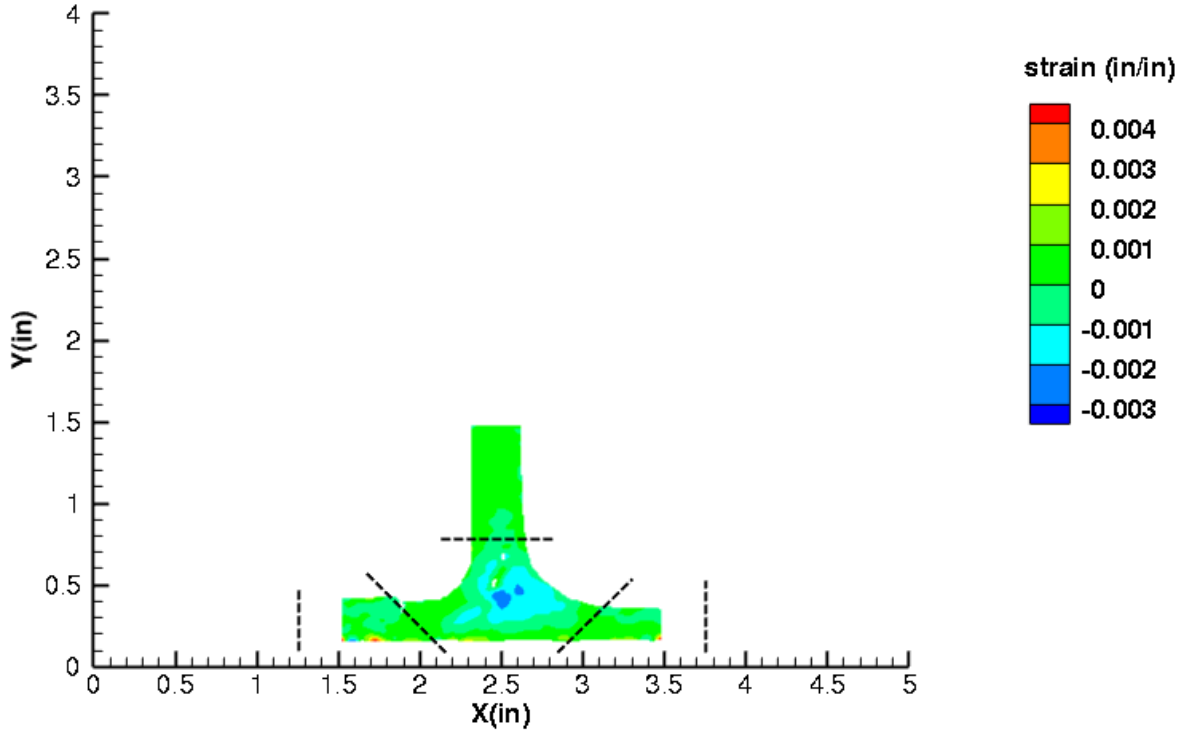

Figure C166. T1N2 strain contours for ε_{yy} at 1808 lb. load, just after initial failure, local 5MP VIC data.

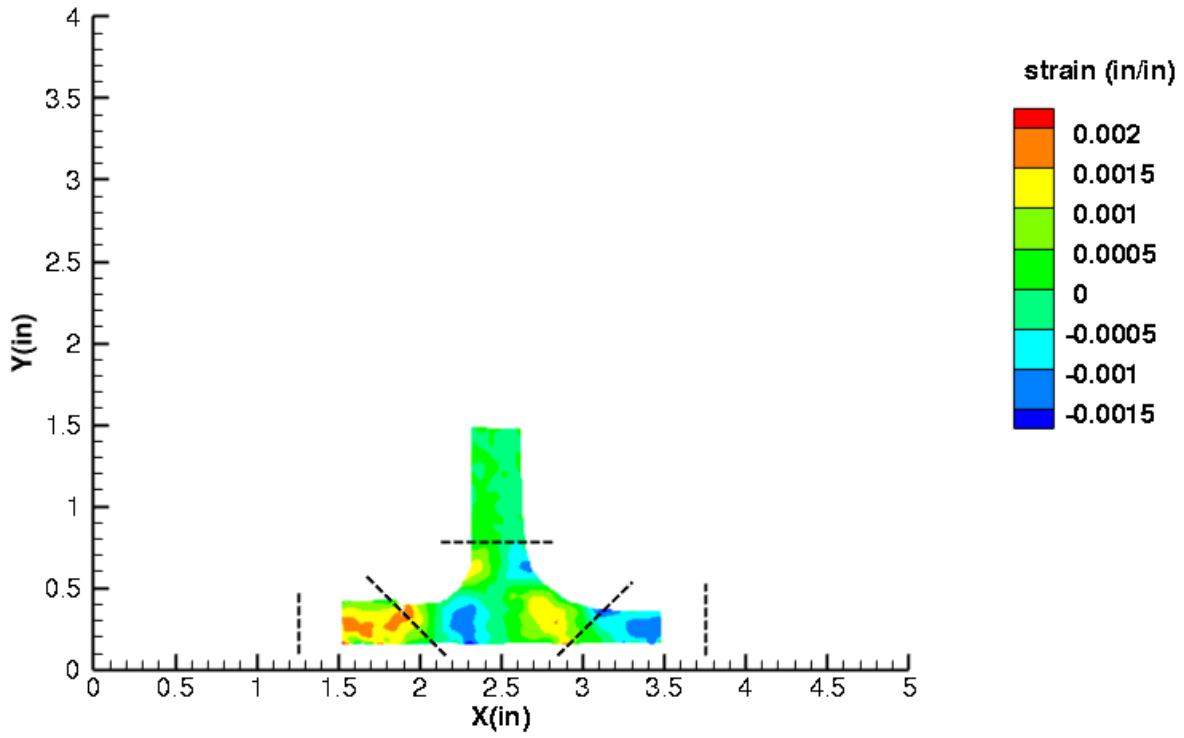

Figure C167. T1N2 strain contours for ε_{xy} at 1978 lb. load, prior to initial failure, local 5MP VIC data.

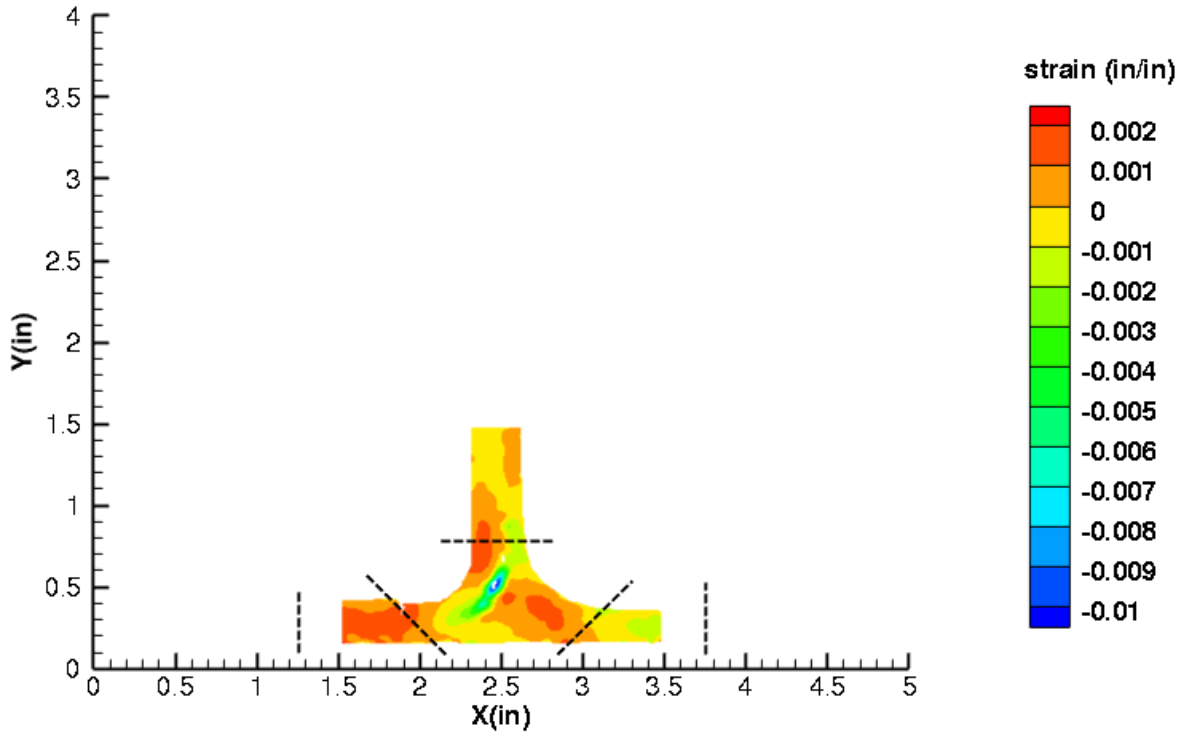

Figure C168. T1N2 strain contours for ε_{xy} at 1808 lb. load, just after initial failure, local 5MP VIC data.

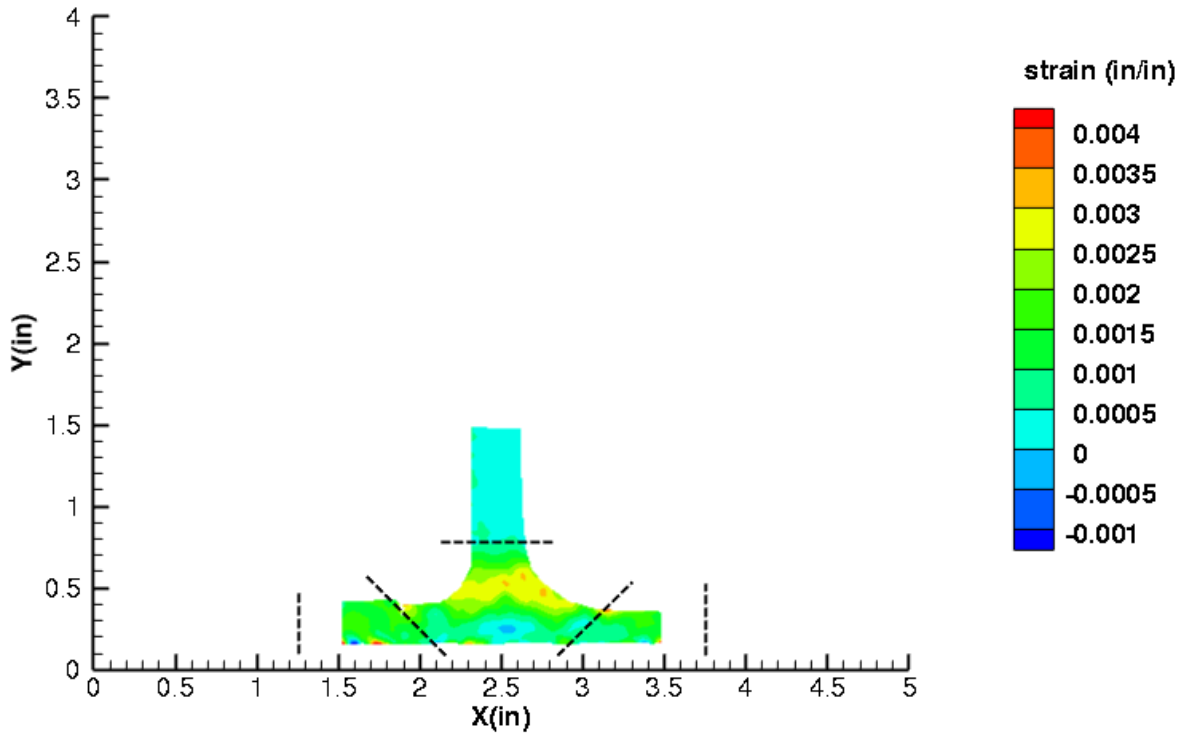

Figure C169. T1N2 strain contours for maximum principal strain at 1978 lb. load, prior to initial failure, local 5MP VIC data.

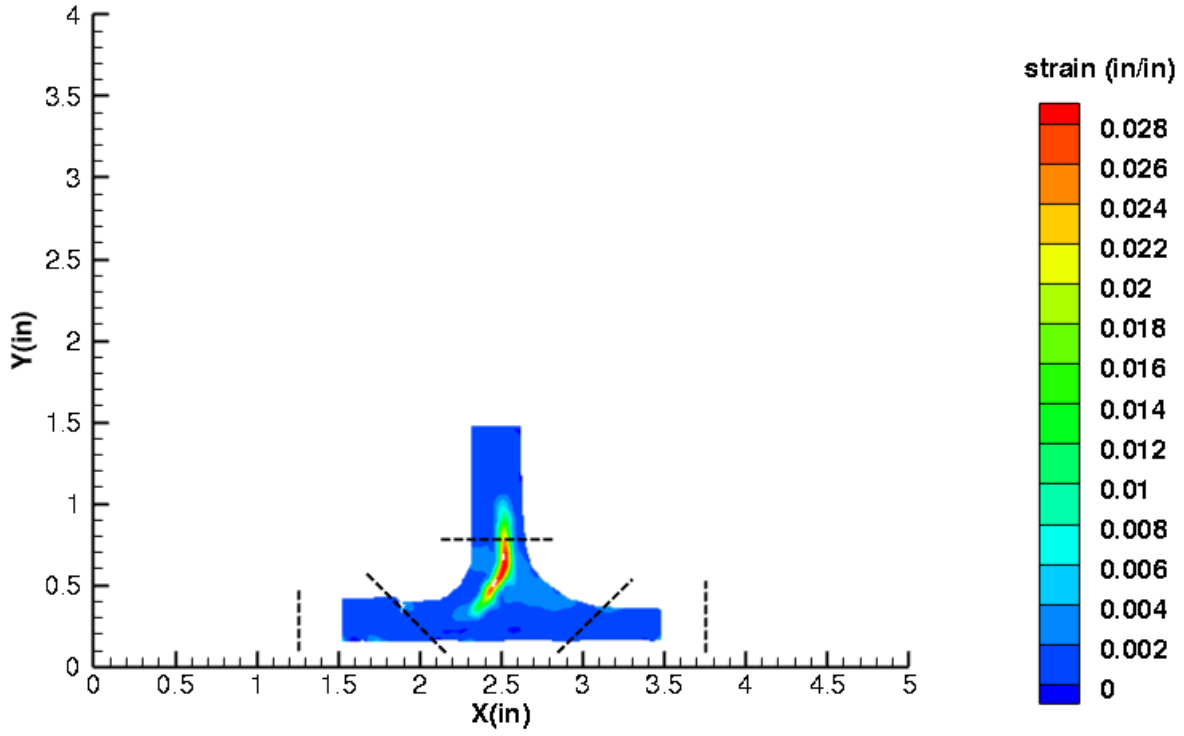

Figure C170. T1N2 strain contours for maximum principal strain at 1808 lb. load, just after initial failure, local 5MP VIC data.

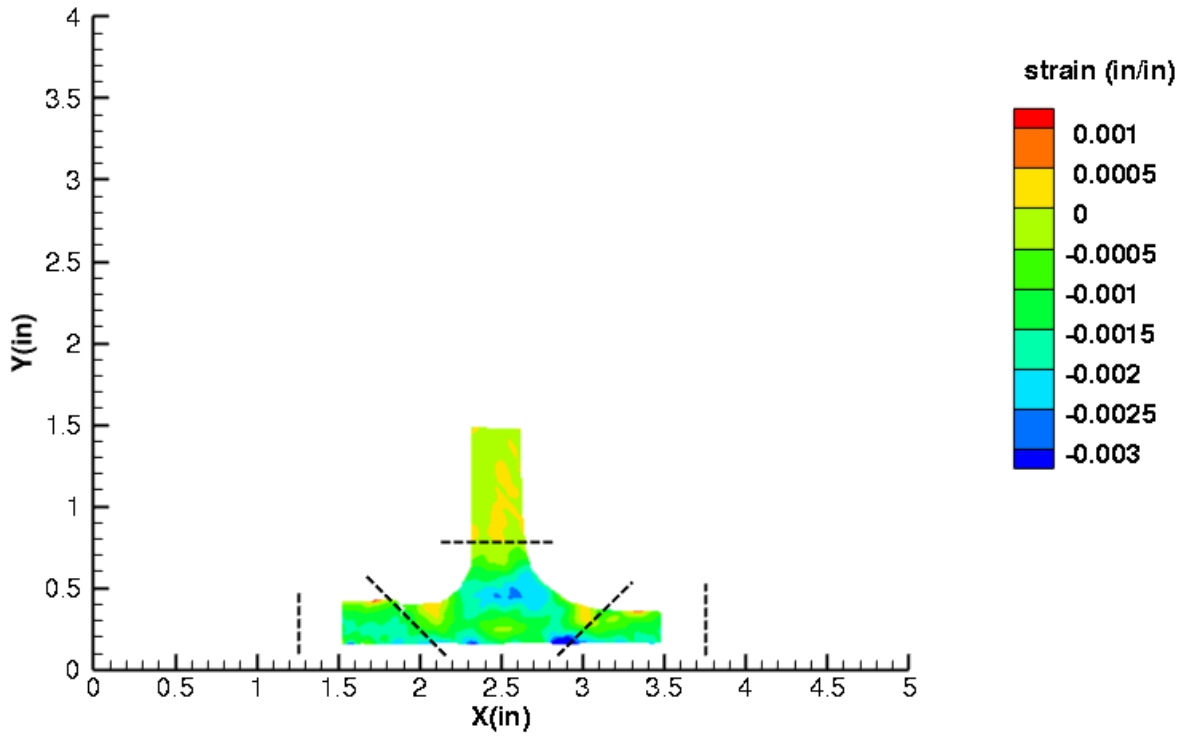

Figure C171. T1N2 strain contours for minimum principal strain at 1978 lb. load, prior to initial failure, local 5MP VIC data.

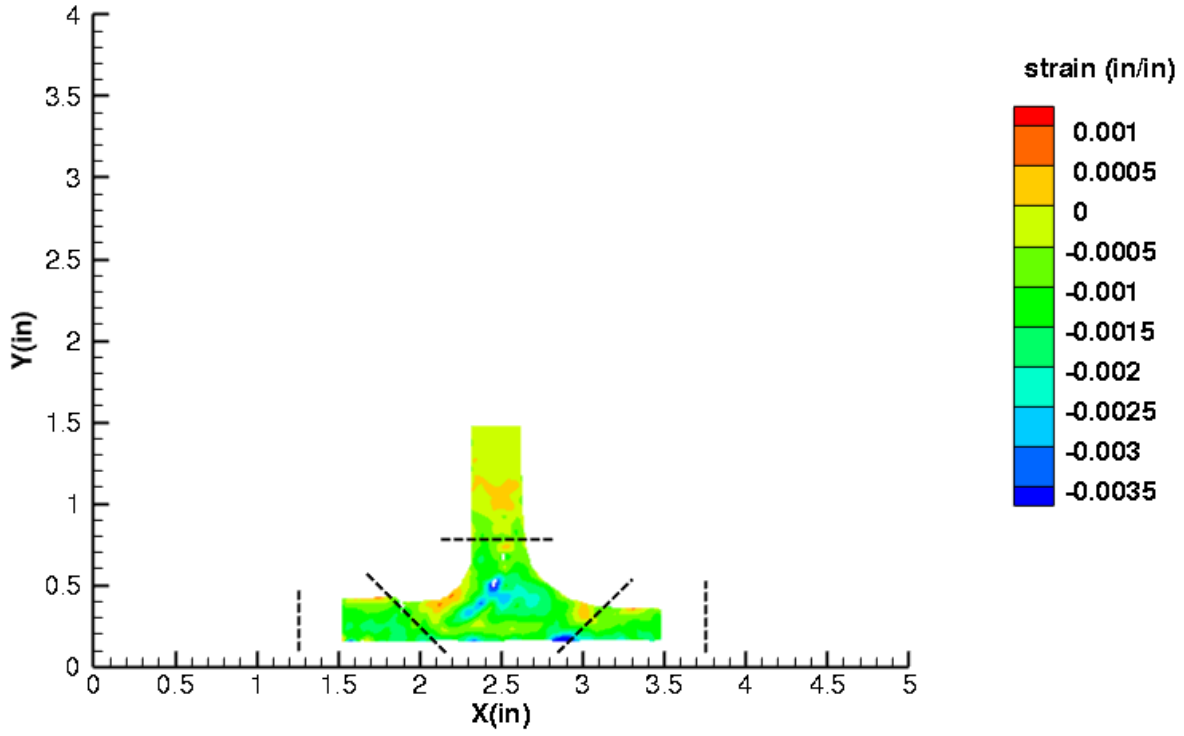

Figure C172. T1N2 strain contours for minimum principal strain at 1808 lb. load, just after initial failure, local 5MP VIC data.

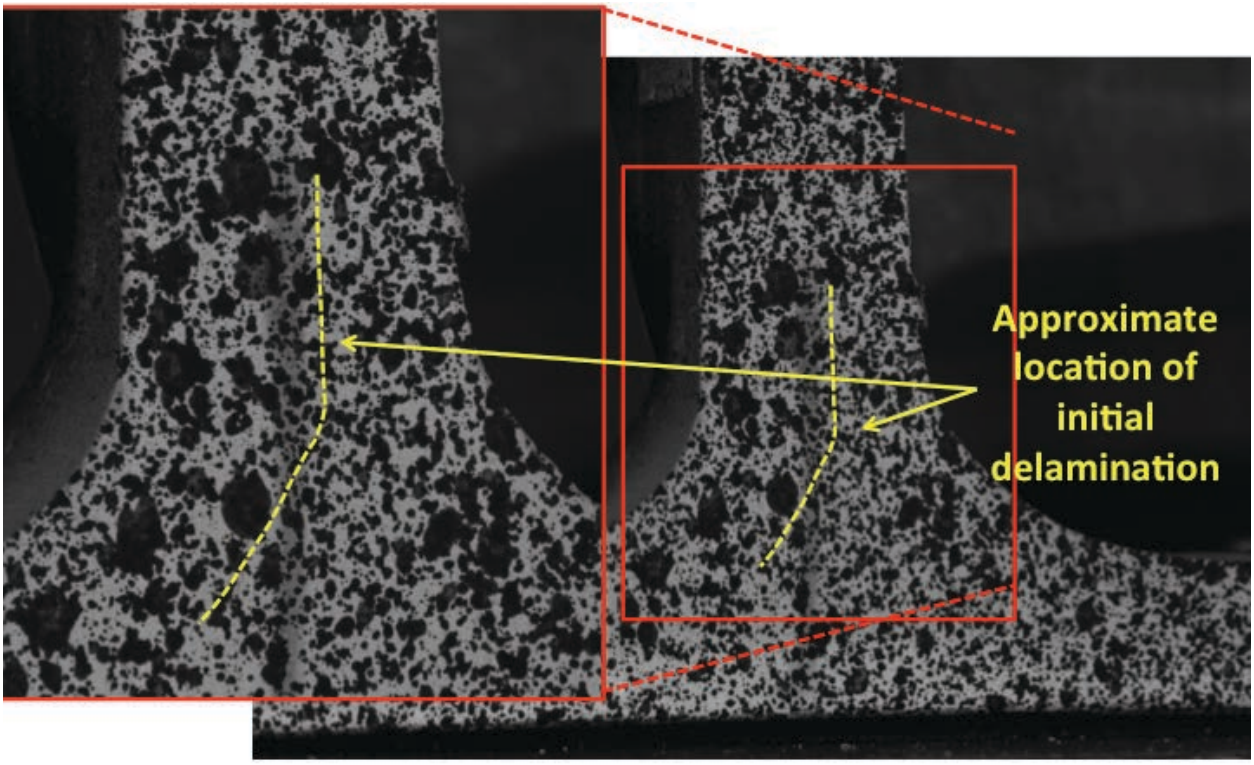

Figure C173. T1N2 image just after initial failure, local 5MP VIC data.

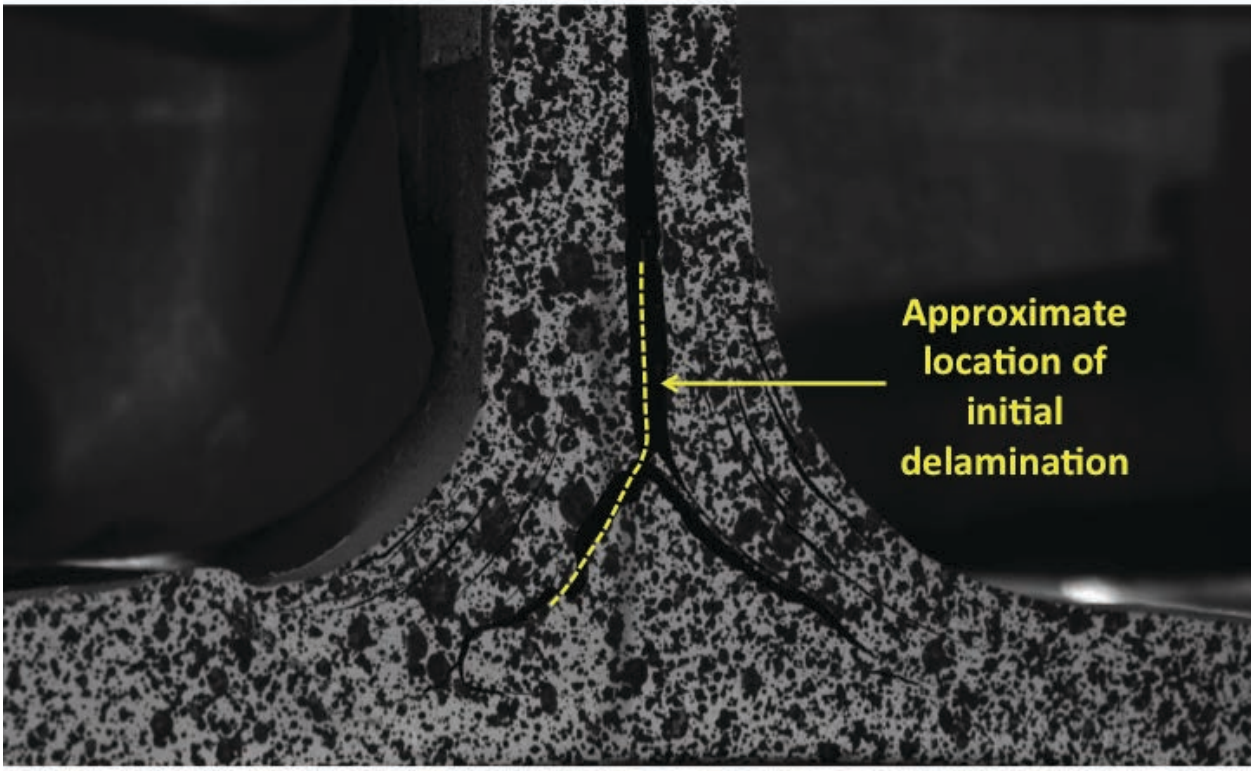

Figure C174. T1N2 image just after maximum load, local 5MP VIC data.

T1N3

This section presents the test data for the T1N3 test article, and includes strain plots and failure images.

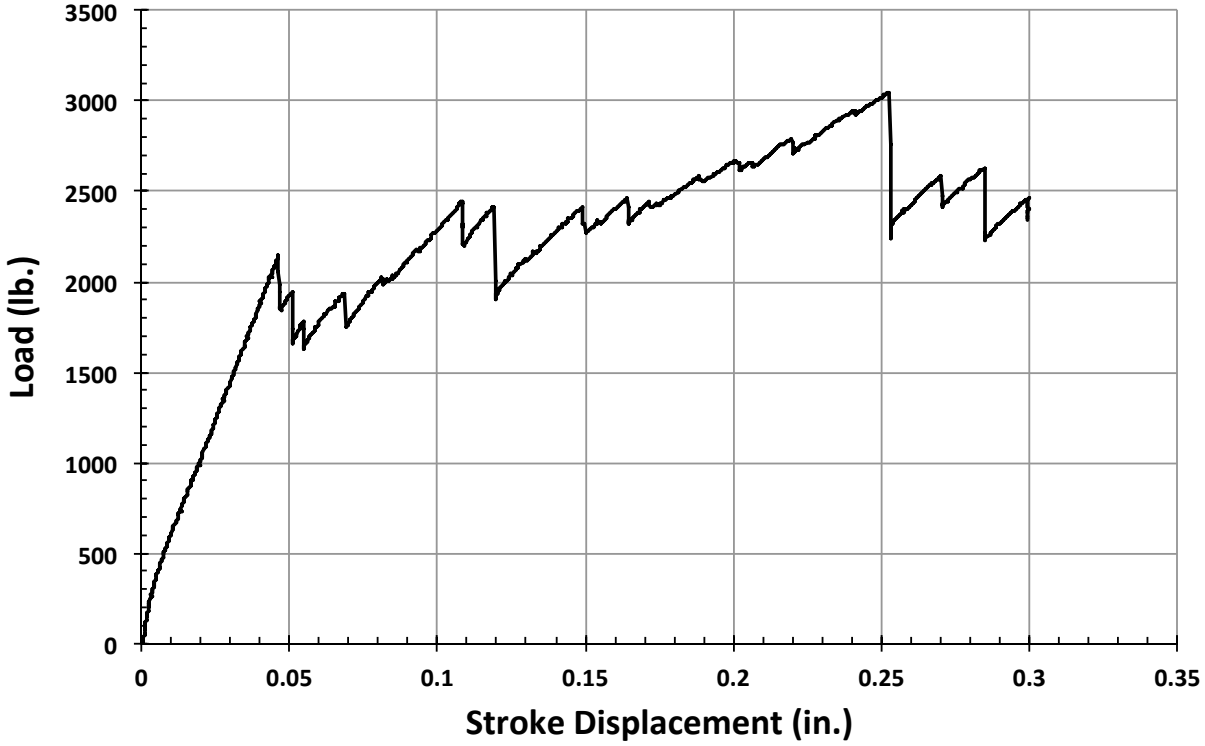

Figure C175. T1N3 load vs. stroke.

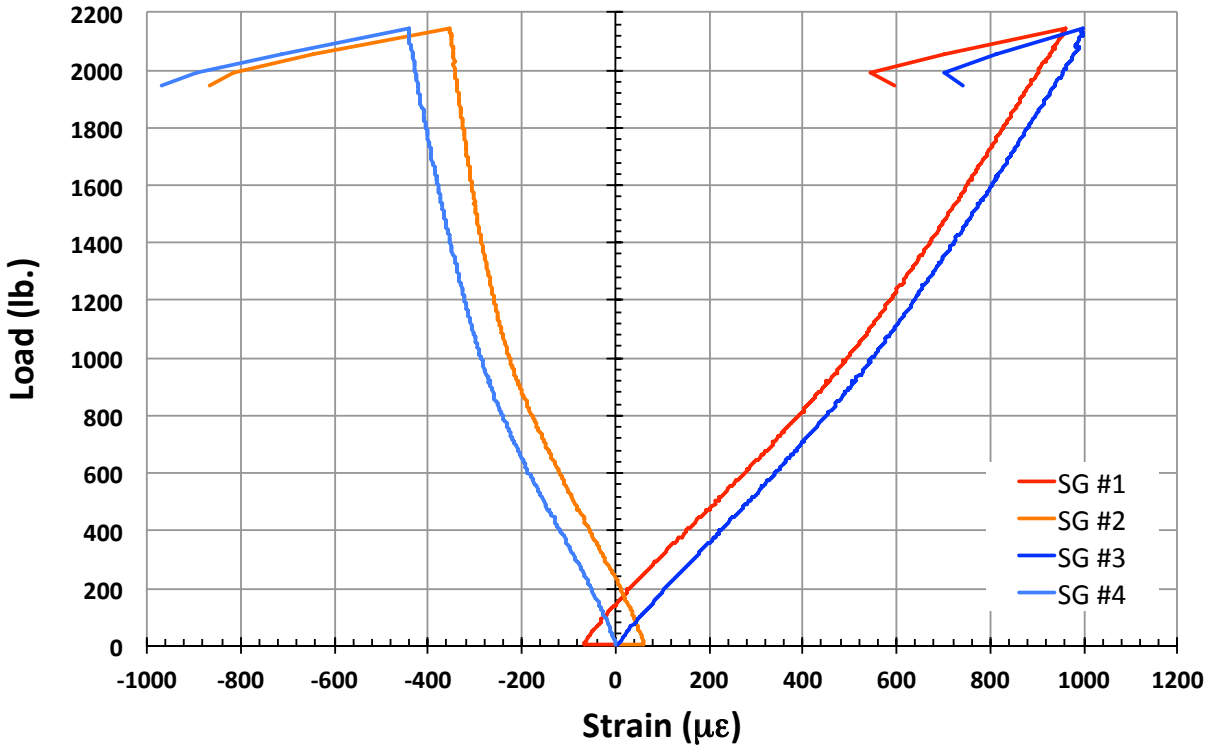

Figure C176. T1N3 load vs. strain, initial loading.

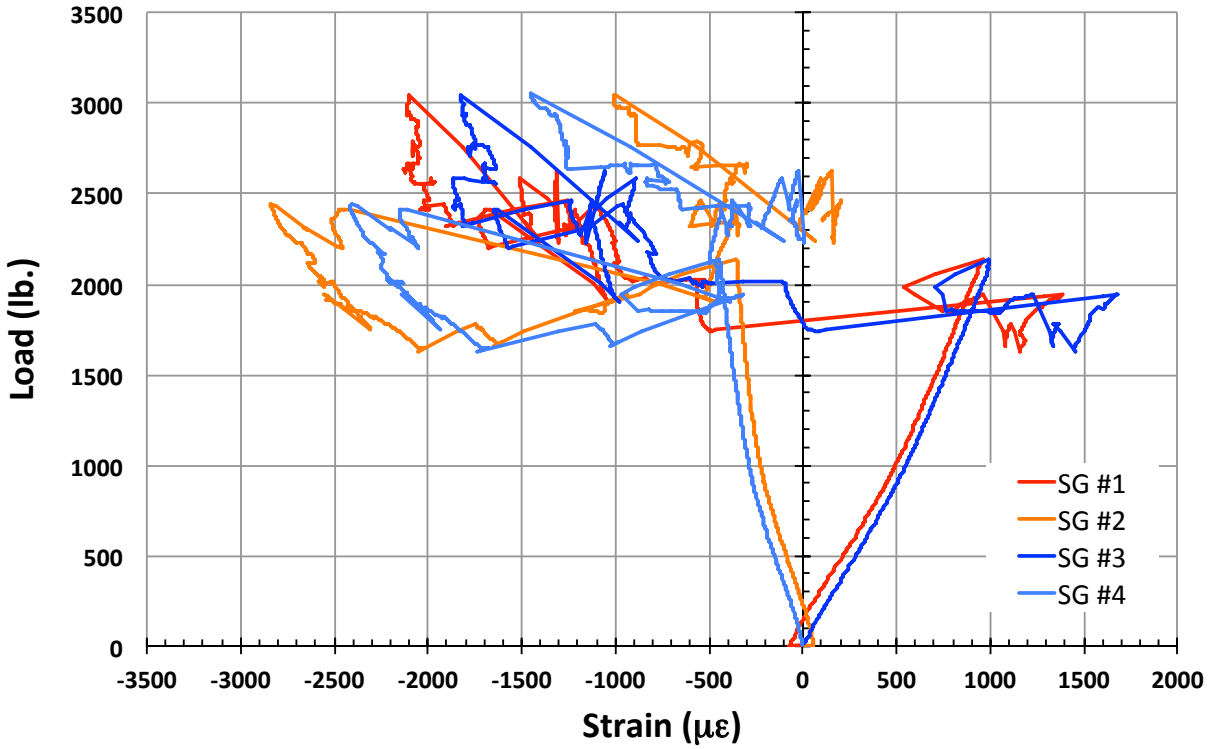

Figure C177. T1N3 load vs. strain.

T5S1

This section presents the test data for the T5S1 test article, and includes strain plots and failure images.

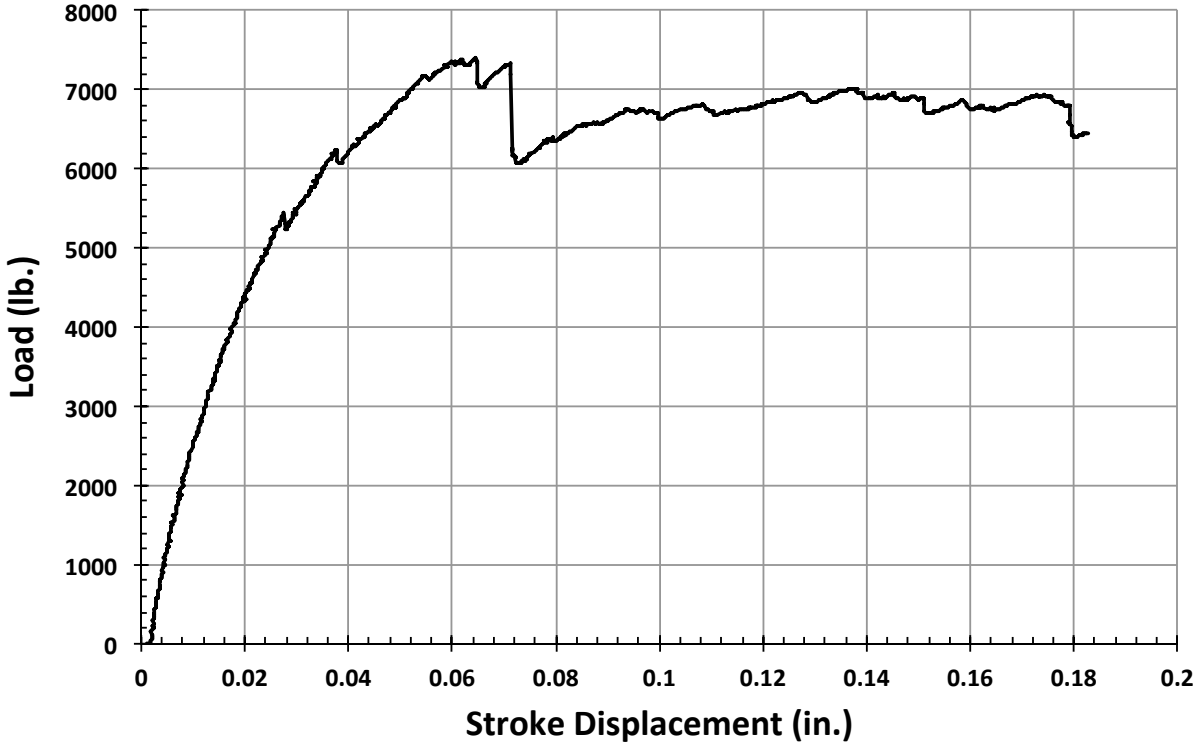

Figure C178. T5S1 load vs. stroke.

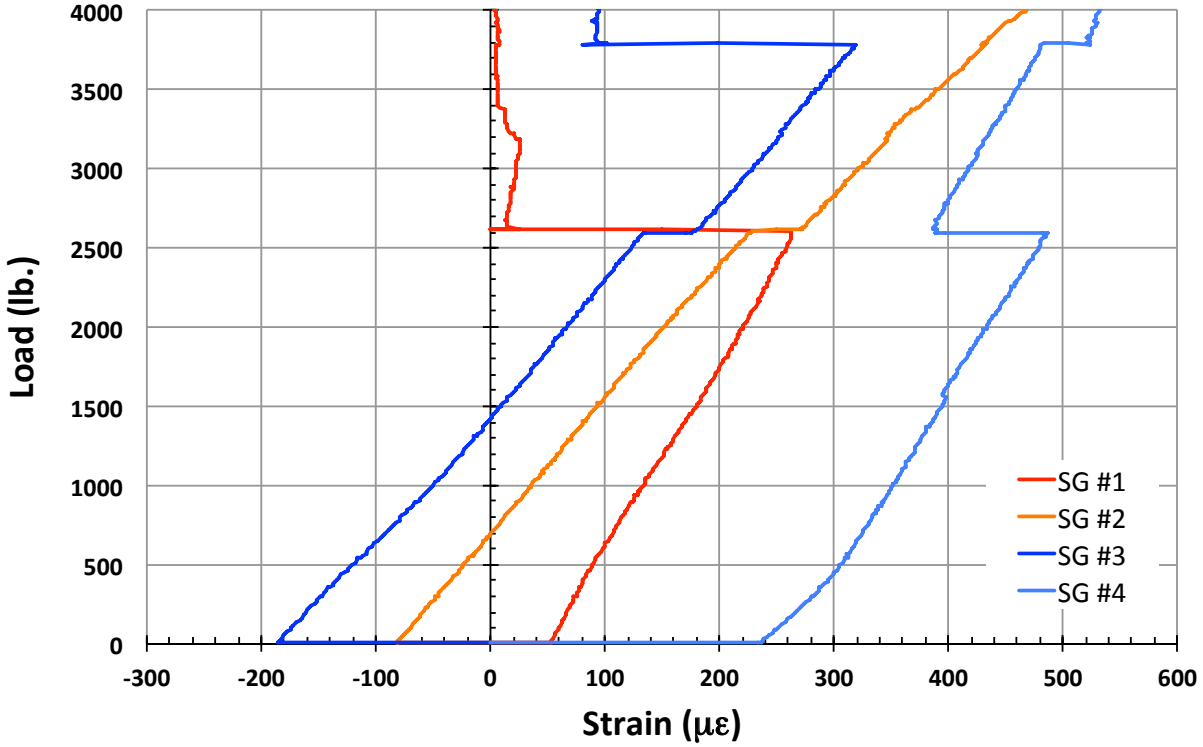

Figure C179. T5S1 load vs. strain, initial loading.

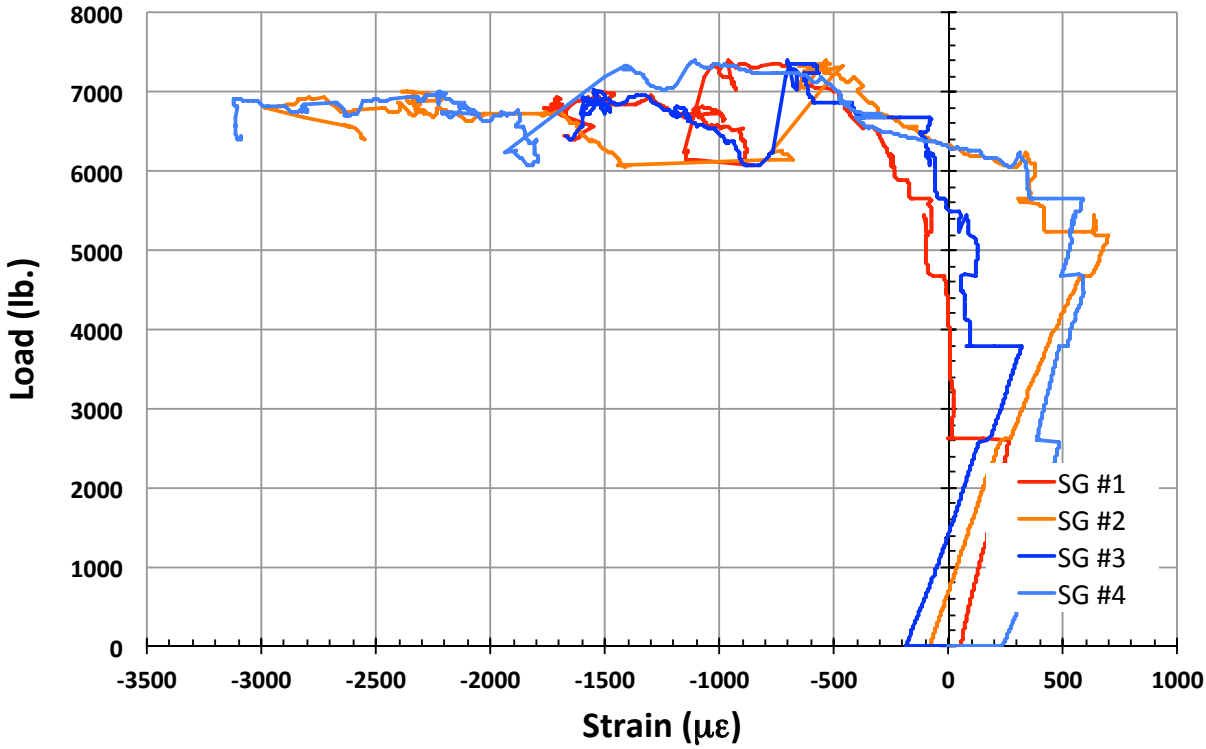

Figure C180. T5S1 load vs. strain.

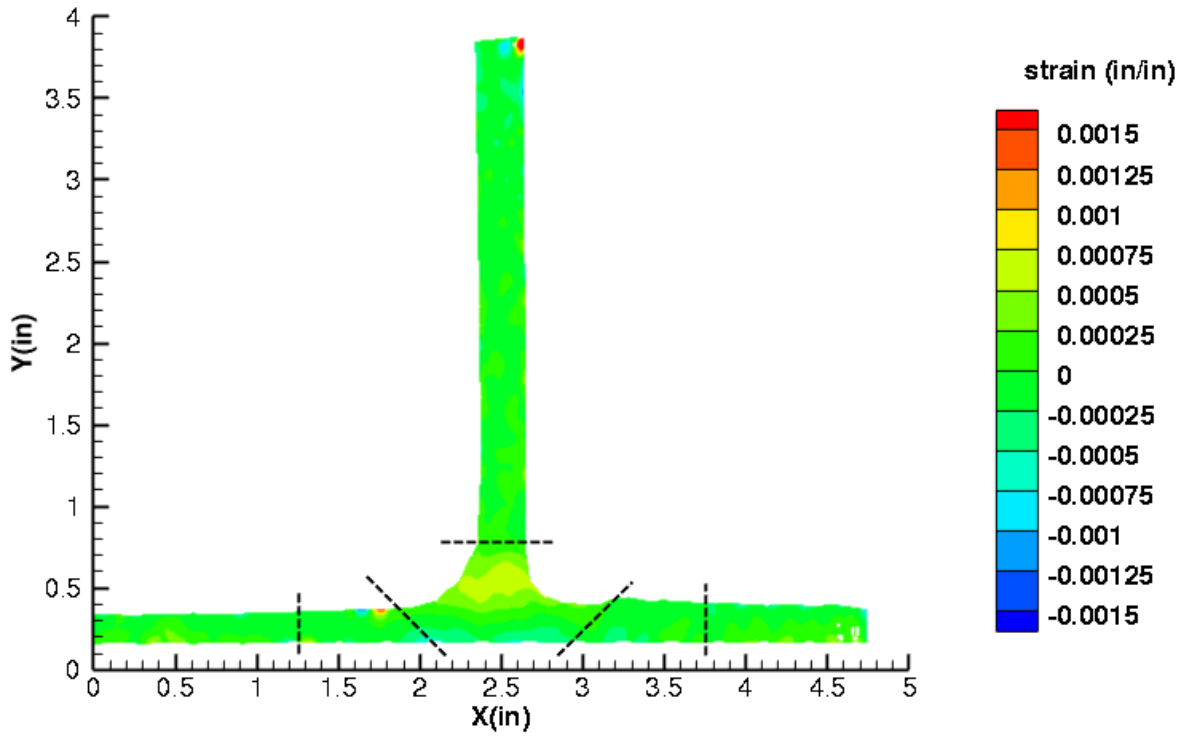

Figure C181. T5S1 strain contours for ε_{xx} at 2615 lb. load, prior to initial failure, 29MP VIC data.

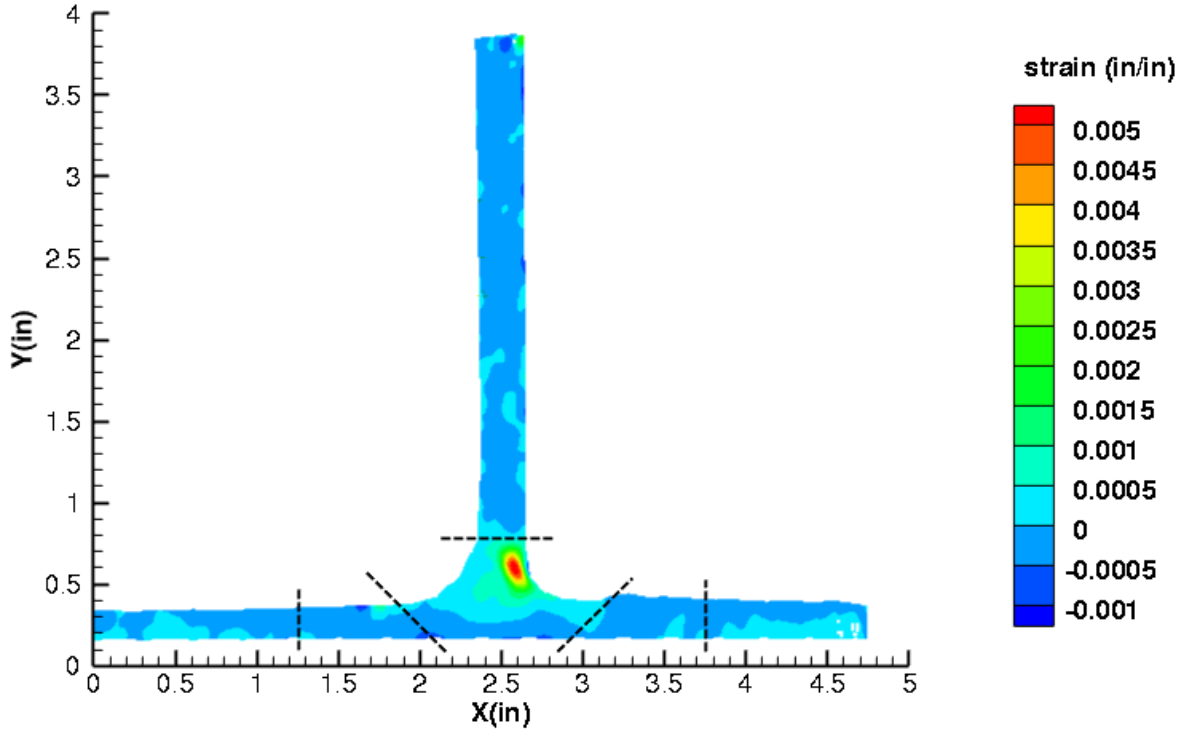

Figure C182. T5S1 strain contours for ε_{xx} at 2632 lb. load, just after initial failure, 29MP VIC data.

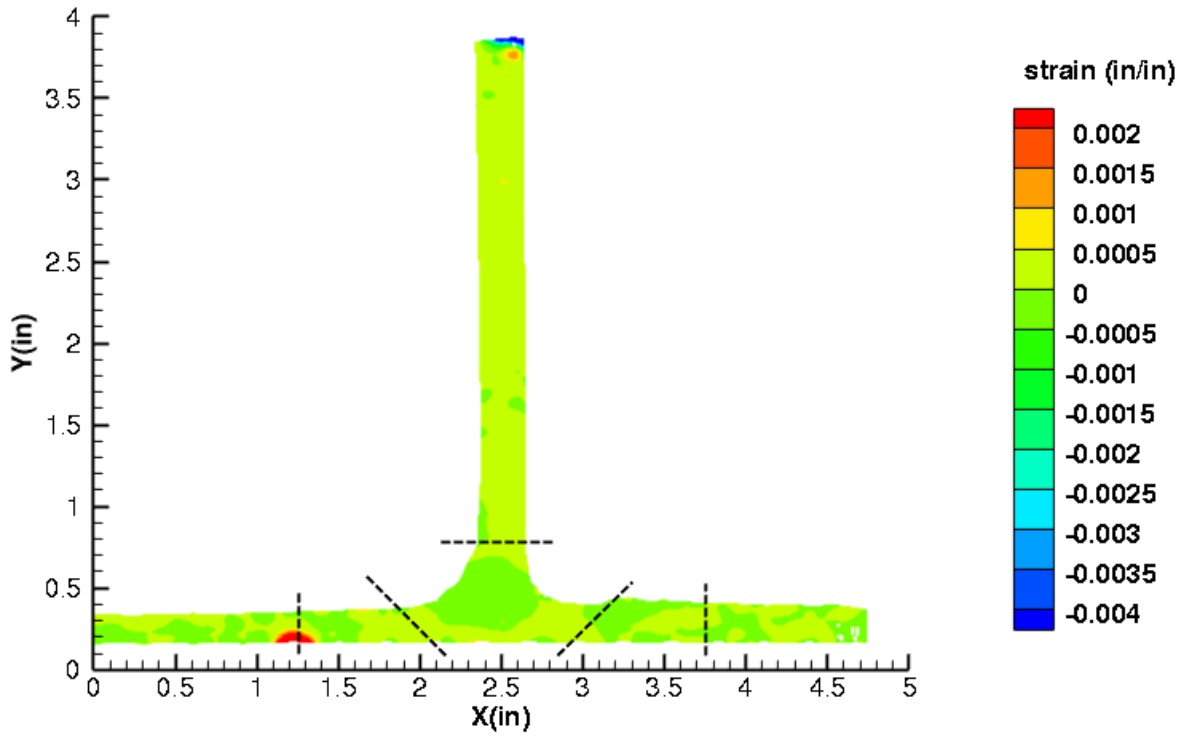

Figure C183. T5S1 strain contours for ε_{yy} at 2615 lb. load, prior to initial failure, 29MP VIC data.

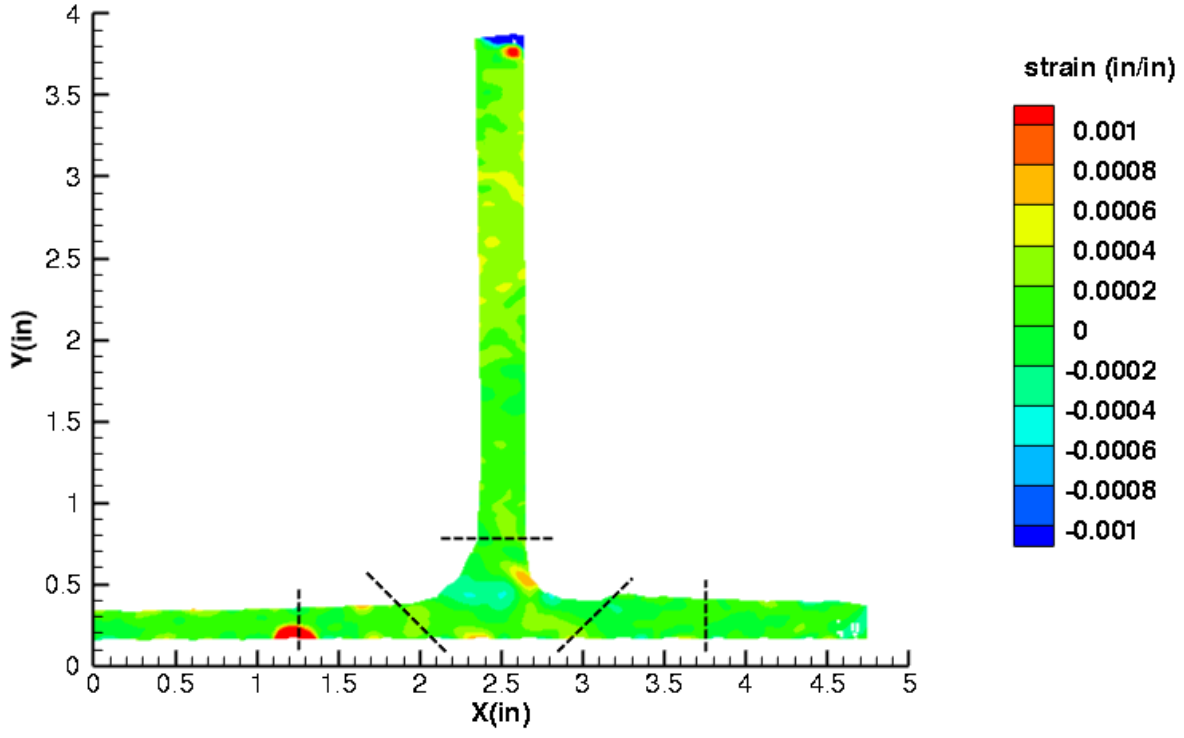

Figure C184. T5S1 strain contours for ε_{yy} at 2632 lb. load, just after initial failure, 29MP VIC data.

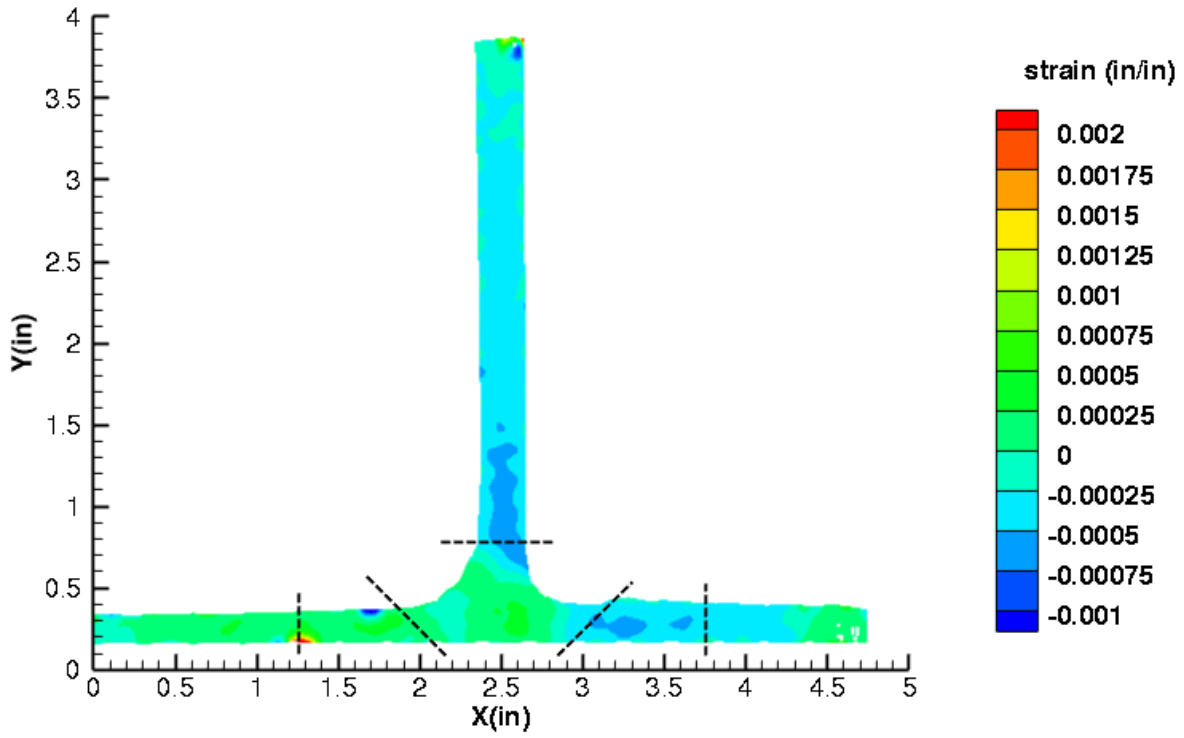

Figure C185. T5S1 strain contours for ε_{xy} at 2615 lb. load, prior to initial failure, 29MP VIC data.

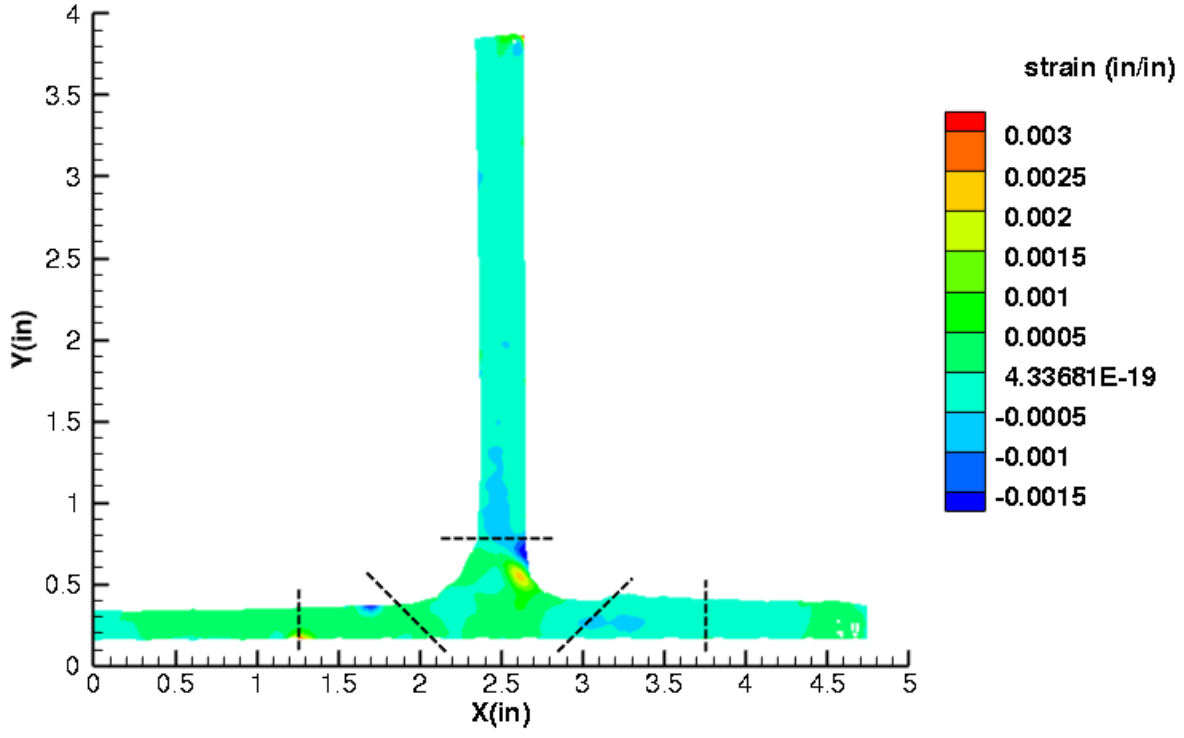

Figure C186. T5S1 strain contours for ε_{xy} at 2632 lb. load, just after initial failure, 29MP VIC data.

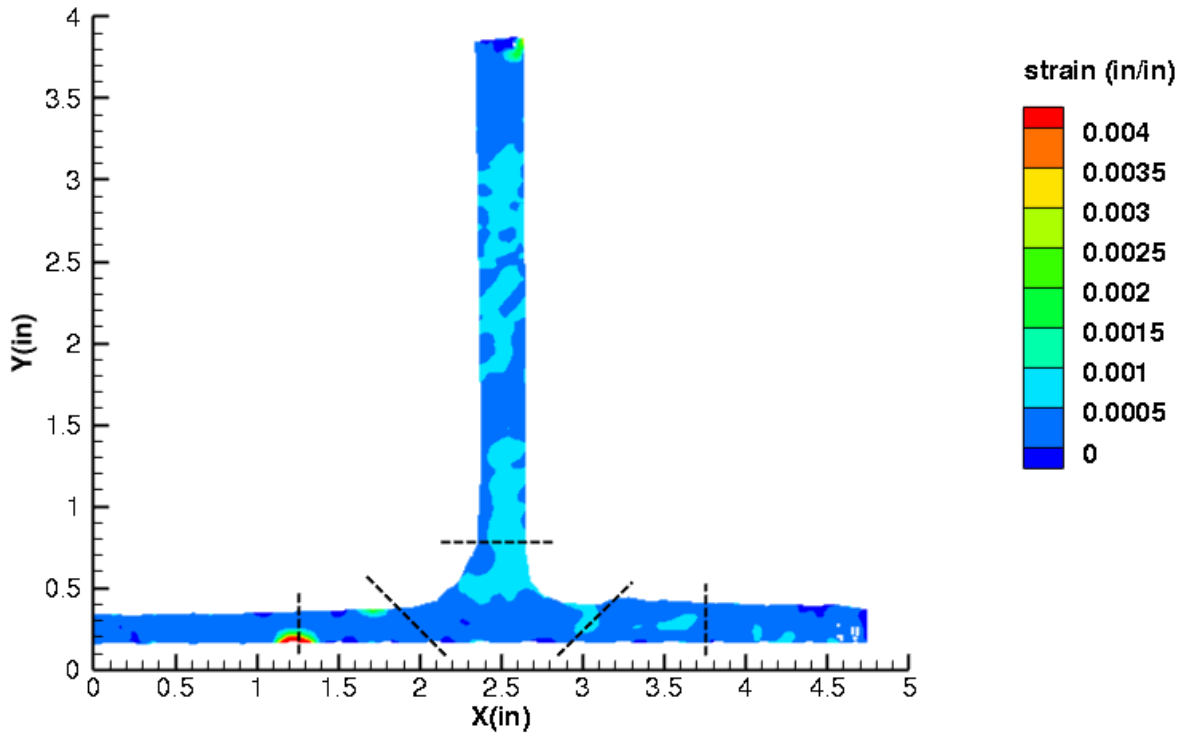

Figure C187. T5S1 strain contours for maximum principal strain at 2615 lb. load, prior to initial failure, 29MP VIC data.

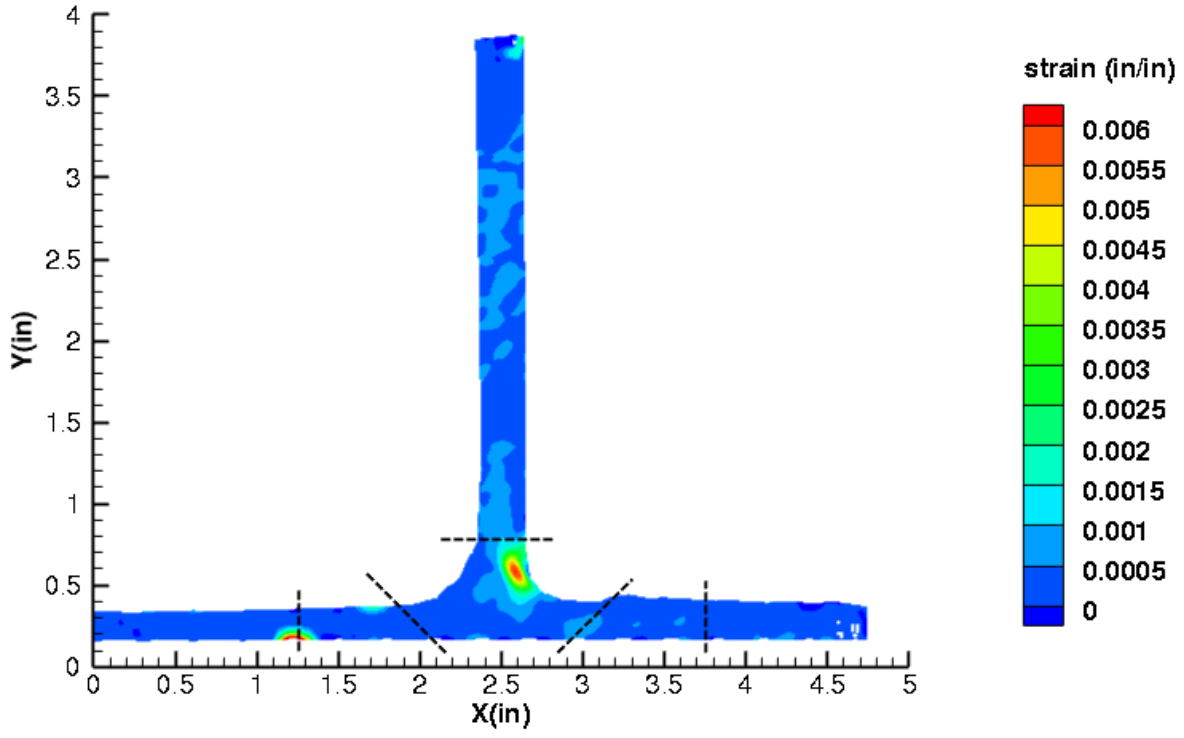

Figure C188. T5S1 strain contours for maximum principal strain at 2632 lb. load, just after initial failure, 29MP VIC data.

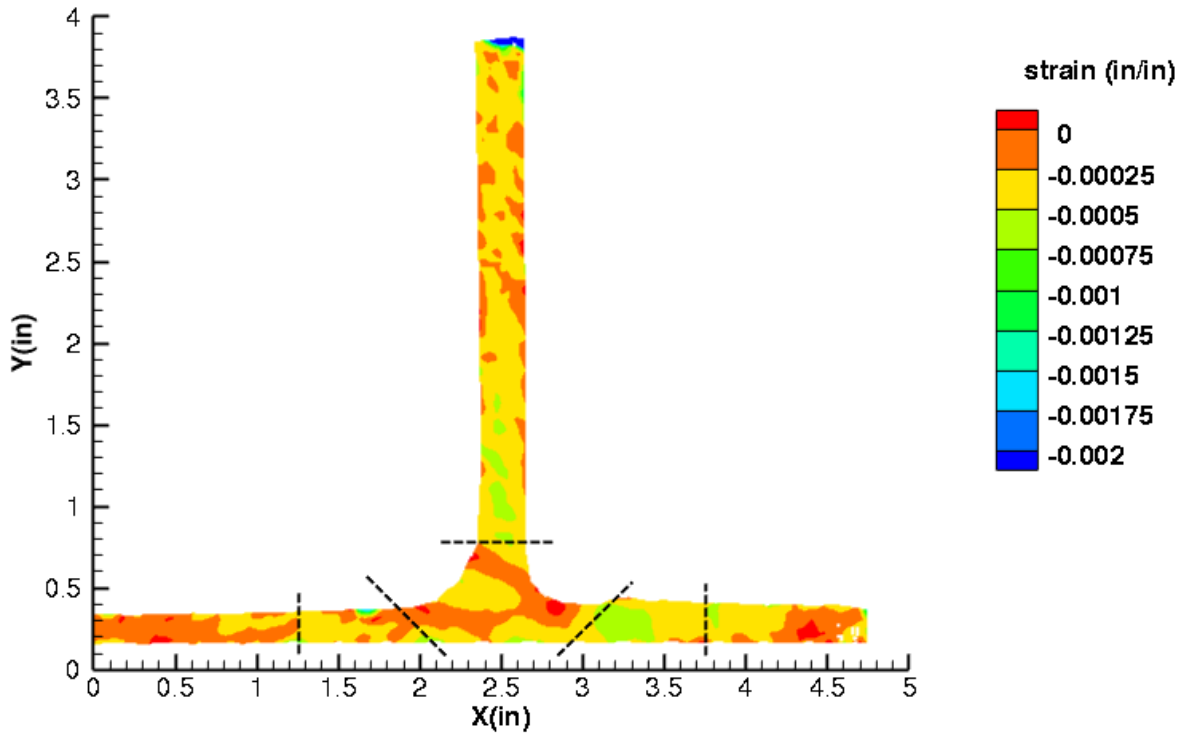

Figure C189. T5S1 strain contours for minimum principal strain at 2615 lb. load, prior to initial failure, 29MP VIC data.

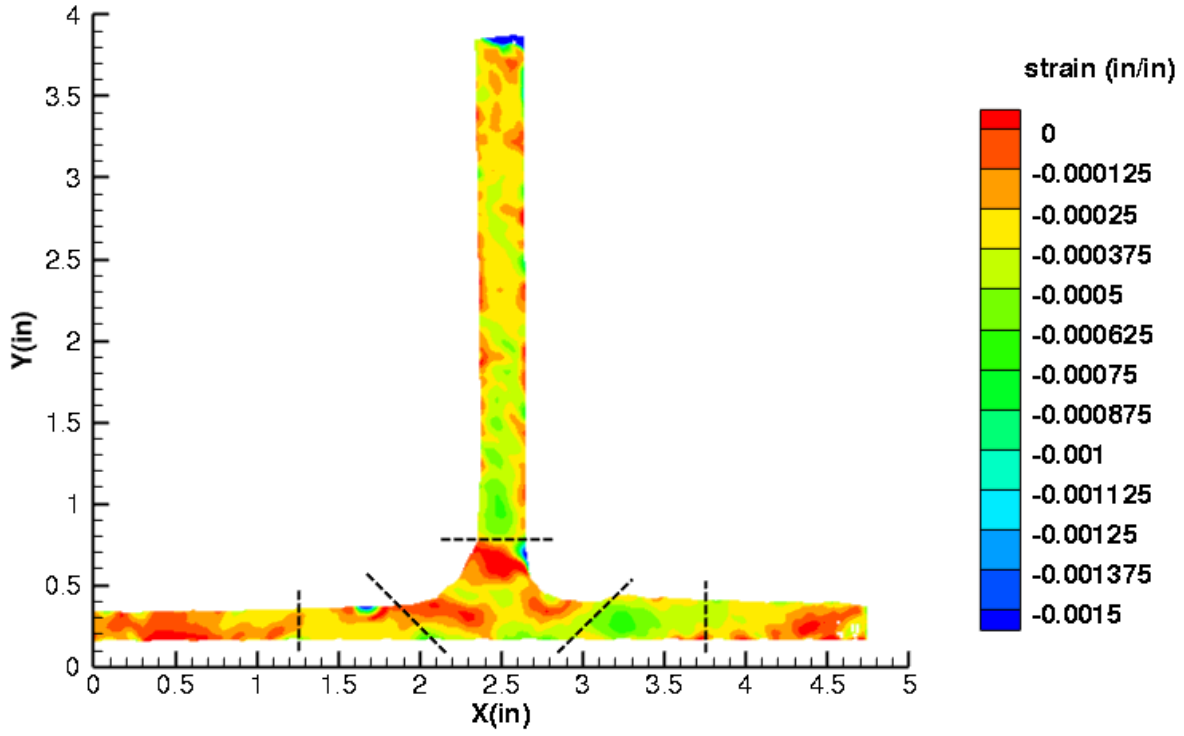

Figure C190. T5S1 strain contours for minimum principal strain at 2632 lb. load, just after initial failure, 29MP VIC data.

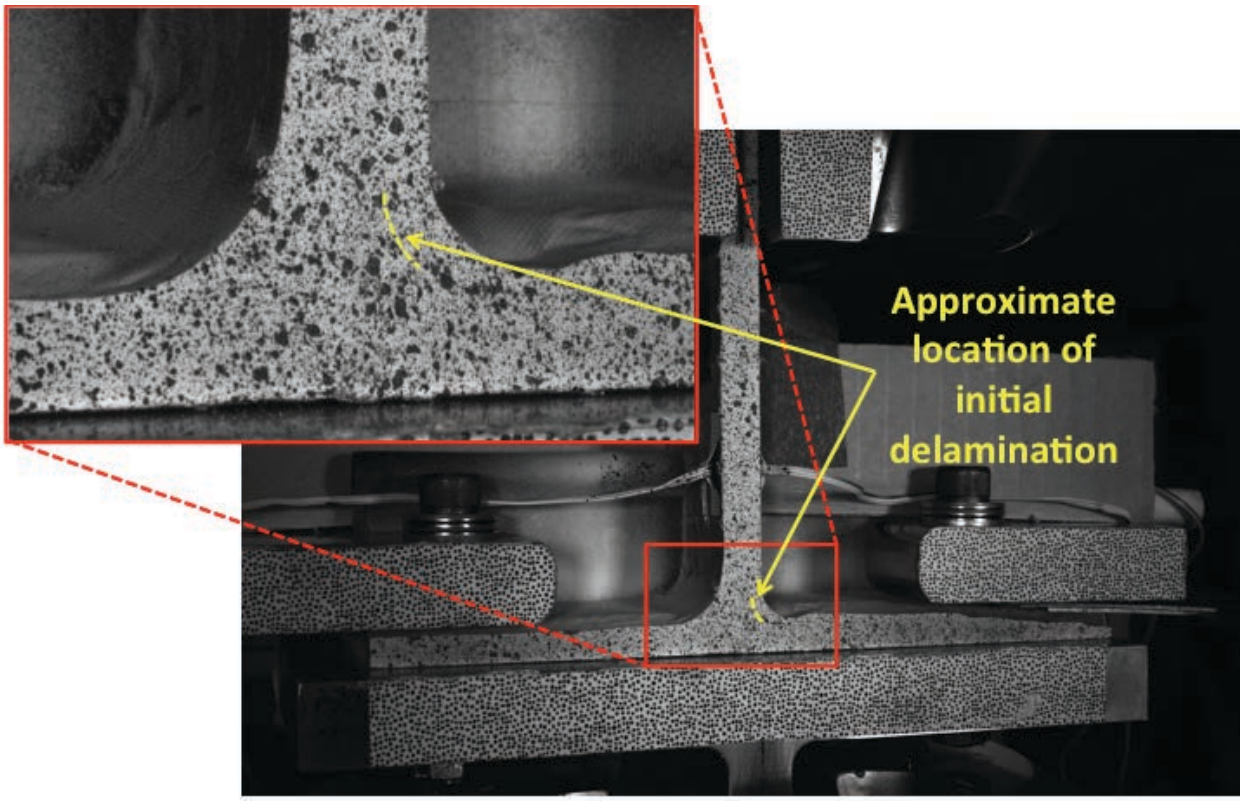

Figure C191. T5S1 image just after initial failure, 29MP VIC data.

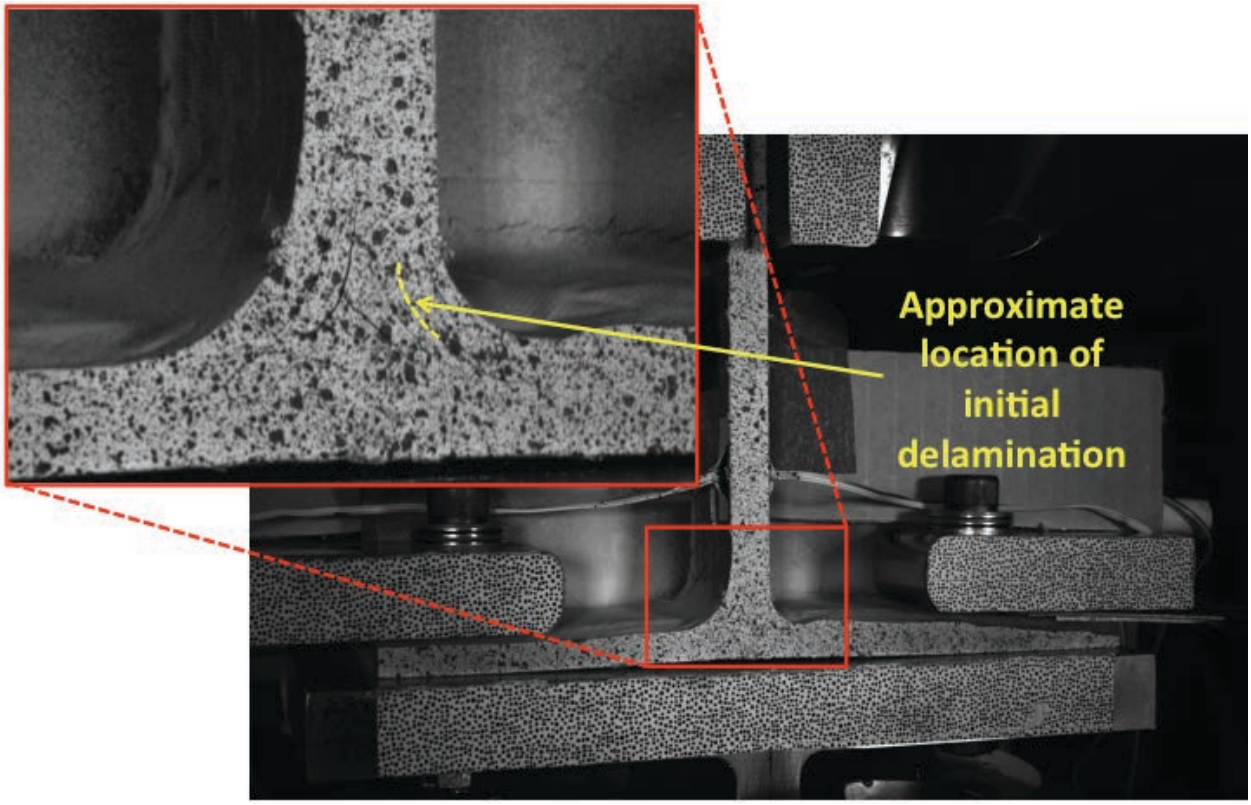

Figure C192. T5S1 image just after maximum load, 29MP VIC data.

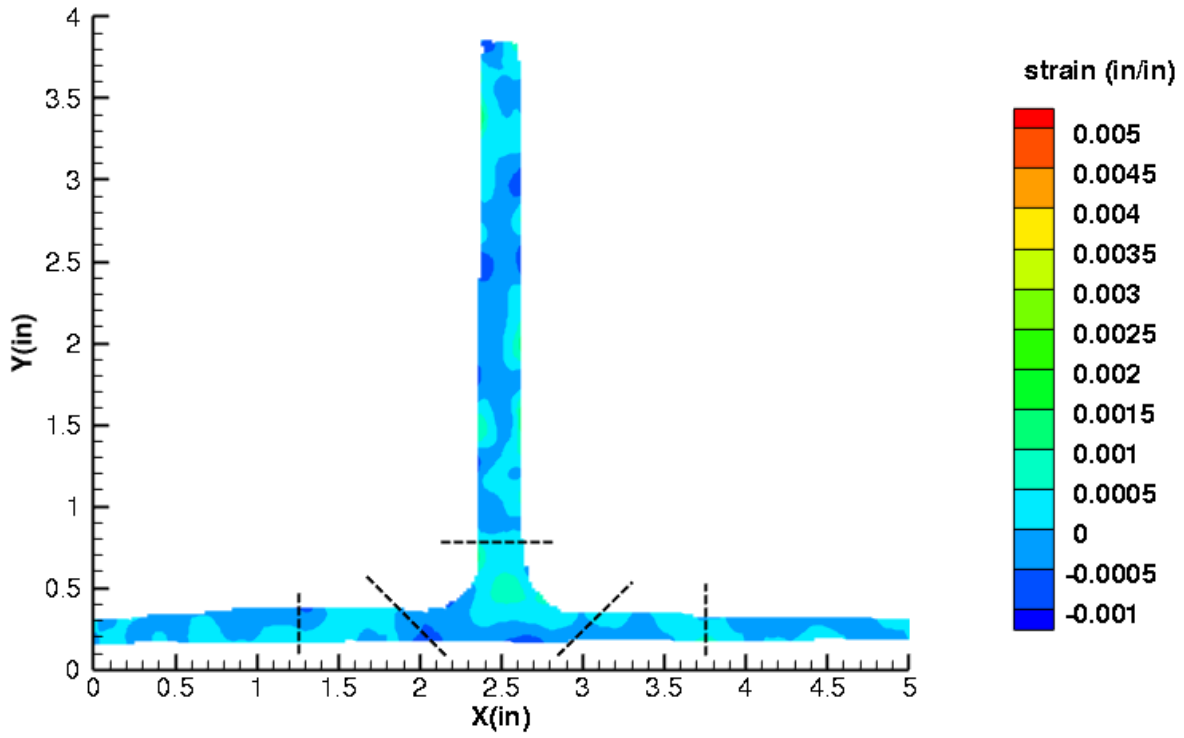

Figure C193. T5S1 strain contours for ε_{xx} at 2597 lb. load, prior to initial failure, 5MP VIC data.

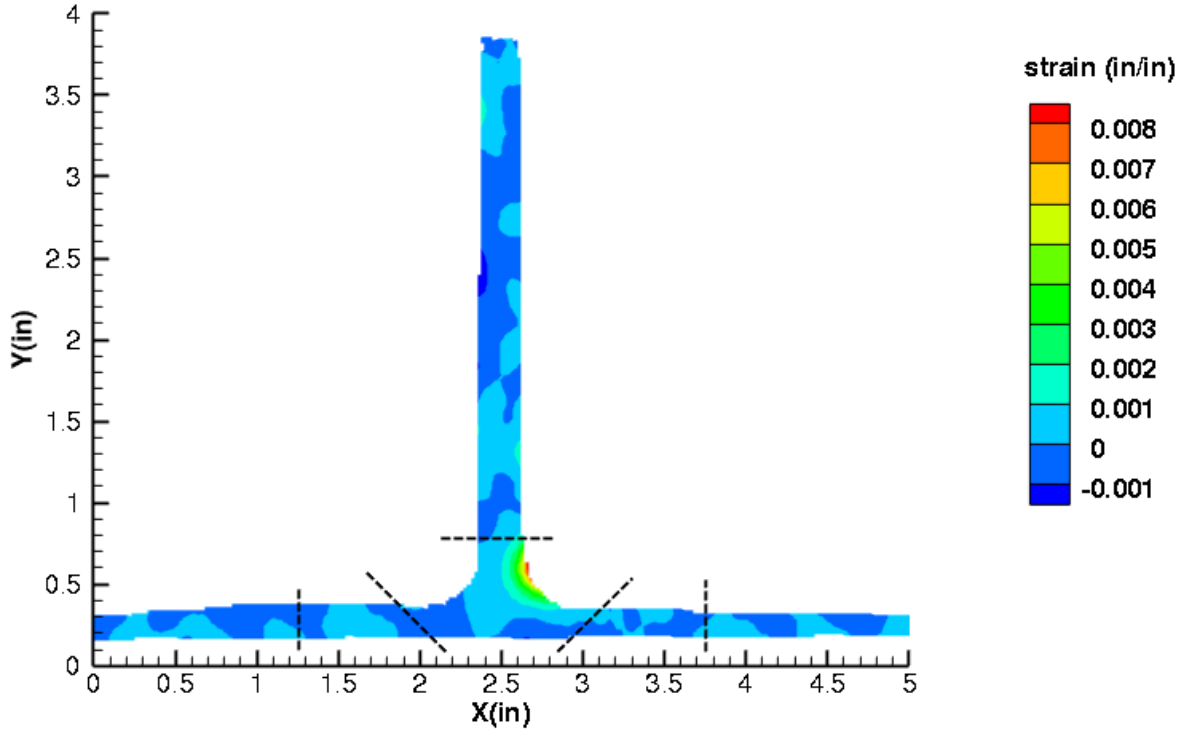

Figure C194. T5S1 strain contours for ε_{xx} at 2534 lb. load, just after initial failure, 5MP VIC data.

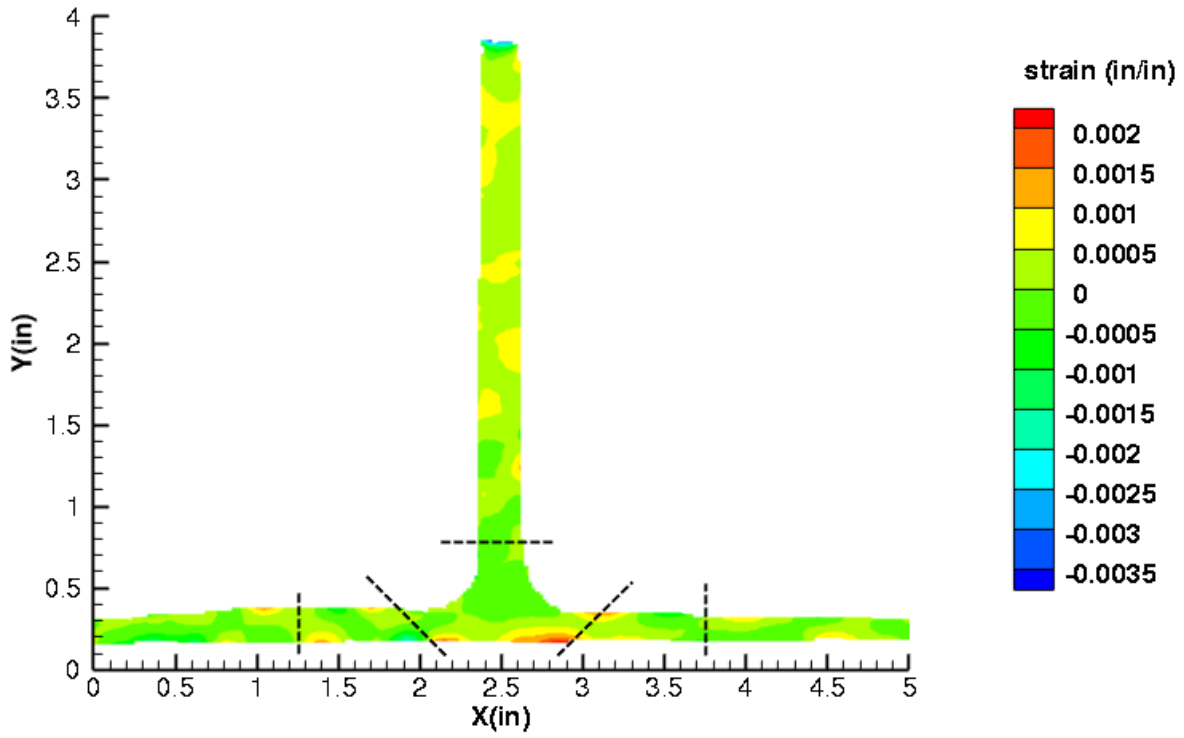

Figure C195. T5S1 strain contours for ε_{yy} at 2597 lb. load, prior to initial failure, 5MP VIC data.

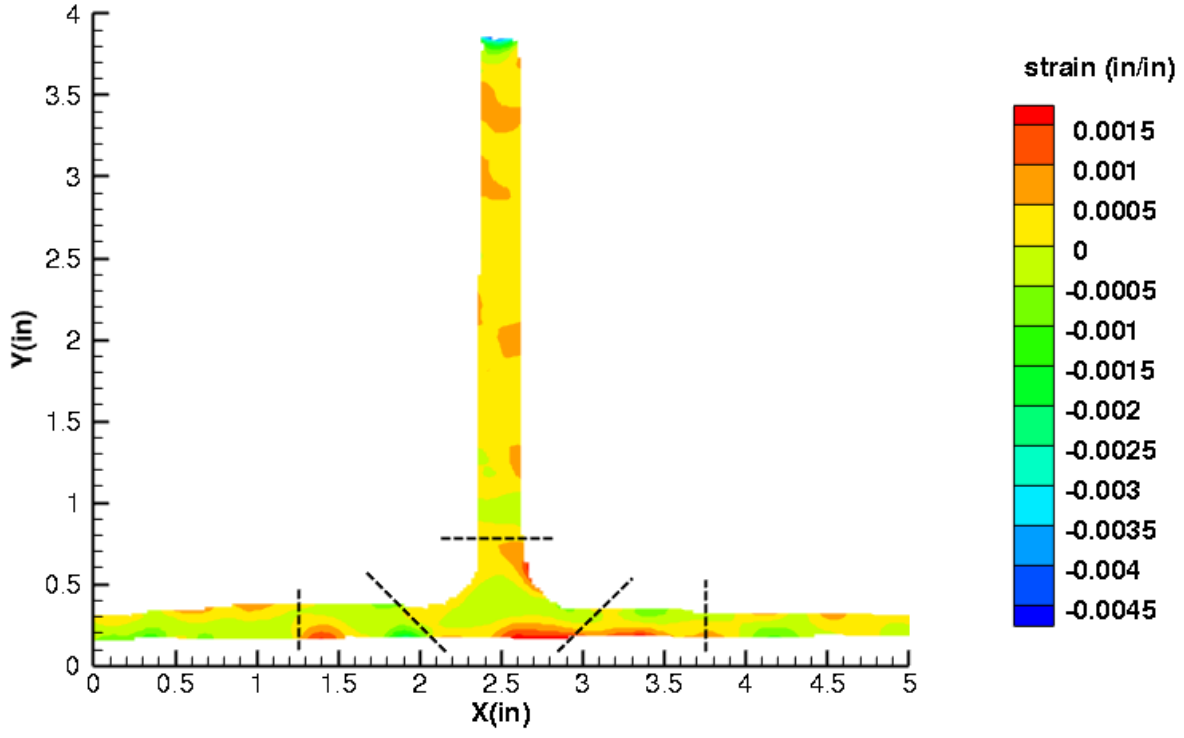

Figure C196. T5S1 strain contours for ε_{yy} at 2534 lb. load, just after initial failure, 5MP VIC data.

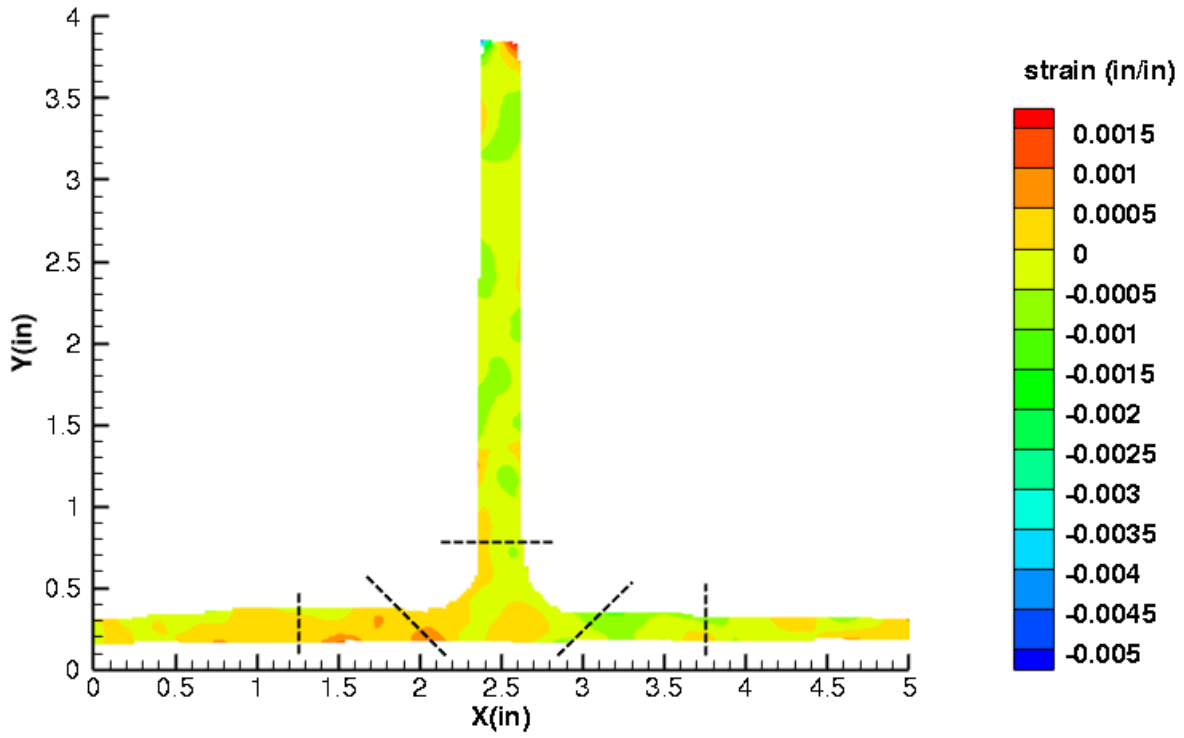

Figure C197. T5S1 strain contours for ε_{xy} at 2597 lb. load, prior to initial failure, 5MP VIC data.

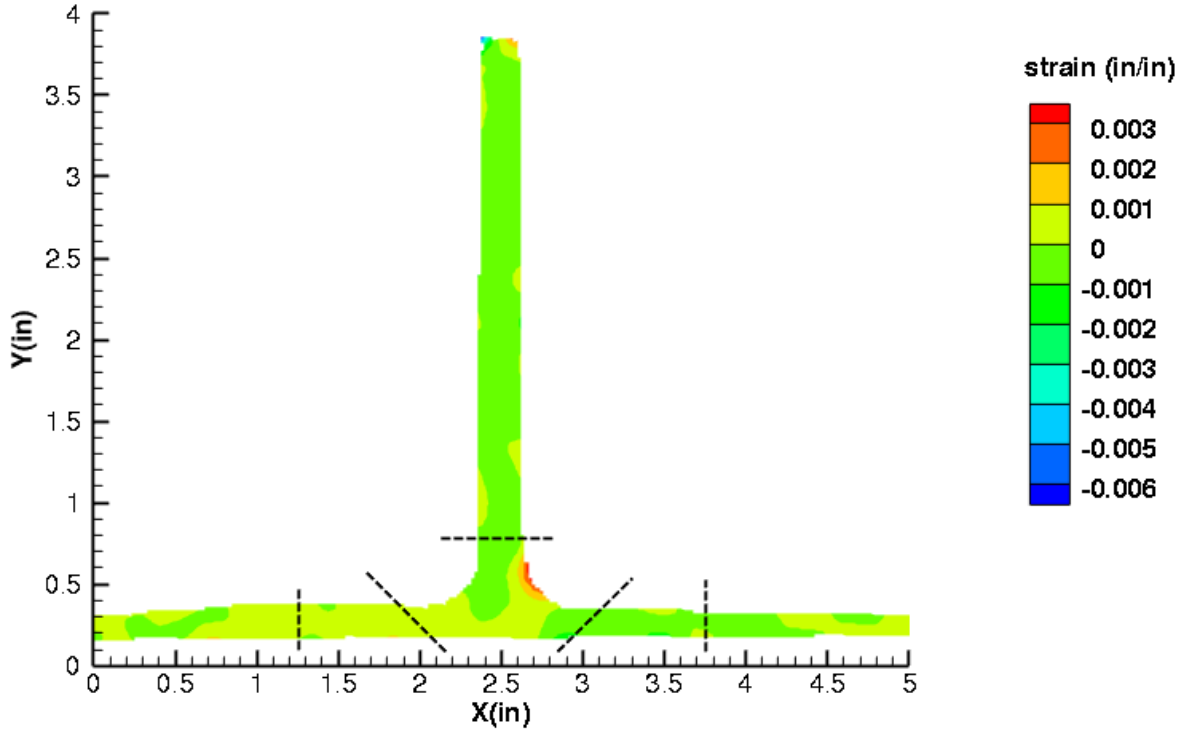

Figure C198. T5S1 strain contours for ε_{xy} at 2534 lb. load, just after initial failure, 5MP VIC data.

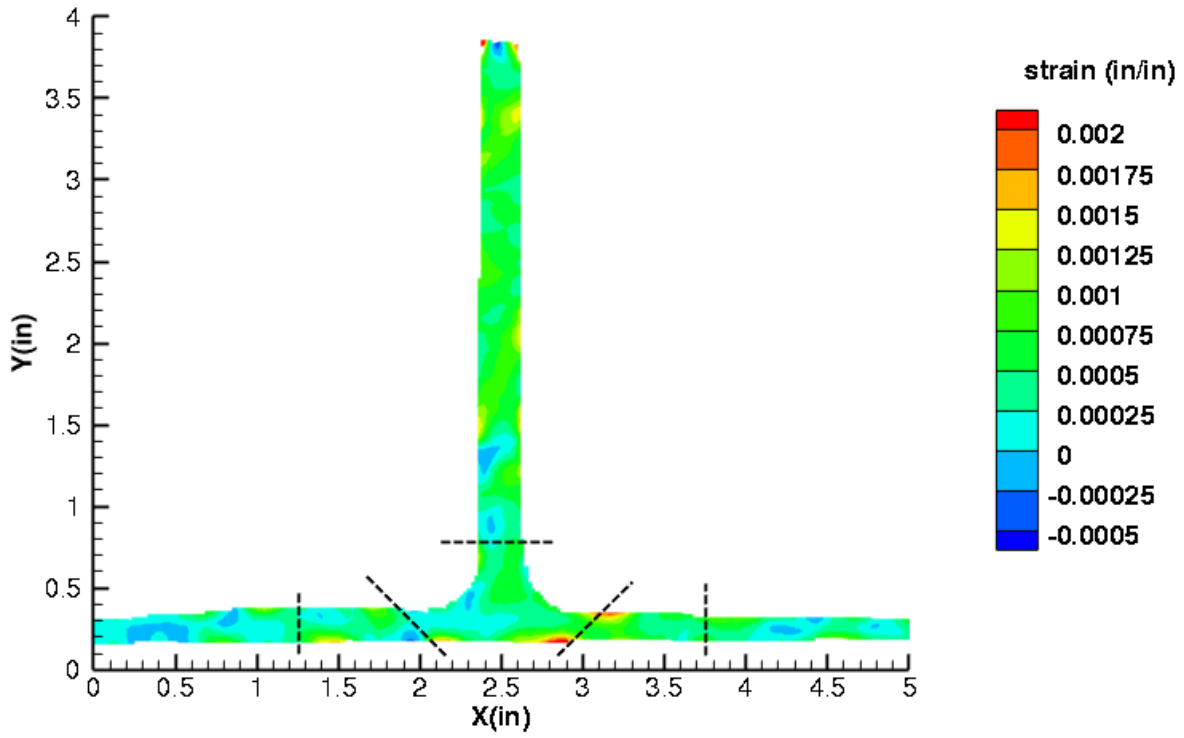

Figure C199. T5S1 strain contours for maximum principal strain at 2597 lb. load, prior to initial failure, 5MP VIC data.

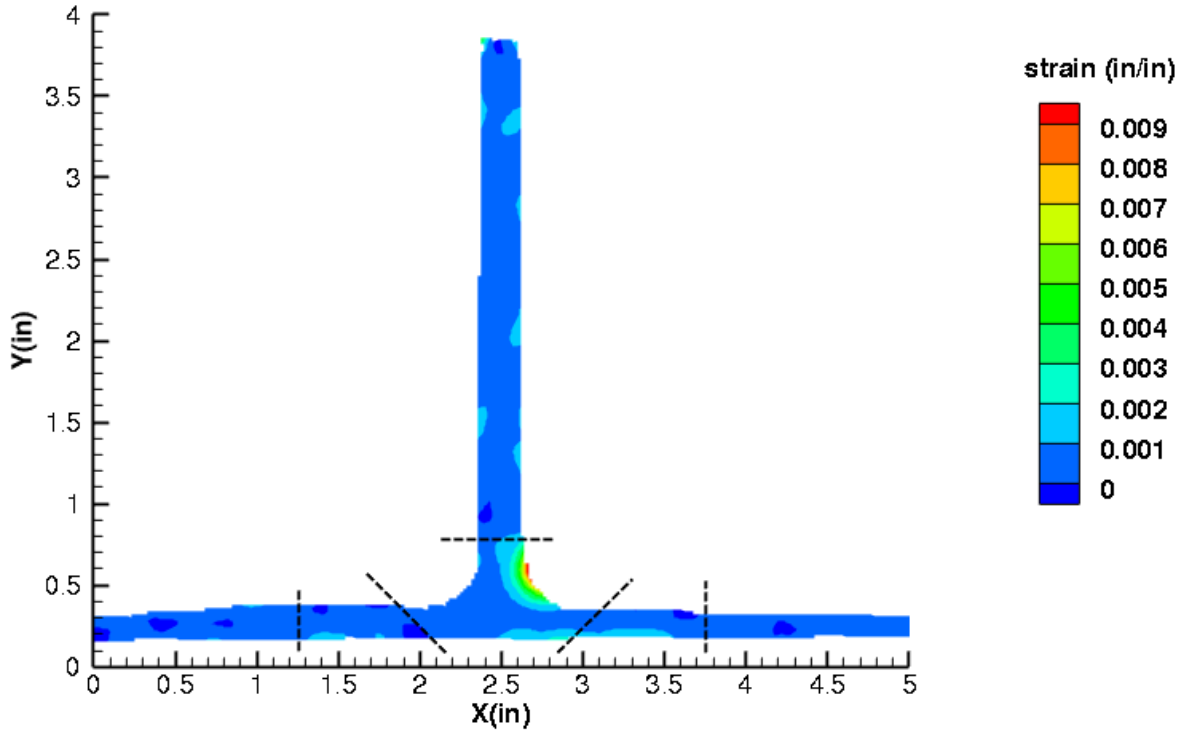

Figure C200. T5S1 strain contours for maximum principal strain at 2534 lb. load, just after initial failure, 5MP VIC data.

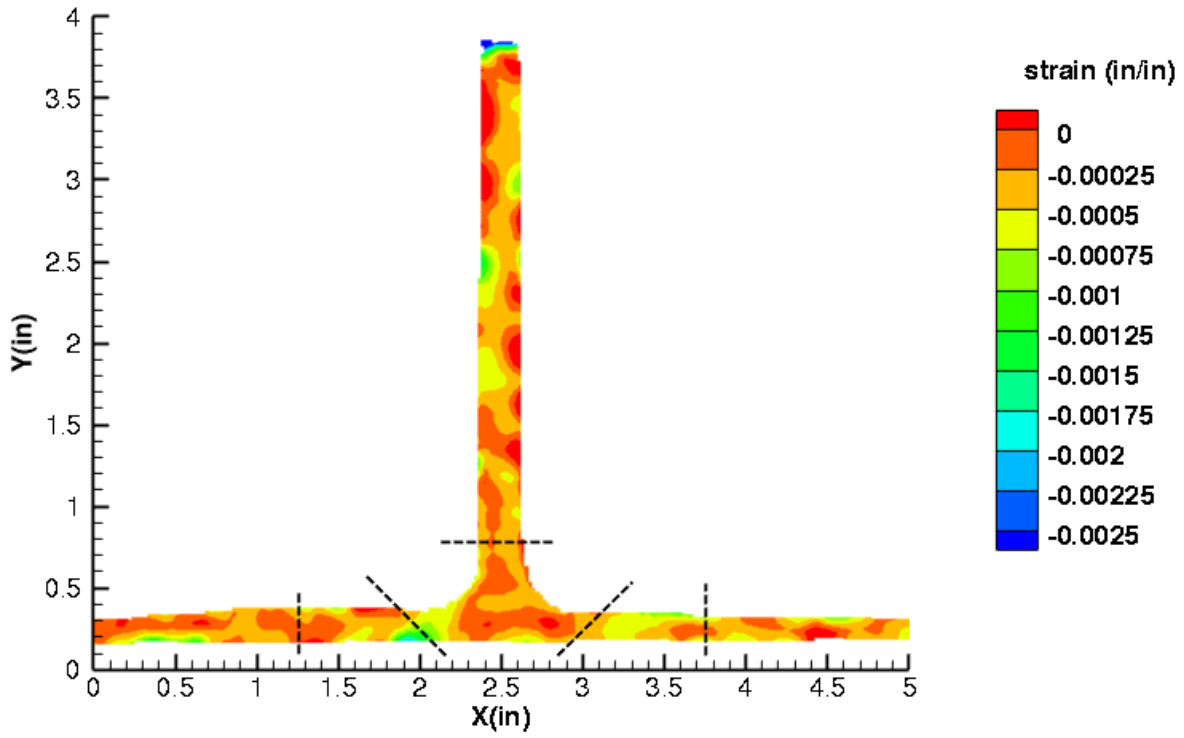

Figure C201. T5S1 strain contours for minimum principal strain at 2597 lb. load, prior to initial failure, 5MP VIC data.

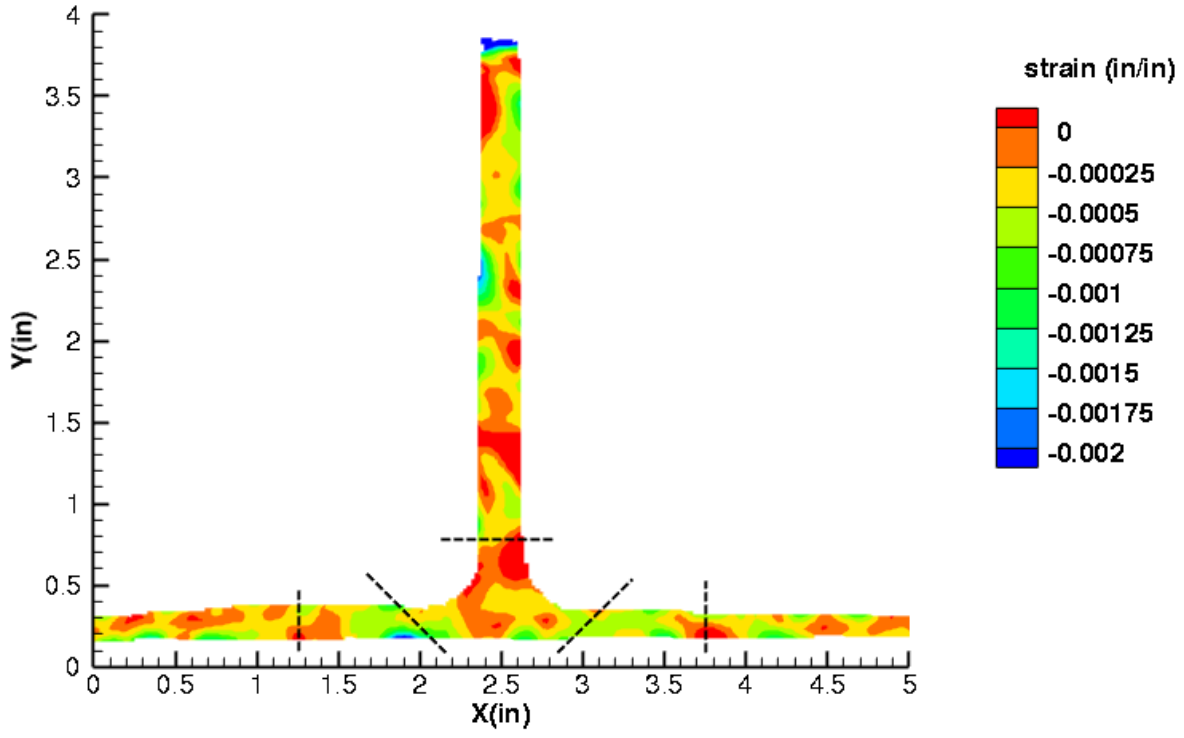

Figure C202. T5S1 strain contours for minimum principal strain at 2534 lb. load, just after initial failure, 5MP VIC data.

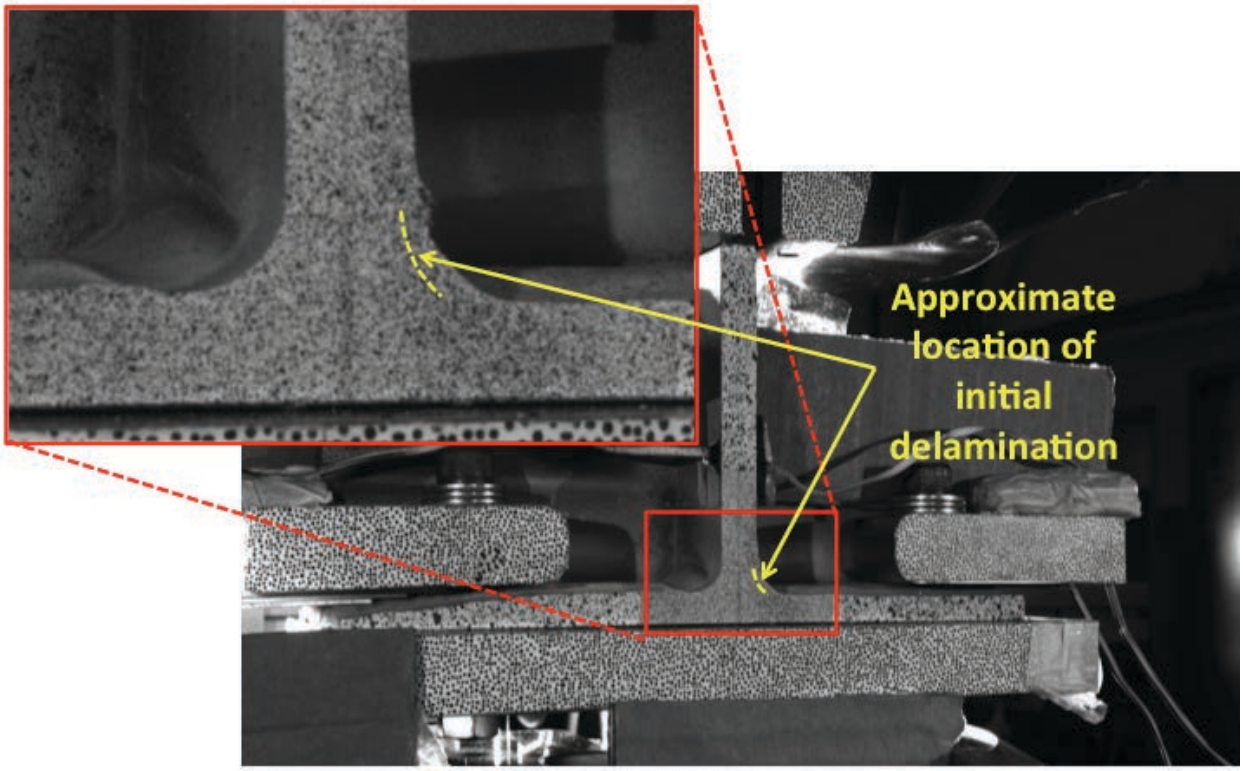

Figure C203. T5S1 image just after initial failure, 5MP VIC data.

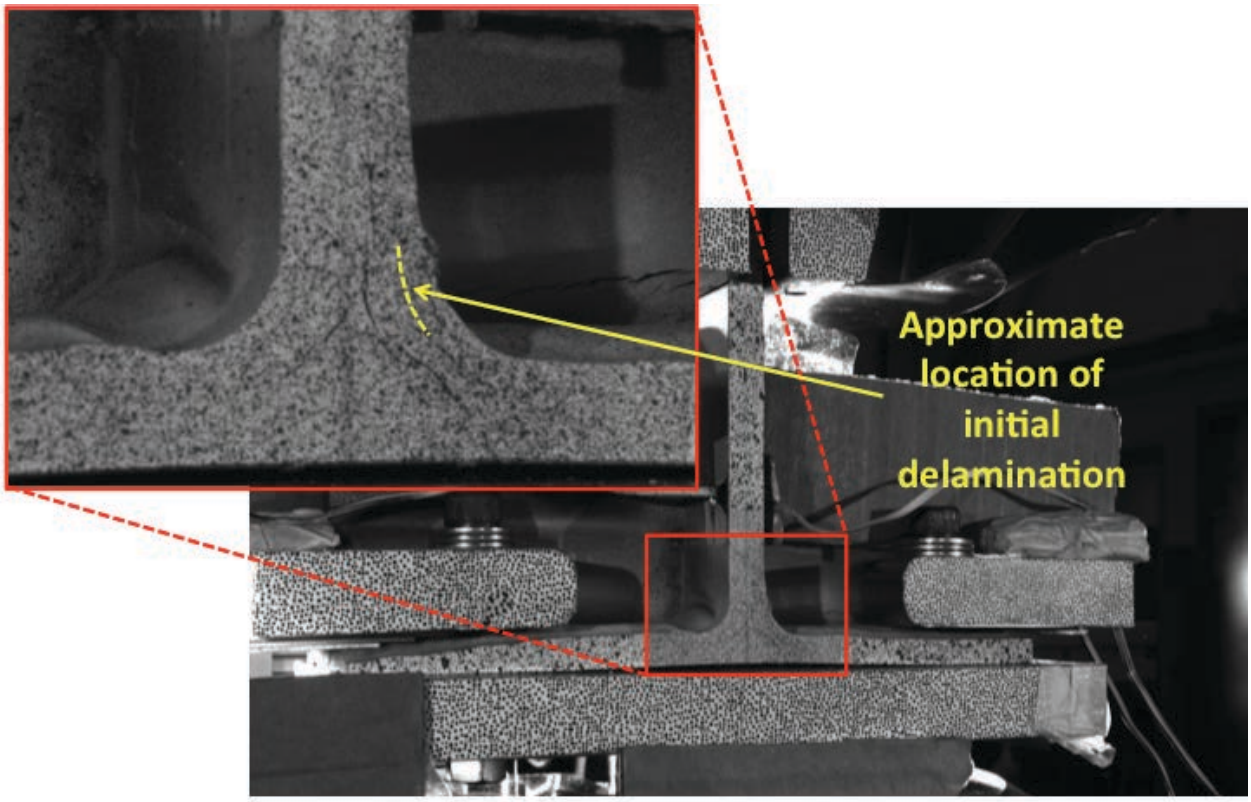

Figure C204. T5S1 image just after maximum load, 5MP VIC data.

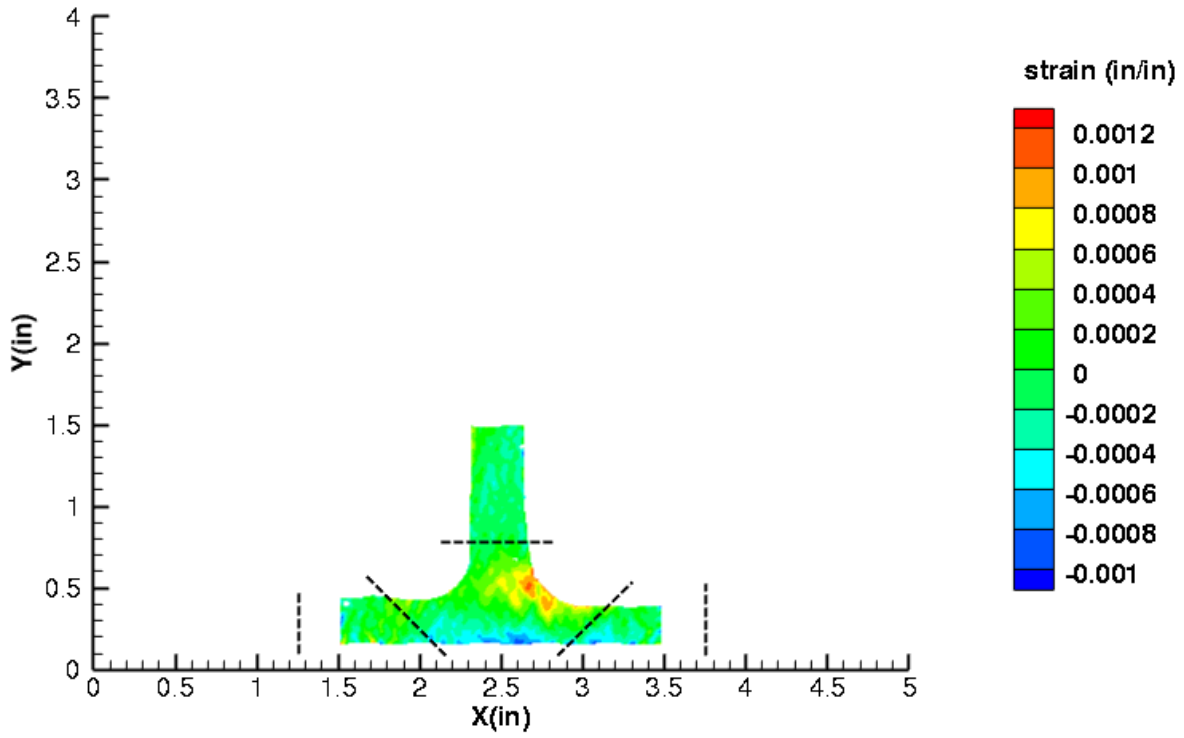

Figure C205. T5S1 strain contours for ε_{xx} at 2597 lb. load, prior to initial failure, local 5MP VIC data.

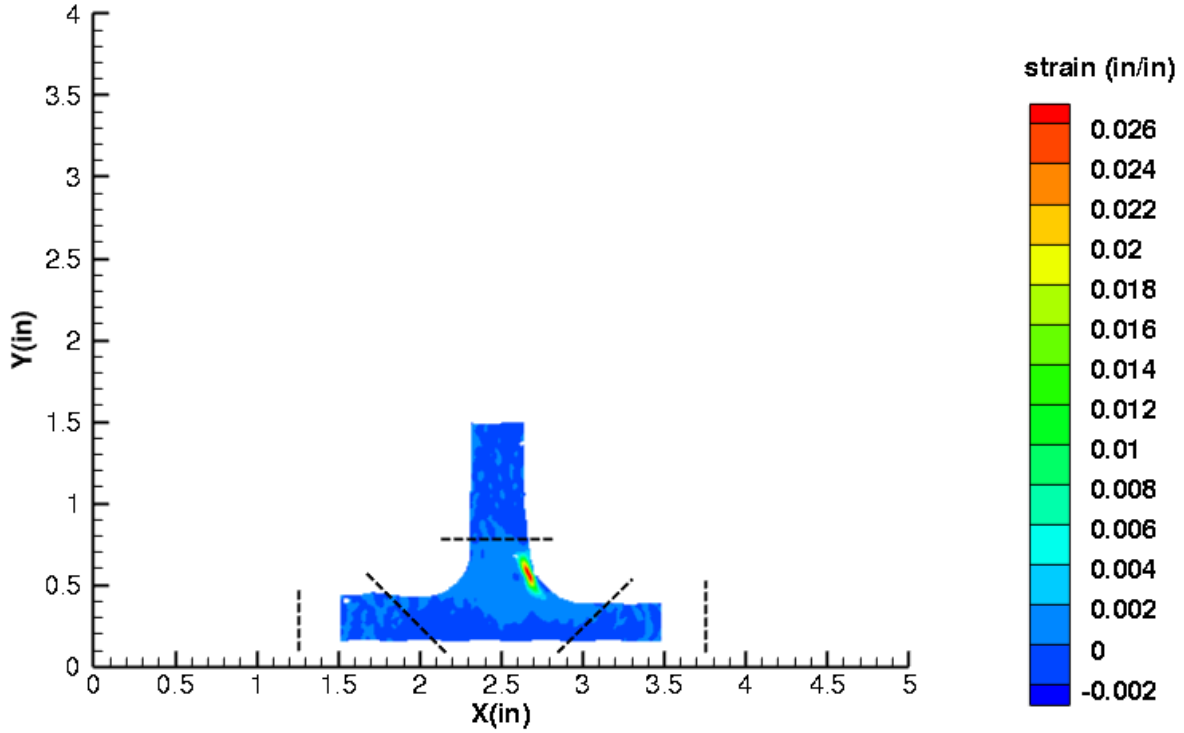

Figure C206. T5S1 strain contours for ε_{xx} at 2534 lb. load, just after initial failure, local 5MP VIC data.

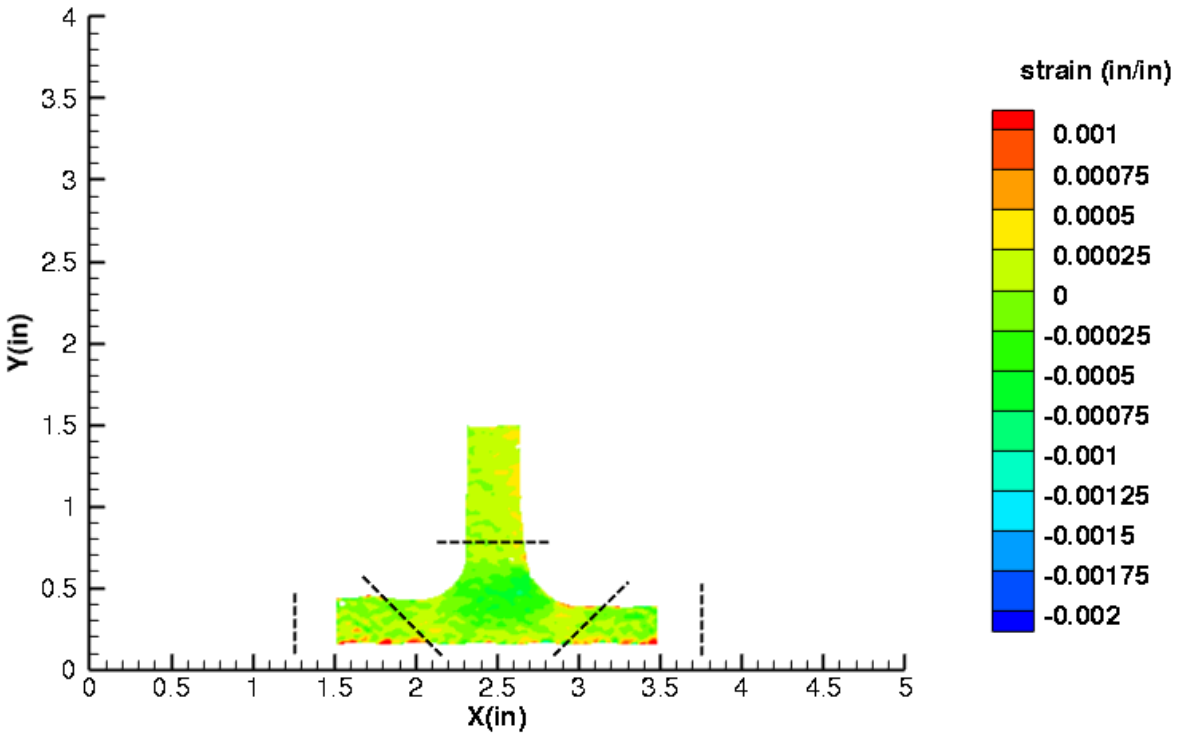

Figure C207. T5S1 strain contours for ε_{yy} at 2597 lb. load, prior to initial failure, local 5MP VIC data.

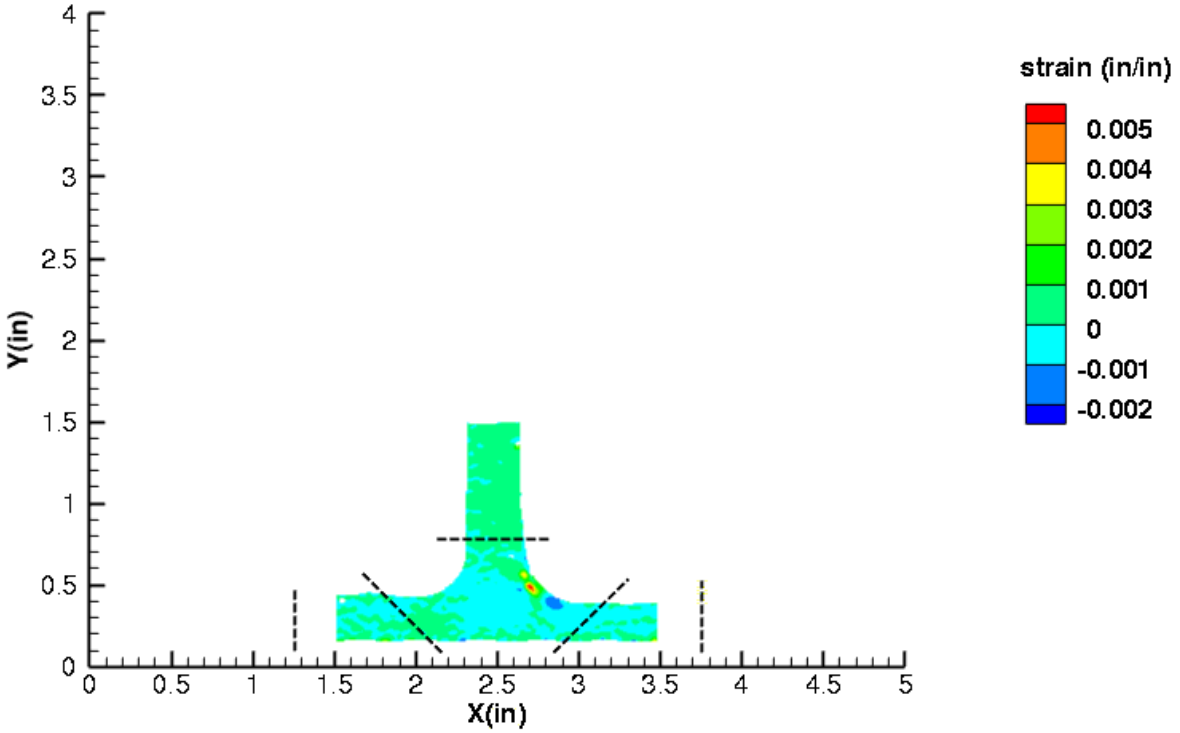

Figure C208. T5S1 strain contours for ε_{yy} at 2534 lb. load, just after initial failure, local 5MP VIC data.

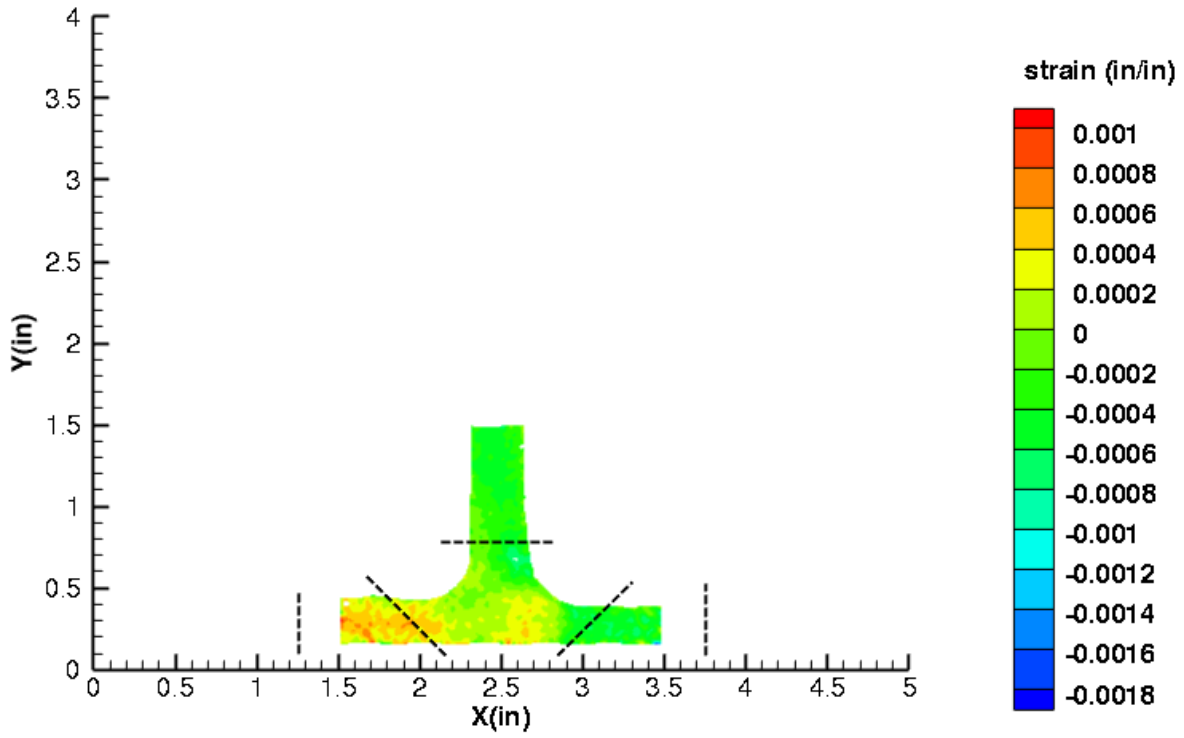

Figure C209. T5S1 strain contours for ε_{xy} at 2597 lb. load, prior to initial failure, local 5MP VIC data.

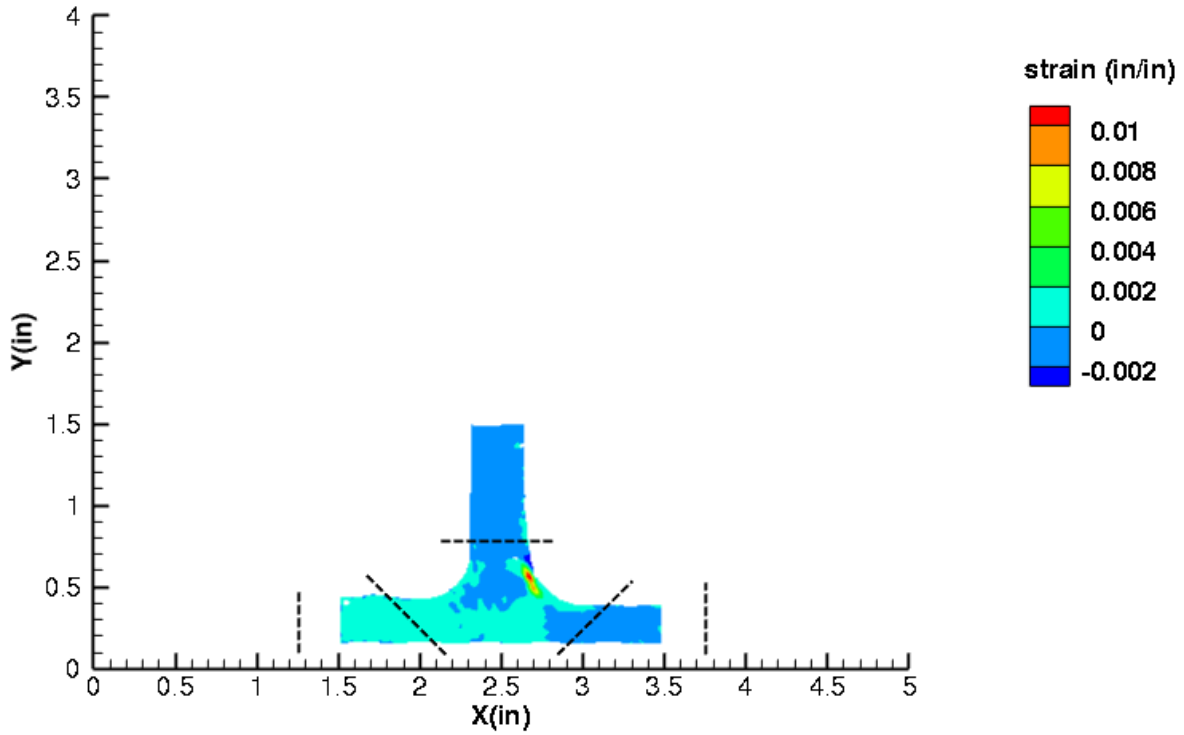

Figure C210. T5S1 strain contours for ε_{xy} at 2534 lb. load, just after initial failure, local 5MP VIC data.

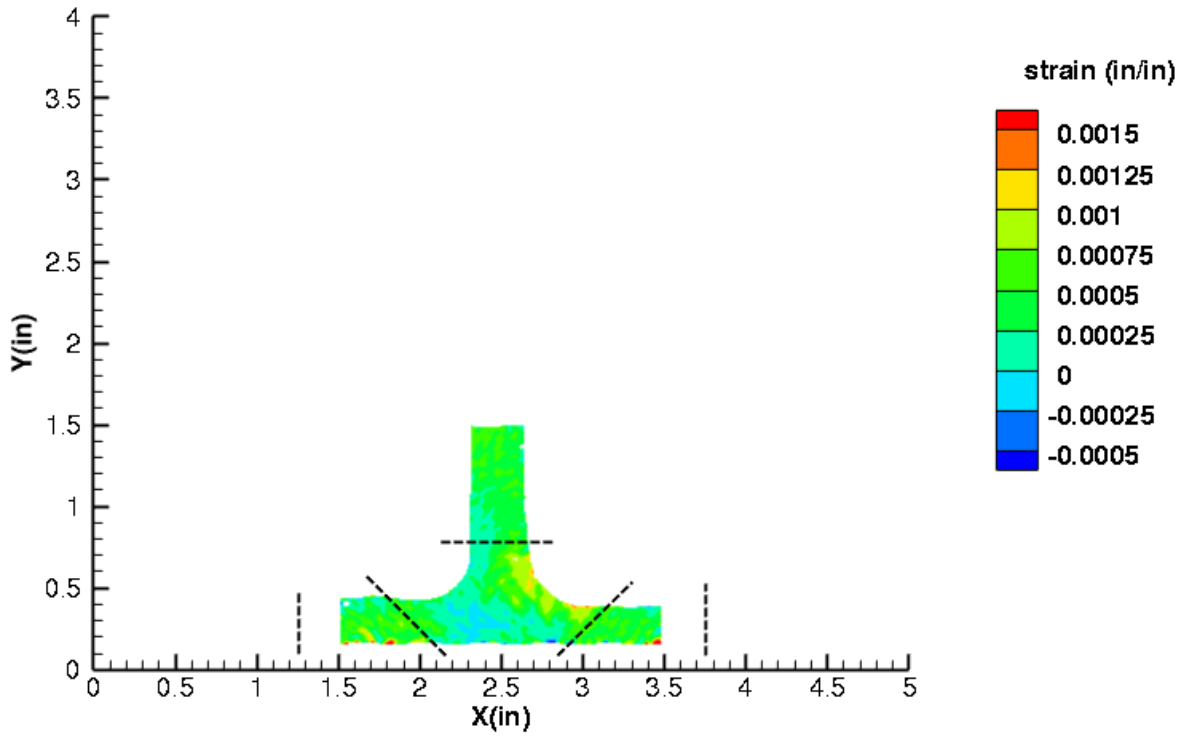

Figure C211. T5S1 strain contours for maximum principal strain at 2597 lb. load, prior to initial failure, local 5MP VIC data.

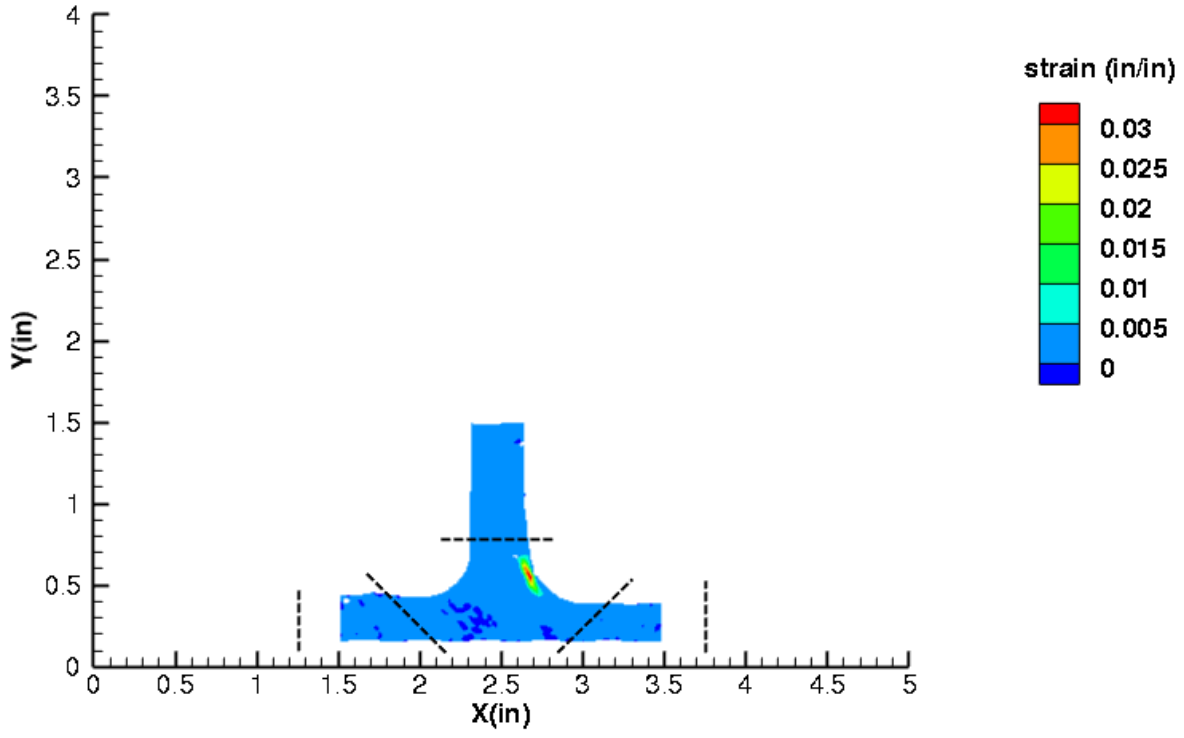

Figure C212. T5S1 strain contours for maximum principal strain at 2534 lb. load, just after initial failure, local 5MP VIC data.

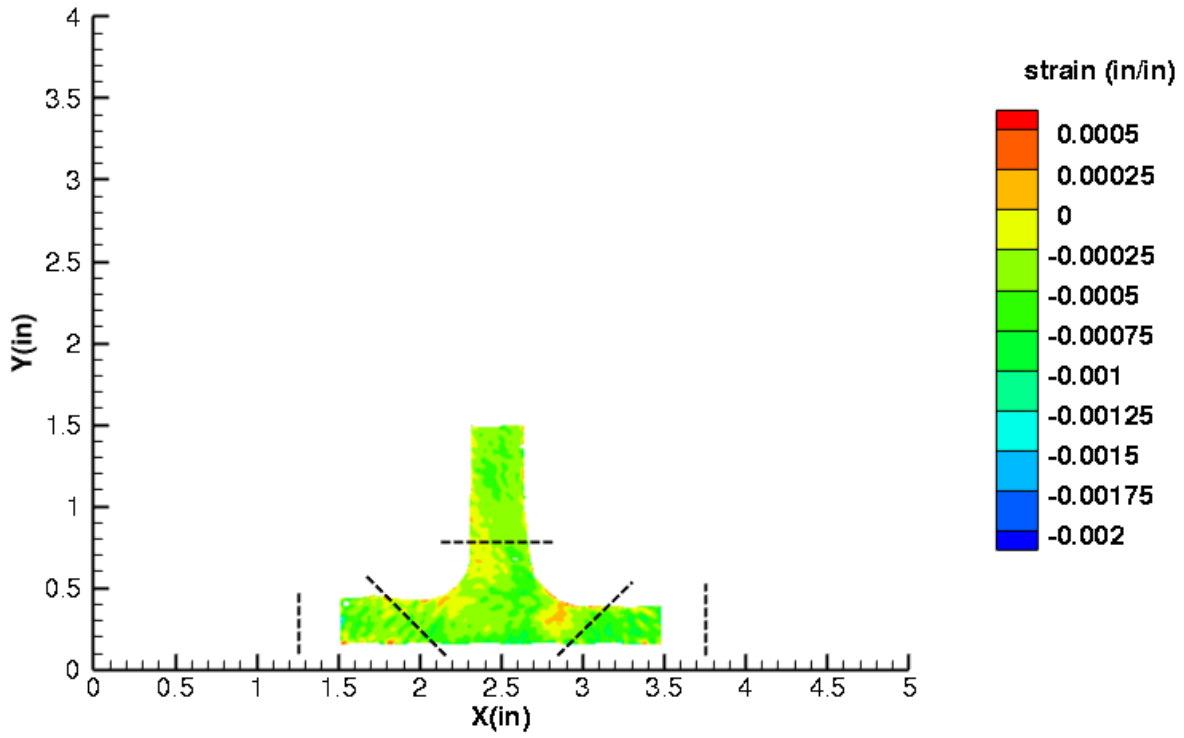

Figure C213. T5S1 strain contours for minimum principal strain at 2597 lb. load, prior to initial failure, local 5MP VIC data.

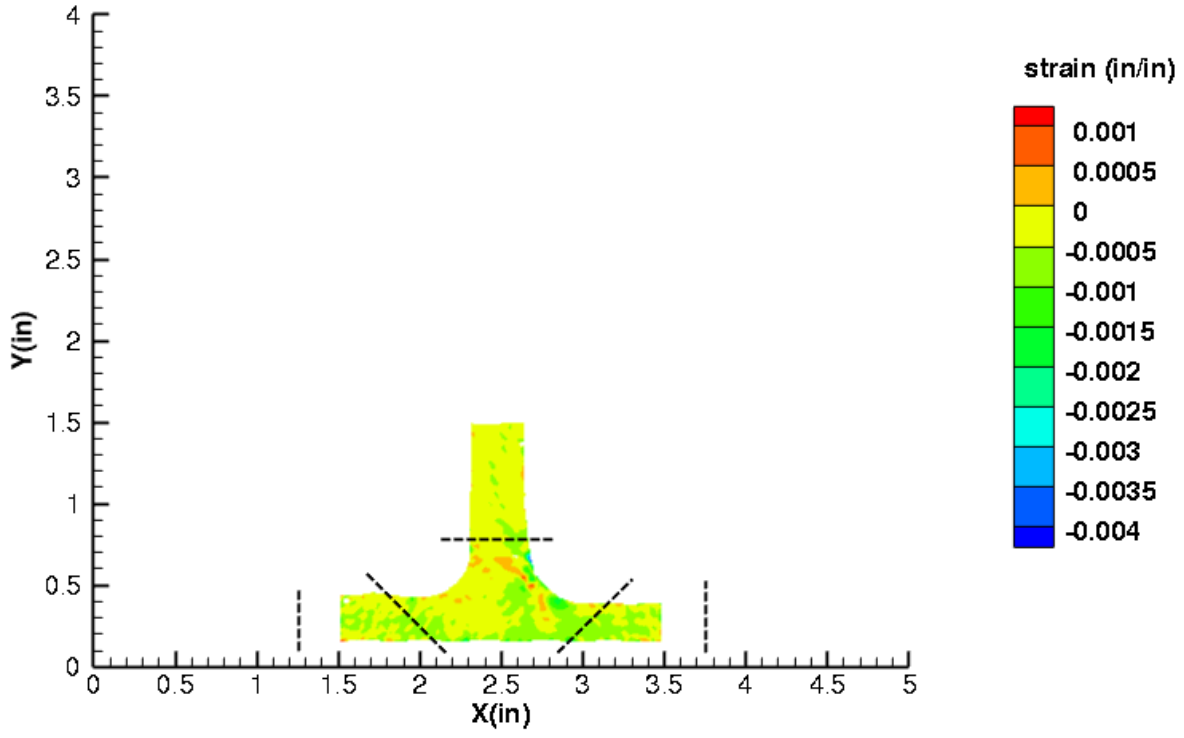

Figure C214. T5S1 strain contours for minimum principal strain at 2534 lb. load, just after initial failure, local 5MP VIC data.

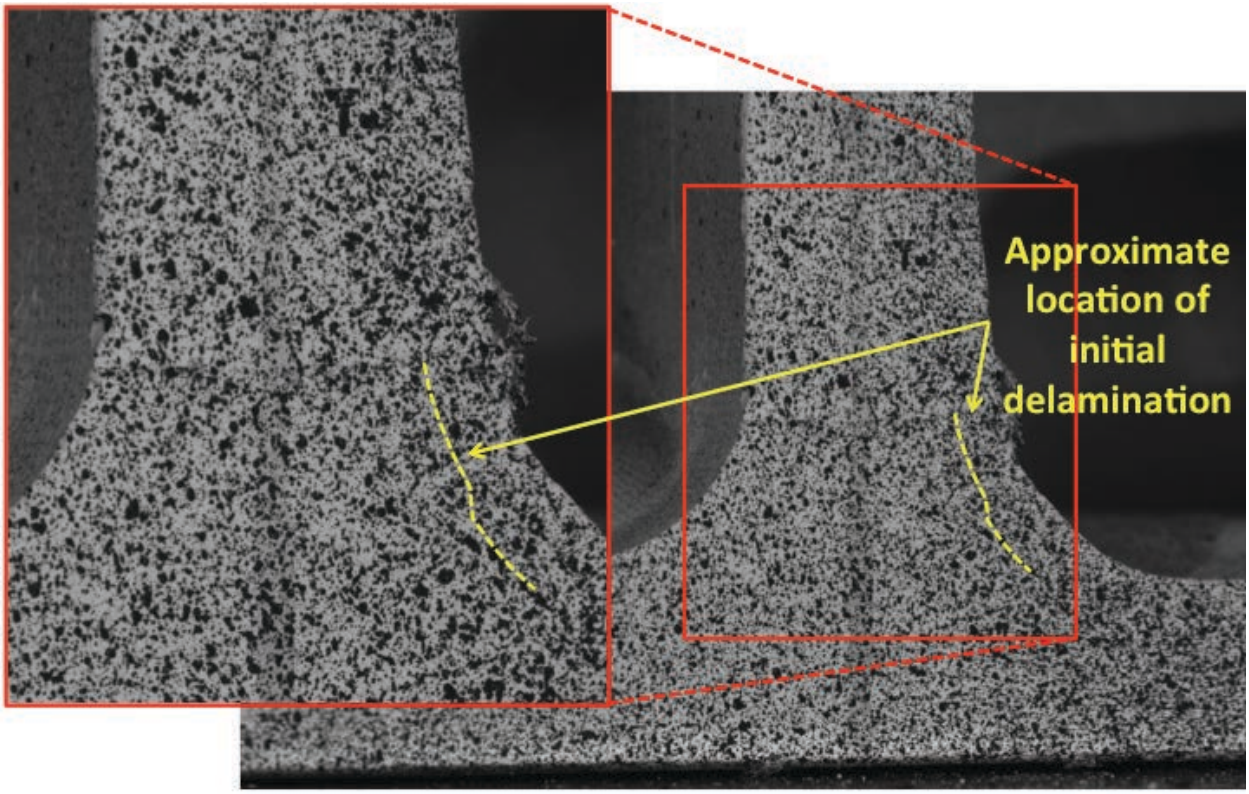

Figure C215. T5S1 image just after initial failure, local 5MP VIC data.

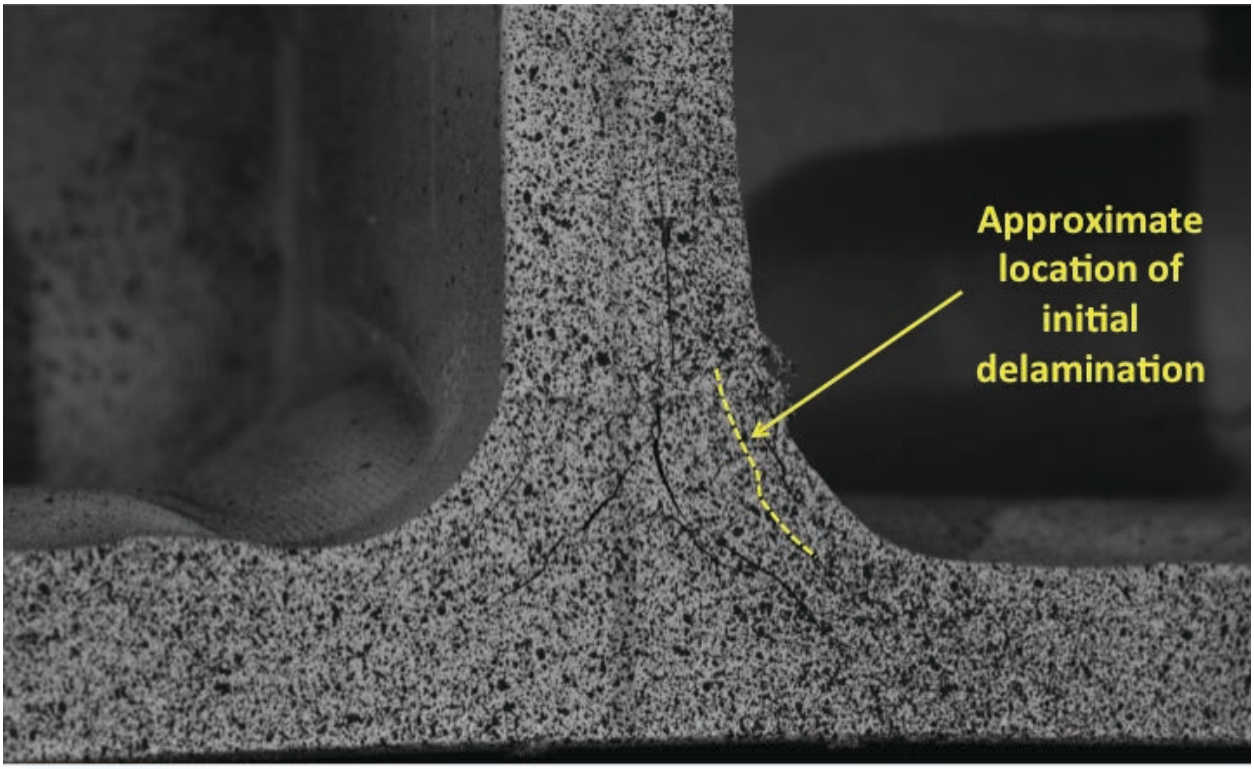

Figure C216. T5S1 image just after maximum load, local 5MP VIC data.

T5S2

This section presents the test data for the T5S2 test article.

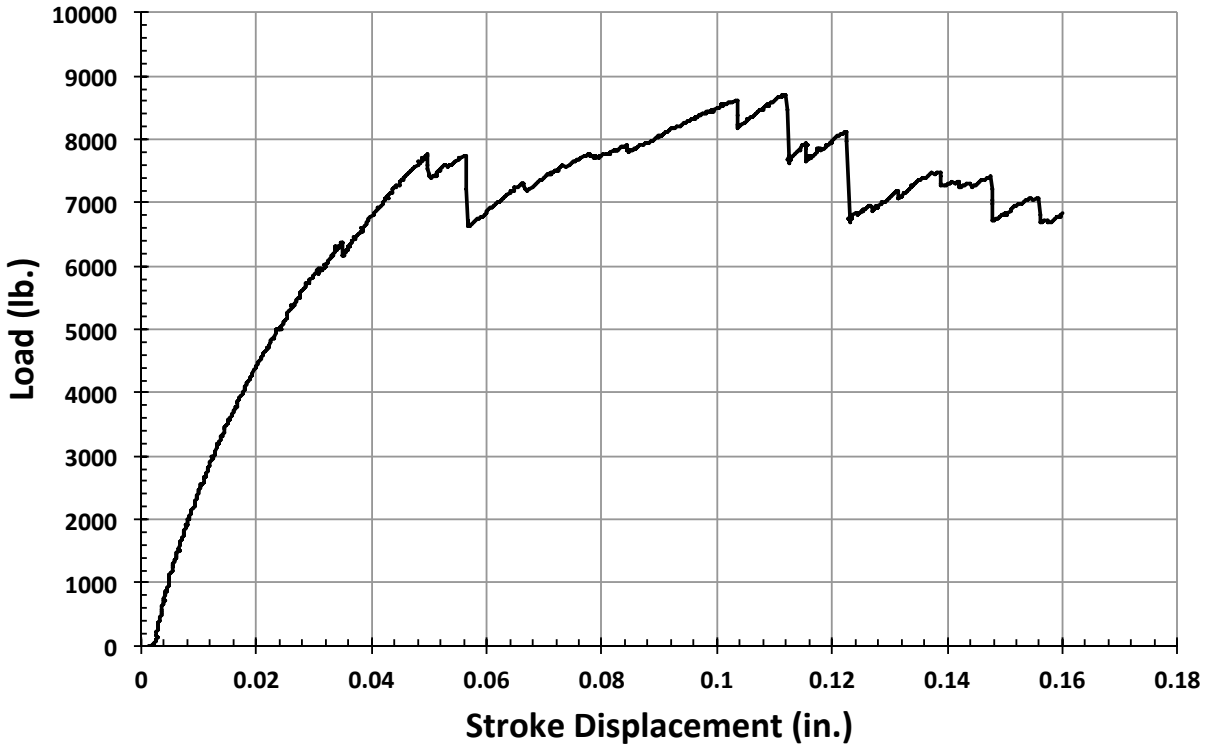

Figure C217. T5S2 load vs. stroke.

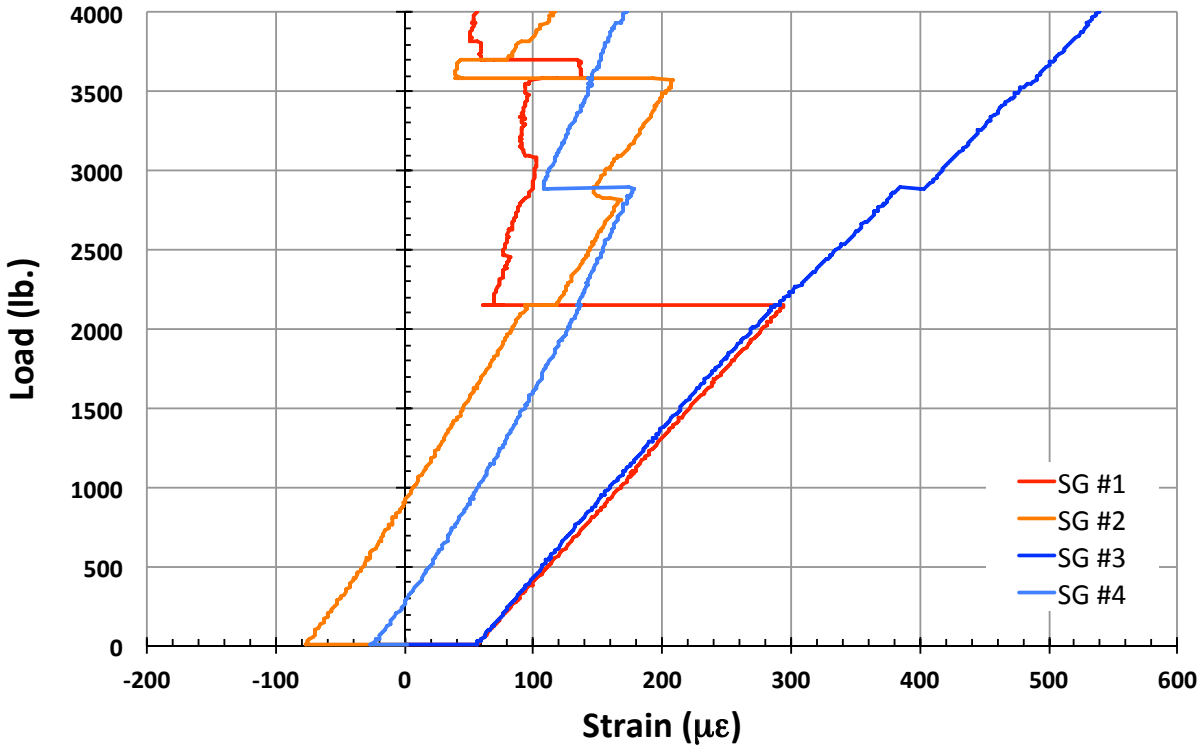

Figure C218. T5S2 load vs. strain, initial loading.

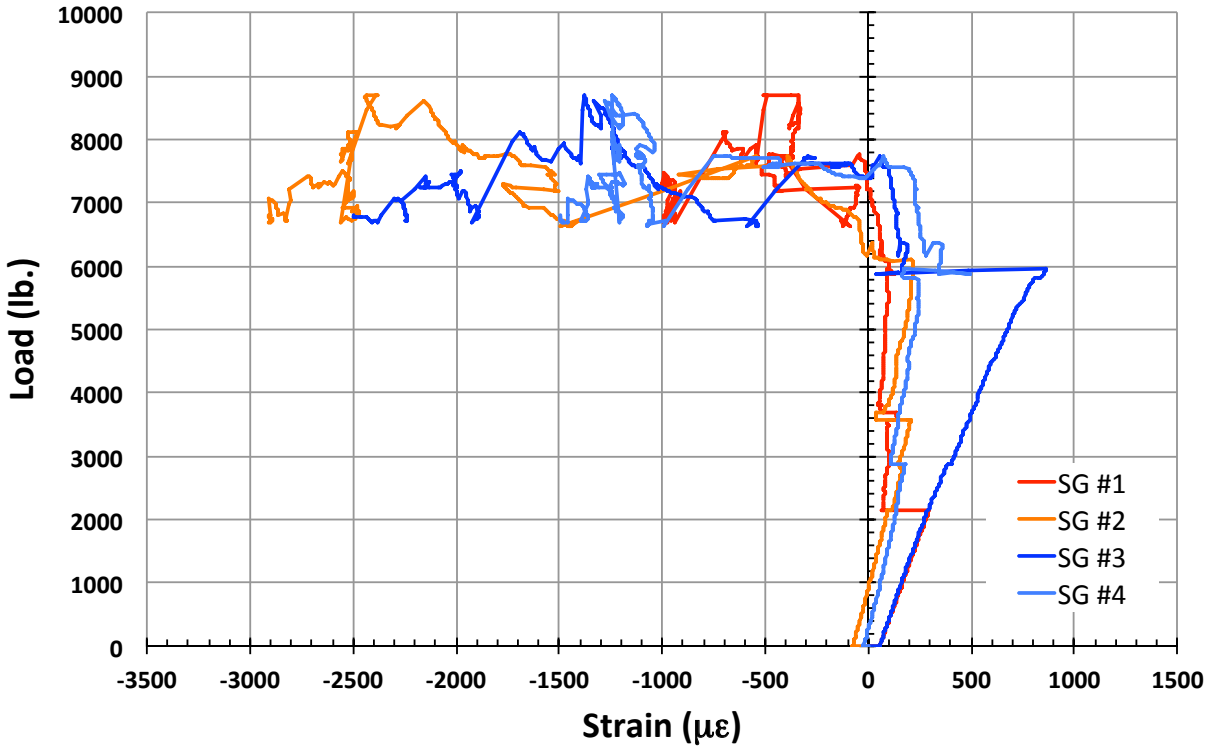

Figure C219. T5S2 load vs. strain.

T5S3

This section presents the test data for the T5S3 test article.

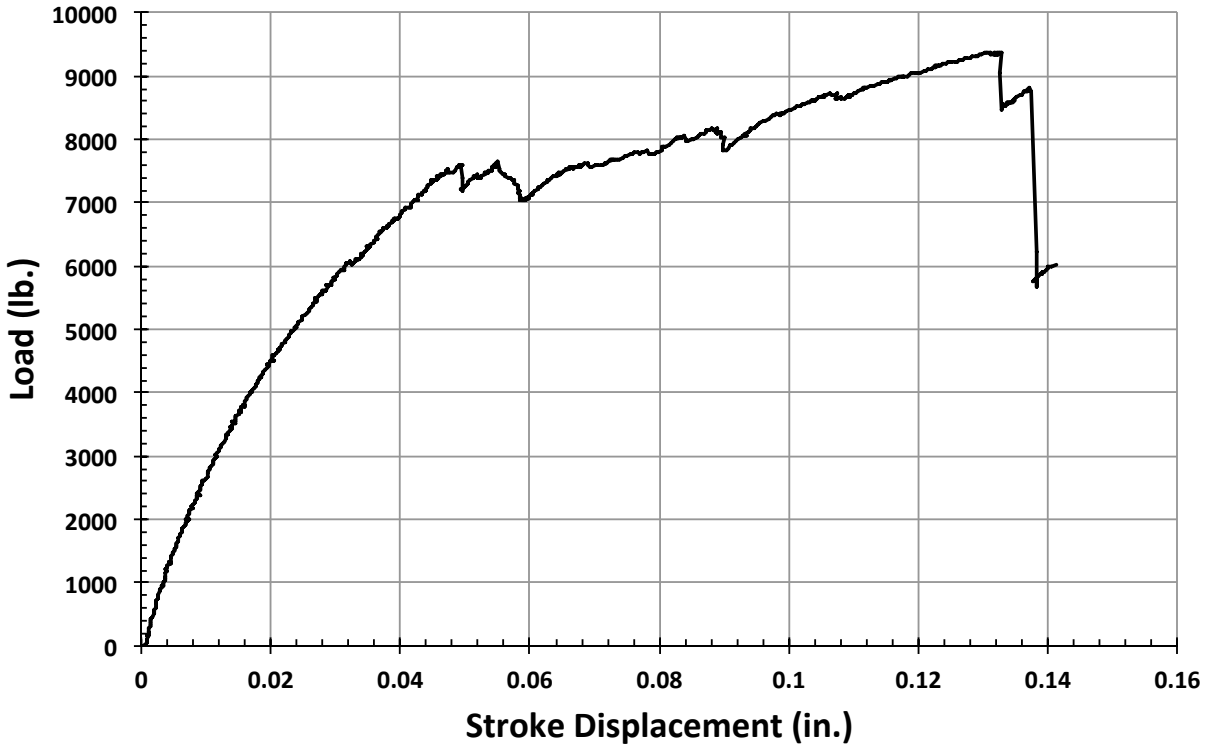

Figure C220. T5S3 load vs. stroke.

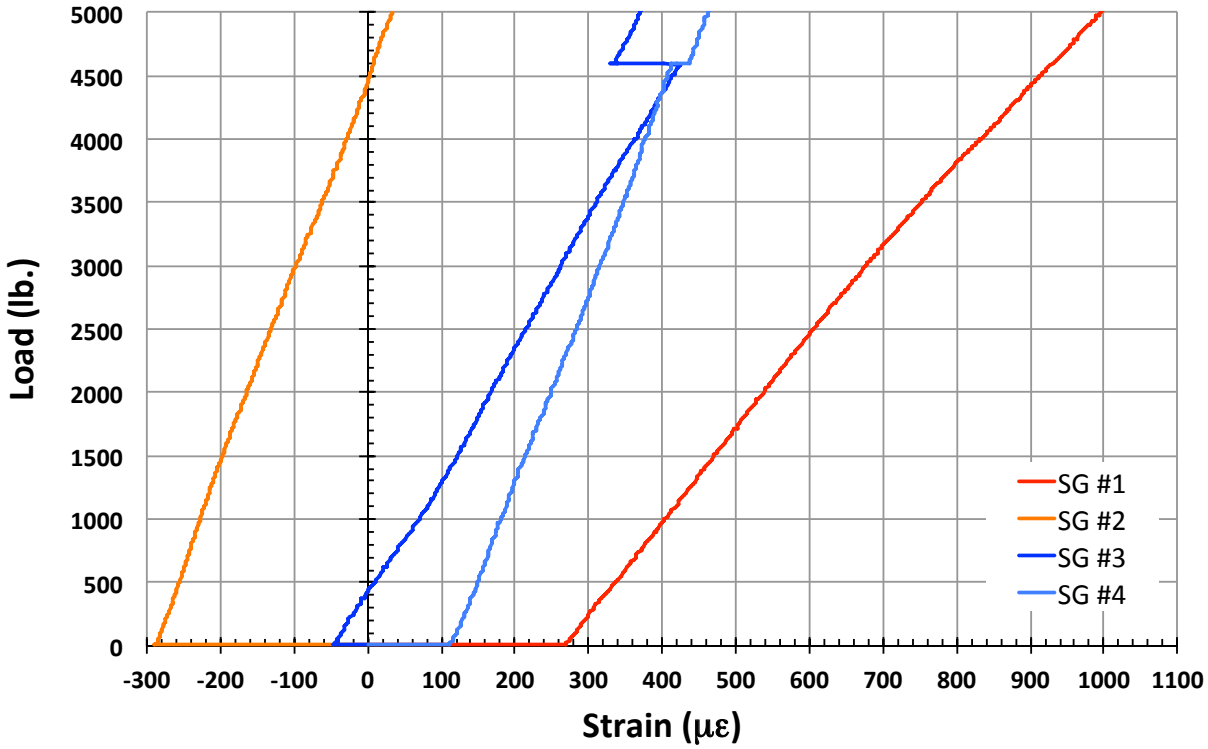

Figure C221. T5S3 load vs. strain, initial loading.

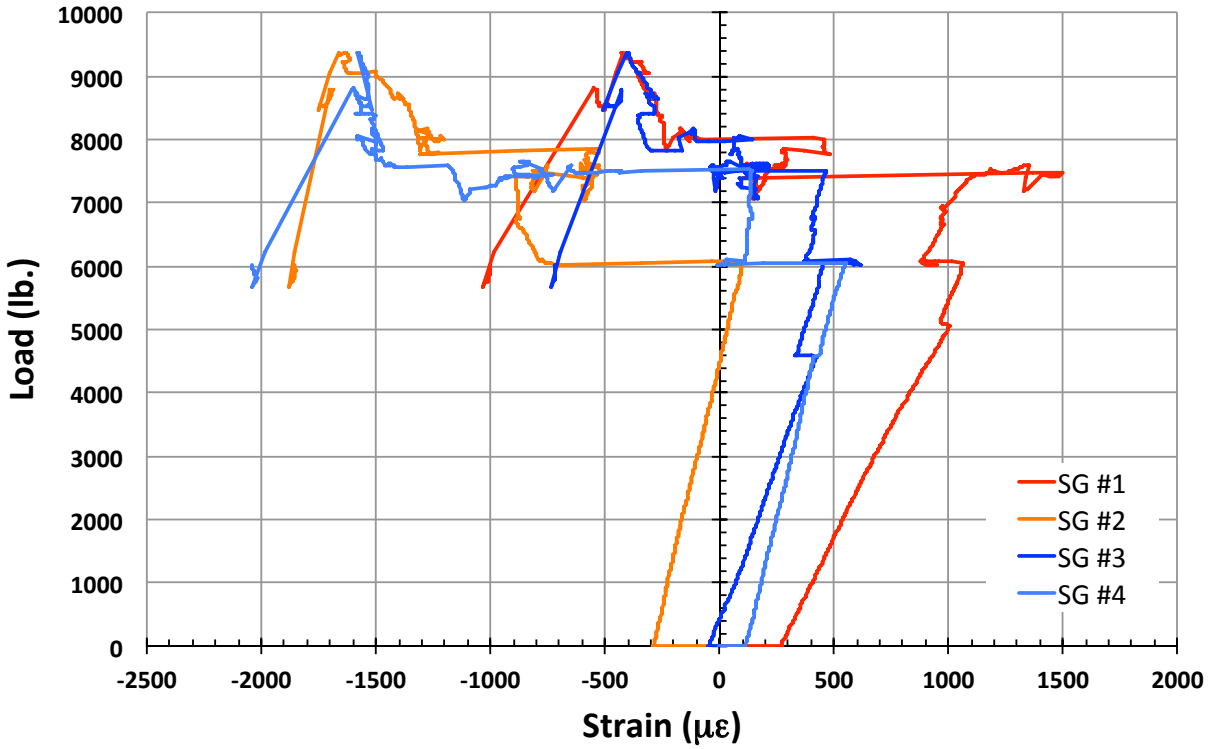

Figure C222. T5S3 load vs. strain.

T5N1

This section presents the test data for the T5N1 test article, and includes strain plots and failure images.

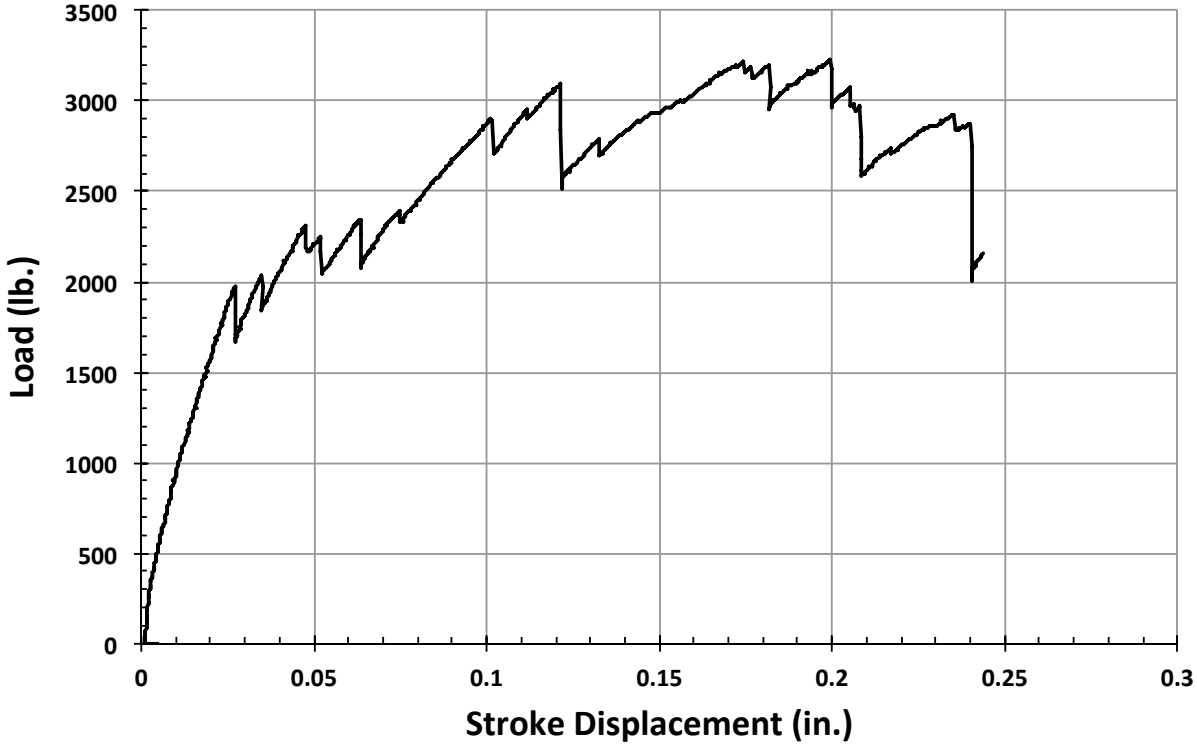

Figure C223. T5N1 load vs. stroke.

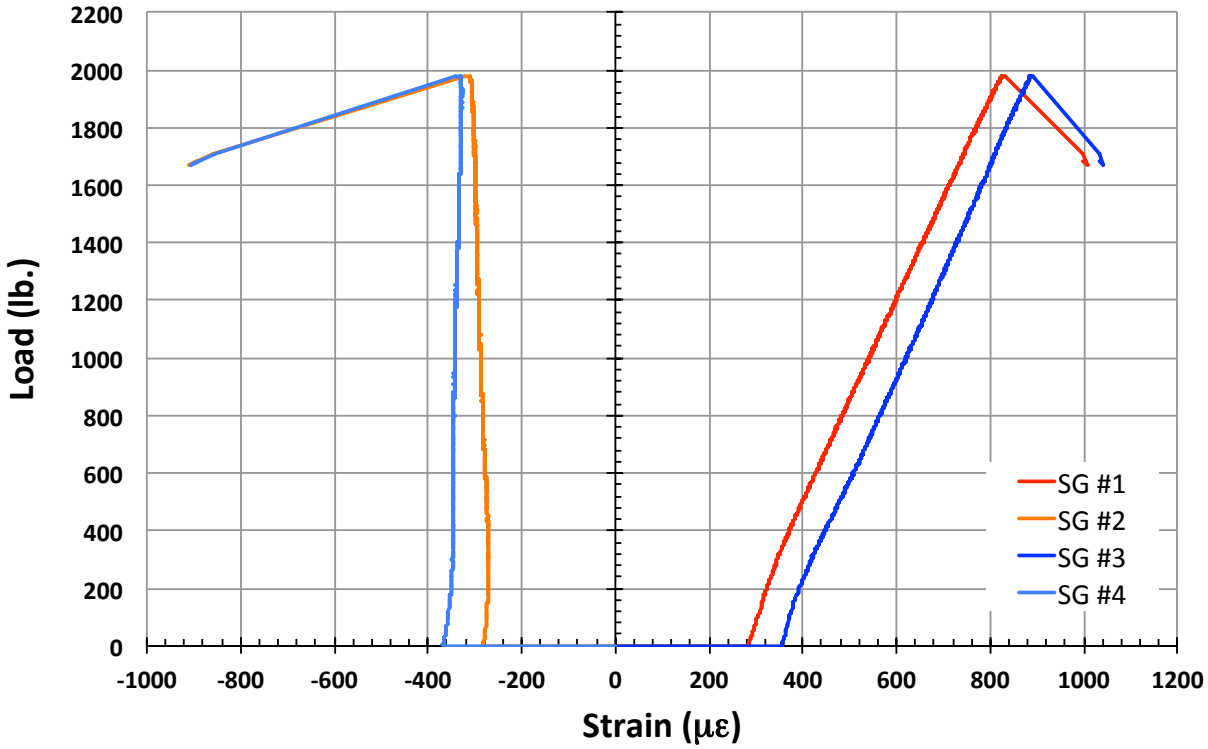

Figure C224. T5N1 load vs. strain, initial loading.

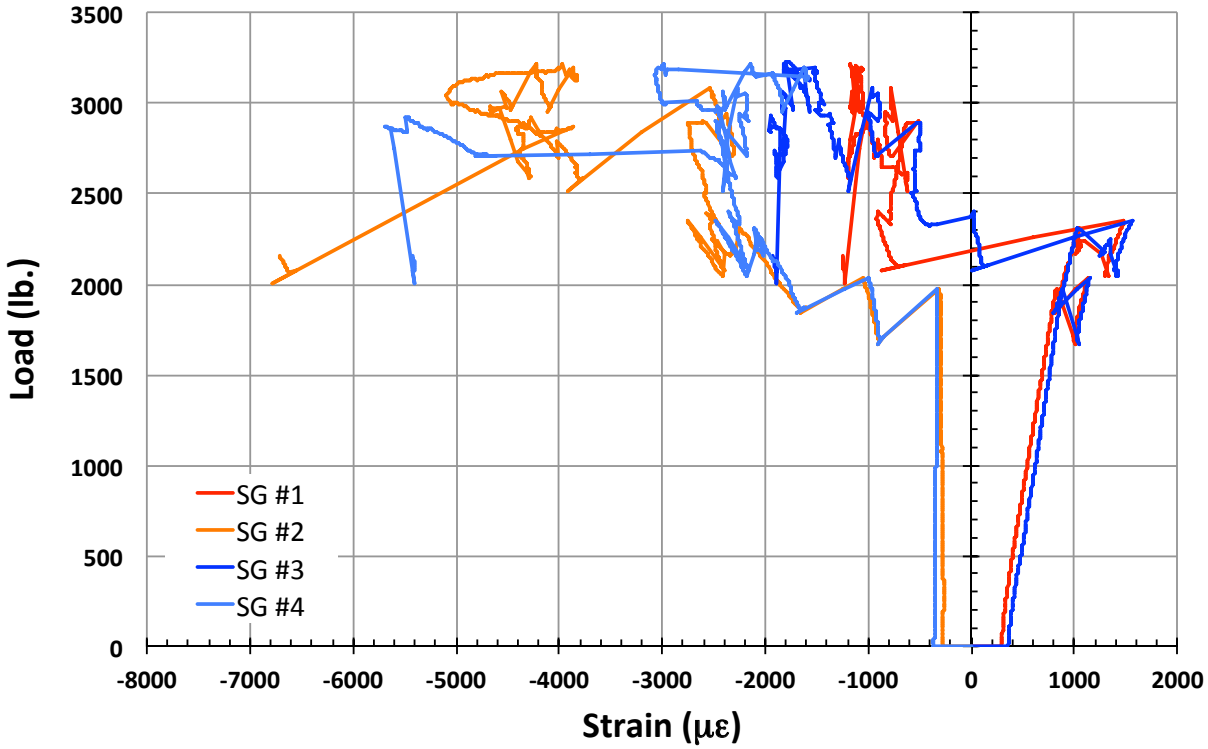

Figure C225. T5N1 load vs. strain.

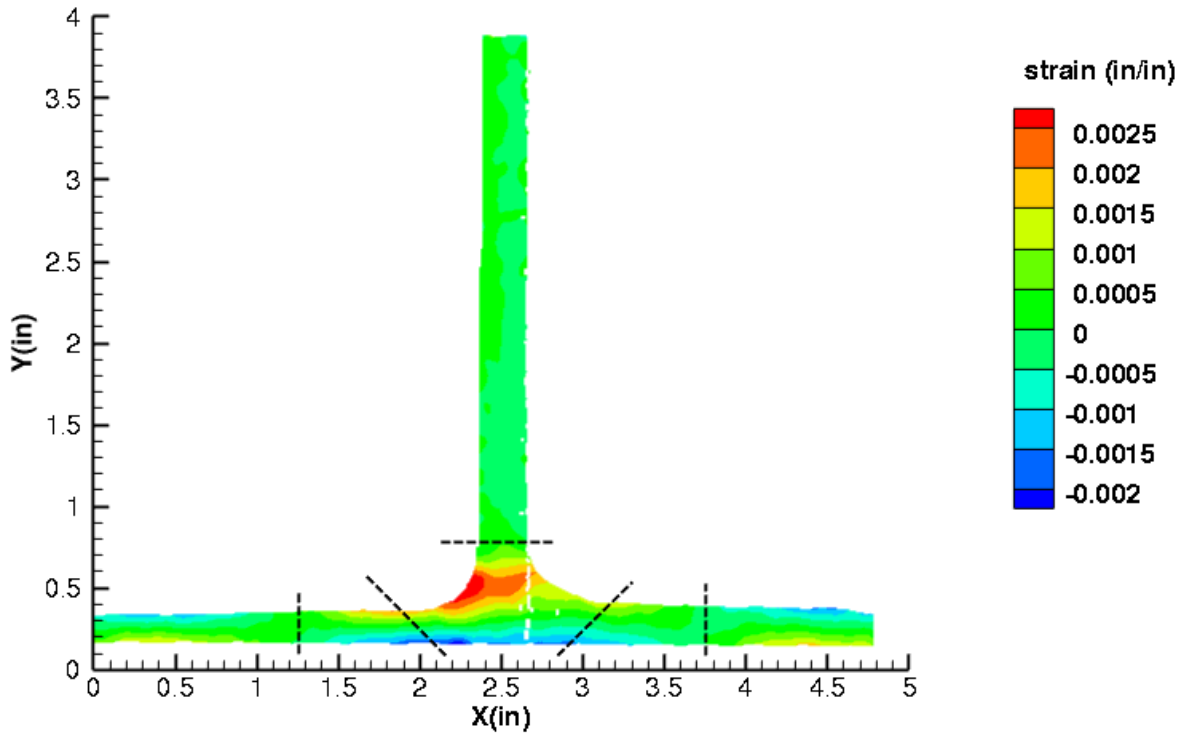

Figure C226. T5N1 strain contours for ε_{xx} at 1986 lb. load, prior to initial failure, 29MP VIC data.

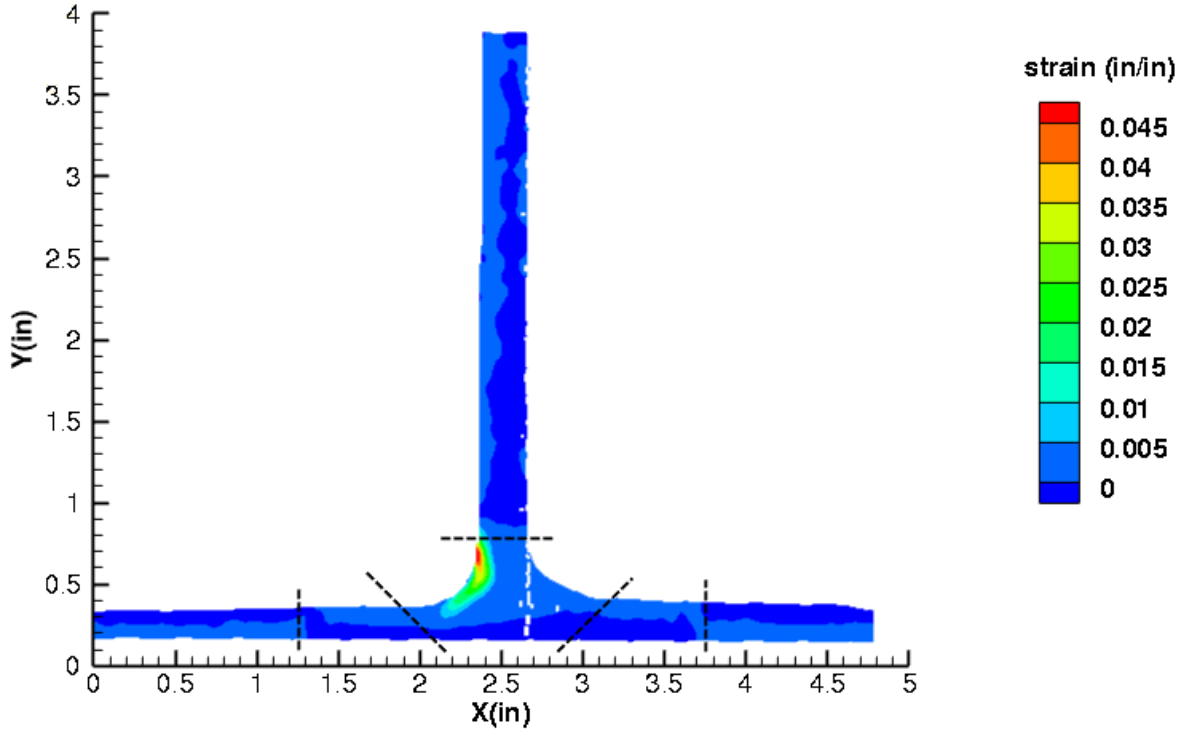

Figure C227. T5N1 strain contours for ε_{xx} at 1670 lb. load, just after initial failure, 29MP VIC data.

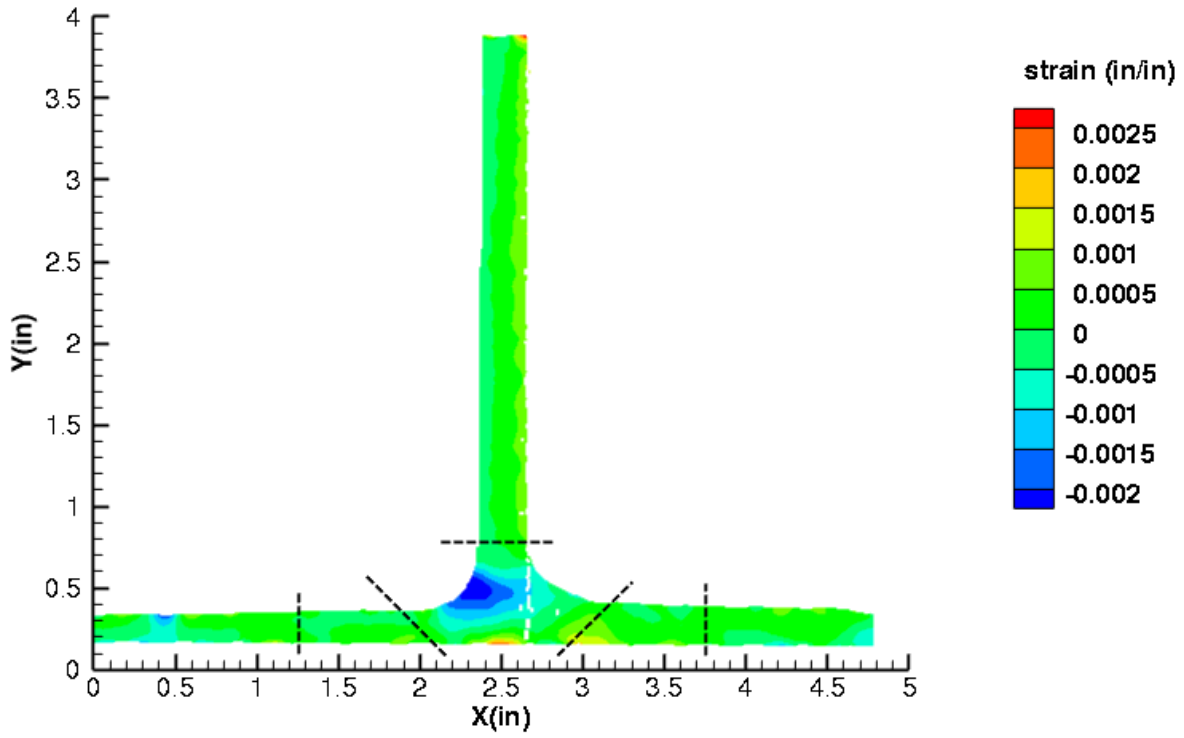

Figure C228. T5N1 strain contours for ε_{yy} at 1986 lb. load, prior to initial failure, 29MP VIC data.

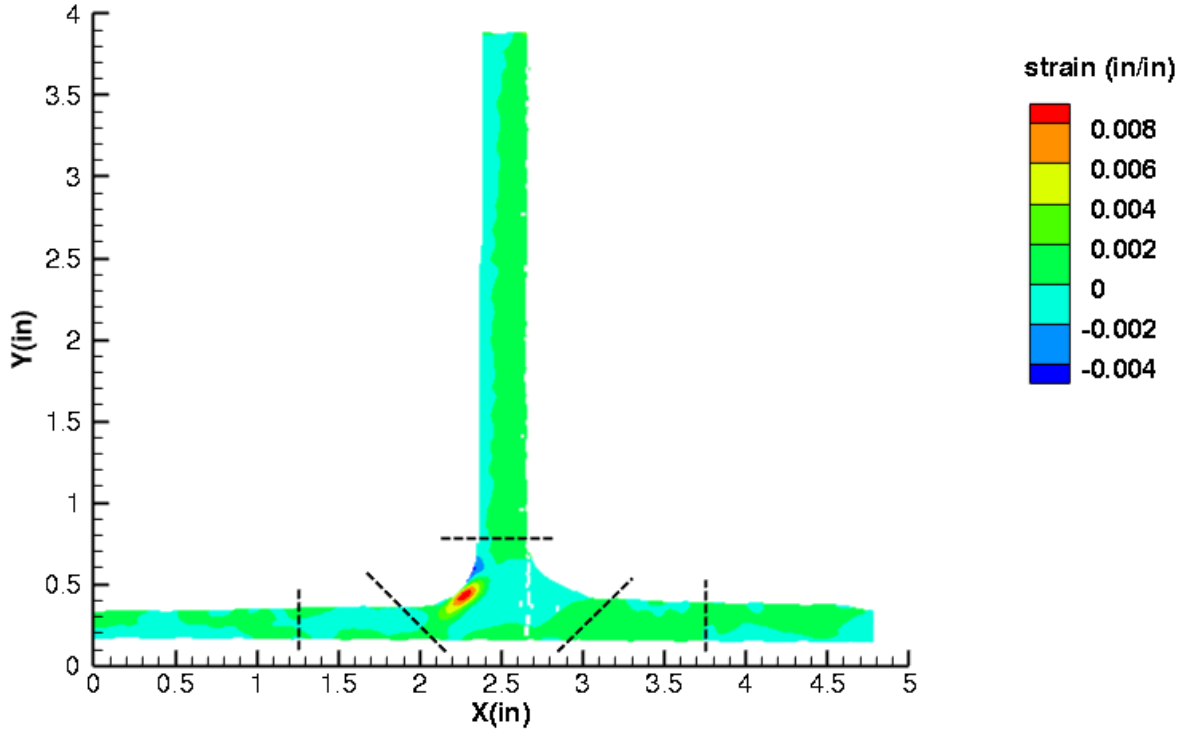

Figure C229. T5N1 strain contours for ε_{yy} at 1670 lb. load, just after initial failure, 29MP VIC data.

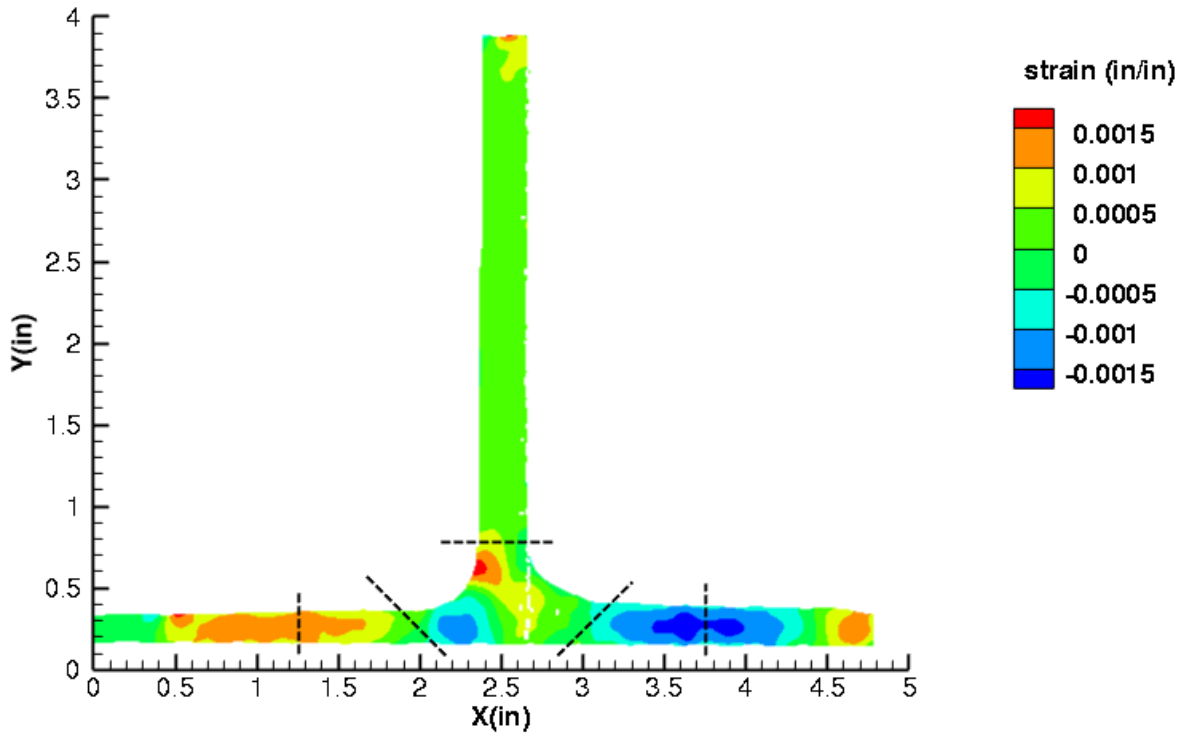

Figure C230. T5N1 strain contours for ε_{xy} at 1986 lb. load, prior to initial failure, 29MP VIC data.

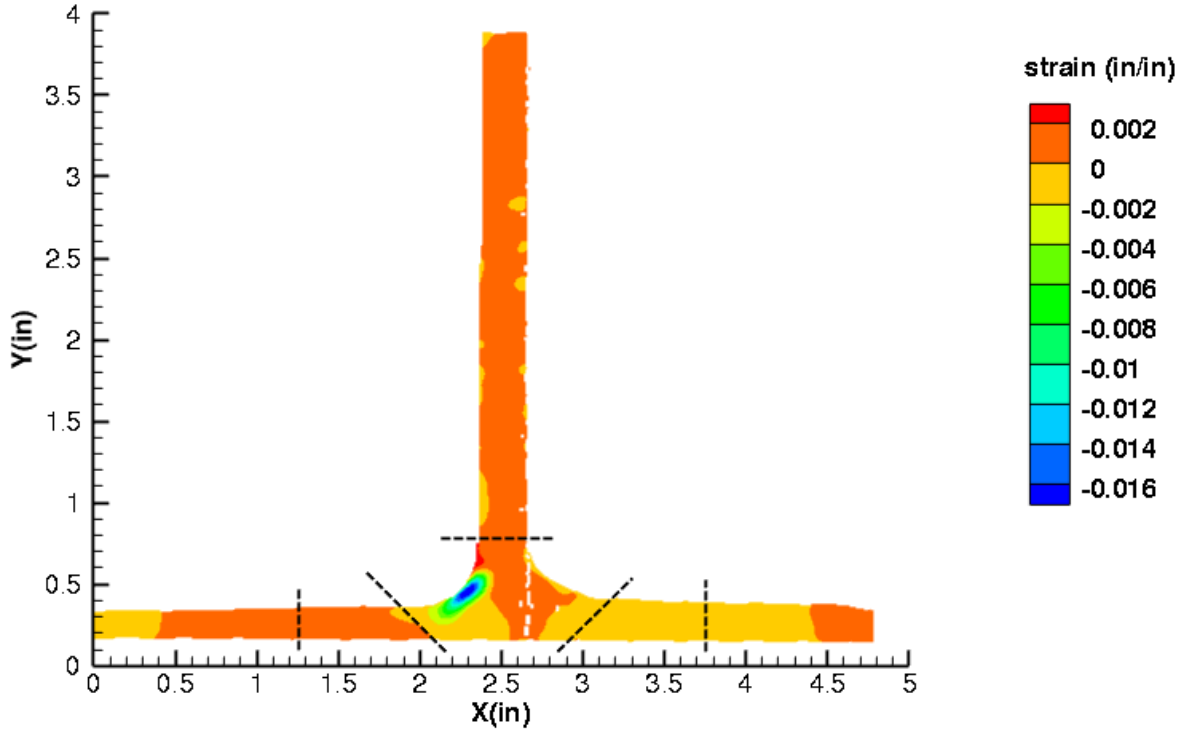

Figure C231. T5N1 strain contours for ε_{xy} at 1670 lb. load, just after initial failure, 29MP VIC data.

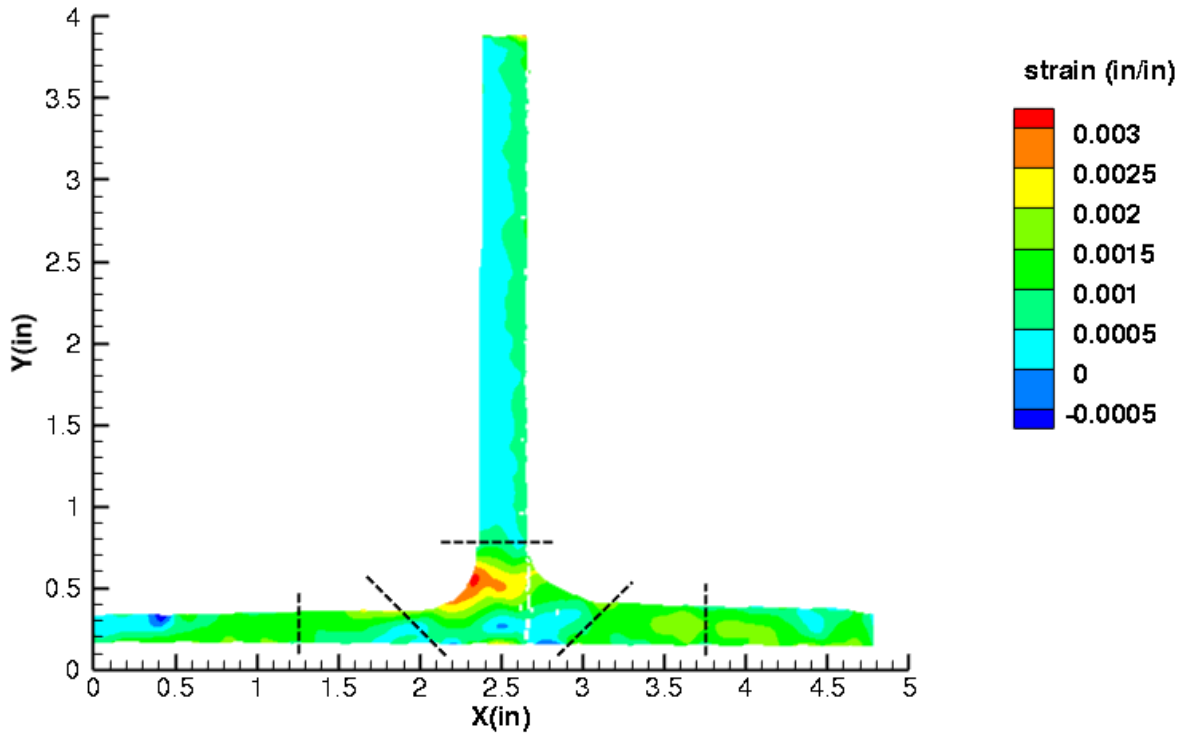

Figure C232. T5N1 strain contours for maximum principal strain at 1986 lb. load, prior to initial failure, 29MP VIC data.

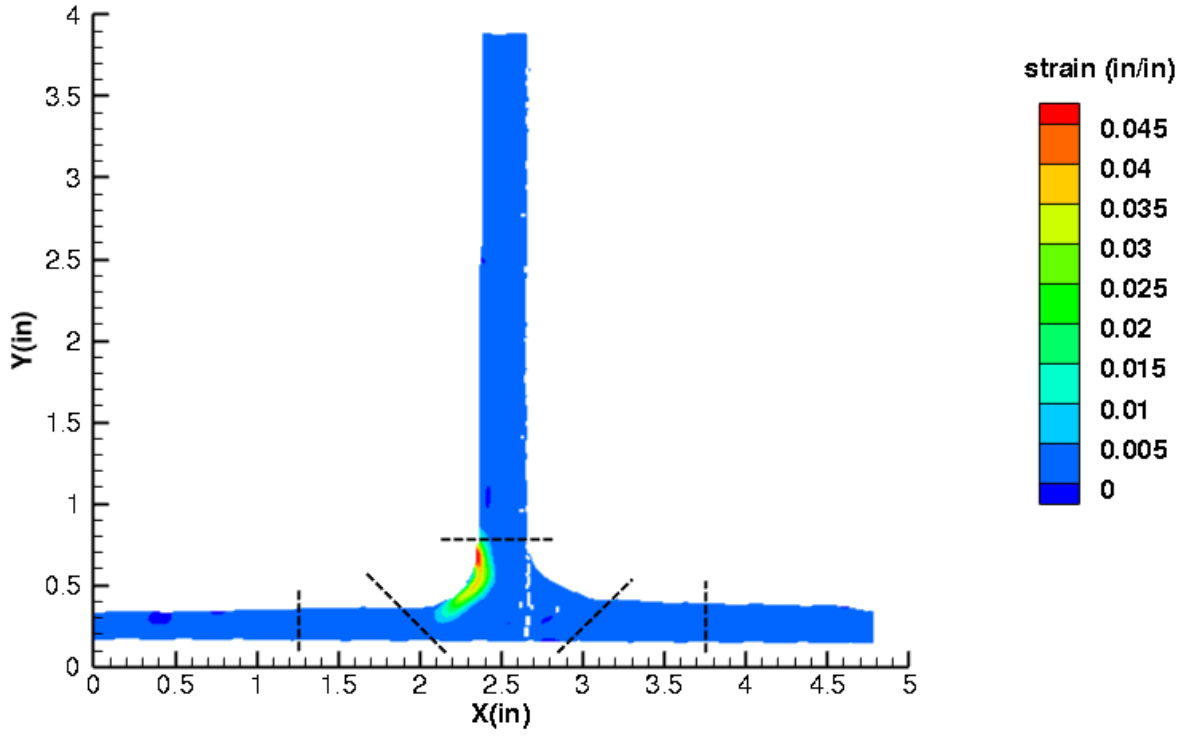

Figure C233. T5N1 strain contours for maximum principal strain at 1670 lb. load, just after initial failure, 29MP VIC data.

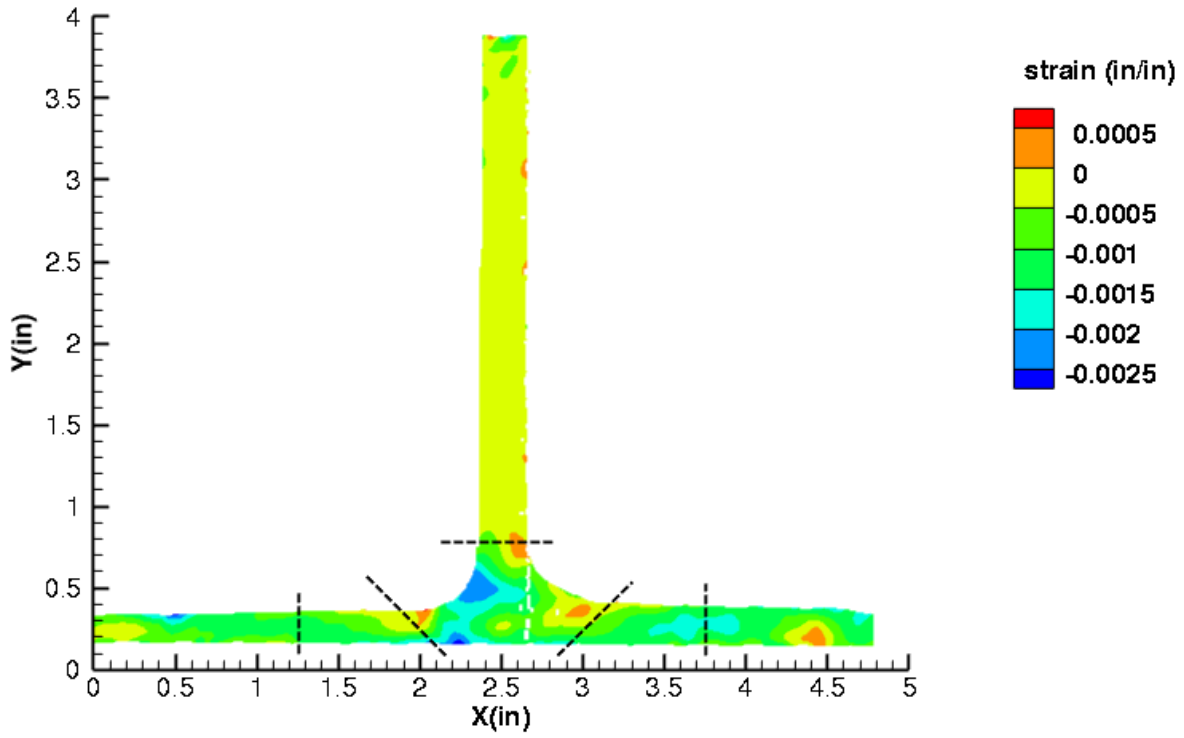

Figure C234. T5N1 strain contours for minimum principal strain at 1986 lb. load, prior to initial failure, 29MP VIC data.

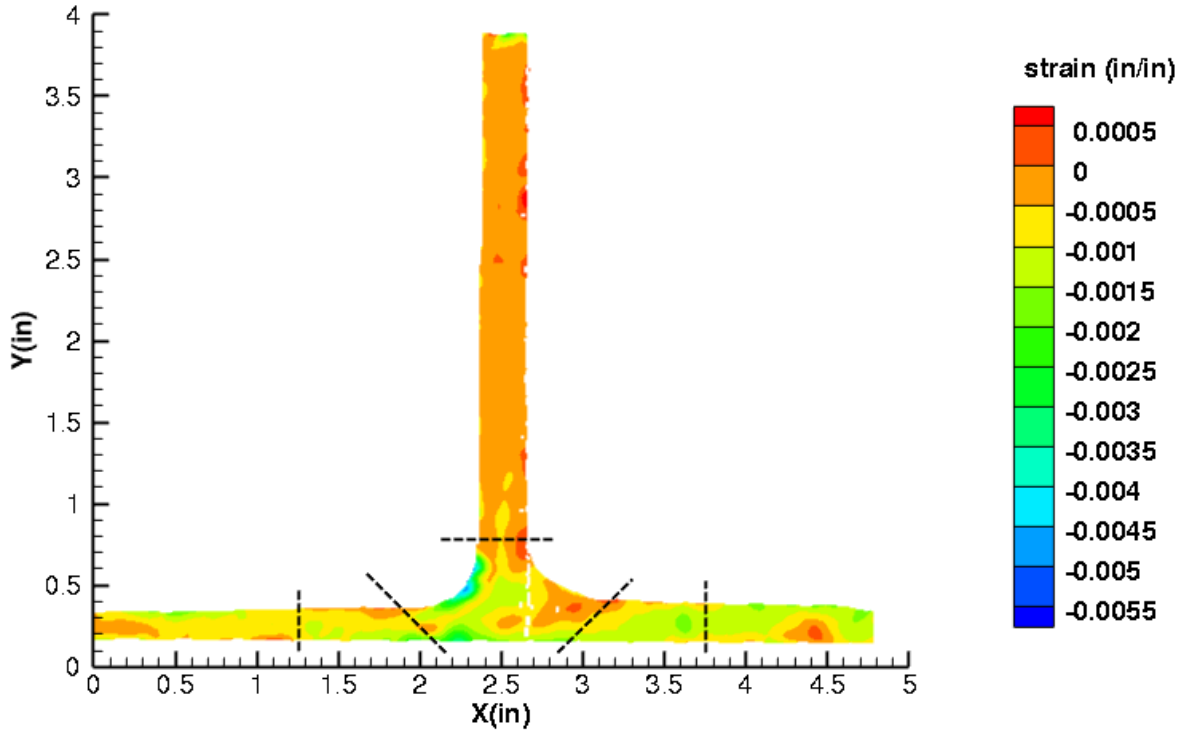

Figure C235. T5N1 strain contours for minimum principal strain at 1670 lb. load, just after initial failure, 29MP VIC data.

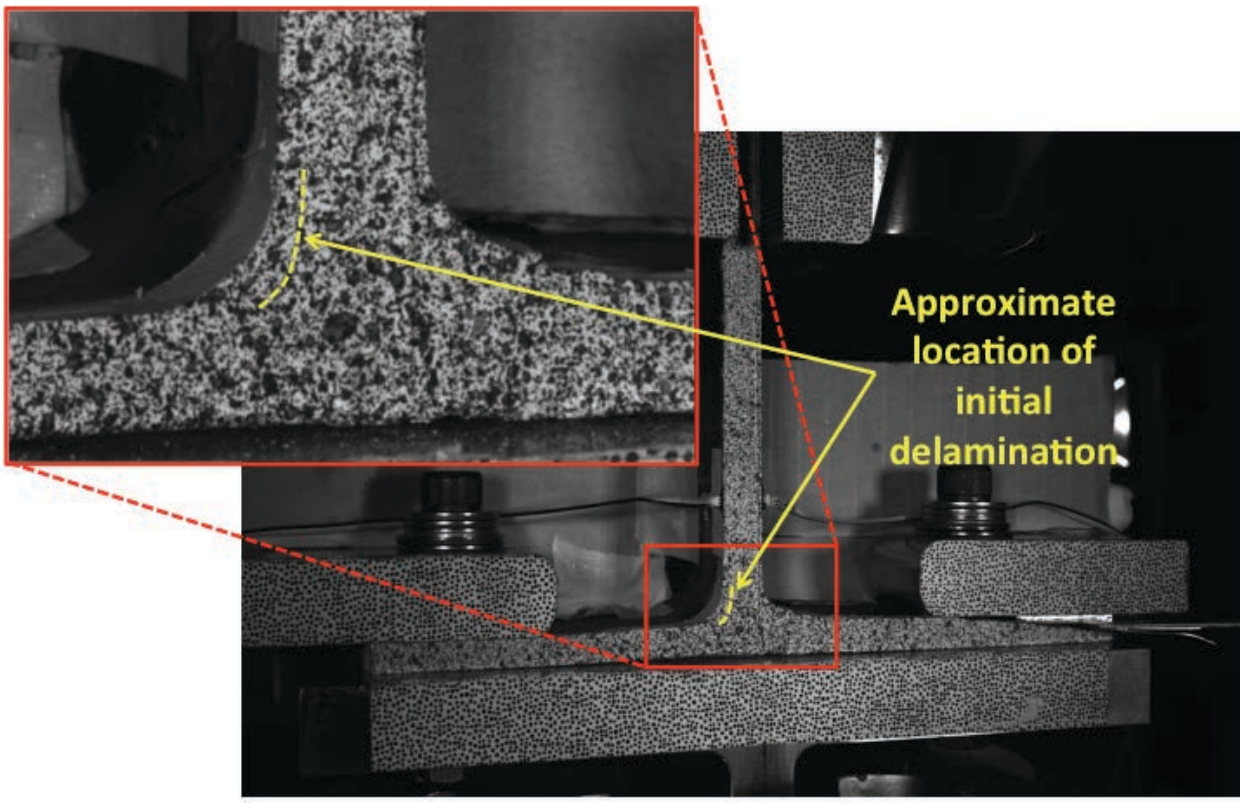

Figure C236. T5N1 image just after initial failure, 29MP VIC data.

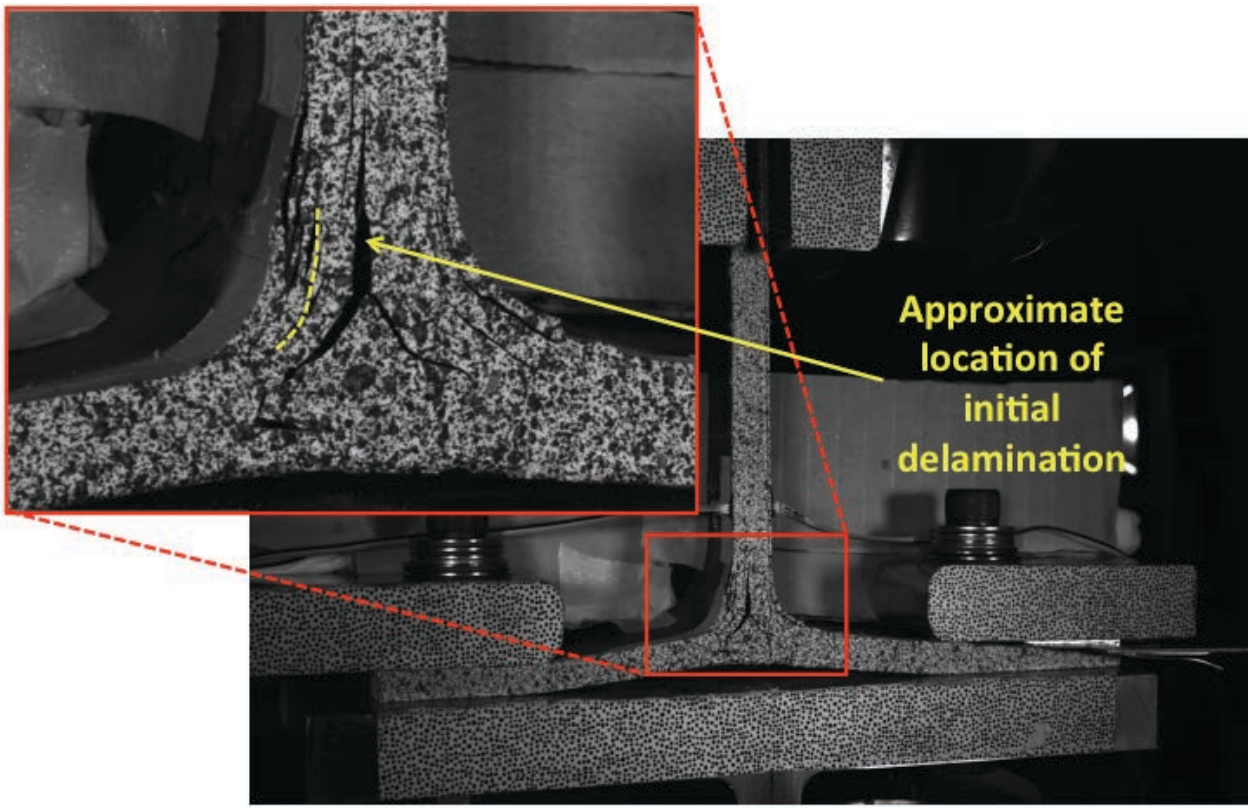

Figure C237. T5N1 image just after maximum load, 29MP VIC data.

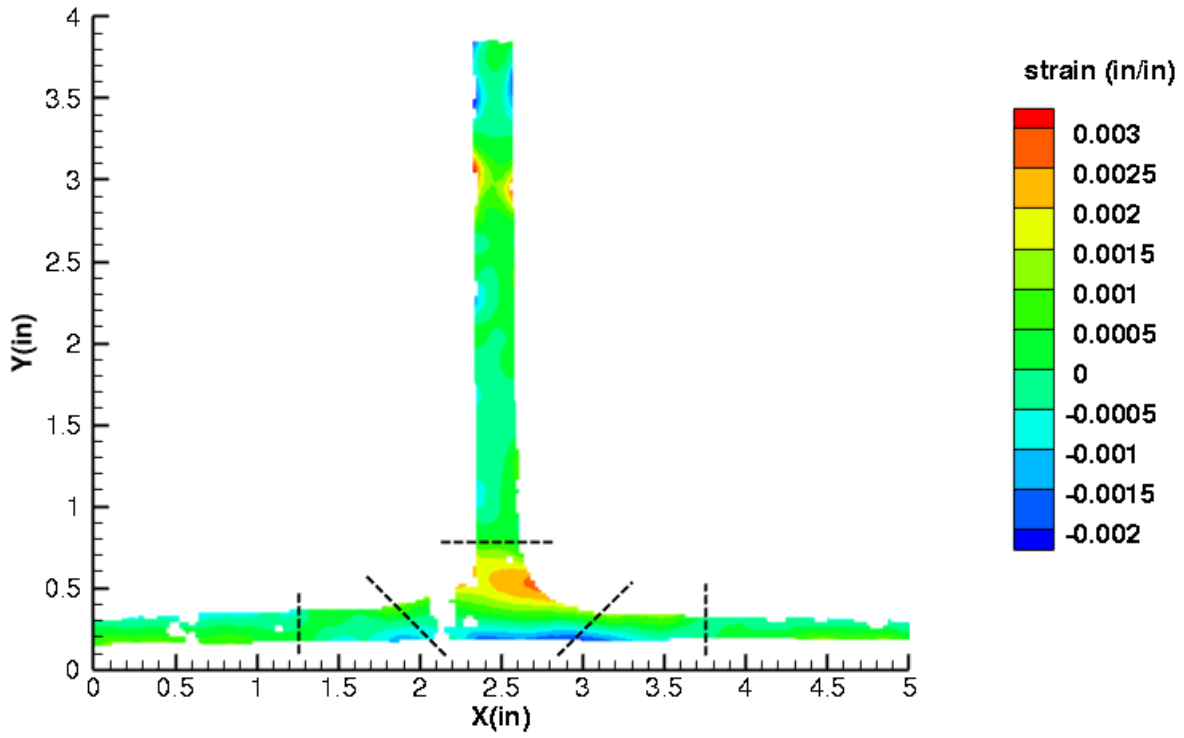

Figure C238. T5N1 strain contours for ε_{xx} at 1986 lb. load, prior to initial failure, 5MP VIC data.

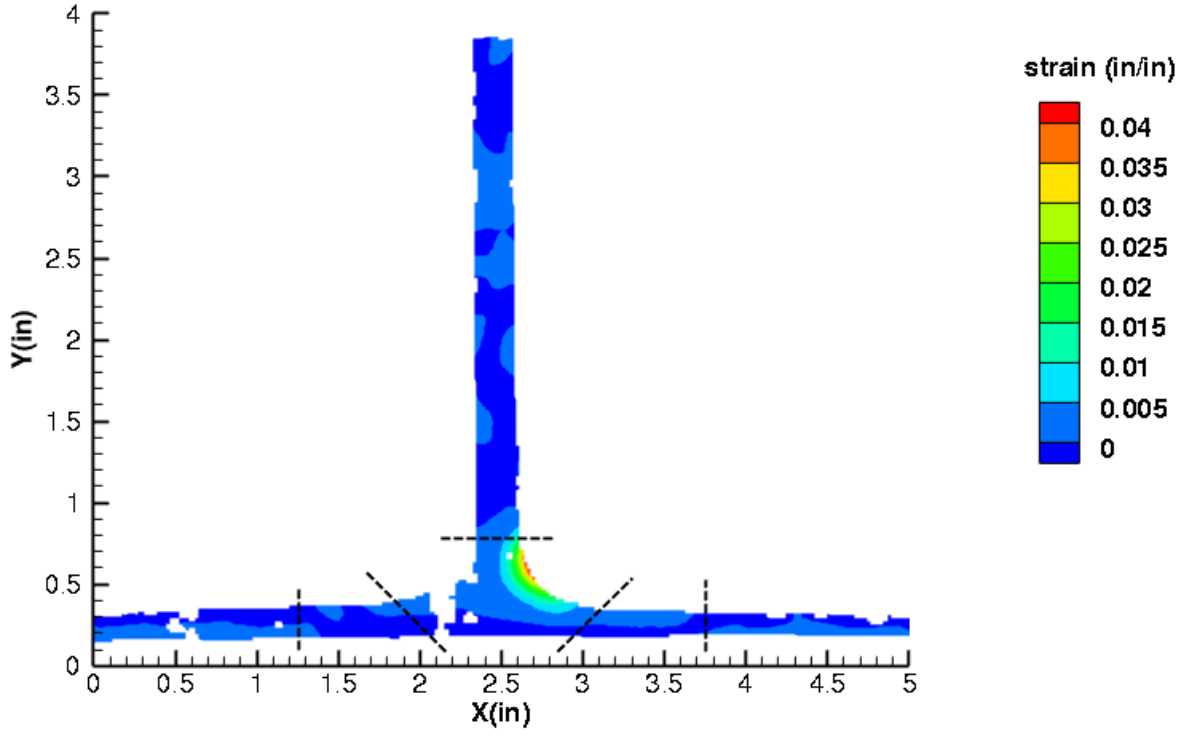

Figure C239. T5N1 strain contours for ε_{xx} at 1670 lb. load, just after initial failure, 5MP VIC data.

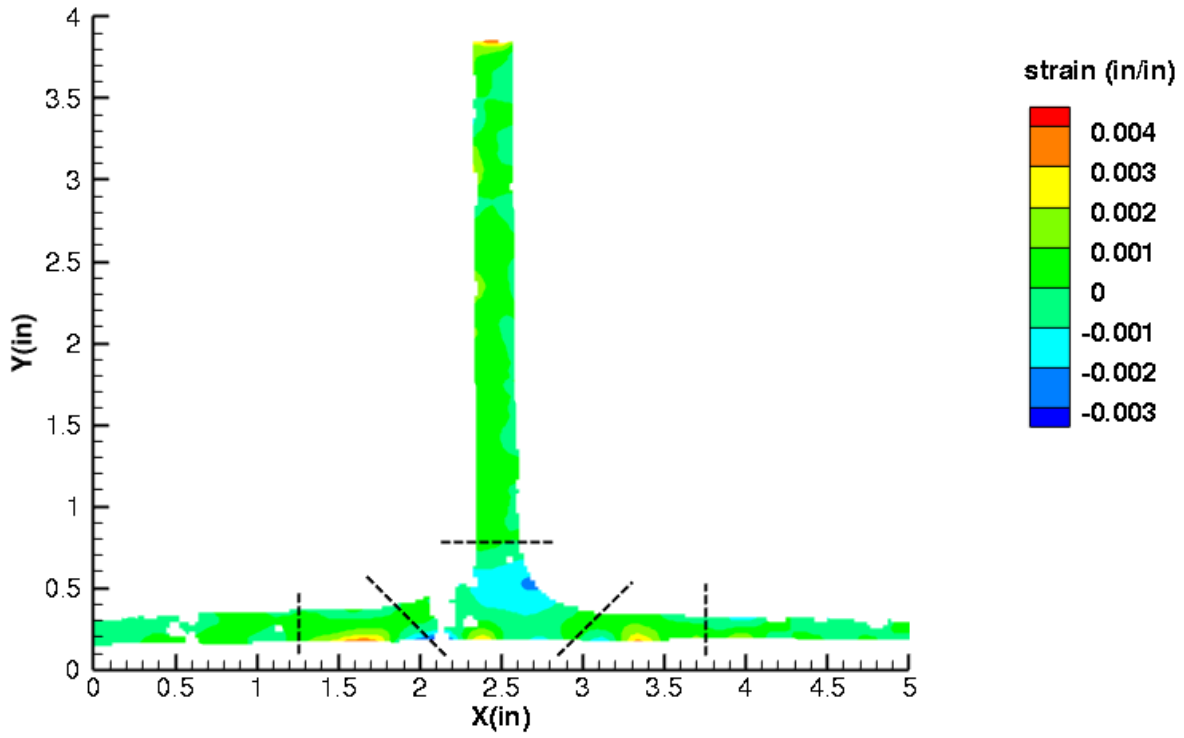

Figure C240. T5N1 strain contours for ε_{yy} at 1986 lb. load, prior to initial failure, 5MP VIC data.

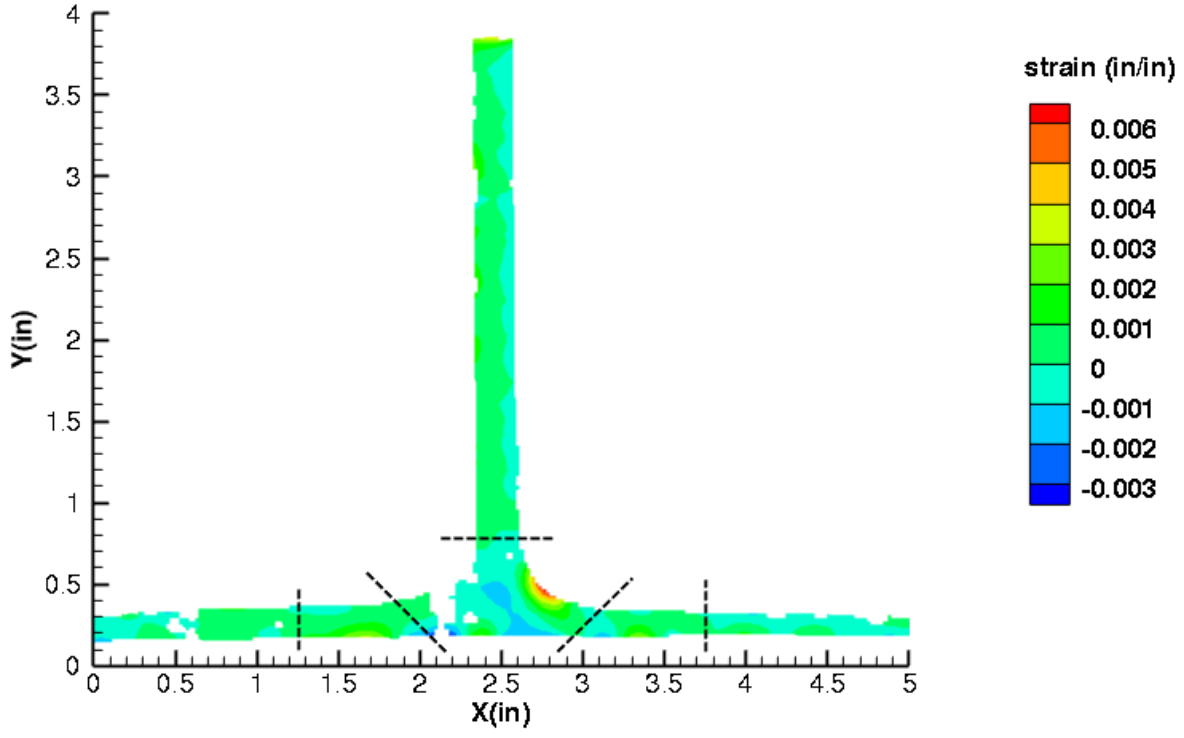

Figure C241. T5N1 strain contours for ε_{yy} at 1670 lb. load, just after initial failure, 5MP VIC data.

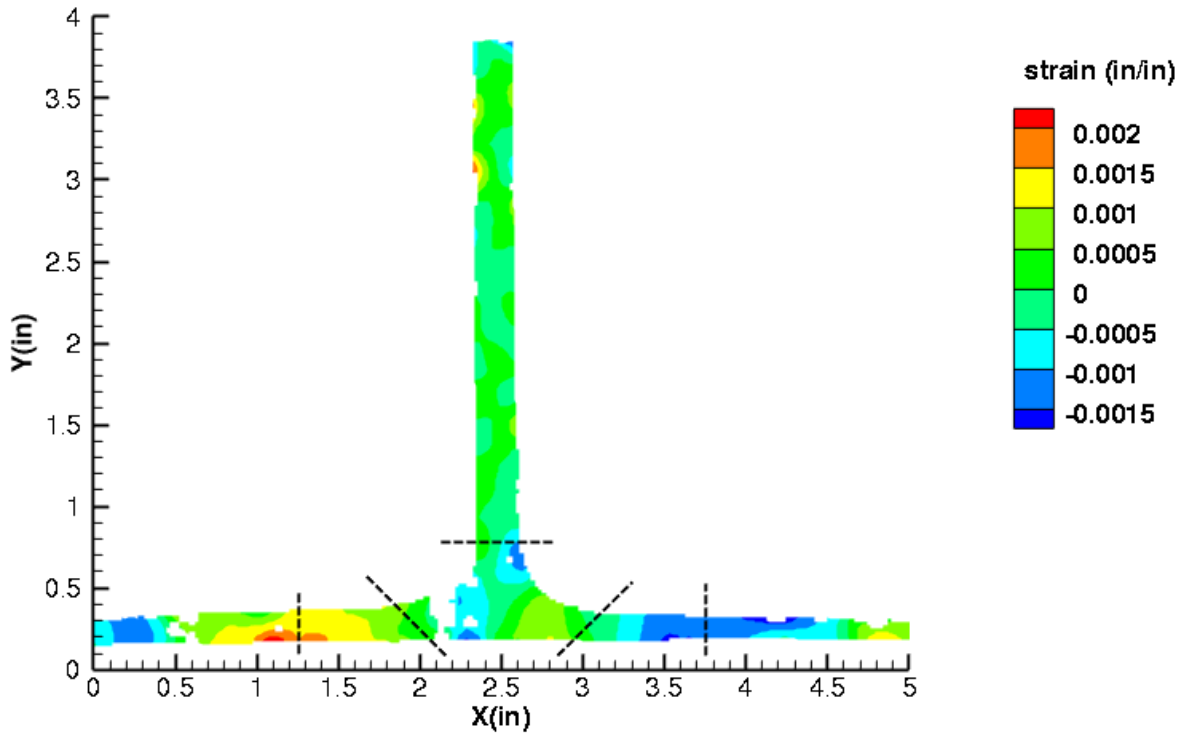

Figure C242. T5N1 strain contours for ε_{xy} at 1986 lb. load, prior to initial failure, 5MP VIC data.

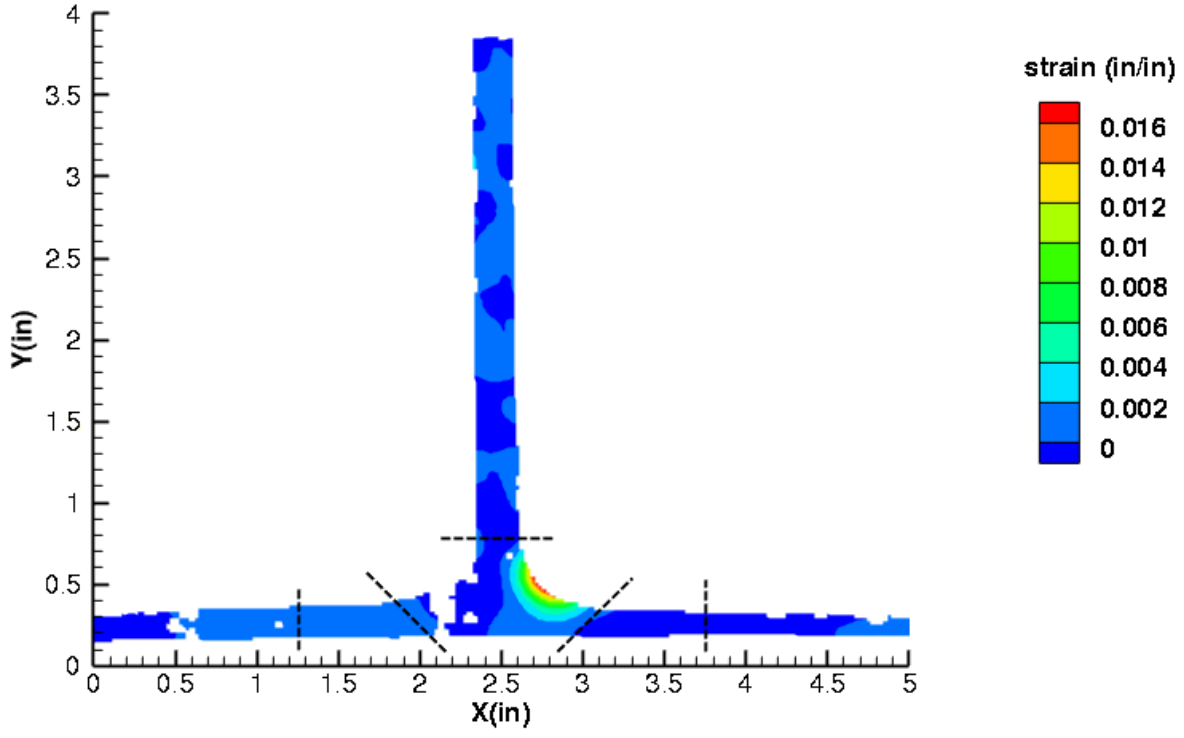

Figure C243. T5N1 strain contours for ε_{xy} at 1670 lb. load, just after initial failure, 5MP VIC data.

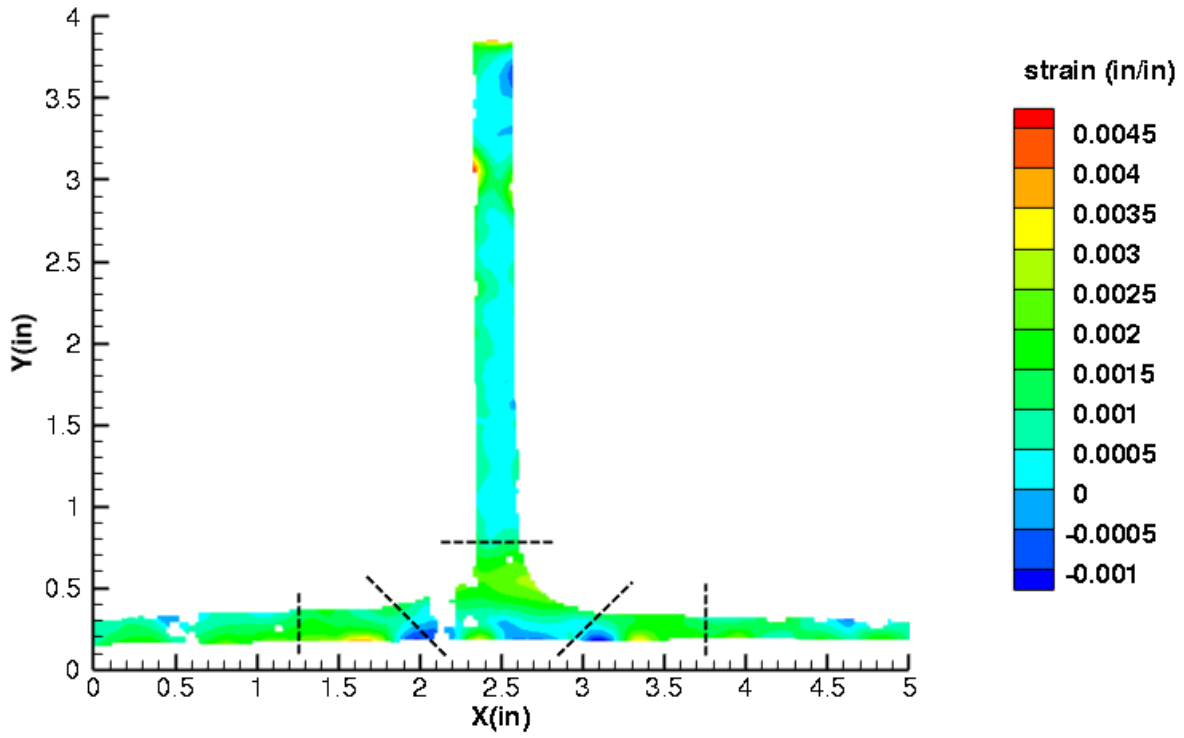

Figure C244. T5N1 strain contours for maximum principal strain at 1986 lb. load, prior to initial failure, 5MP VIC data.

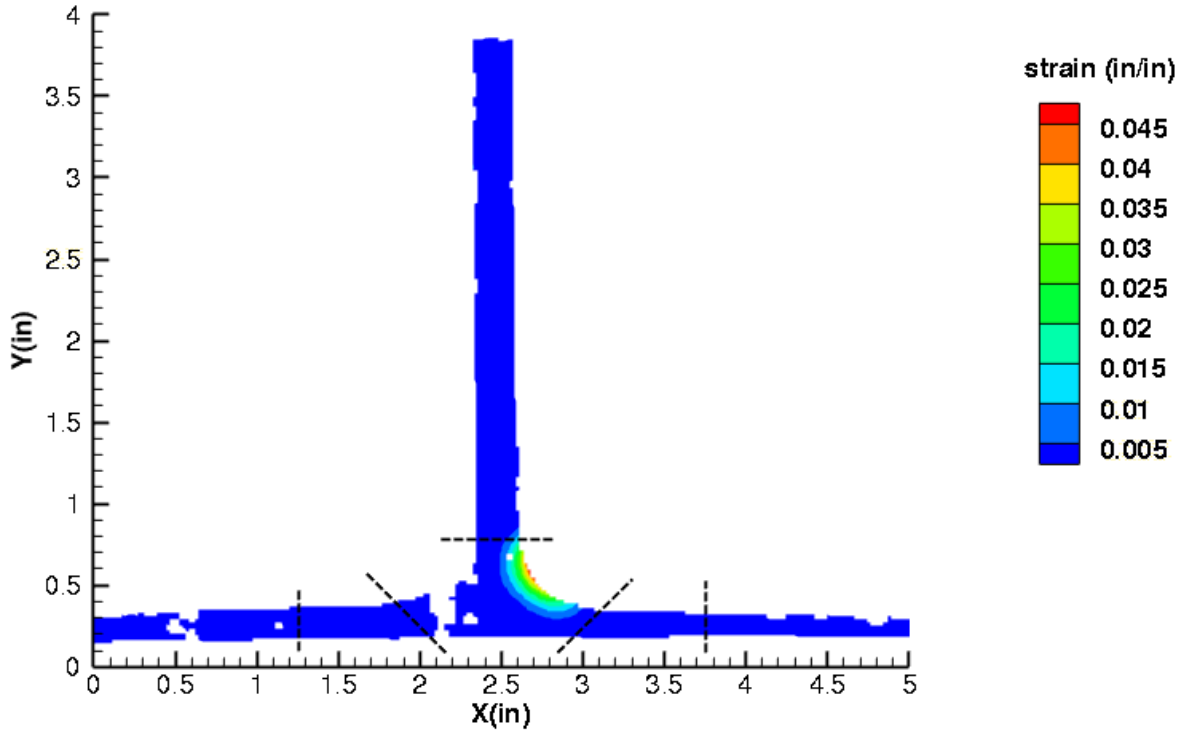

Figure C245. T5N1 strain contours for maximum principal strain at 1670 lb. load, just after initial failure, 5MP VIC data.

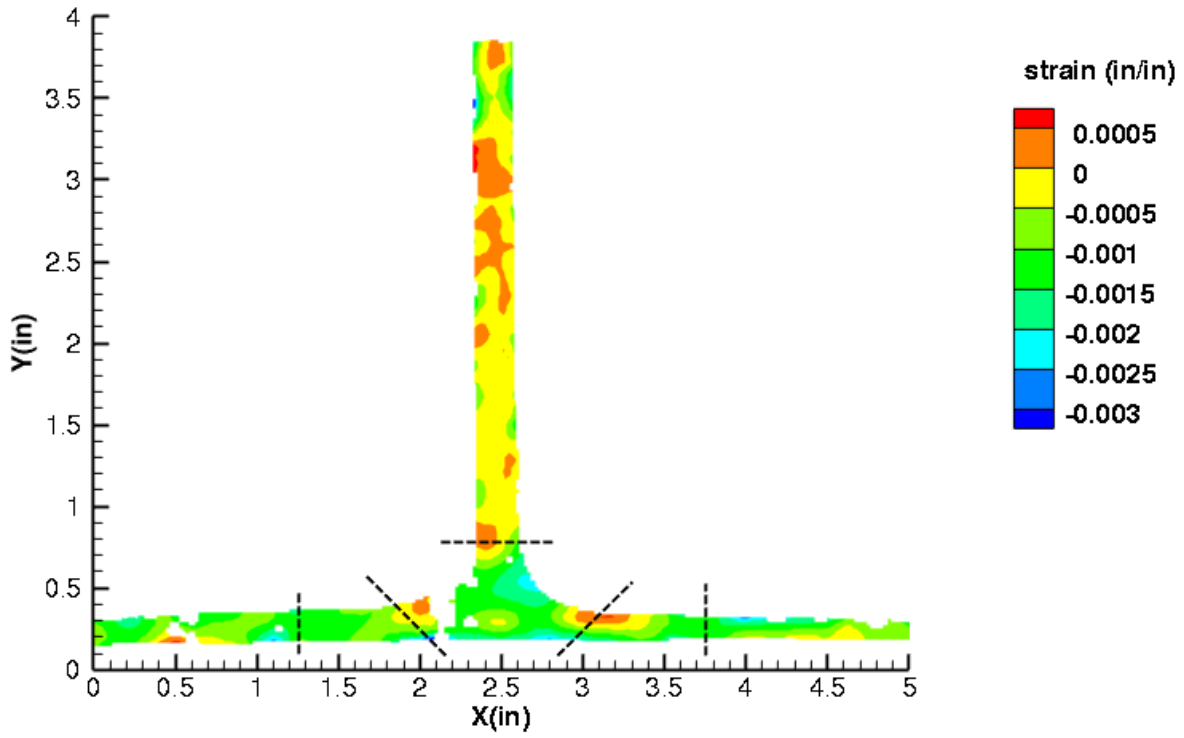

Figure C246. T5N1 strain contours for minimum principal strain at 1986 lb. load, prior to initial failure, 5MP VIC data.

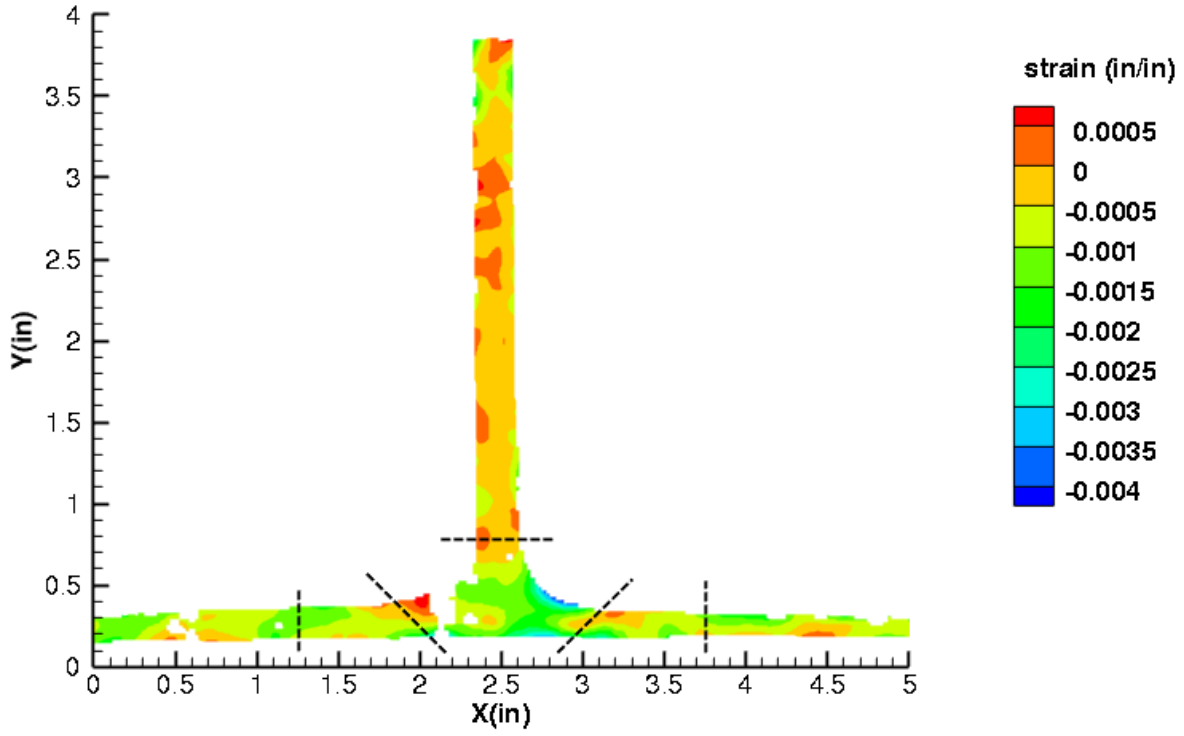

Figure C247. T5N1 strain contours for minimum principal strain at 1670 lb. load, just after initial failure, 5MP VIC data.

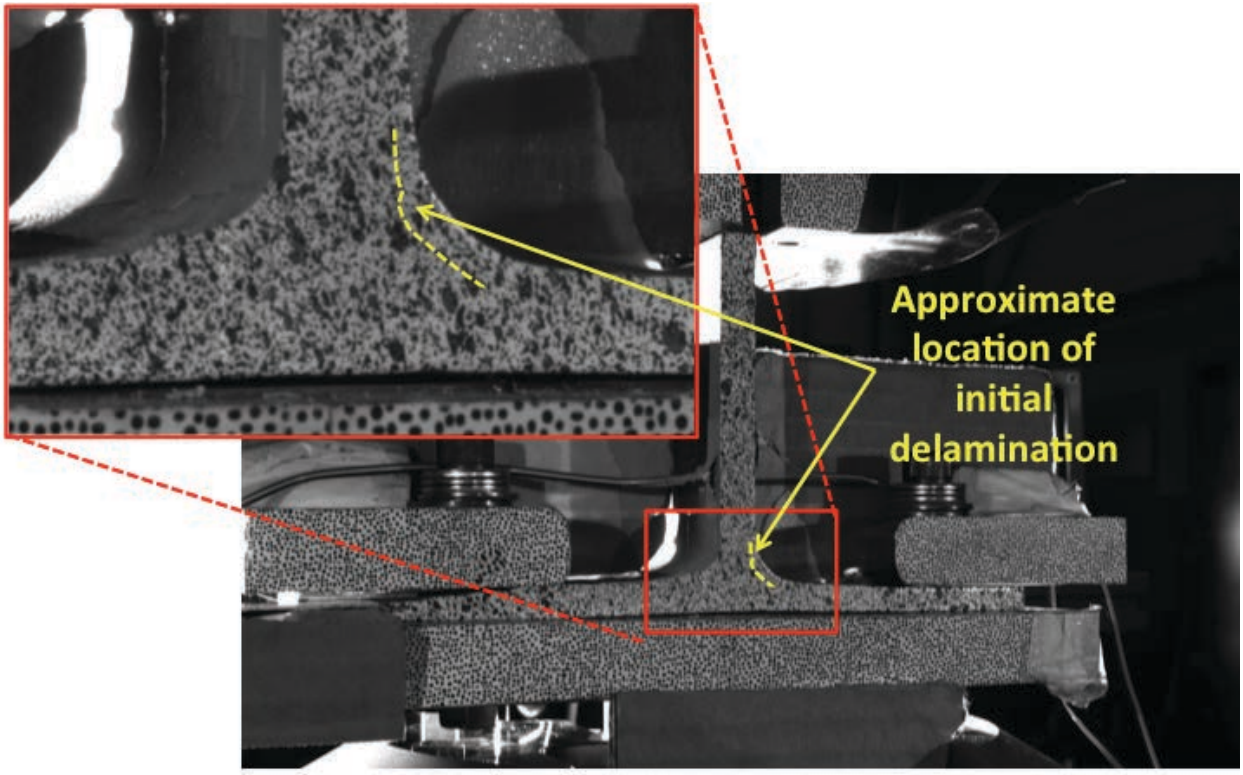

Figure C248. T5N1 image just after initial failure, 5MP VIC data.

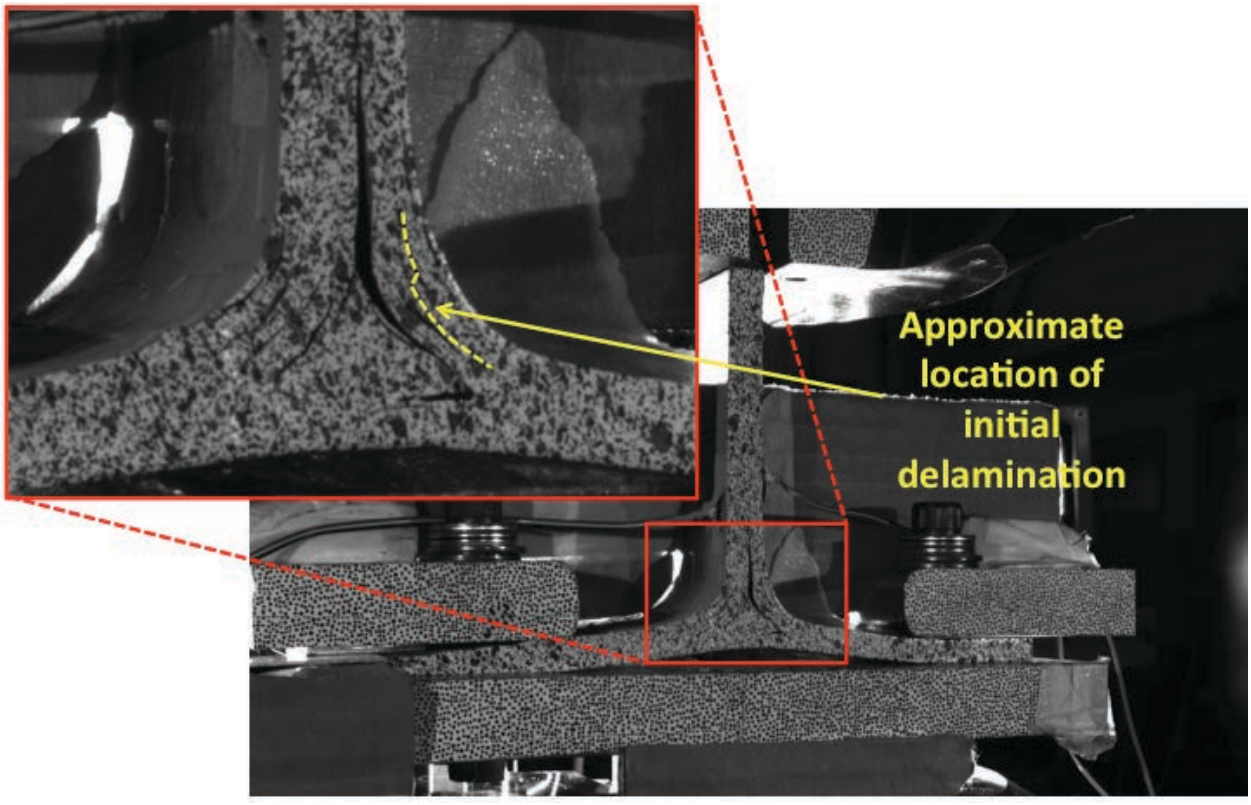

Figure C249. T5N1 image just after maximum load, 5MP VIC data.

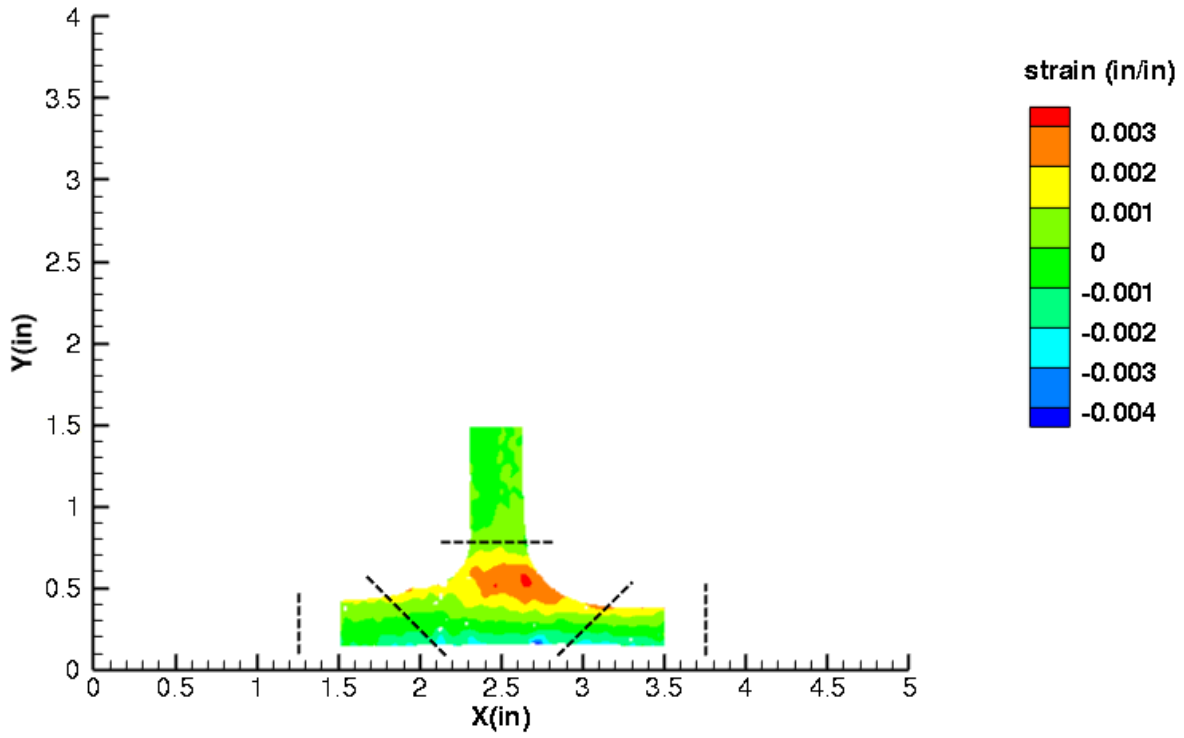

Figure C250. T5N1 strain contours for ε_{xx} at 1986 lb. load, prior to initial failure, local 5MP VIC data.

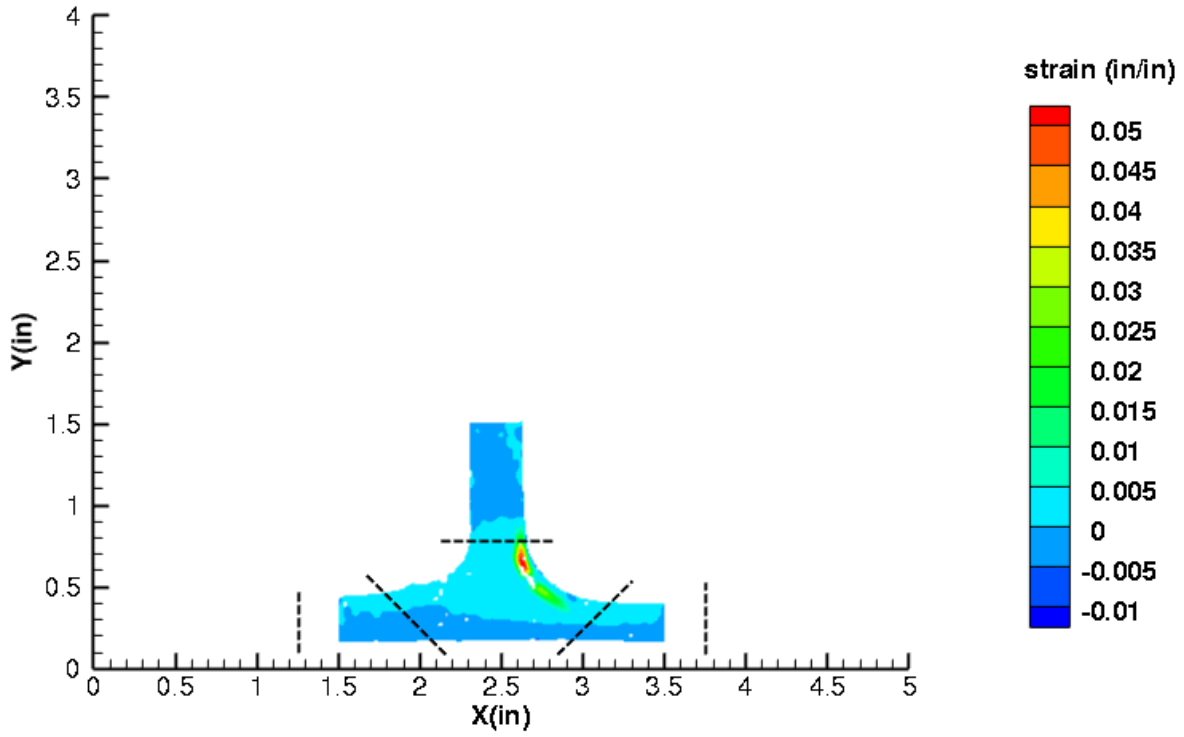

Figure C251. T5N1 strain contours for ε_{xx} at 1670 lb. load, just after initial failure, local 5MP VIC data.

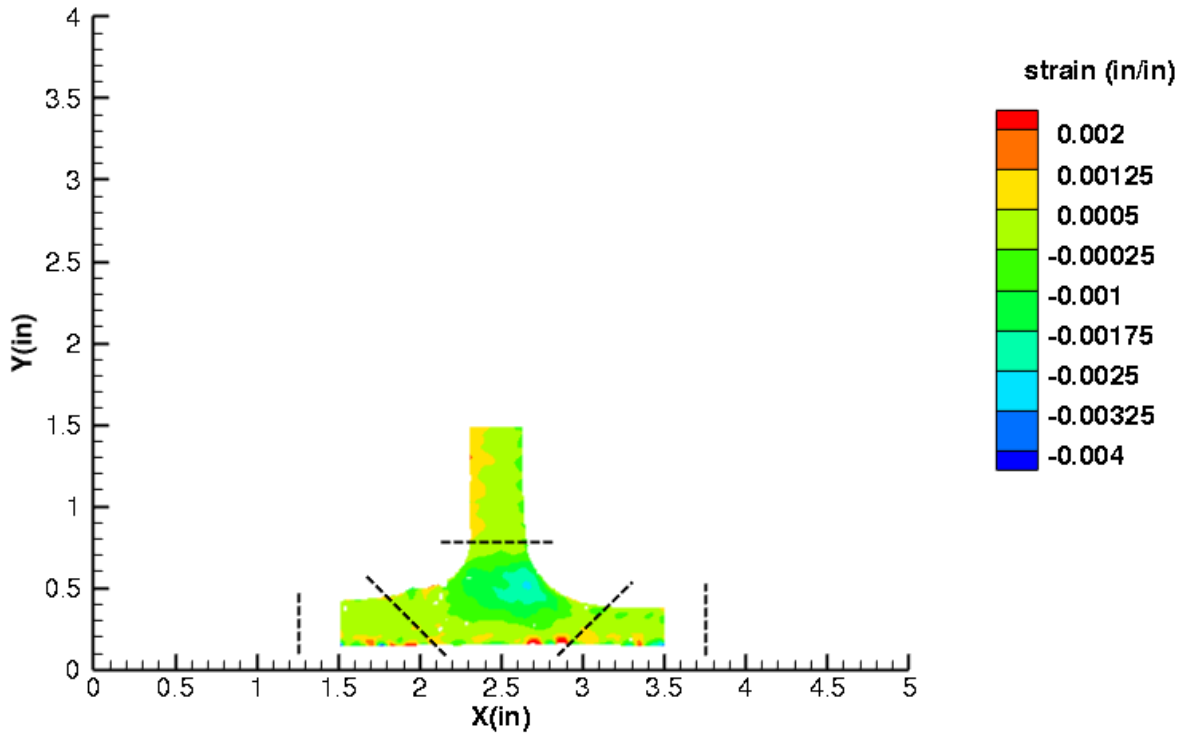

Figure C252. T5N1 strain contours for ε_{yy} at 1986 lb. load, prior to initial failure, local 5MP VIC data.

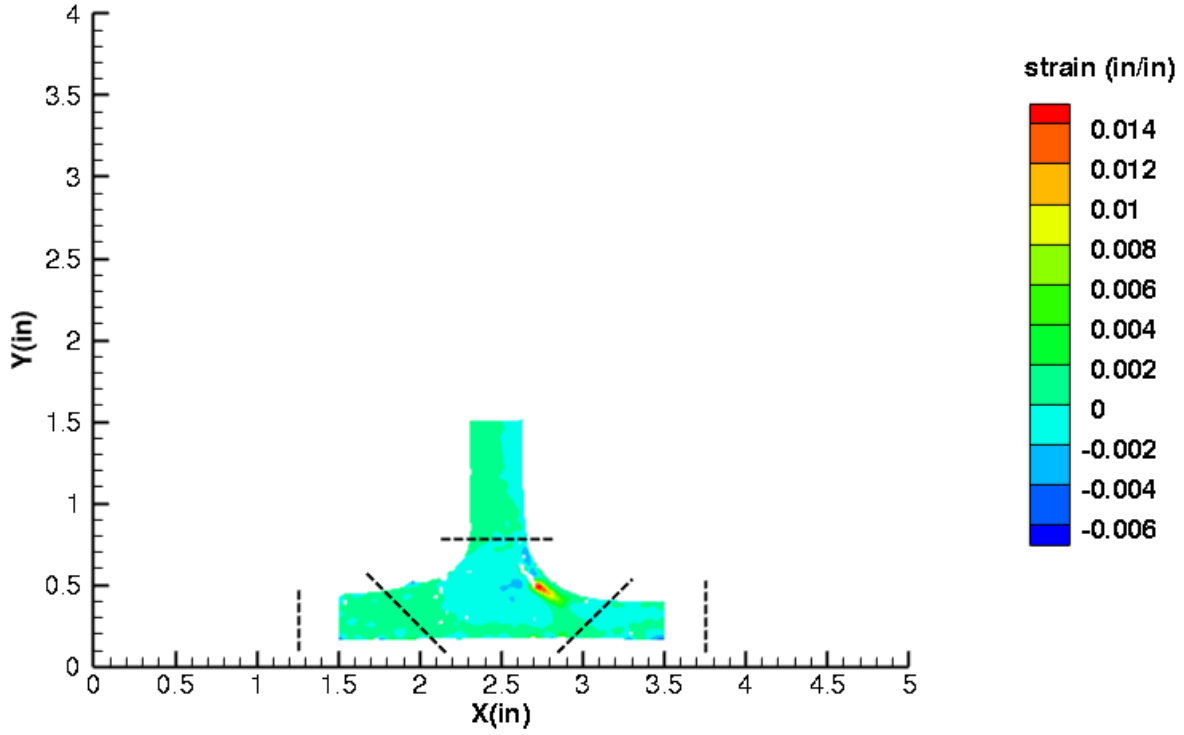

Figure C253. T5N1 strain contours for ε_{yy} at 1670 lb. load, just after initial failure, local 5MP VIC data.

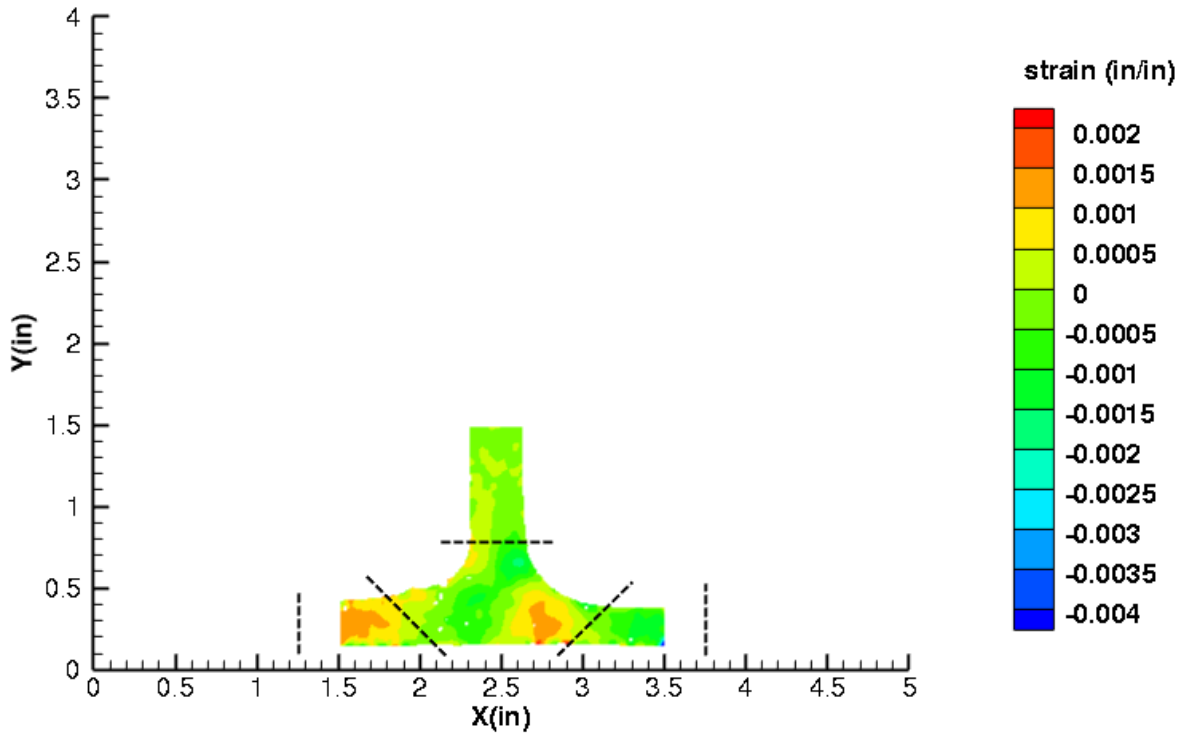

Figure C254. T5N1 strain contours for ε_{xy} at 1986 lb. load, prior to initial failure, local 5MP VIC data.

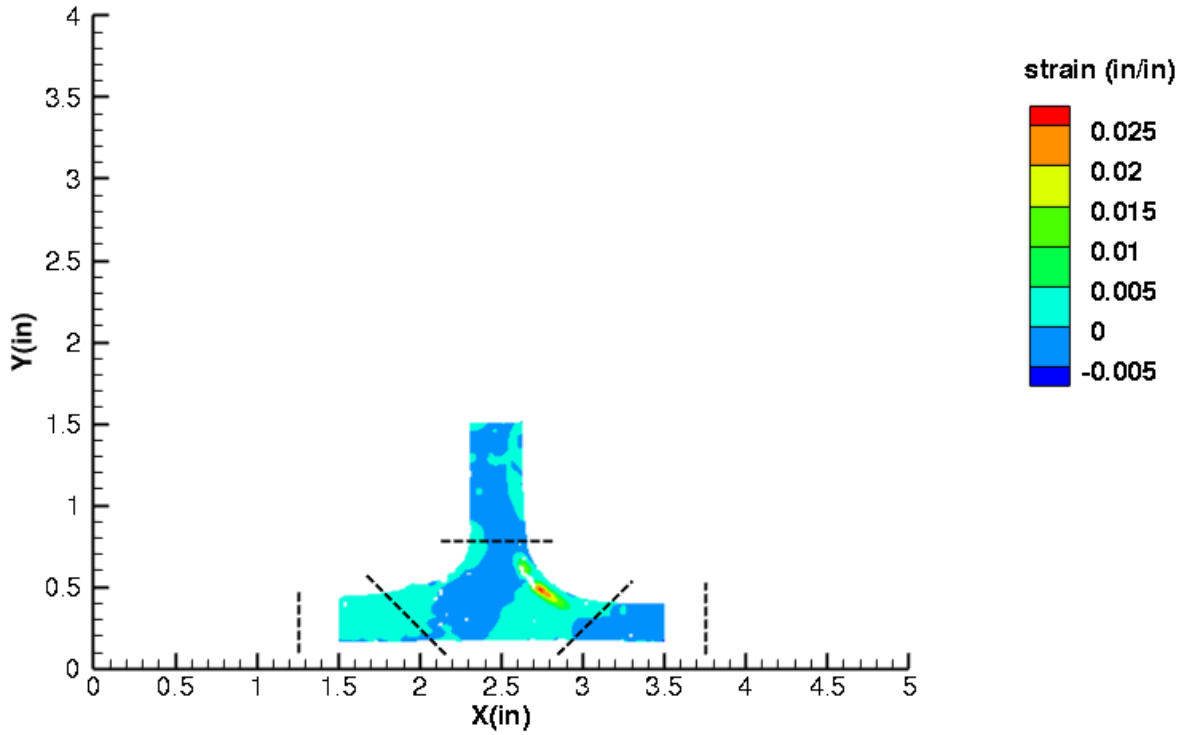

Figure C255. T5N1 strain contours for ε_{xy} at 1670 lb. load, just after initial failure, local 5MP VIC data.

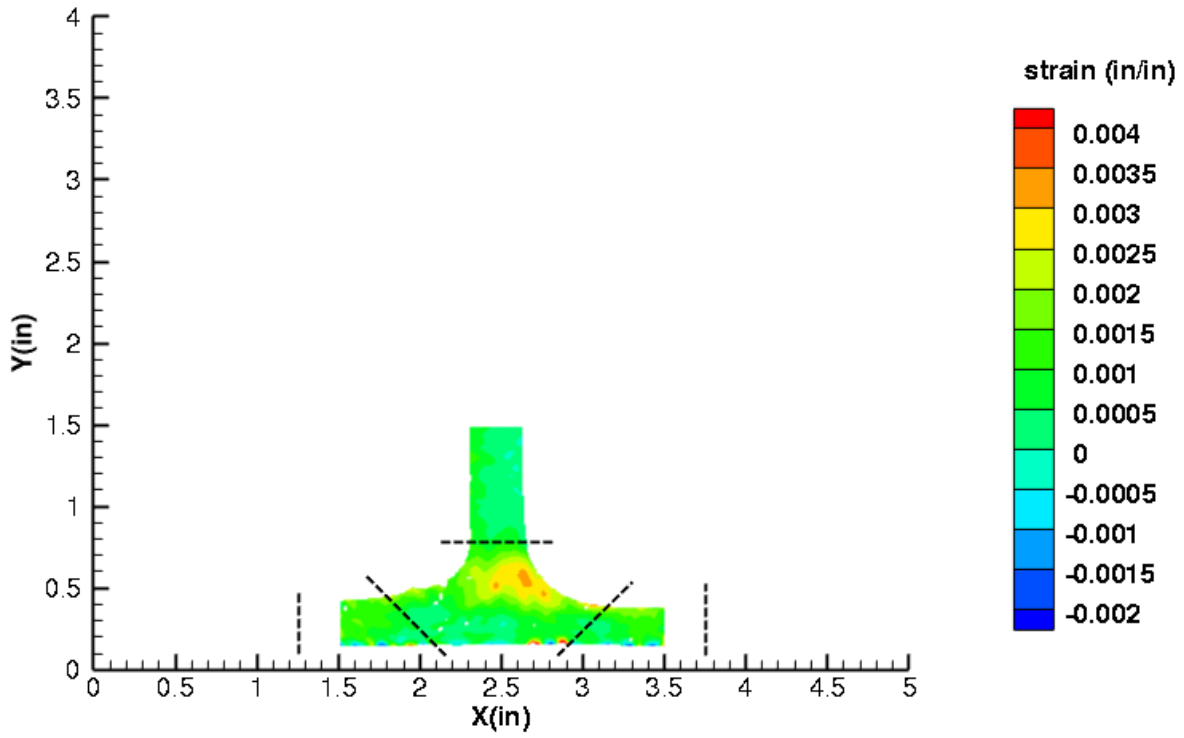

Figure C256. T5N1 strain contours for maximum principal strain at 1986 lb. load, prior to initial failure, local 5MP VIC data.

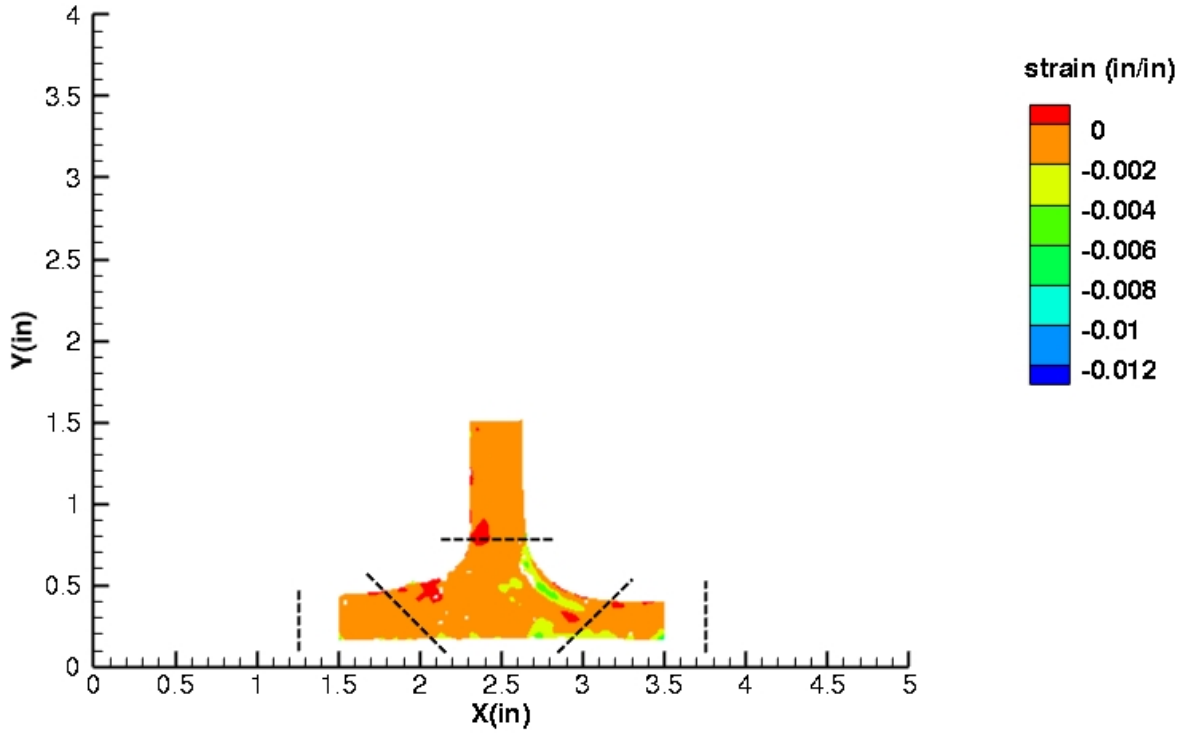

Figure C257. T5N1 strain contours for maximum principal strain at 1670 lb. load, just after initial failure, local 5MP VIC data.

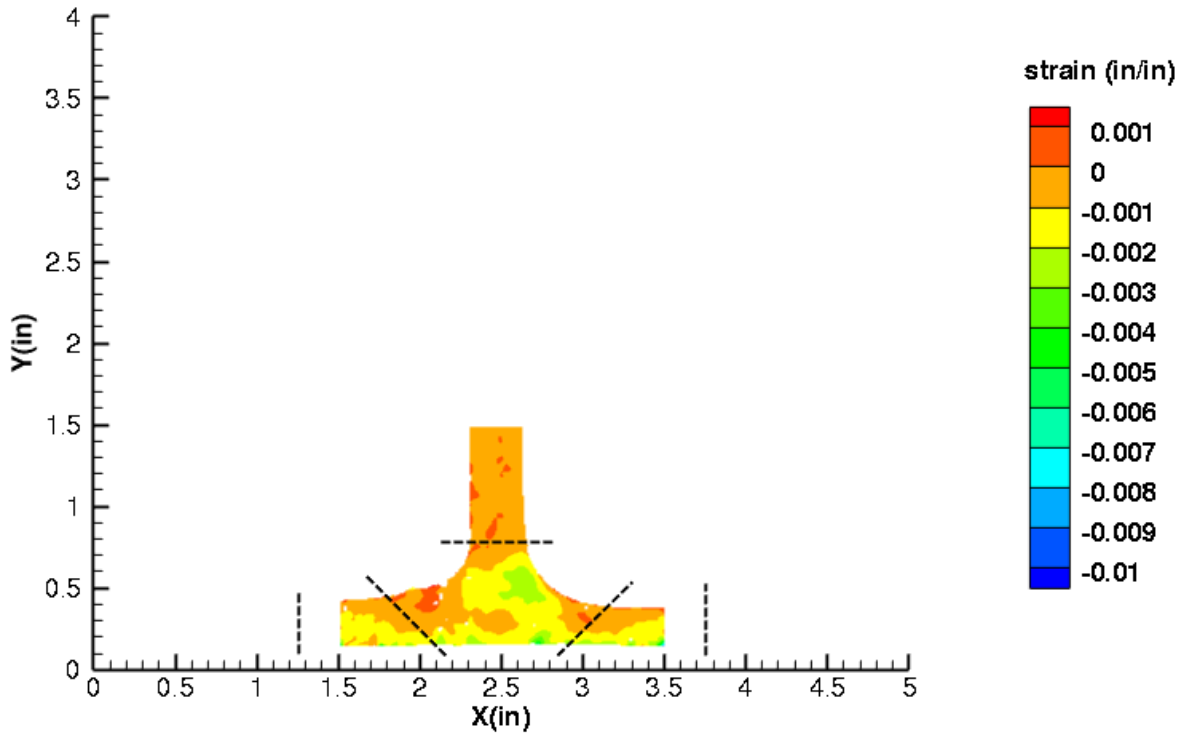

Figure C258. T5N1 strain contours for minimum principal strain at 1986 lb. load, prior to initial failure, local 5MP VIC data.

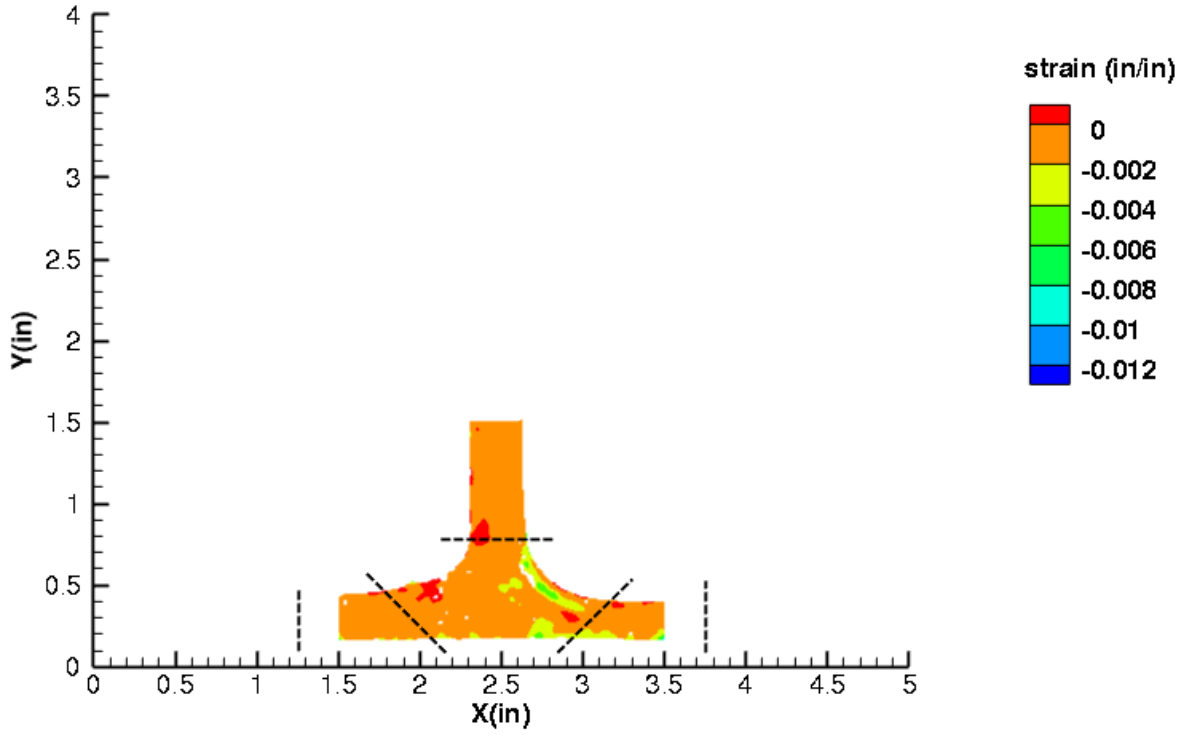

Figure C259. T5N1 strain contours for minimum principal strain at 1670 lb. load, just after initial failure, local 5MP VIC data.

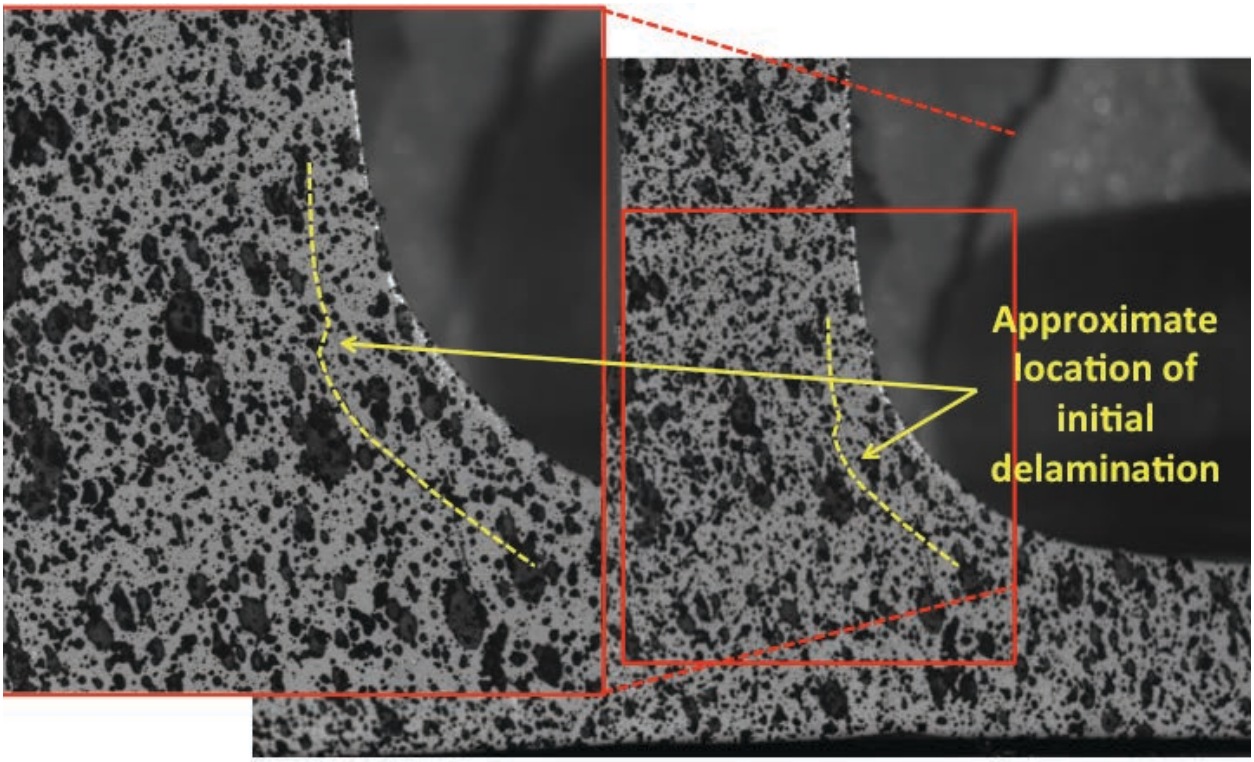

Figure C260. T5N1 image just after initial failure, local 5MP VIC data.

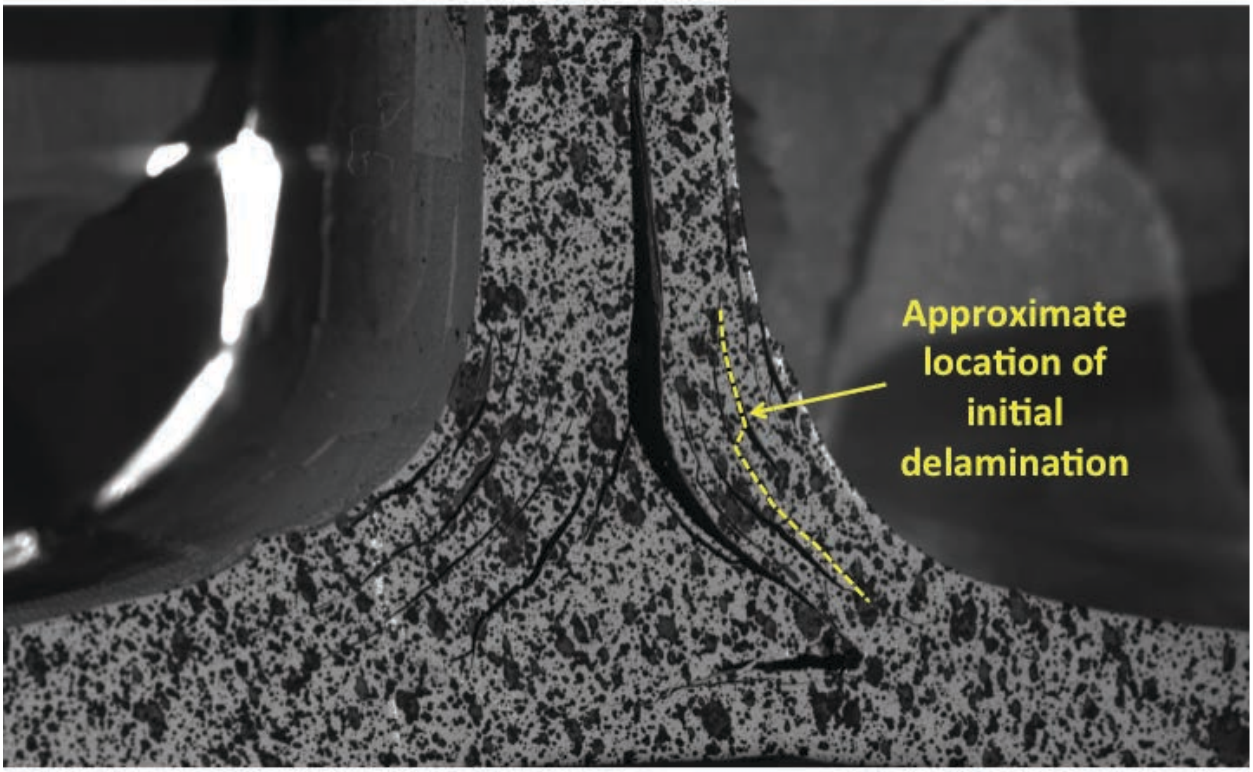

Figure C261. T5N1 image just after maximum load, local 5MP VIC data.

T5N2

This section presents the test data for the T5N2 test article.

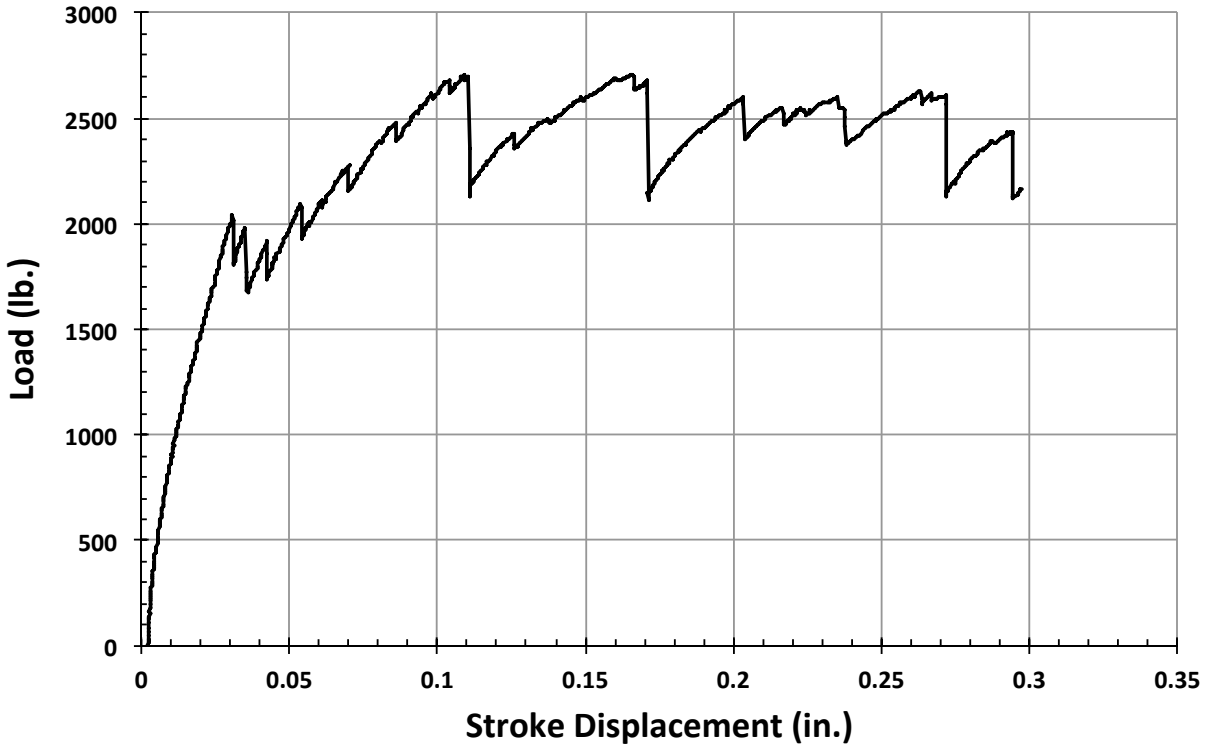

Figure C262. T5N2 load vs. stroke.

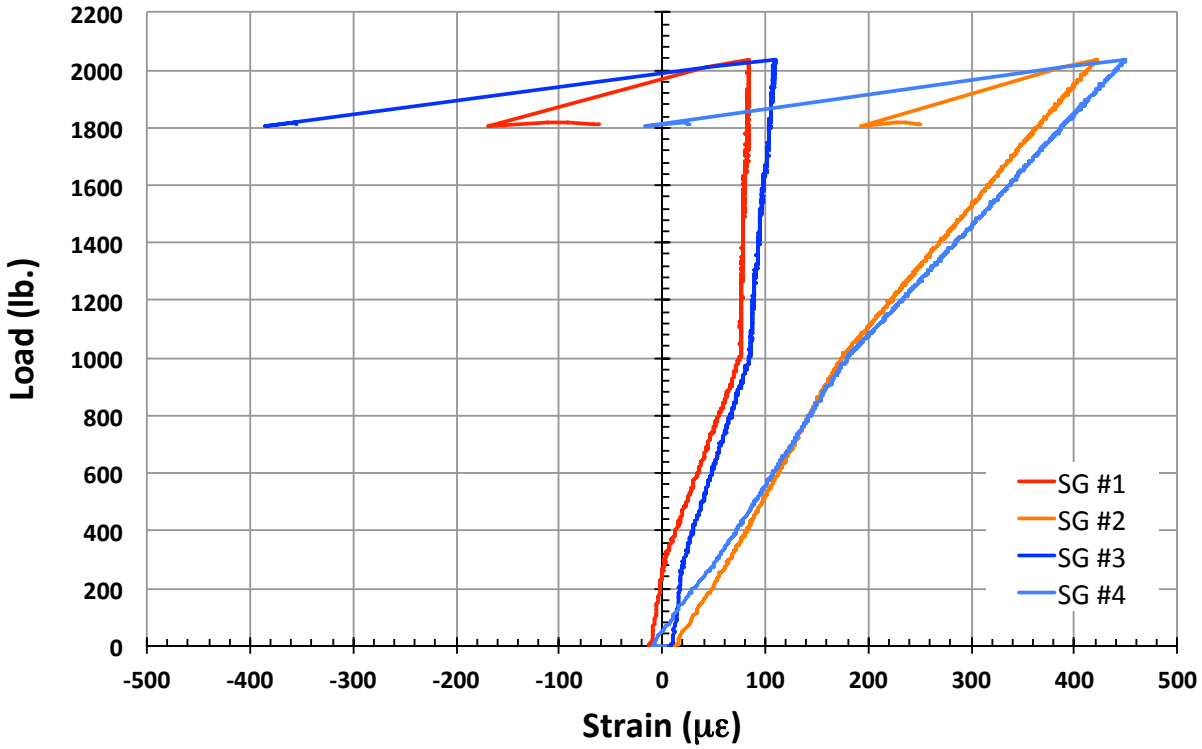

Figure C263. T5N2 load vs. strain, initial loading.

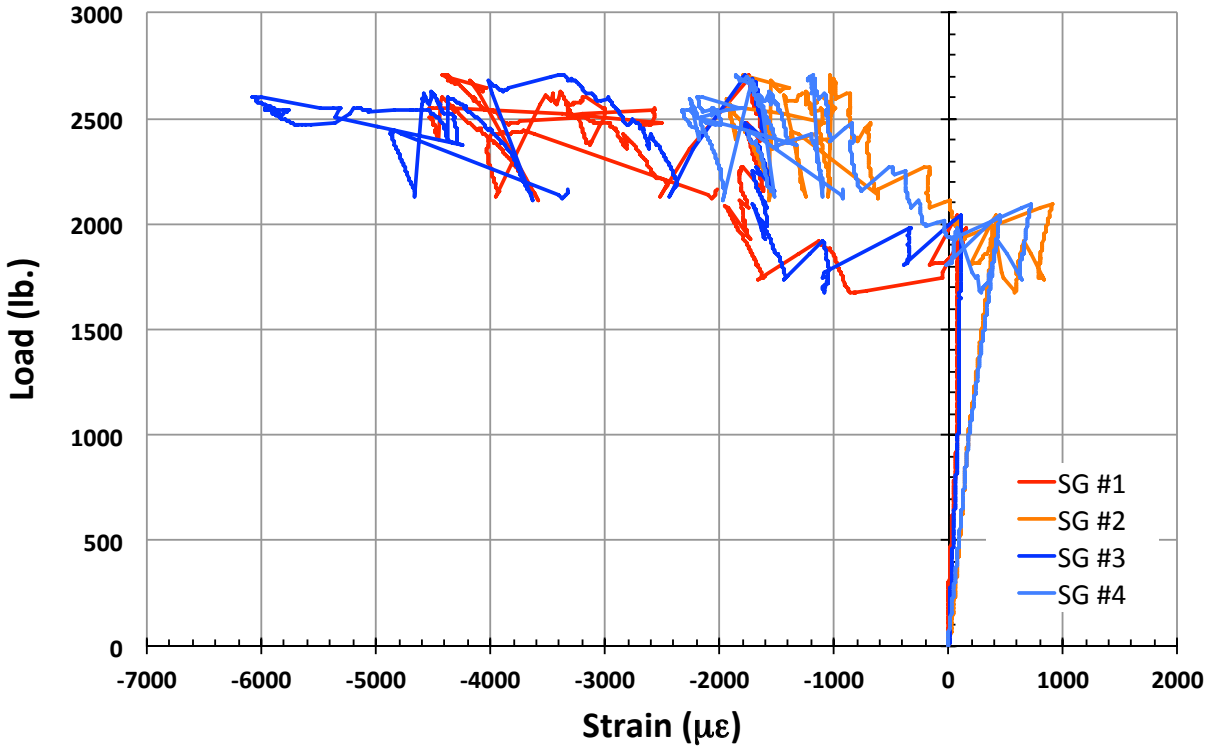

Figure C264. T5N2 load vs. strain.

T5N3

This section presents the test data for the T5N3 test article.

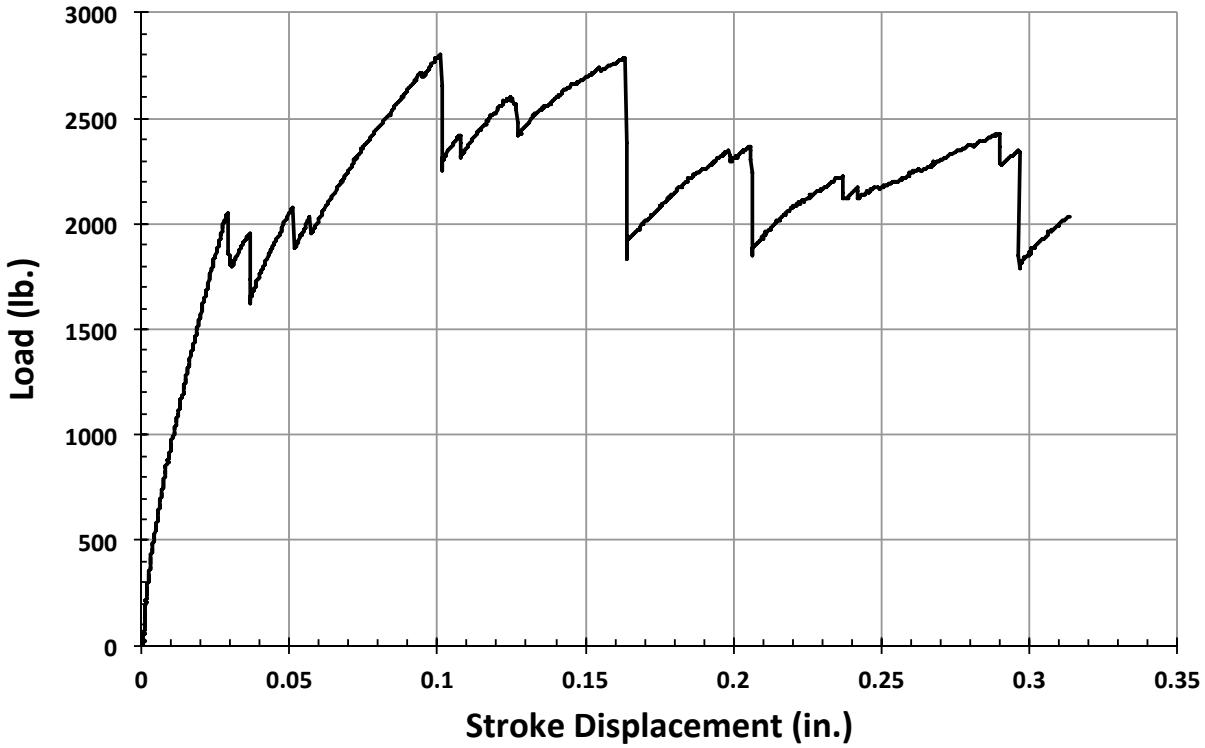

Figure C265. T5N3 load vs. stroke.

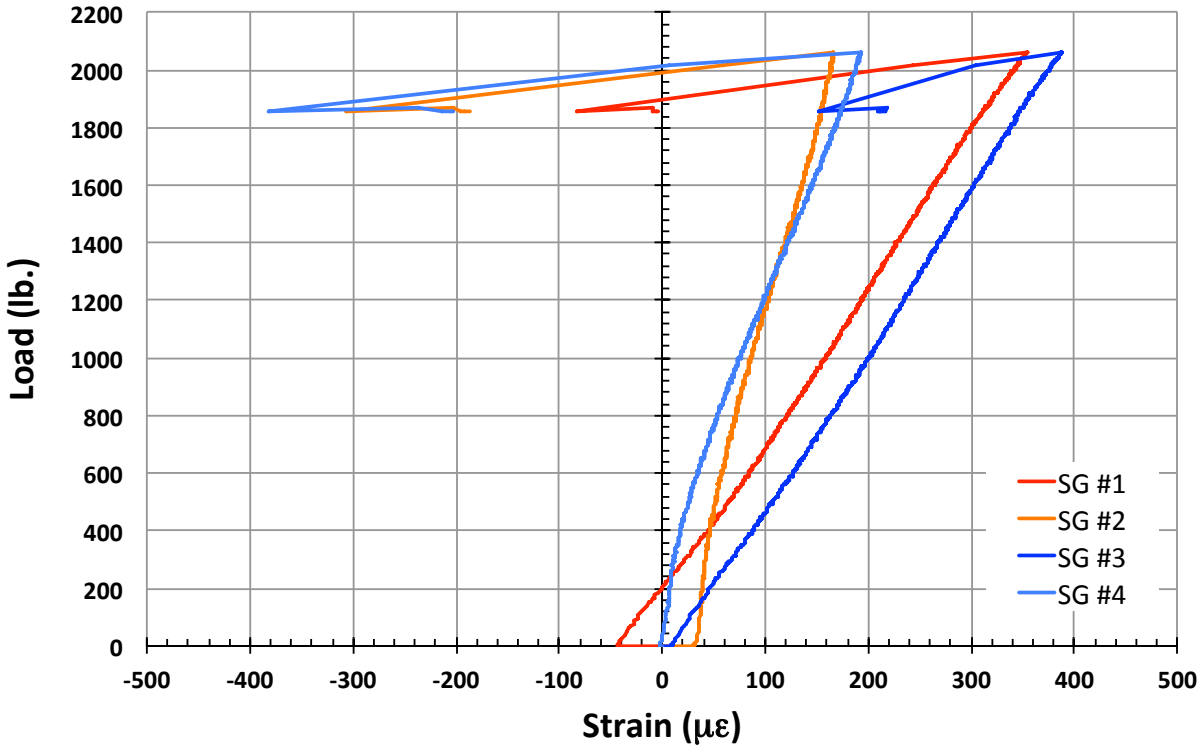

Figure C266. T5N3 load vs. strain, initial loading.

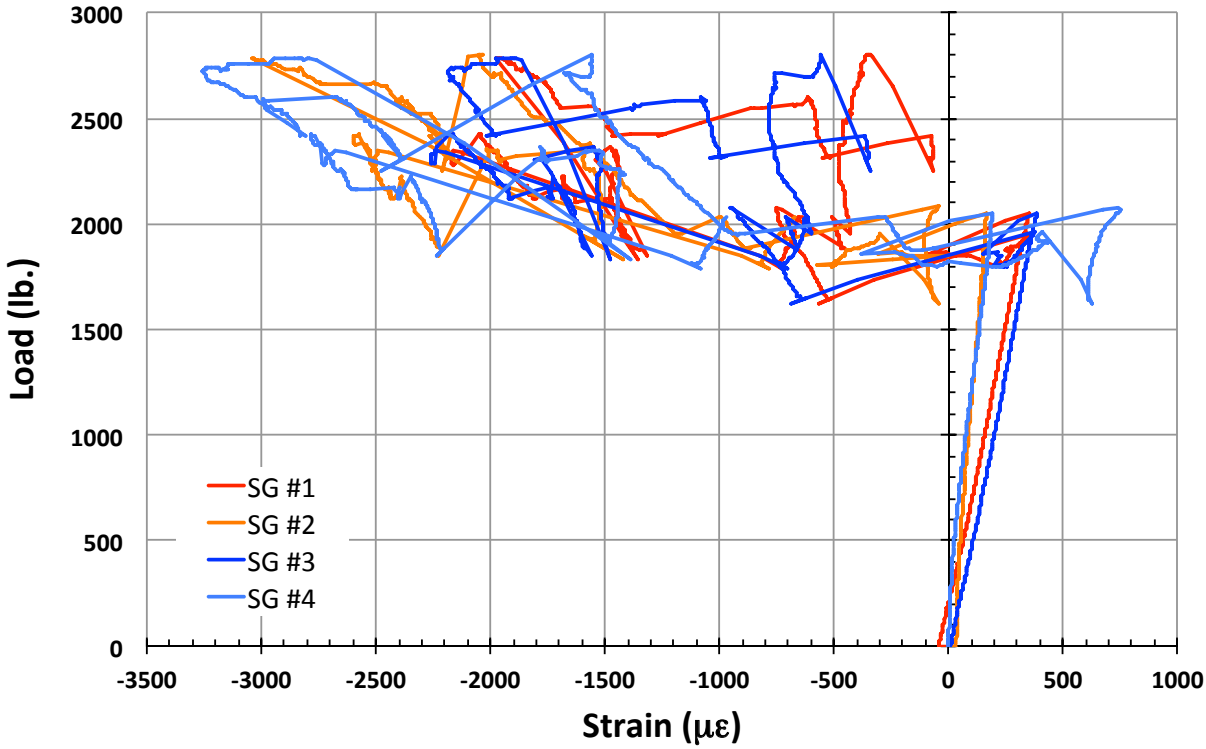

Figure C267. T5N3 load vs. strain.

Bending Tests

BNS1

This section presents the test data for the BNS1 test article, and includes strain plots and failure images.

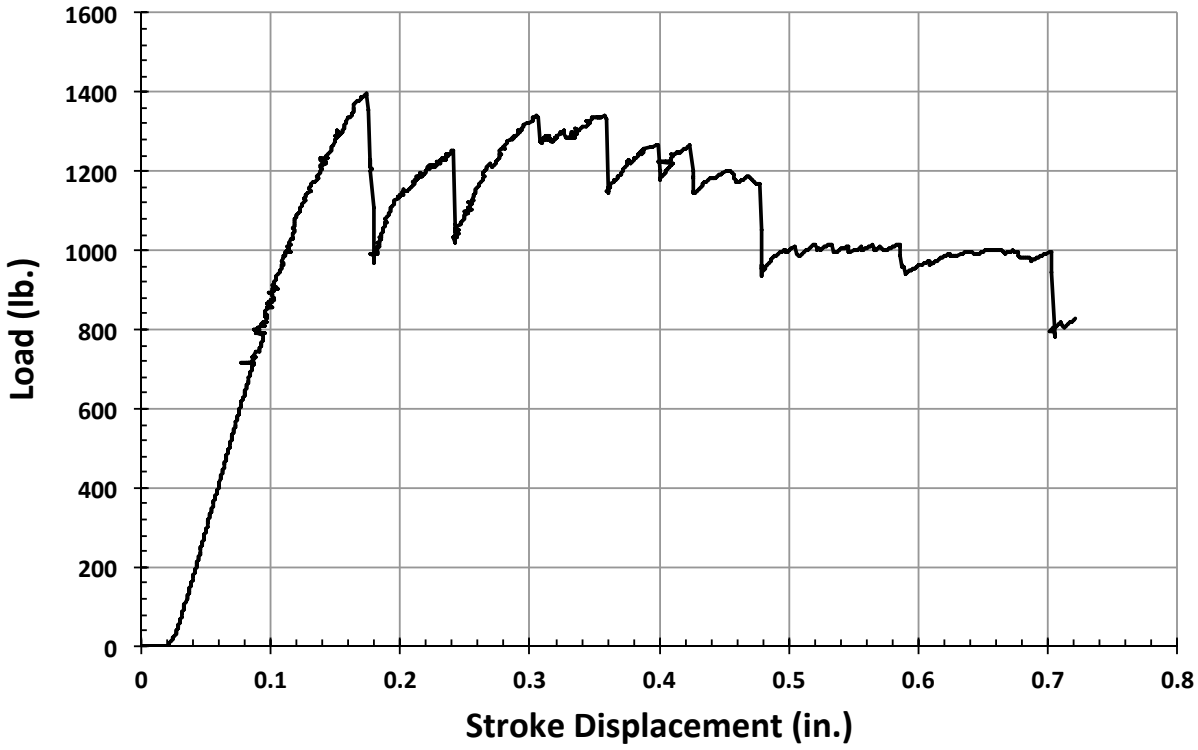

Figure C268. BNS1 load vs. stroke.

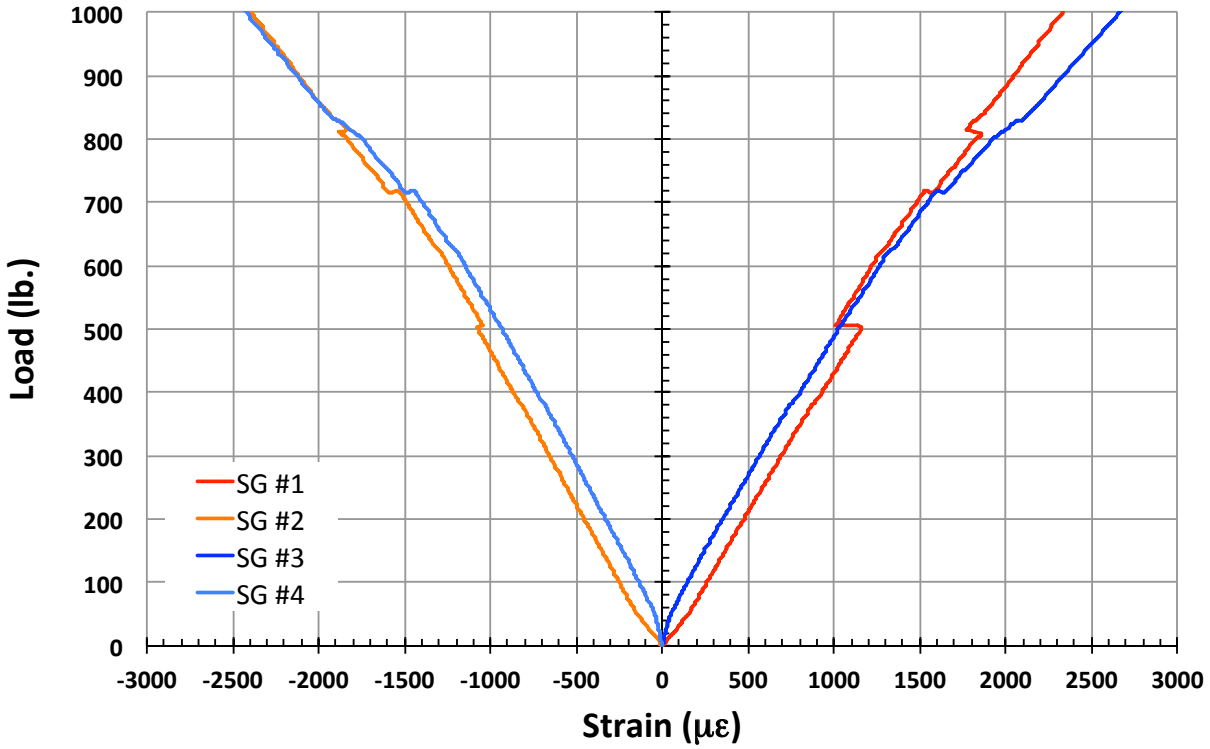

Figure C269. BNS1 load vs. strain, initial loading.

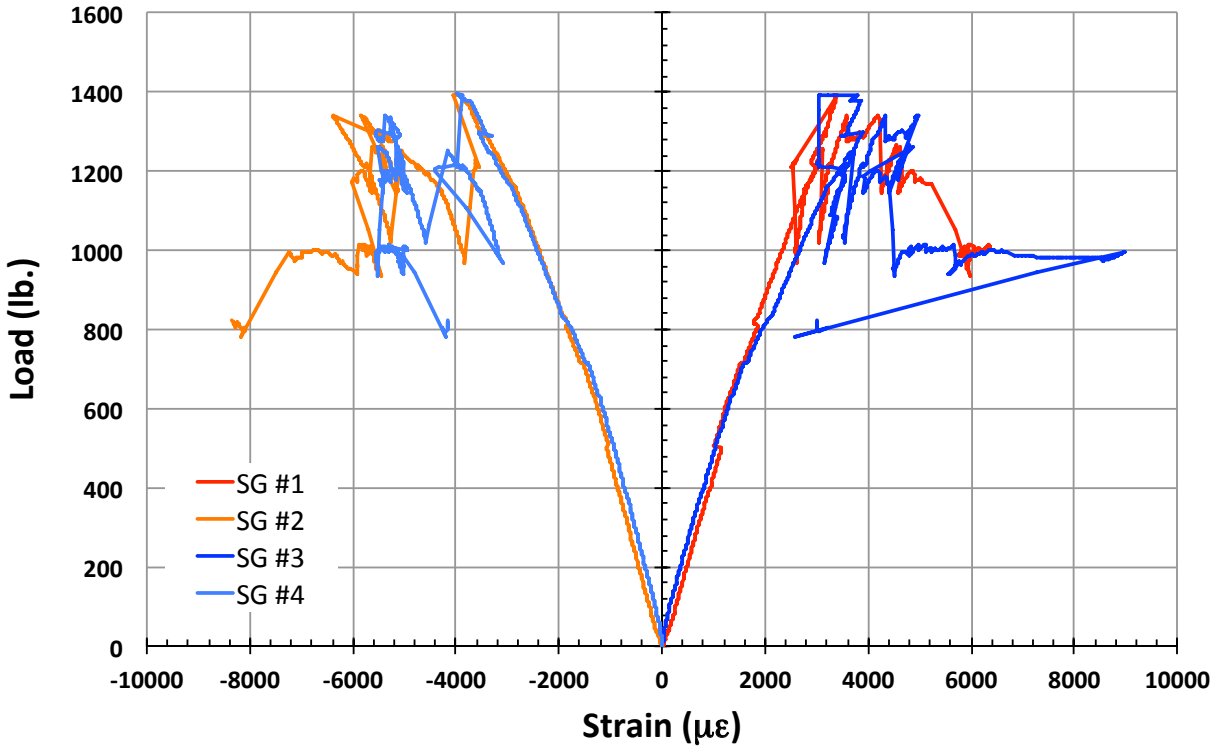

Figure C270. BNS1 load vs. strain.

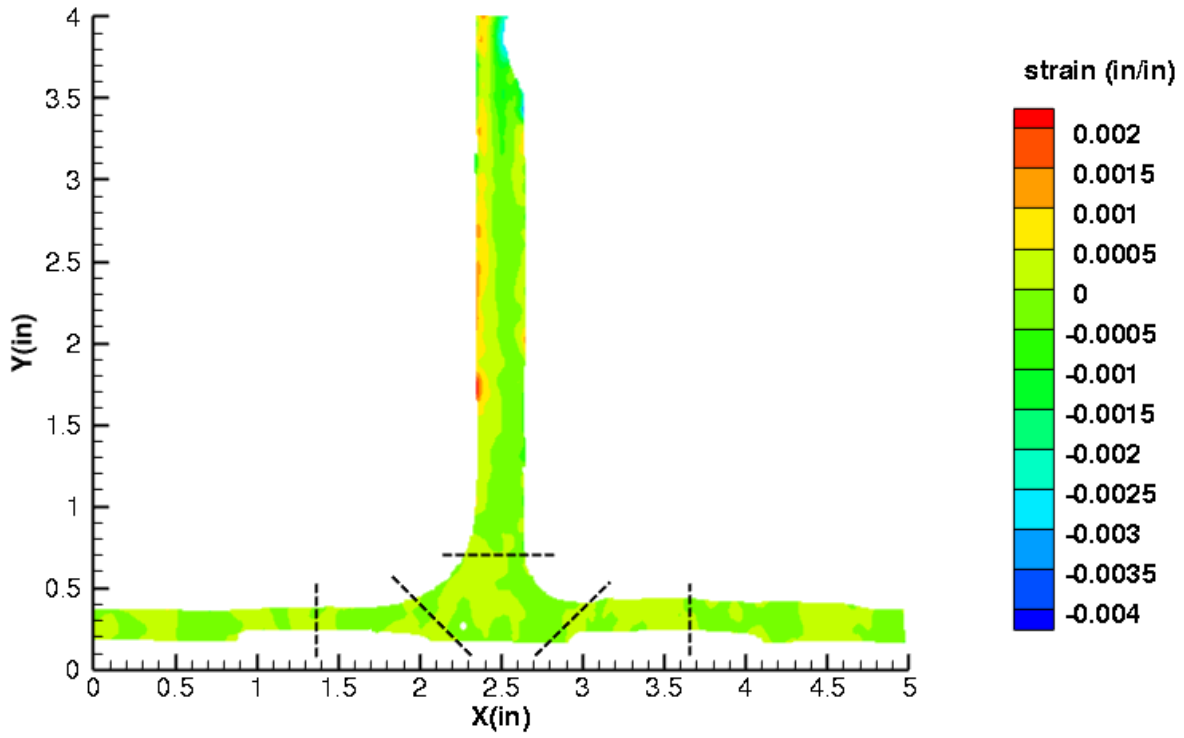

Figure C271. BNS1 strain contours for ε_{xx} at 517 lb. load, prior to initial failure, front 12MP VIC data.

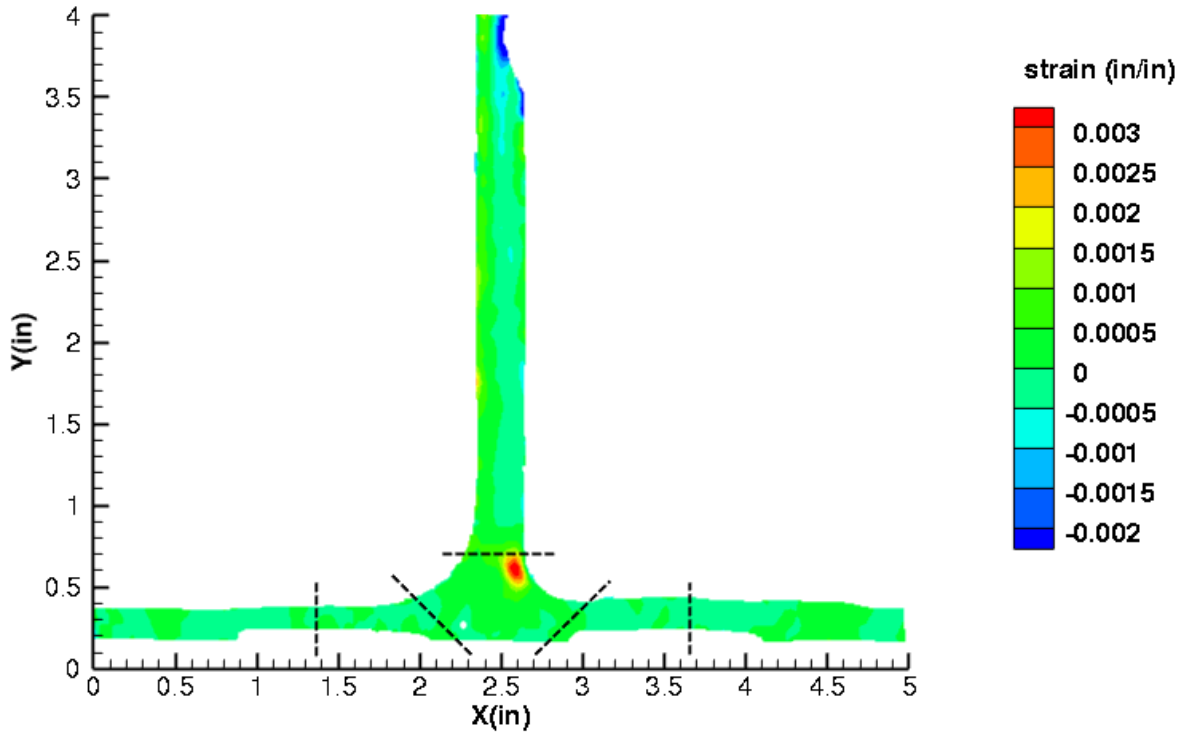

Figure C272. BNS1 strain contours for ε_{xx} at 527 lb. load, just after initial failure, front 12MP VIC data.

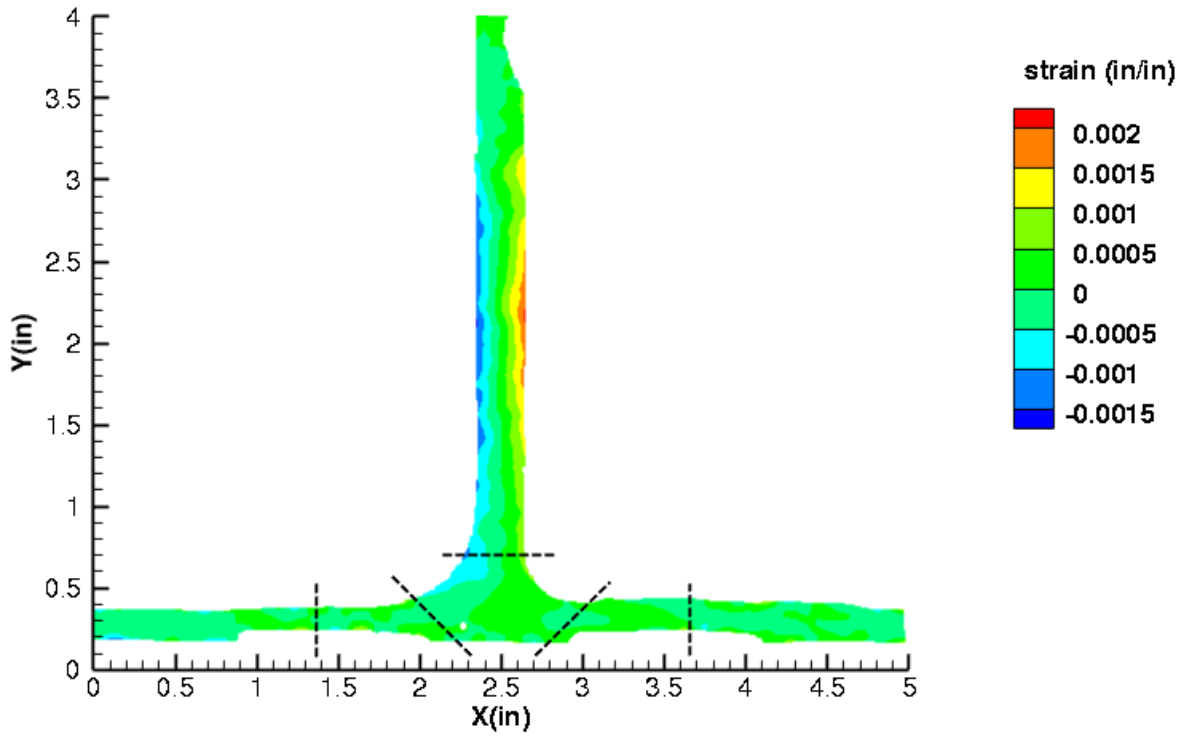

Figure C273. BNS1 strain contours for ε_{yy} at 517 lb. load, prior to initial failure, front 12MP VIC data.

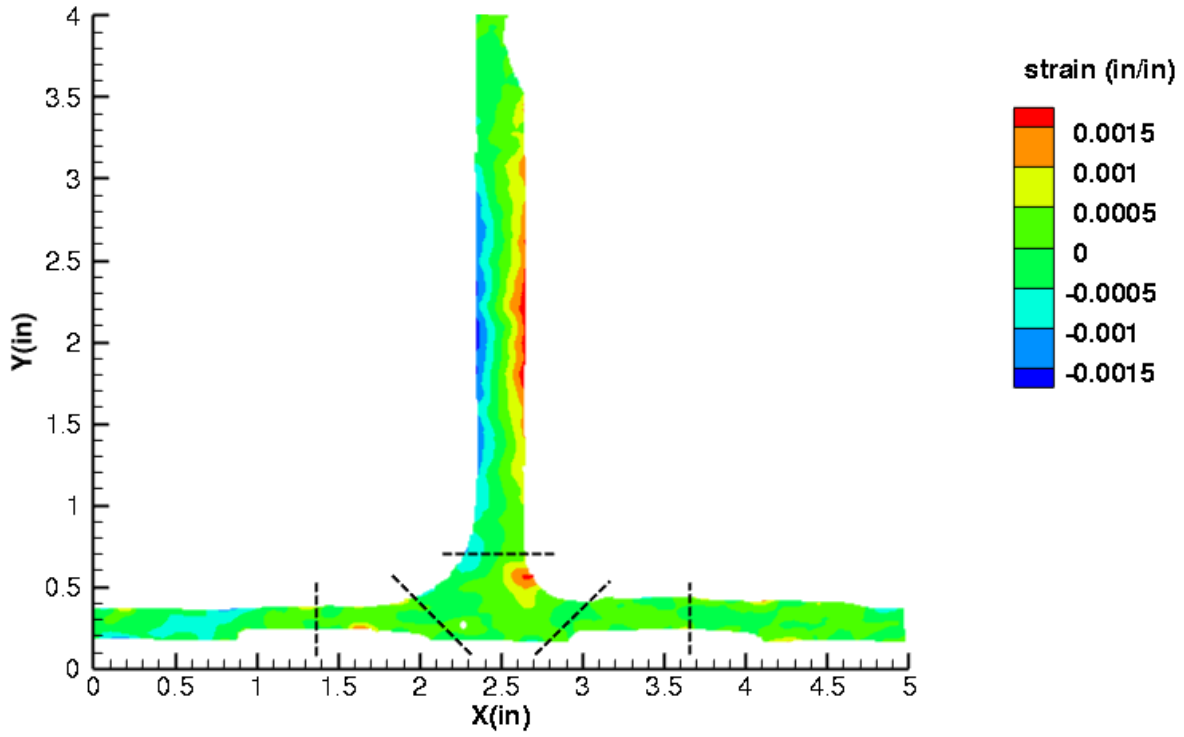

Figure C274. BNS1 strain contours for ε_{yy} at 527 lb. load, just after initial failure, front 12MP VIC data.

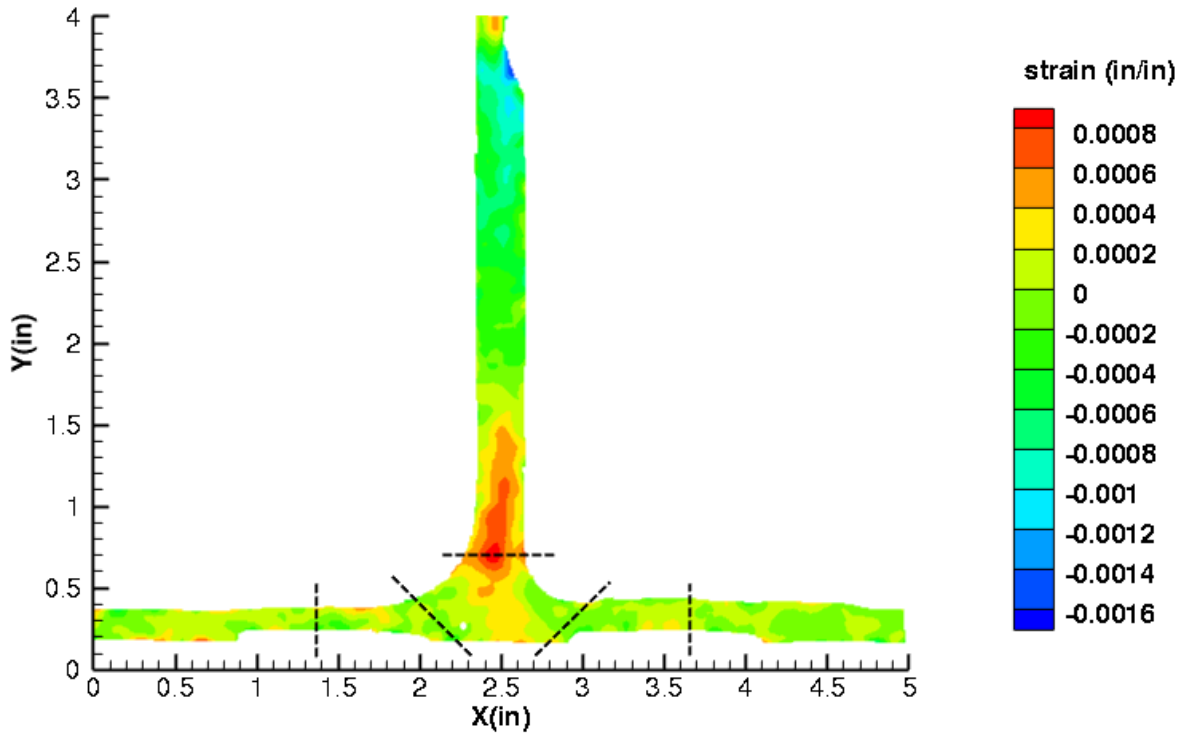

Figure C275. BNS1 strain contours for ε_{xy} at 517 lb. load, prior to initial failure, front 12MP VIC data.

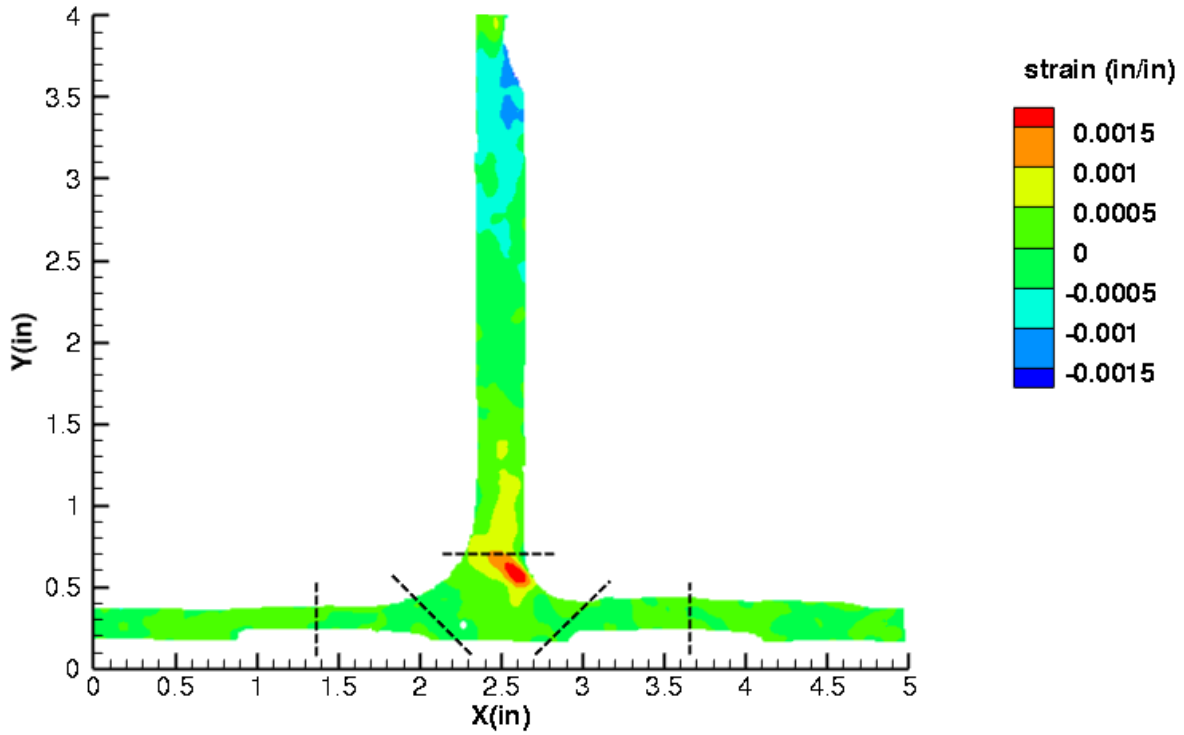

Figure C276. BNS1 strain contours for ε_{xy} at 527 lb. load, just after initial failure, front 12MP VIC data.

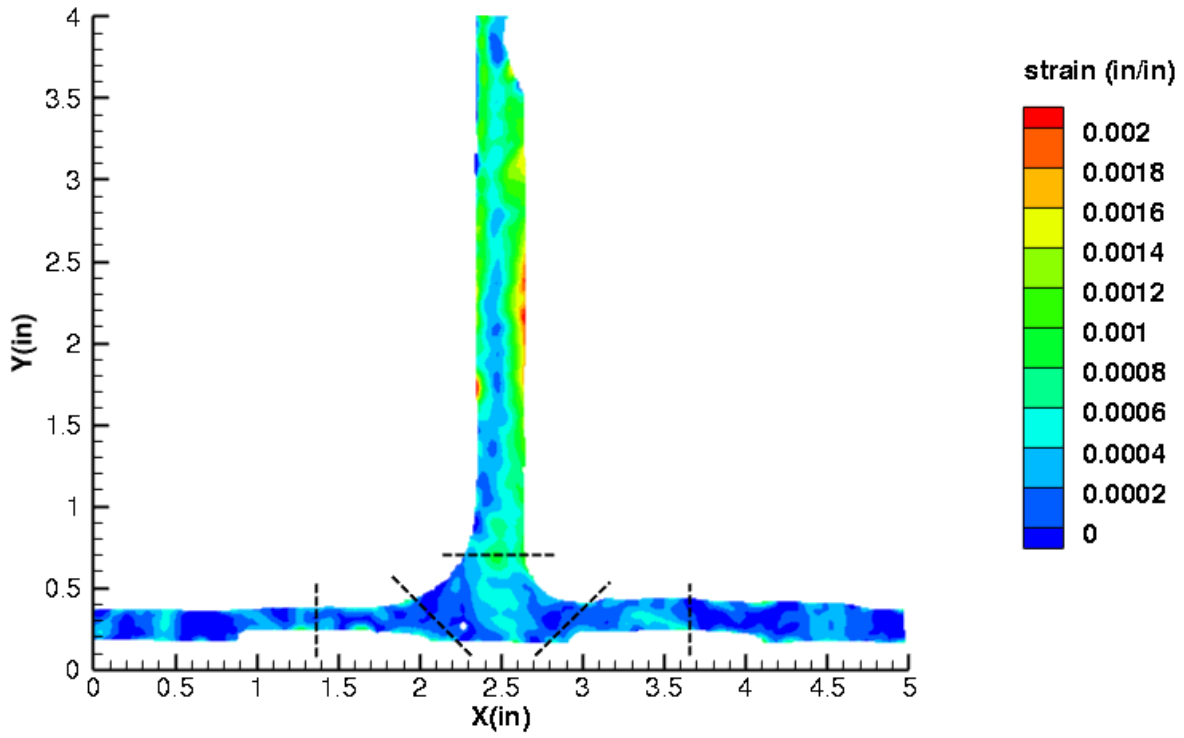

Figure C277. BNS1 strain contours for maximum principal strain at 517 lb. load, prior to initial failure, front 12MP VIC data.

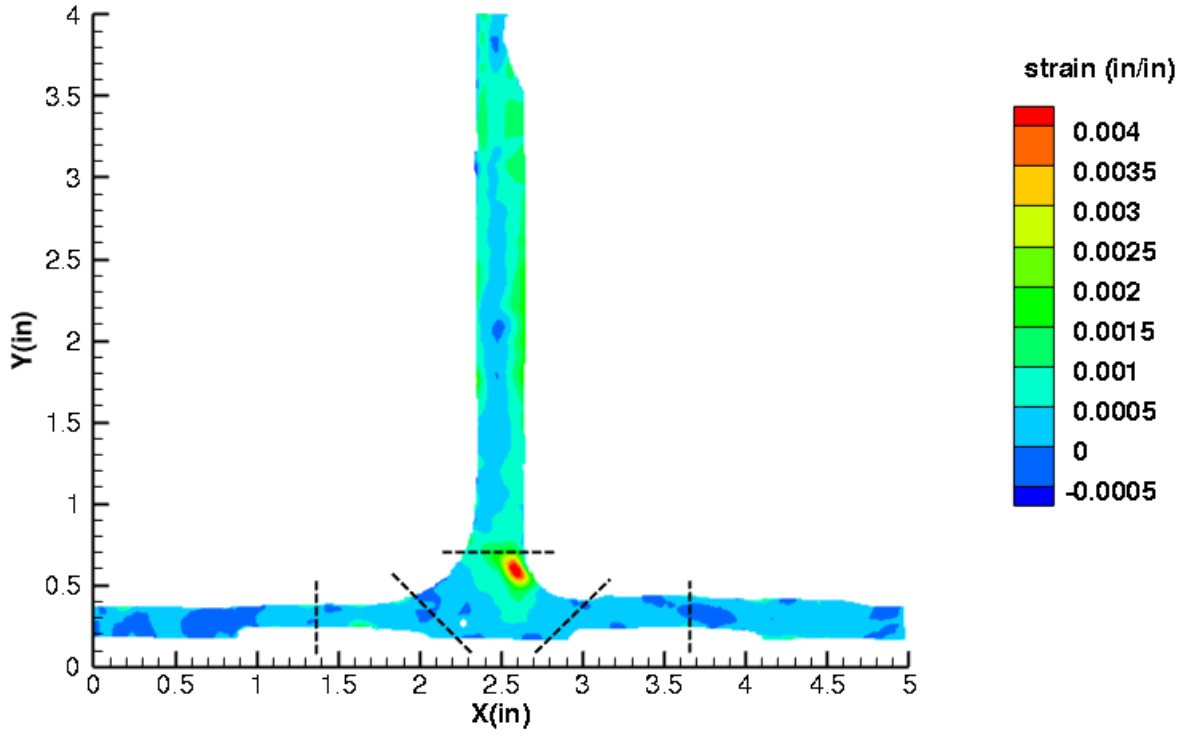

Figure C278. BNS1 strain contours for maximum principal strain at 527 lb. load, just after initial failure, front 12MP VIC data.

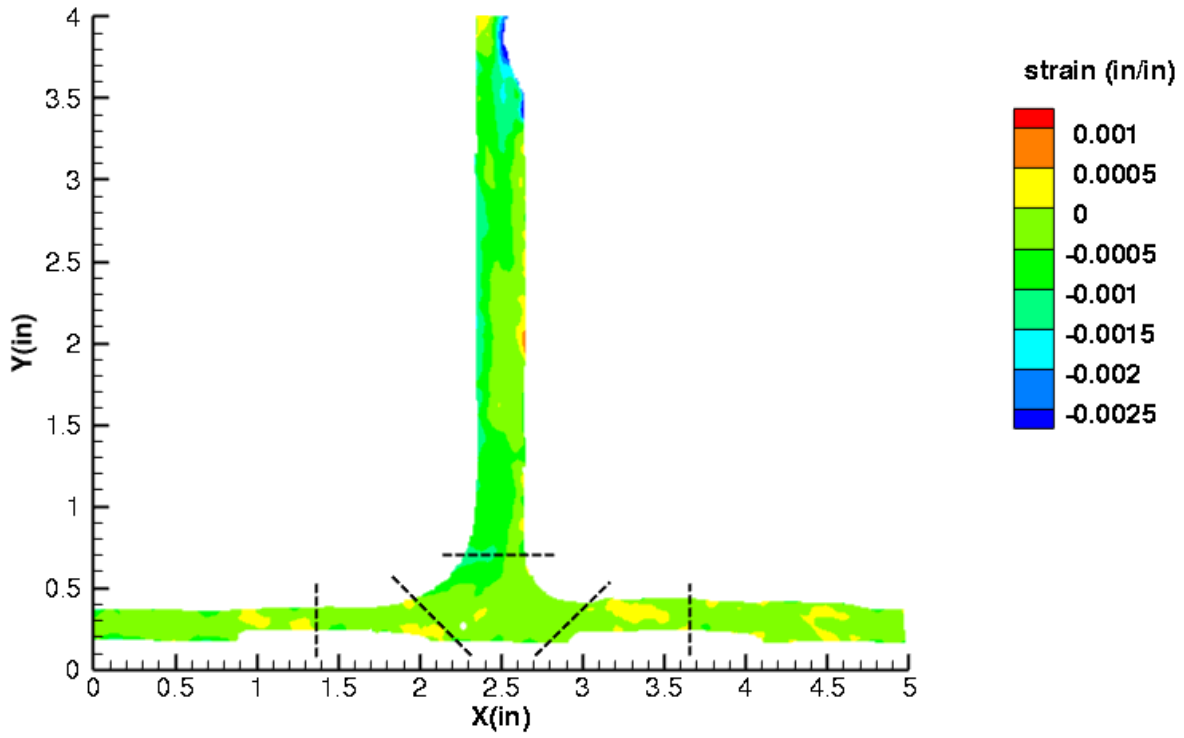

Figure C279. BNS1 strain contours for minimum principal strain at 517 lb. load, prior to initial failure, front 12MP VIC data.

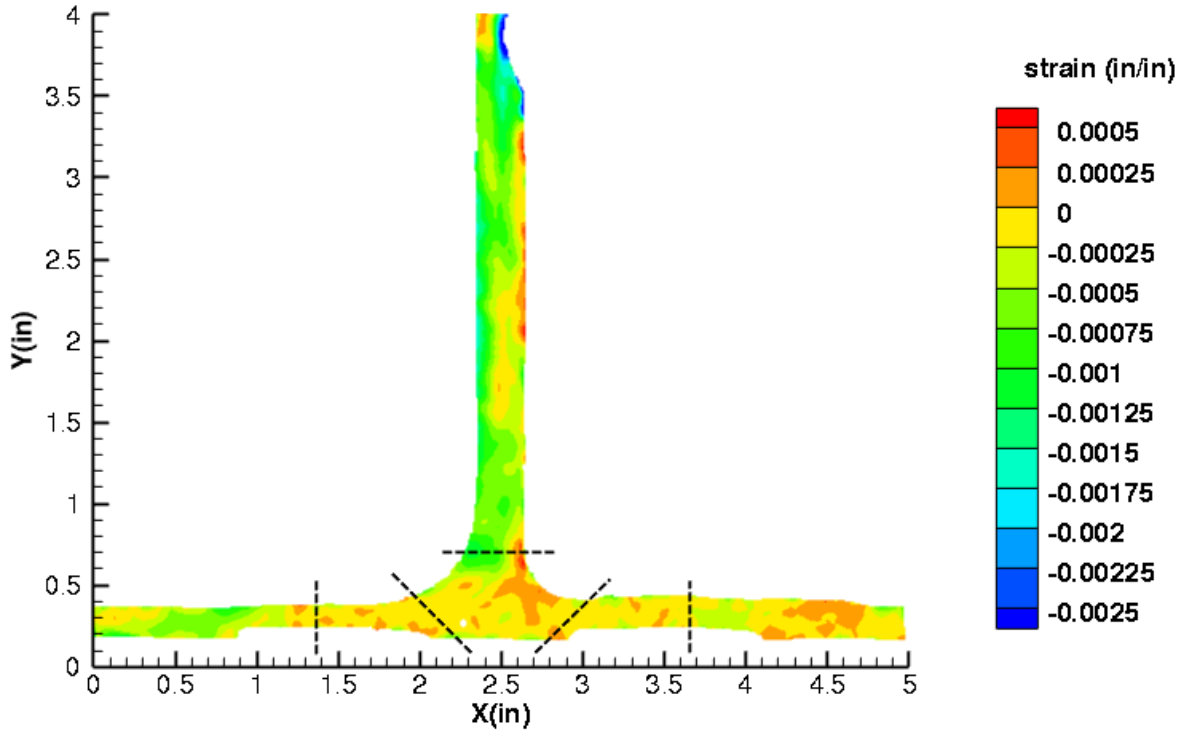

Figure C280. BNS1 strain contours for minimum principal strain at 527 lb. load, just after initial failure, front 12MP VIC data.

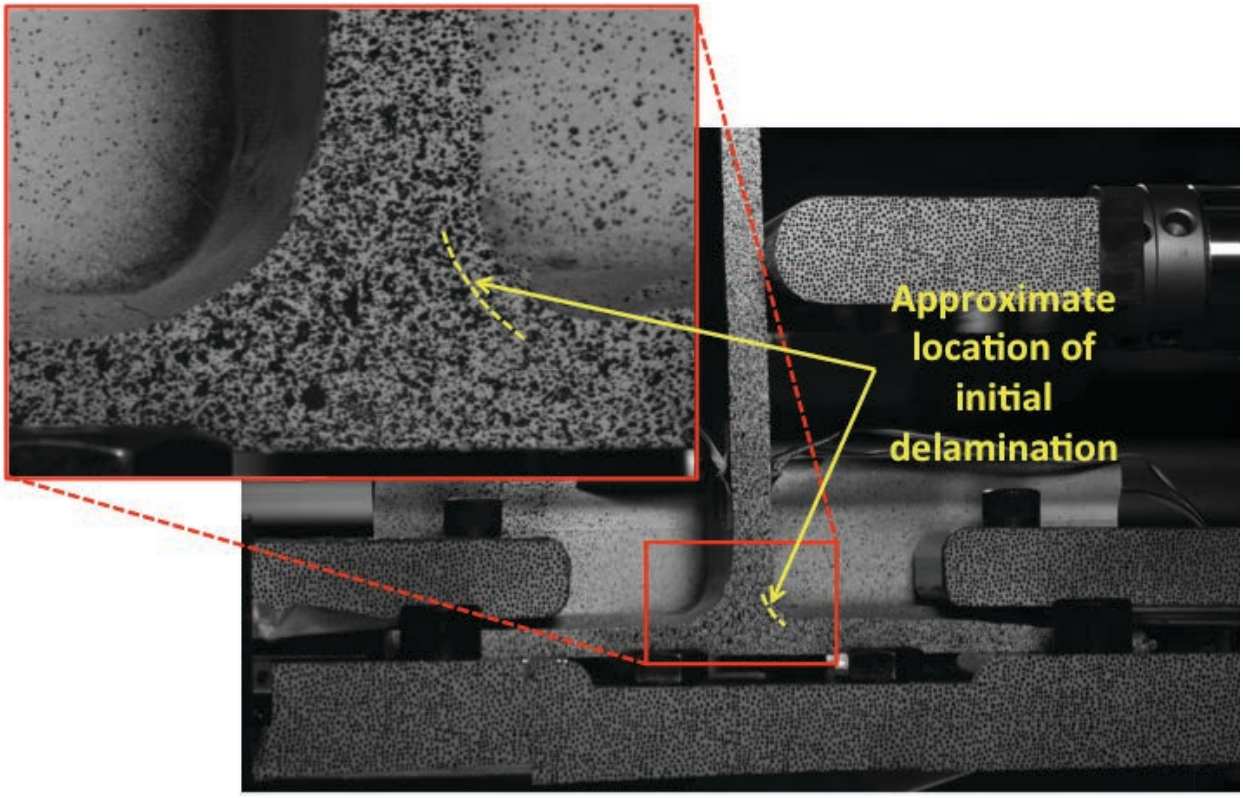

Figure C281. BNS1 image just after initial failure, front 12MP VIC data.

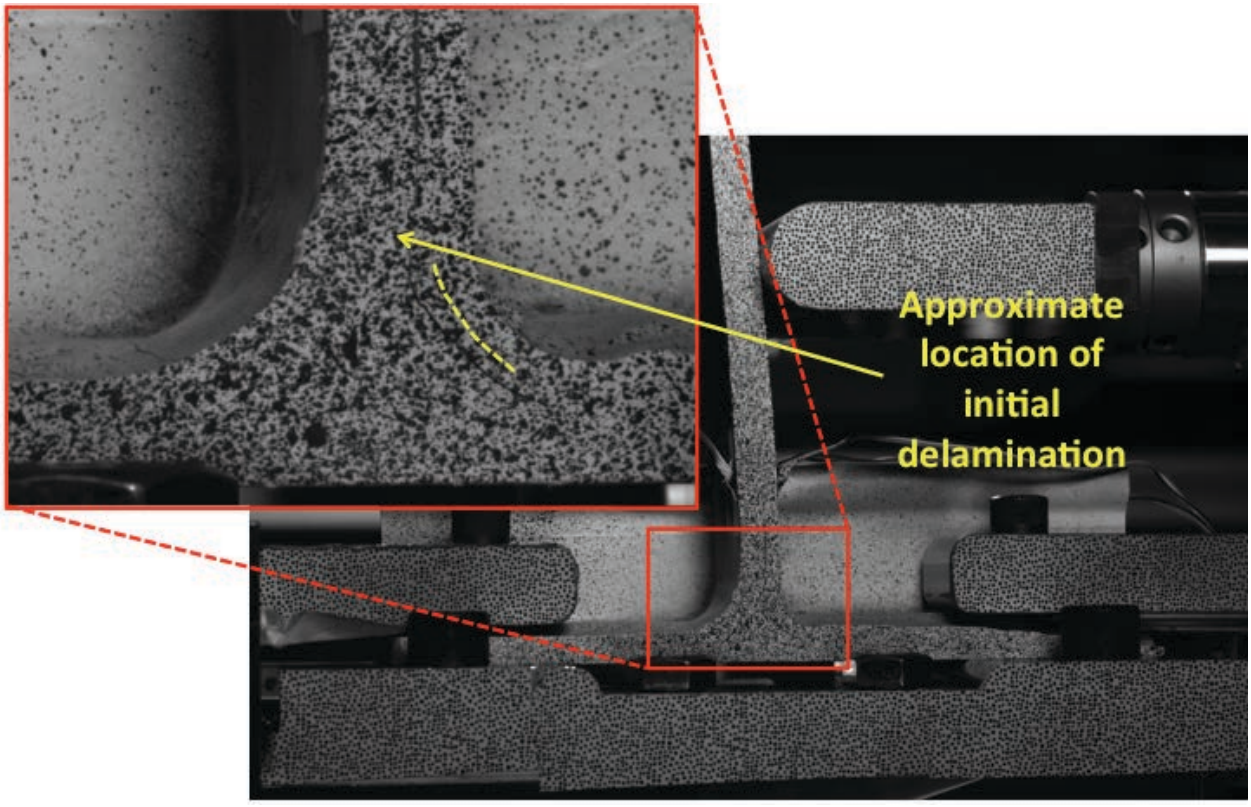

Figure C282. BNS1 image just after maximum load, front 12MP VIC data.

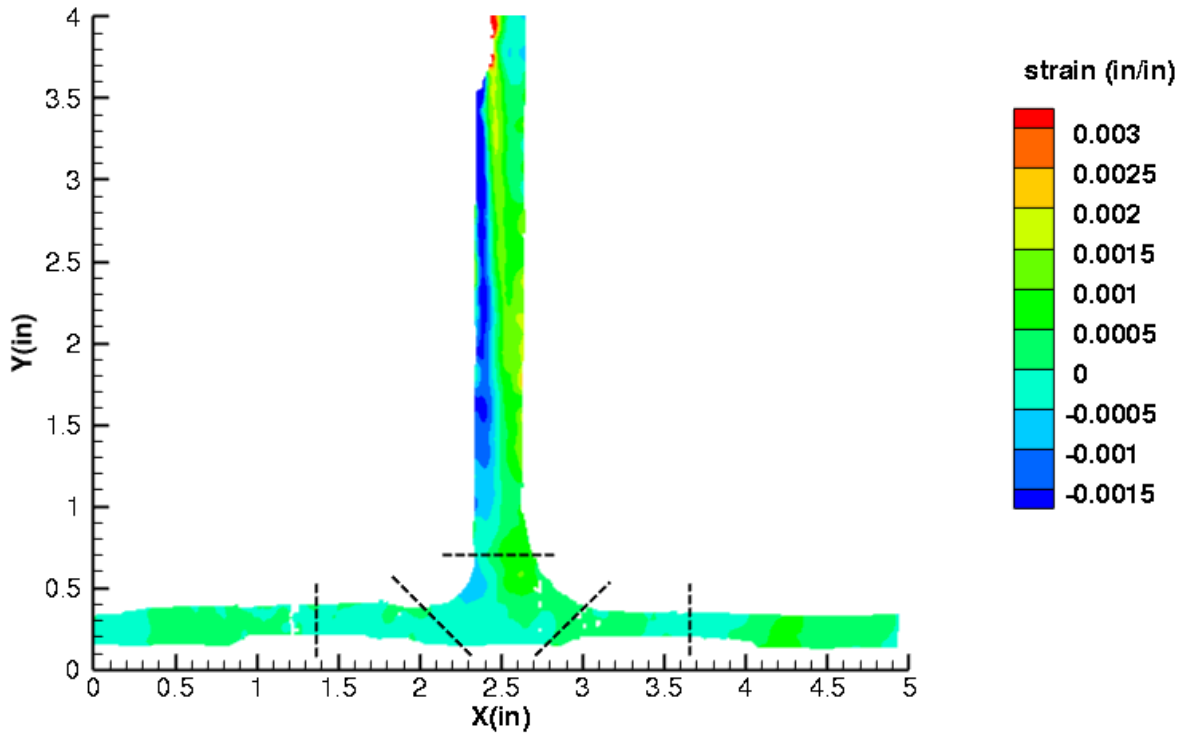

Figure C283. BNS1 strain contours for ε_{xx} at 1296 lb. load, prior to initial failure, back 12MP VIC data.

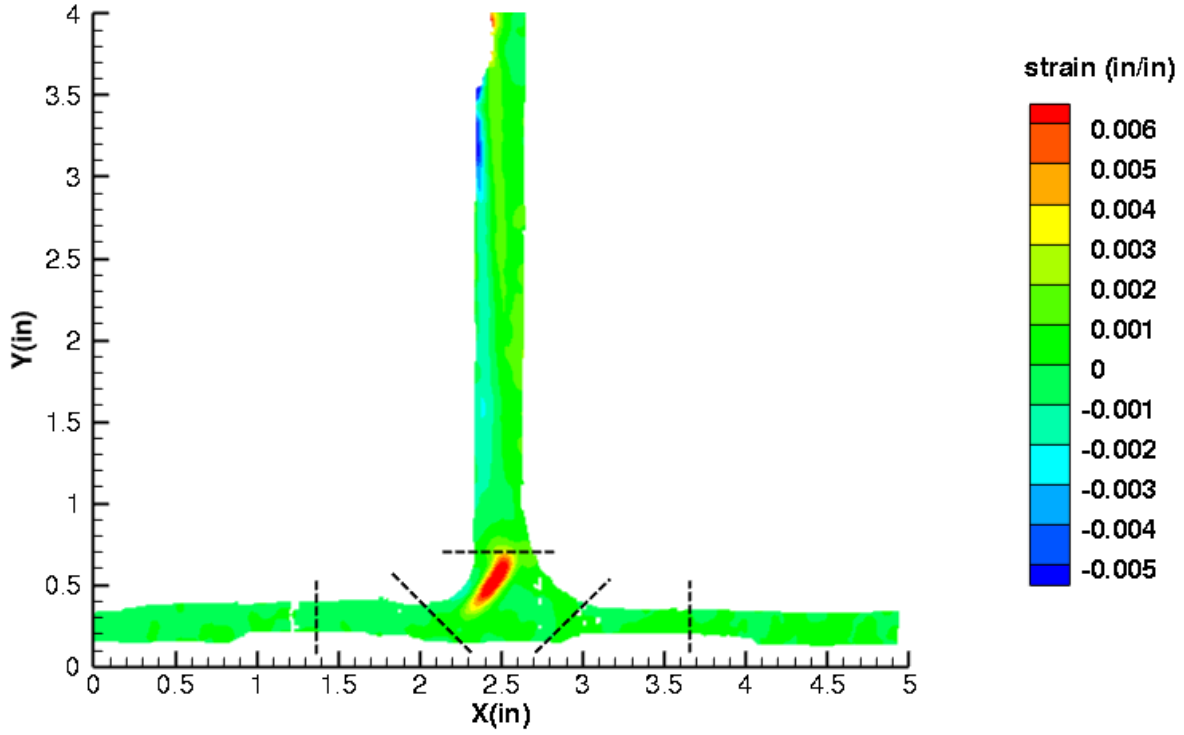

Figure C284. BNS1 strain contours for ε_{xx} at 1292 lb. load, just after initial failure, back 12MP VIC data.

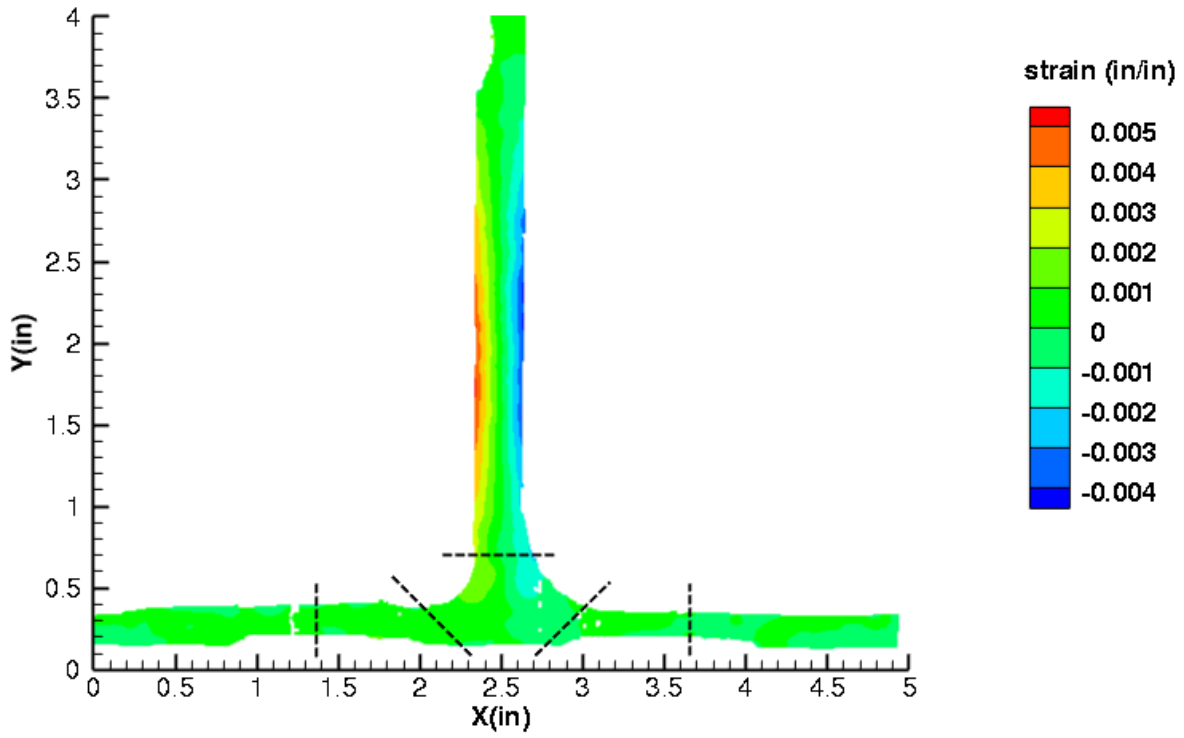

Figure C285. BNS1 strain contours for ε_{yy} at 1296 lb. load, prior to initial failure, back 12MP VIC data.

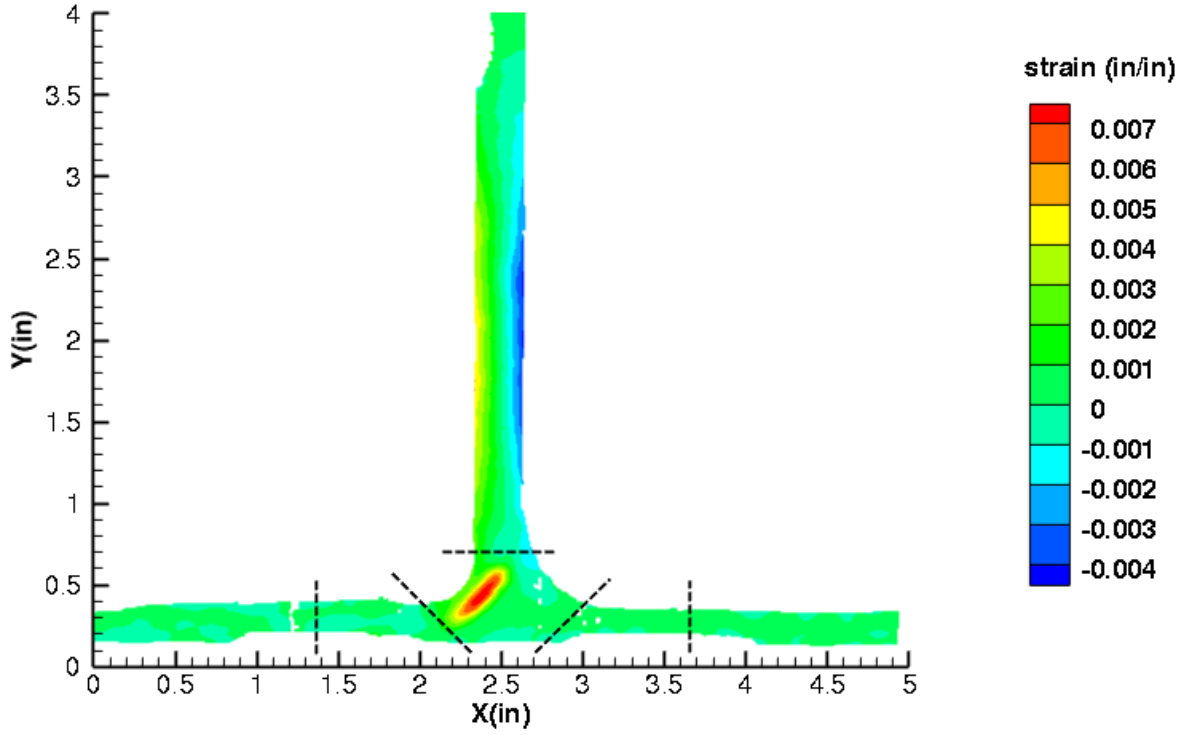

Figure C286. BNS1 strain contours for ε_{yy} at 1292 lb. load, just after initial failure, back 12MP VIC data.

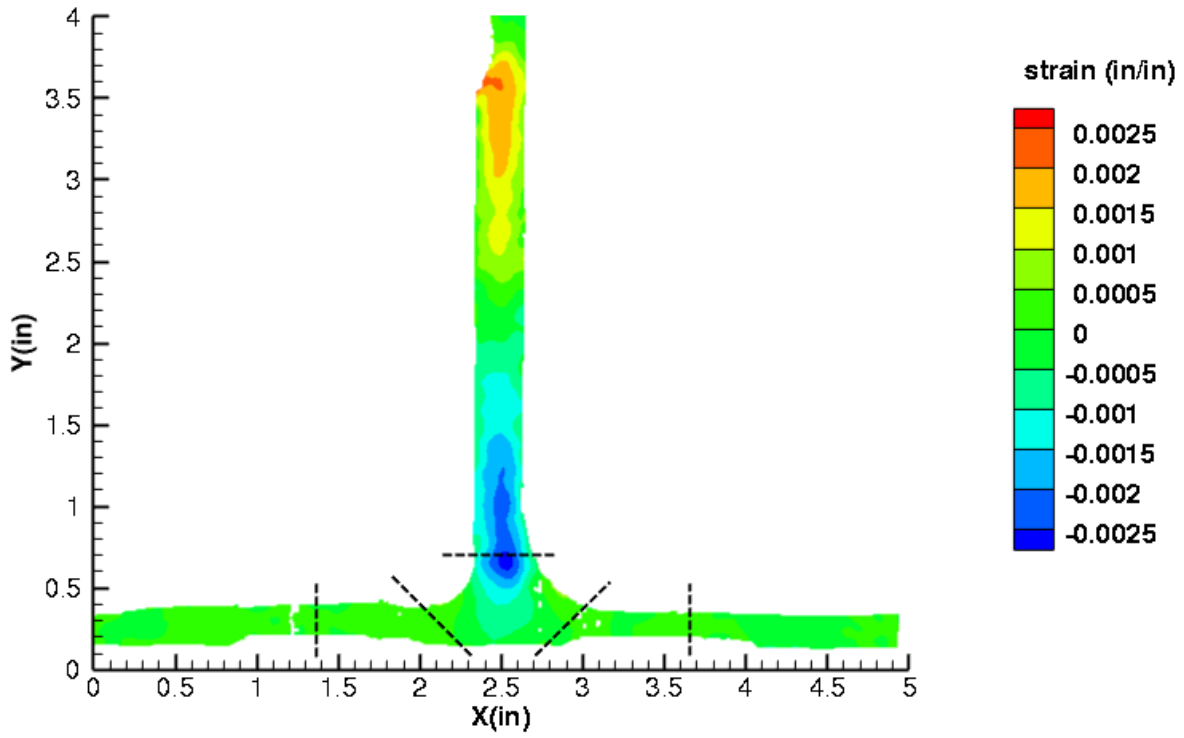

Figure C287. BNS1 strain contours for ε_{xy} at 1296 lb. load, prior to initial failure, back 12MP VIC data.

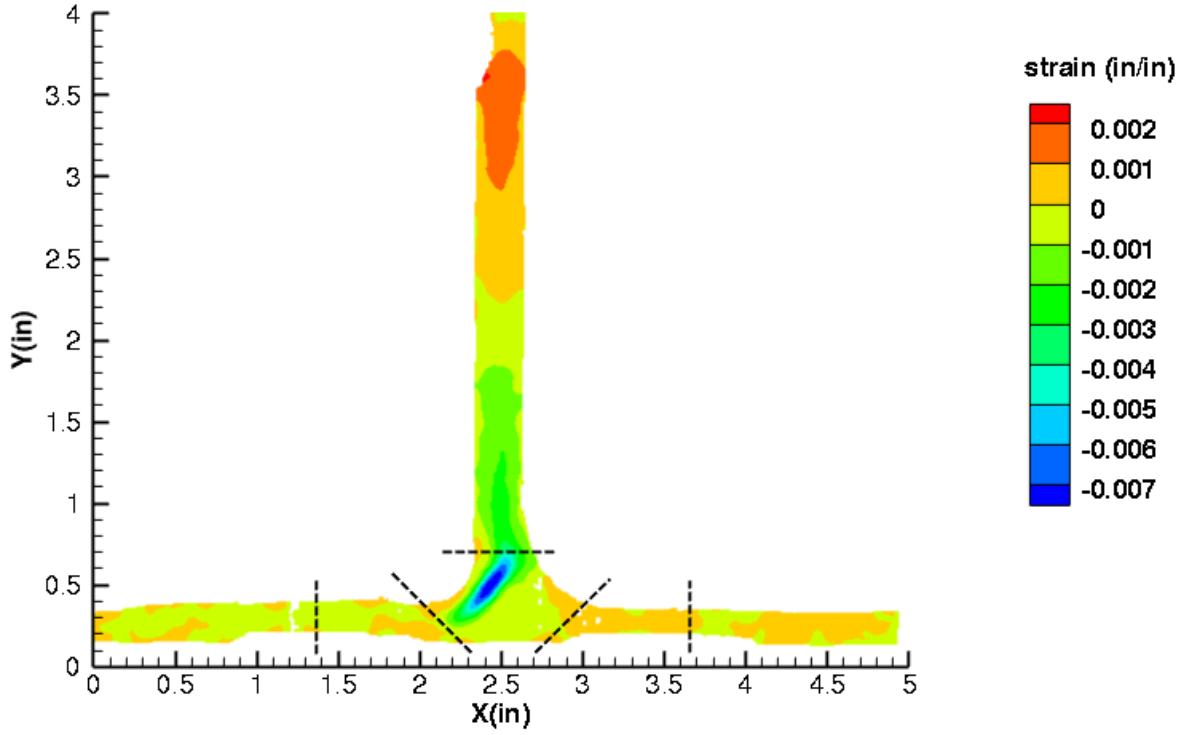

Figure C288. BNS1 strain contours for ε_{xy} at 1292 lb. load, just after initial failure, back 12MP VIC data.

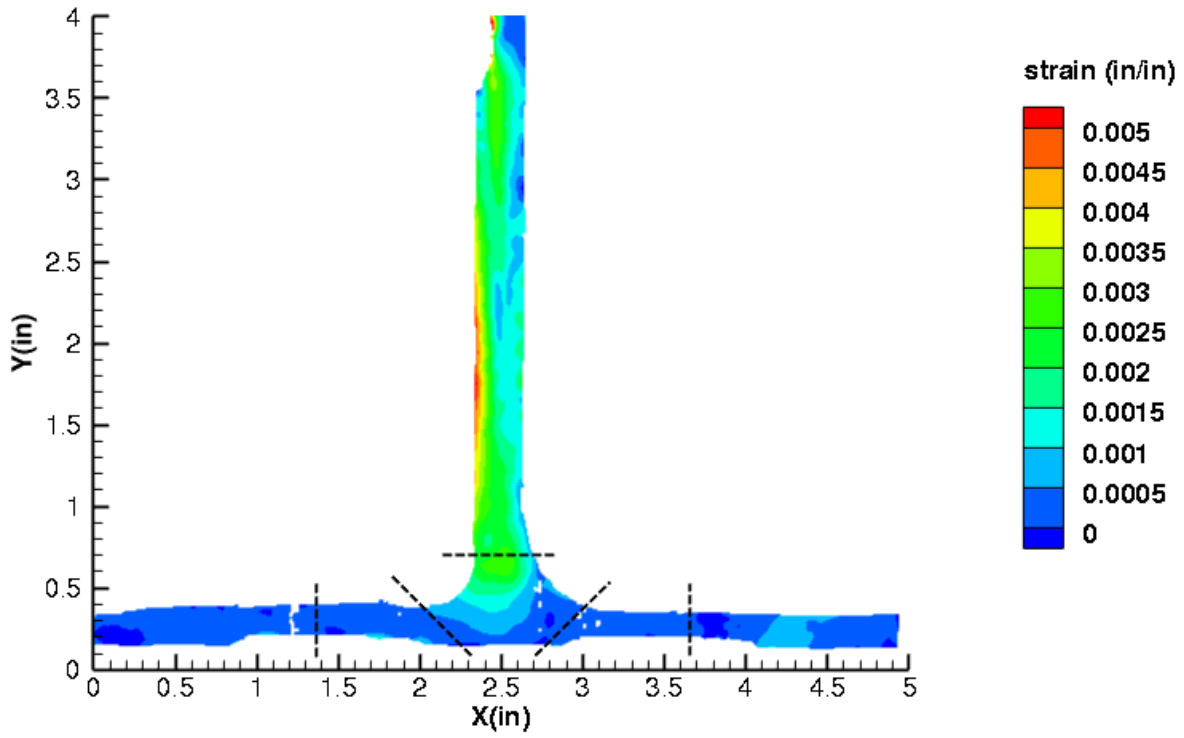

Figure C289. BNS1 strain contours for maximum principal strain at 1296 lb. load, prior to initial failure, back 12MP VIC data.

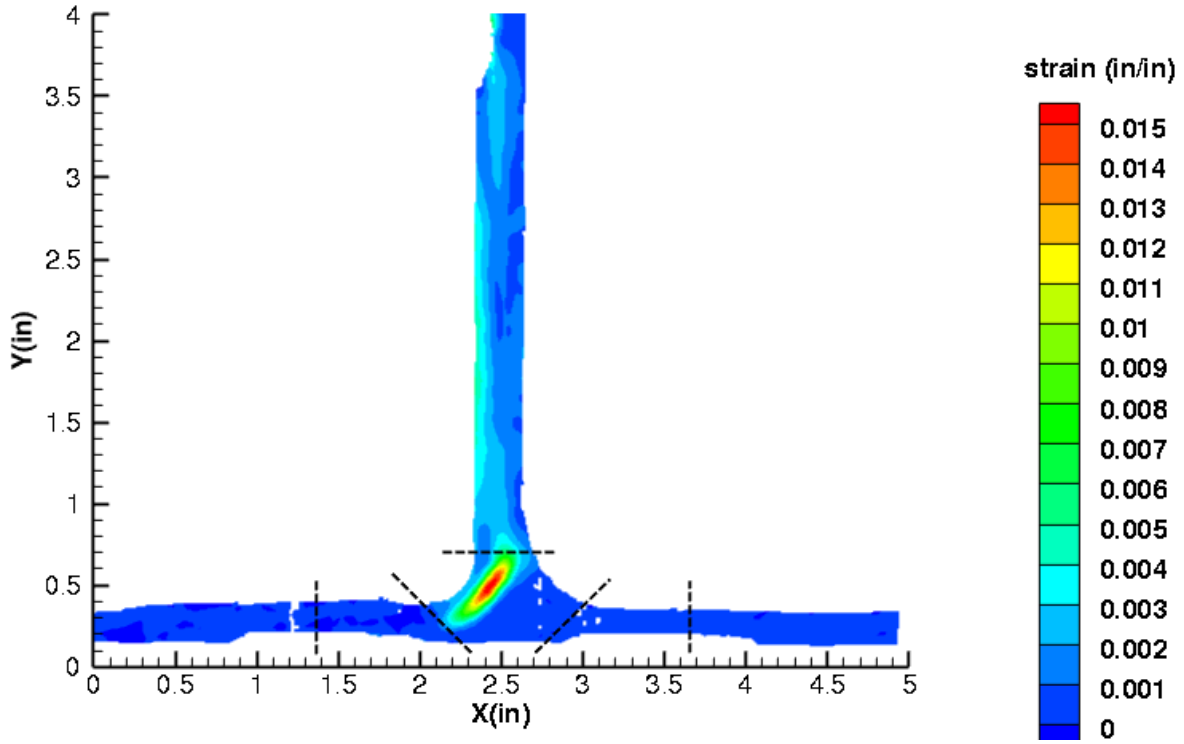

Figure C290. BNS1 strain contours for maximum principal strain at 1292 lb. load, just after initial failure, back 12MP VIC data.

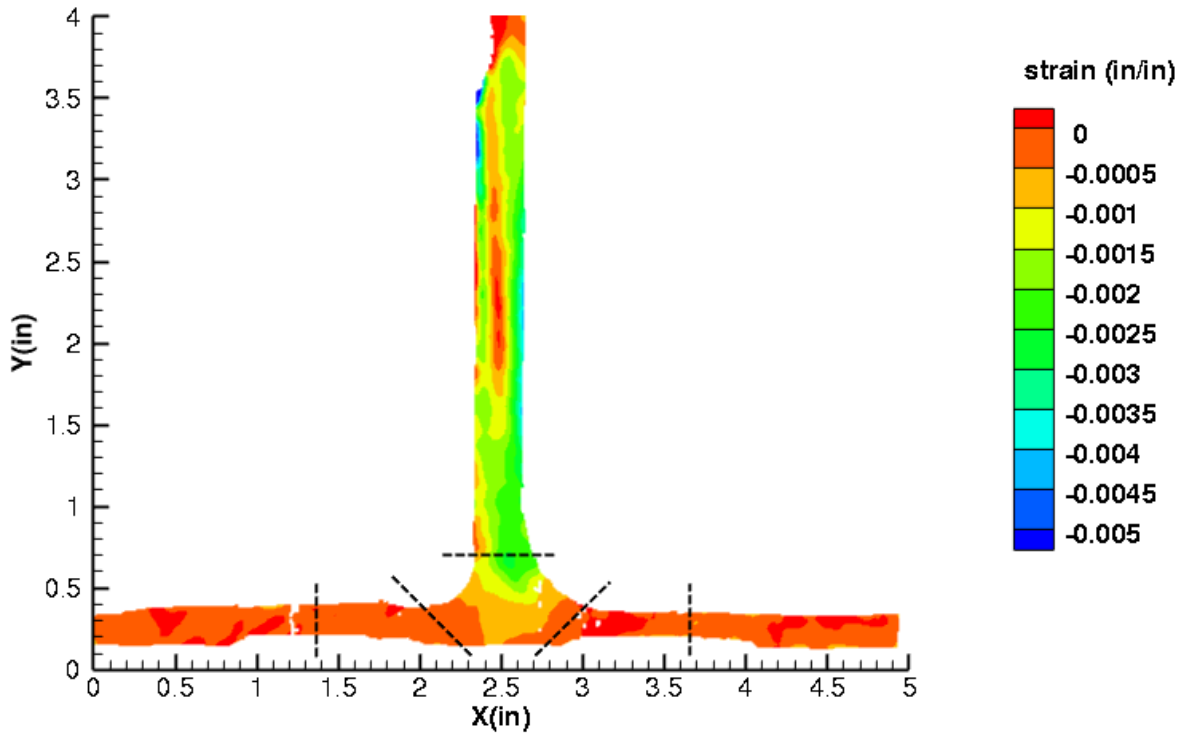

Figure C291. BNS1 strain contours for minimum principal strain at 1296 lb. load, prior to initial failure, back 12MP VIC data.

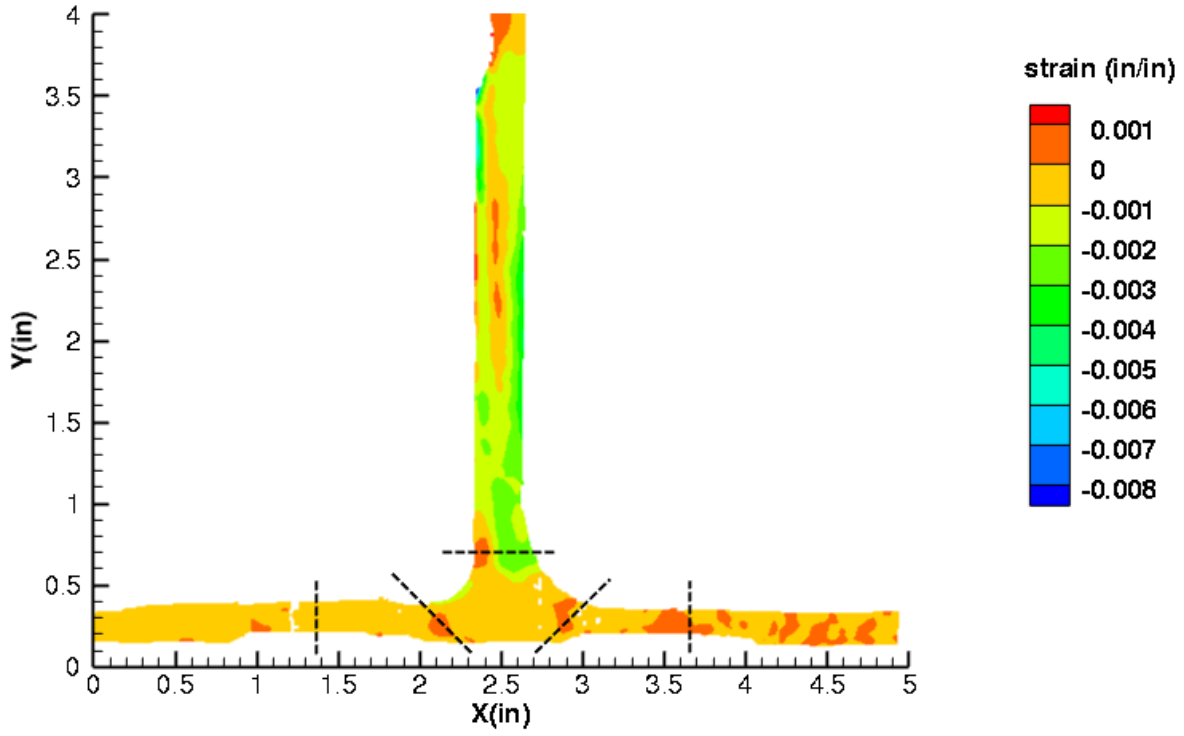

Figure C292. BNS1 strain contours for minimum principal strain at 1292 lb. load, just after initial failure, back 12MP VIC data.

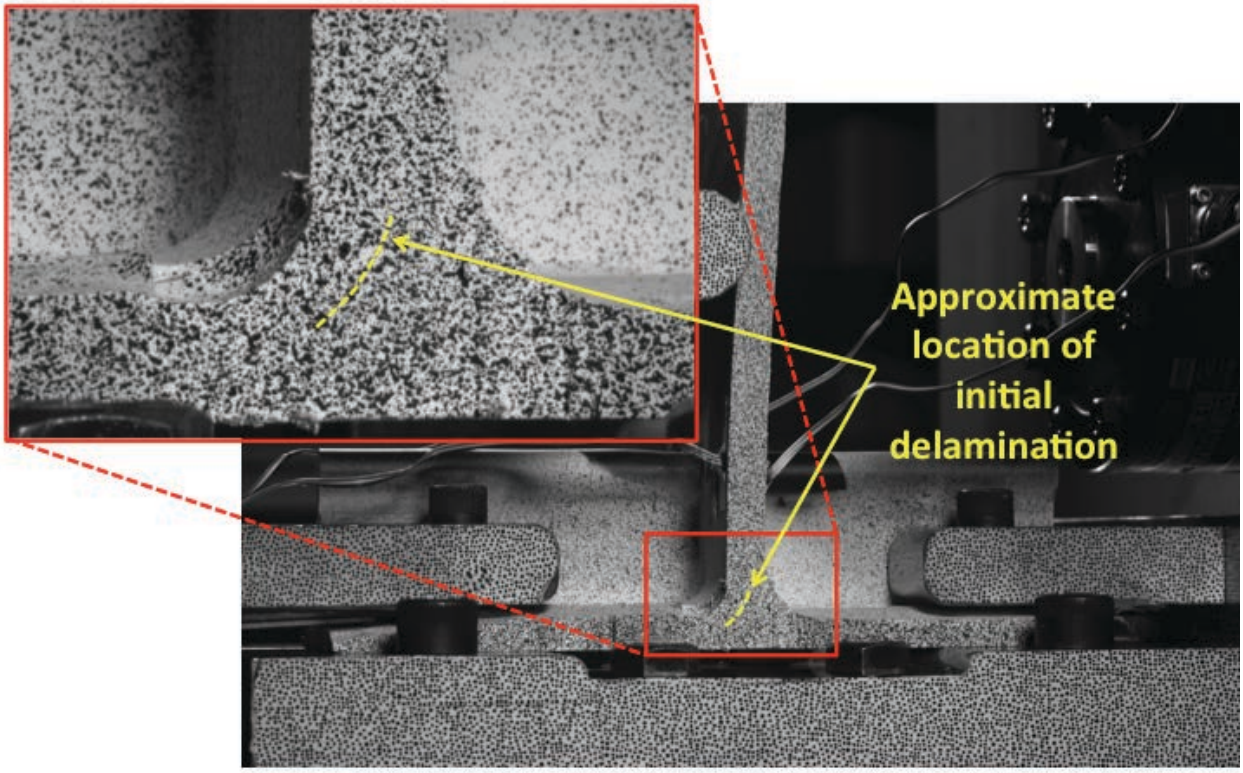

Figure C293. BNS1 image just after initial failure, back 12MP VIC data.

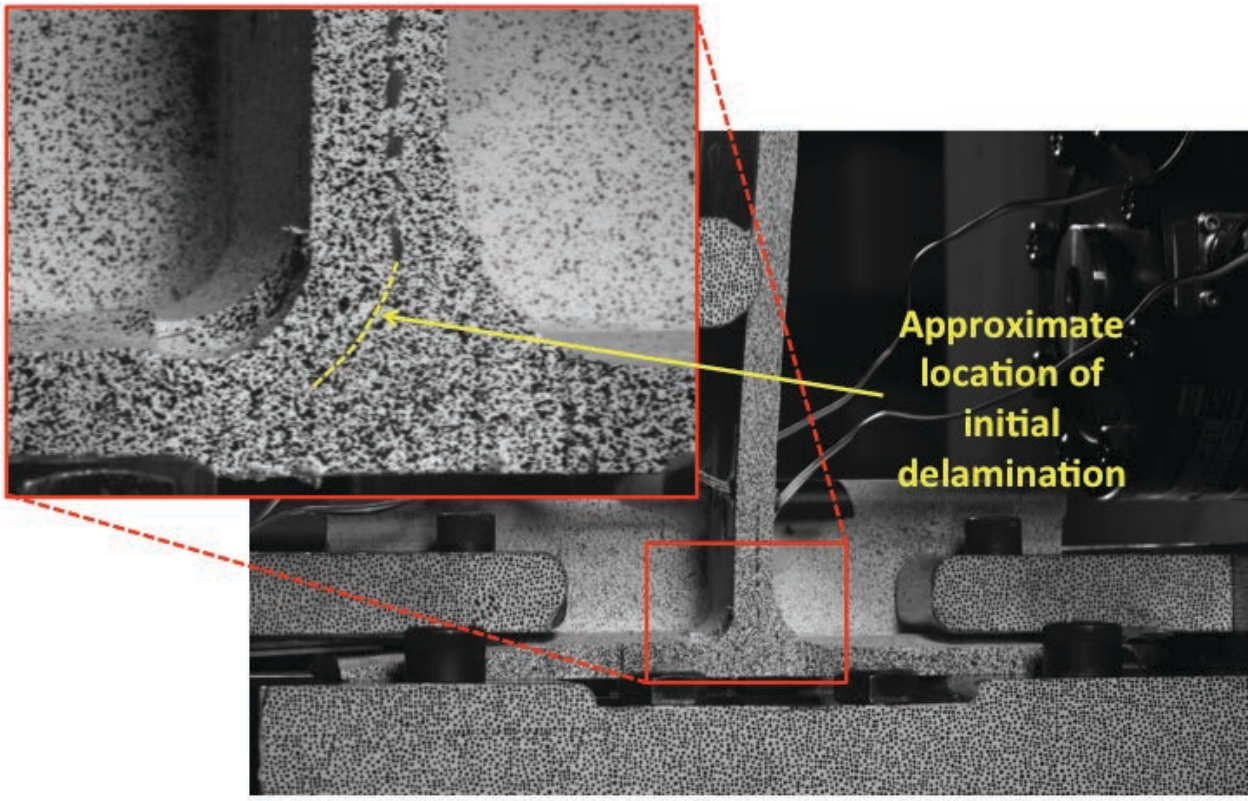

Figure C294. BNS1 image just after maximum load, back 12MP VIC data.

BNS2

This section presents the test data for the BNS2 test article.

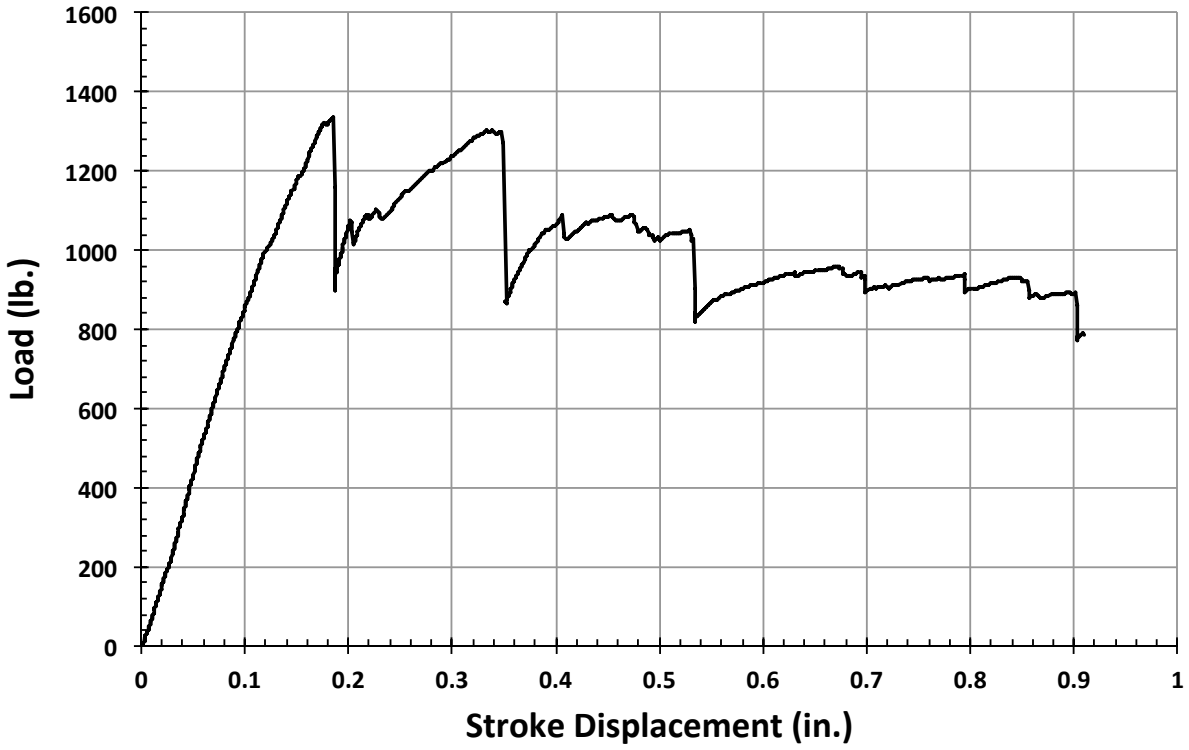

Figure C295. BNS2 load vs. stroke.

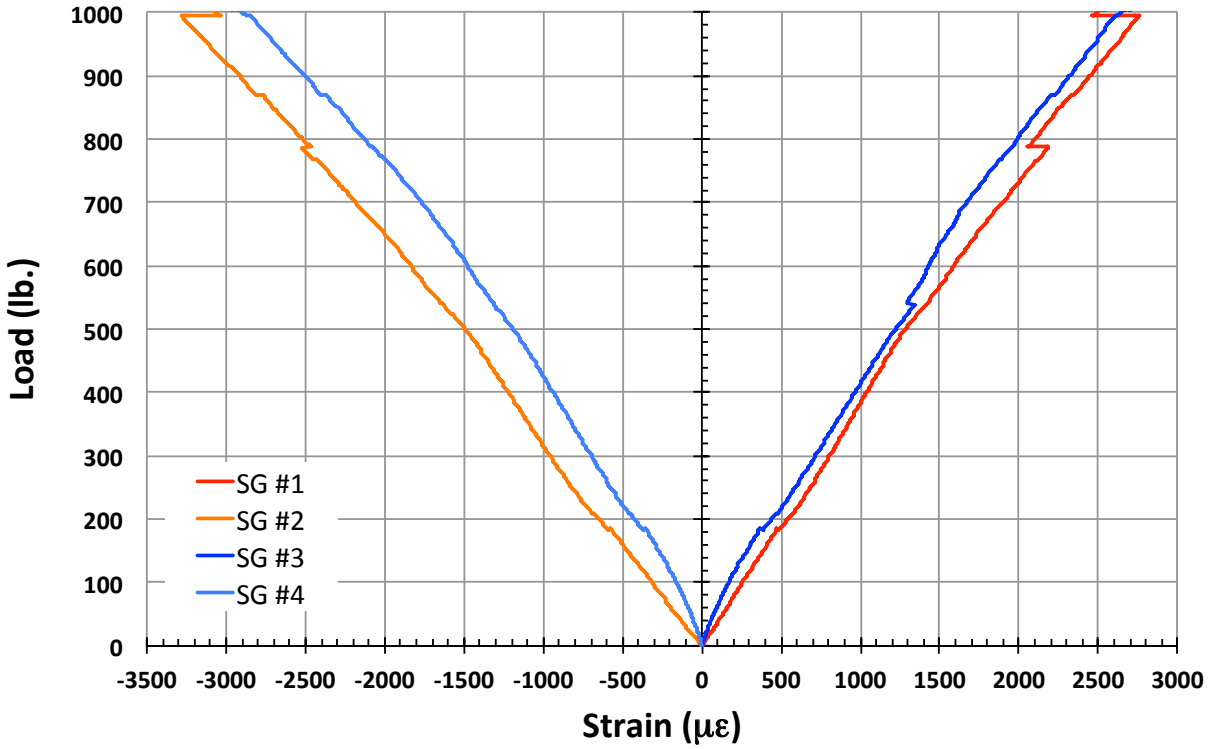

Figure C296. BNS2 load vs. strain, initial loading.

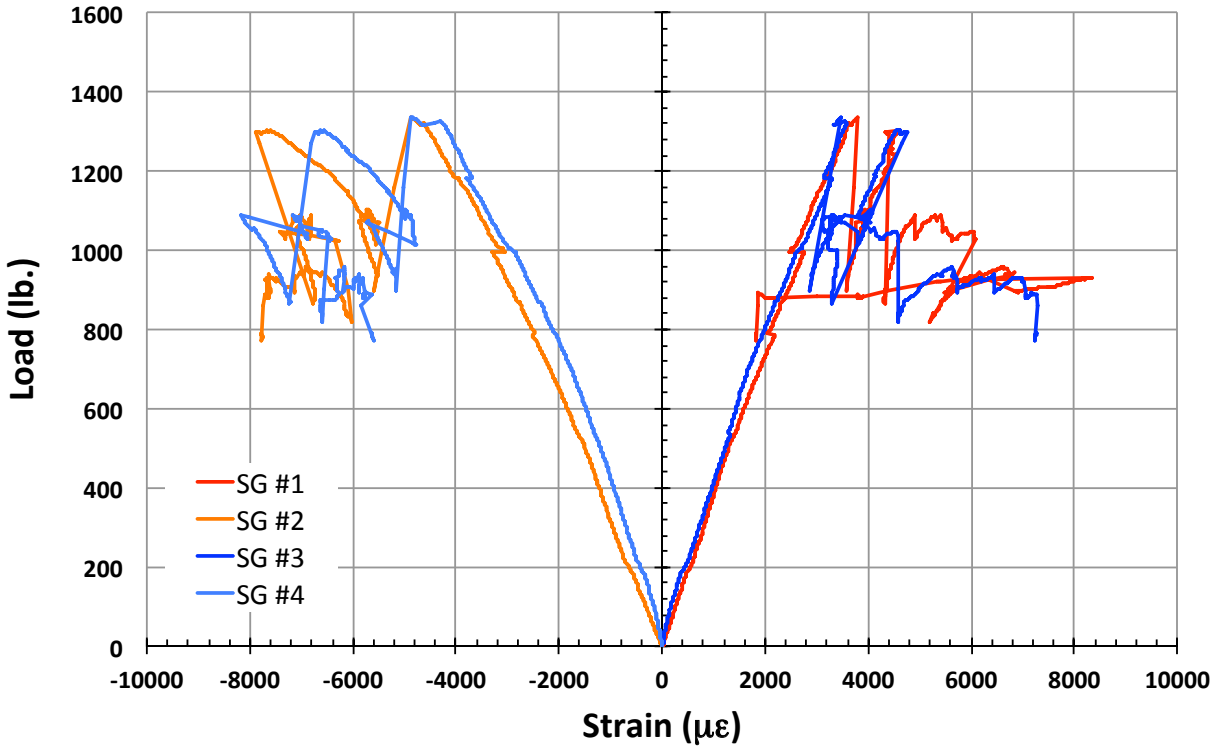

Figure C297. BNS2 load vs. strain.

BNS3

This section presents the test data for the BNS3 test article.

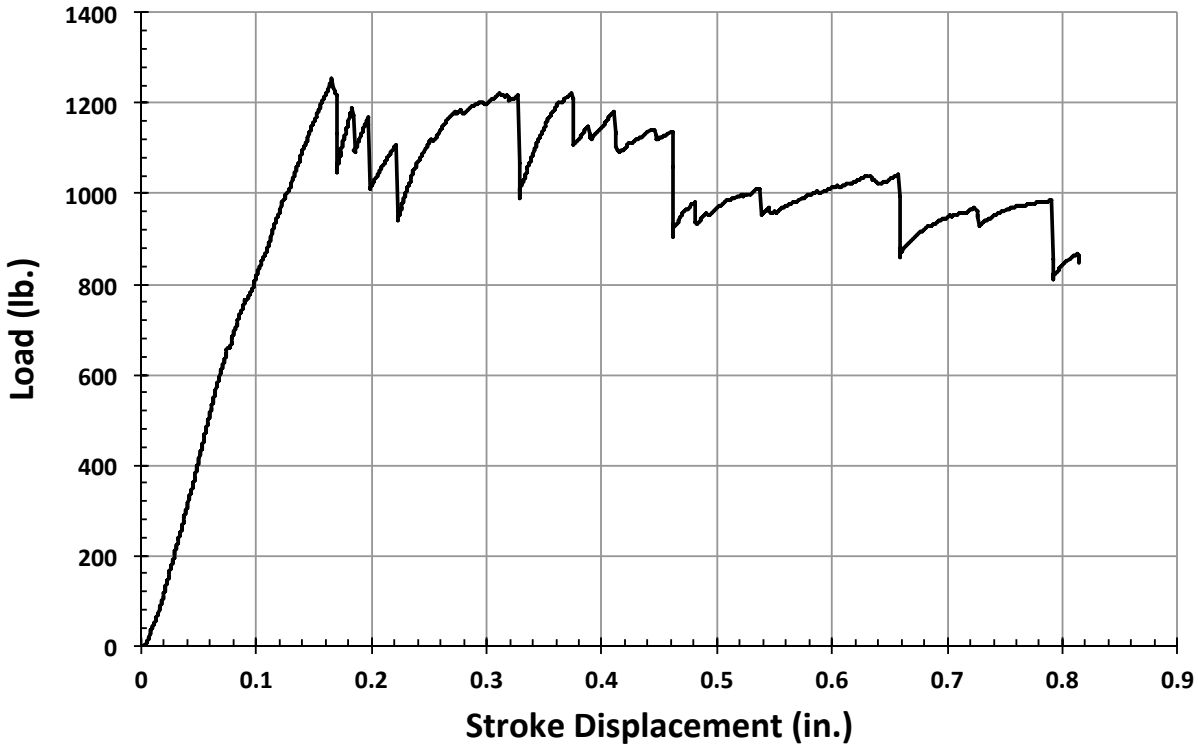

Figure C298. BNS3 load vs. stroke.

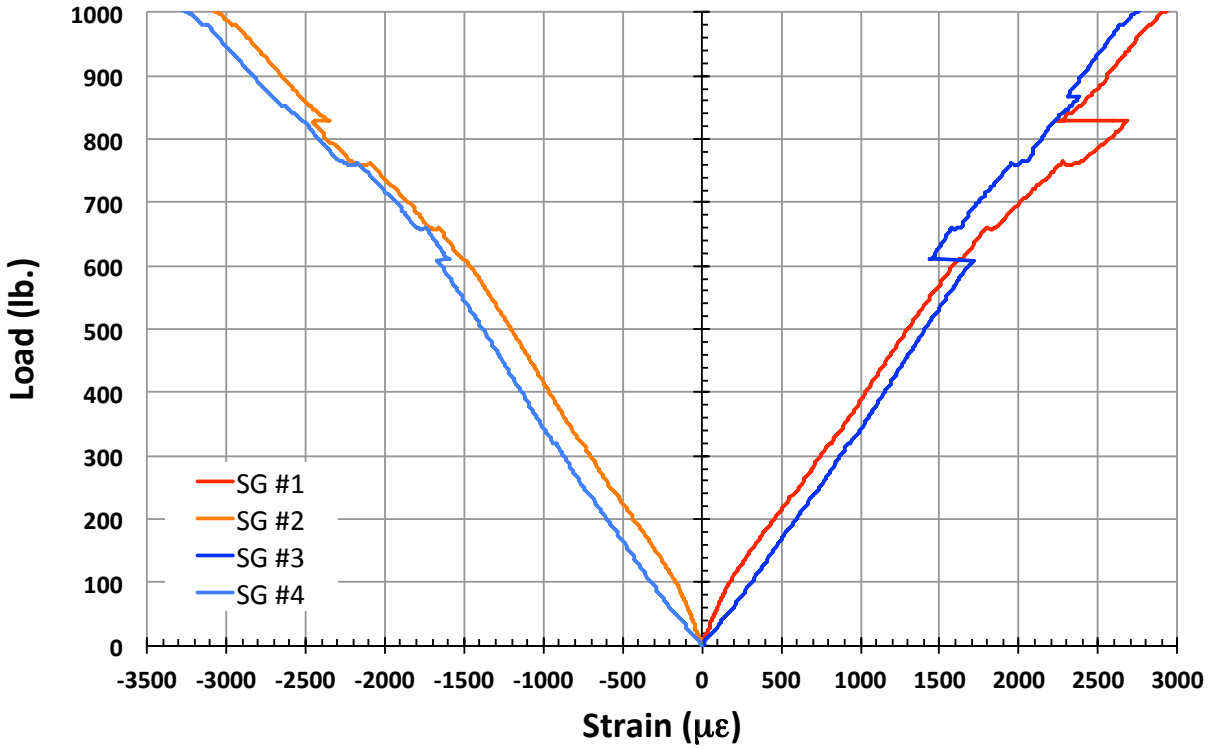

Figure C299. BNS3 load vs. strain, initial loading.

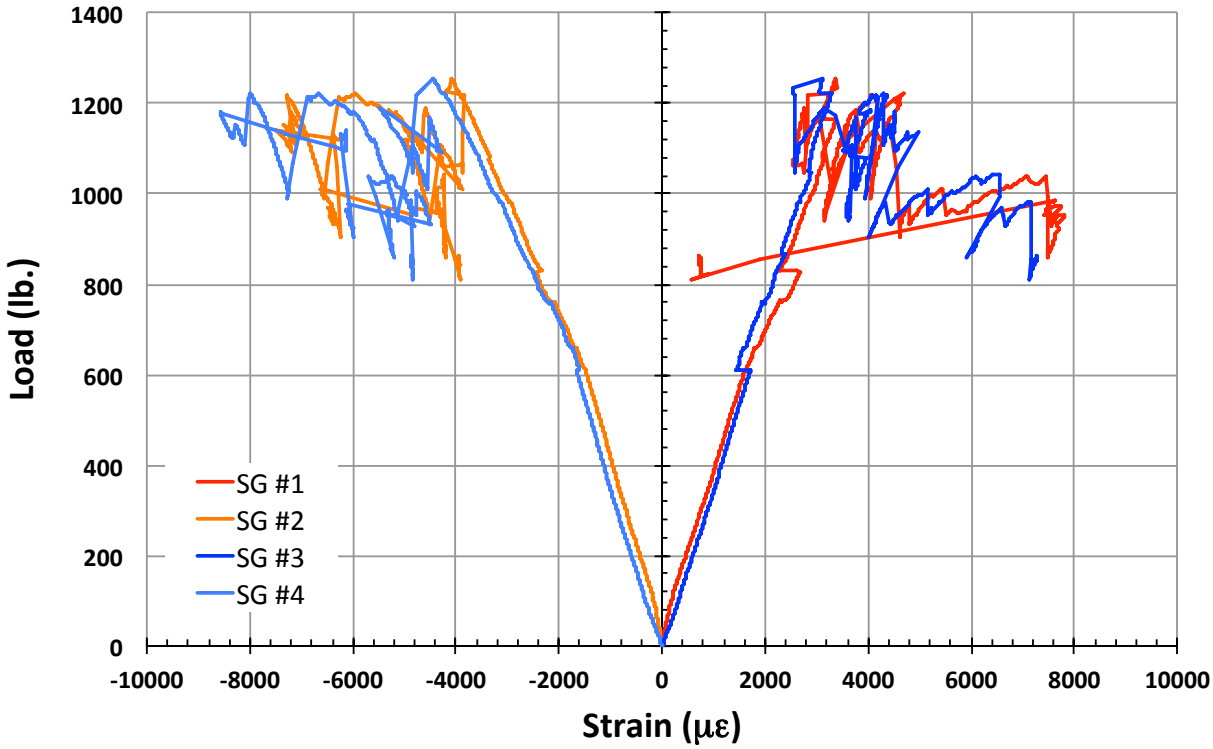

Figure C300. BNS3 load vs. strain.

BNN1

This section presents the test data for the BNN1 test article.

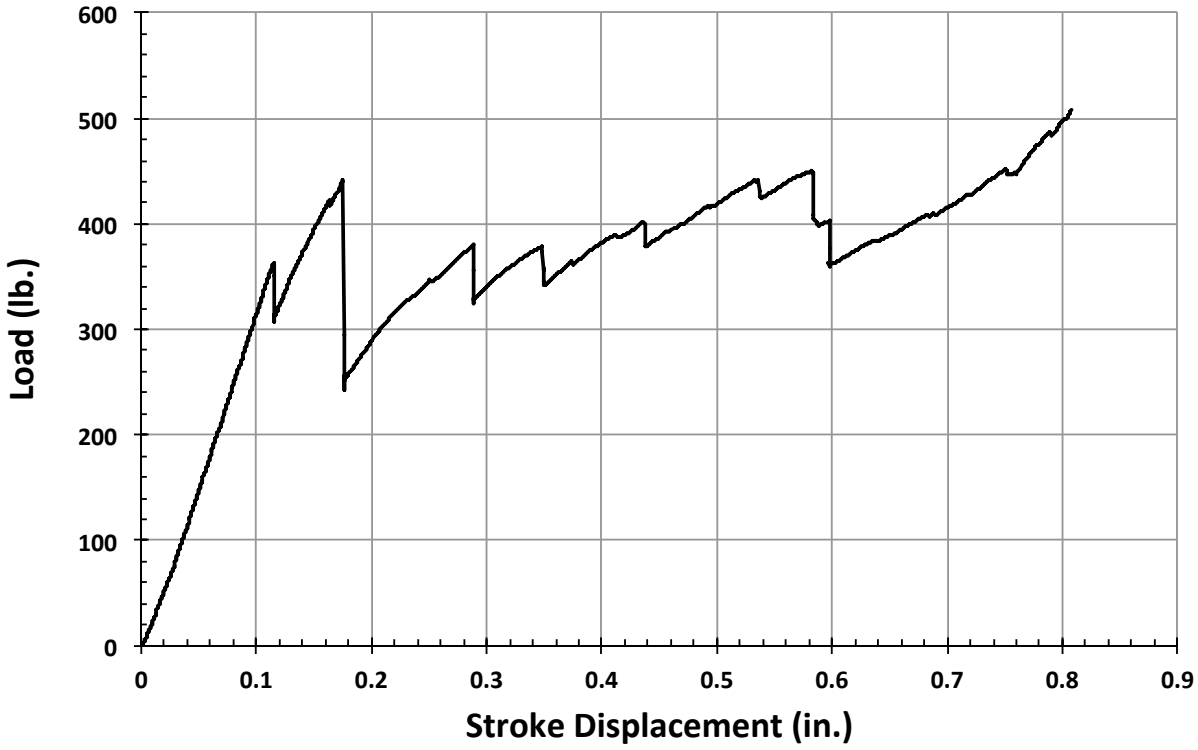

Figure C301. BNN1 load vs. stroke.

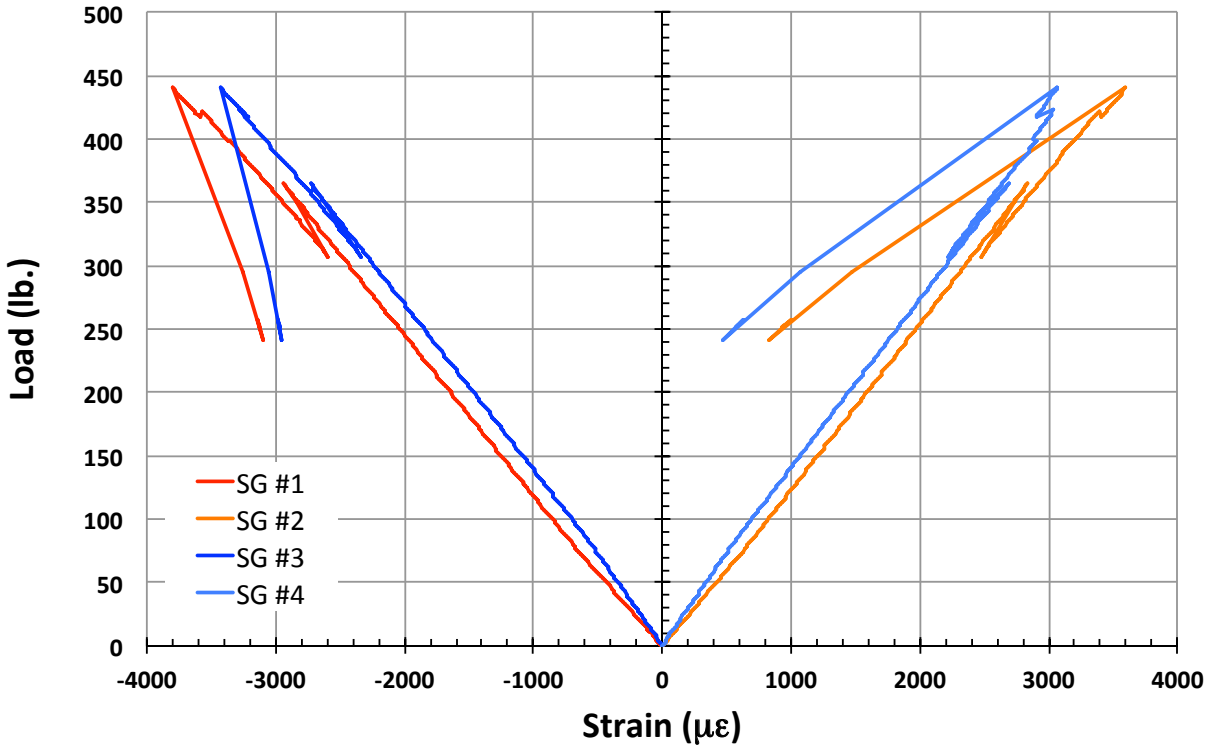

Figure C302. BNN1 load vs. strain, initial loading.

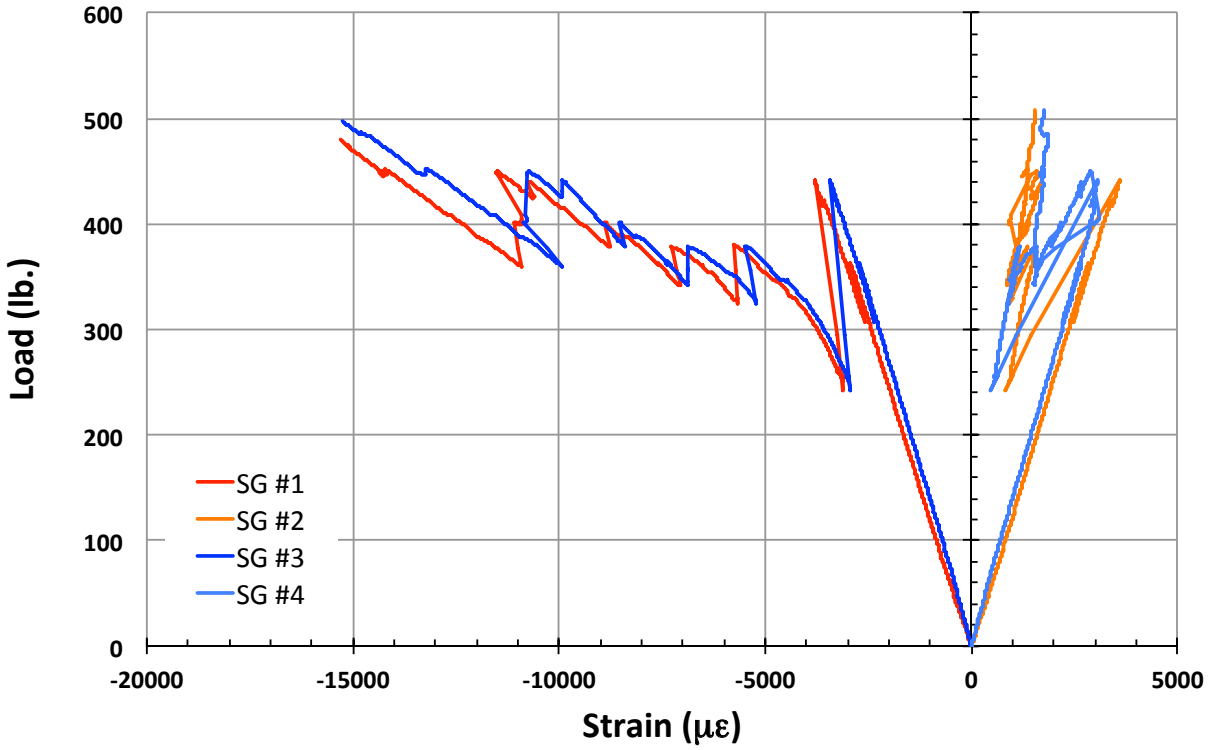

Figure C303. BNN1 load vs. strain.

BNN2

This section presents the test data for the BNS2 test article, and includes strain plots and failure images.

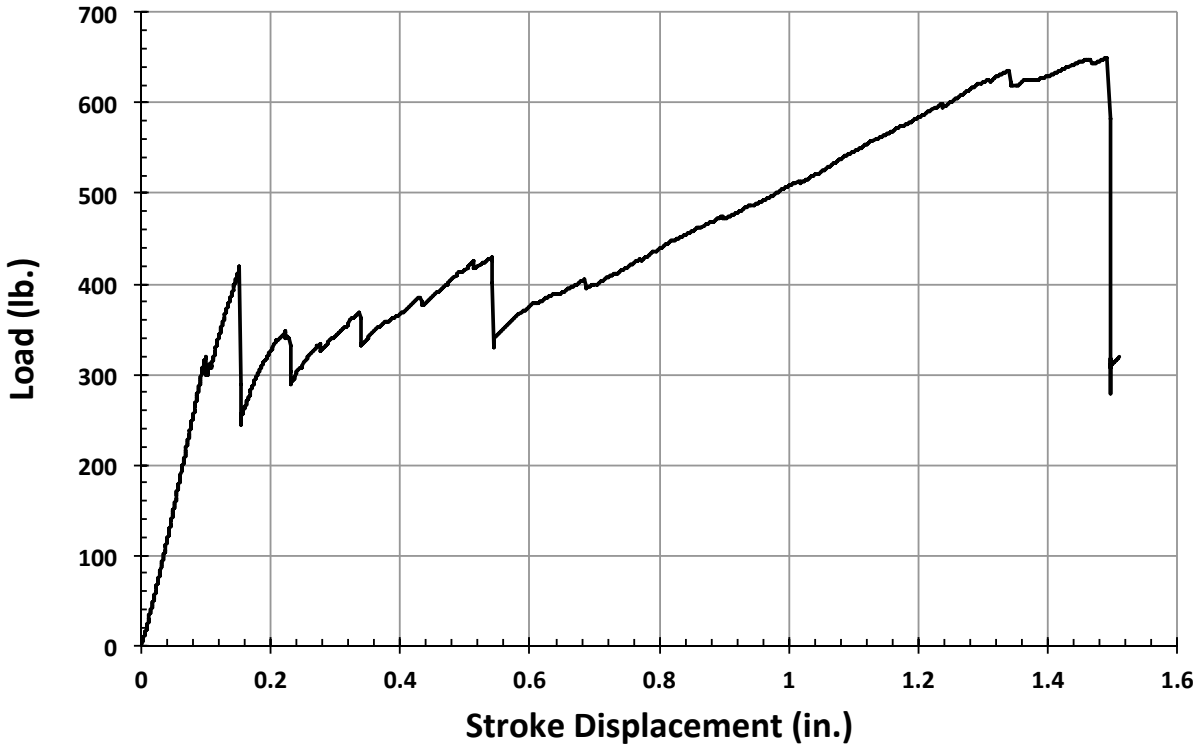

Figure C304. BNN2 load vs. stroke.

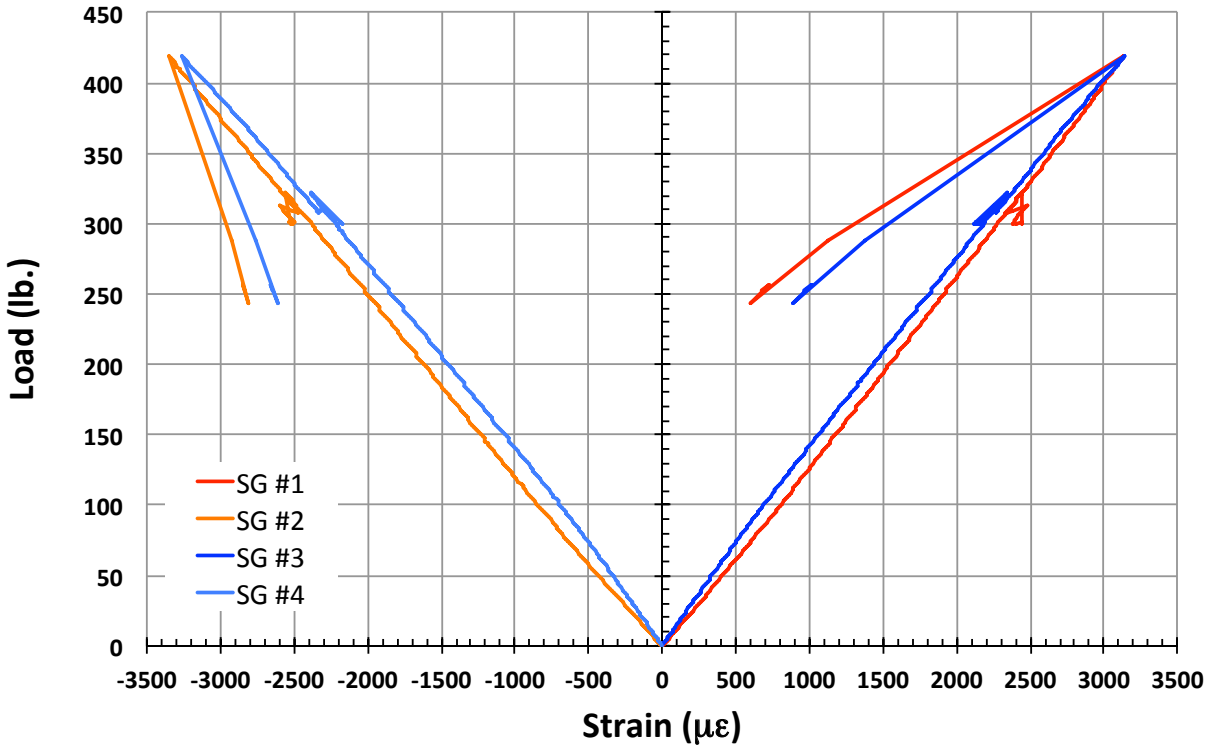

Figure C305. BNN2 load vs. strain, initial loading.

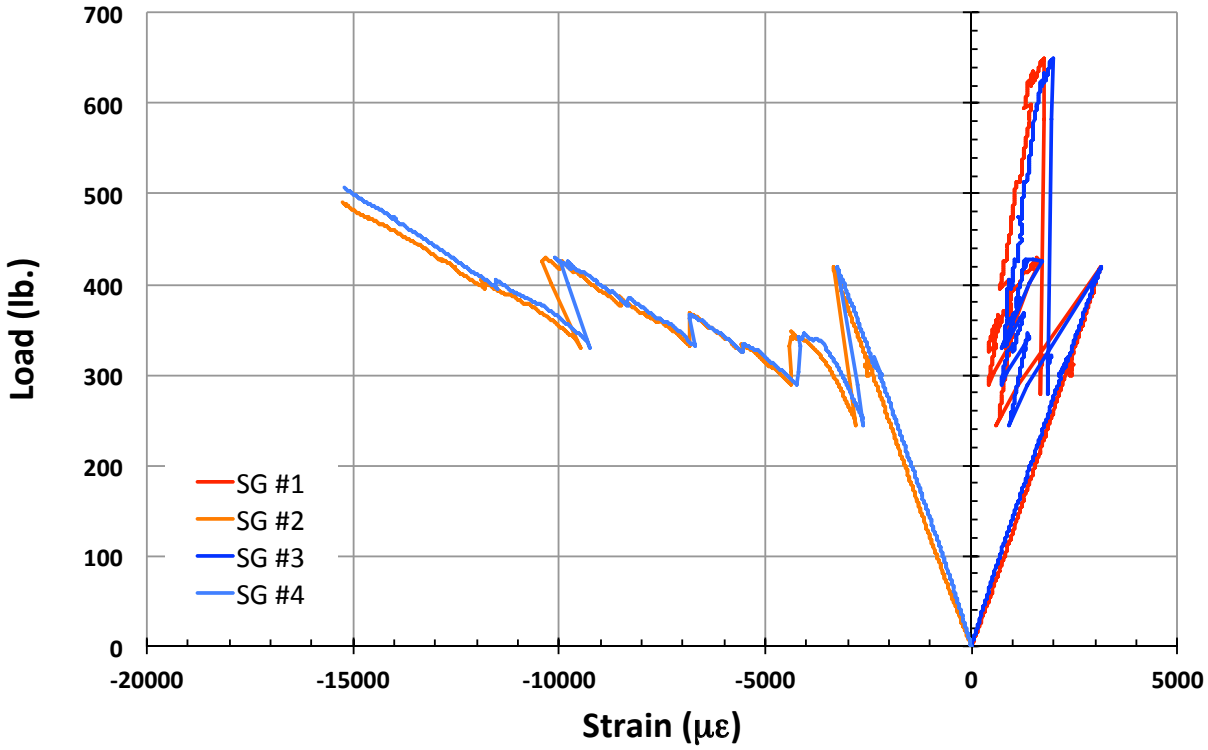

Figure C306. BNN2 load vs. strain.

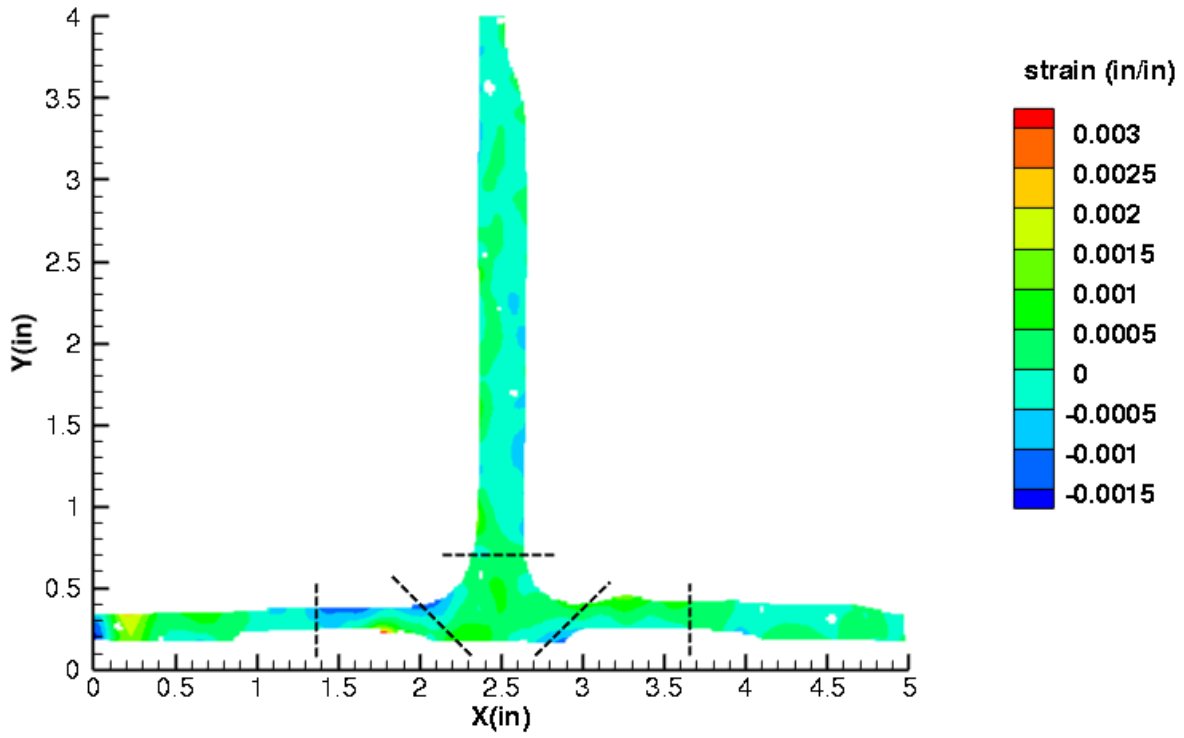

Figure C307. BNN2 strain contours for ε_{xx} at 323 lb. load, prior to initial failure, front 12MP VIC data.

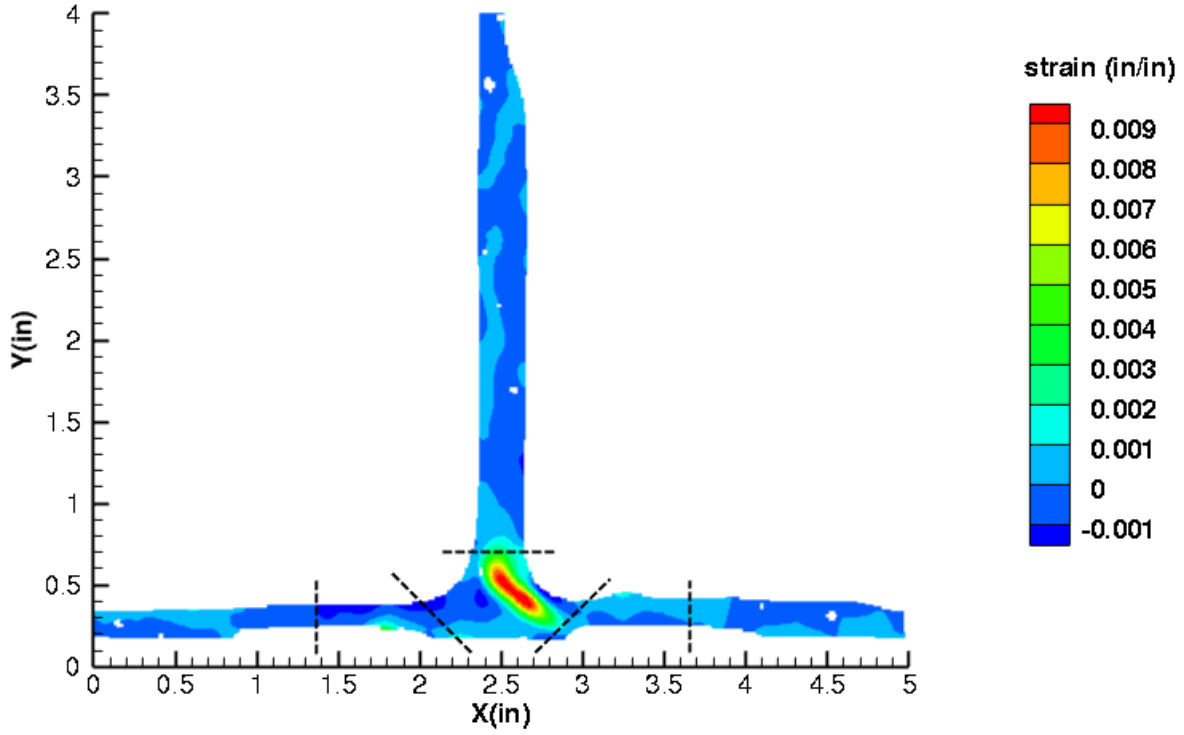

Figure C308. BNN2 strain contours for ε_{xx} at 297 lb. load, just after initial failure, front 12MP VIC data.

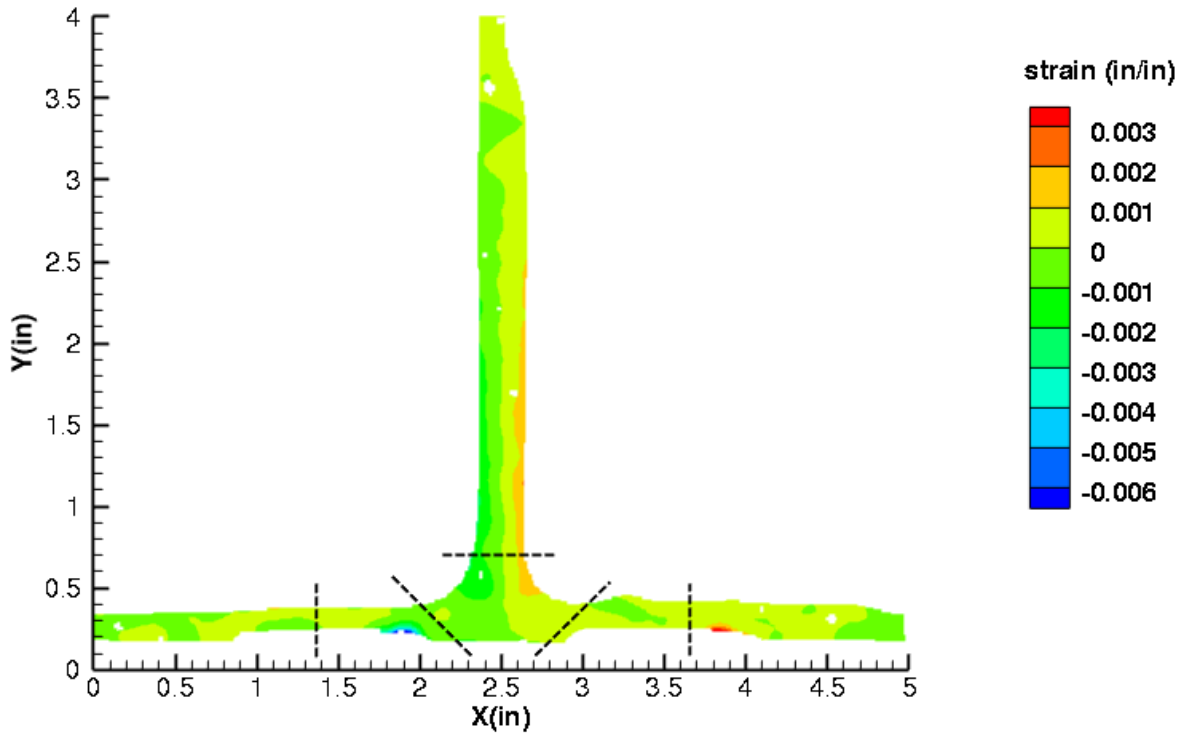

Figure C309. BNN2 strain contours for ε_{yy} at 323 lb. load, prior to initial failure, front 12MP VIC data.

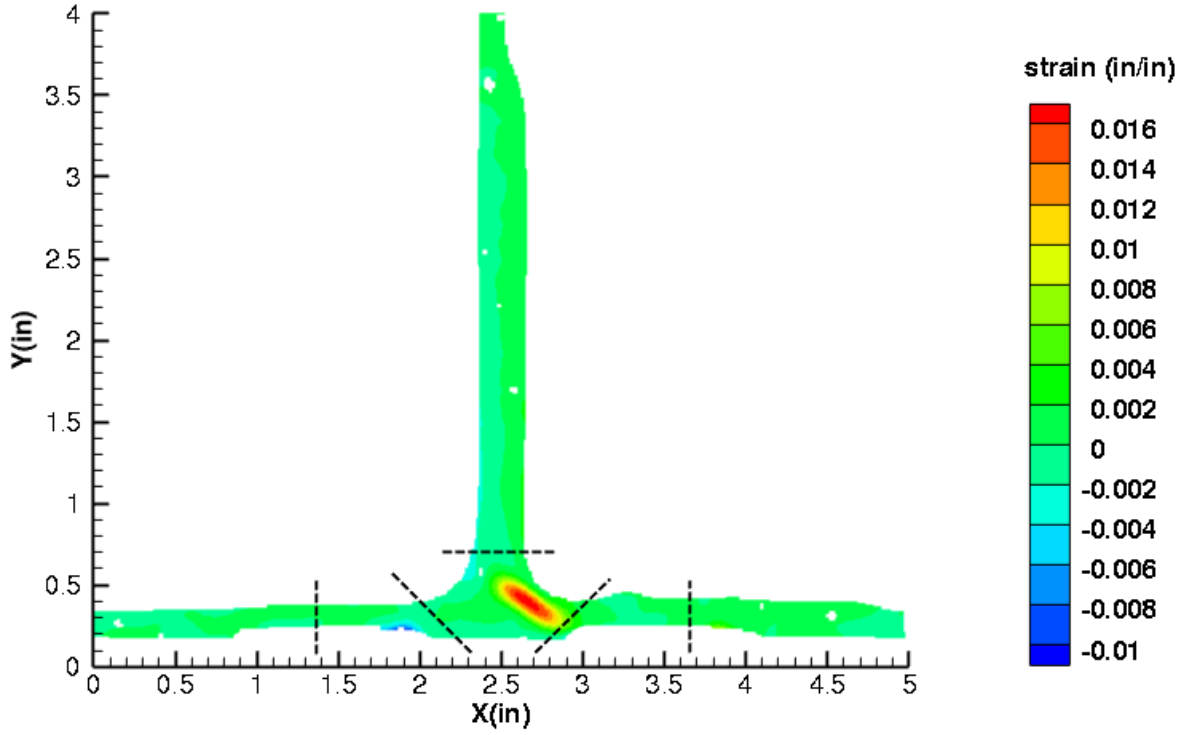

Figure C310. BNN2 strain contours for ε_{yy} at 297 lb. load, just after initial failure, front 12MP VIC data.

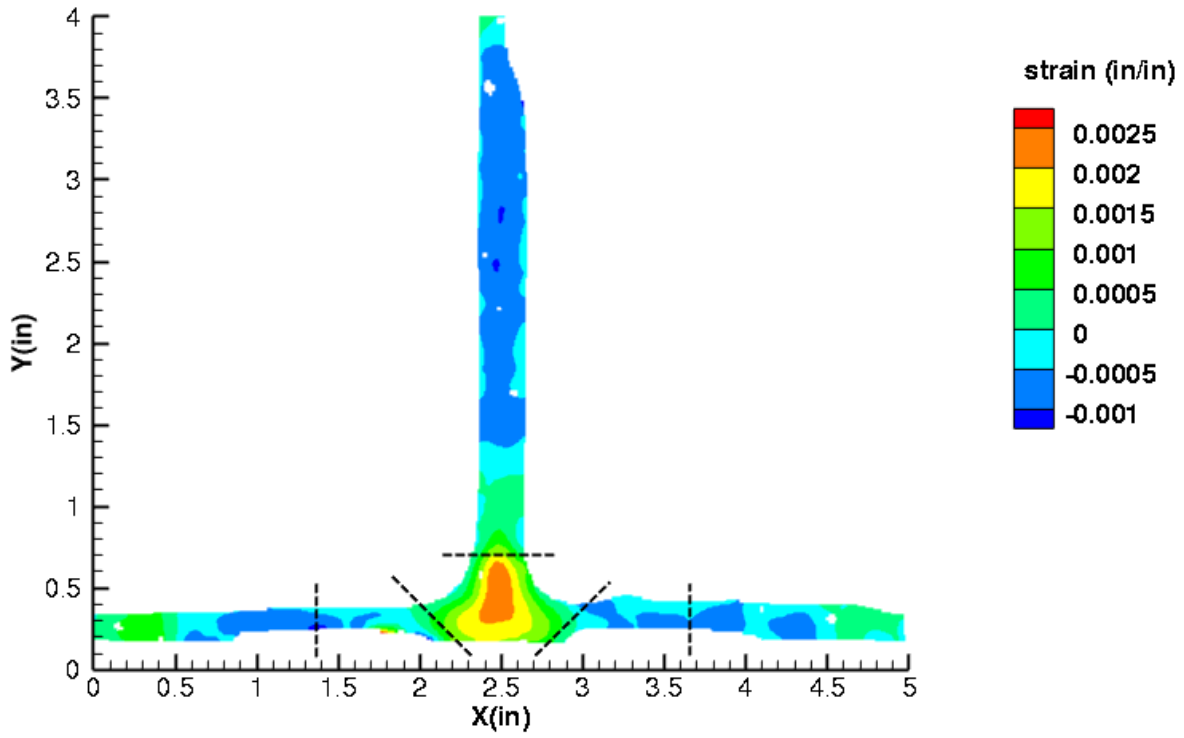

Figure C311. BNN2 strain contours for ε_{xy} at 323 lb. load, prior to initial failure, front 12MP VIC data.

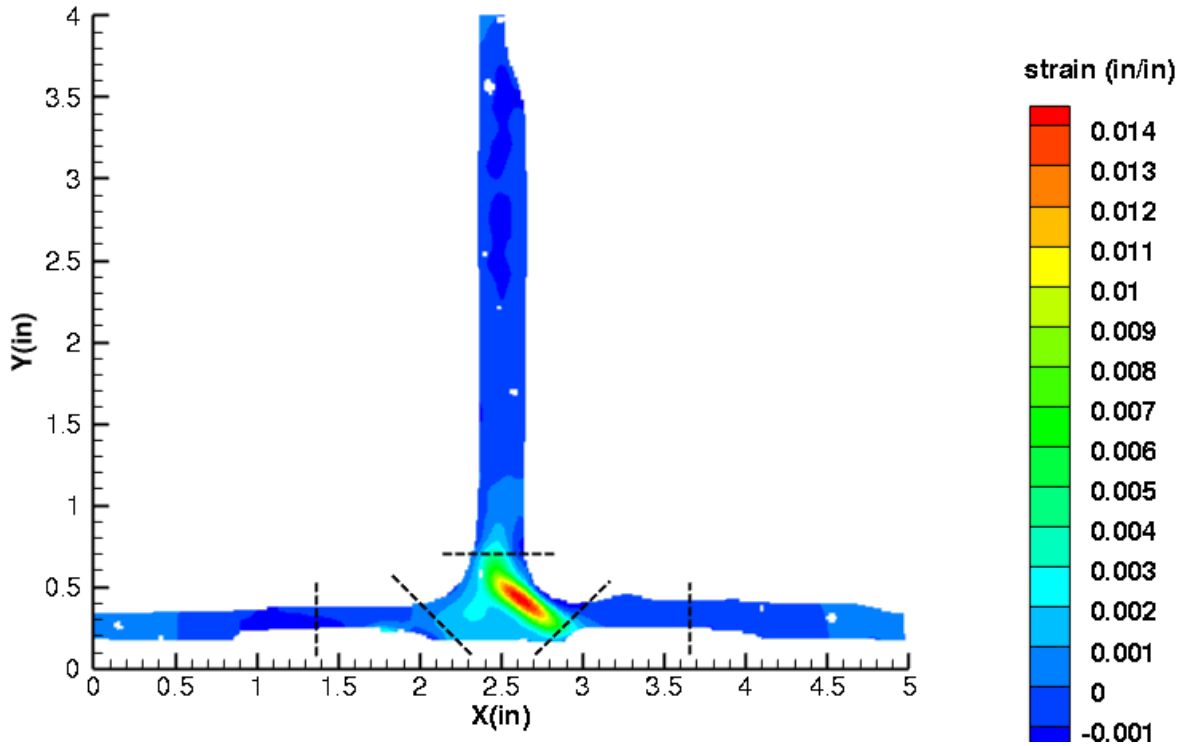

Figure C312. BNN2 strain contours for ε_{xy} at 297 lb. load, just after initial failure, front 12MP VIC data.

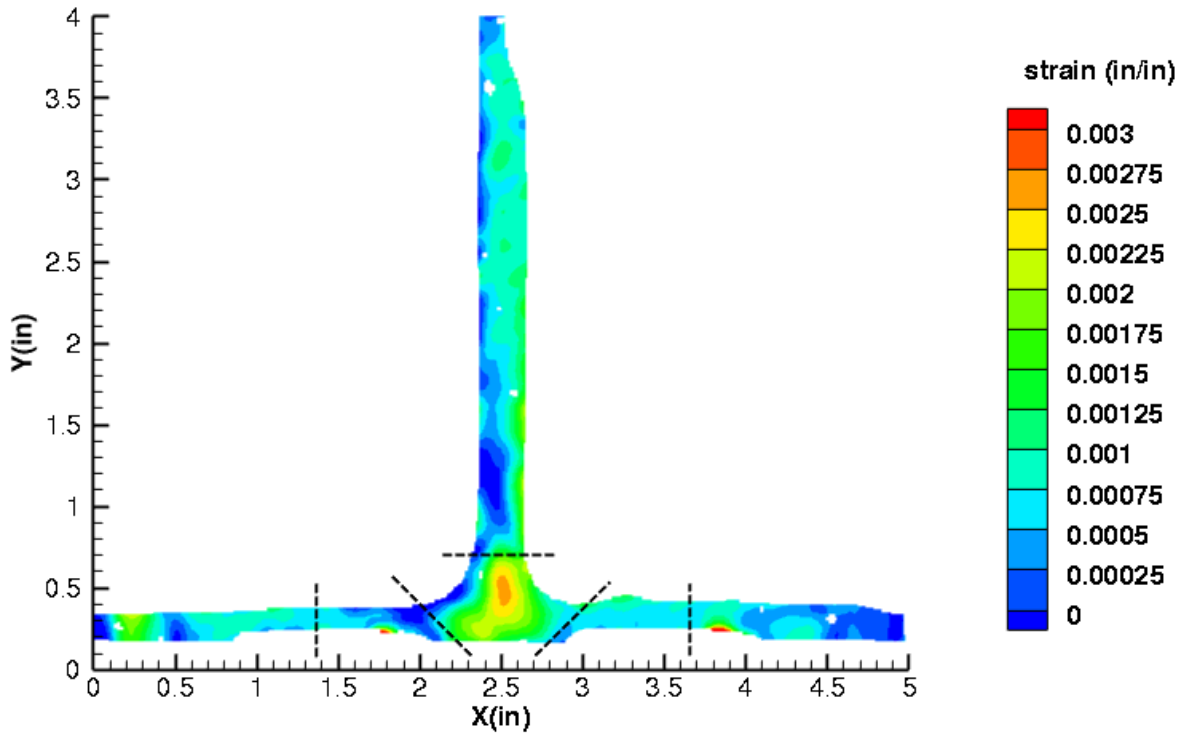

Figure C313. BNN2 strain contours for maximum principal strain at 323 lb. load, prior to initial failure, front 12MP VIC data.

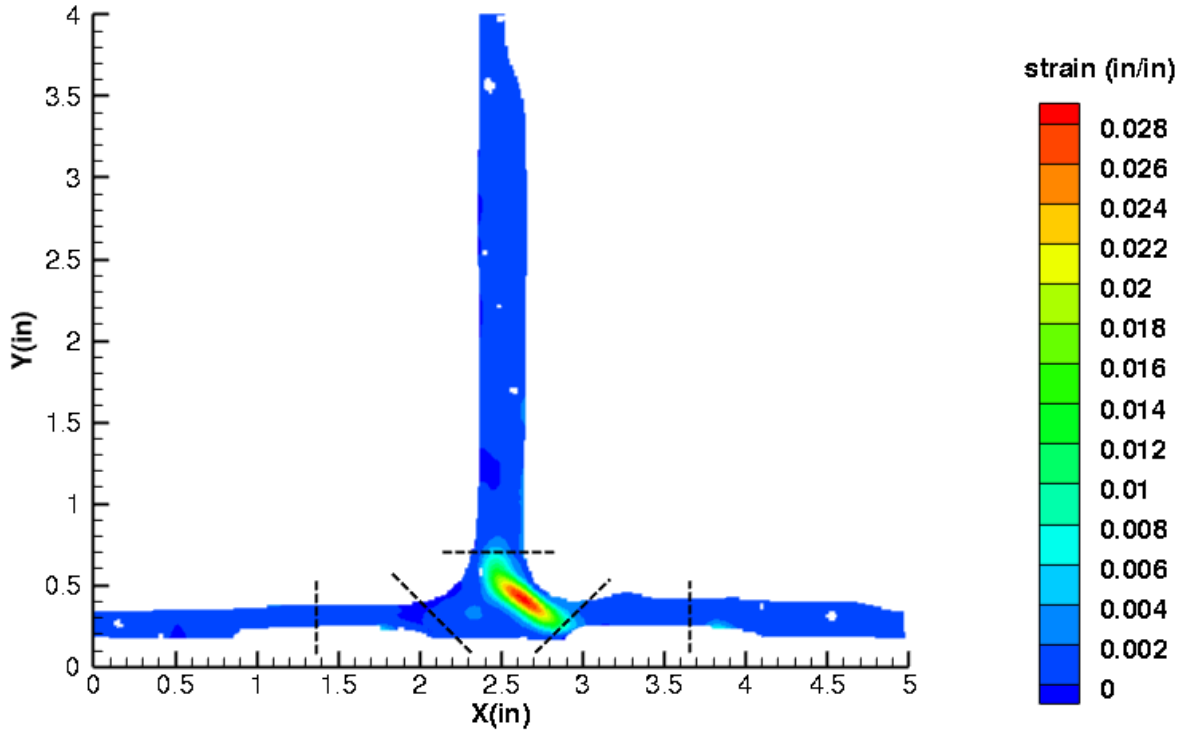

Figure C314. BNN2 strain contours for maximum principal strain at 297 lb. load, just after initial failure, front 12MP VIC data.

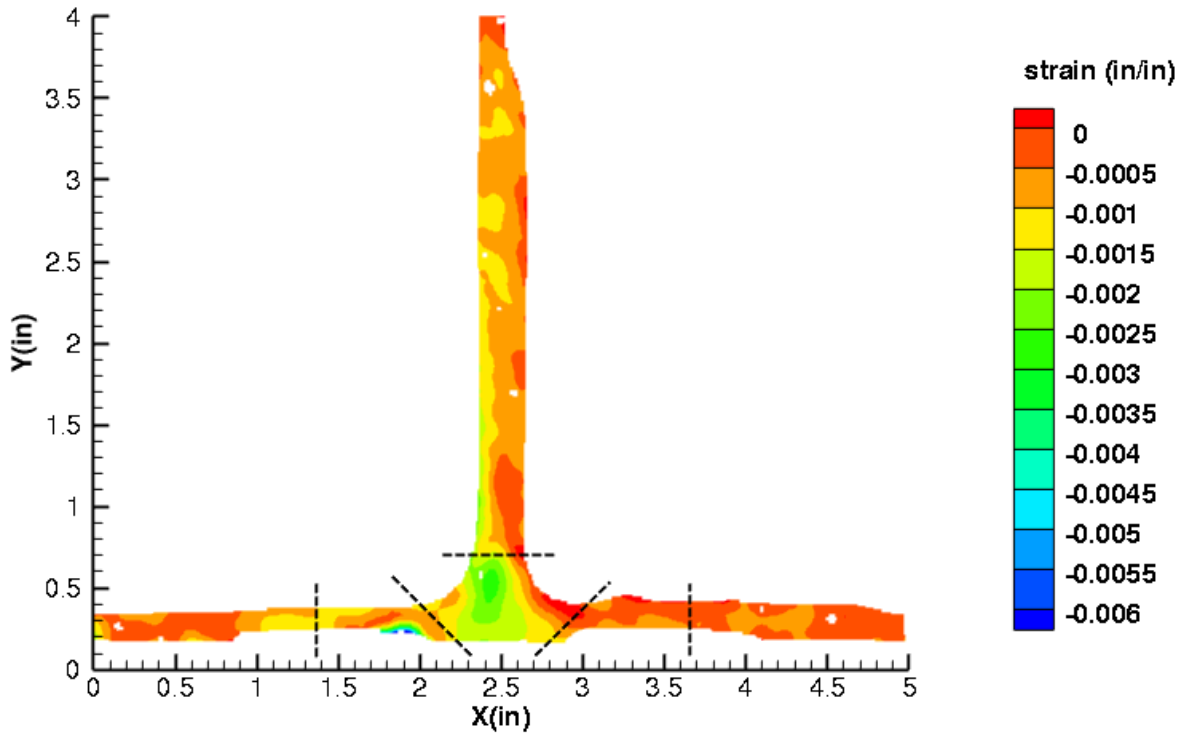

Figure C315. BNN2 strain contours for minimum principal strain at 323 lb. load, prior to initial failure, front 12MP VIC data.

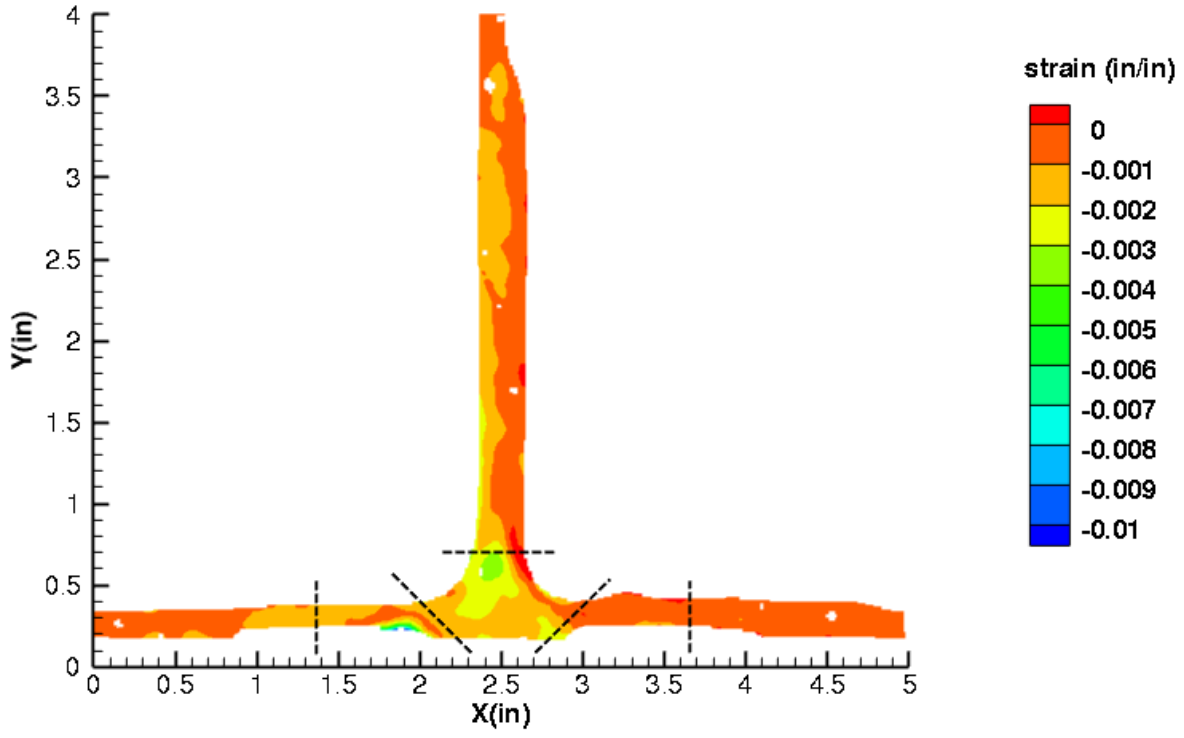

Figure C316. BNN2 strain contours for minimum principal strain at 297 lb. load, just after initial failure, front 12MP VIC data.

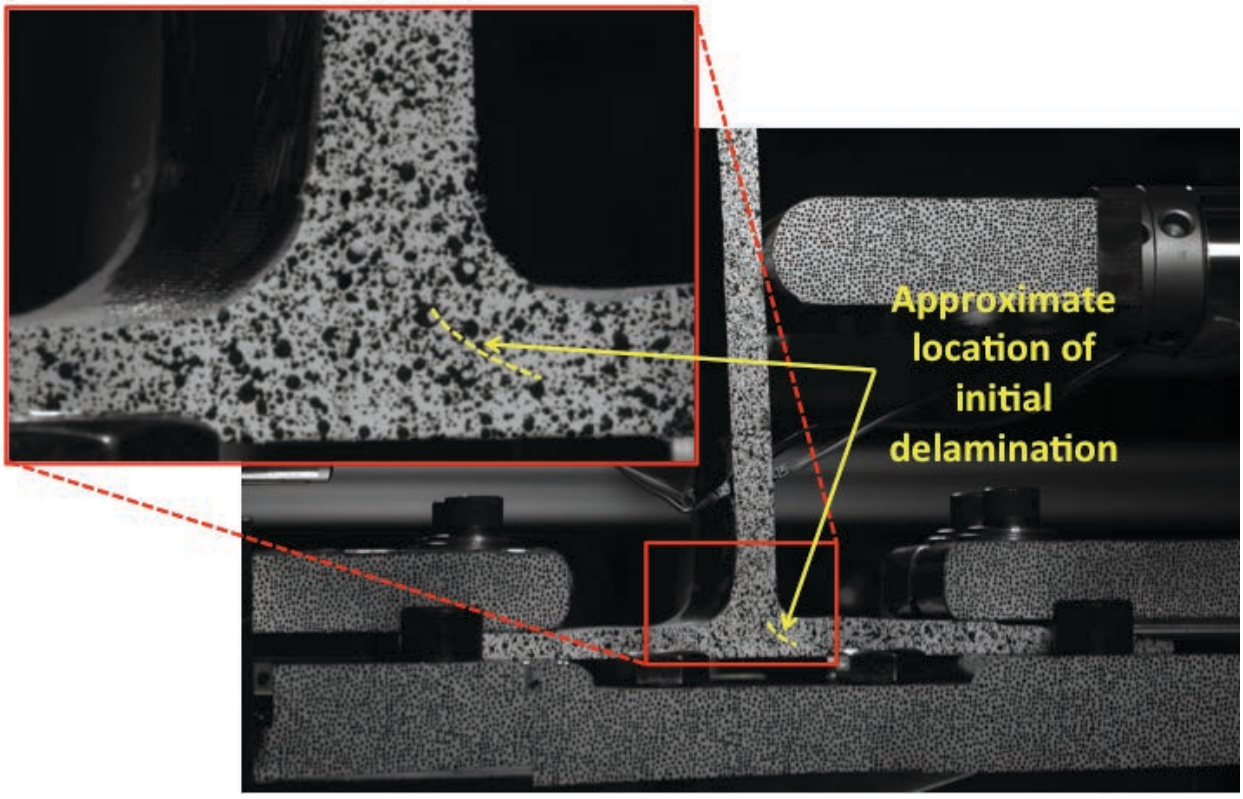

Figure C317. BNN2 image just after initial failure, front 12MP VIC data.

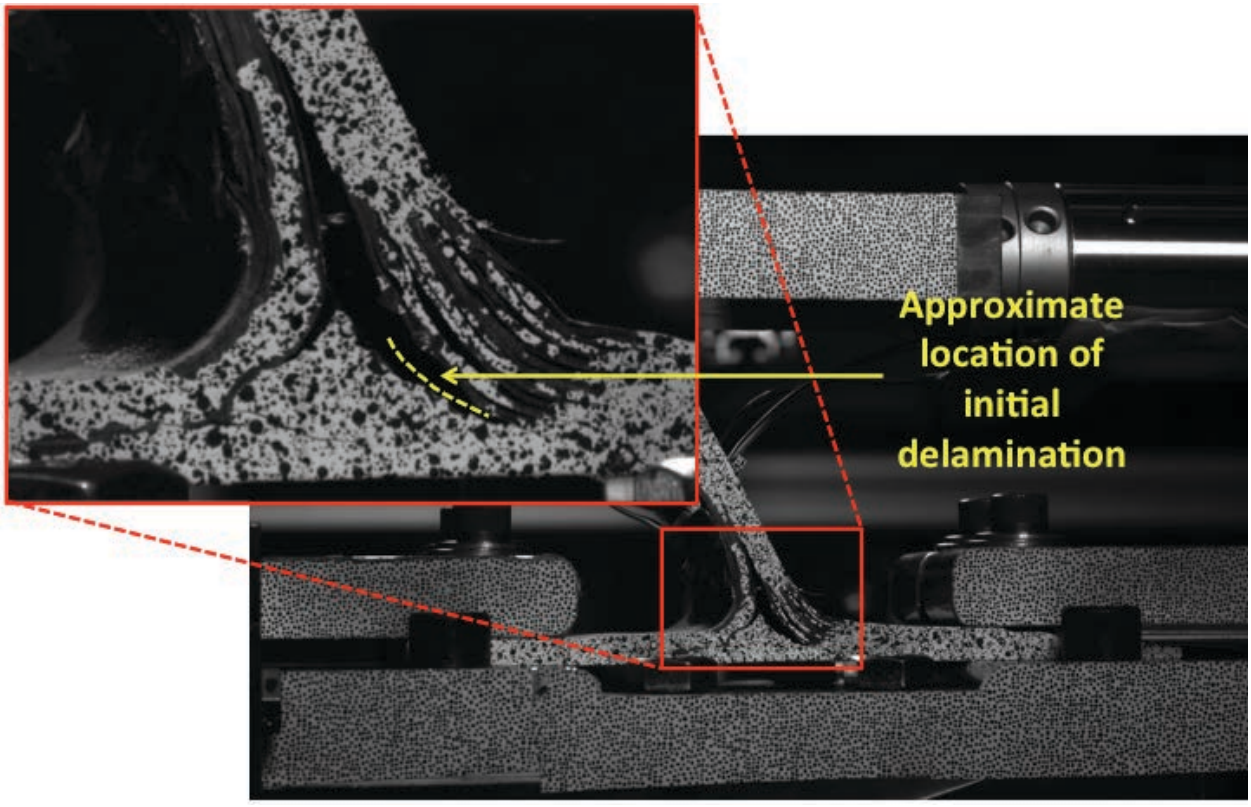

Figure C318. BNN2 image just after maximum load, front 12MP VIC data.

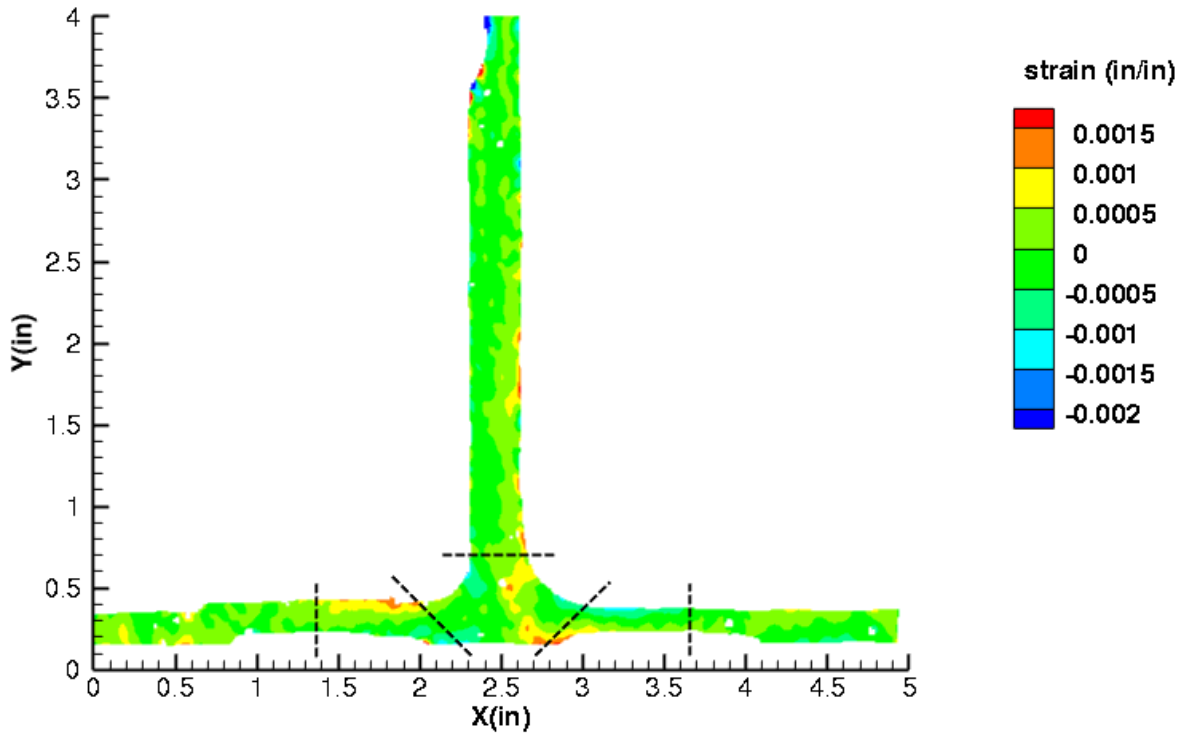

Figure C319. BNN2 strain contours for ε_{xx} at 323 lb. load, prior to initial failure, back 12MP VIC data.

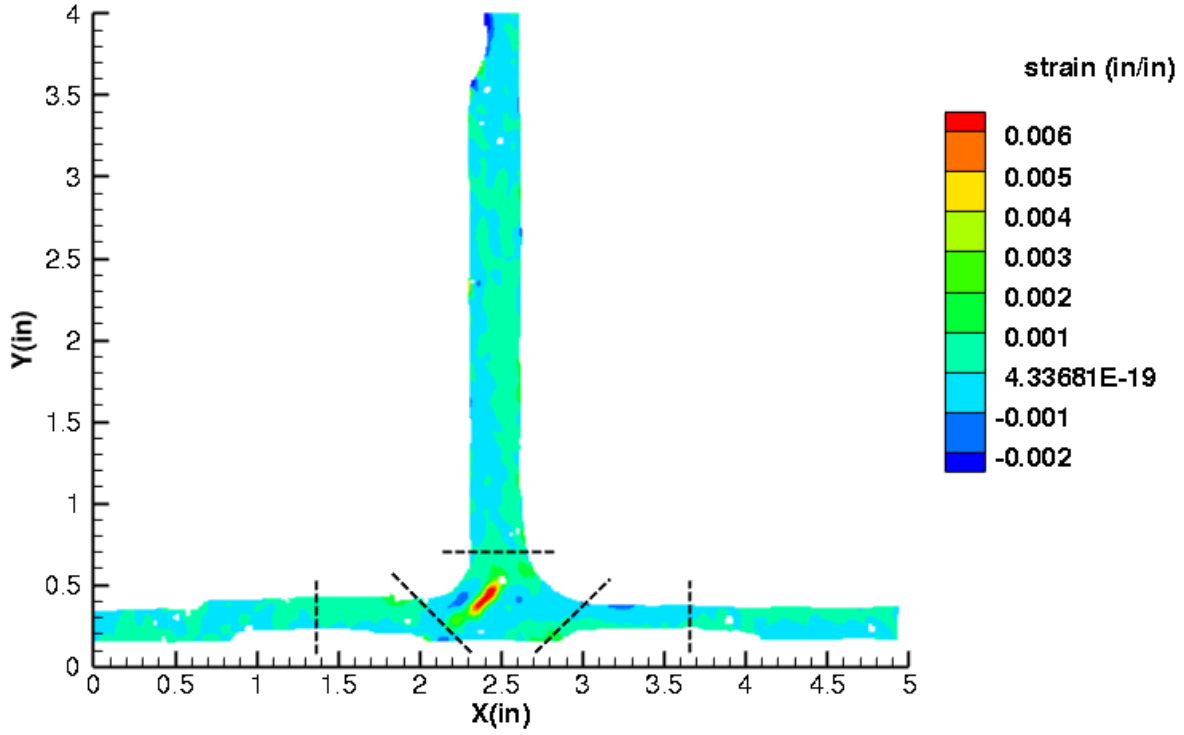

Figure C320. BNN2 strain contours for ε_{xx} at 297 lb. load, just after initial failure, back 12MP VIC data.

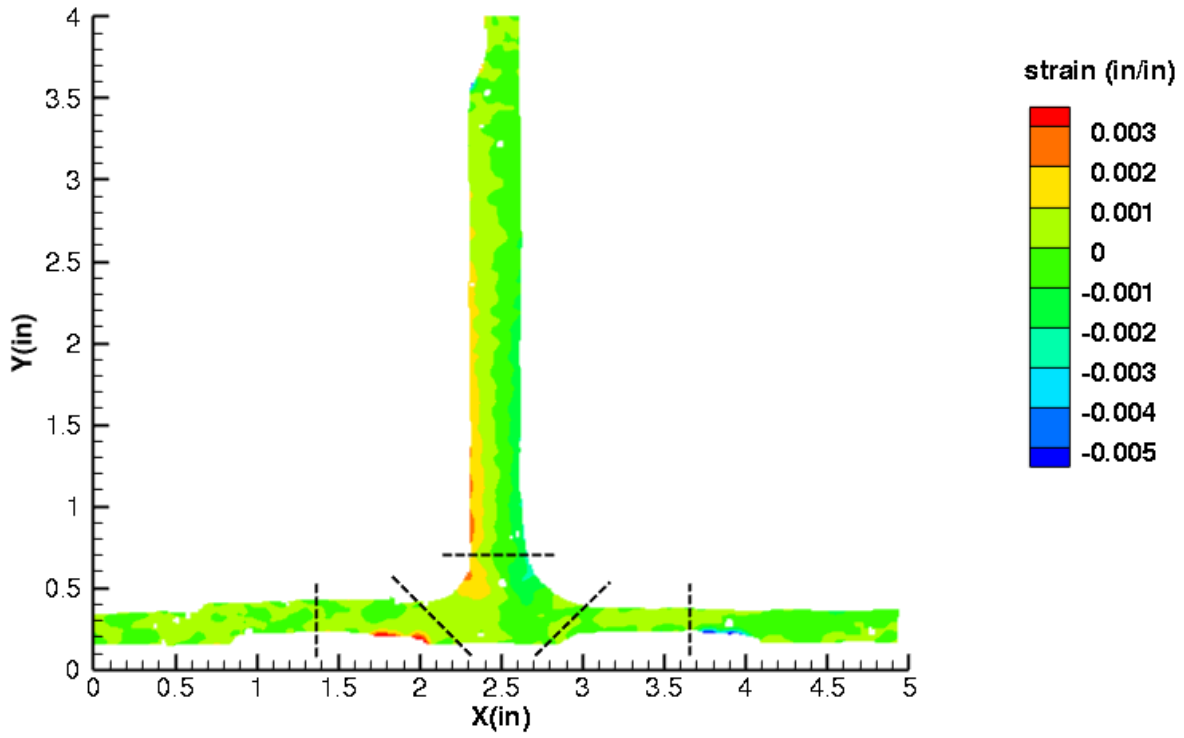

Figure C321. BNN2 strain contours for ε_{yy} at 323 lb. load, prior to initial failure, back 12MP VIC data.

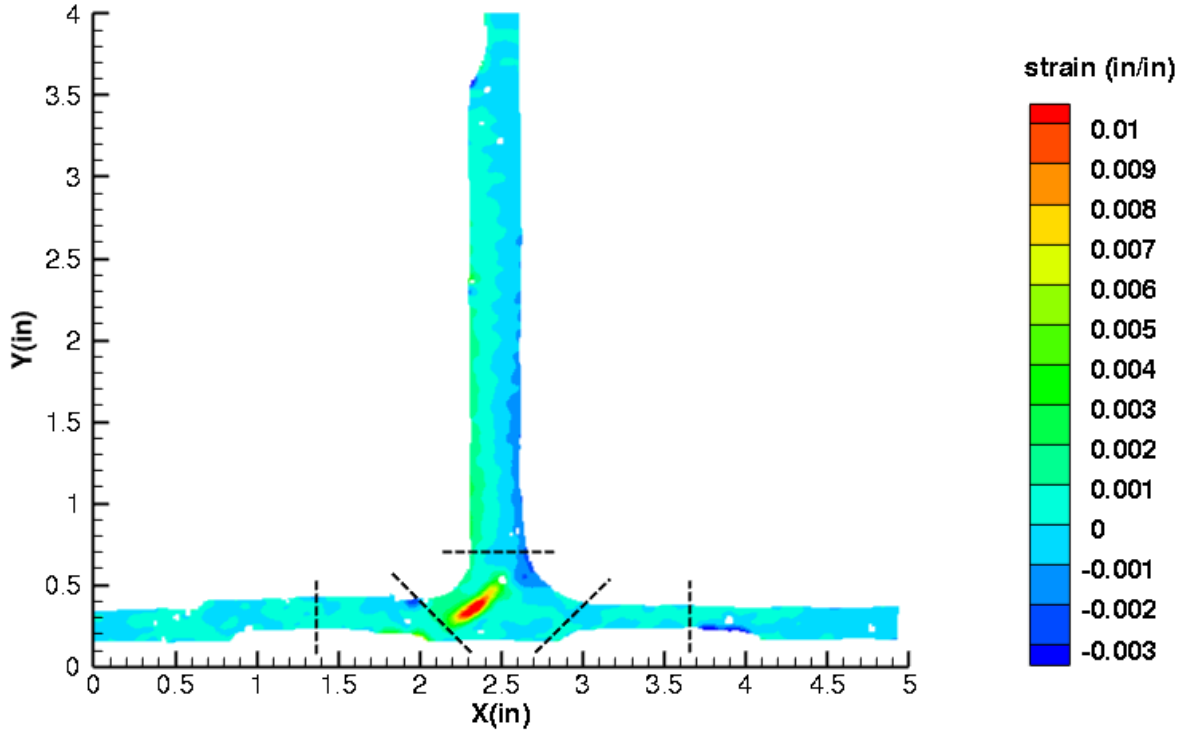

Figure C322. BNN2 strain contours for ε_{yy} at 297 lb. load, just after initial failure, back 12MP VIC data.

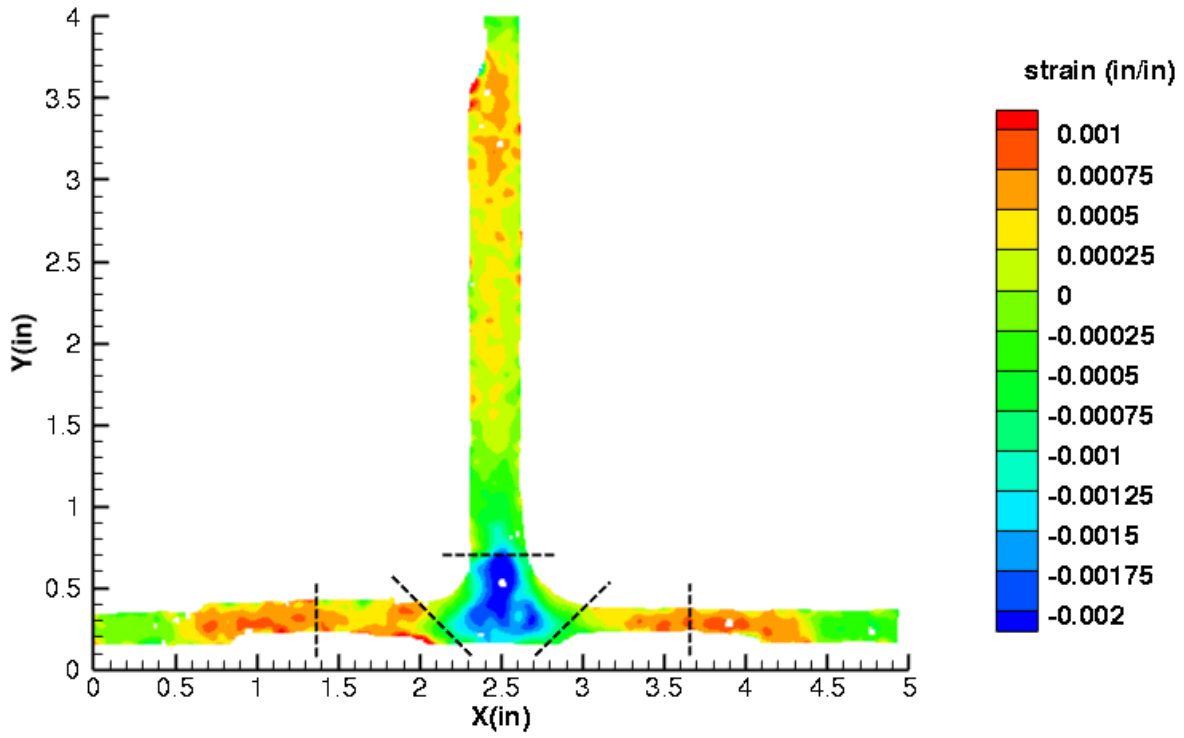

Figure C323. BNN2 strain contours for ε_{xy} at 323 lb. load, prior to initial failure, back 12MP VIC data.

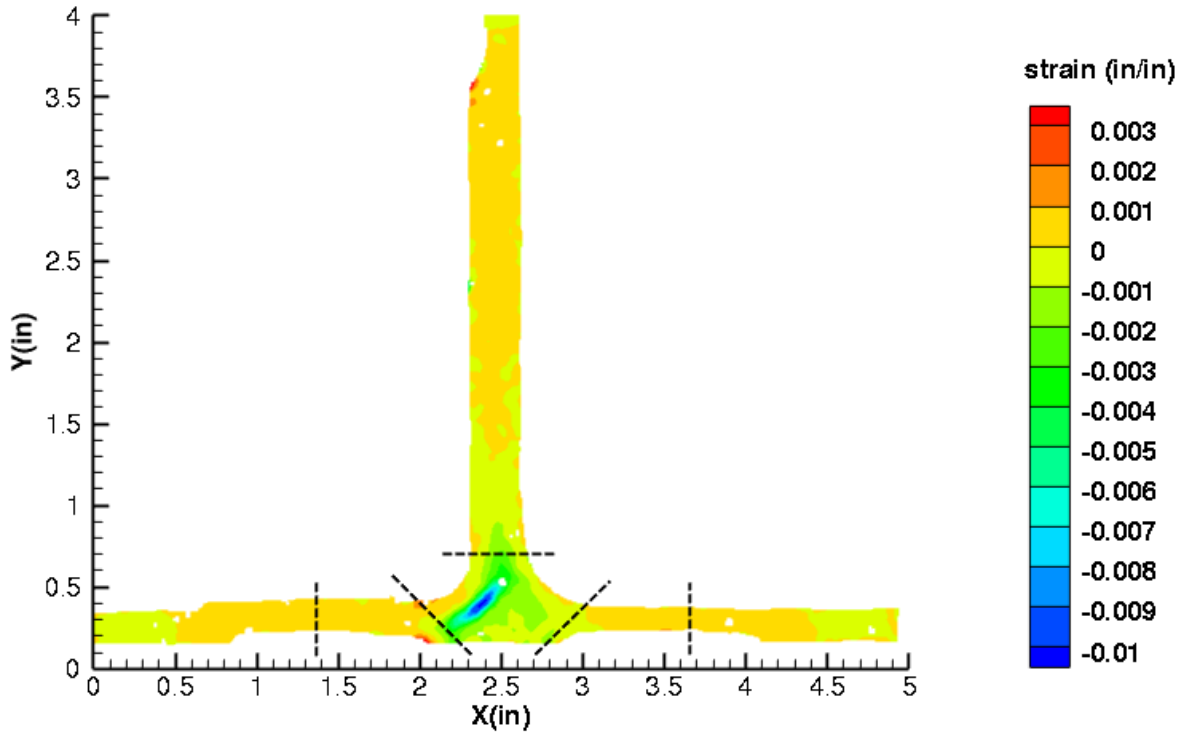

Figure C324. BNN2 strain contours for ε_{xy} at 297 lb. load, just after initial failure, back 12MP VIC data.

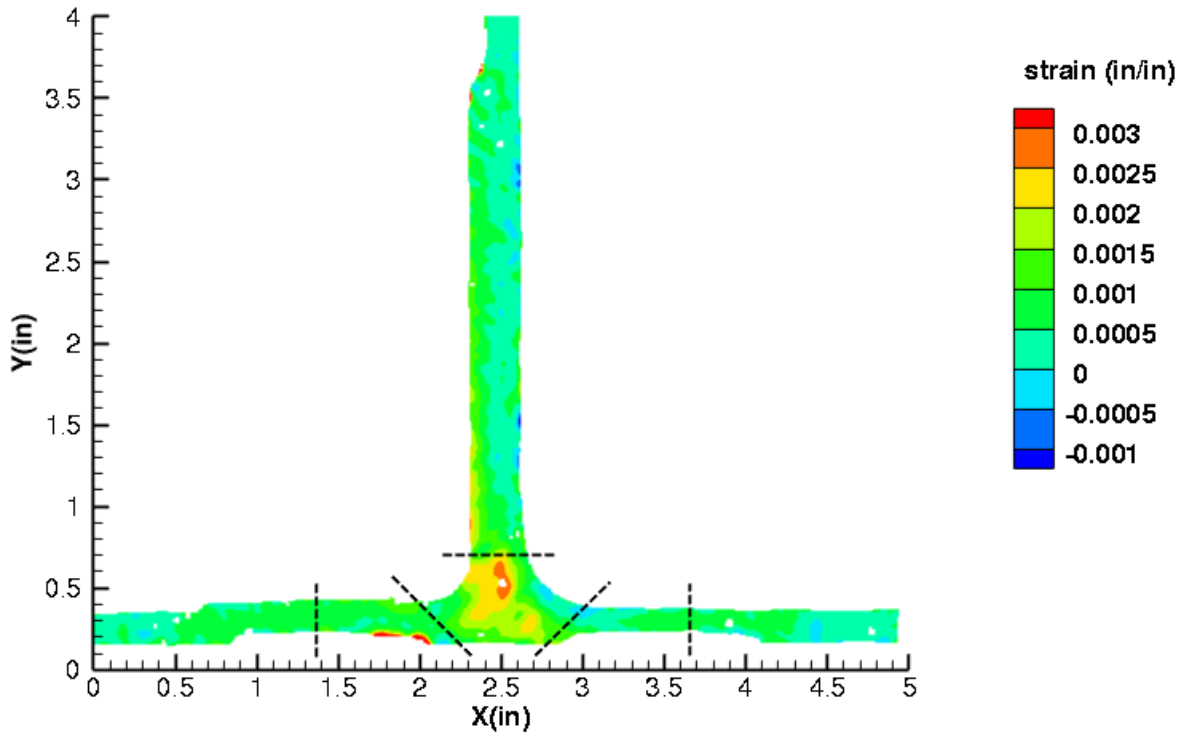

Figure C325. BNN2 strain contours for maximum principal strain at 323 lb. load, prior to initial failure, back 12MP VIC data.

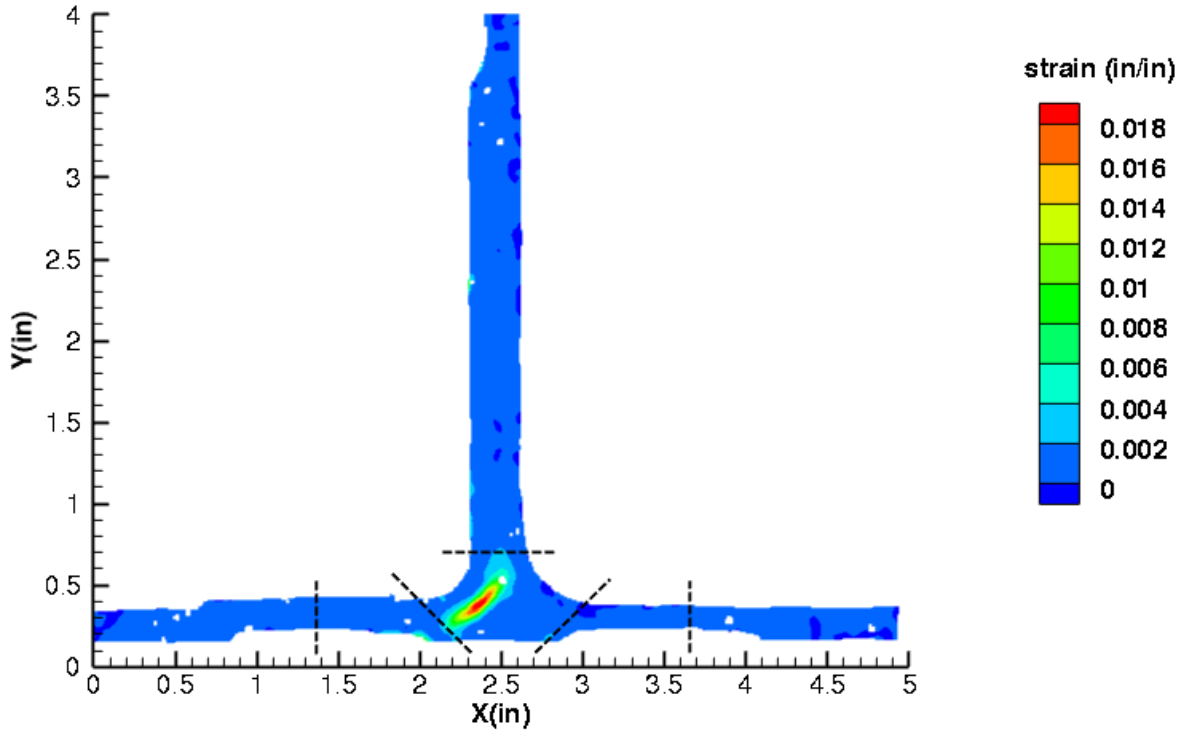

Figure C326. BNN2 strain contours for maximum principal strain at 297 lb. load, just after initial failure, back 12MP VIC data.

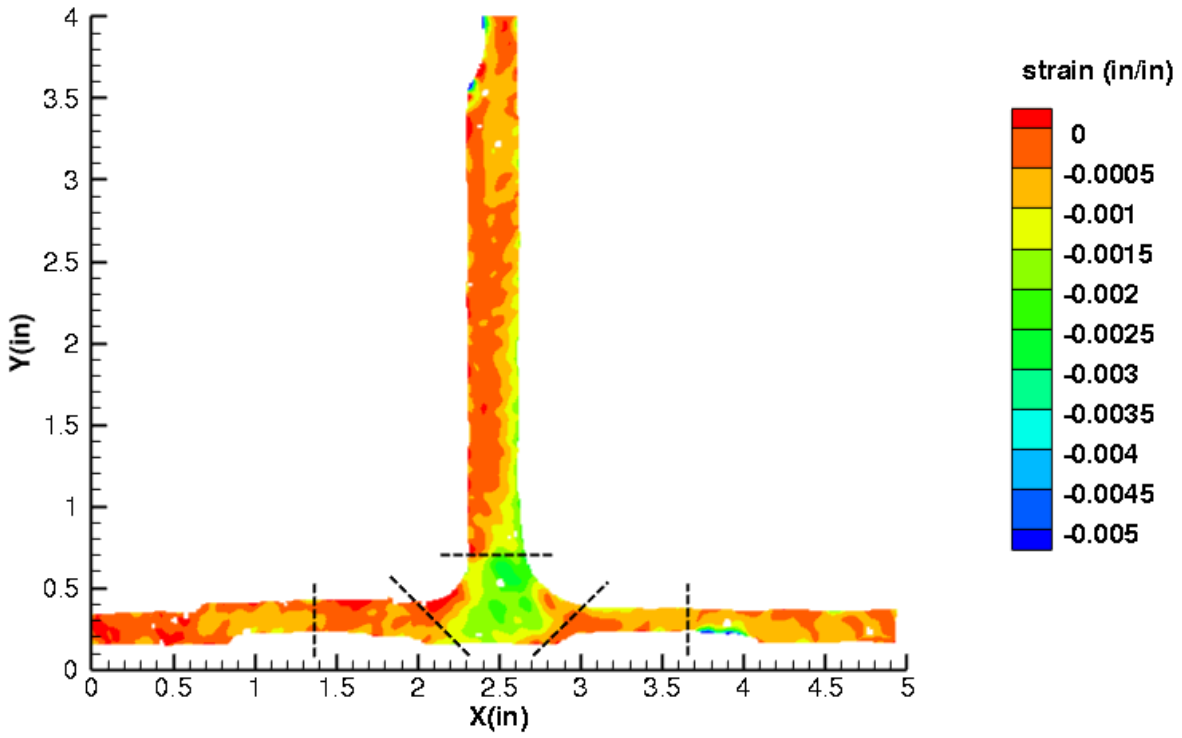

Figure C327. BNN2 strain contours for minimum principal strain at 323 lb. load, prior to initial failure, back 12MP VIC data.

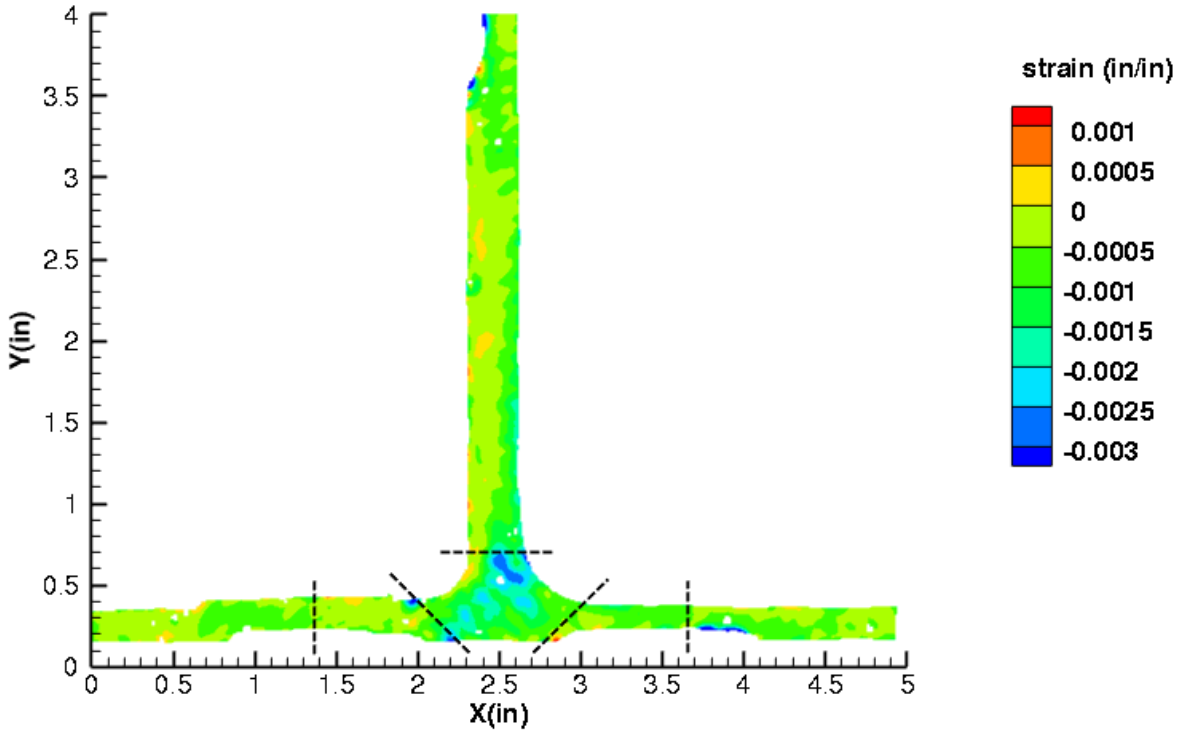

Figure C328. BNN2 strain contours for minimum principal strain at 297 lb. load, just after initial failure, back 12MP VIC data.

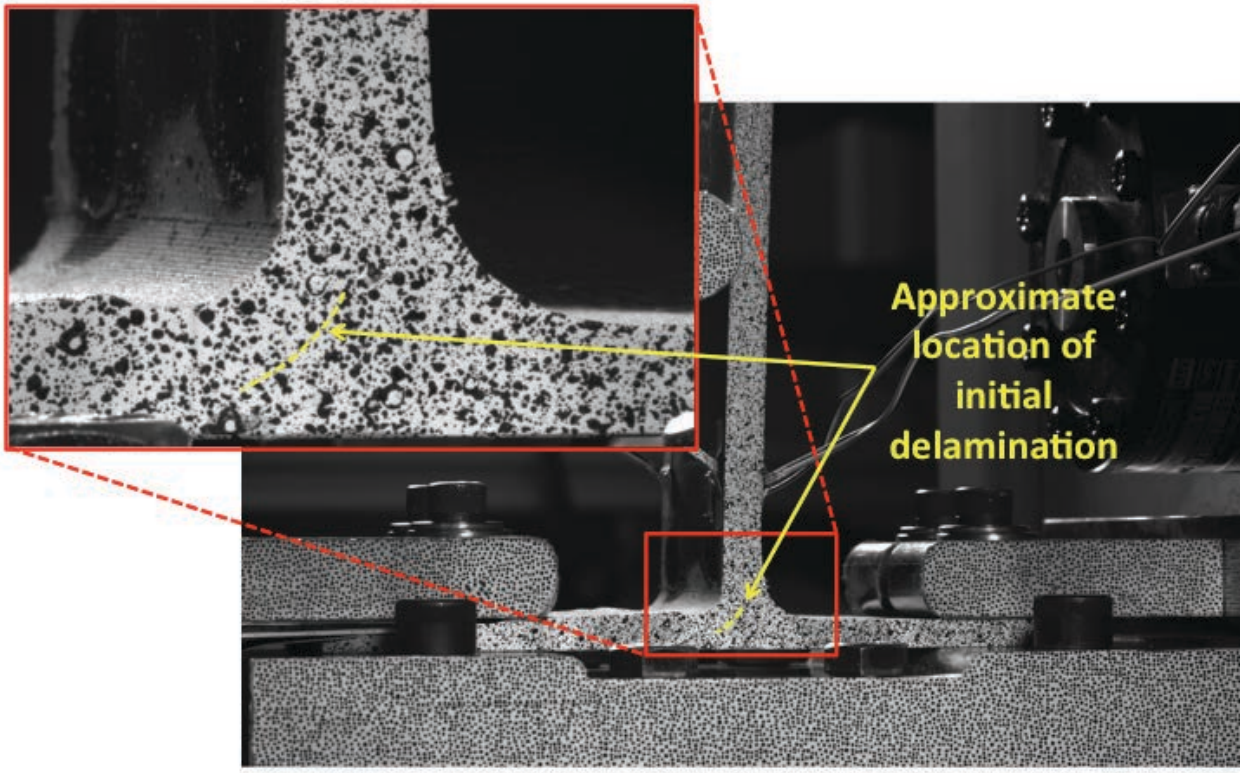

Figure C329. BNN2 image just after initial failure, back 12MP VIC data.

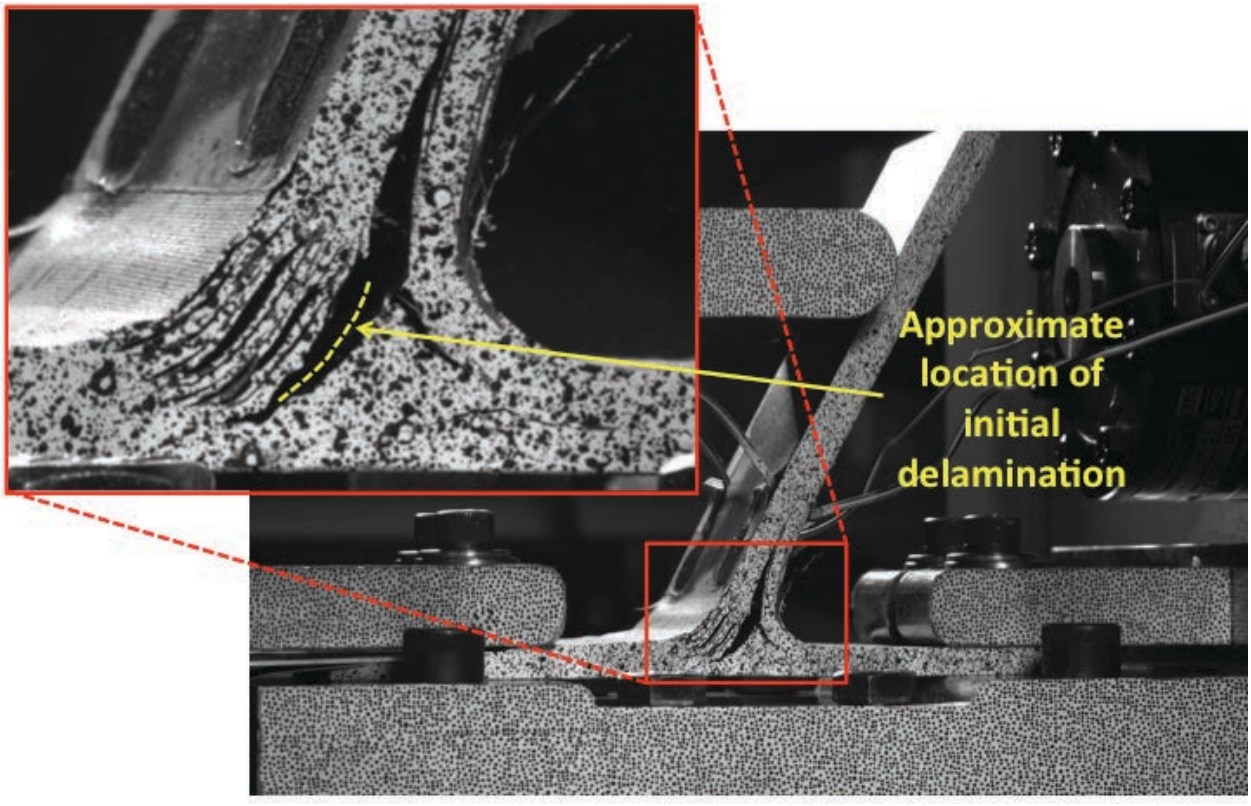

Figure C330. BNN2 image just after maximum load, back 12MP VIC data.

B1S1

This section presents the test data for the B1S1 test article, and includes strain plots and failure images.

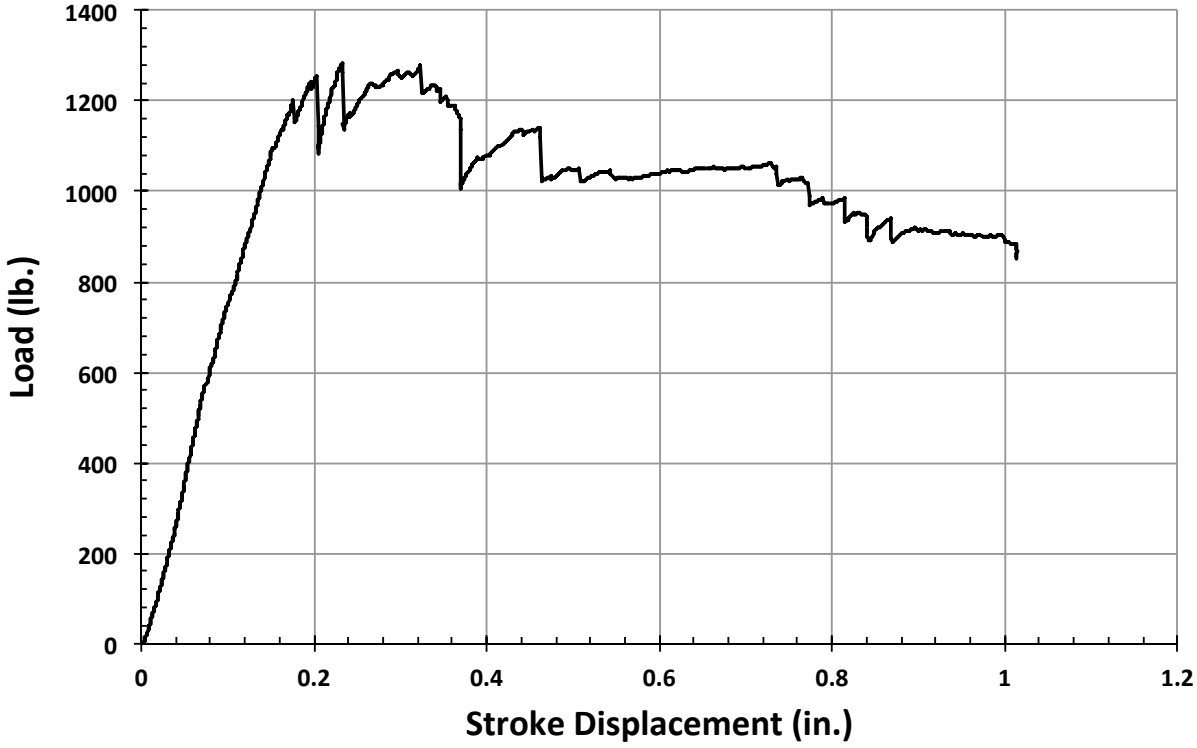

Figure C331. B1S1 load vs. stroke.

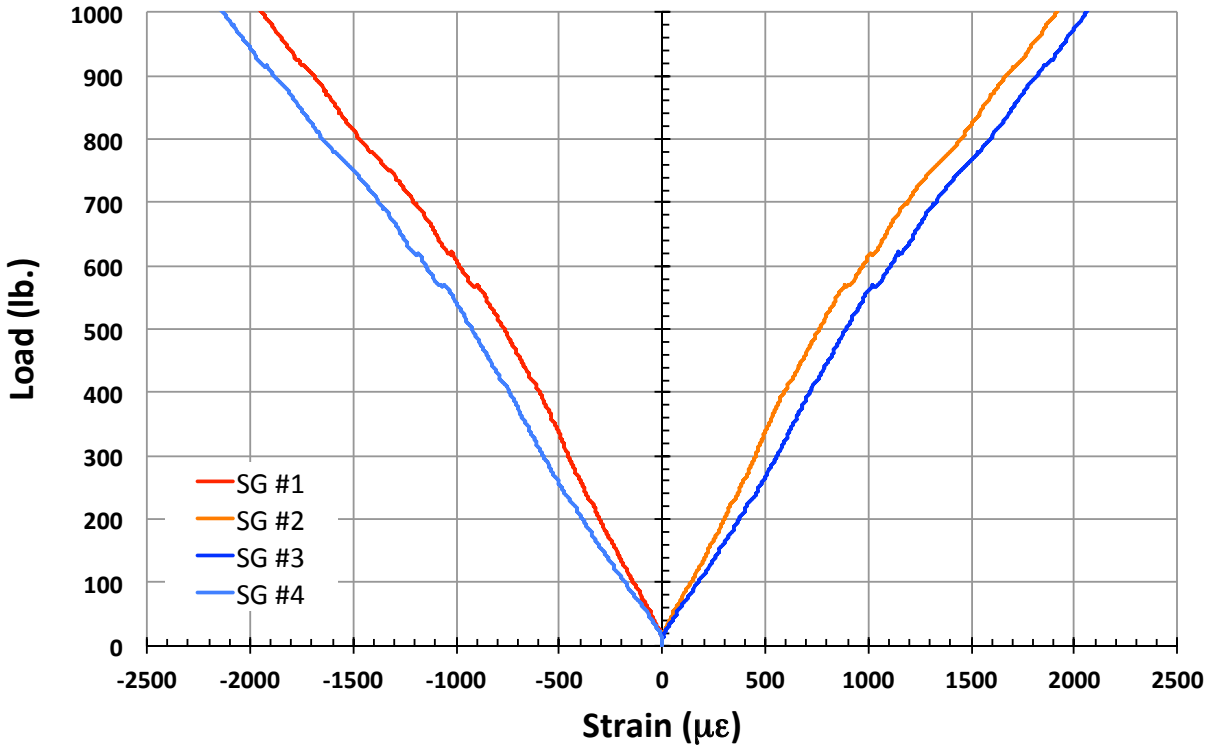

Figure C332. B1S1 load vs. strain, initial loading.

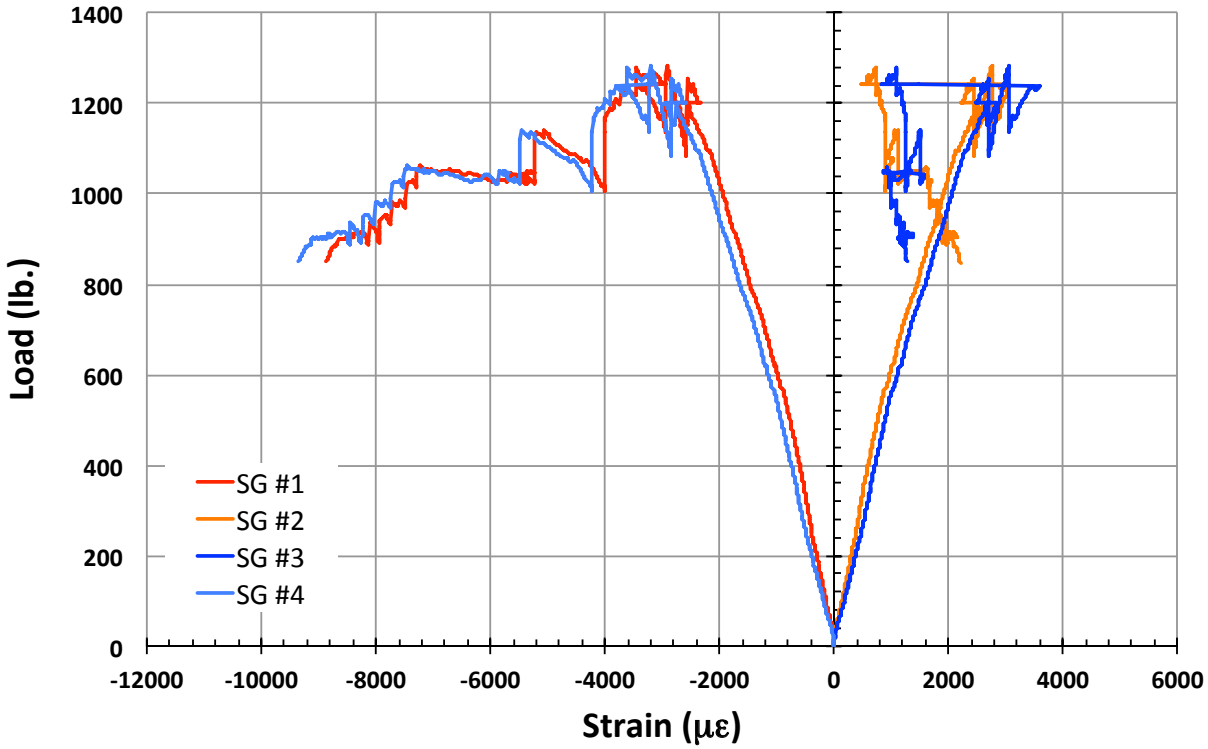

Figure C333. B1S1 load vs. strain.

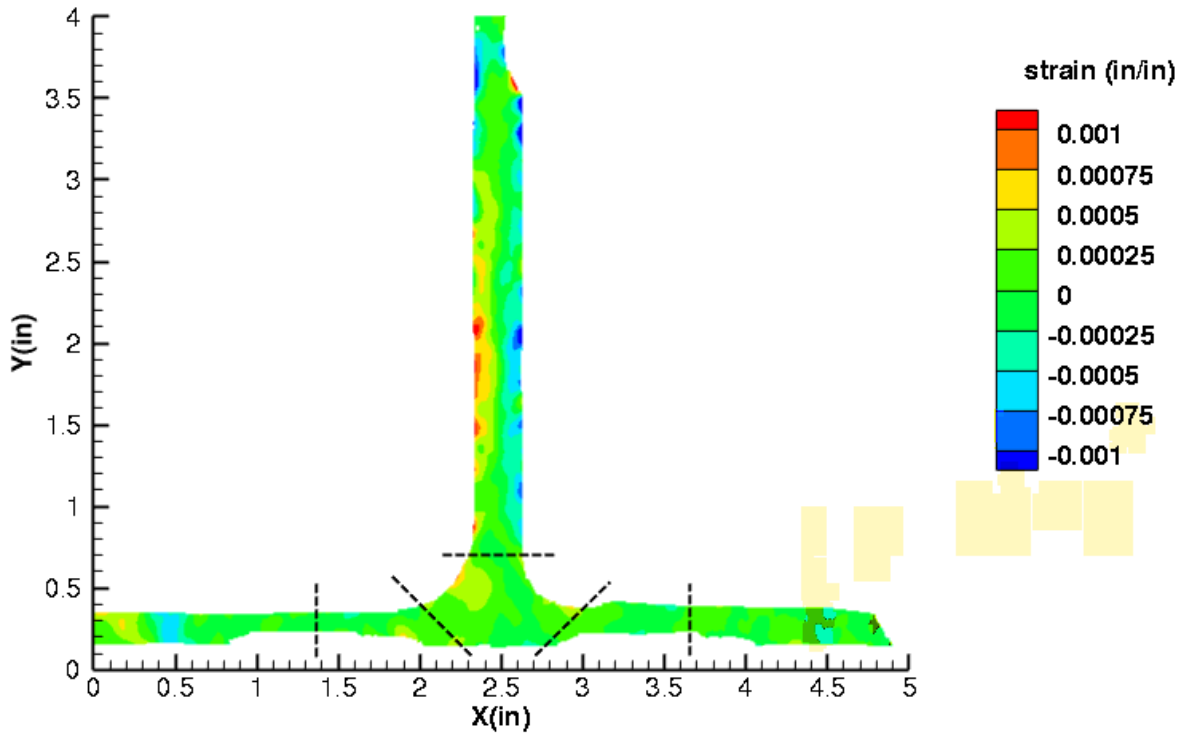

Figure C334. B1S1 strain contours for ε_{xx} at 590 lb. load, prior to initial failure, front 12MP VIC data.

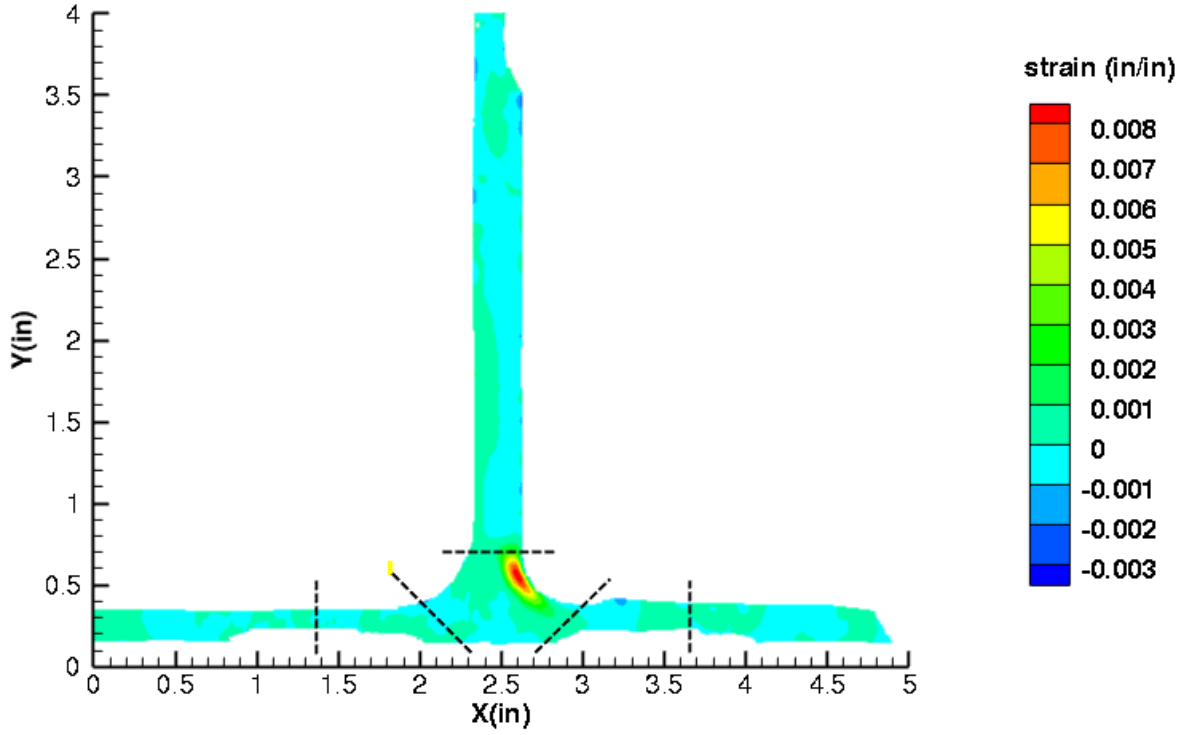

Figure C335. B1S1 strain contours for ε_{xx} at 597 lb. load, just after initial failure, front 12MP VIC data.

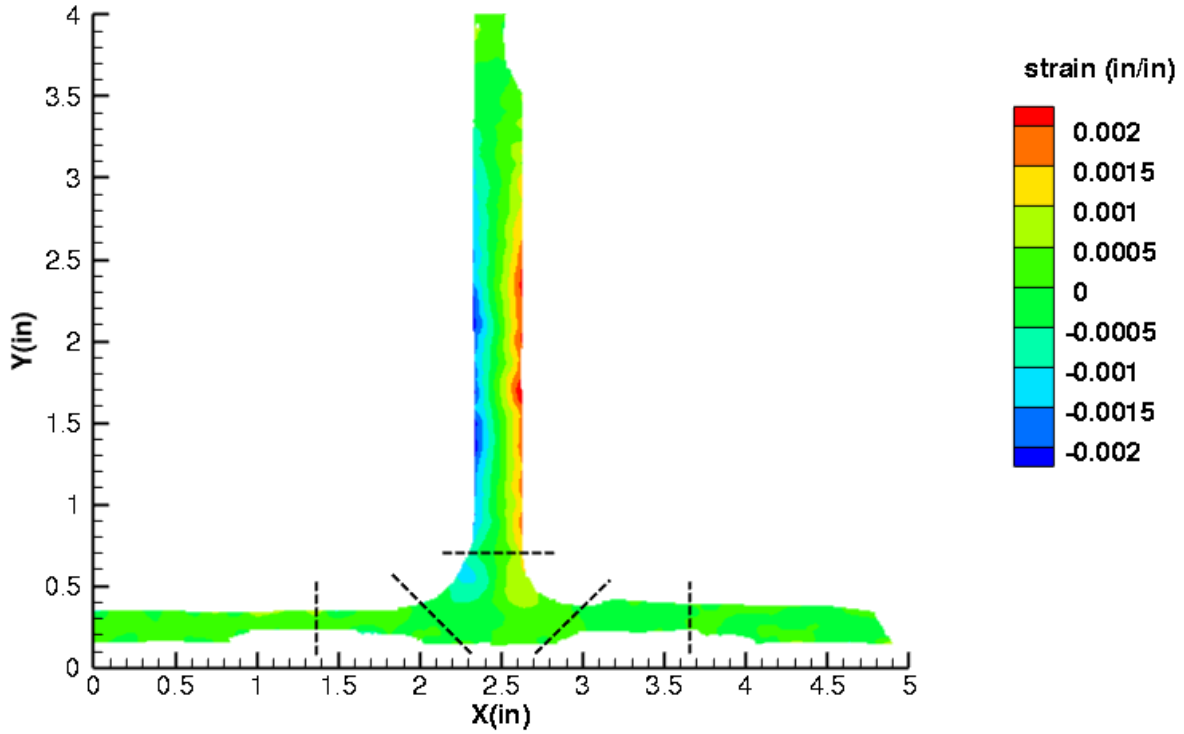

Figure C336. B1S1 strain contours for ε_{yy} at 590 lb. load, prior to initial failure, front 12MP VIC data.

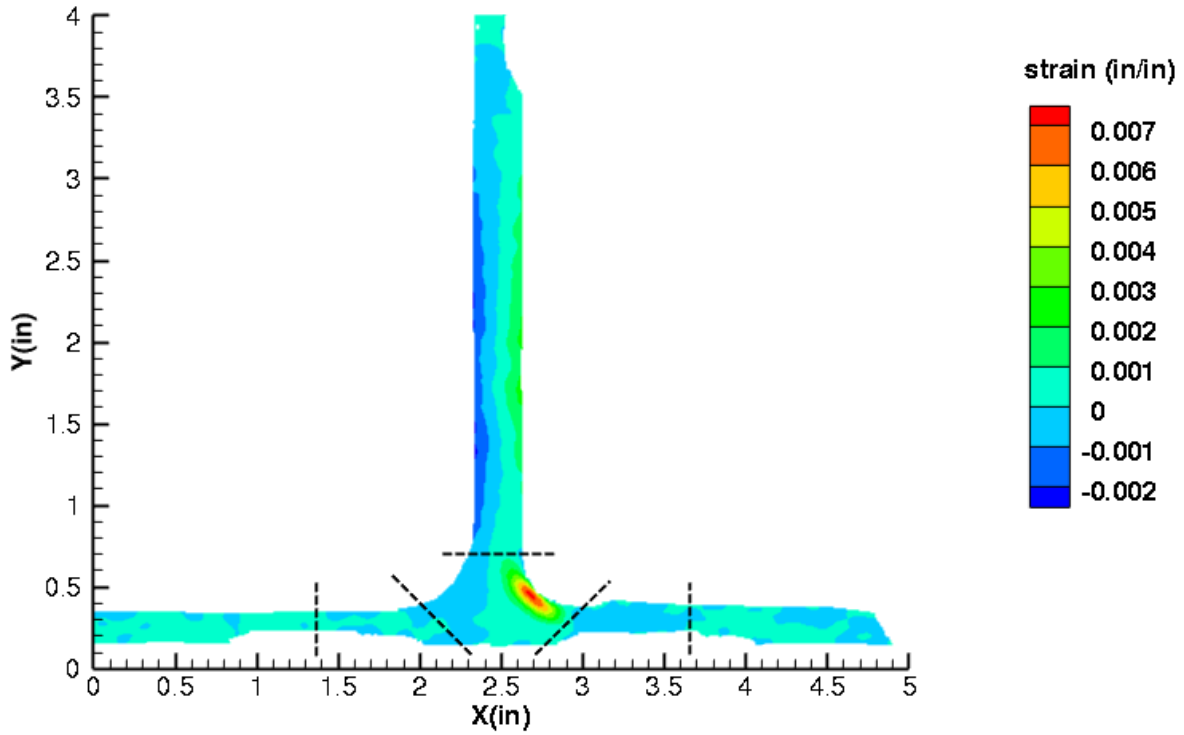

Figure C337. B1S1 strain contours for ε_{yy} at 597 lb. load, just after initial failure, front 12MP VIC data.

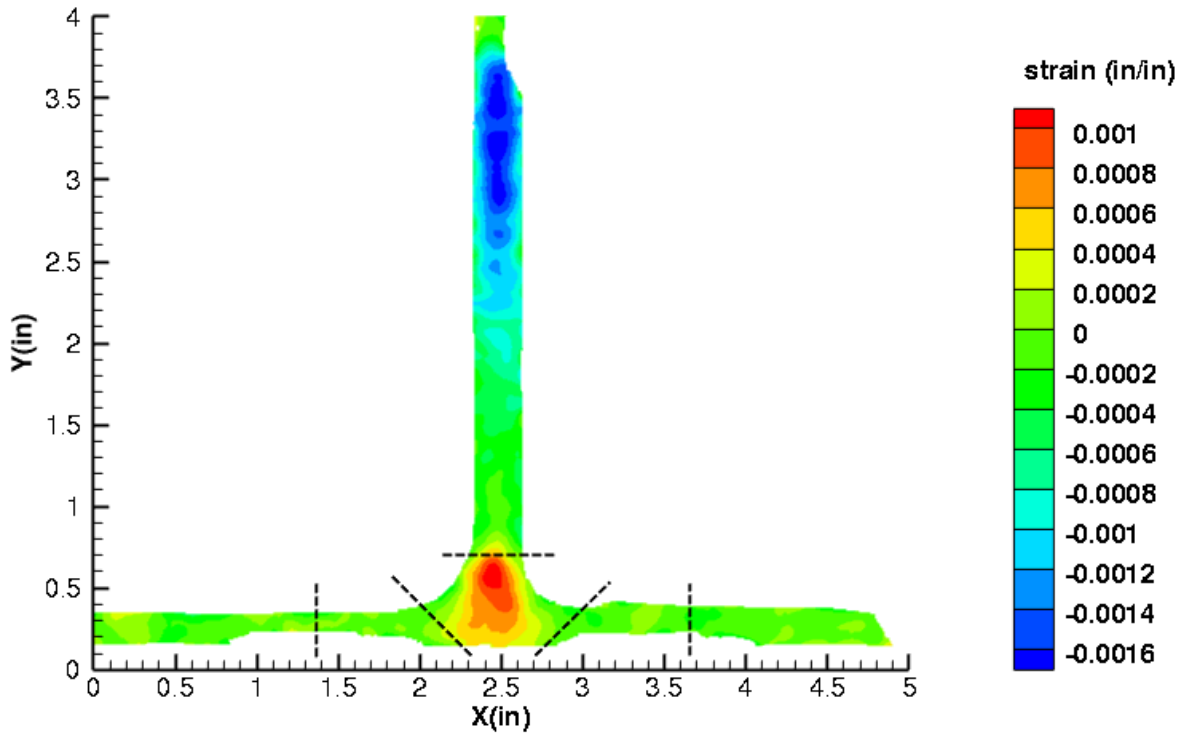

Figure C338. B1S1 strain contours for ε_{xy} at 590 lb. load, prior to initial failure, front 12MP VIC data.

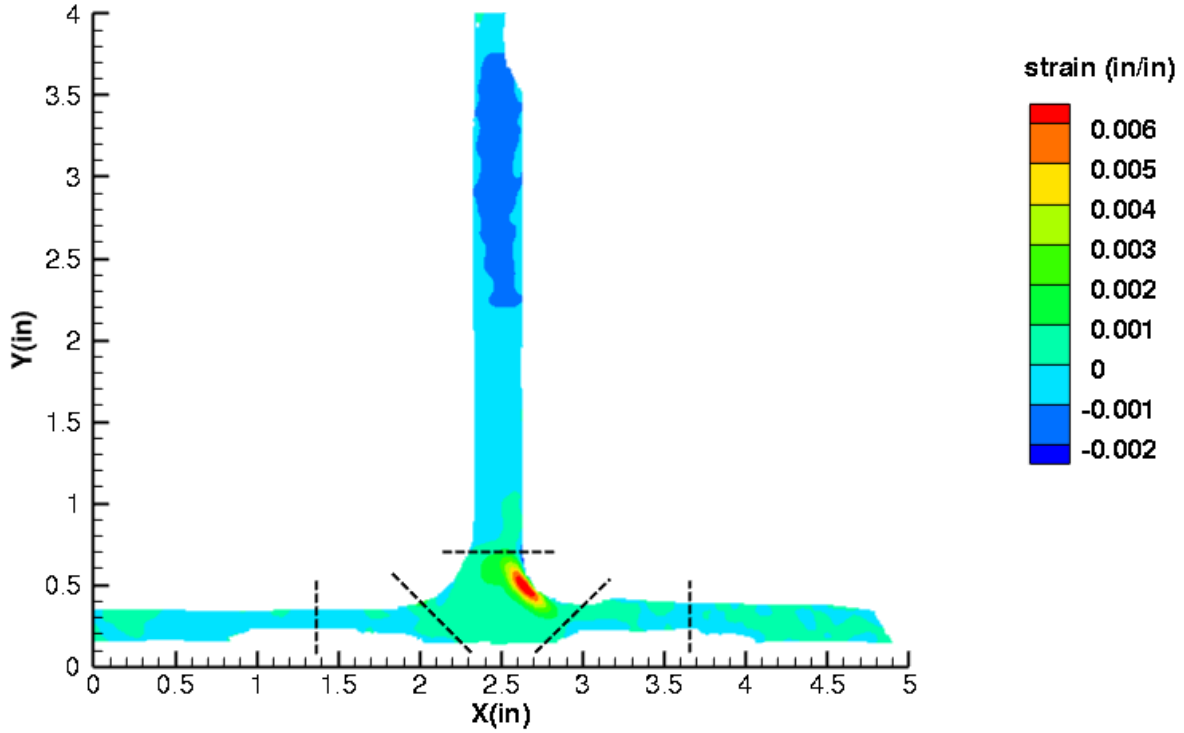

Figure C339. B1S1 strain contours for ε_{xy} at 597 lb. load, just after initial failure, front 12MP VIC data.

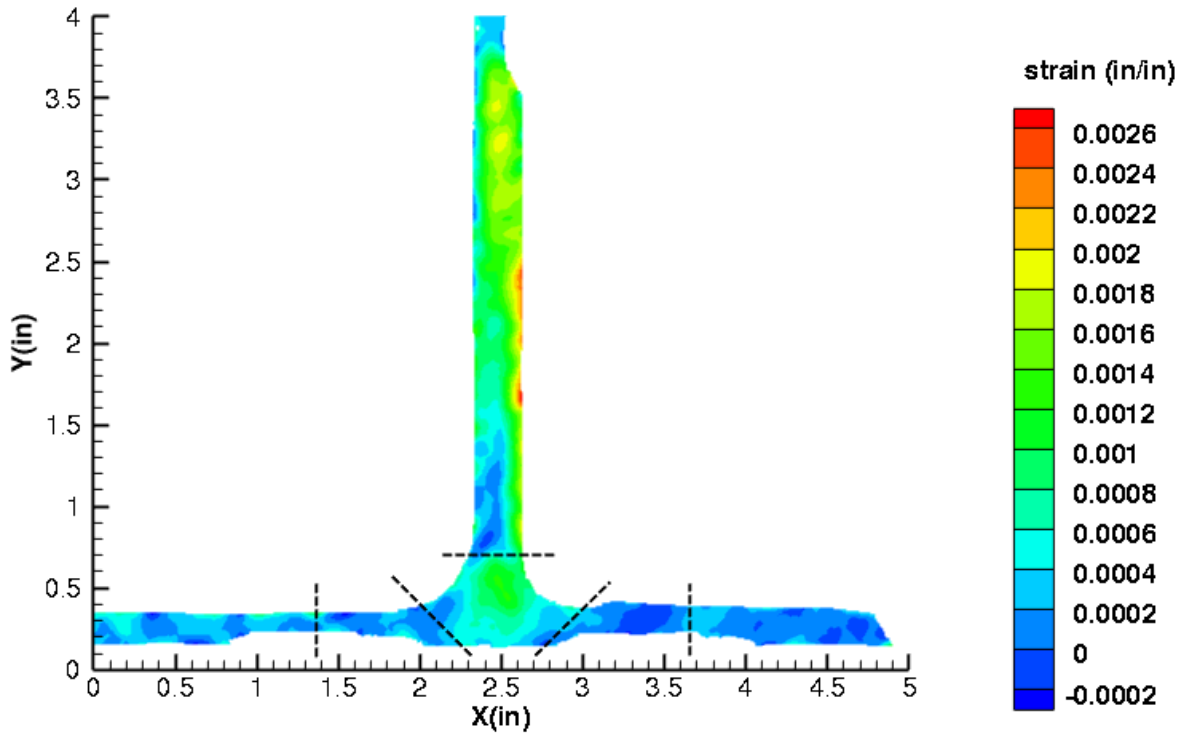

Figure C340. B1S1 strain contours for maximum principal strain at 590 lb. load, prior to initial failure, front 12MP VIC data.

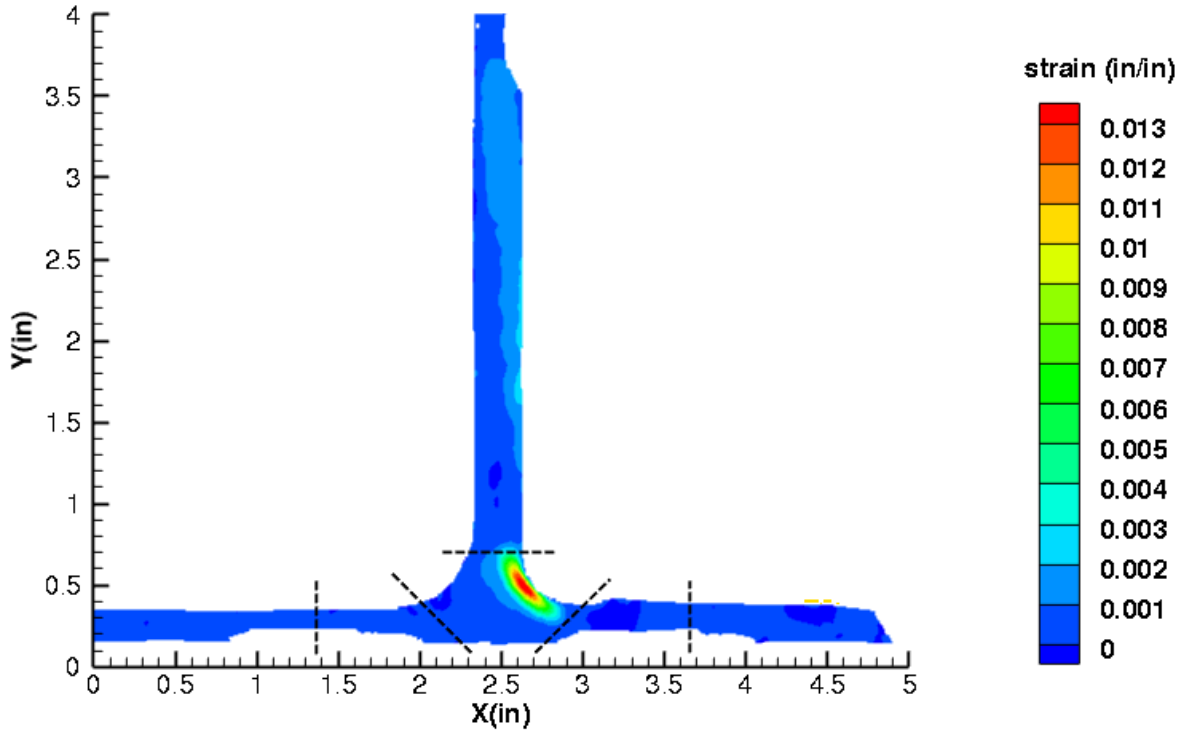

Figure C341. B1S1 strain contours for maximum principal strain at 597 lb. load, just after initial failure, front 12MP VIC data.

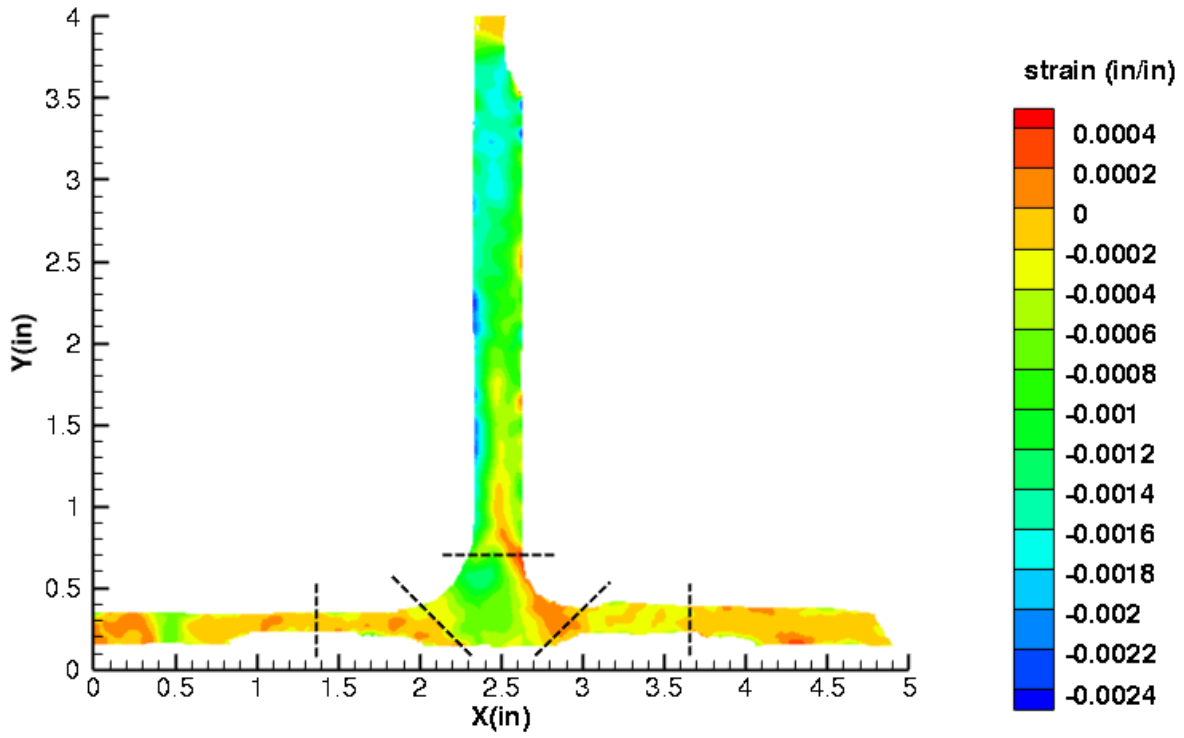

Figure C342. B1S1 strain contours for minimum principal strain at 590 lb. load, prior to initial failure, front 12MP VIC data.

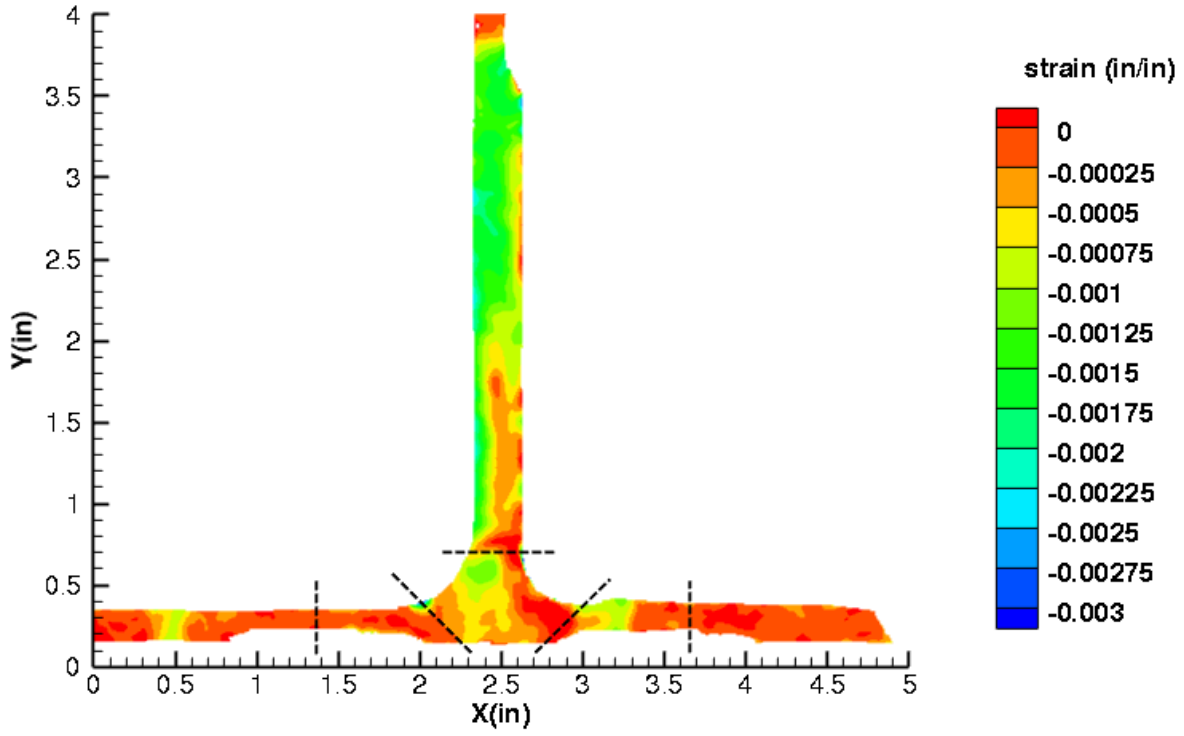

Figure C343. B1S1 strain contours for minimum principal strain at 597 lb. load, just after initial failure, front 12MP VIC data.

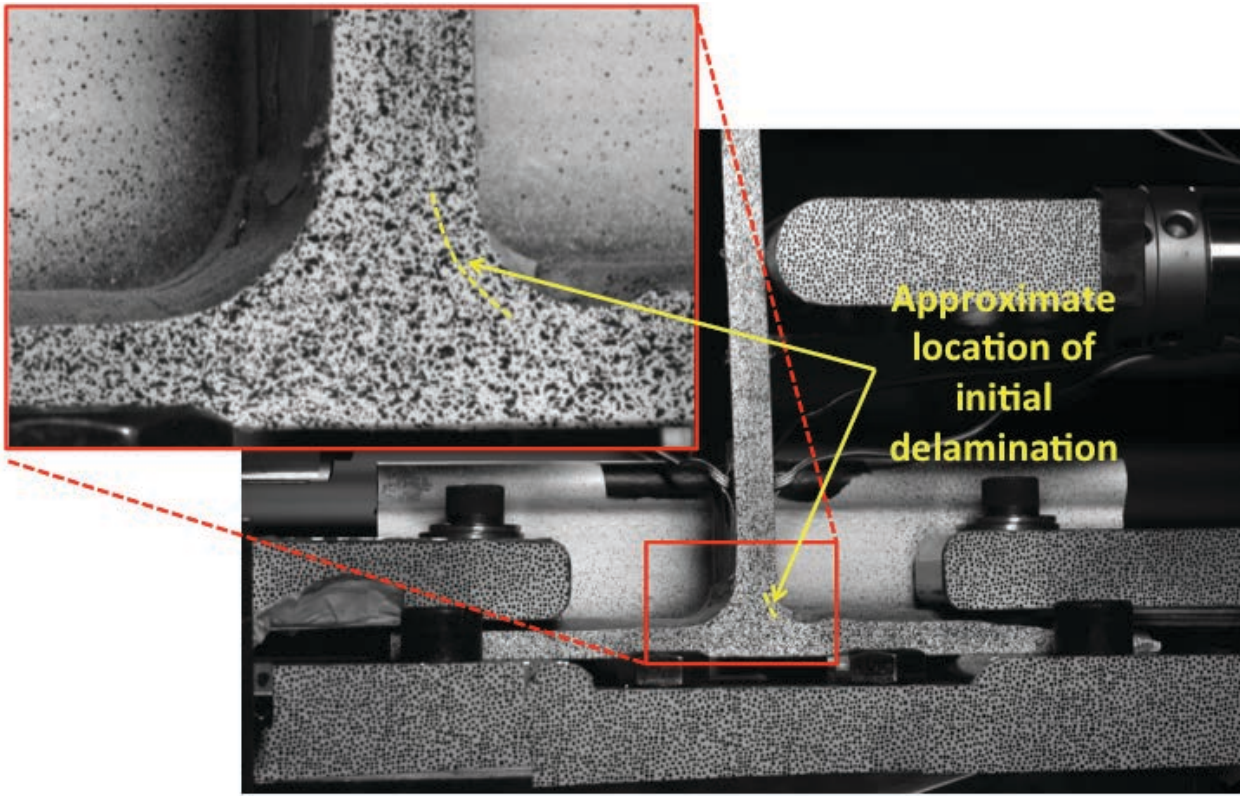

Figure C344. B1S1 image just after initial failure, front 12MP VIC data.

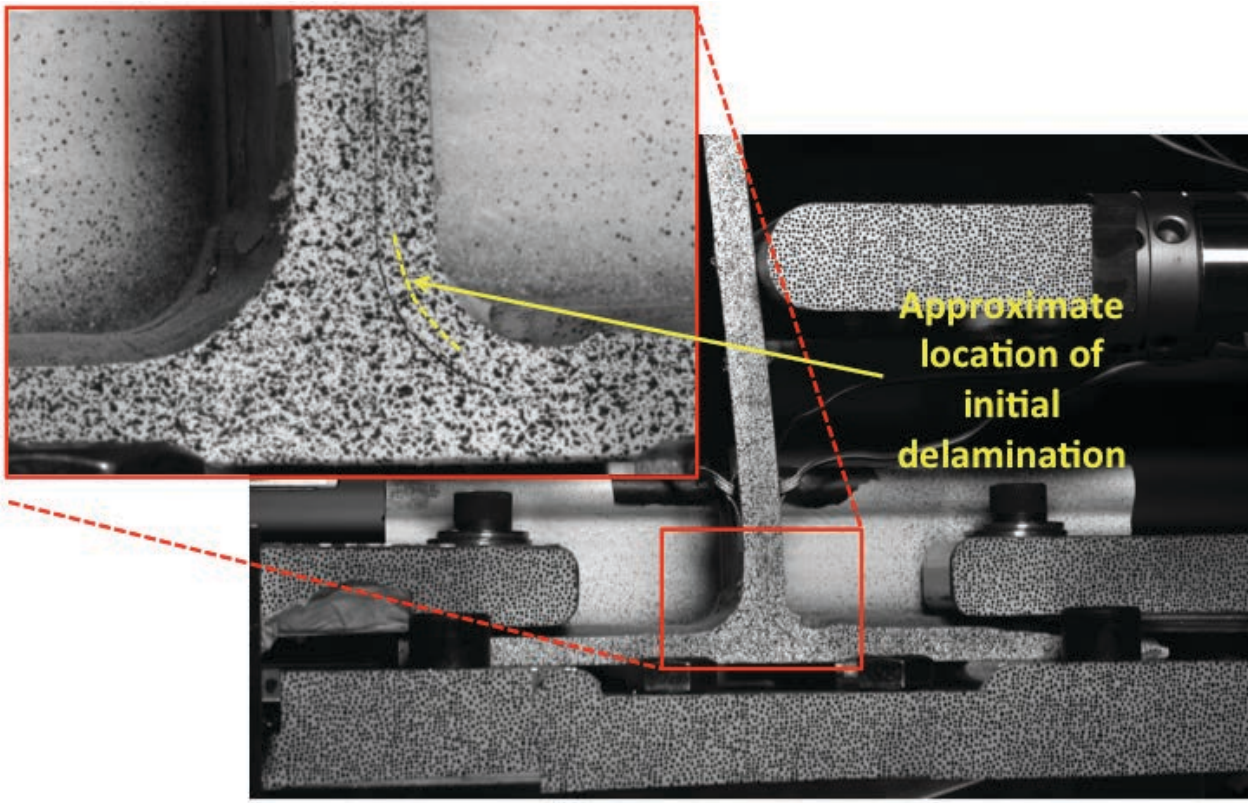

Figure C345. B1S1 image just after maximum load, front 12MP VIC data.

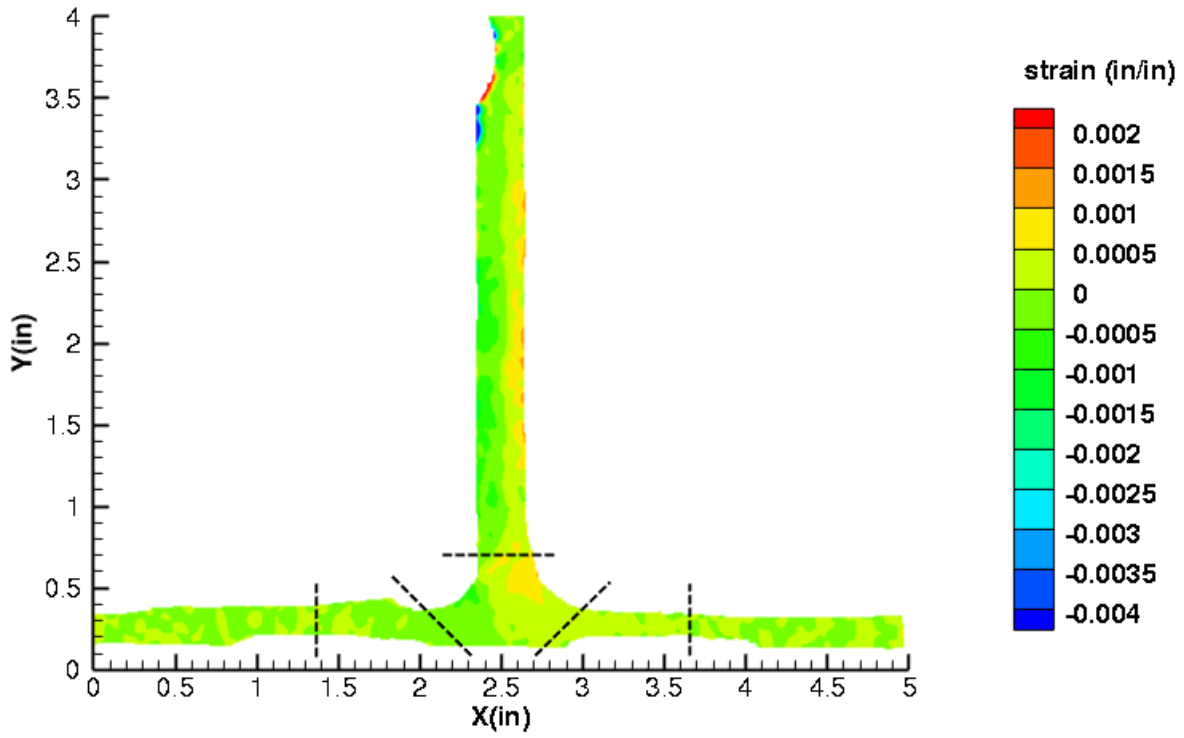

Figure C346. B1S1 strain contours for ε_{xx} at 736 lb. load, prior to initial failure, back 12MP VIC data.

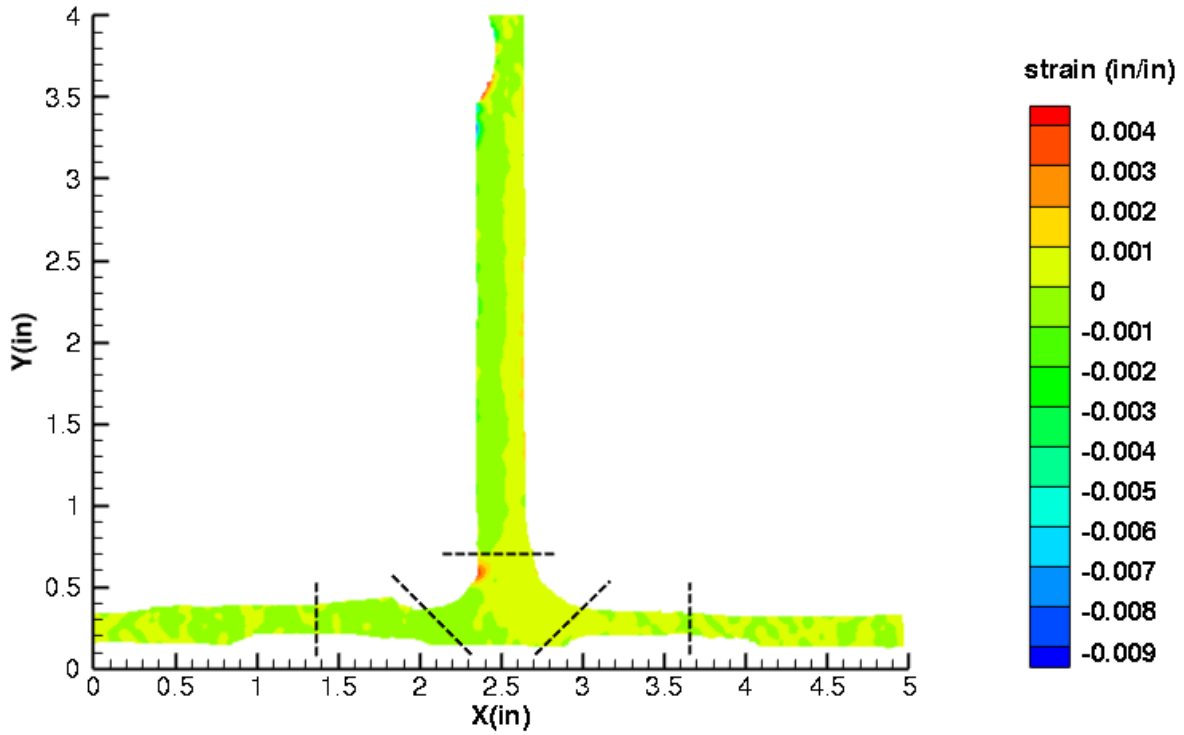

Figure C347. B1S1 strain contours for ε_{xx} at 740 lb. load, just after initial failure, back 12MP VIC data.

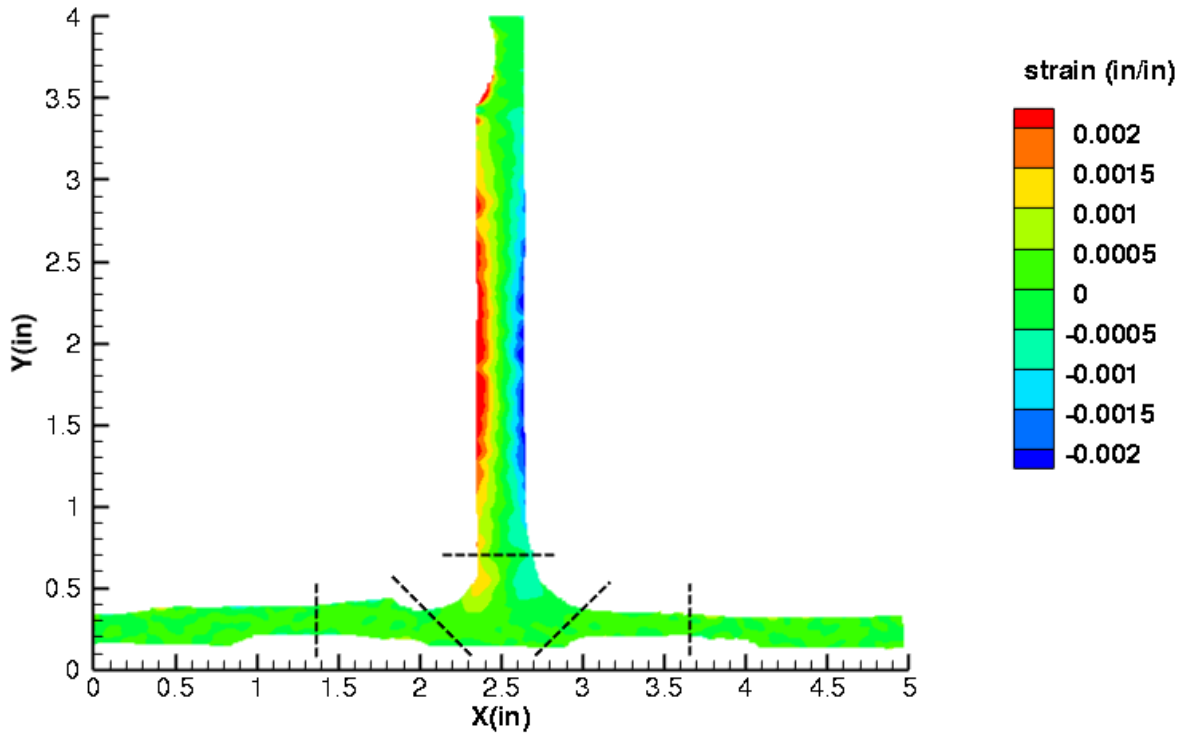

Figure C348. B1S1 strain contours for ε_{yy} at 736 lb. load, prior to initial failure, back 12MP VIC data.

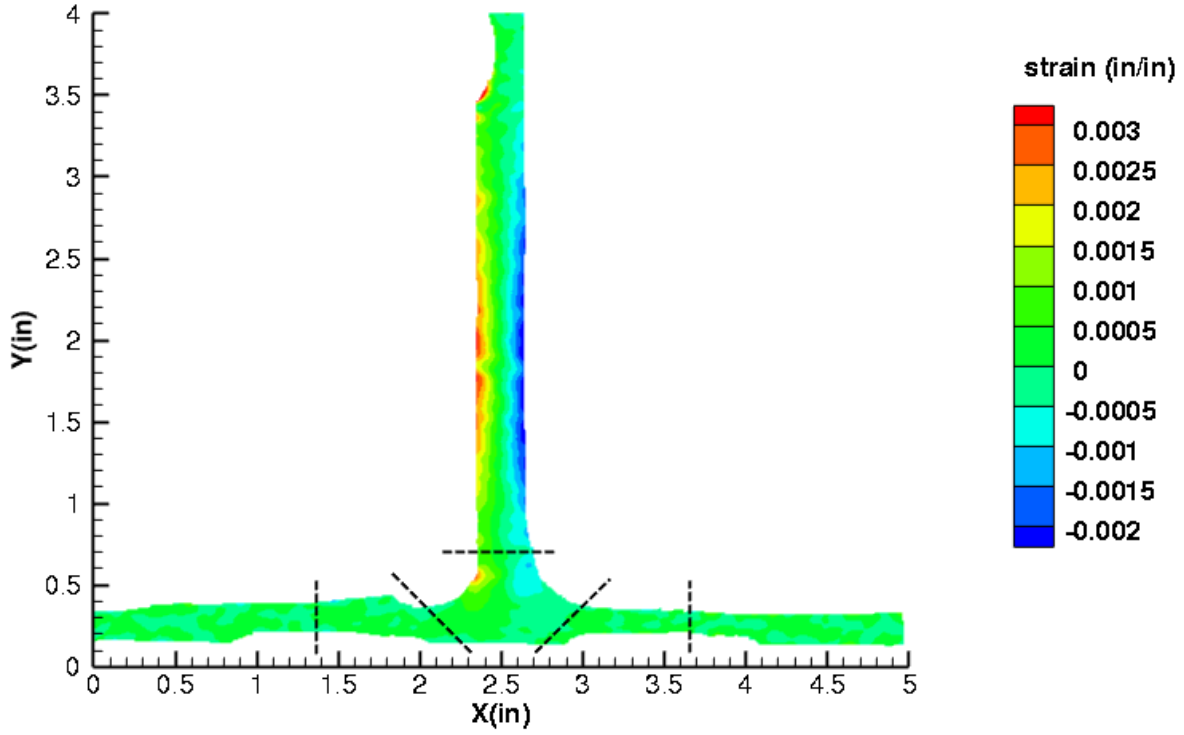

Figure C349. B1S1 strain contours for ε_{yy} at 740 lb. load, just after initial failure, back 12MP VIC data.

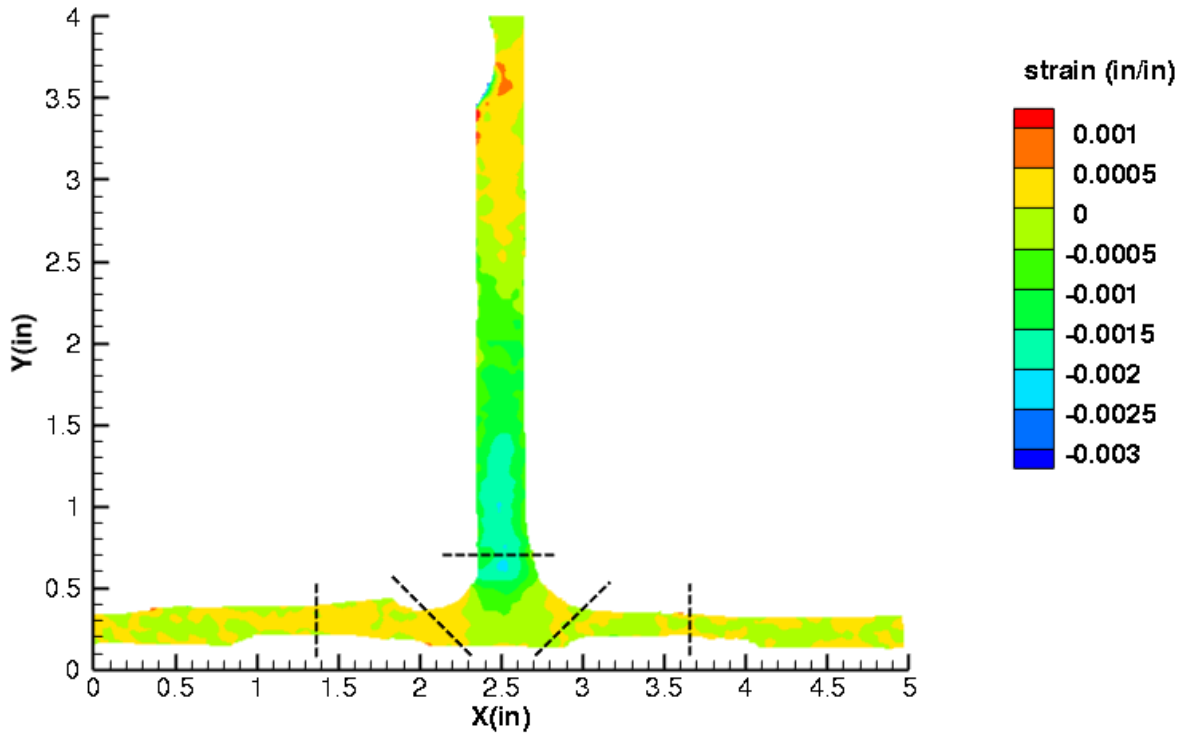

Figure C350. B1S1 strain contours for ε_{xy} at 736 lb. load, prior to initial failure, back 12MP VIC data.

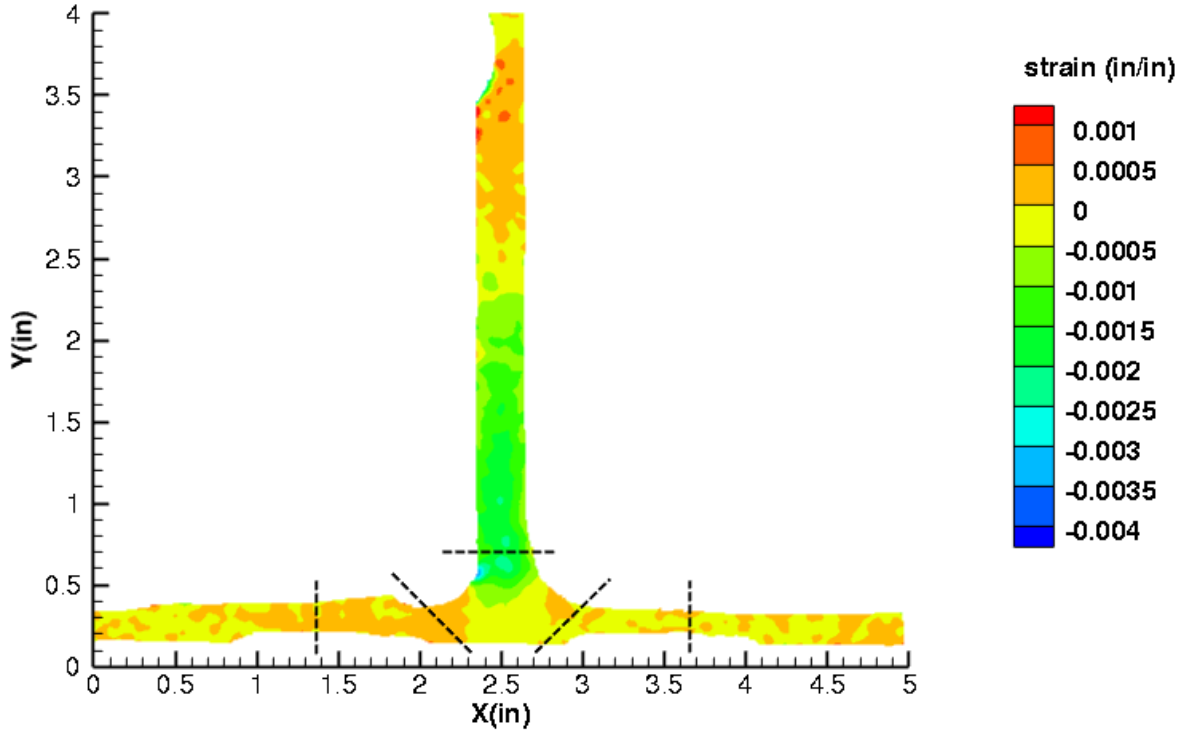

Figure C351. B1S1 strain contours for ε_{xy} at 740 lb. load, just after initial failure, back 12MP VIC data.

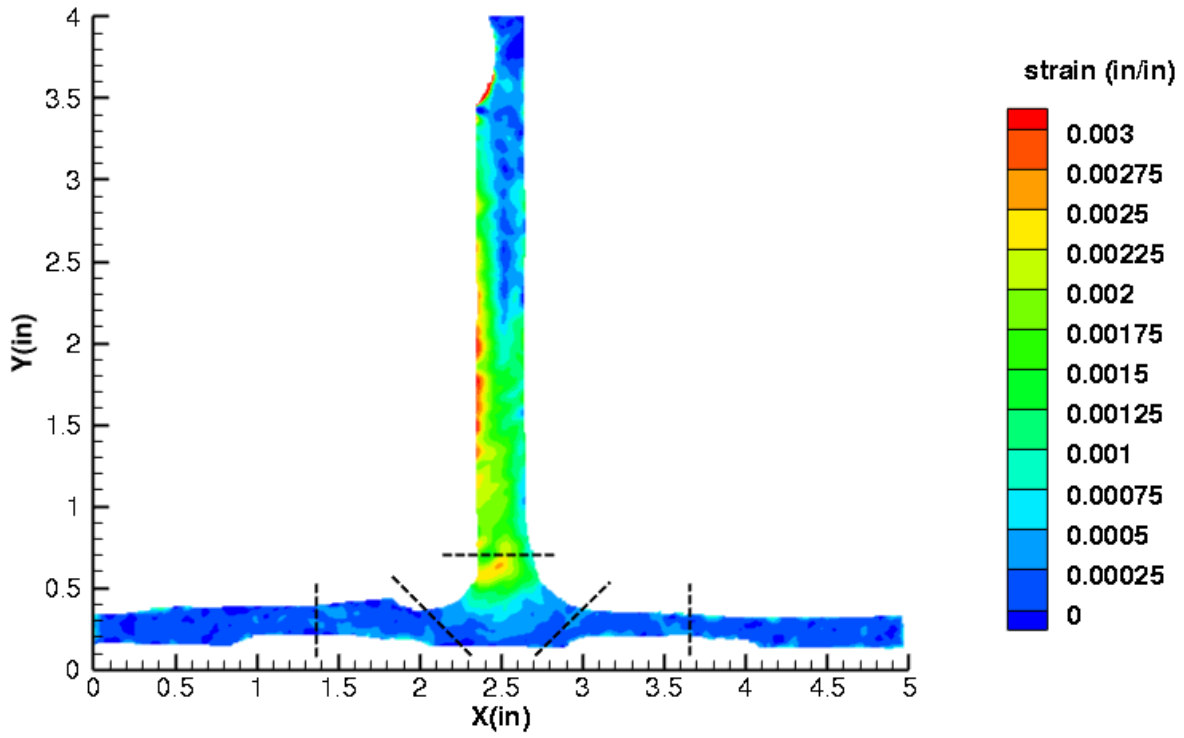

Figure C352. B1S1 strain contours for maximum principal strain at 736 lb. load, prior to initial failure, back 12MP VIC data.

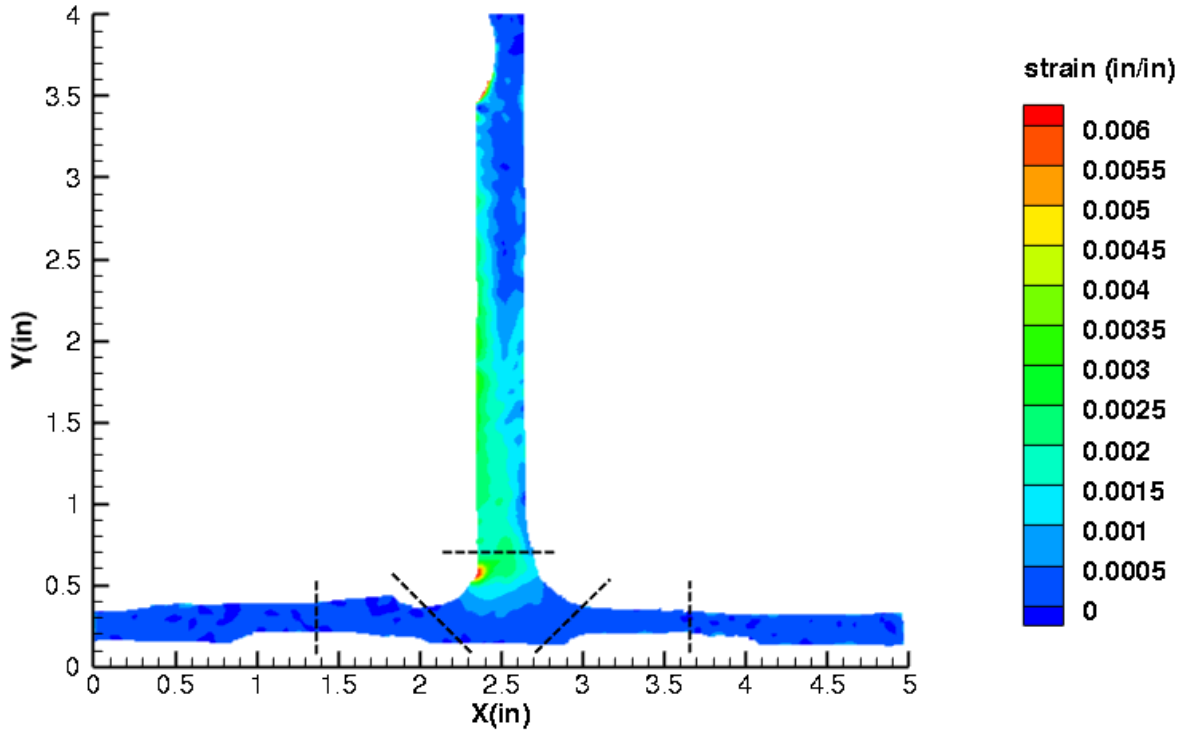

Figure C353. B1S1 strain contours for maximum principal strain at 740 lb. load, just after initial failure, back 12MP VIC data.

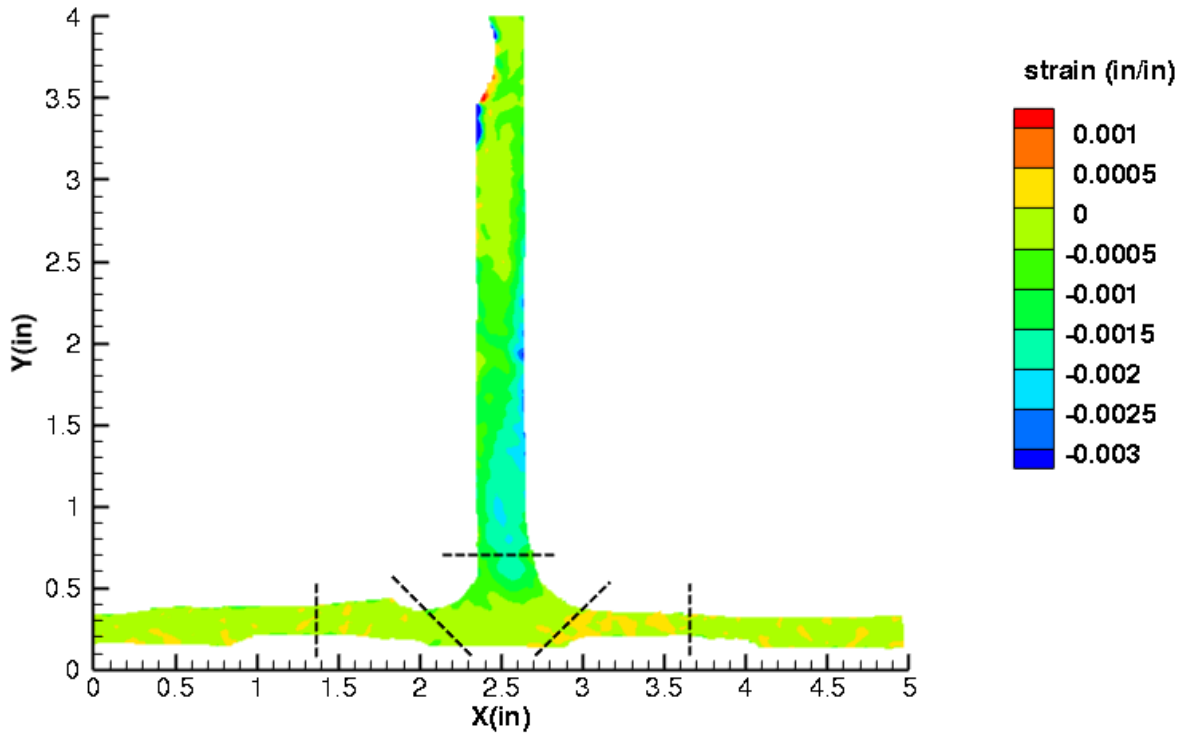

Figure C354. B1S1 strain contours for minimum principal strain at 736 lb. load, prior to initial failure, back 12MP VIC data.

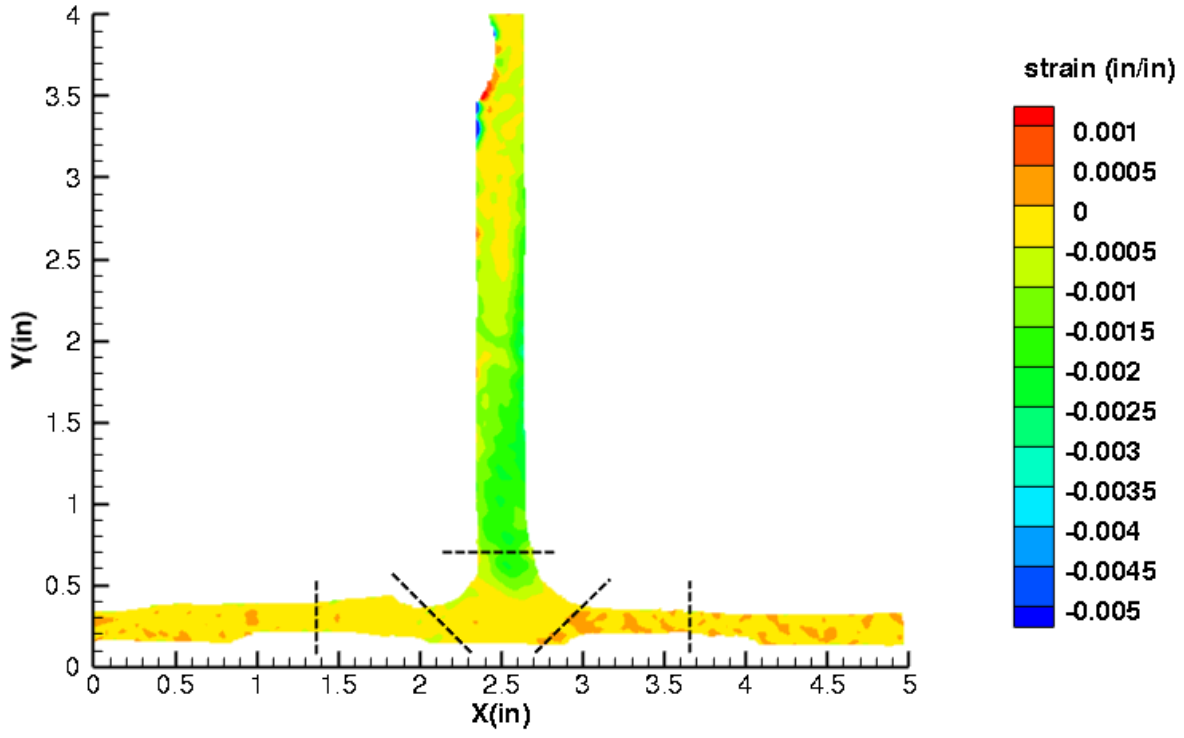

Figure C355. B1S1 strain contours for minimum principal strain at 740 lb. load, just after initial failure, back 12MP VIC data.

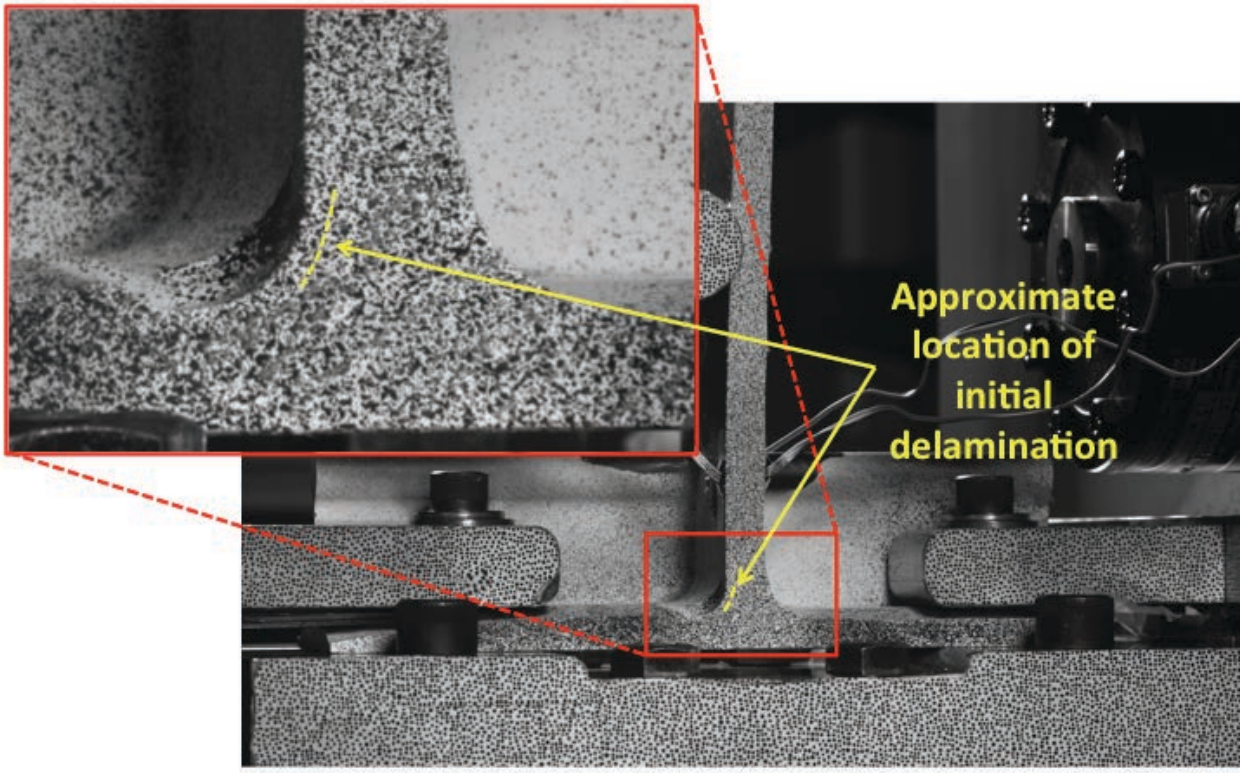

Figure C356. B1S1 image just after initial failure, back 12MP VIC data.

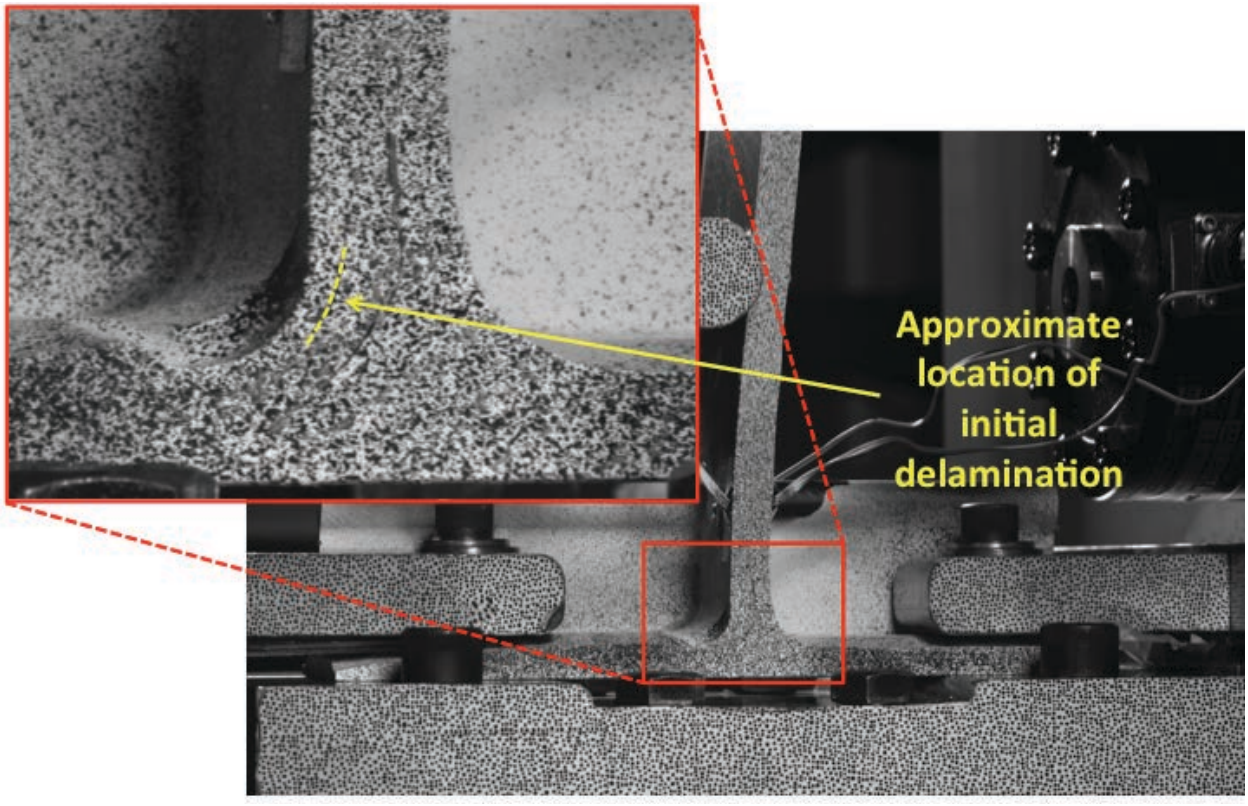

Figure C357. B1S1 image just after maximum load, back 12MP VIC data.

B1S2

This section presents the test data for the B1S2 test article.

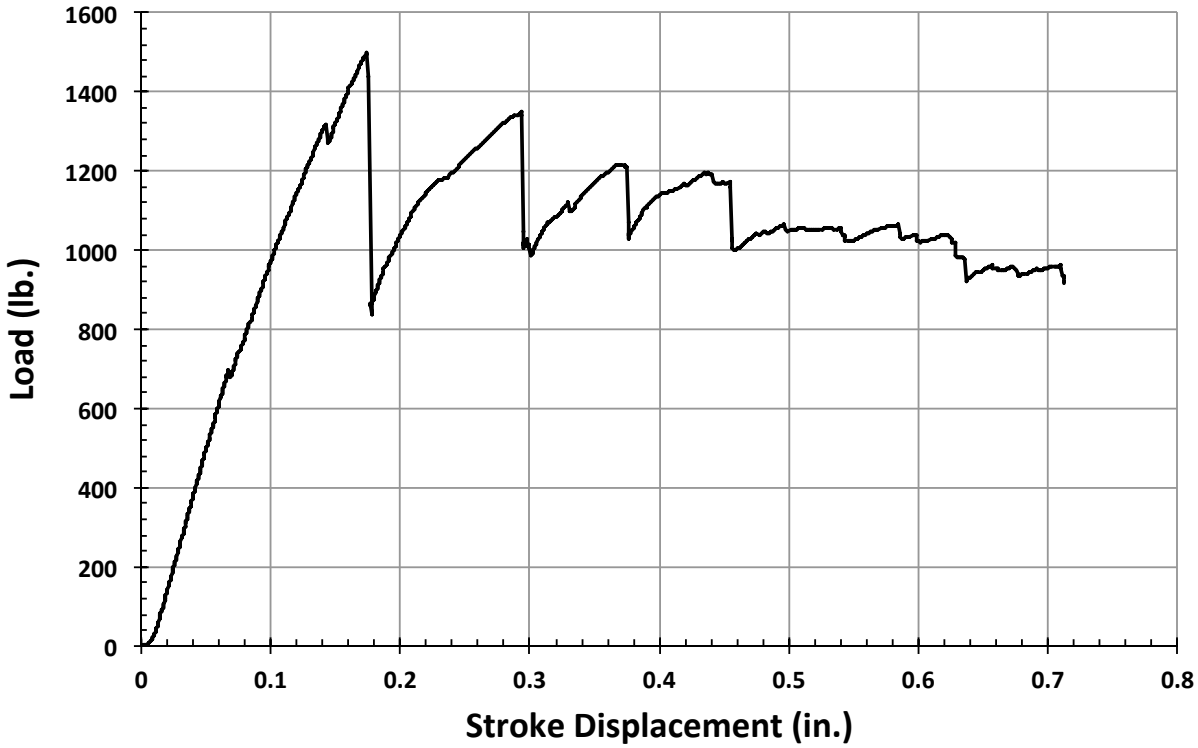

Figure C358. B1S2 load vs. stroke.

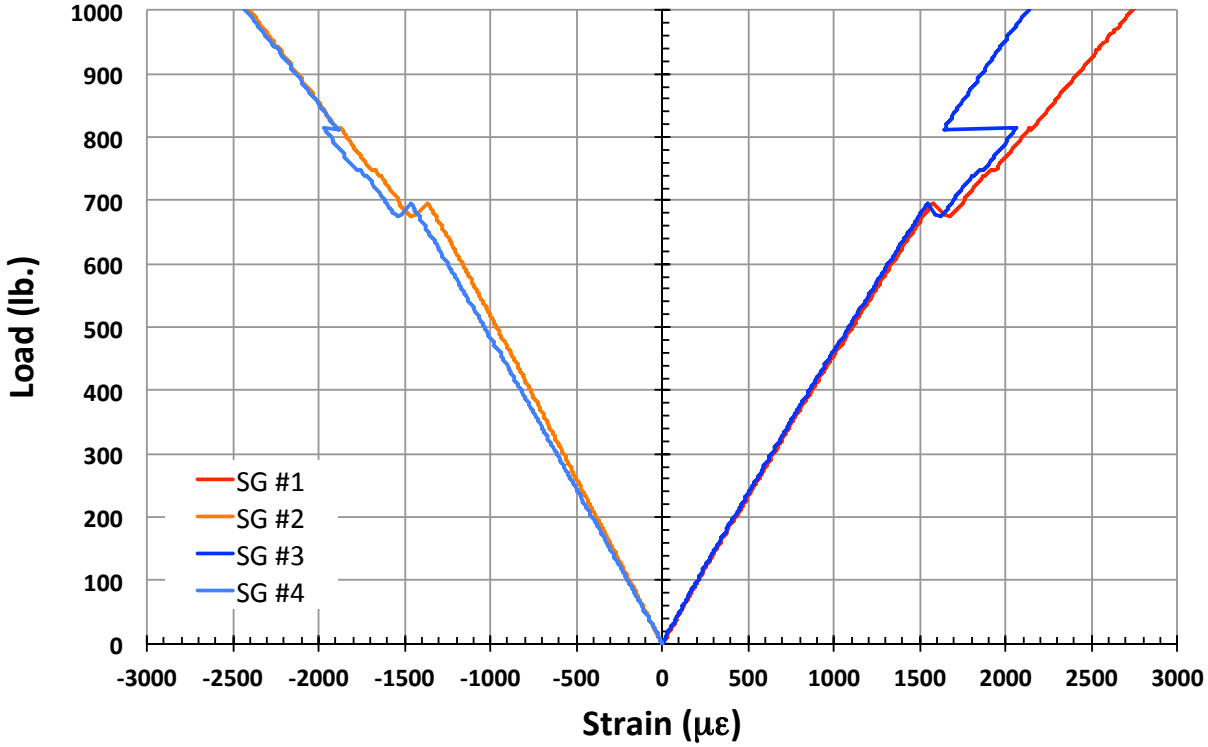

Figure C359. B1S2 load vs. strain, initial loading.

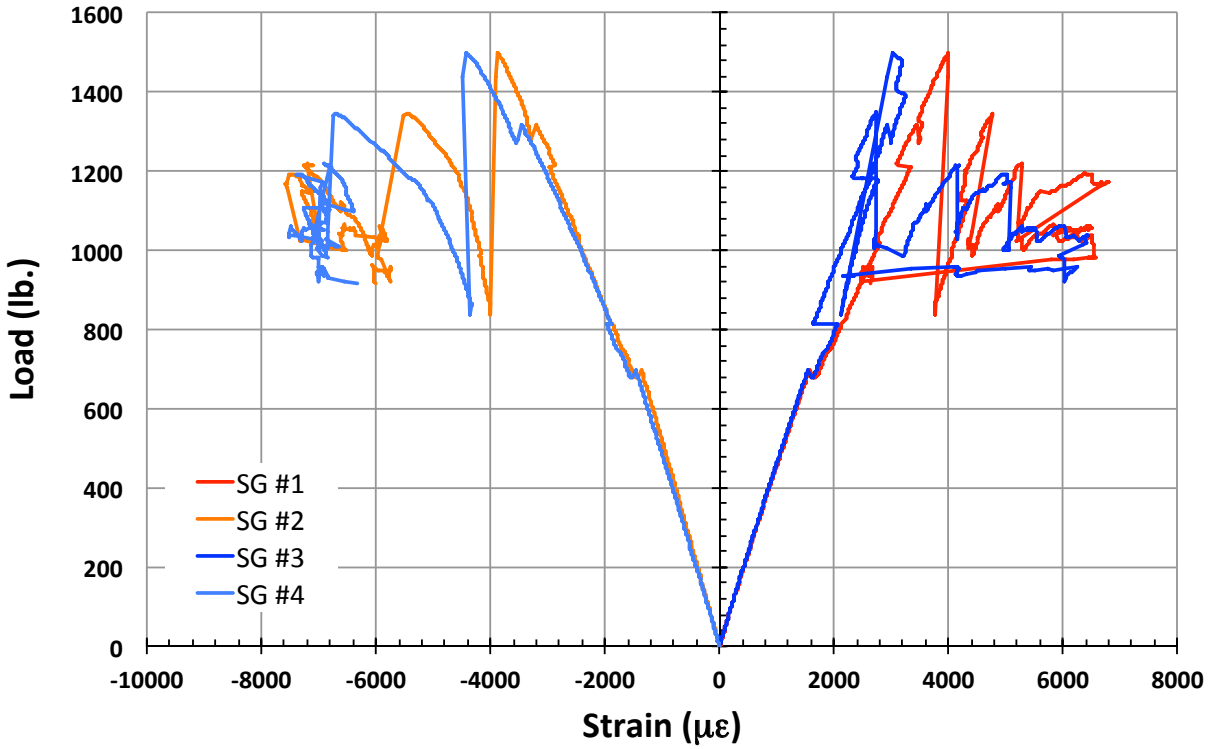

Figure C360. B1S2 load vs. strain.

B1S3

This section presents the test data for the B1S3 test article.

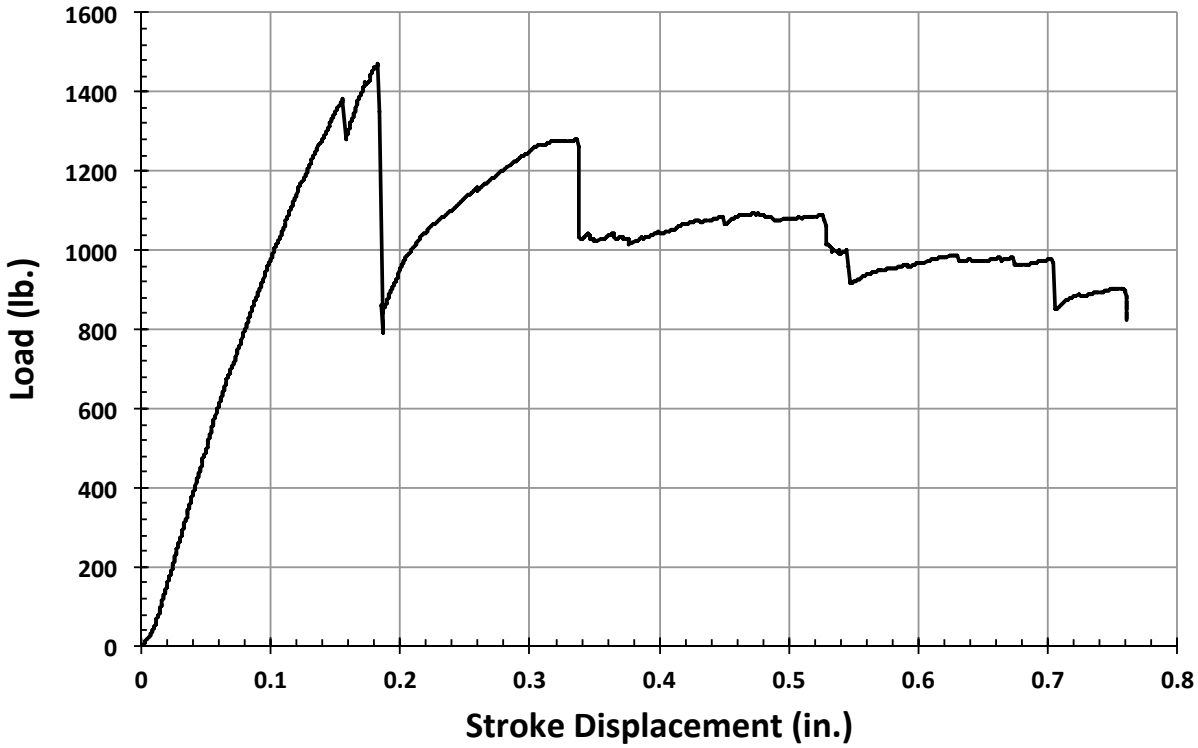

Figure C361. B1S3 load vs. stroke.

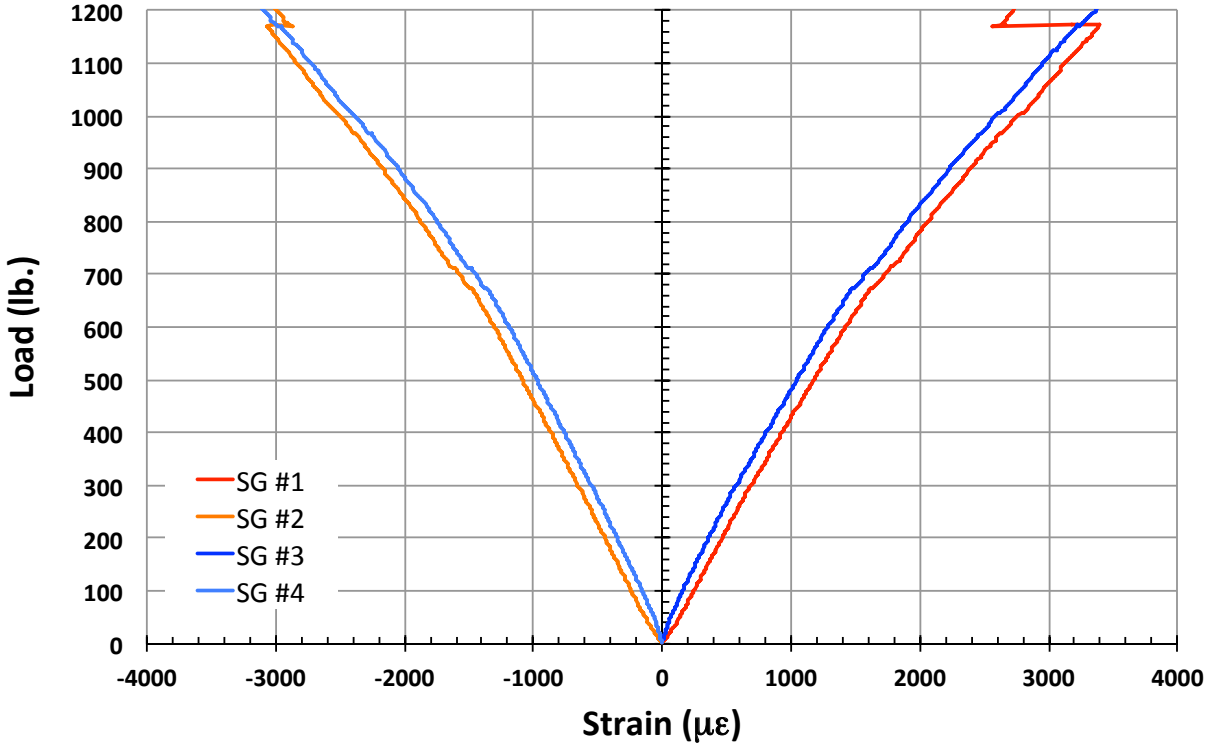

Figure C362. B1S3 load vs. strain, initial loading.

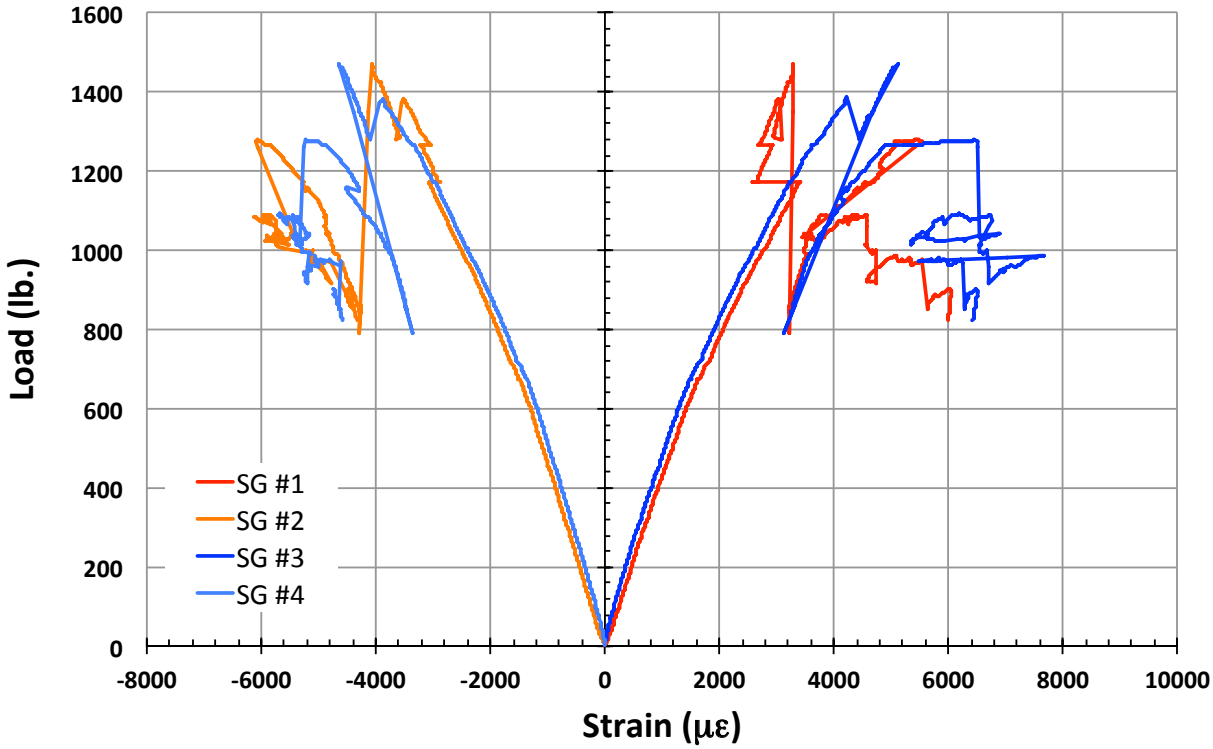

Figure C363. B1S3 load vs. strain.

B1N1

This section presents the test data for the B1N1 test article, and includes strain plots and failure images.

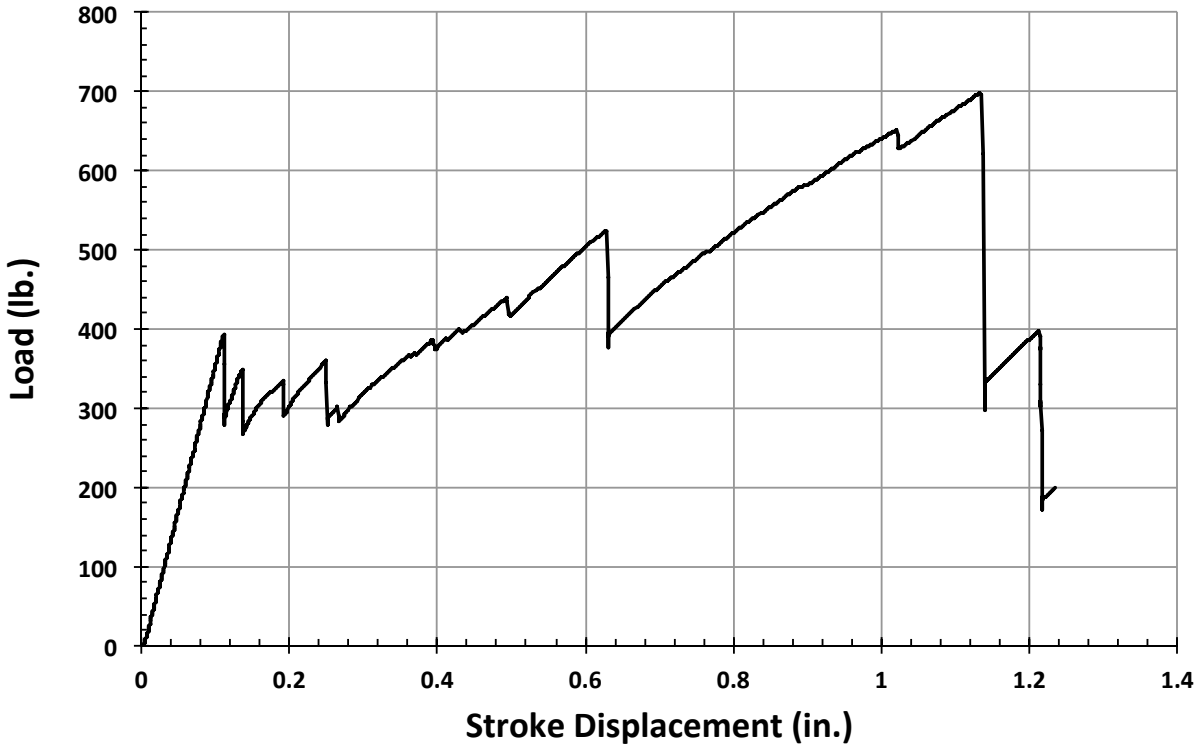

Figure C364. B1N1 load vs. stroke.

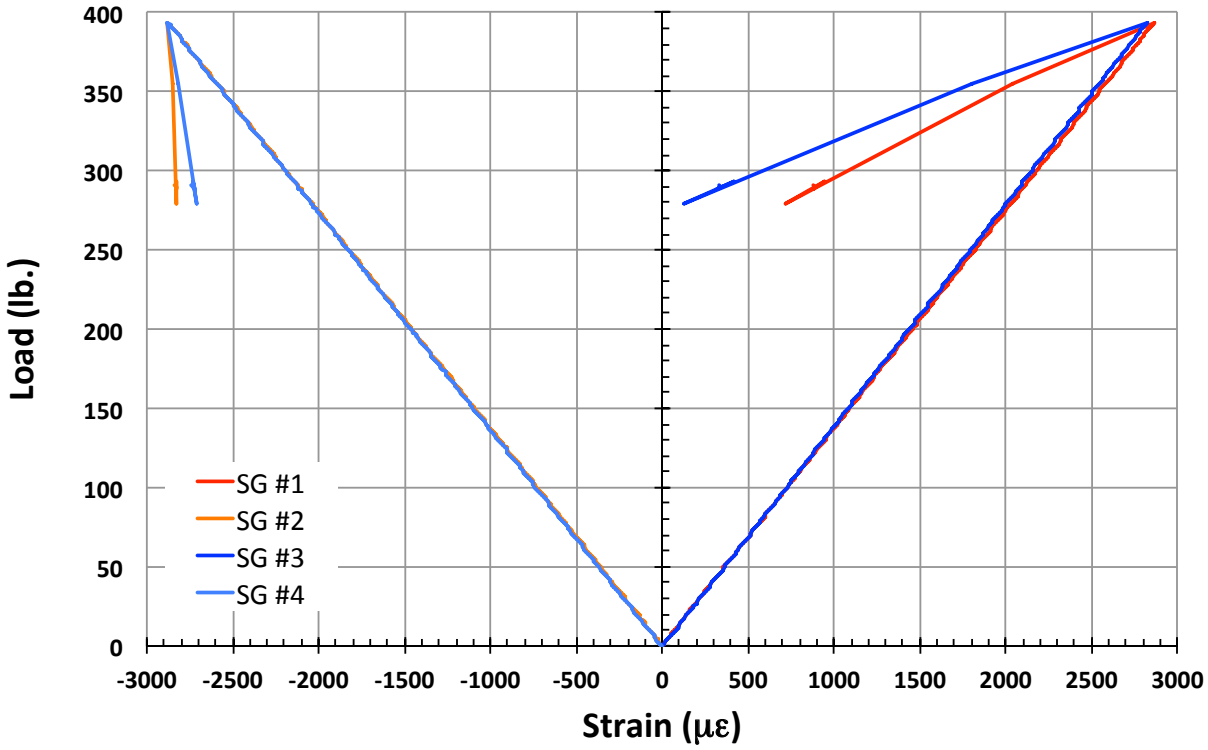

Figure C365. B1N1 load vs. strain, initial loading.

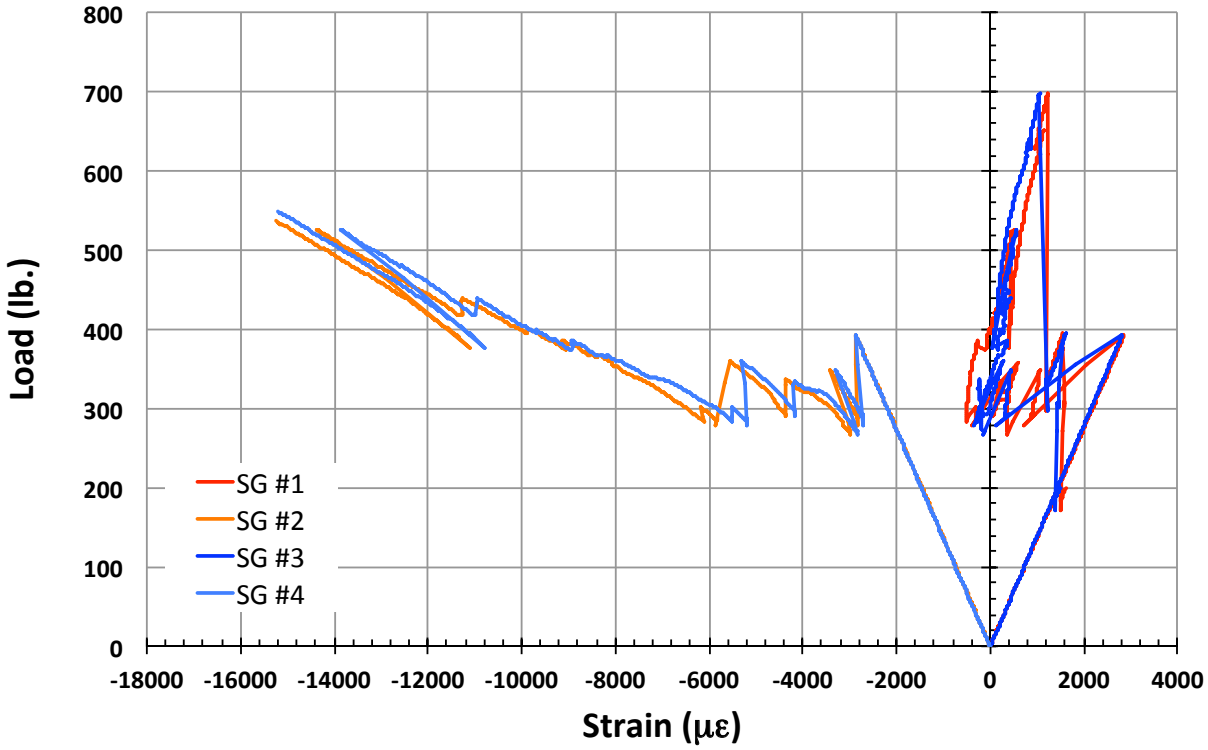

Figure C366. B1N1 load vs. strain.

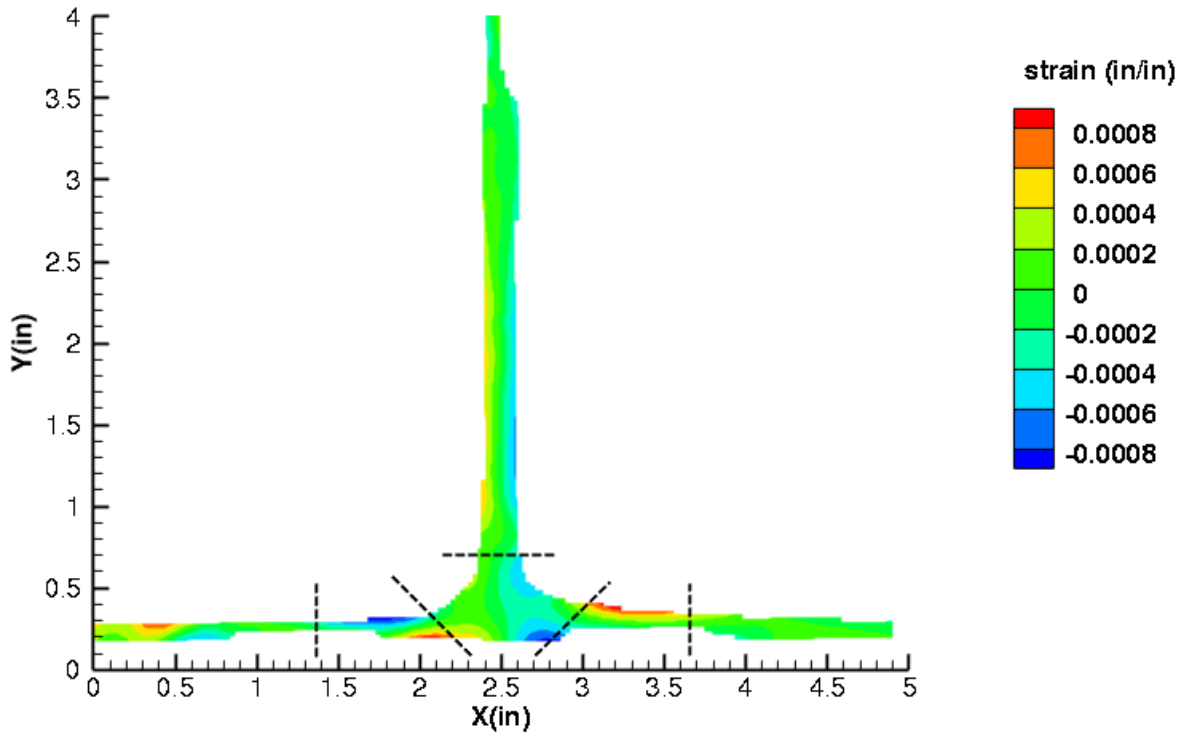

Figure C367. B1N1 strain contours for ε_{xx} at 395 lb. load, prior to initial failure, front 12MP VIC data.

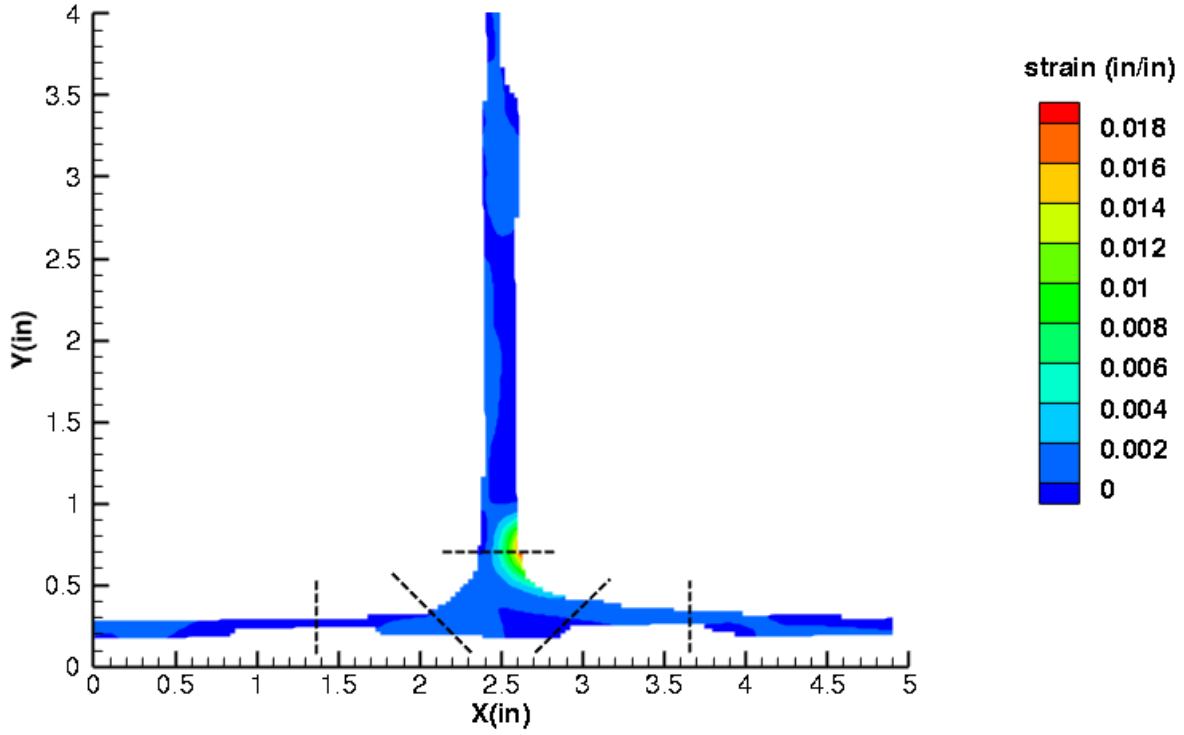

Figure C368. B1N1 strain contours for ε_{xx} at 289 lb. load, just after initial failure, front 12MP VIC data.

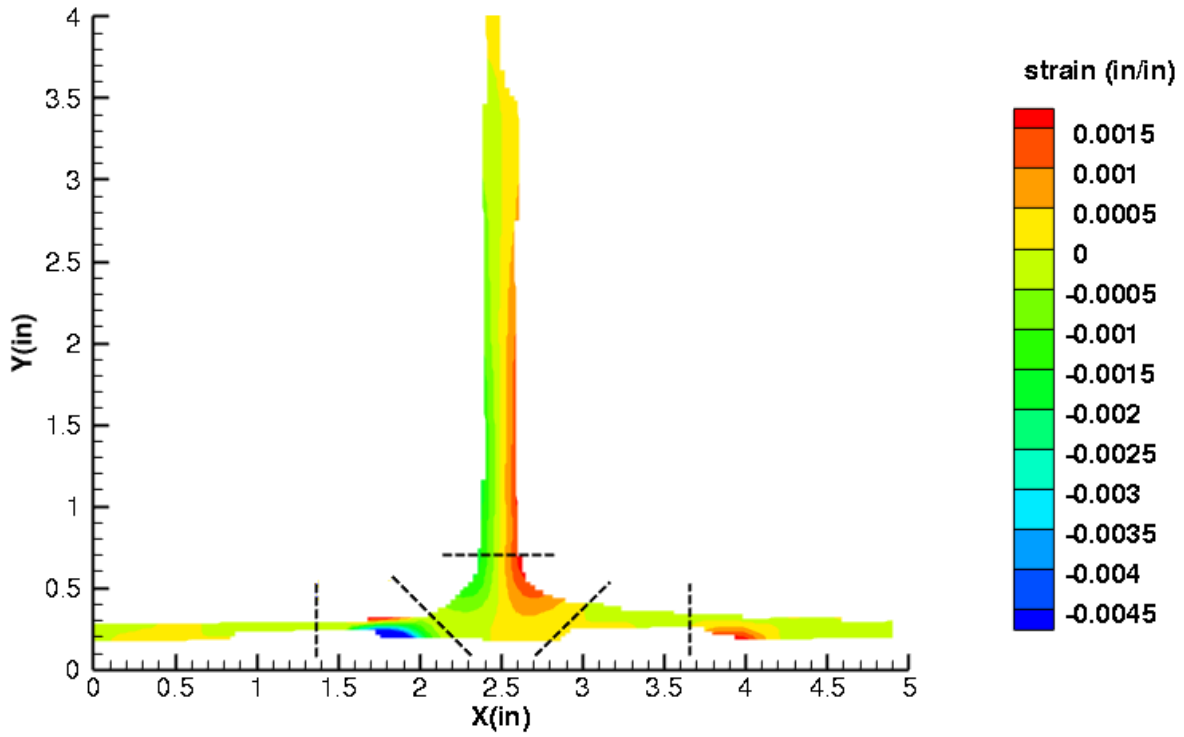

Figure C369. B1N1 strain contours for ε_{yy} at 395 lb. load, prior to initial failure, front 12MP VIC data.

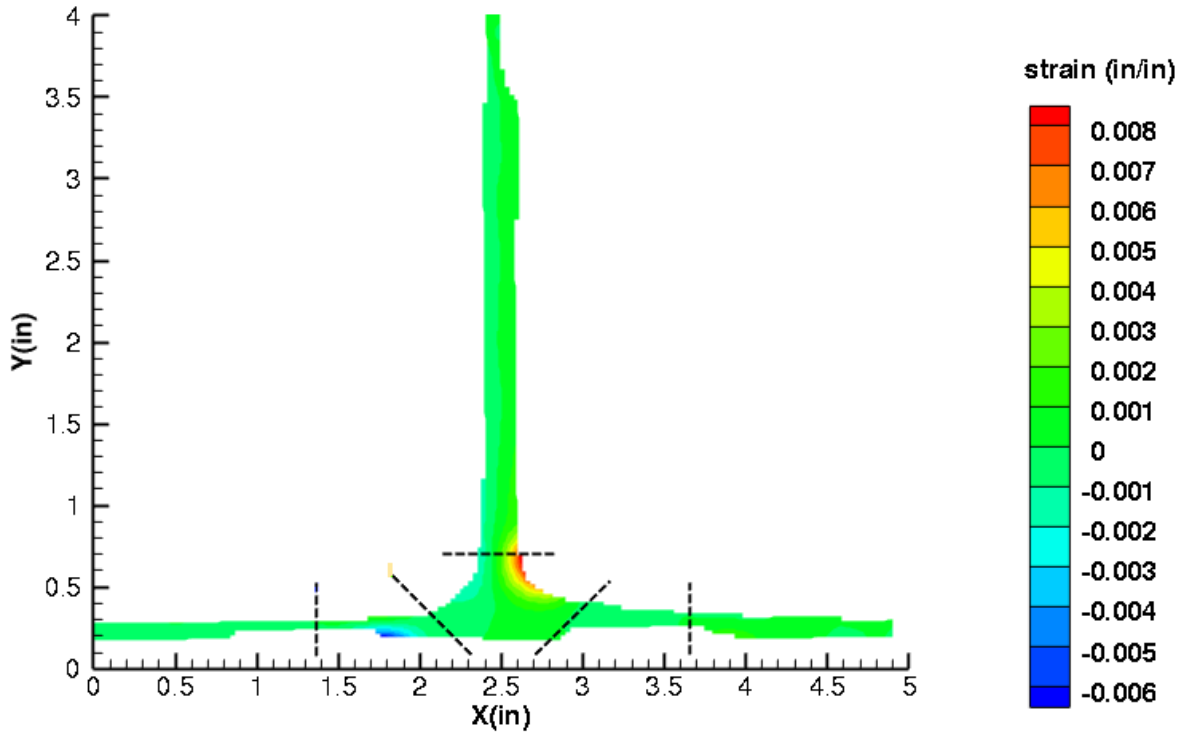

Figure C370. B1N1 strain contours for ε_{yy} at 289 lb. load, just after initial failure, front 12MP VIC data.

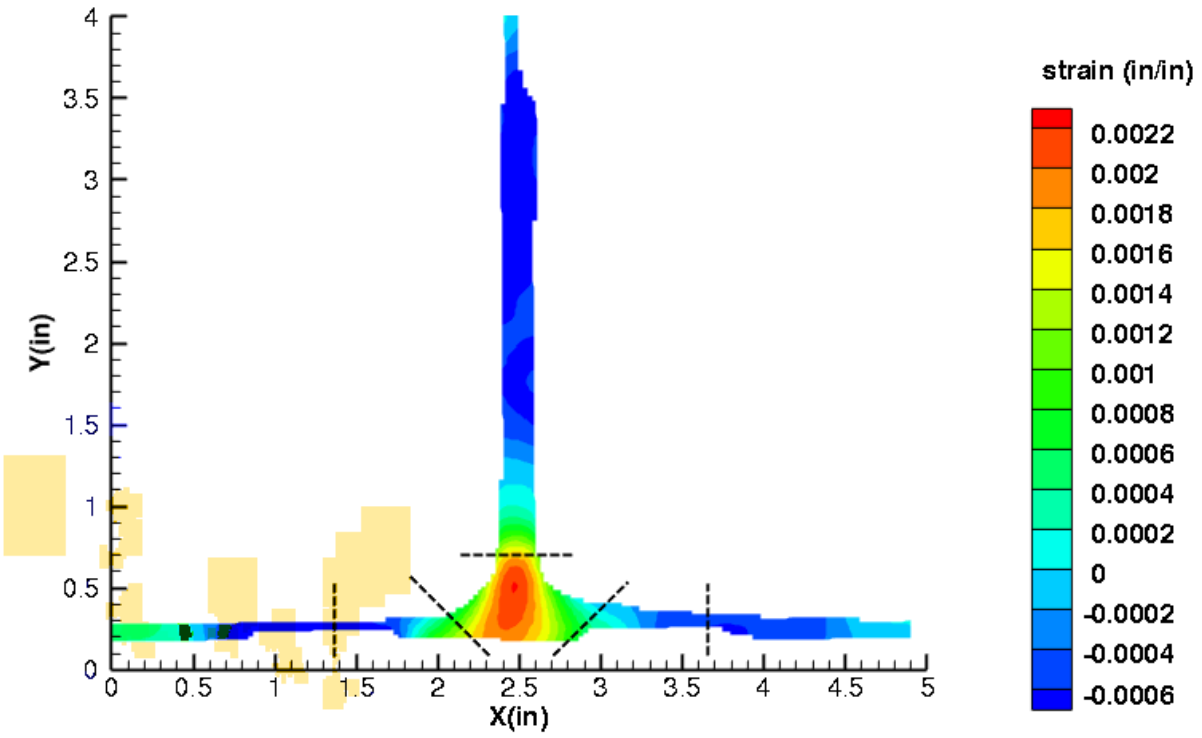

Figure C371. B1N1 strain contours for ε_{xy} at 395 lb. load, prior to initial failure, front 12MP VIC data.

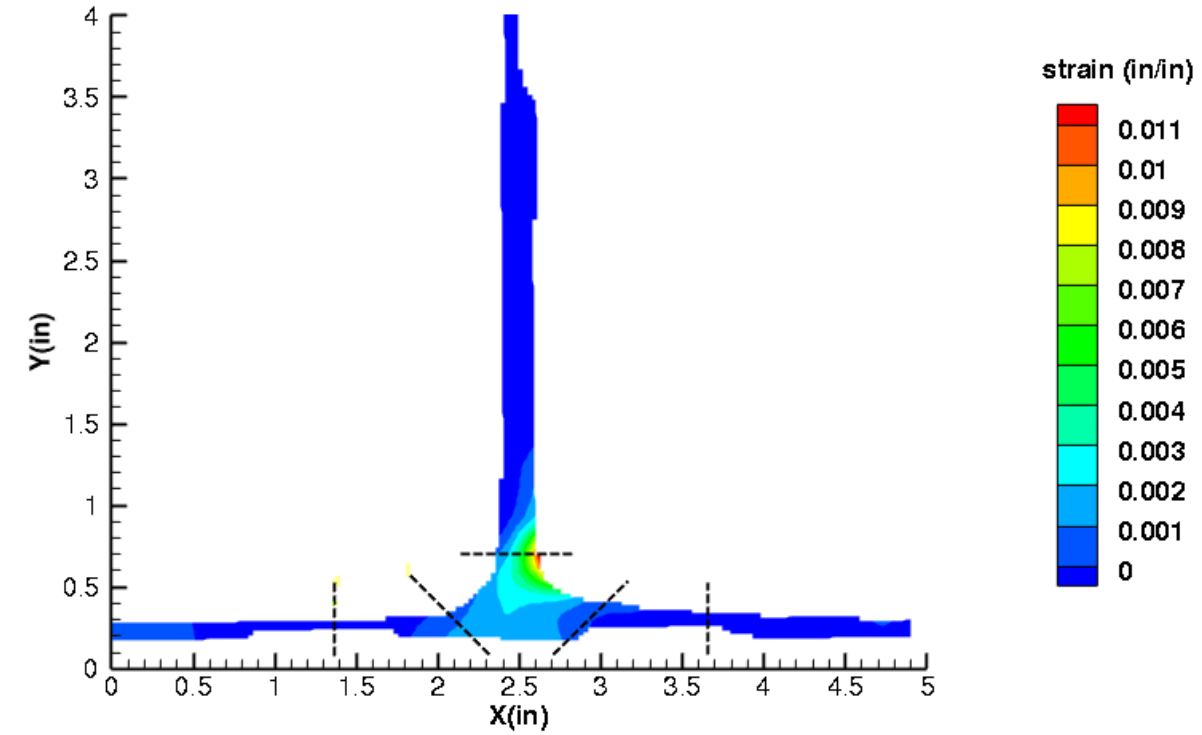

Figure C372. B1N1 strain contours for ε_{xy} at 289 lb. load, just after initial failure, front 12MP VIC data.

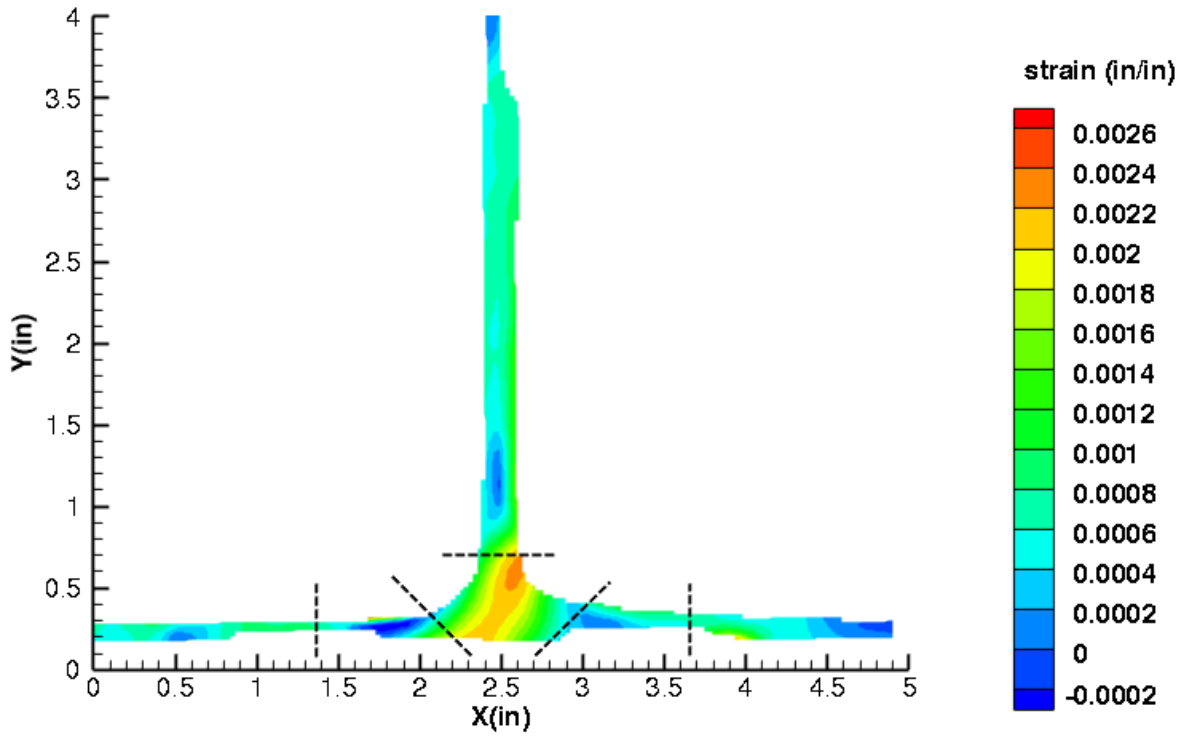

Figure C373. B1N1 strain contours for maximum principal strain at 395 lb. load, prior to initial failure, front 12MP VIC data.

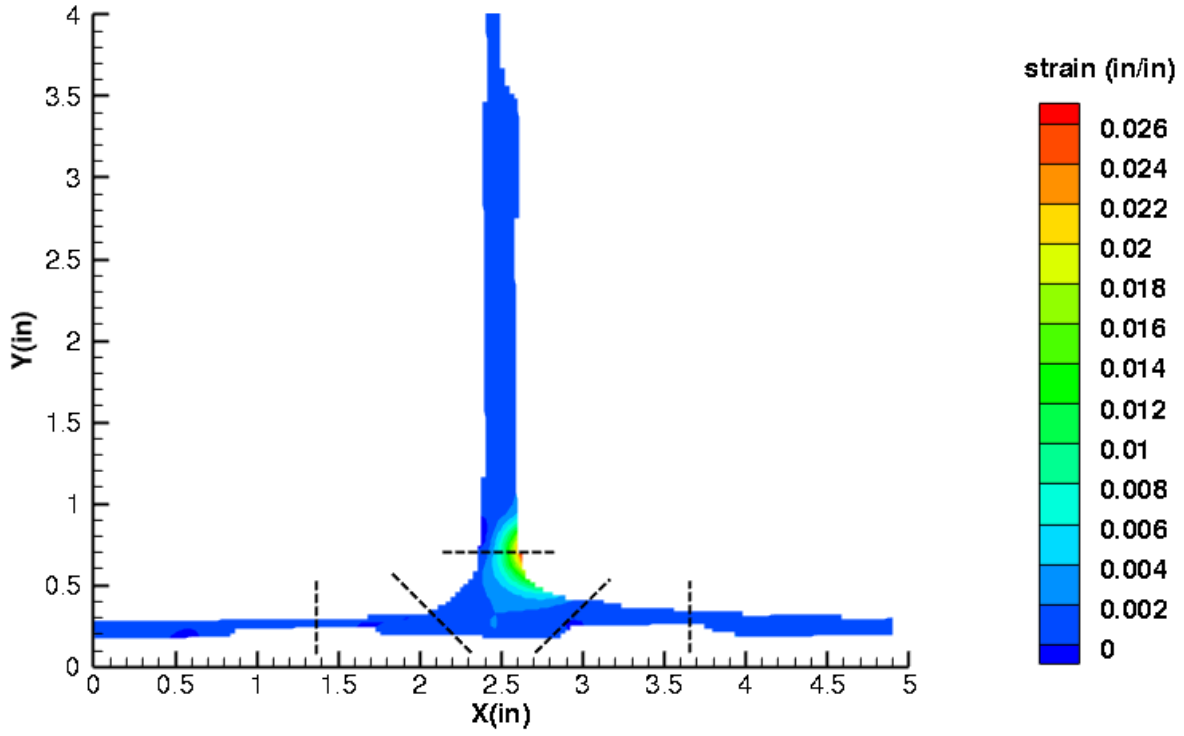

Figure C374. B1N1 strain contours for maximum principal strain at 289 lb. load, just after initial failure, front 12MP VIC data.

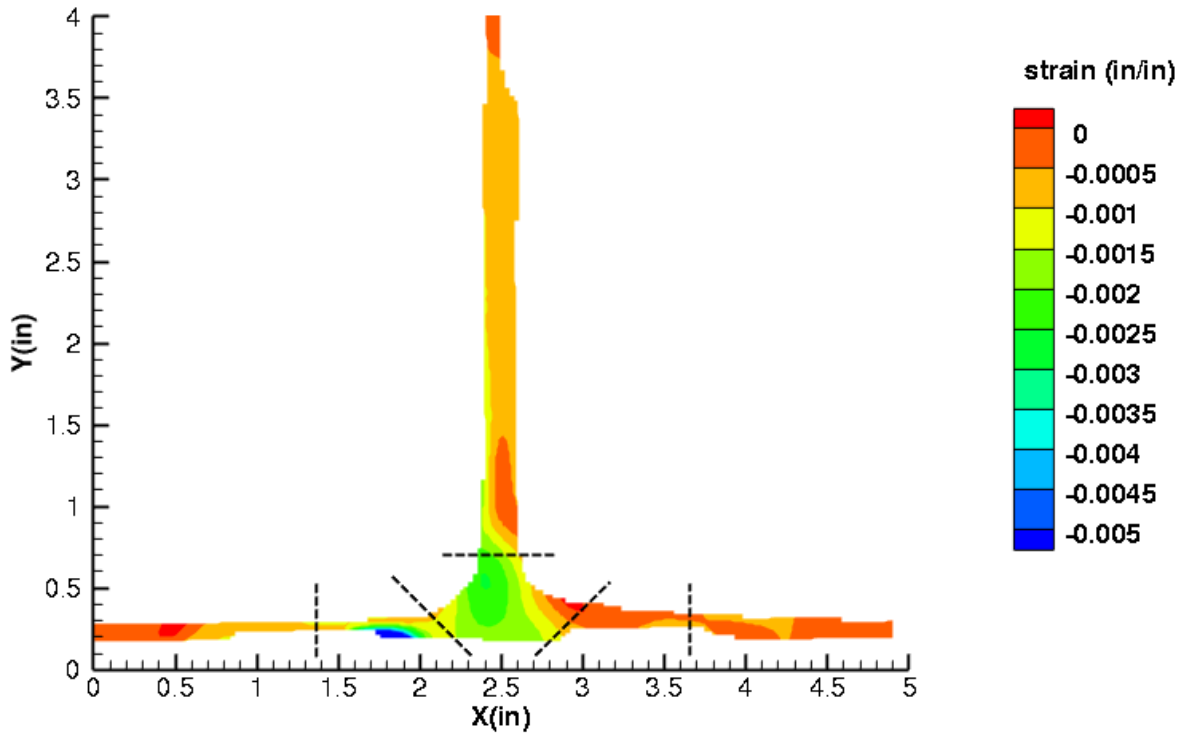

Figure C375. B1N1 strain contours for minimum principal strain at 395 lb. load, prior to initial failure, front 12MP VIC data.

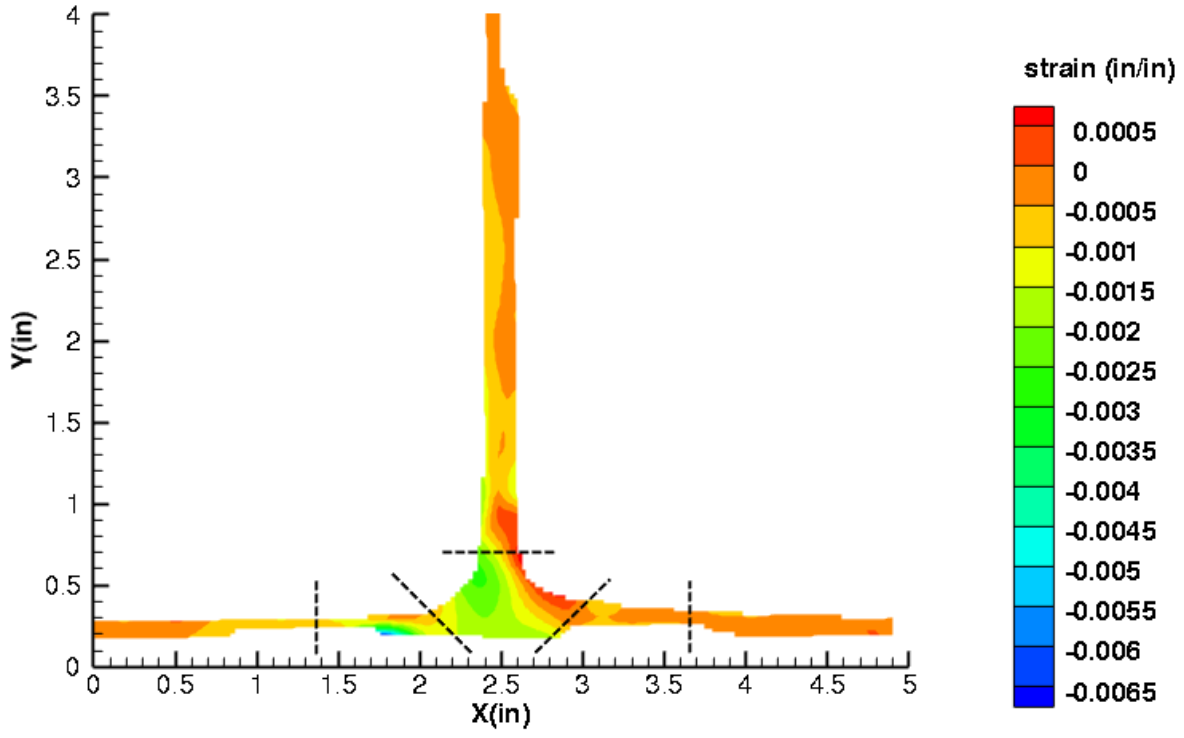

Figure C376. B1N1 strain contours for minimum principal strain at 289 lb. load, just after initial failure, front 12MP VIC data.

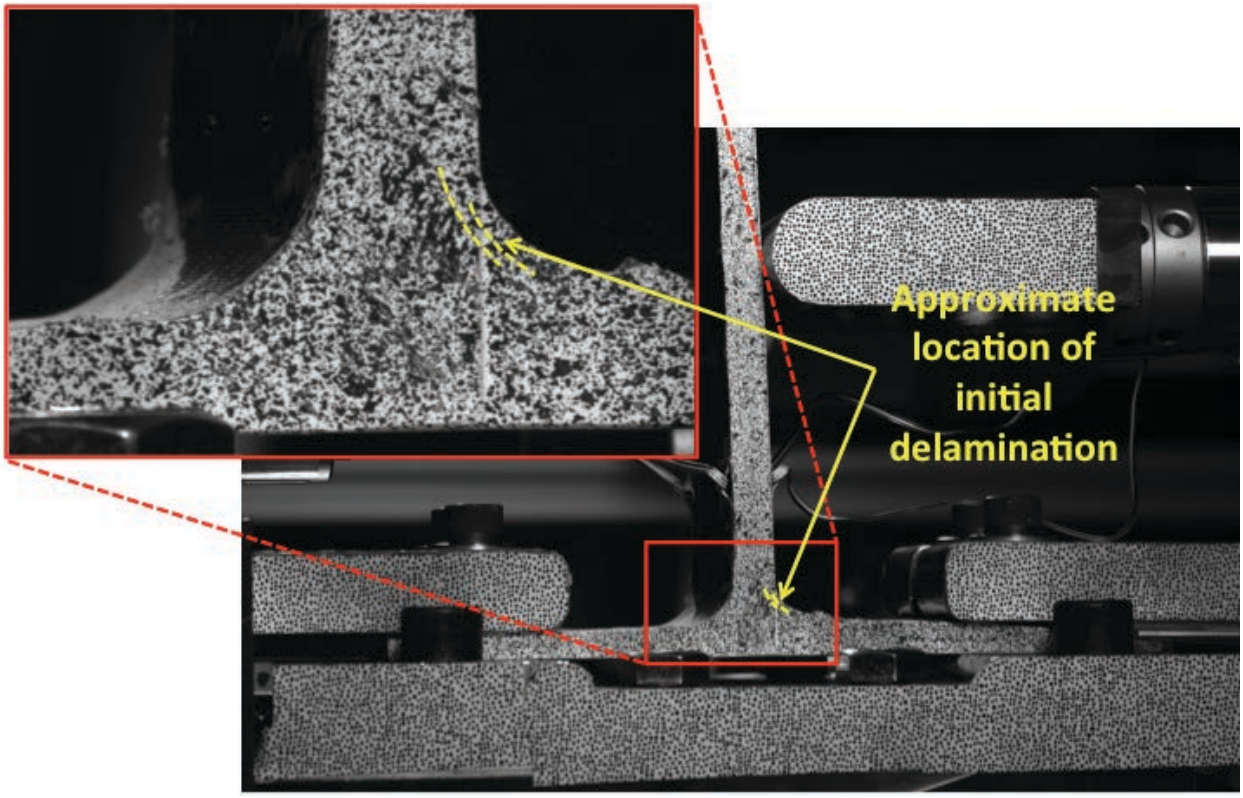

Figure C377. B1N1 image just after initial failure, front 12MP VIC data.

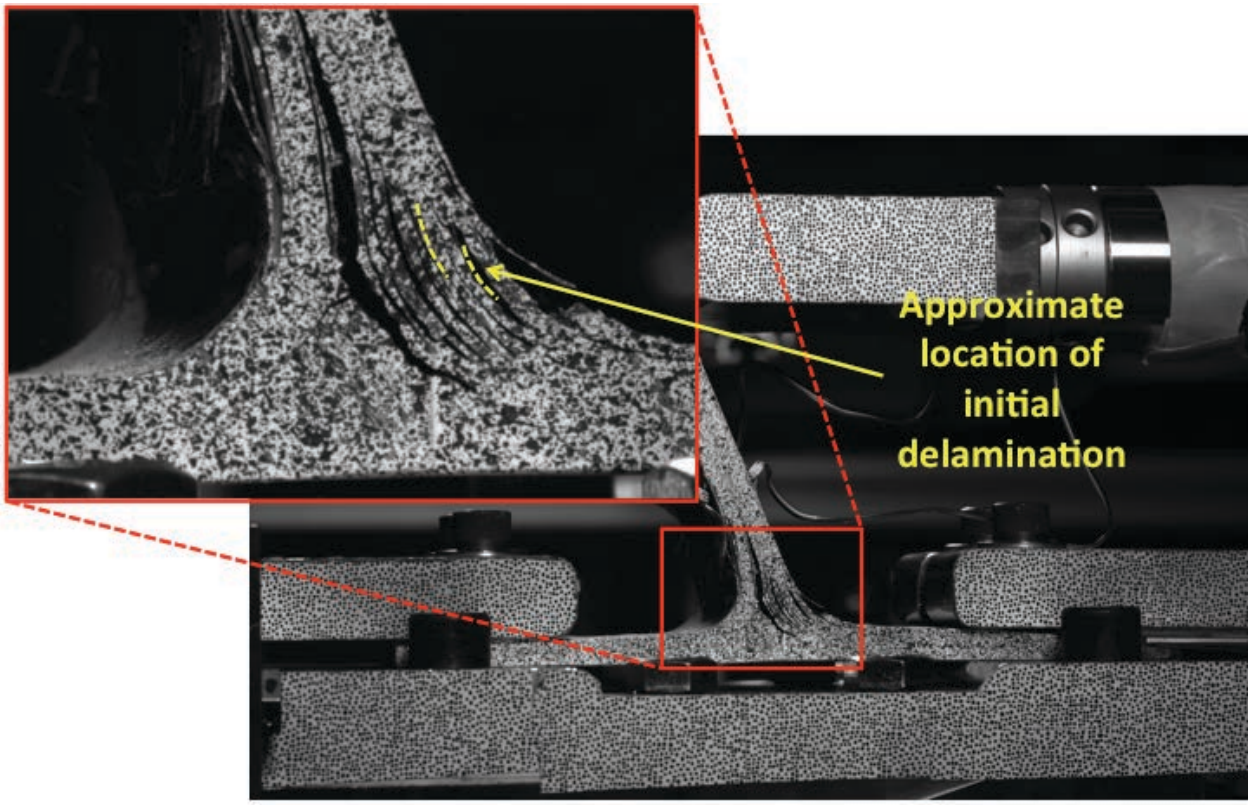

Figure C378. B1N1 image just after maximum load, front 12MP VIC data.

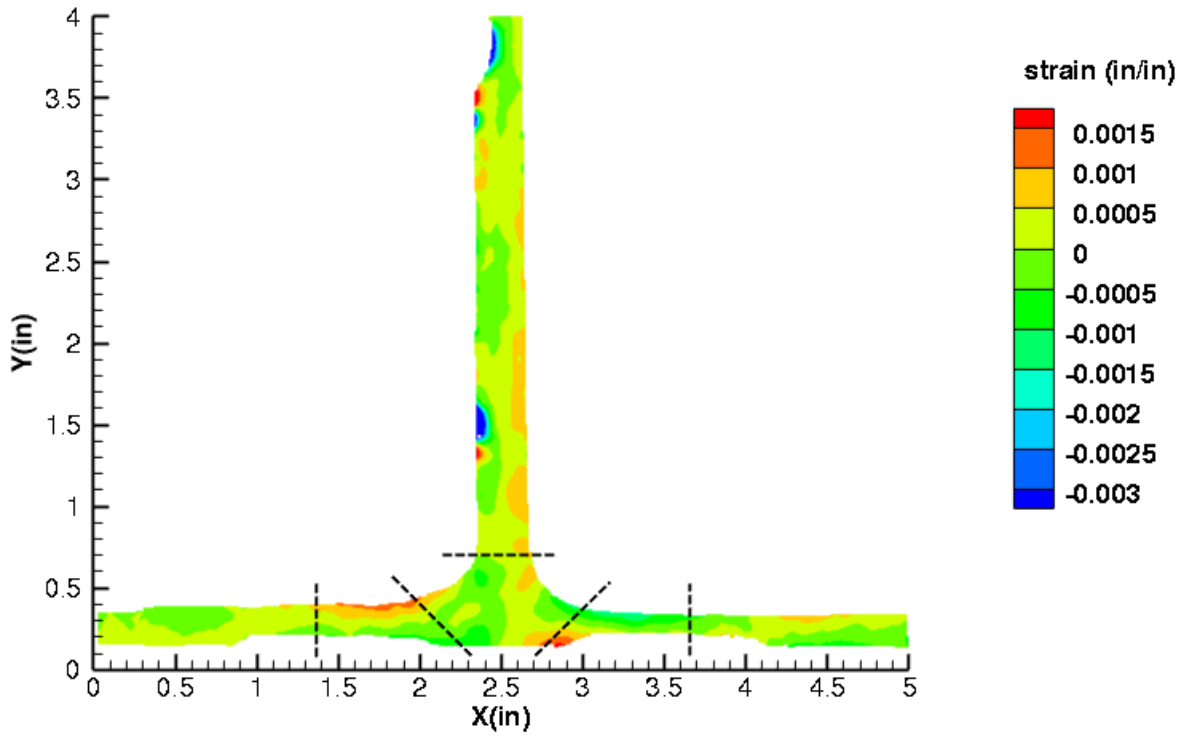

Figure C379. B1N1 strain contours for ε_{xx} at 395 lb. load, prior to initial failure, back 12MP VIC data.

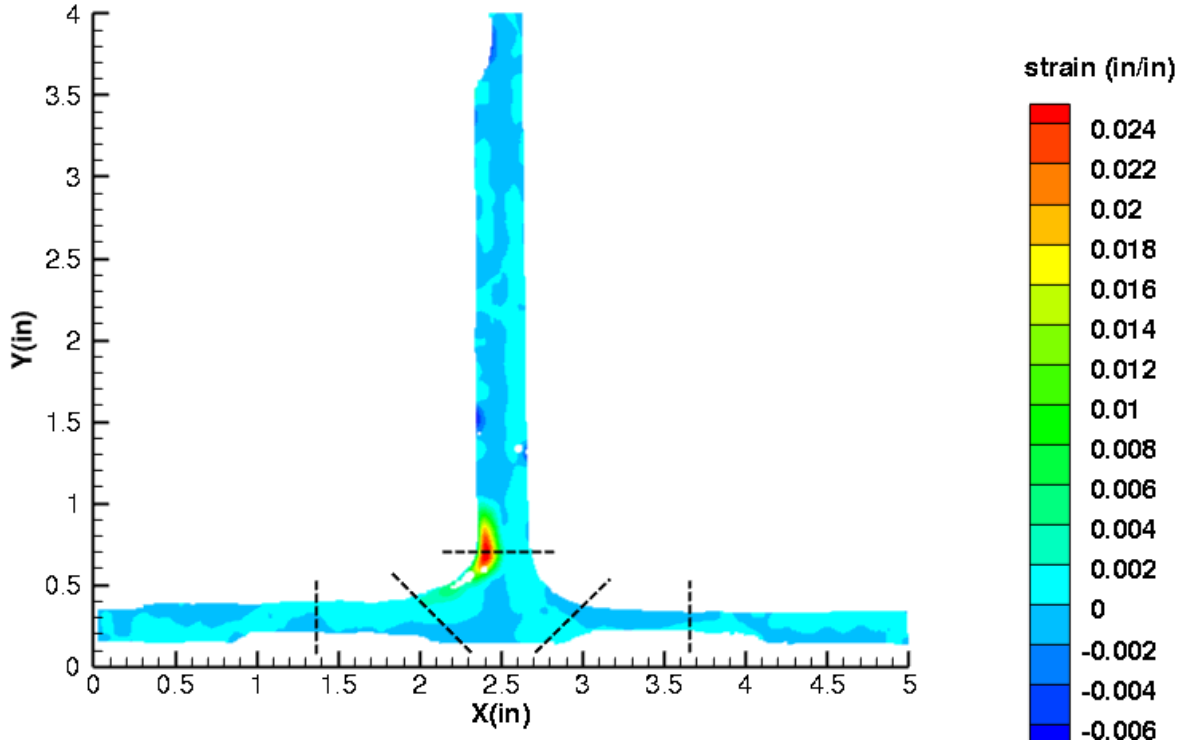

Figure C380. B1N1 strain contours for ε_{xx} at 289 lb. load, just after initial failure, back 12MP VIC data.

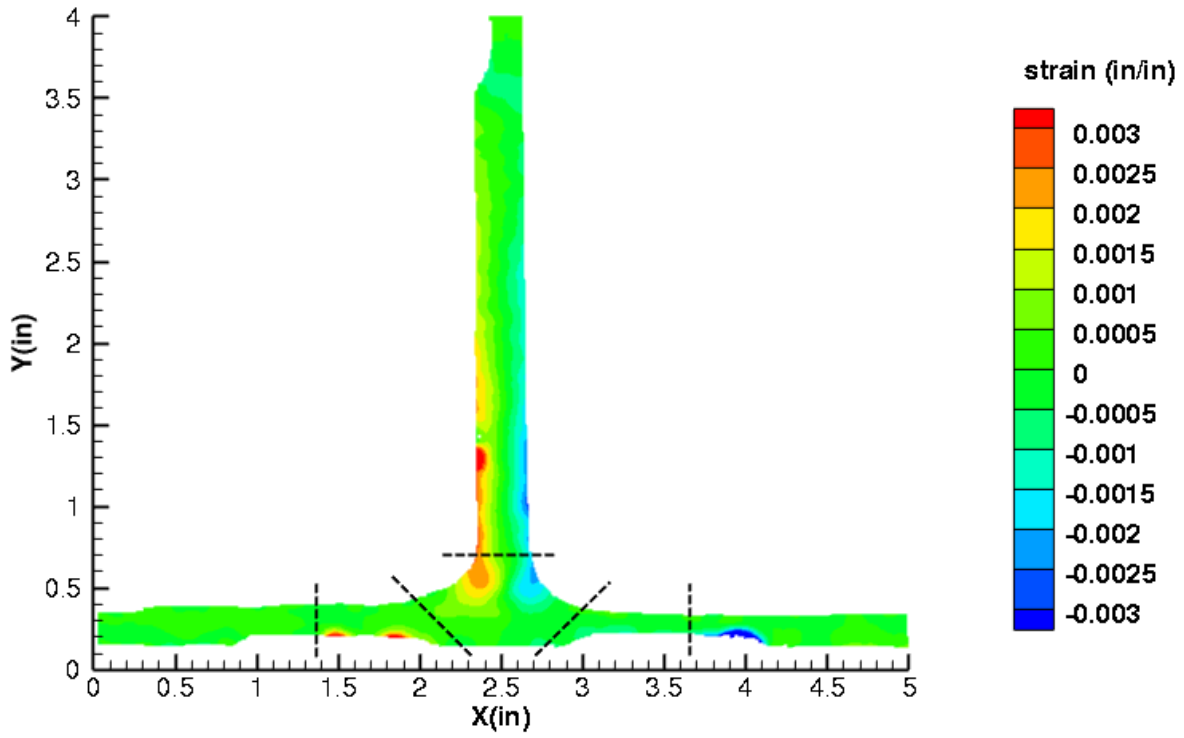

Figure C381. B1N1 strain contours for ε_{yy} at 395 lb. load, prior to initial failure, back 12MP VIC data.

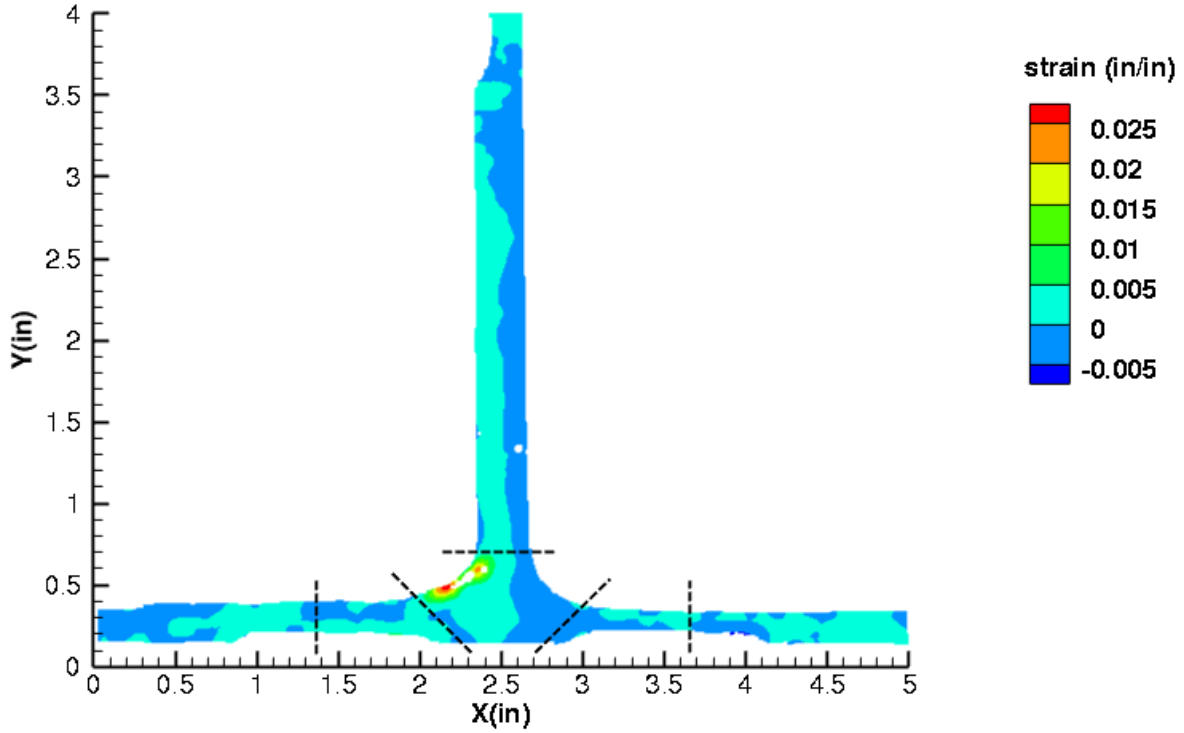

Figure C382. B1N1 strain contours for ε_{yy} at 289 lb. load, just after initial failure, back 12MP VIC data.

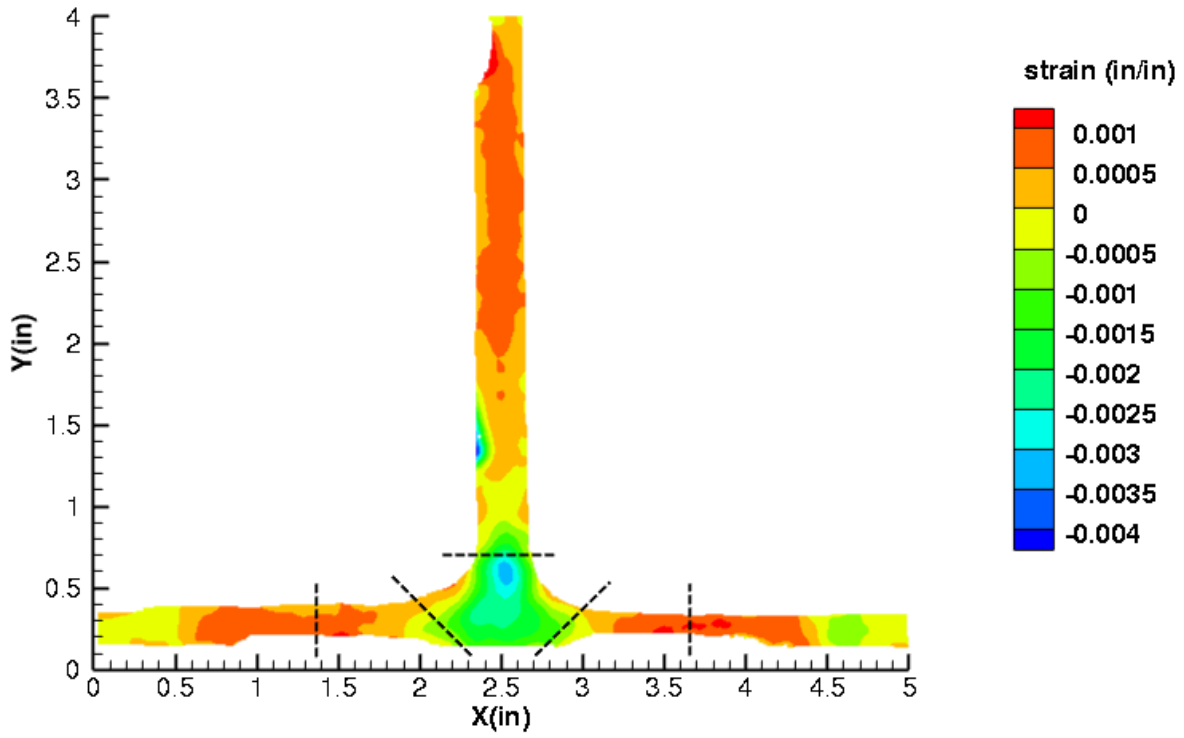

Figure C383. B1N1 strain contours for ε_{xy} at 295 lb. load, prior to initial failure, back 12MP VIC data.

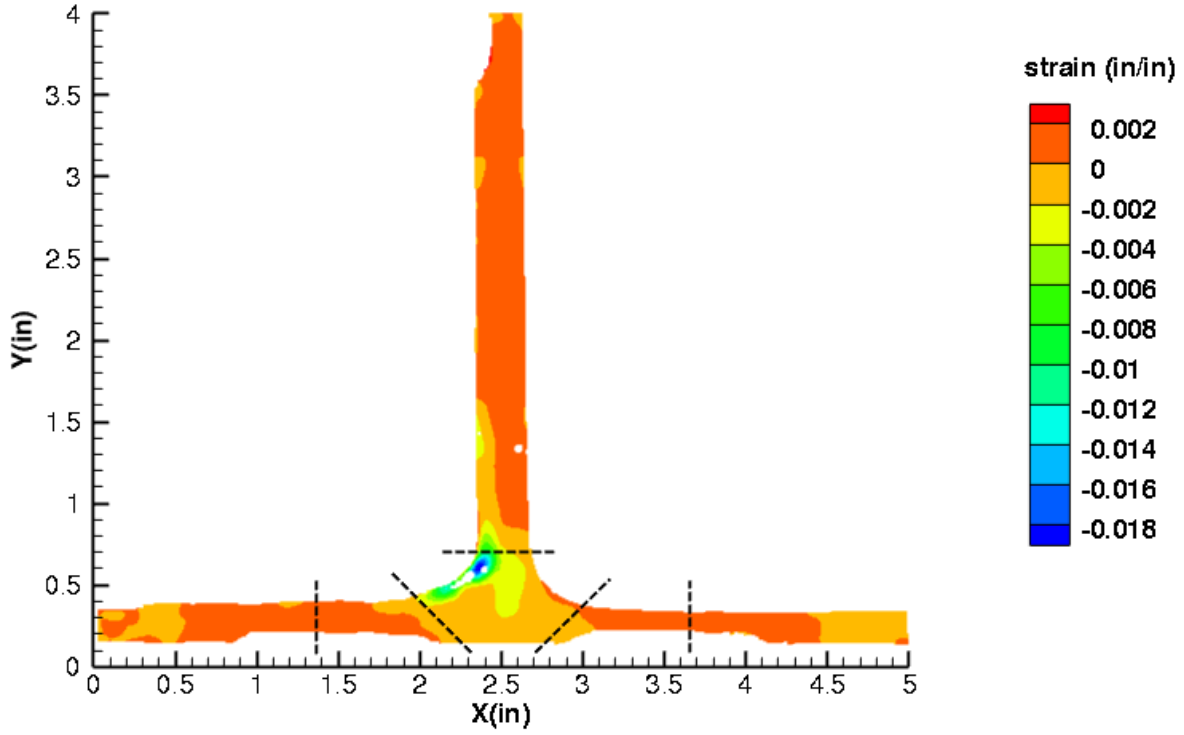

Figure C384. B1N1 strain contours for ε_{xy} at 289 lb. load, just after initial failure, back 12MP VIC data.

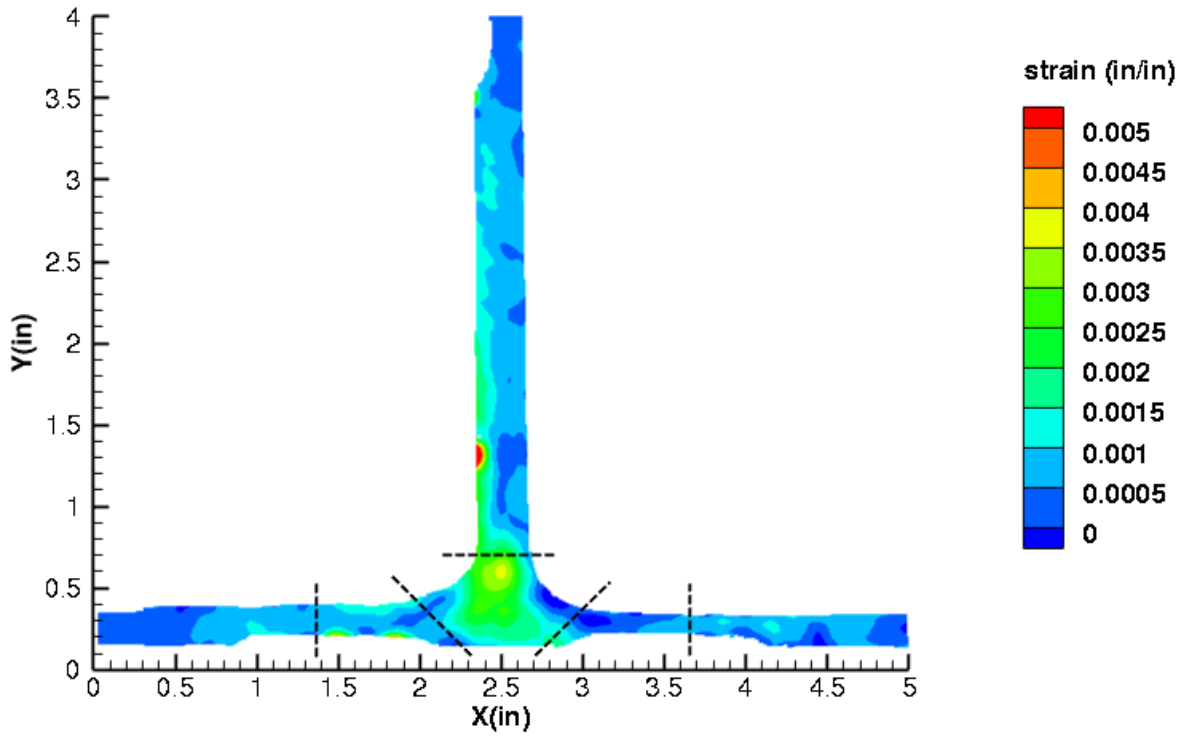

Figure C385. B1N1 strain contours for maximum principal strain at 395 lb. load, prior to initial failure, back 12MP VIC data.

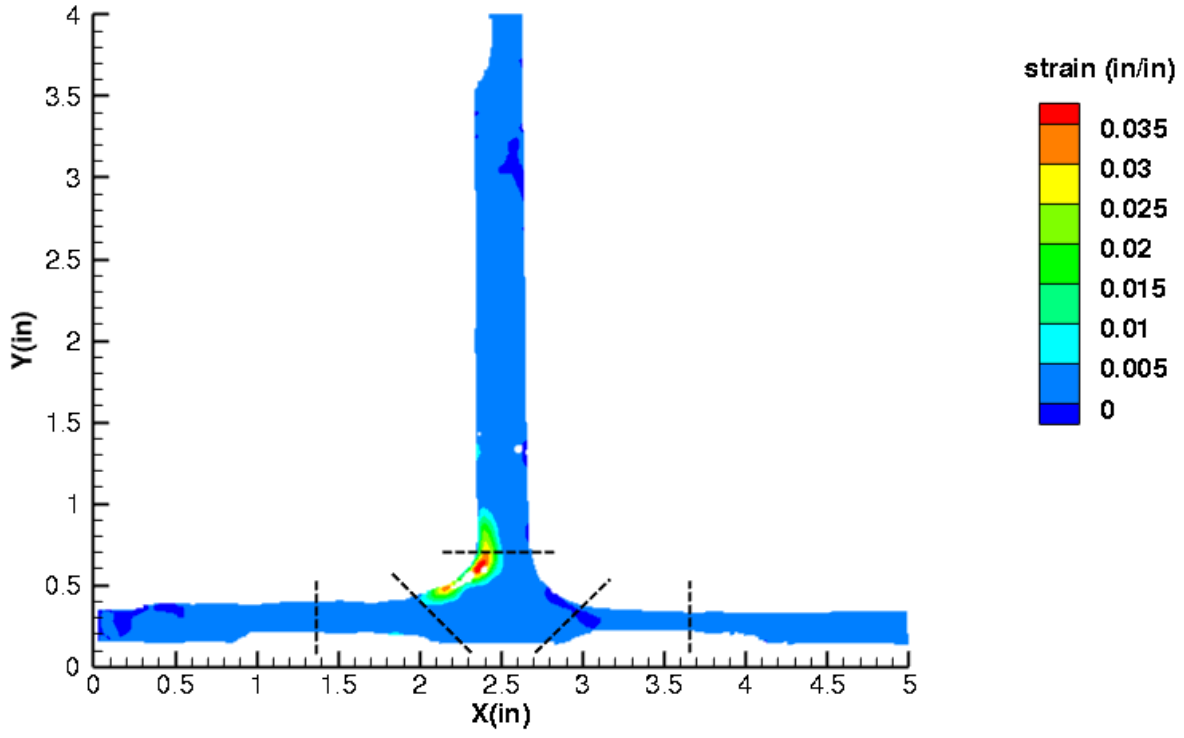

Figure C386. B1N1 strain contours for maximum principal strain at 289 lb. load, just after initial failure, back 12MP VIC data.

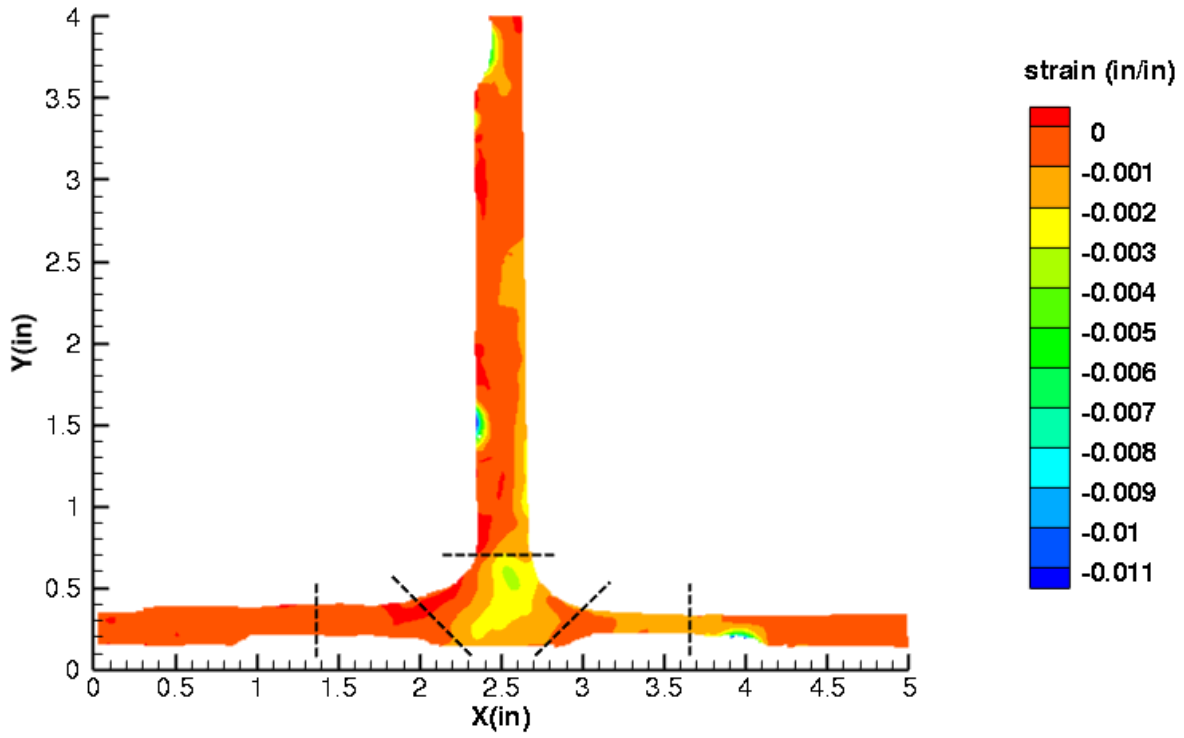

Figure C387. B1N1 strain contours for minimum principal strain at 395 lb. load, prior to initial failure, back 12MP VIC data.

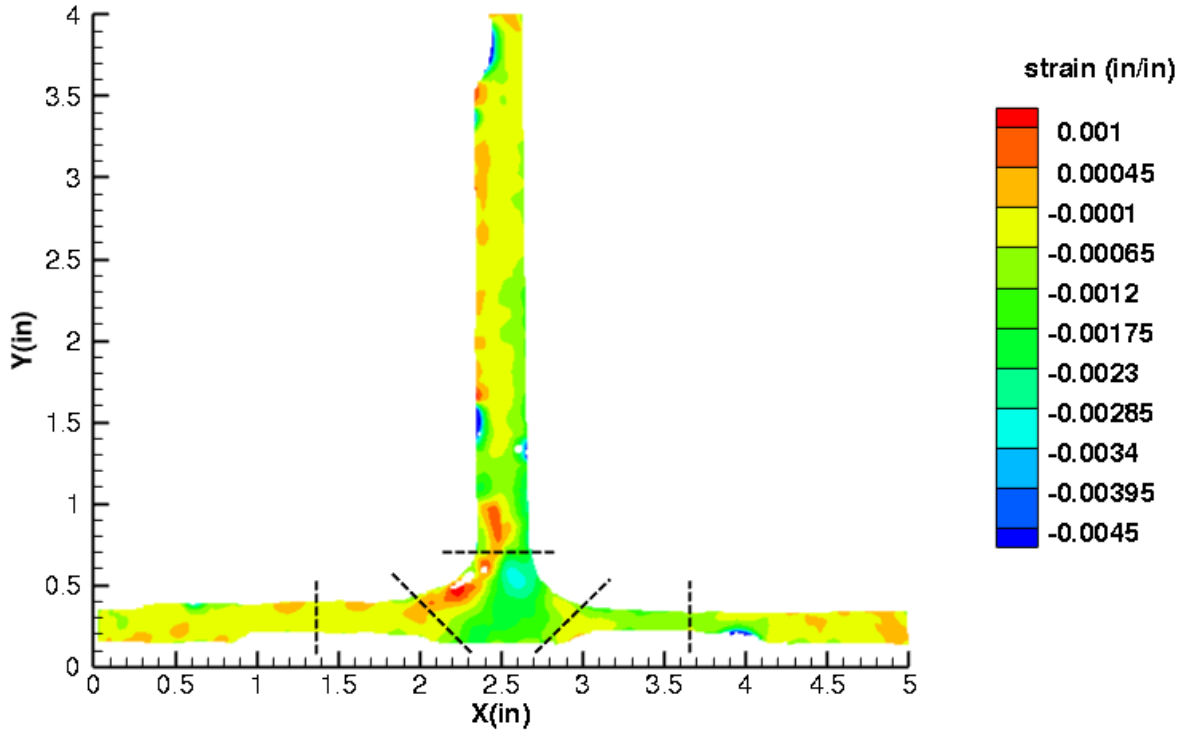

Figure C388. B1N1 strain contours for minimum principal strain at 289 lb. load, just after initial failure, back 12MP VIC data.

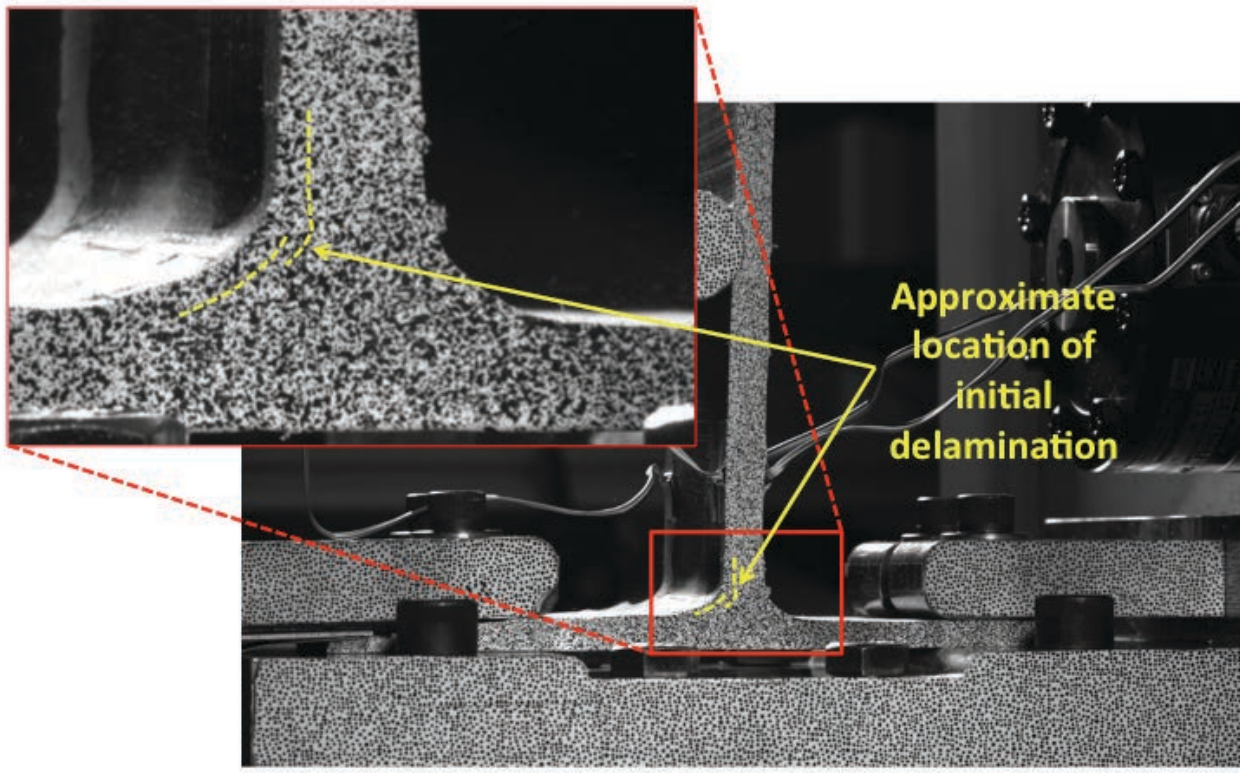

Figure C389. B1N1 image just after initial failure, back 12MP VIC data.

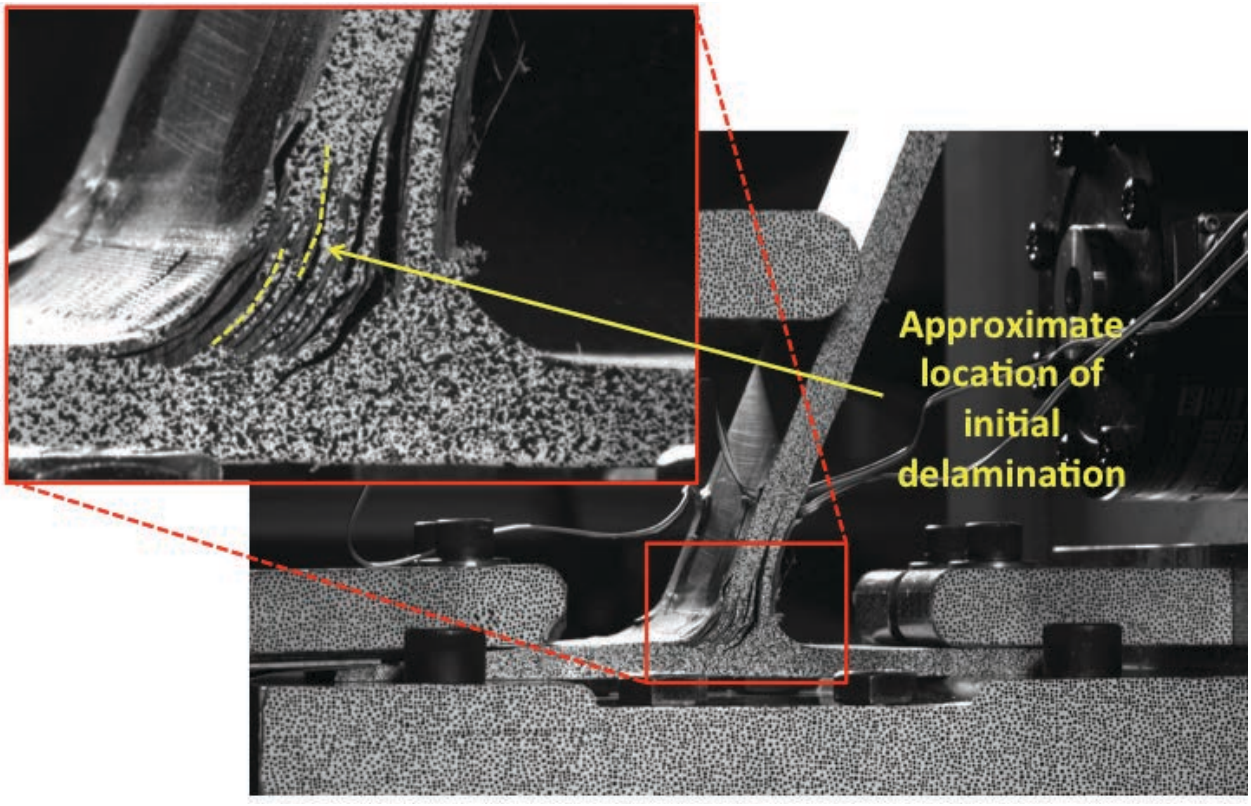

Figure C390. B1N1 image just after maximum load, back 12MP VIC data.

B1N2

This section presents the test data for the B1N2 test article.

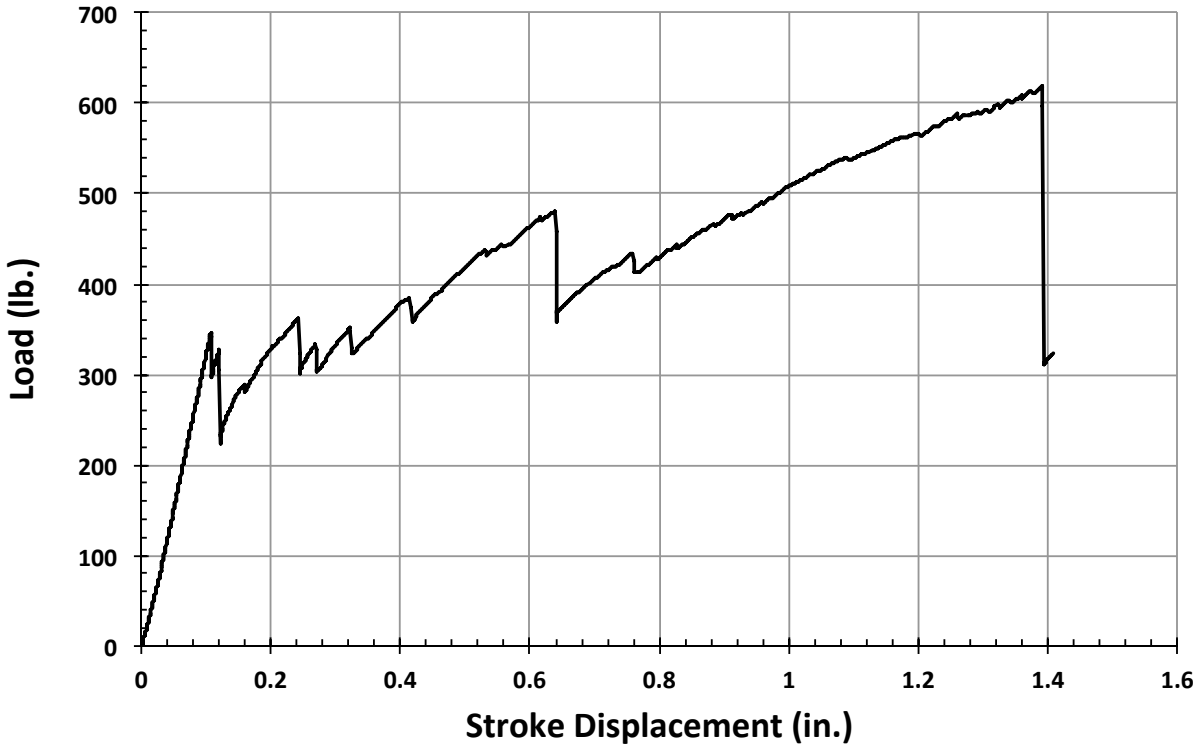

Figure C391. B1N2 load vs. stroke.

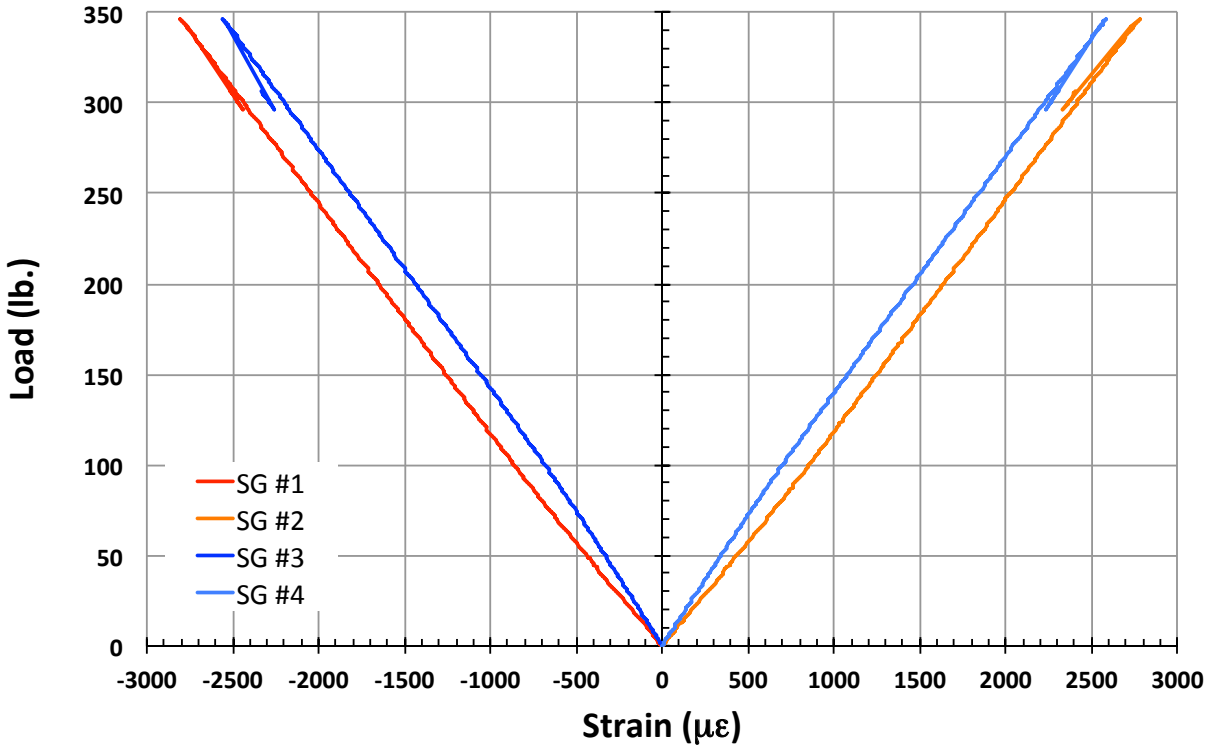

Figure C392. B1N2 load vs. strain, initial loading.

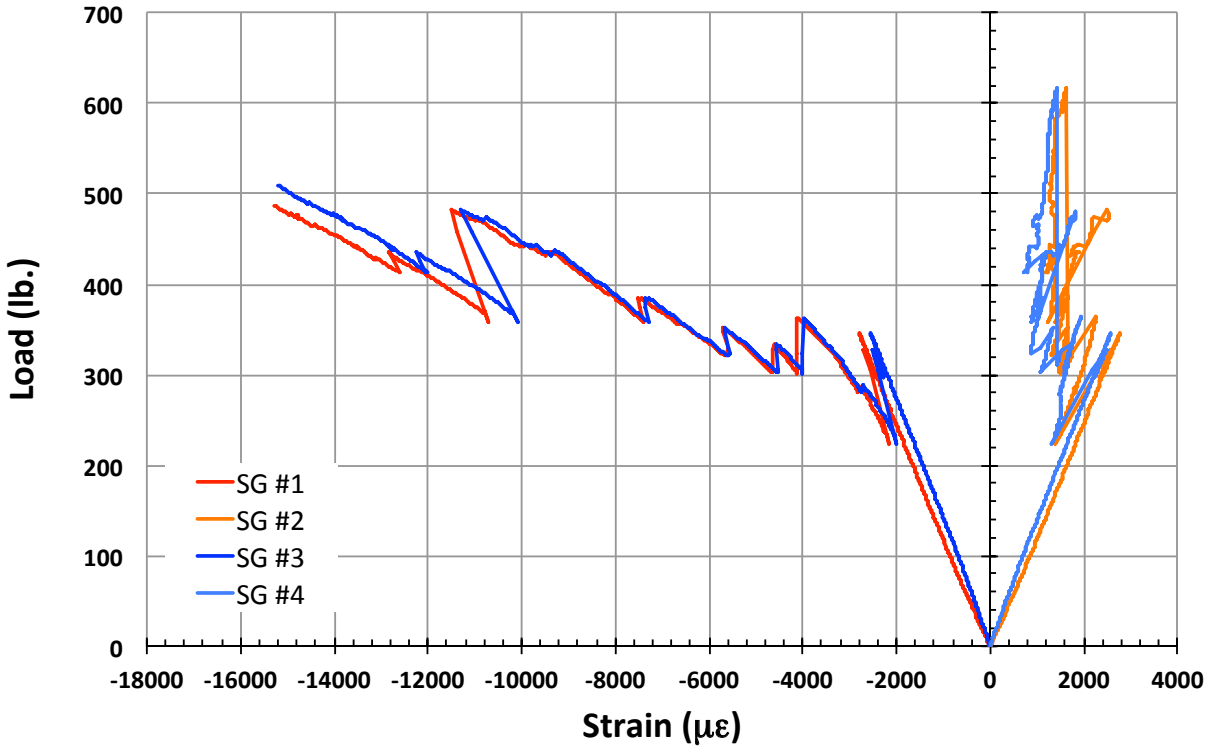

Figure C393. B1N2 load vs. strain.

B1N3

This section presents the test data for the B1N3 test article.

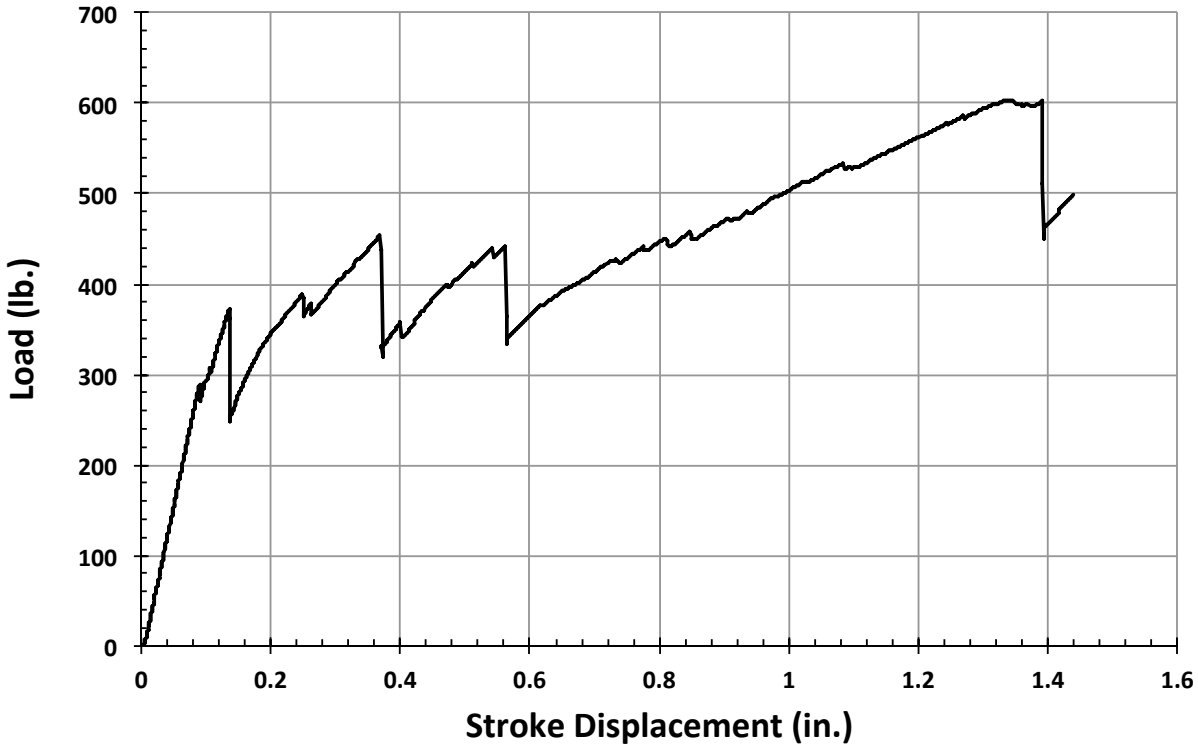

Figure C394. B1N3 load vs. stroke.

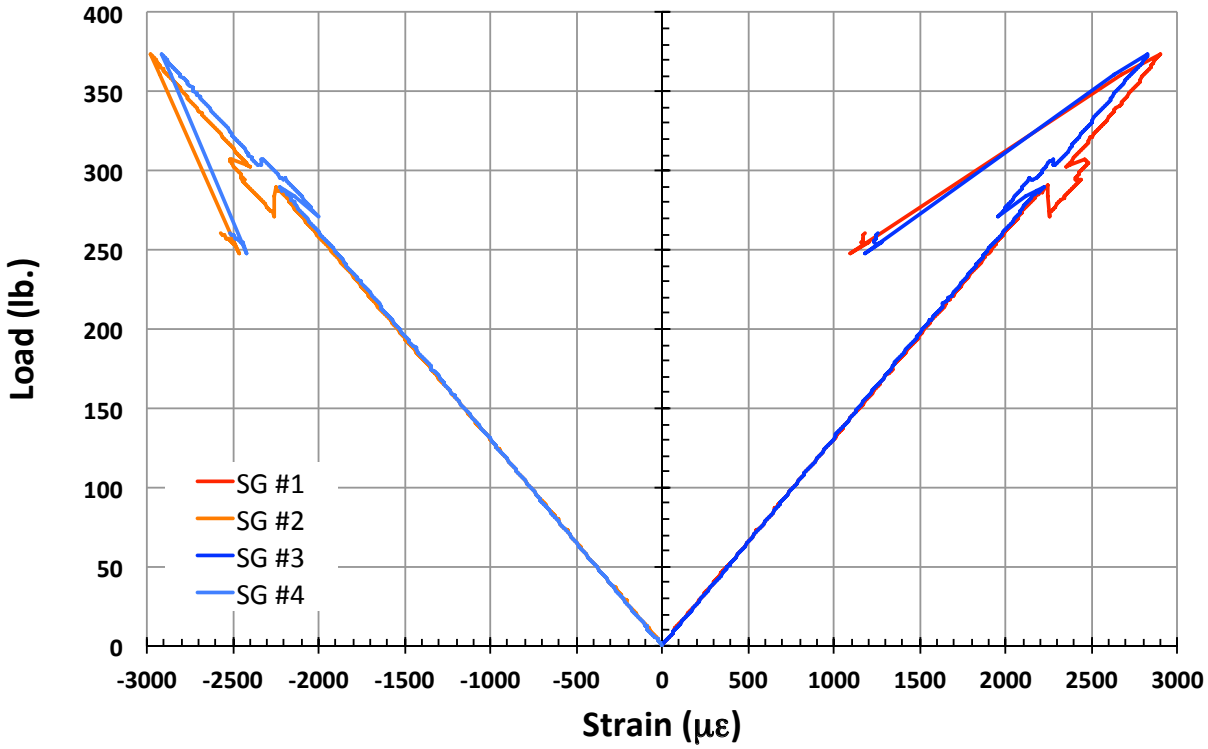

Figure C395. B1N3 load vs. strain, initial loading.

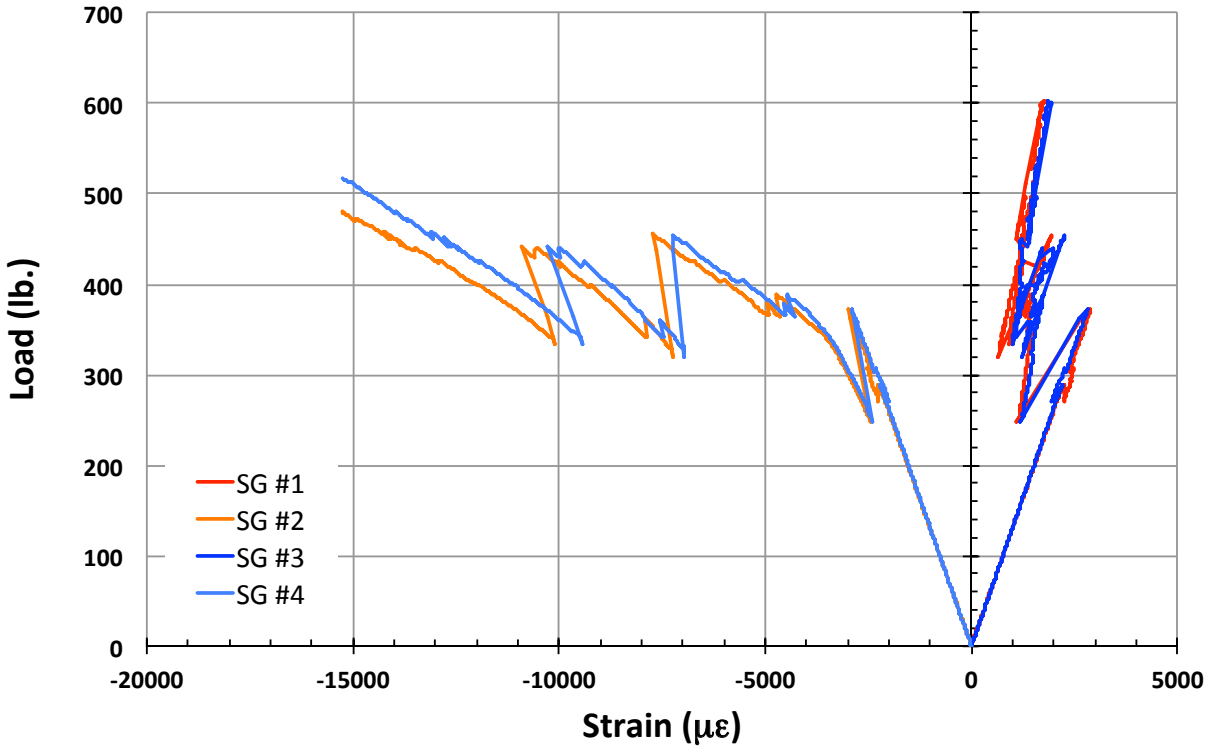

Figure C396. B1N3 load vs. strain.

B5S1

This section presents the test data for the B5S1 test article, and includes strain plots and failure images.

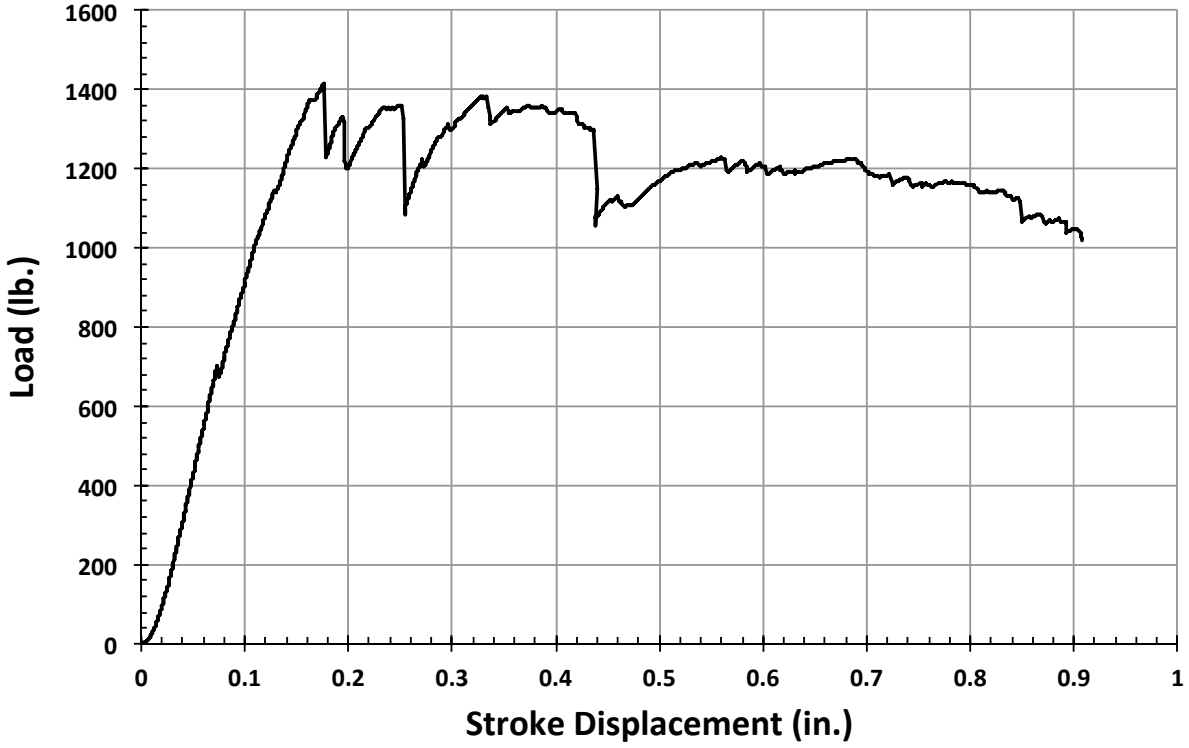

Figure C397. B5S1 load vs. stroke.

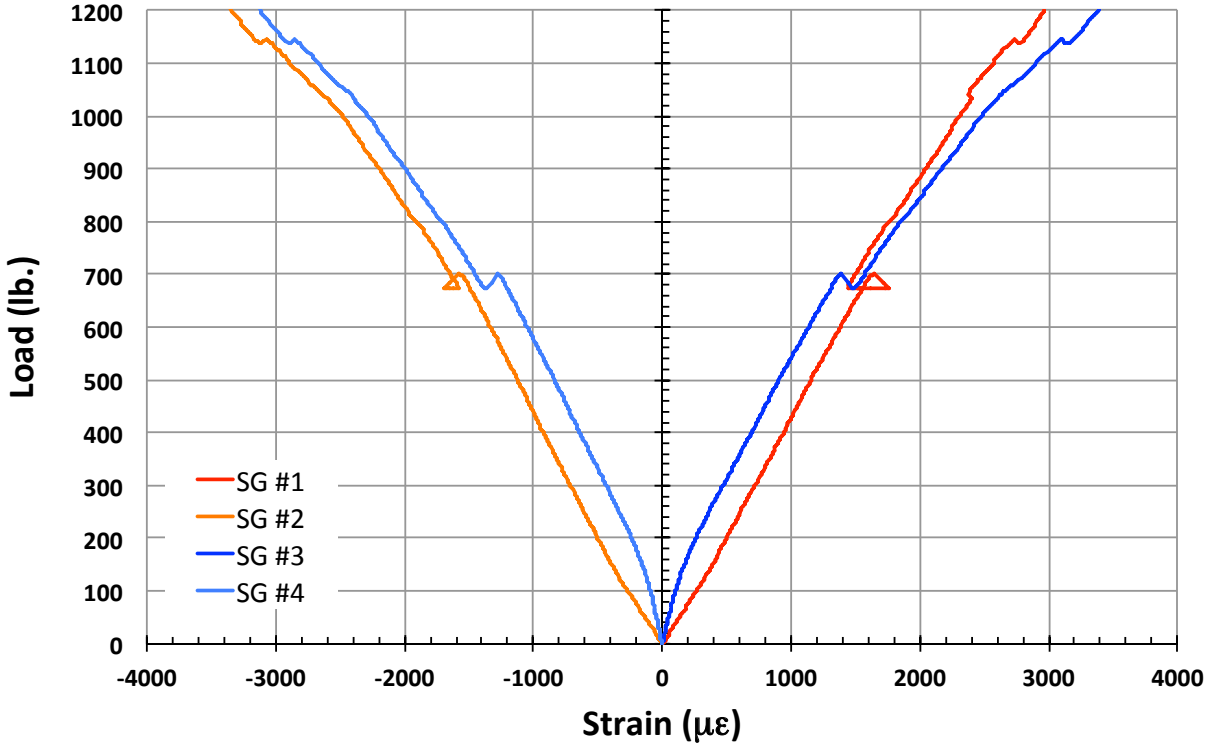

Figure C398. B5S1 load vs. strain, initial loading.

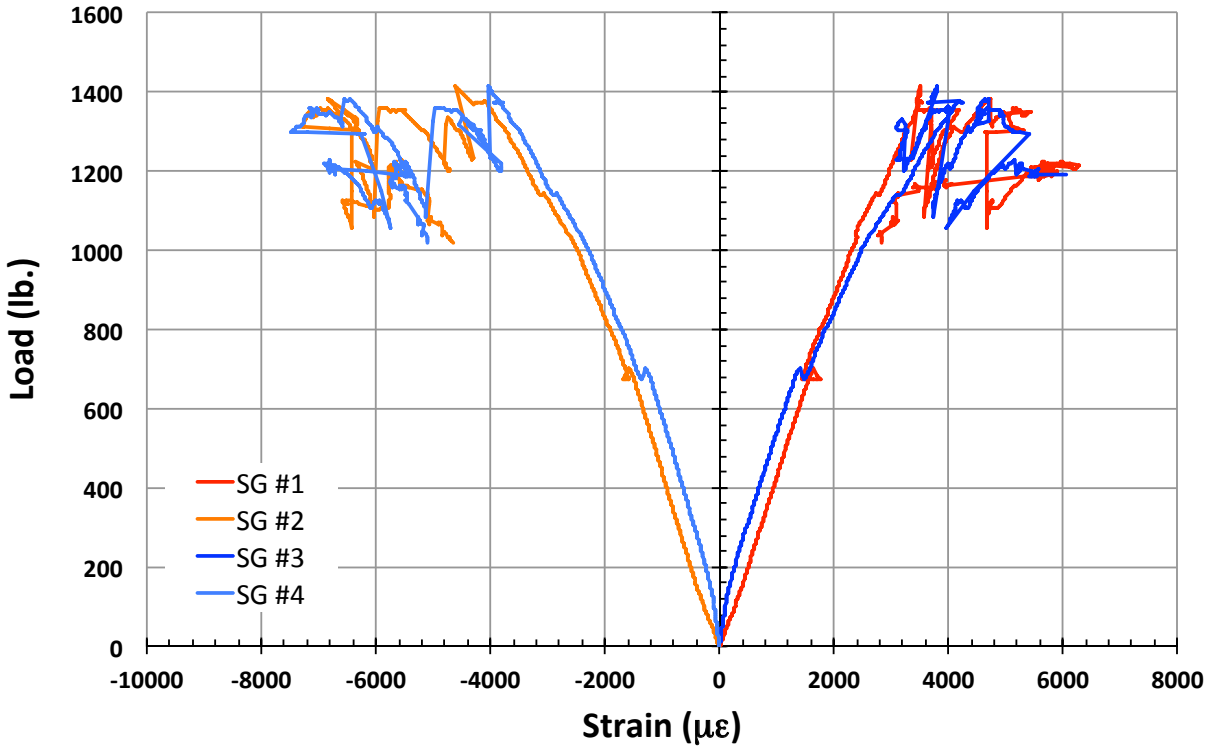

Figure C399. B5S1 load vs. strain.

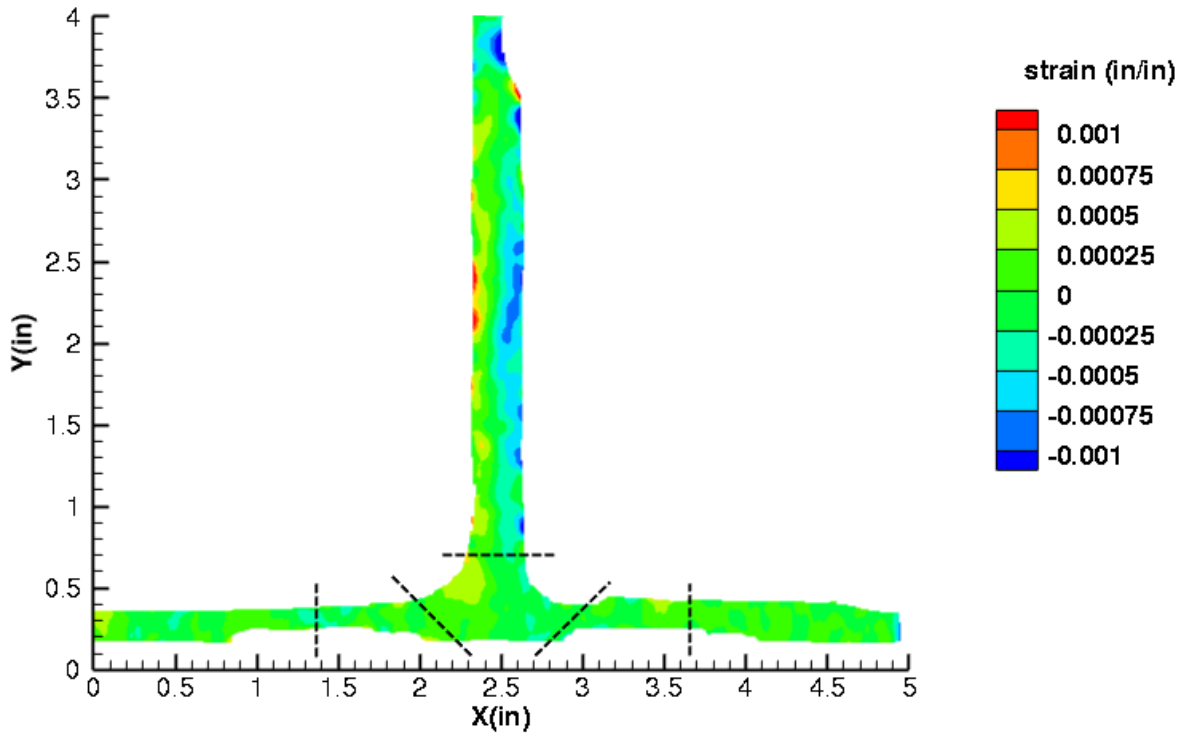

Figure C400. B5S1 strain contours for ε_{xx} at 703 lb. load, prior to initial failure, front 12MP VIC data.

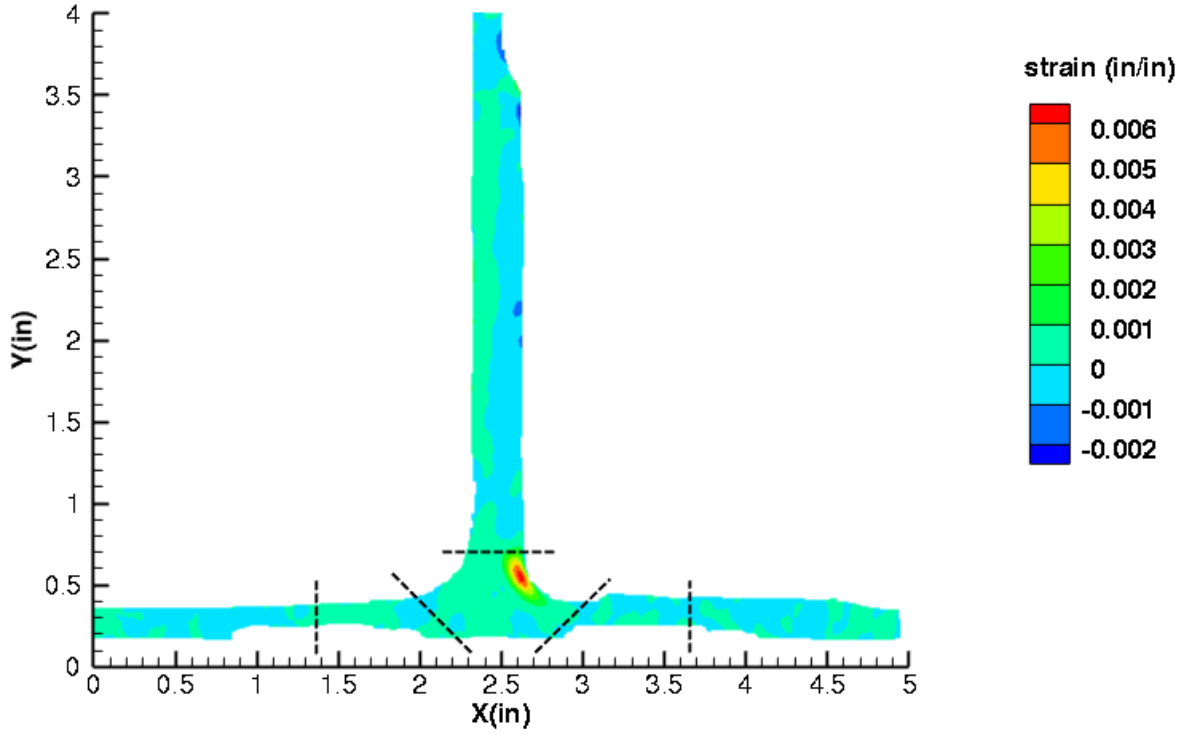

Figure C401. B5S1 strain contours for ε_{xx} at 675 lb. load, just after initial failure, front 12MP VIC data.

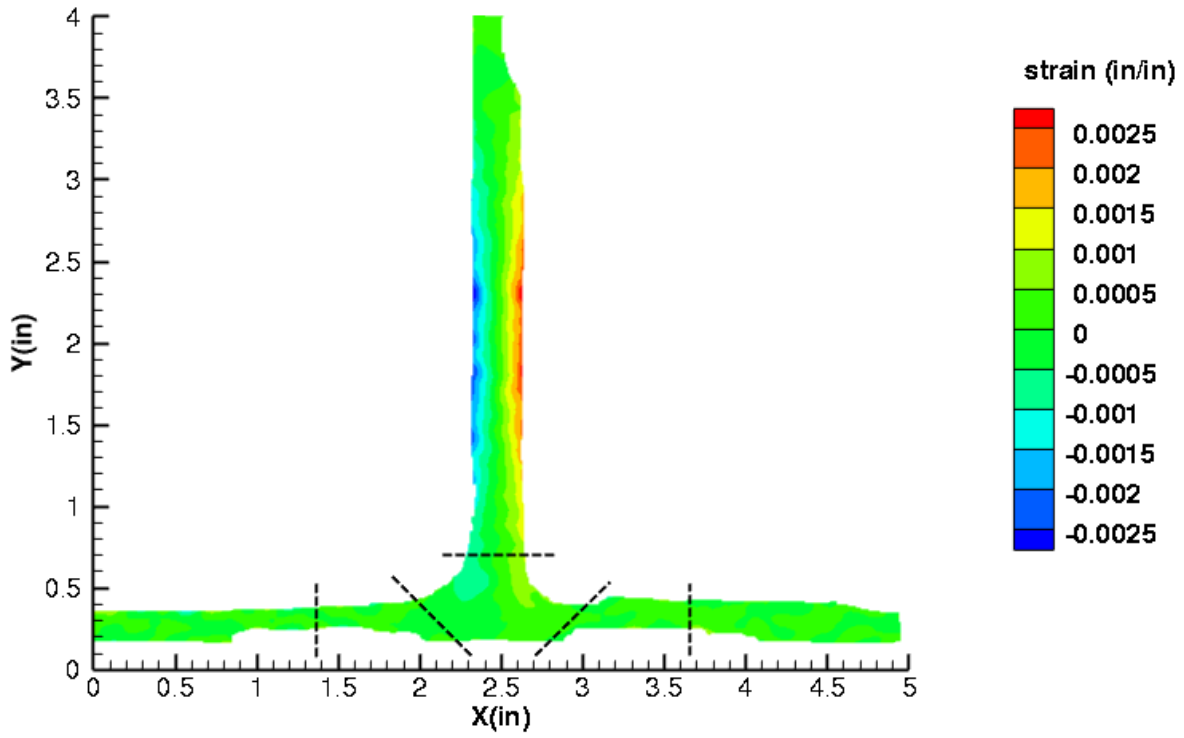

Figure C402. B5S1 strain contours for ε_{yy} at 703 lb. load, prior to initial failure, front 12MP VIC data.

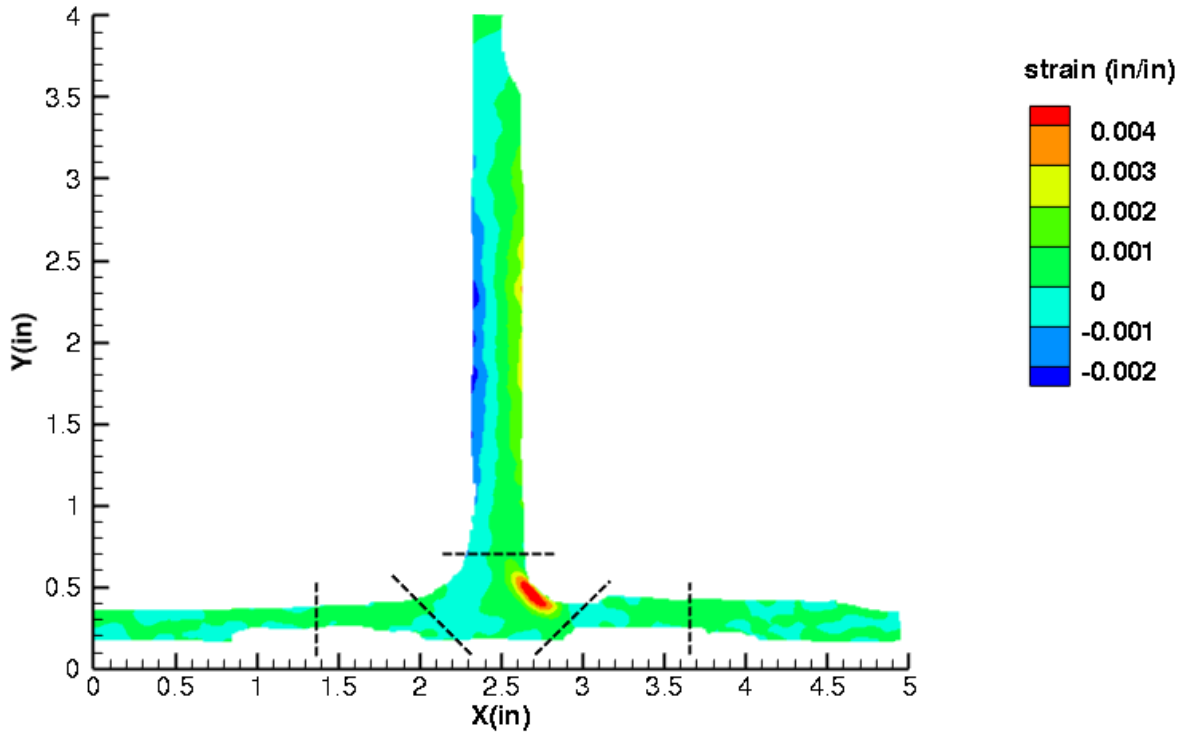

Figure C403. B5S1 strain contours for ε_{yy} at 675 lb. load, just after initial failure, front 12MP VIC data.

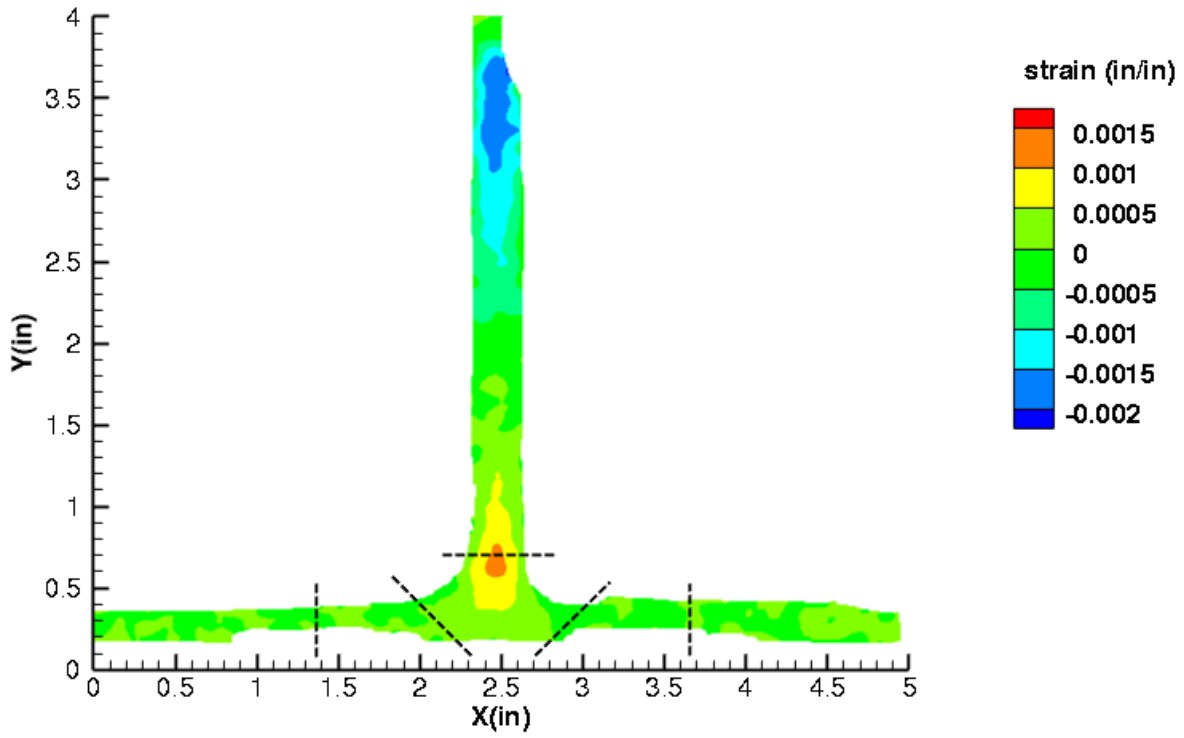

Figure C404. B5S1 strain contours for ε_{xy} at 703 lb. load, prior to initial failure, front 12MP VIC data.

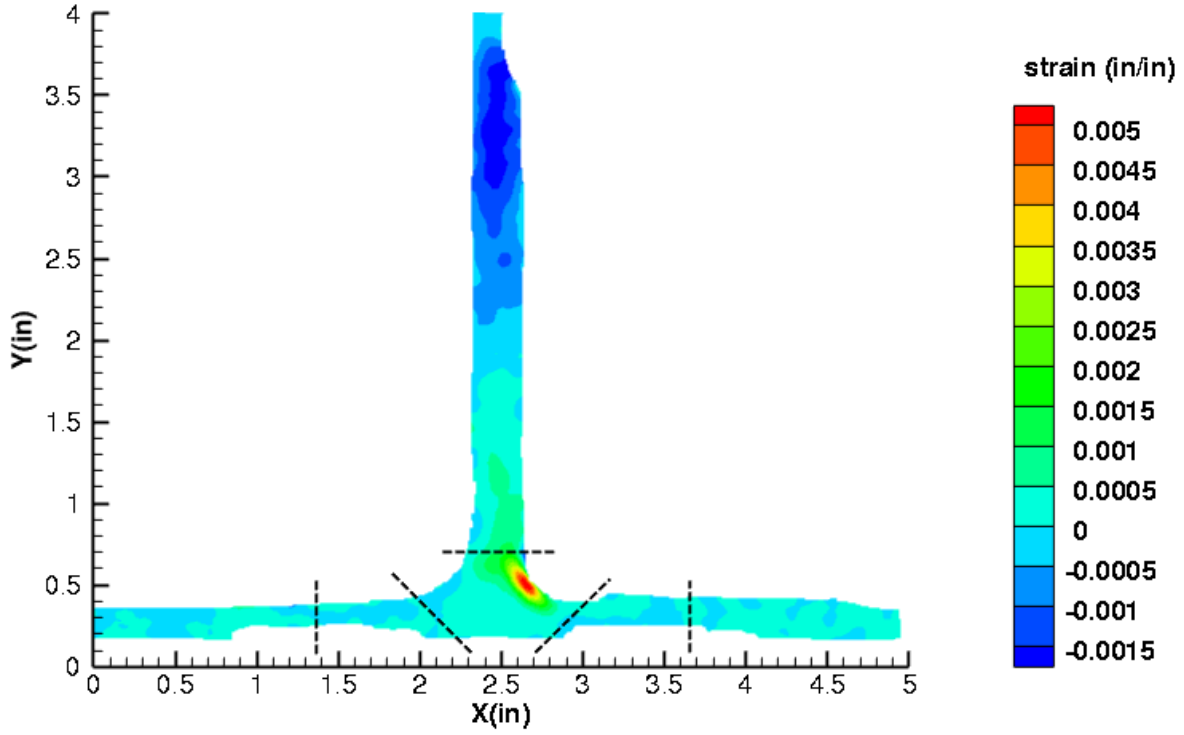

Figure C405. B5S1 strain contours for ε_{xy} at 675 lb. load, just after initial failure, front 12MP VIC data.

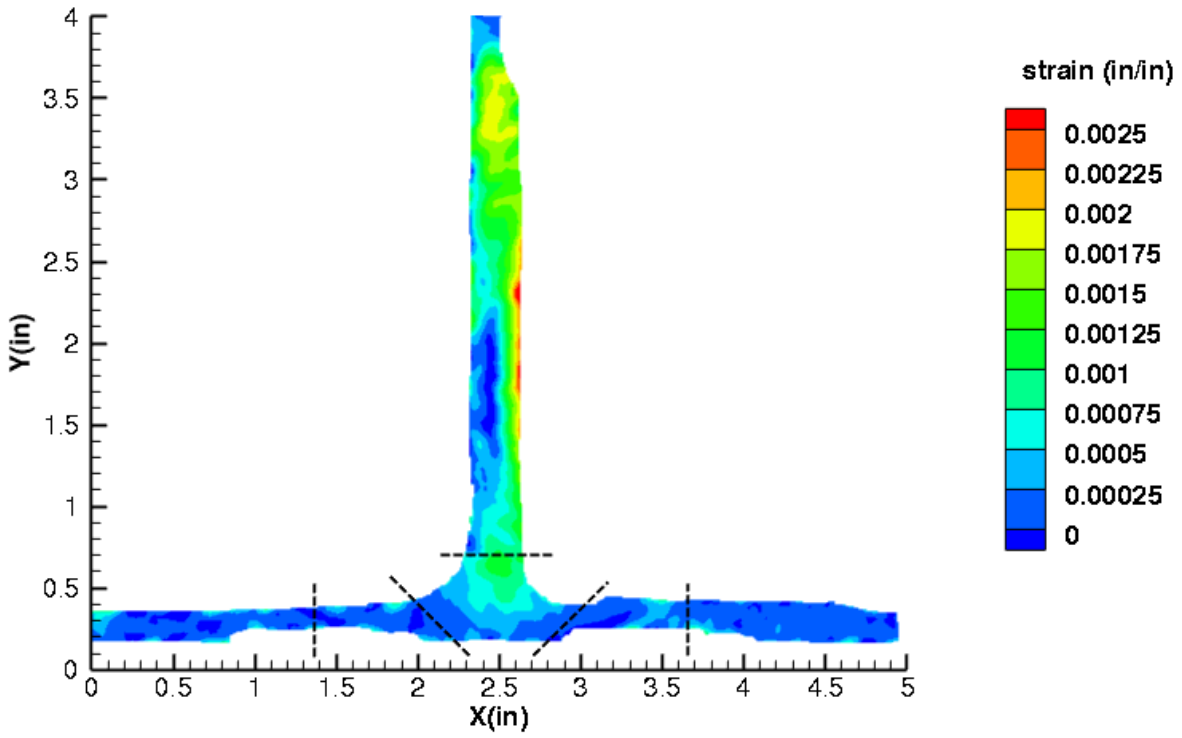

Figure C406. B5S1 strain contours for maximum principal strain at 703 lb. load, prior to initial failure, front 12MP VIC data.

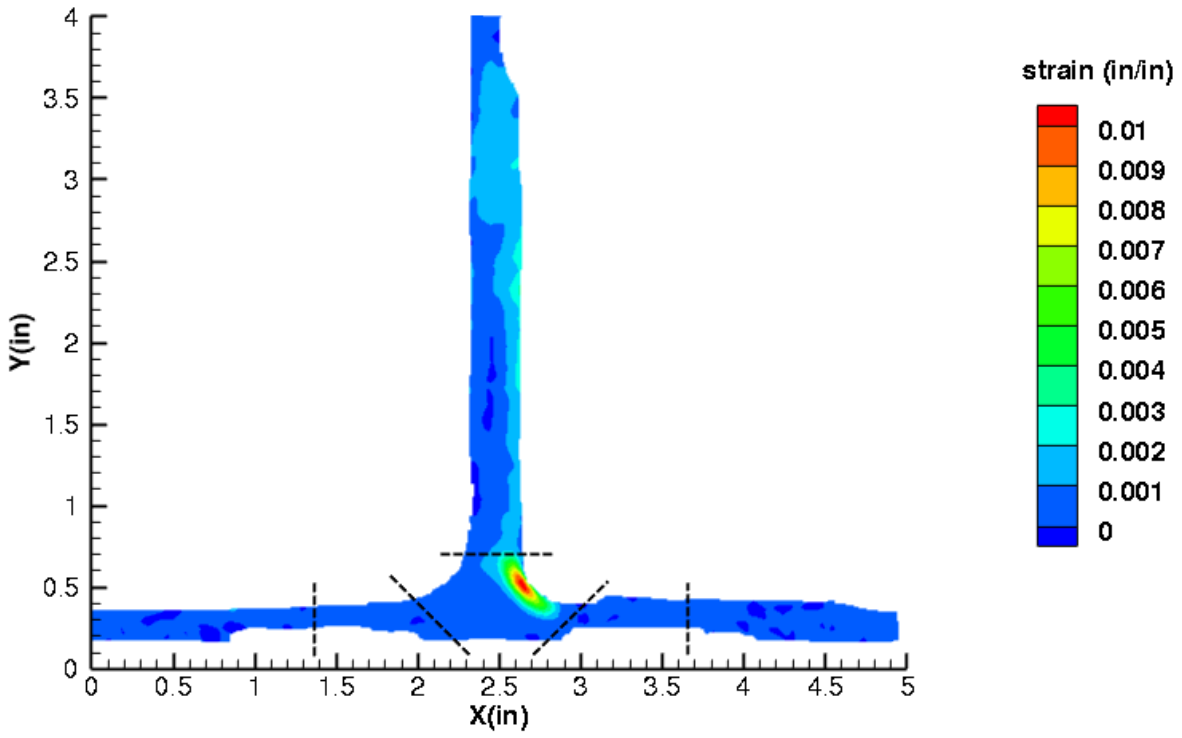

Figure C407. B5S1 strain contours for maximum principal strain at 675 lb. load, just after initial failure, front 12MP VIC data.

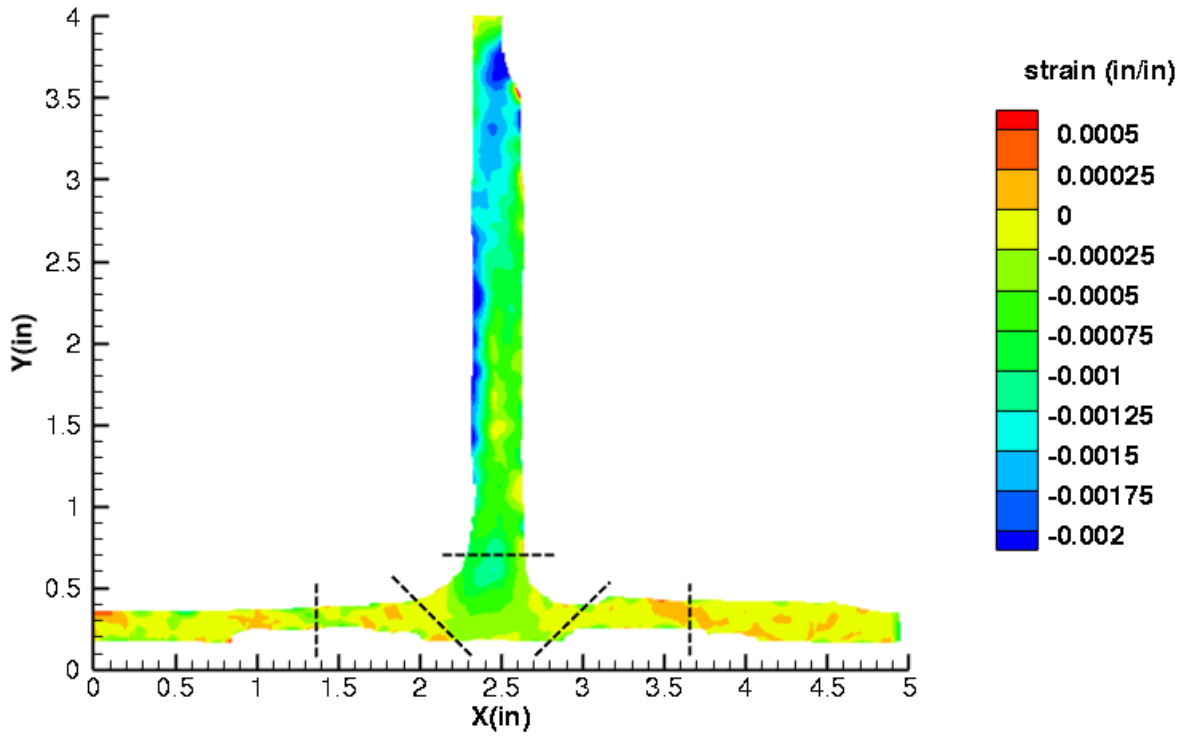

Figure C408. B5S1 strain contours for minimum principal strain at 703 lb. load, prior to initial failure, front 12MP VIC data.

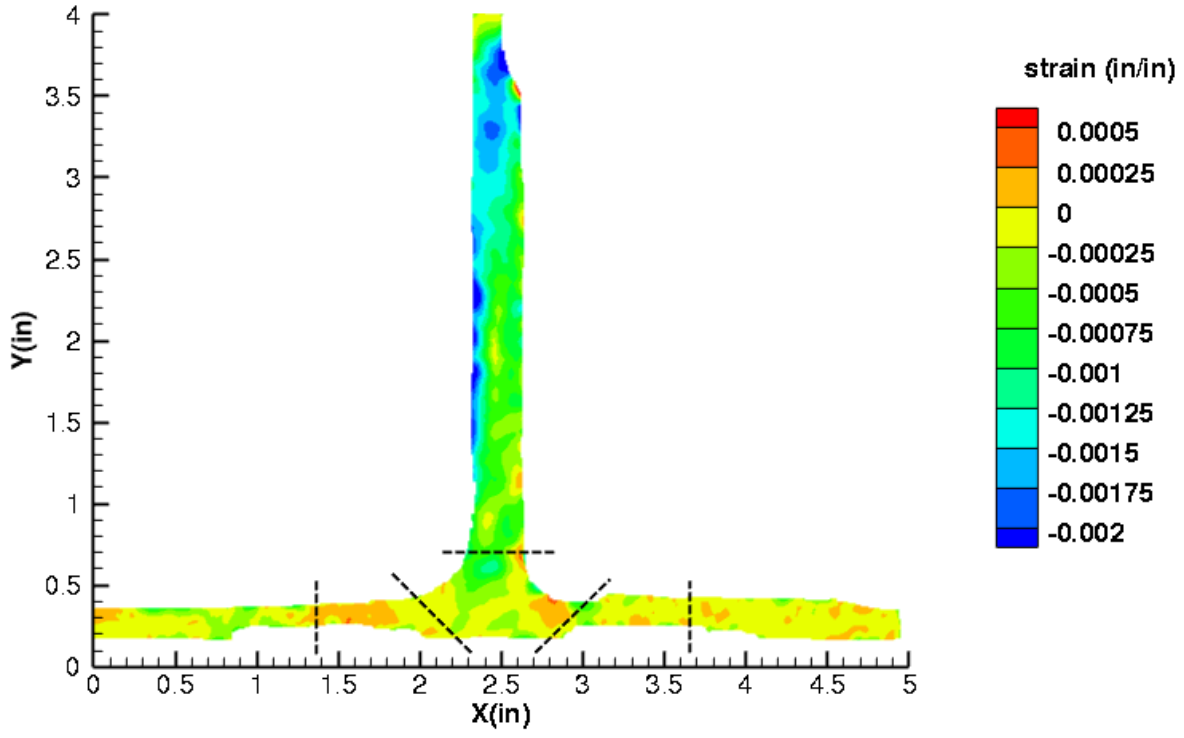

Figure C409. B5S1 strain contours for minimum principal strain at 675 lb. load, just after initial failure, front 12MP VIC data.

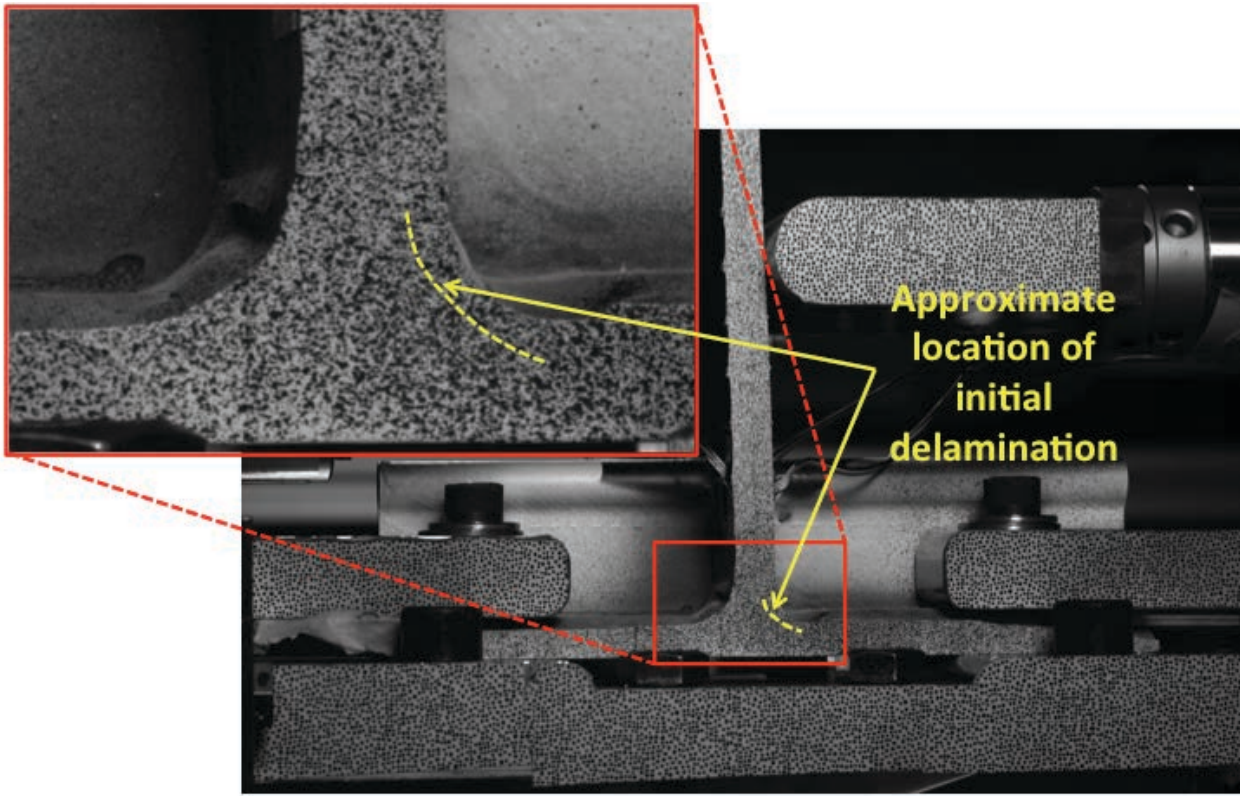

Figure C410. B5S1 image just after initial failure, front 12MP VIC data.

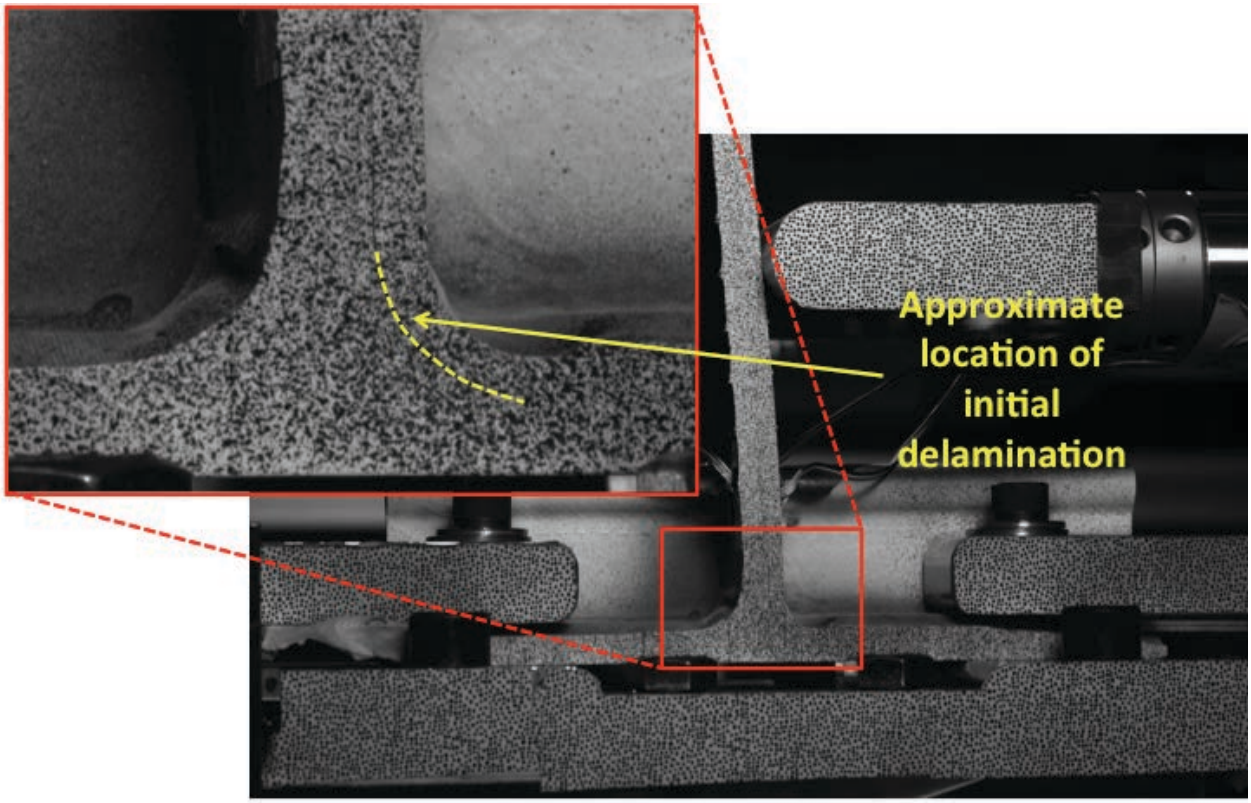

Figure C411. B5S1 image just after maximum load, front 12MP VIC data.

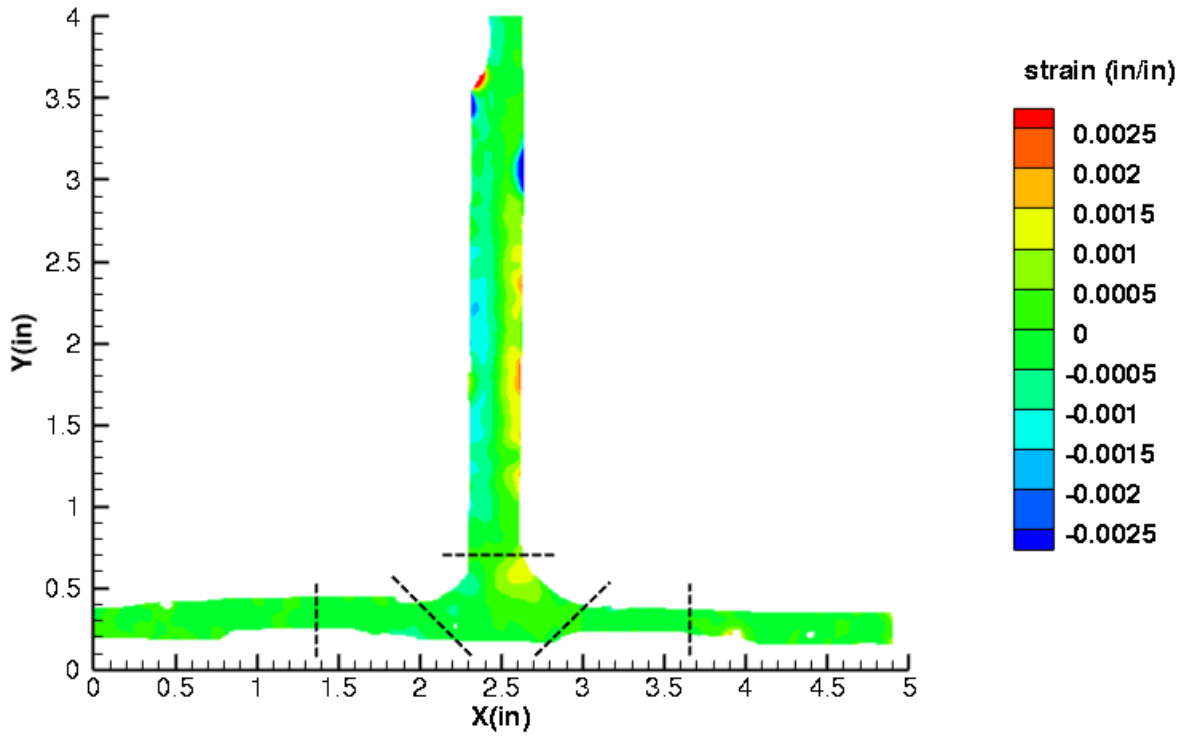

Figure C412. B5S1 strain contours for ε_{xx} at 1383 lb. load, prior to initial failure, back 12MP VIC data.

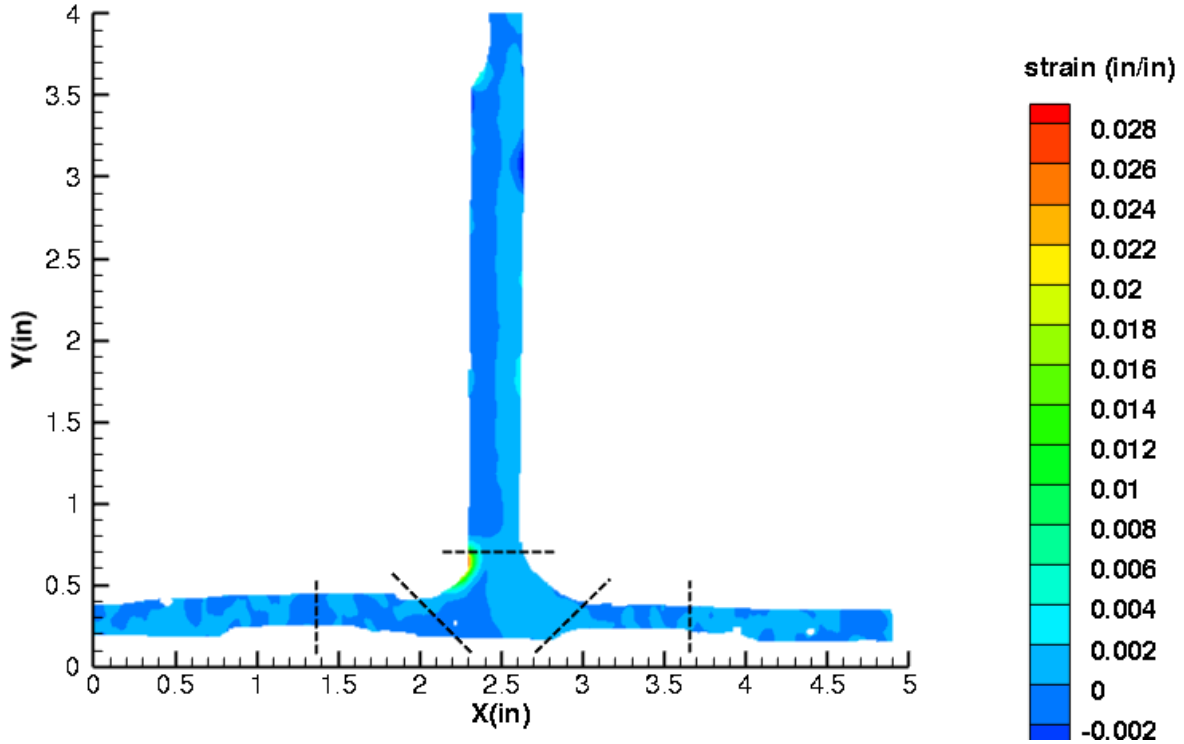

Figure C413. B5S1 strain contours for ε_{xx} at 1380 lb. load, just after initial failure, back 12MP VIC data.

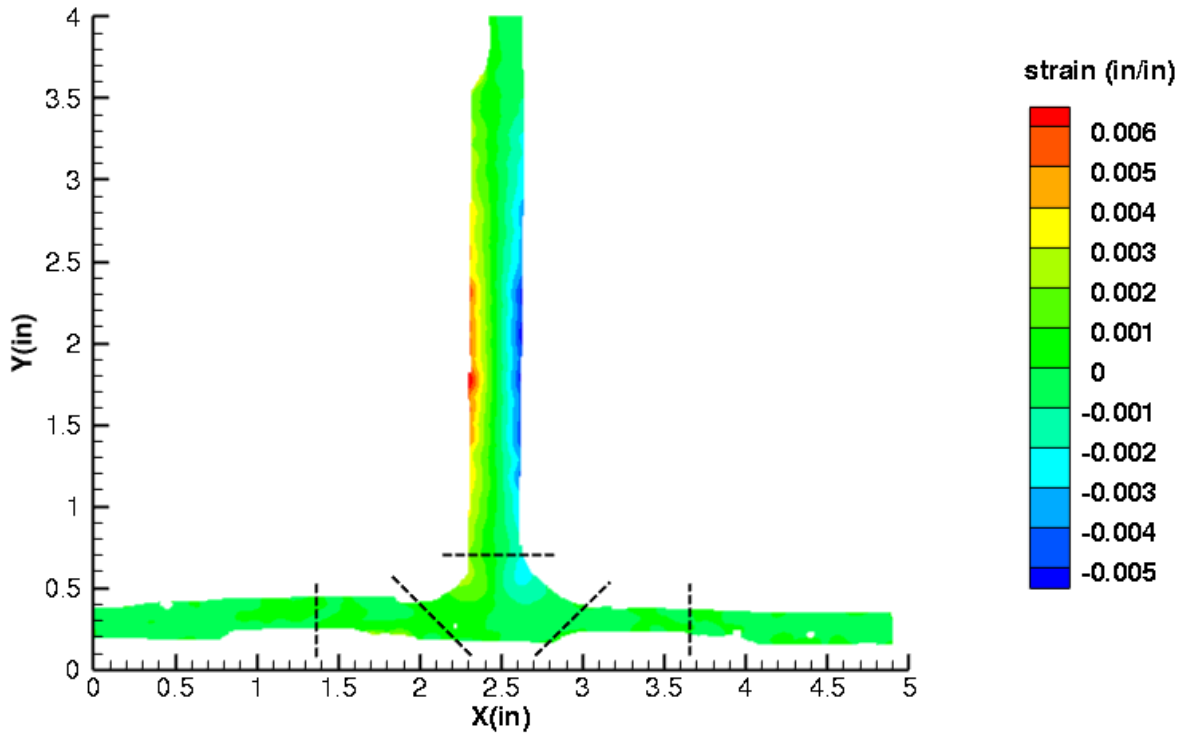

Figure C414. B5S1 strain contours for ε_{yy} at 1383 lb. load, prior to initial failure, back 12MP VIC data.

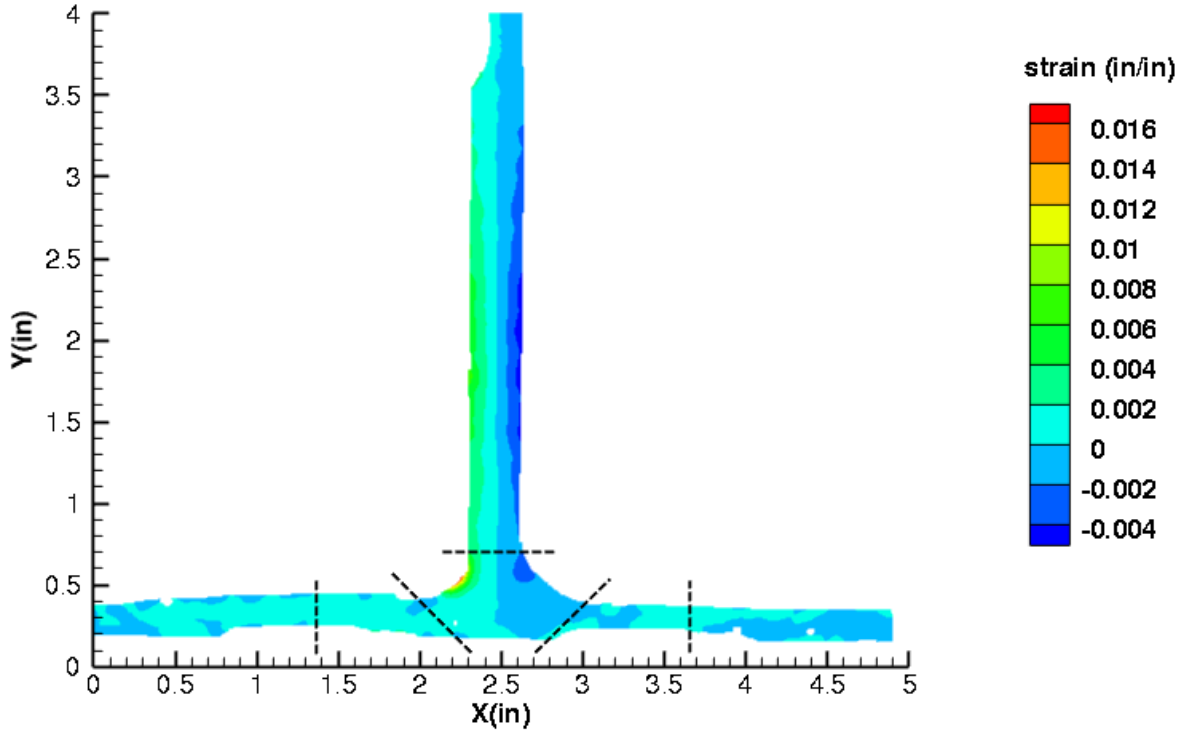

Figure C415. B5S1 strain contours for ε_{yy} at 1380 lb. load, just after initial failure, back 12MP VIC data.

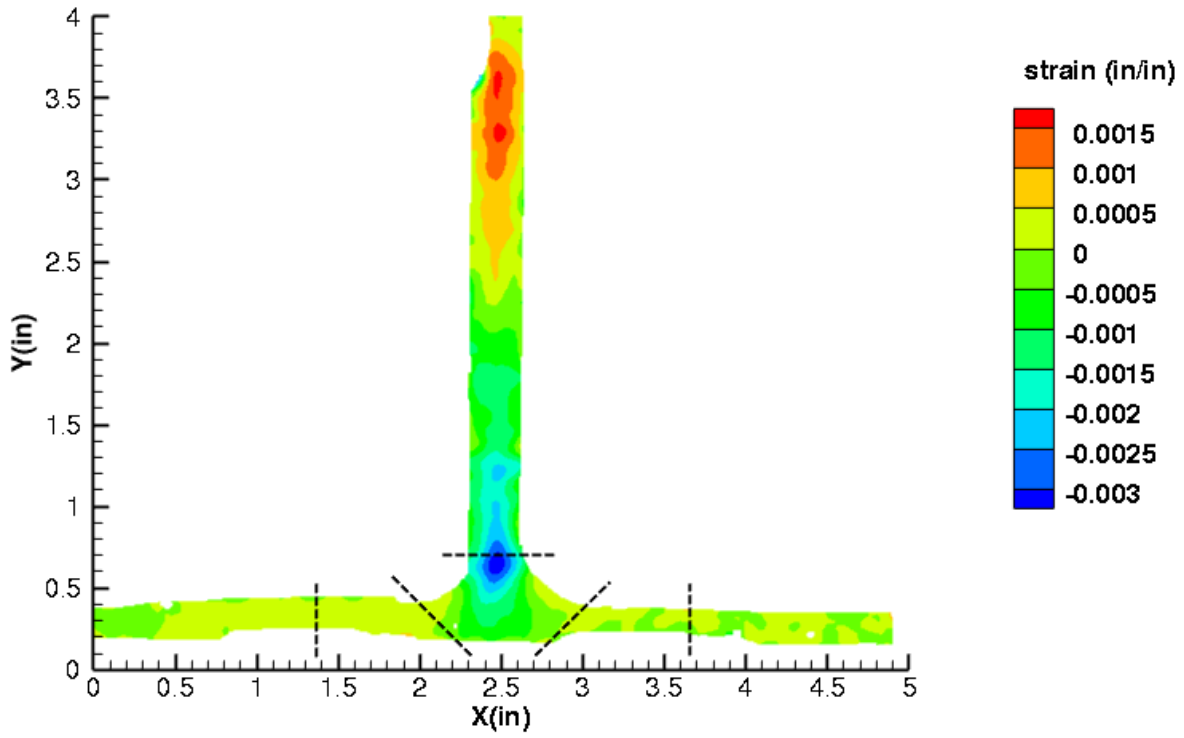

Figure C416. B5S1 strain contours for ε_{xy} at 1383 lb. load, prior to initial failure, back 12MP VIC data.

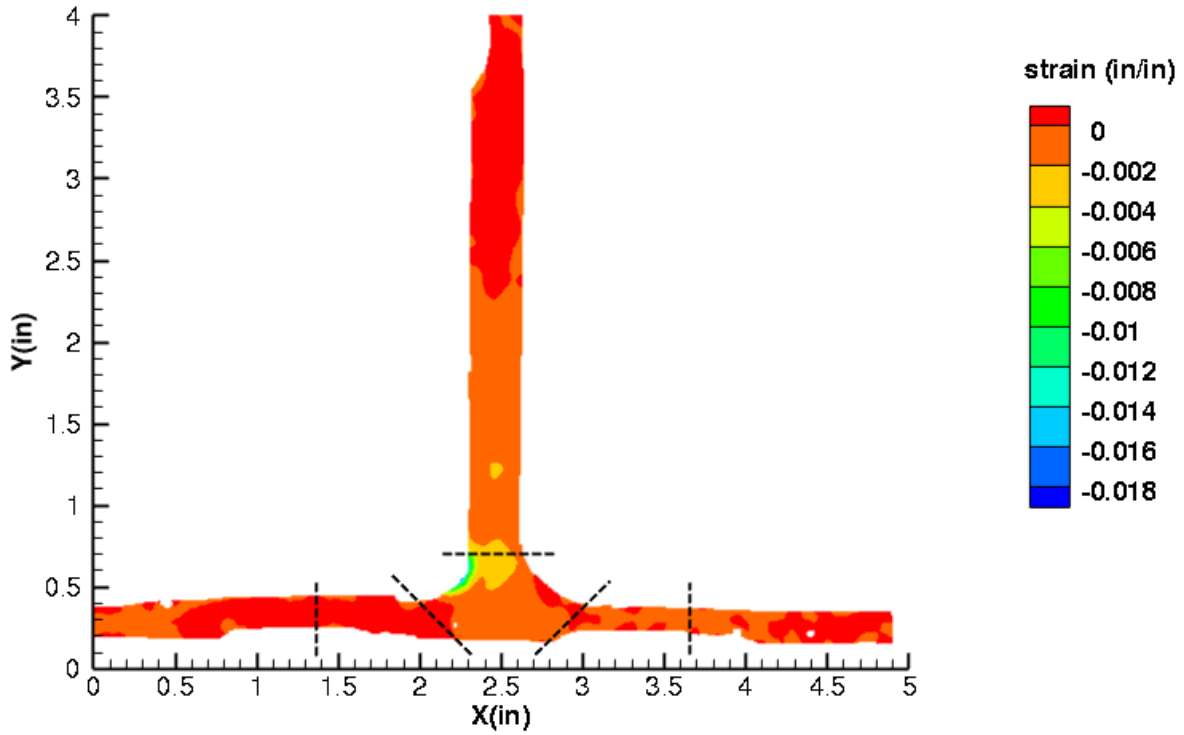

Figure C417. B5S1 strain contours for ε_{xy} at 1380 lb. load, just after initial failure, back 12MP VIC data.

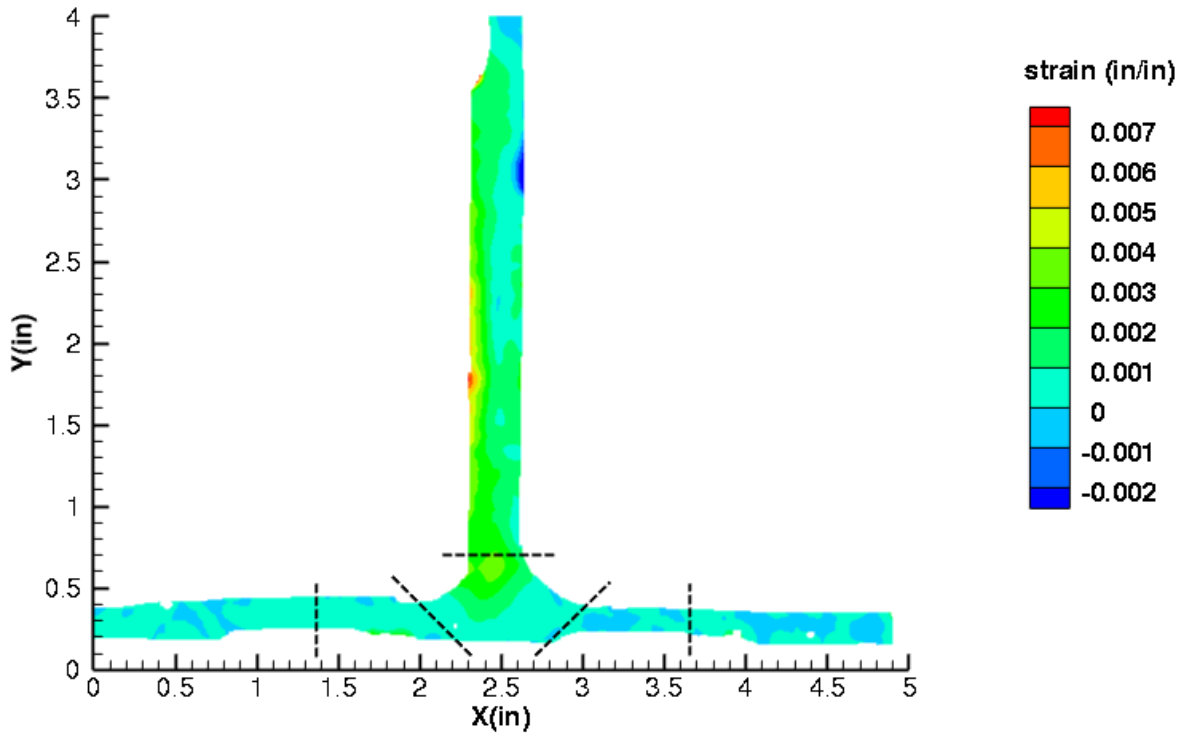

Figure C418. B5S1 strain contours for maximum principal strain at 1383 lb. load, prior to initial failure, back 12MP VIC data.

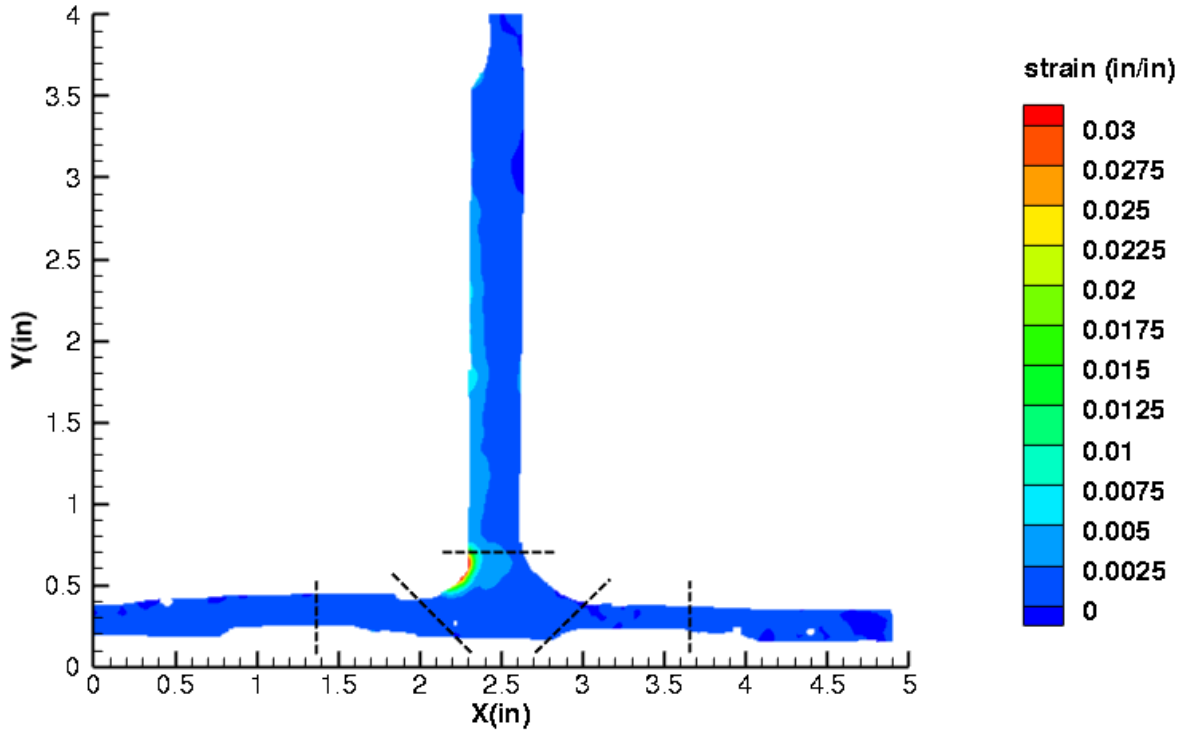

Figure C419. B5S1 strain contours for maximum principal strain at 1380 lb. load, just after initial failure, back 12MP VIC data.

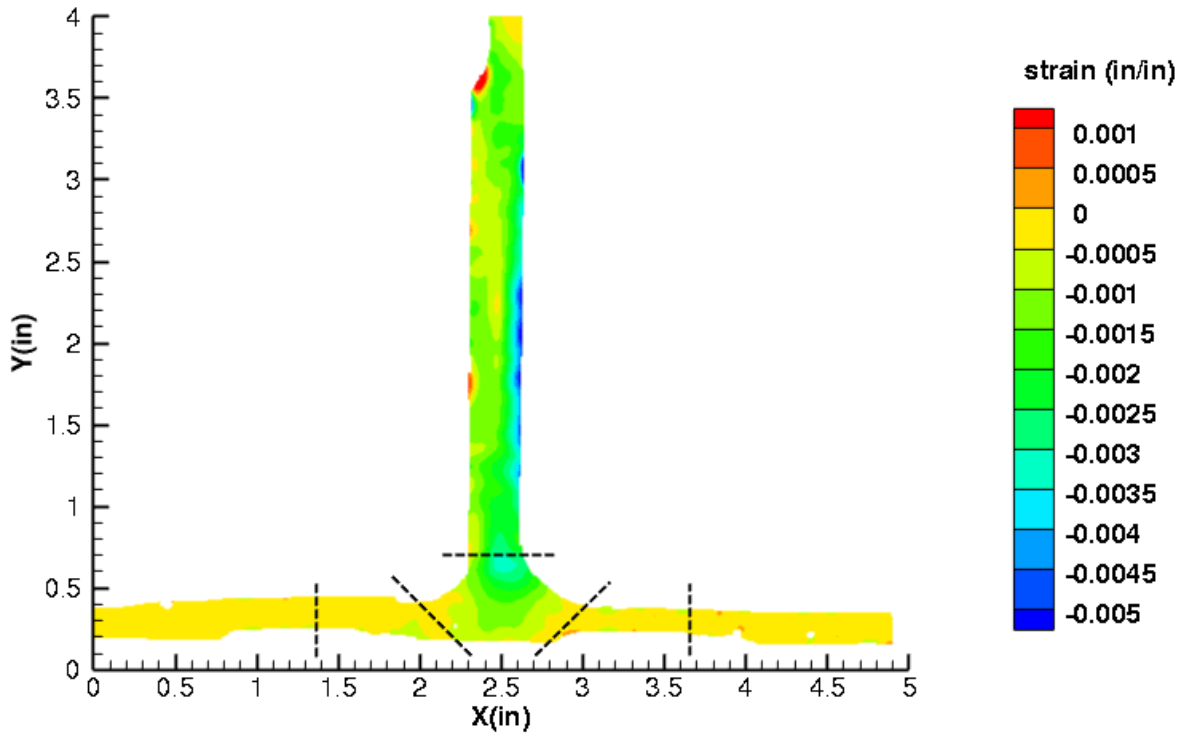

Figure C420. B5S1 strain contours for minimum principal strain at 1383 lb. load, prior to initial failure, back 12MP VIC data.

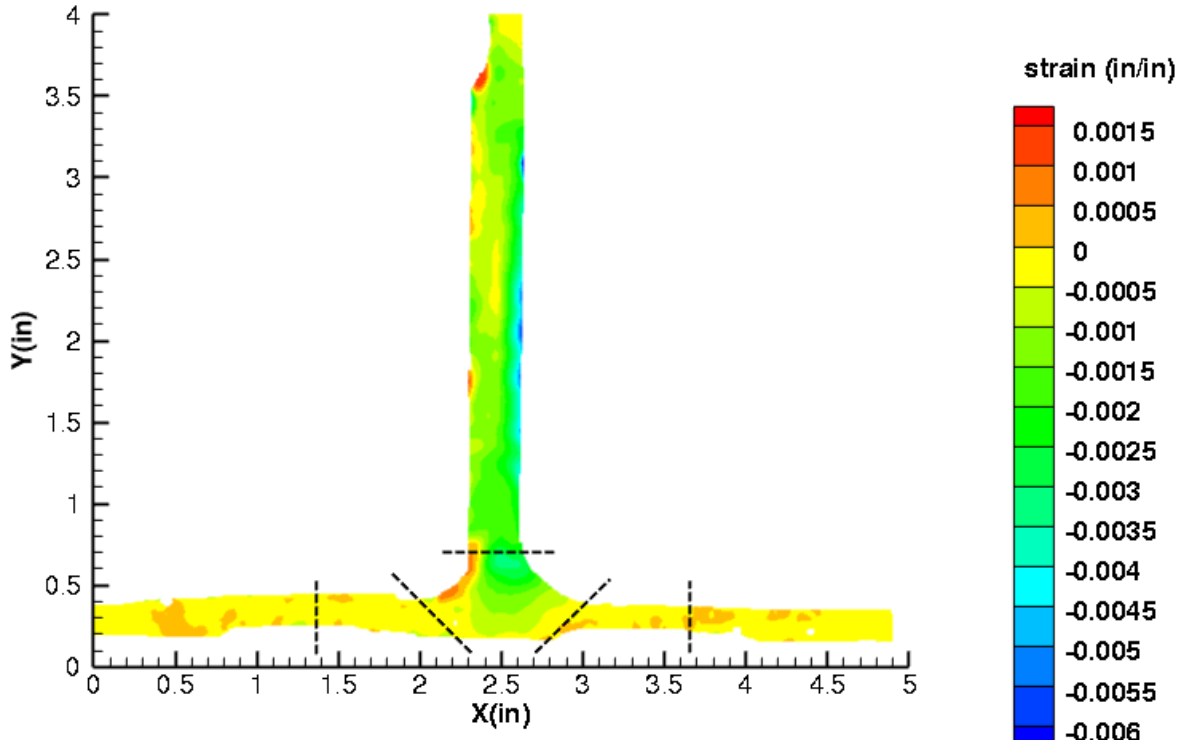

Figure C421. B5S1 strain contours for minimum principal strain at 1380 lb. load, just after initial failure, back 12MP VIC data.

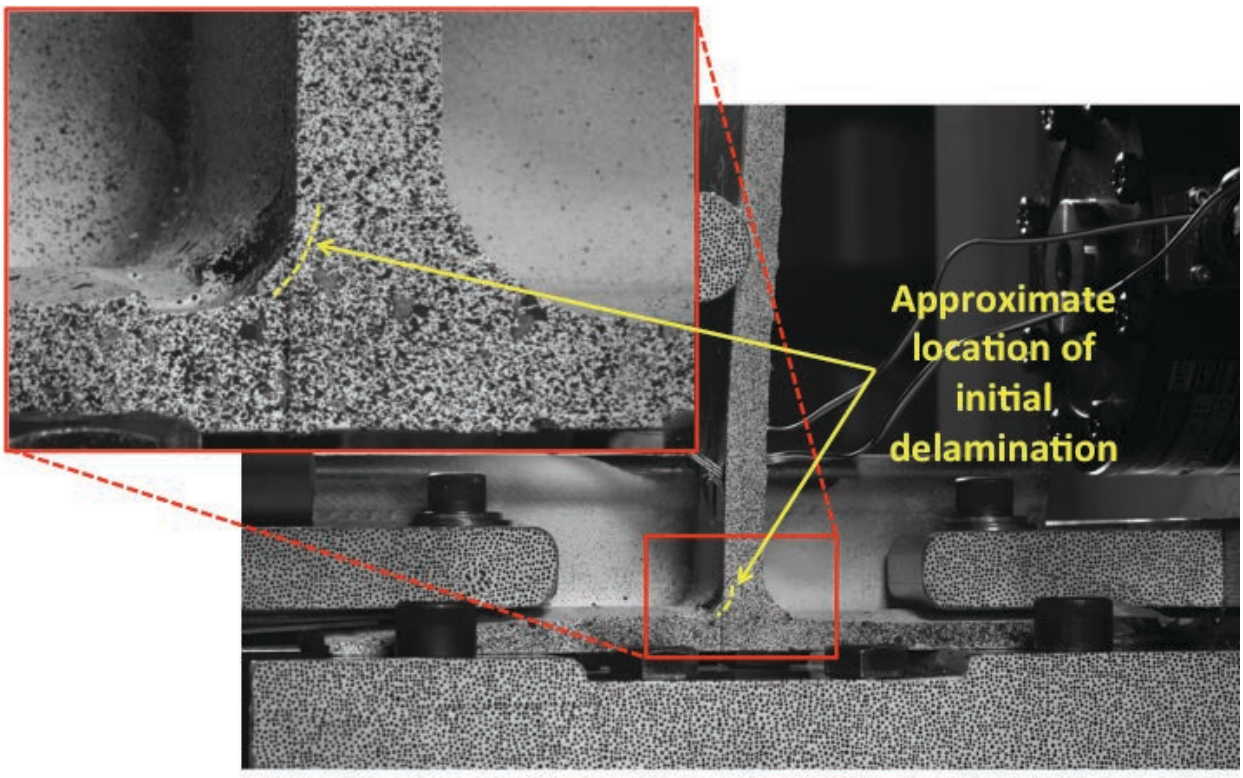

Figure C422. B5S1 image just after initial failure, back 12MP VIC data.

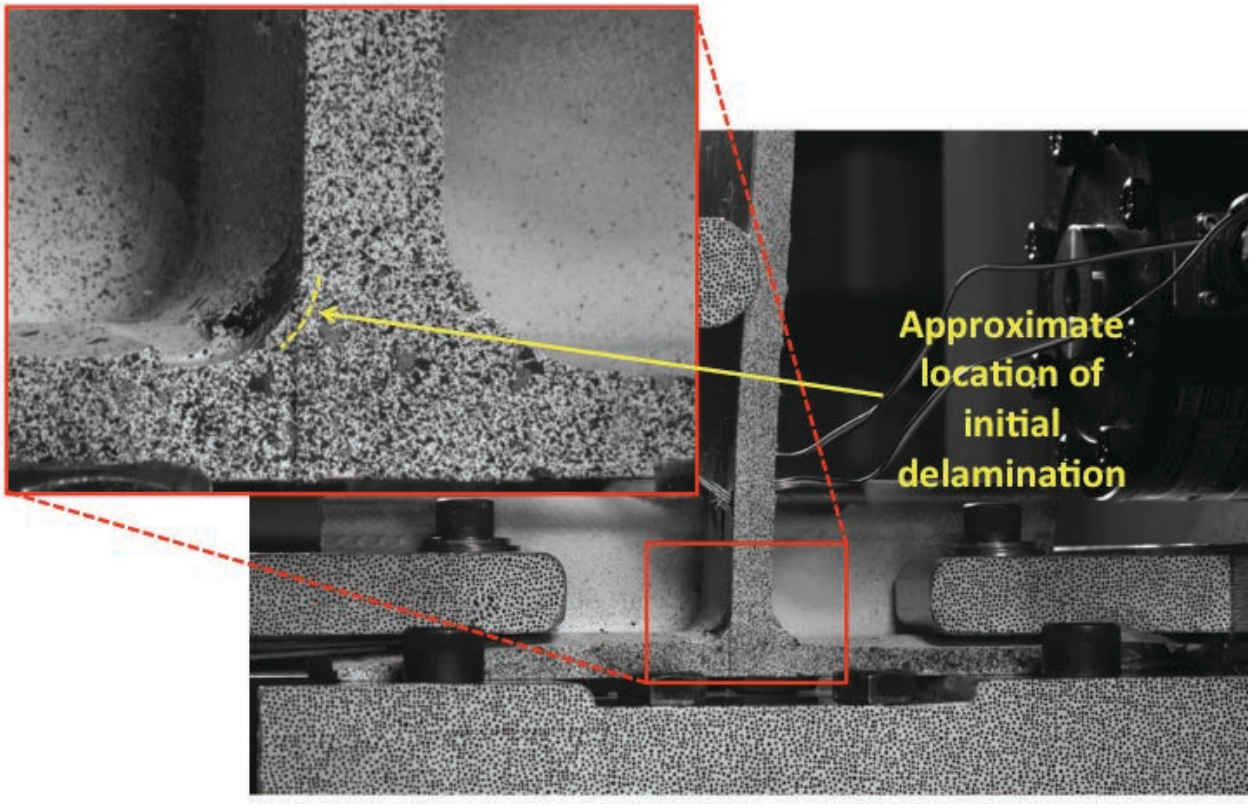

Figure C423. B5S1 image just after maximum load, back 12MP VIC data.

B5S2

This section presents the test data for the B5S2 test article.

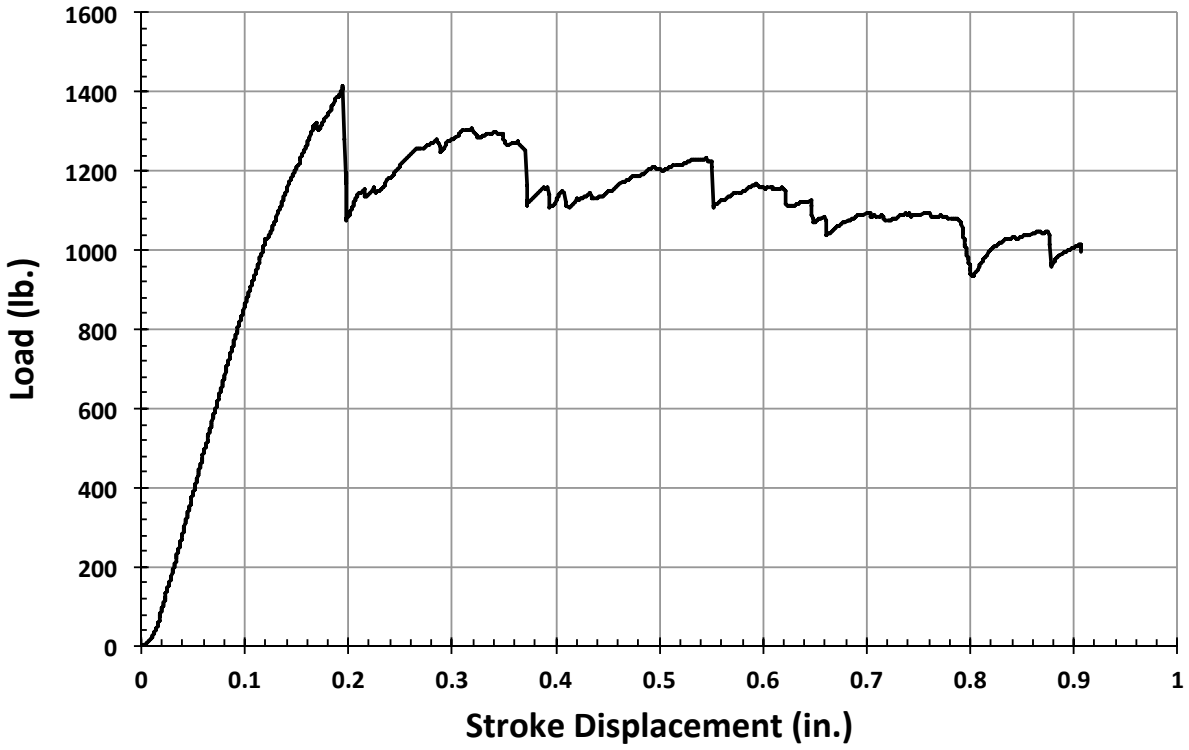

Figure C424. B5S2 load vs. stroke.

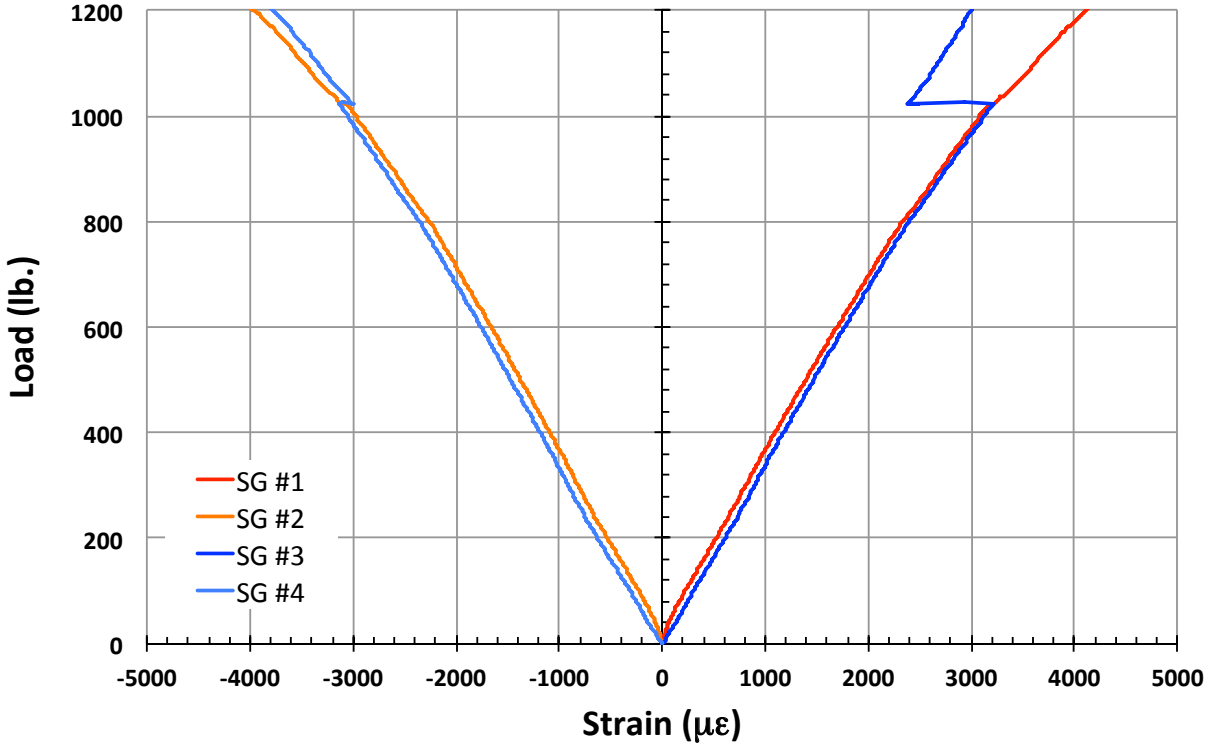

Figure C425. B5S2 load vs. strain, initial loading.

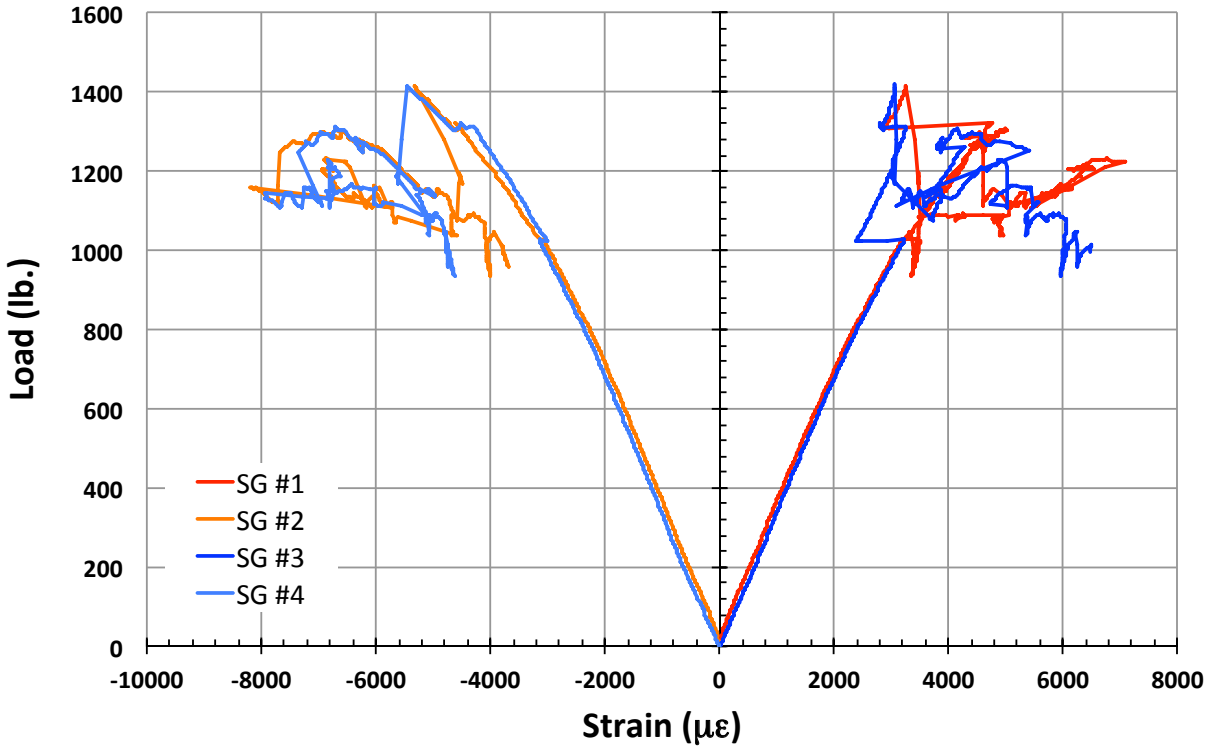

Figure C426. B5S2 load vs. strain.

B5S3

This section presents the test data for the B5S3 test article.

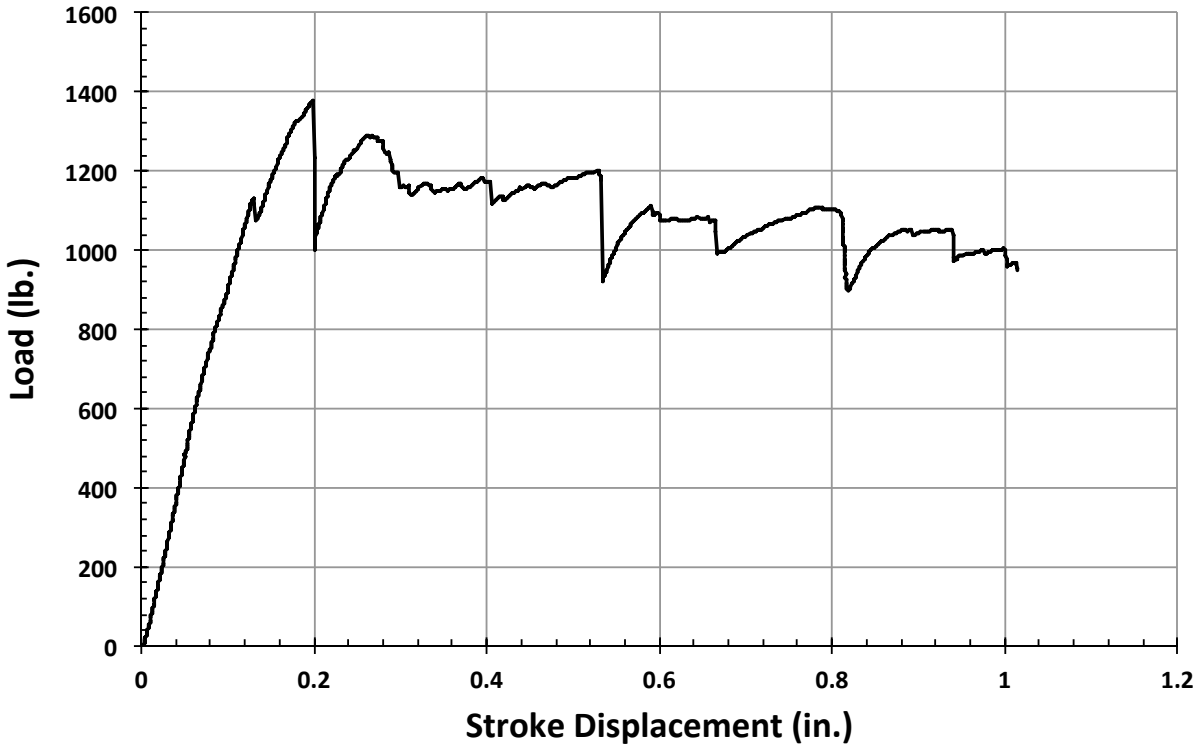

Figure C427. B5S3 load vs. stroke.

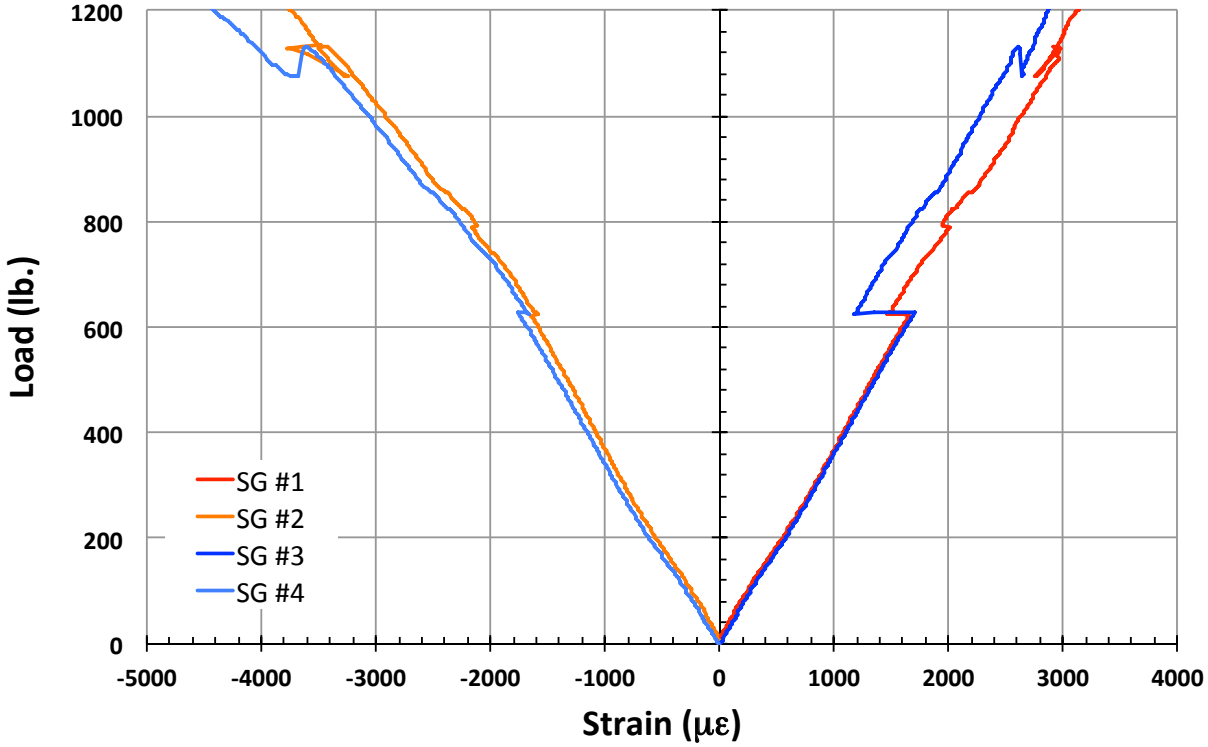

Figure C428. B5S3 load vs. strain, initial loading.

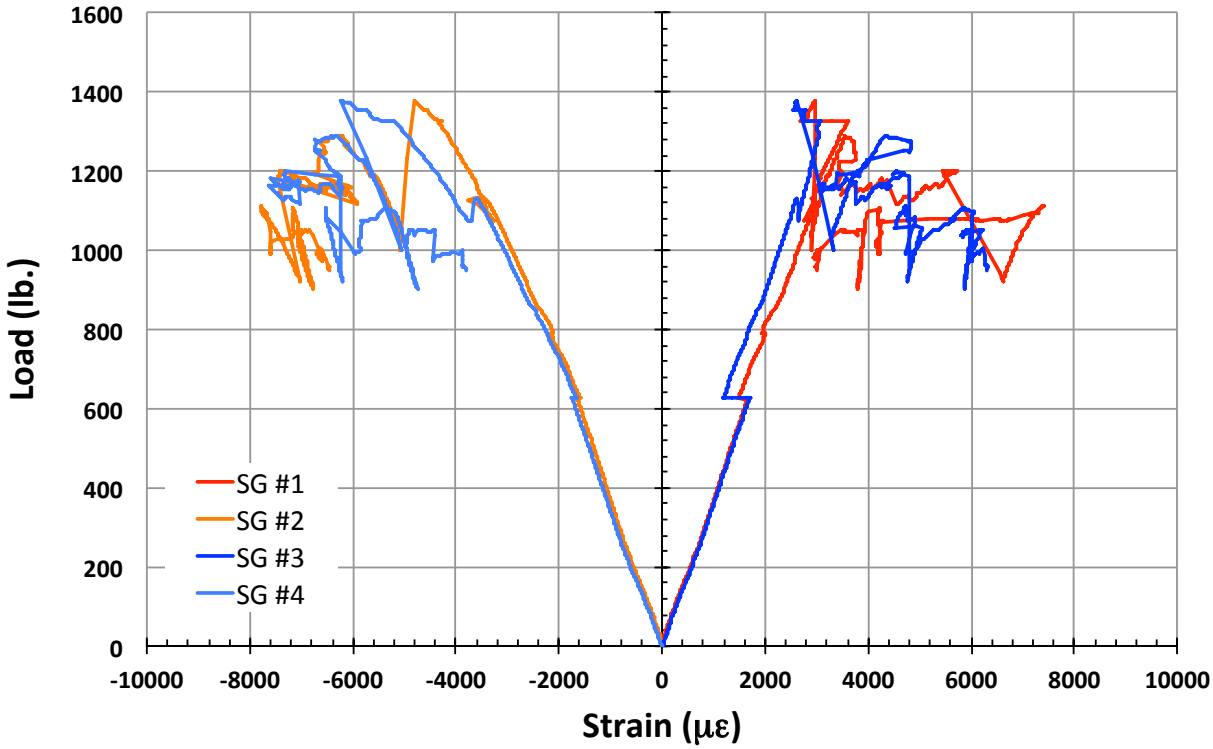

Figure C429. B5S3 load vs. strain.

B5N1

This section presents the test data for the B5N1 test article, and includes strain plots and failure images.

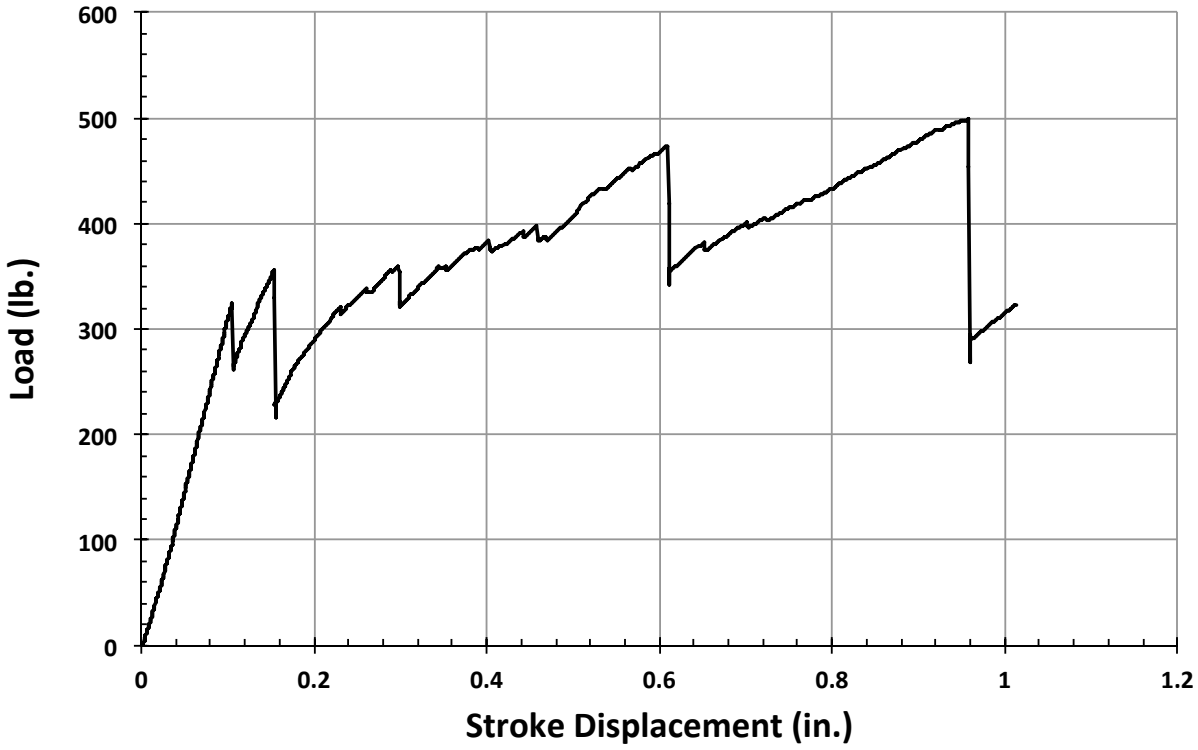

Figure C430. B5N1 load vs. stroke.

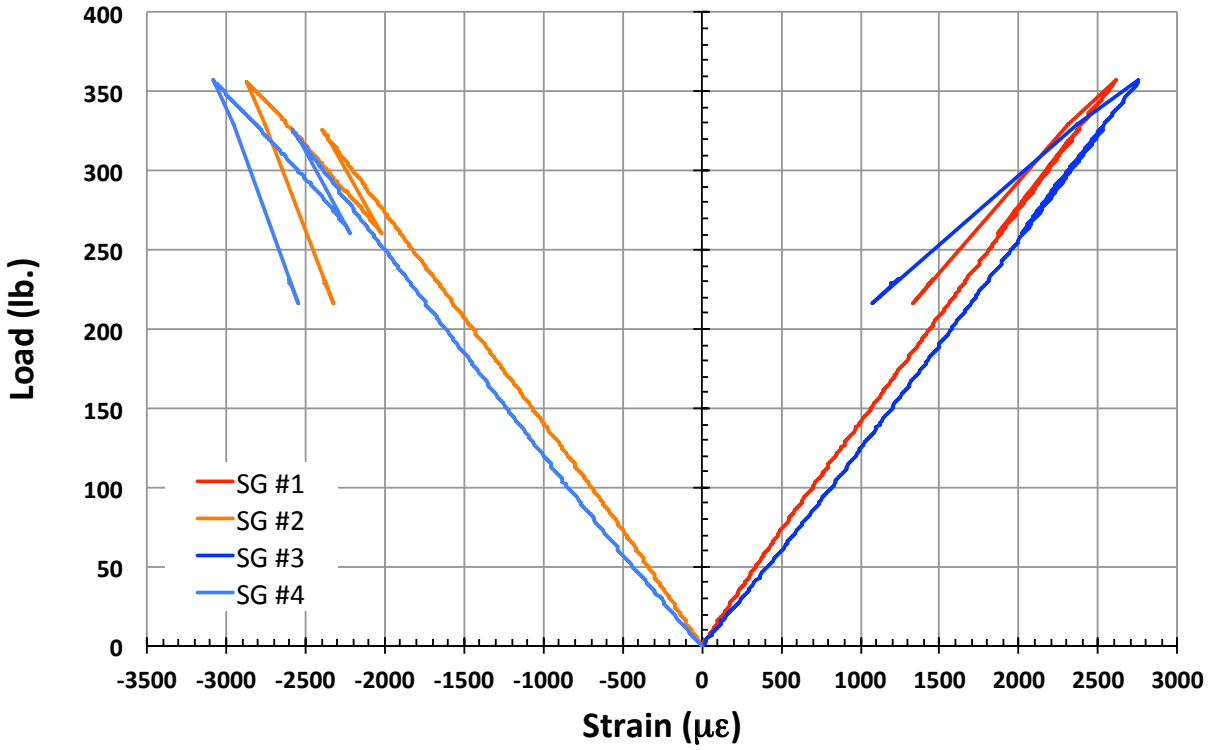

Figure C431. B5N1 load vs. strain, initial loading.

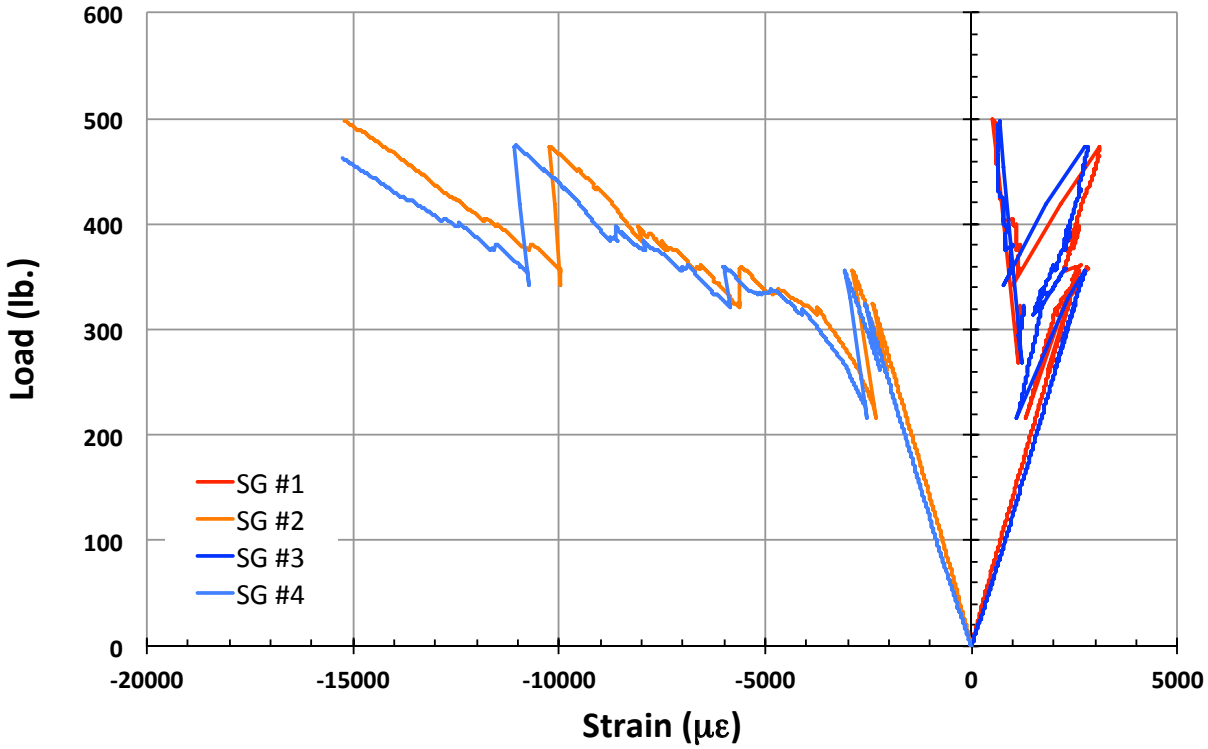

Figure C432. B5N1 load vs. strain.

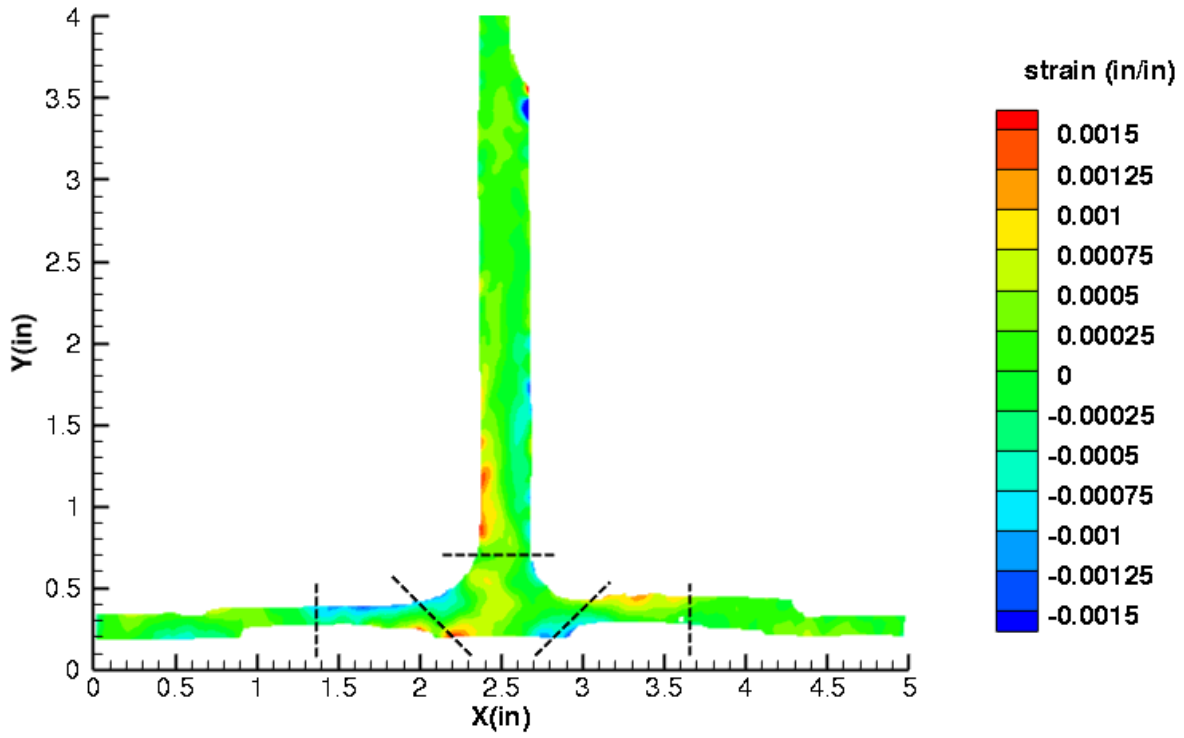

Figure C433. B5N1 strain contours for ε_{xx} at 327 lb. load, prior to initial failure, front 12MP VIC data.

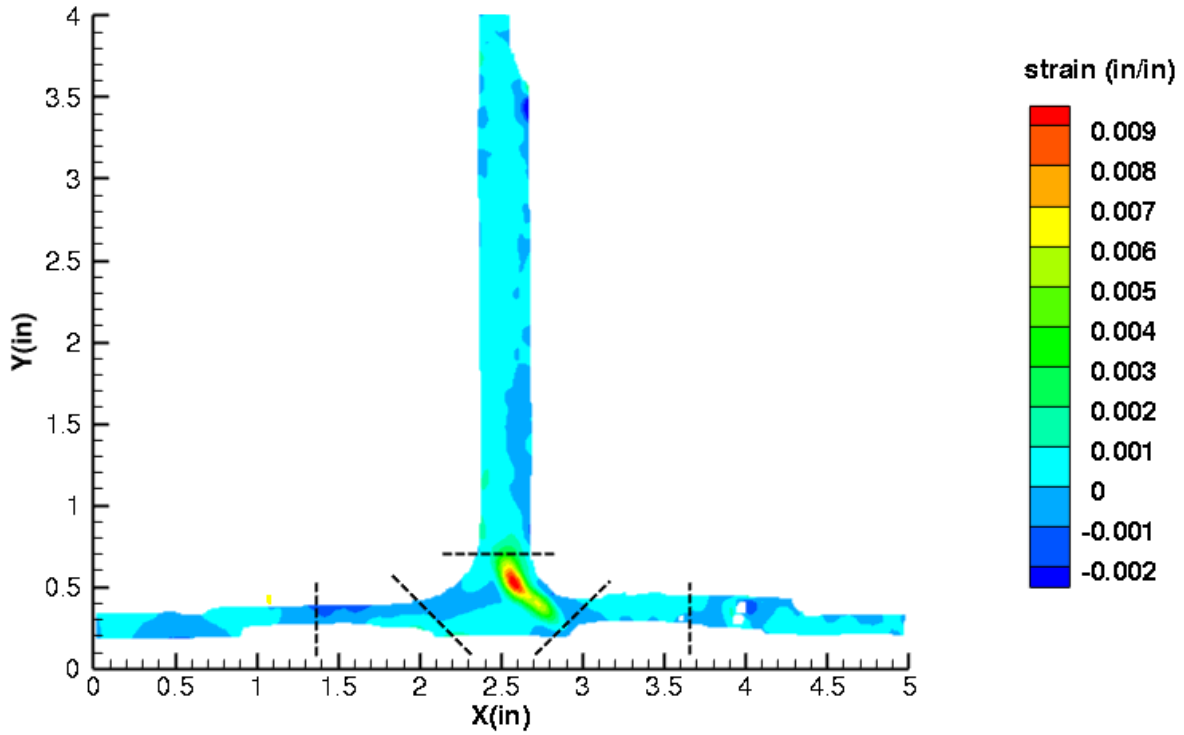

Figure C434. B5N1 strain contours for ε_{xx} at 263 lb. load, just after initial failure, front 12MP VIC data.

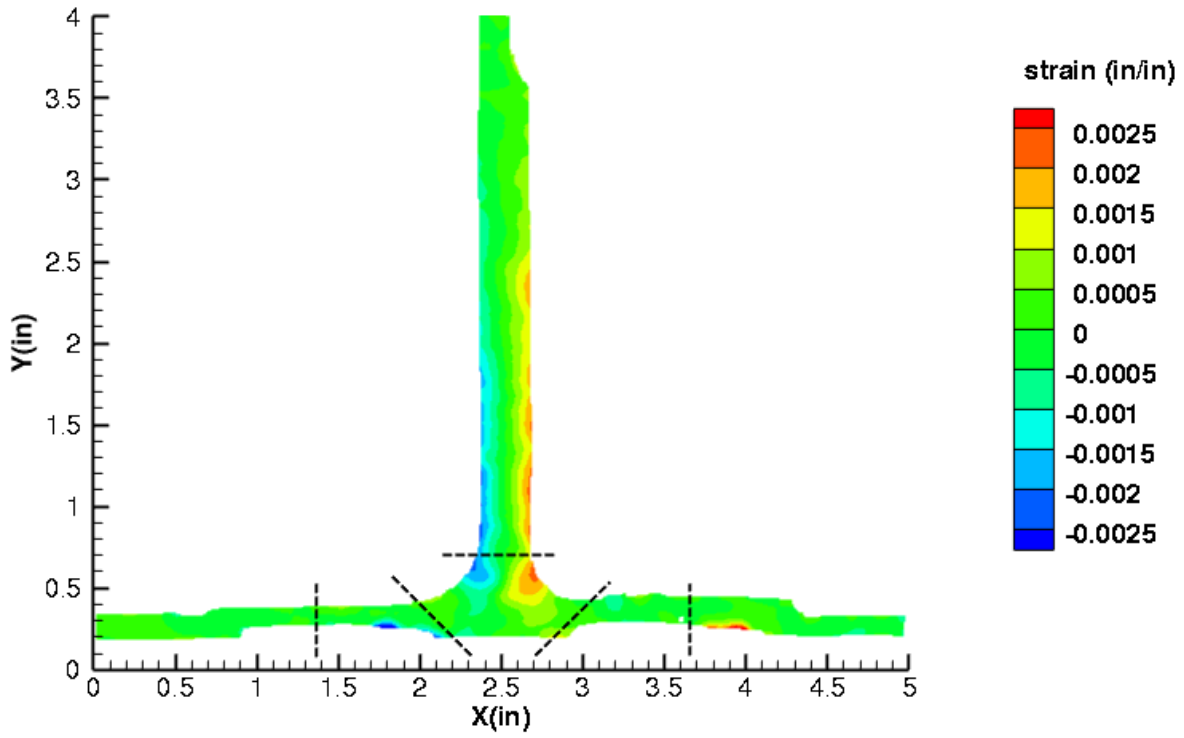

Figure C435. B5N1 strain contours for ε_{yy} at 327 lb. load, prior to initial failure, front 12MP VIC data.

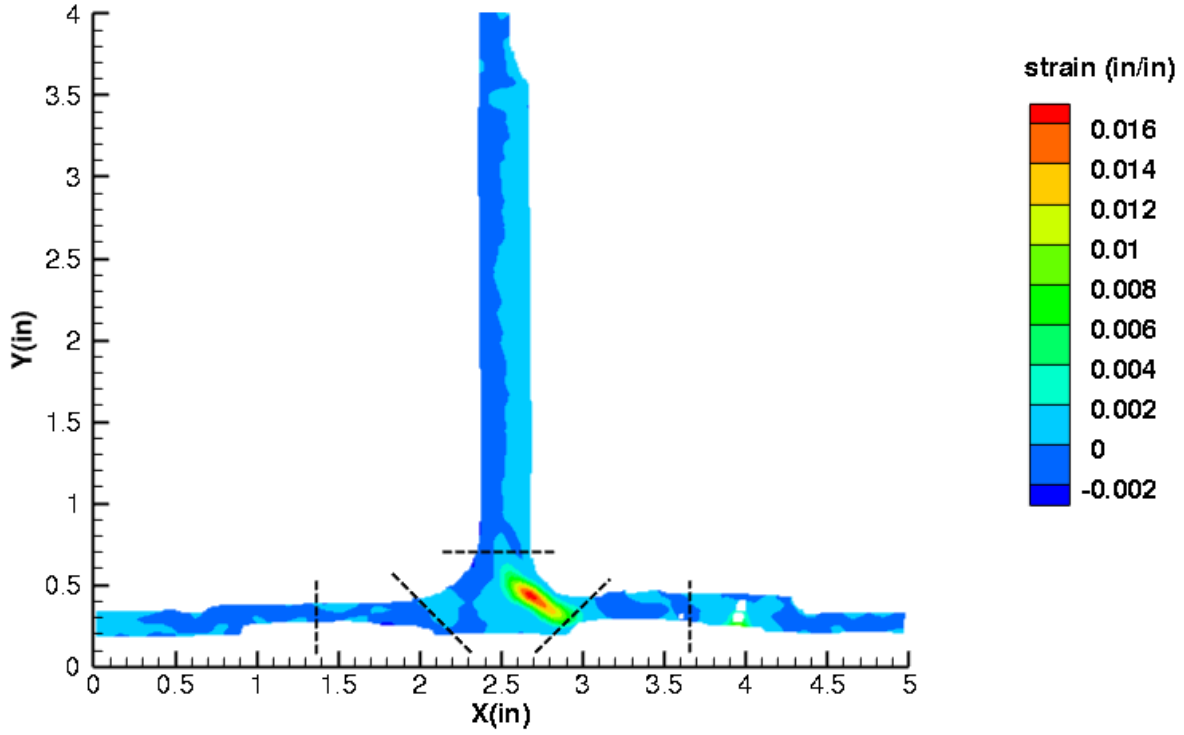

Figure C436. B5N1 strain contours for ε_{yy} at 263 lb. load, just after initial failure, front 12MP VIC data.

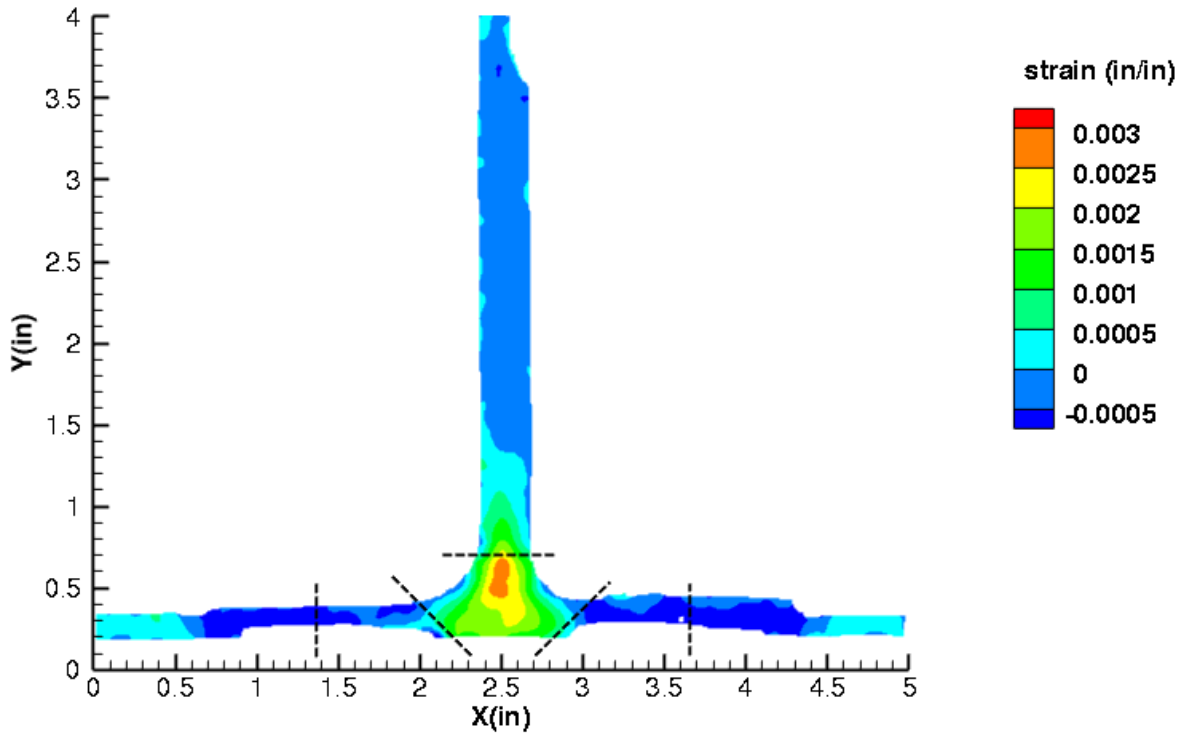

Figure C437. B5N1 strain contours for ε_{xy} at 327 lb. load, prior to initial failure, front 12MP VIC data.

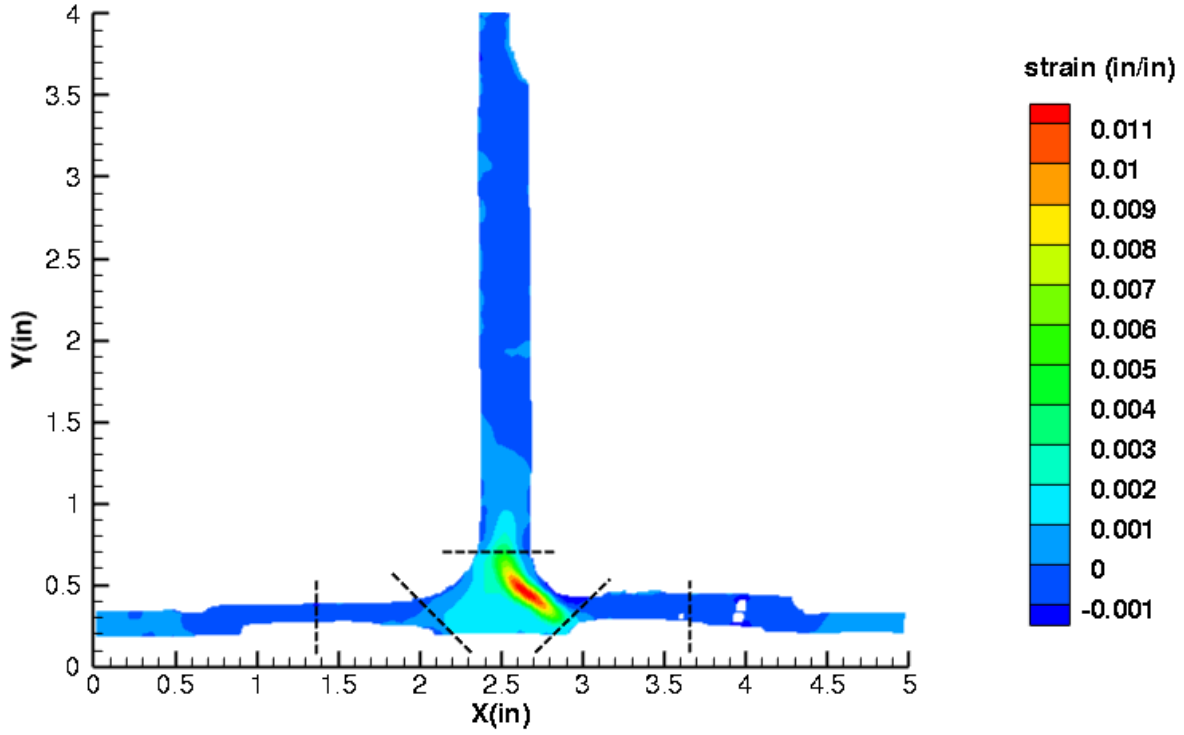

Figure C438. B5N1 strain contours for ε_{xy} at 263 lb. load, just after initial failure, front 12MP VIC data.

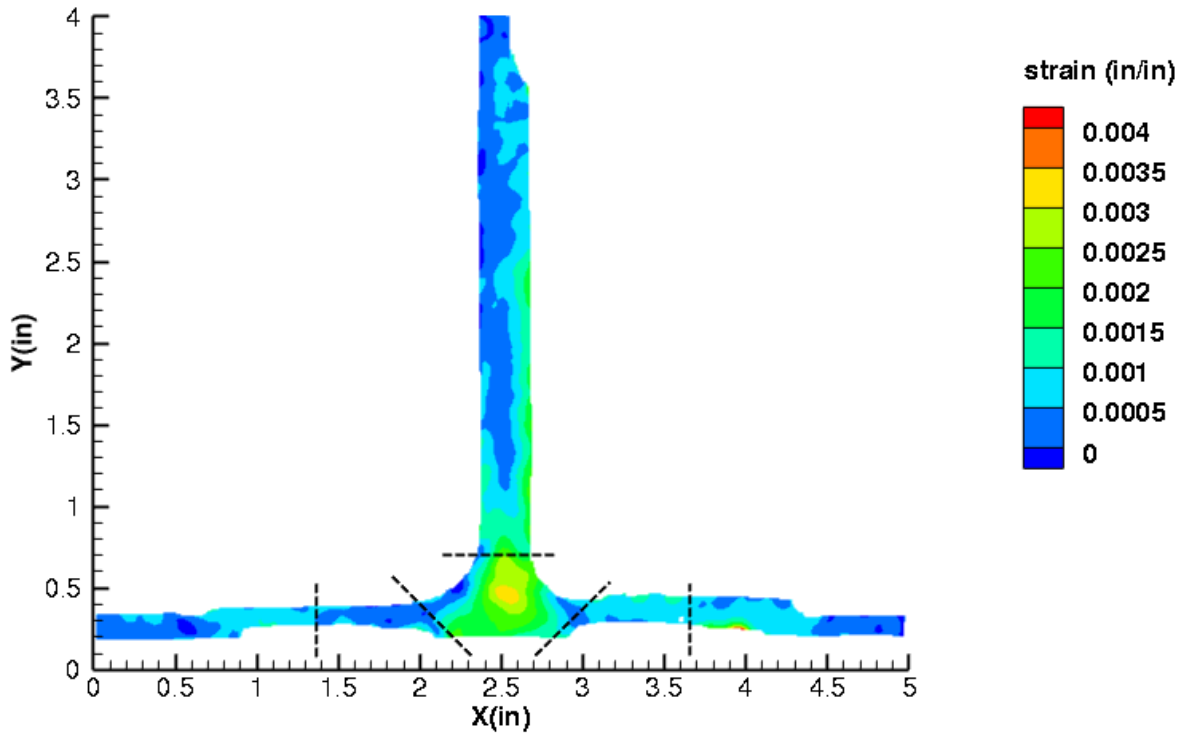

Figure C439. B5N1 strain contours for maximum principal strain at 327 lb. load, prior to initial failure, front 12MP VIC data.

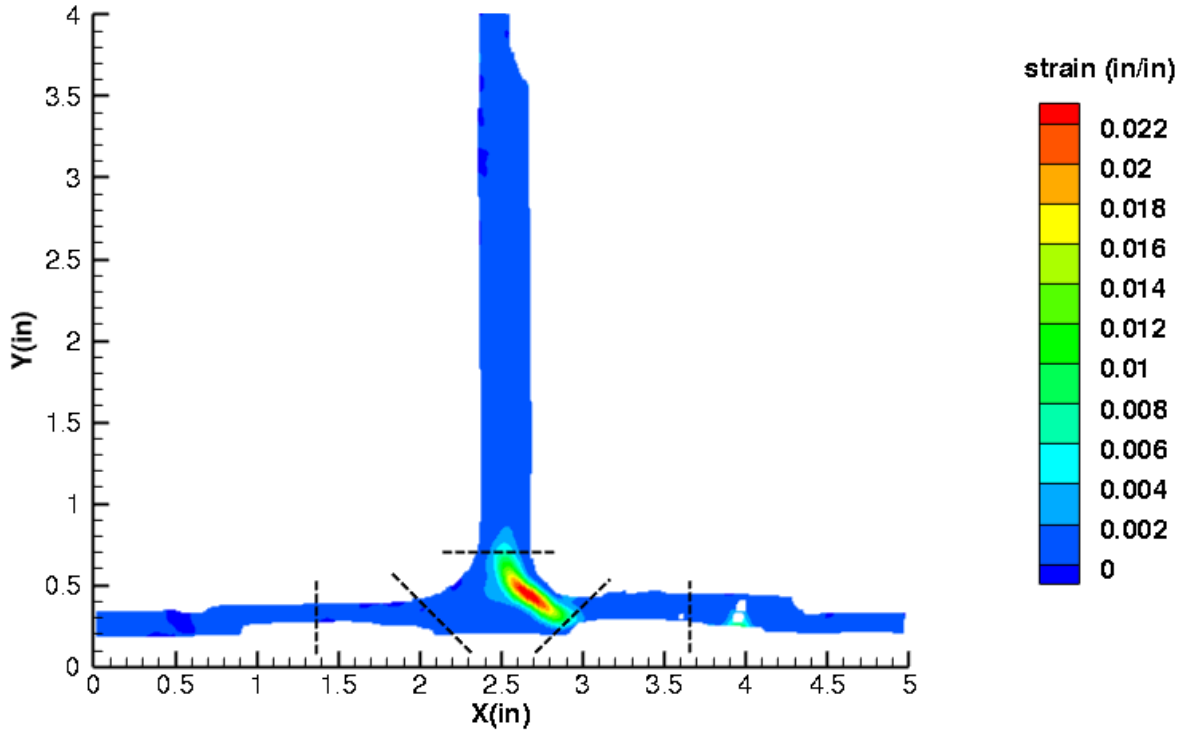

Figure C440. B5N1 strain contours for maximum principal strain at 263 lb. load, just after initial failure, front 12MP VIC data.

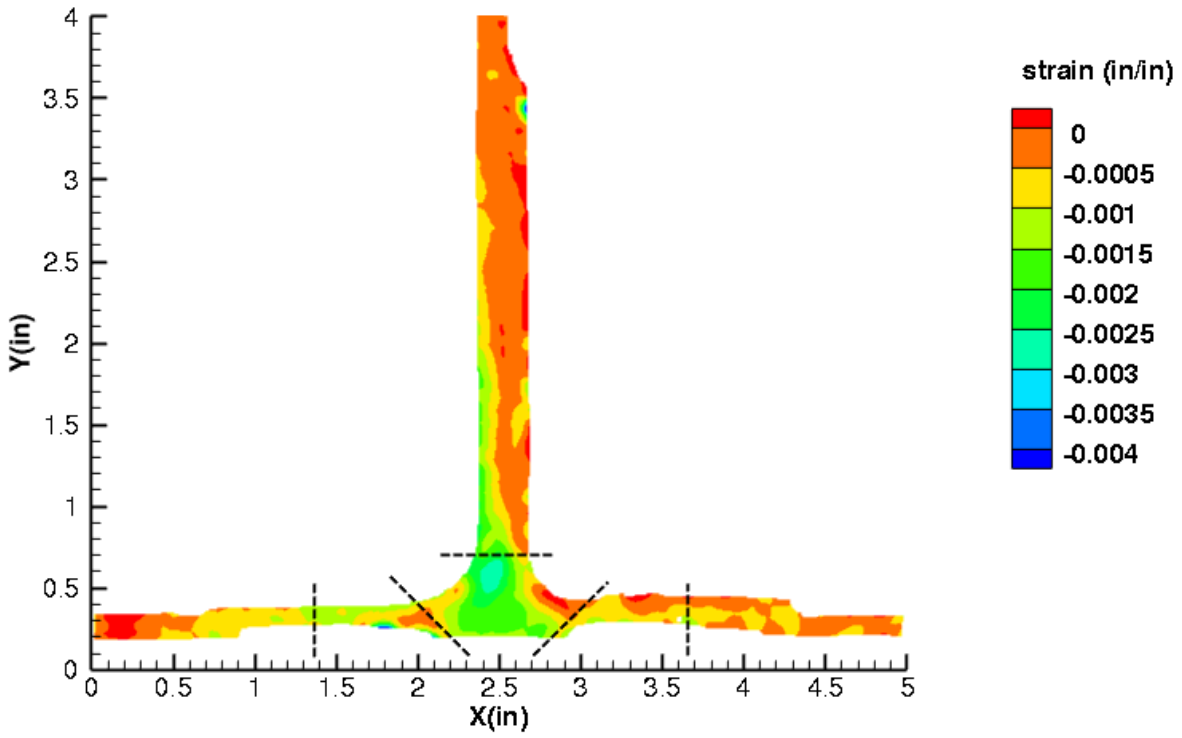

Figure C441. B5N1 strain contours for minimum principal strain at 327 lb. load, prior to initial failure, front 12MP VIC data.

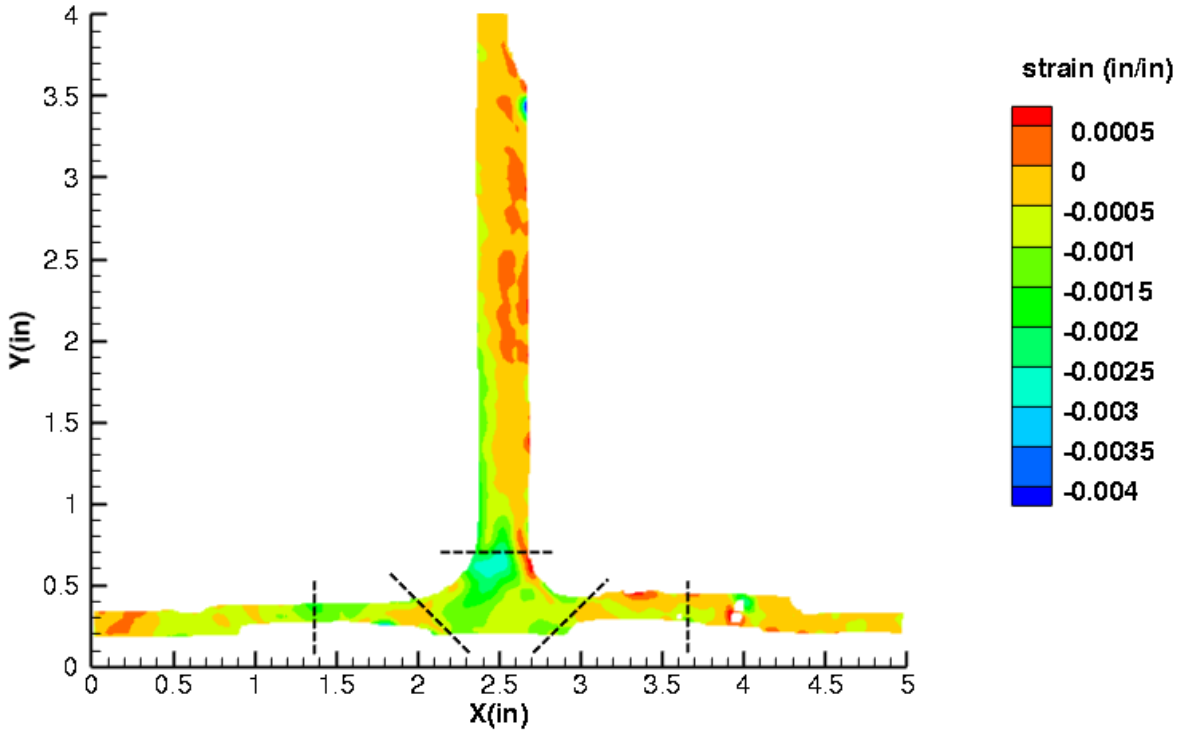

Figure C442. B5N1 strain contours for minimum principal strain at 263 lb. load, just after initial failure, front 12MP VIC data.

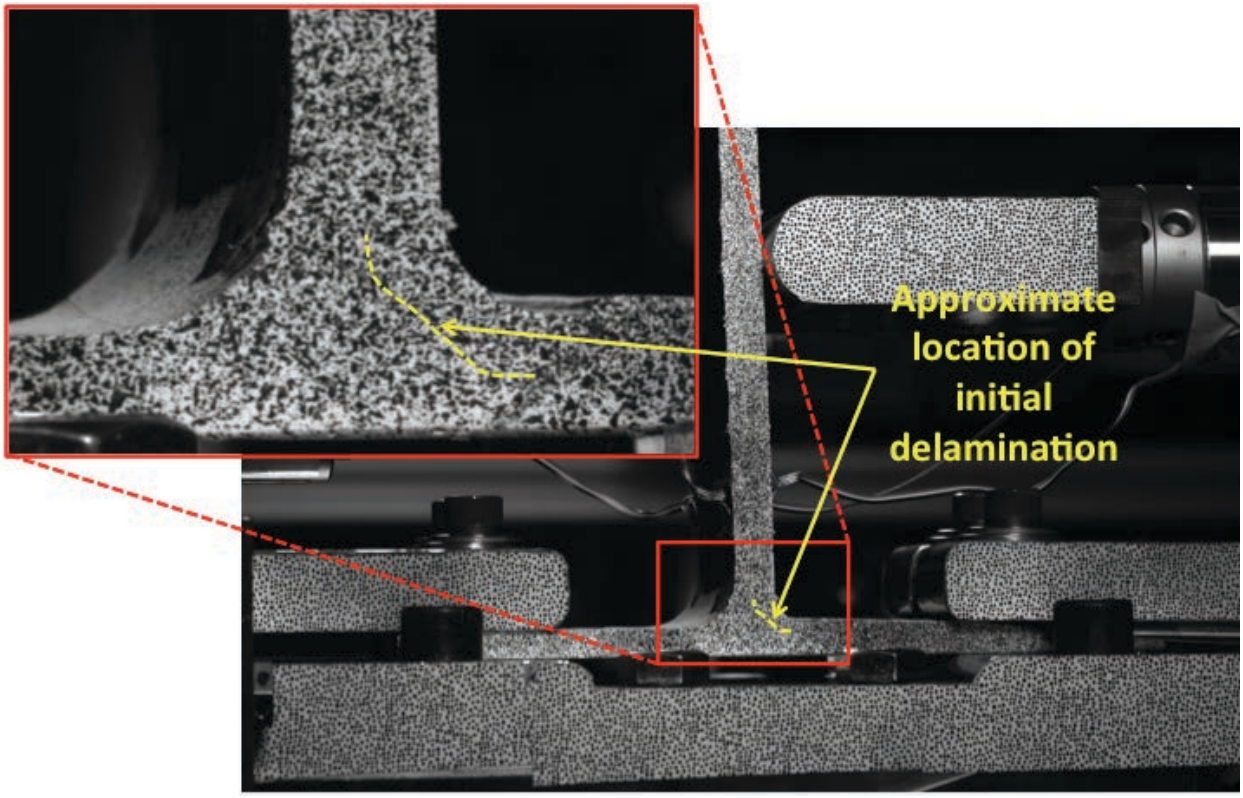

Figure C443. B5N1 image just after initial failure, front 12MP VIC data.

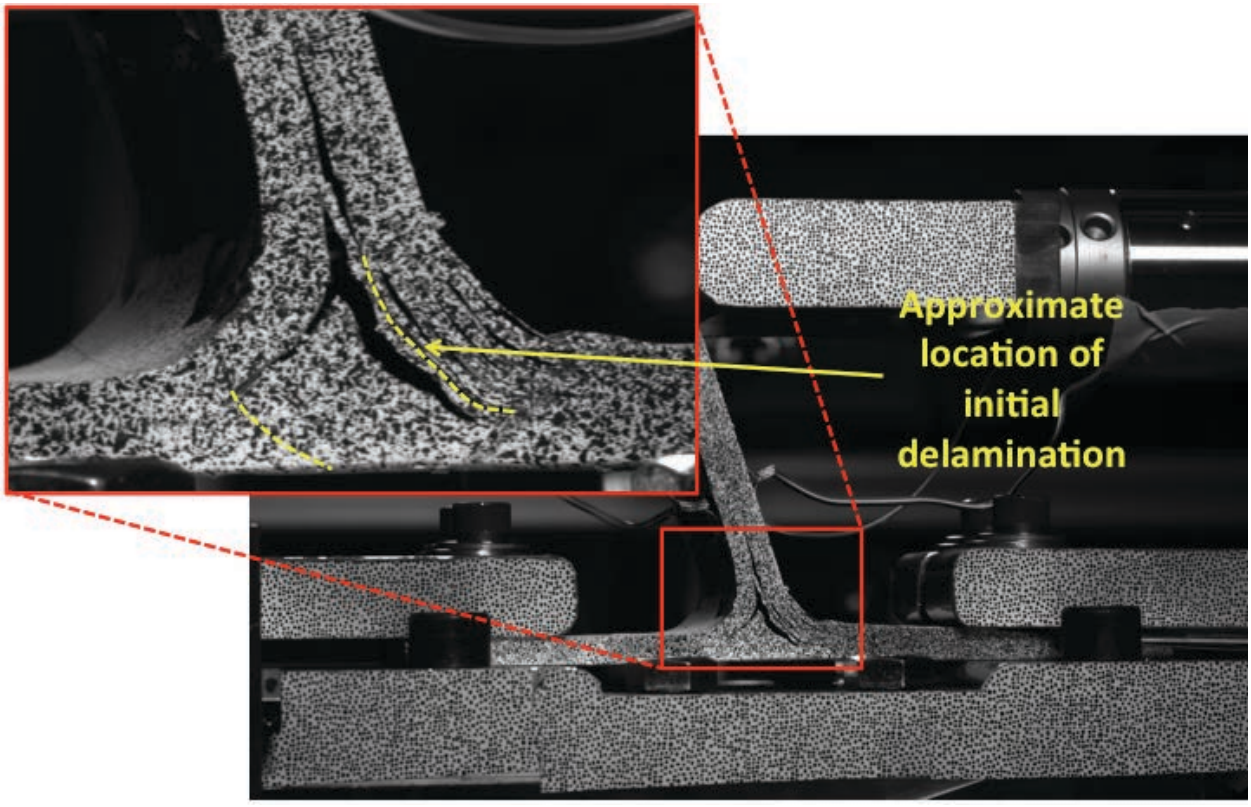

Figure C444. B5N1 image just after maximum load, front 12MP VIC data.

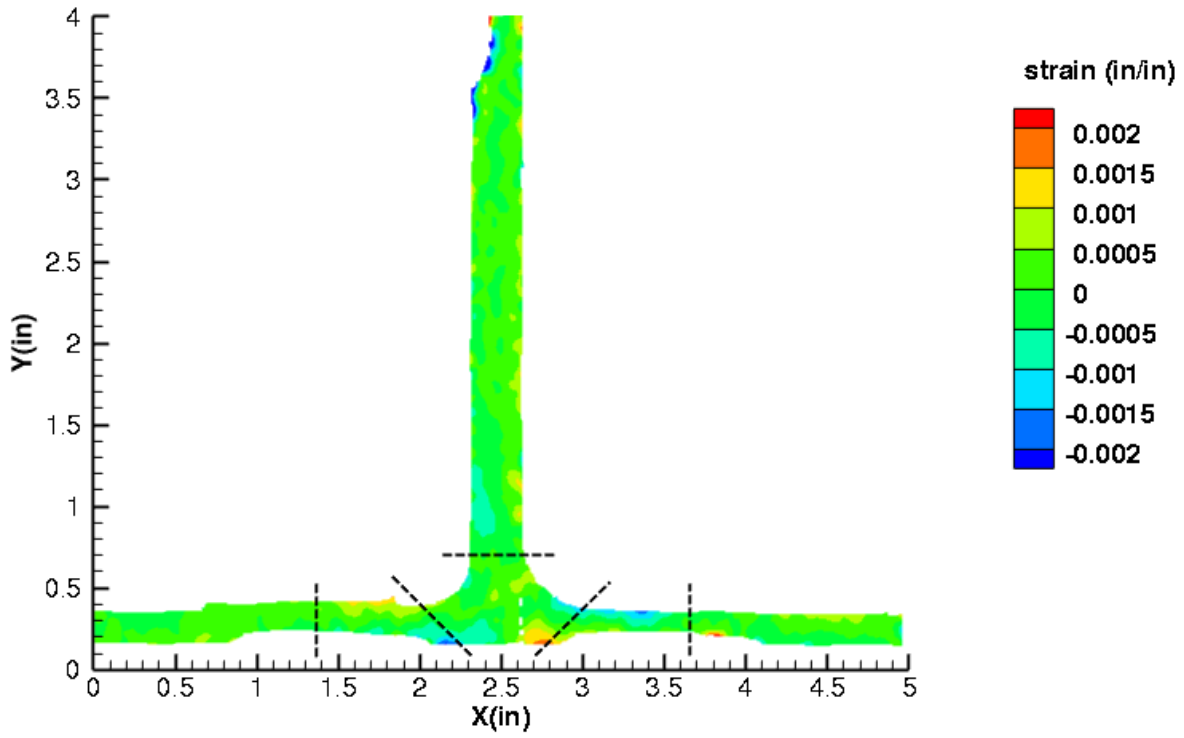

Figure C445. B5N1 strain contours for ε_{xx} at 327 lb. load, prior to initial failure, back 12MP VIC data.

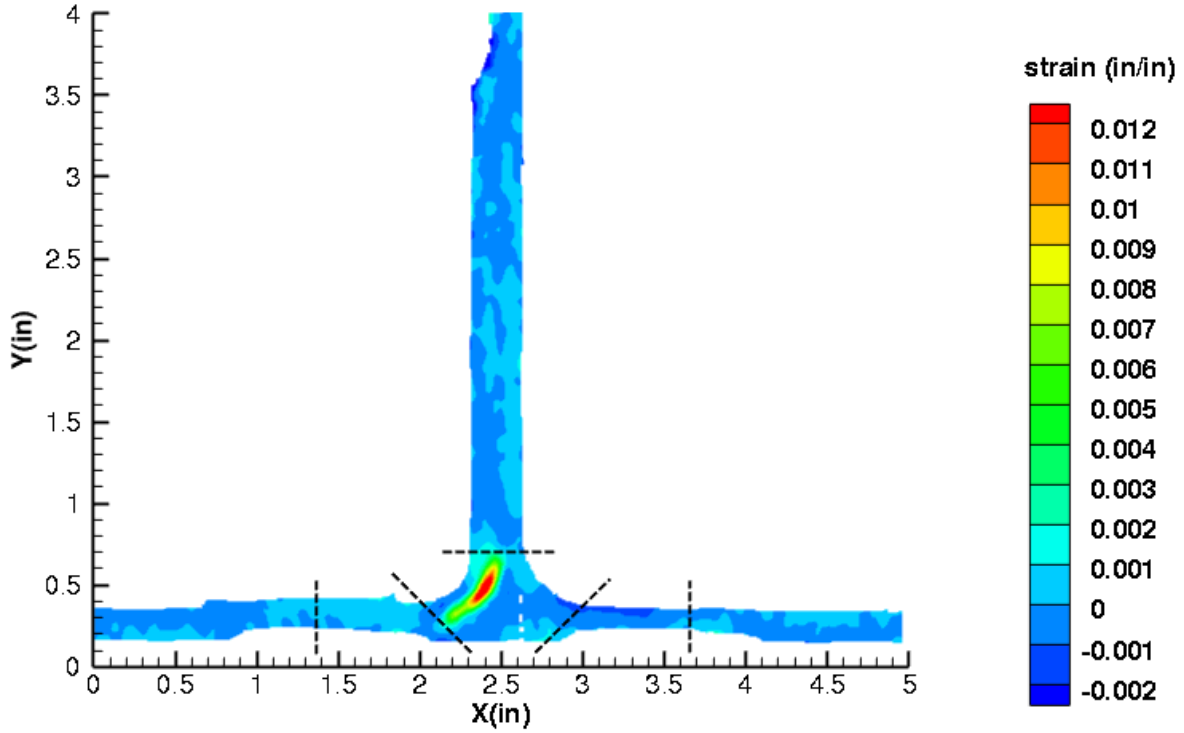

Figure C446. B5N1 strain contours for ε_{xx} at 263 lb. load, just after initial failure, back 12MP VIC data.

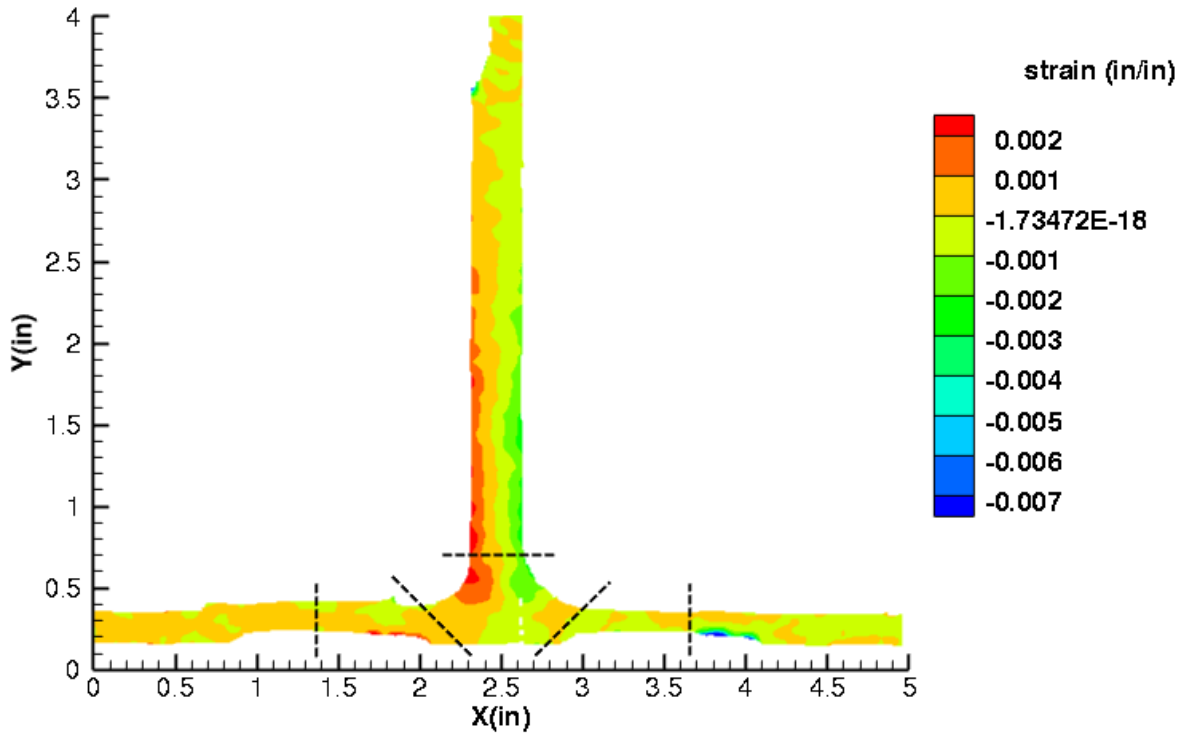

Figure C447. B5N1 strain contours for ε_{yy} at 327 lb. load, prior to initial failure, back 12MP VIC data.

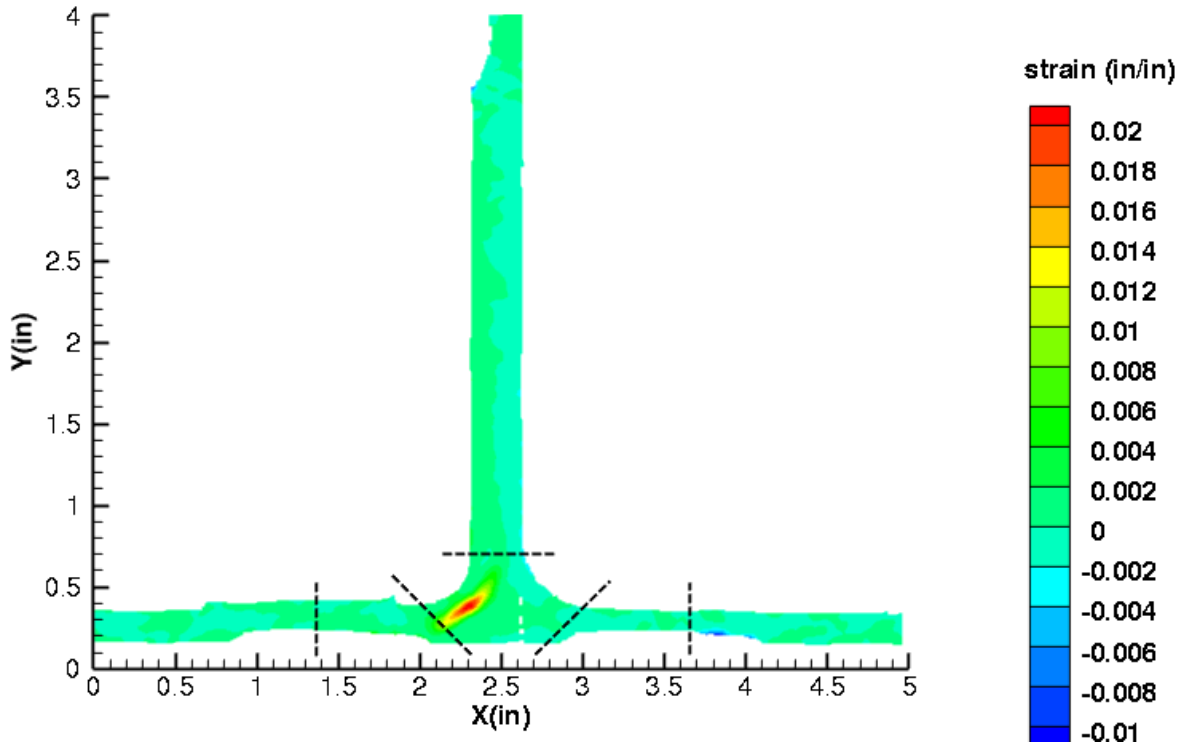

Figure C448. B5N1 strain contours for ε_{yy} at 263 lb. load, just after initial failure, back 12MP VIC data.

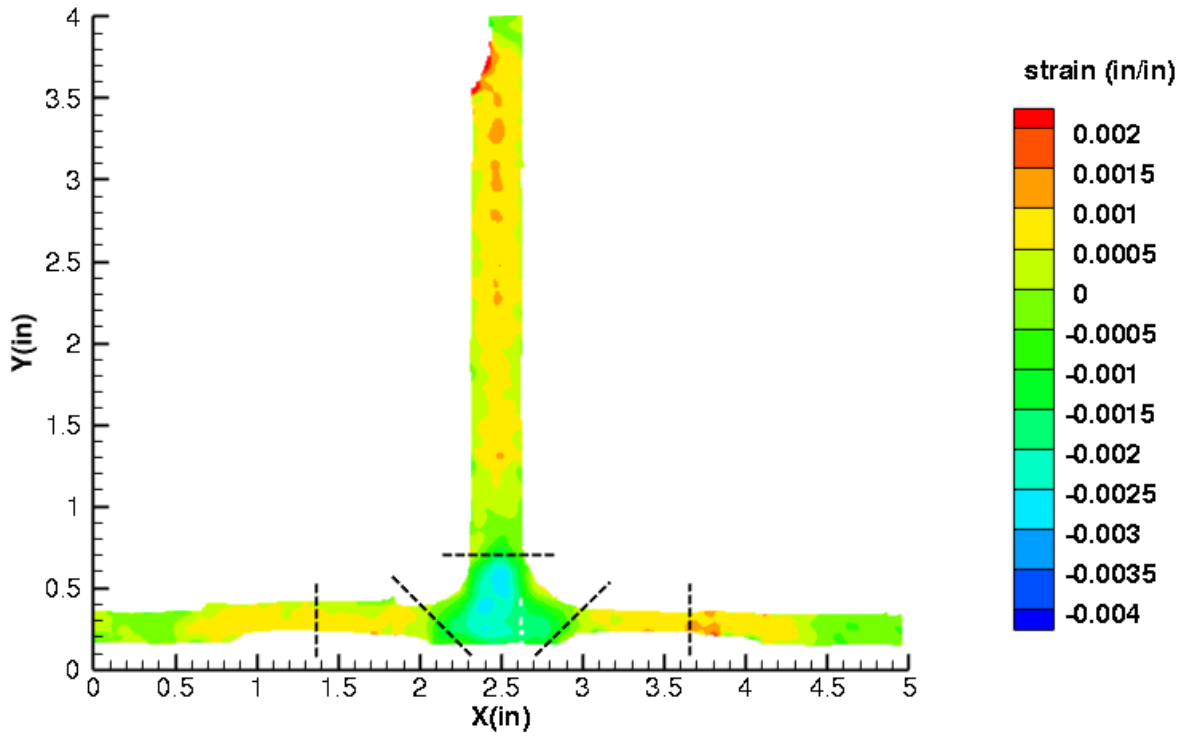

Figure C449. B5N1 strain contours for ε_{xy} at 327 lb. load, prior to initial failure, back 12MP VIC data.

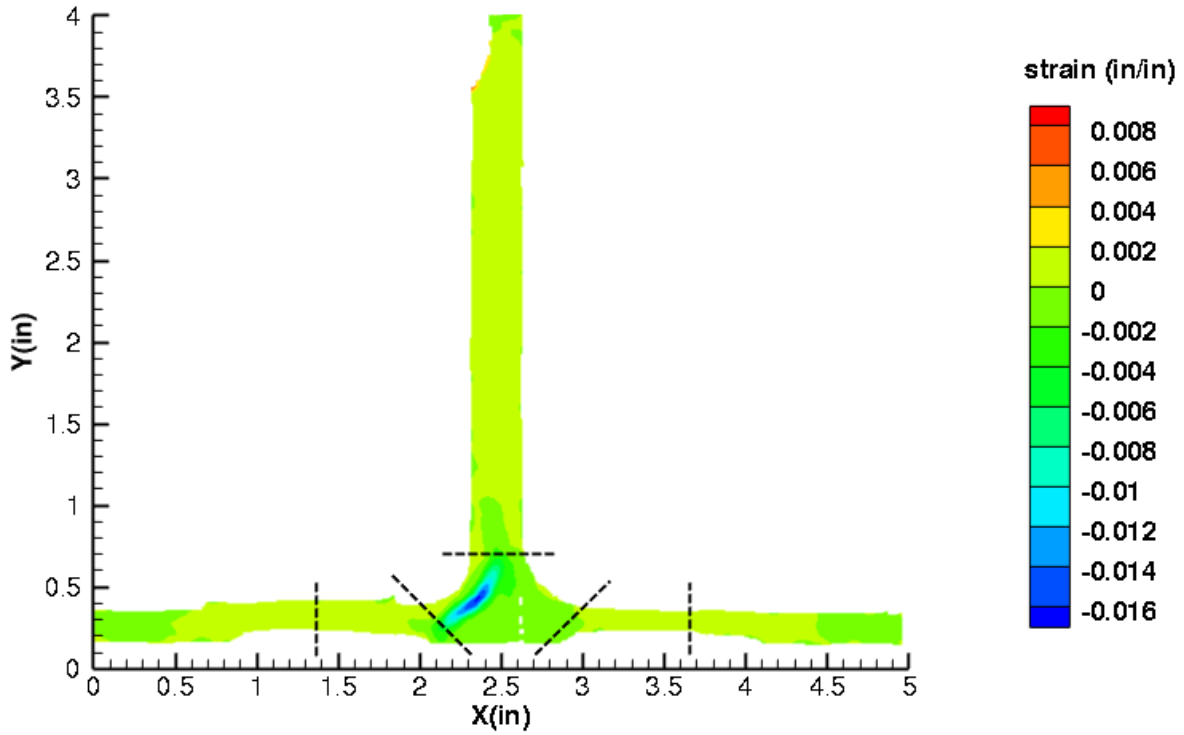

Figure C450. B5N1 strain contours for ε_{xy} at 263 lb. load, just after initial failure, back 12MP VIC data.

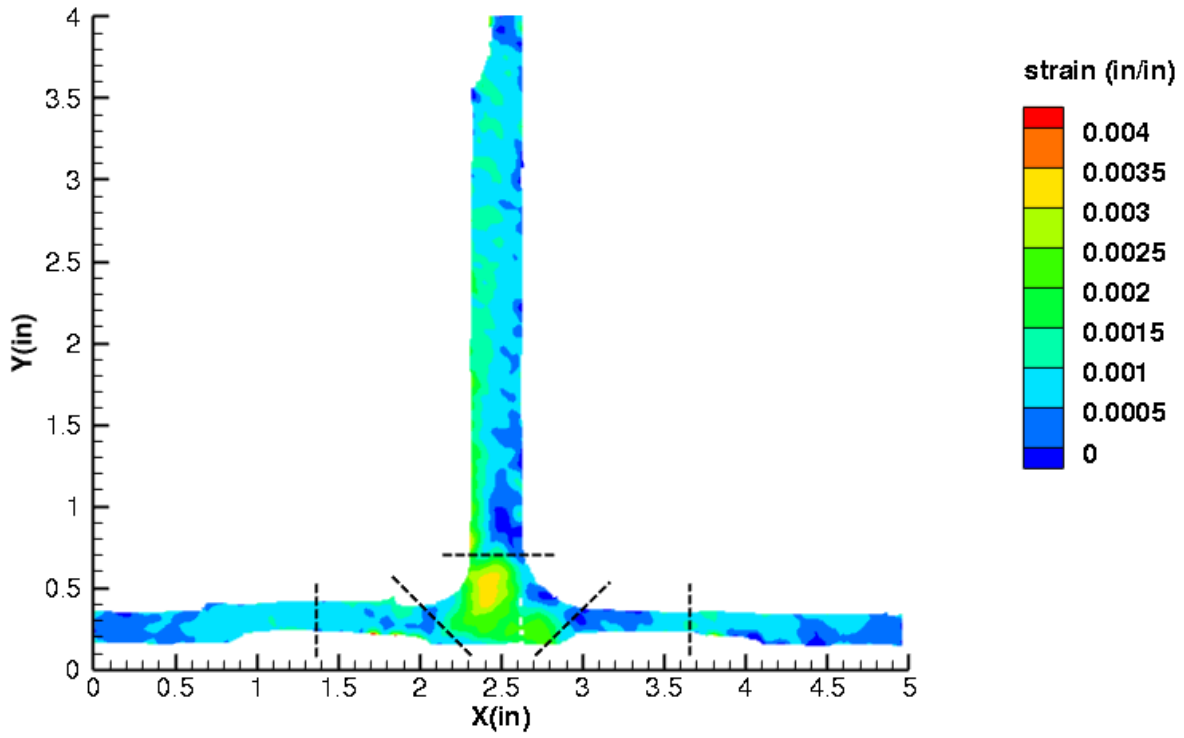

Figure C451. B5N1 strain contours for maximum principal strain at 327 lb. load, prior to initial failure, back 12MP VIC data.

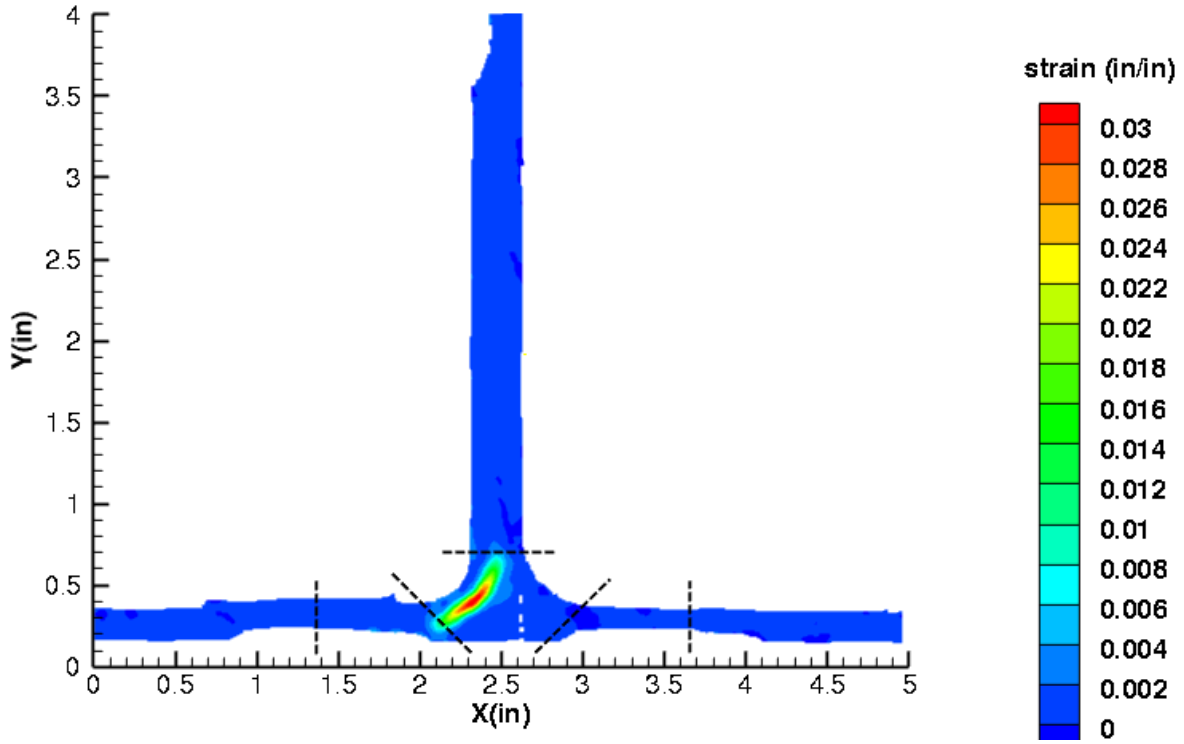

Figure C452. B5N1 strain contours for maximum principal strain at 263 lb. load, just after initial failure, back 12MP VIC data.

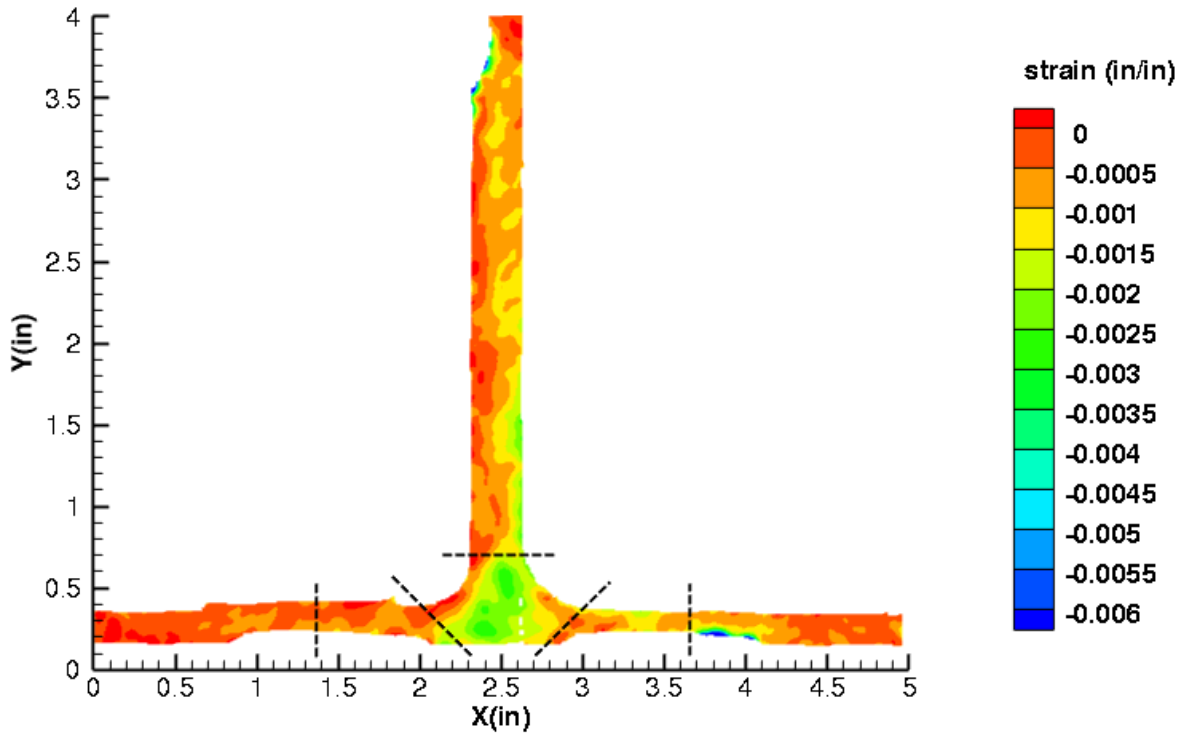

Figure C453. B5N1 strain contours for minimum principal strain at 327 lb. load, prior to initial failure, back 12MP VIC data.

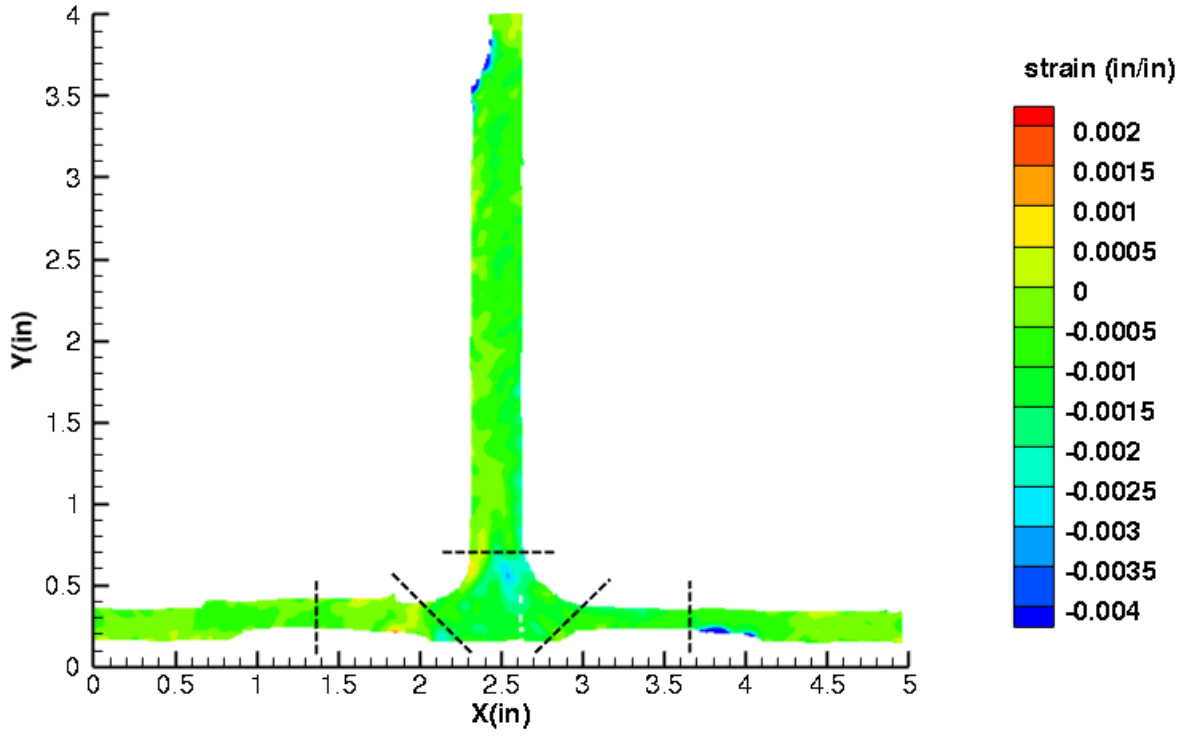

Figure C454. B5N1 strain contours for minimum principal strain at 263 lb. load, just after initial failure, back 12MP VIC data.

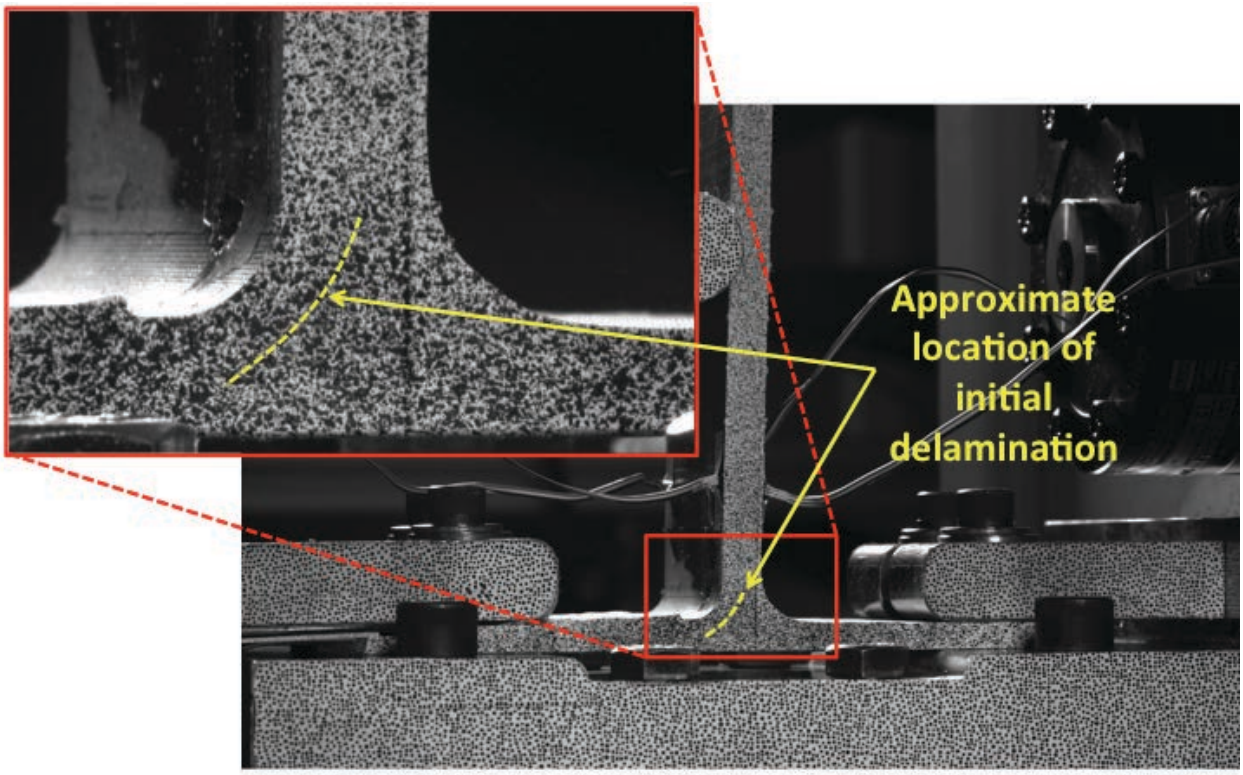

Figure C455. B5N1 image just after initial failure, back 12MP VIC data.

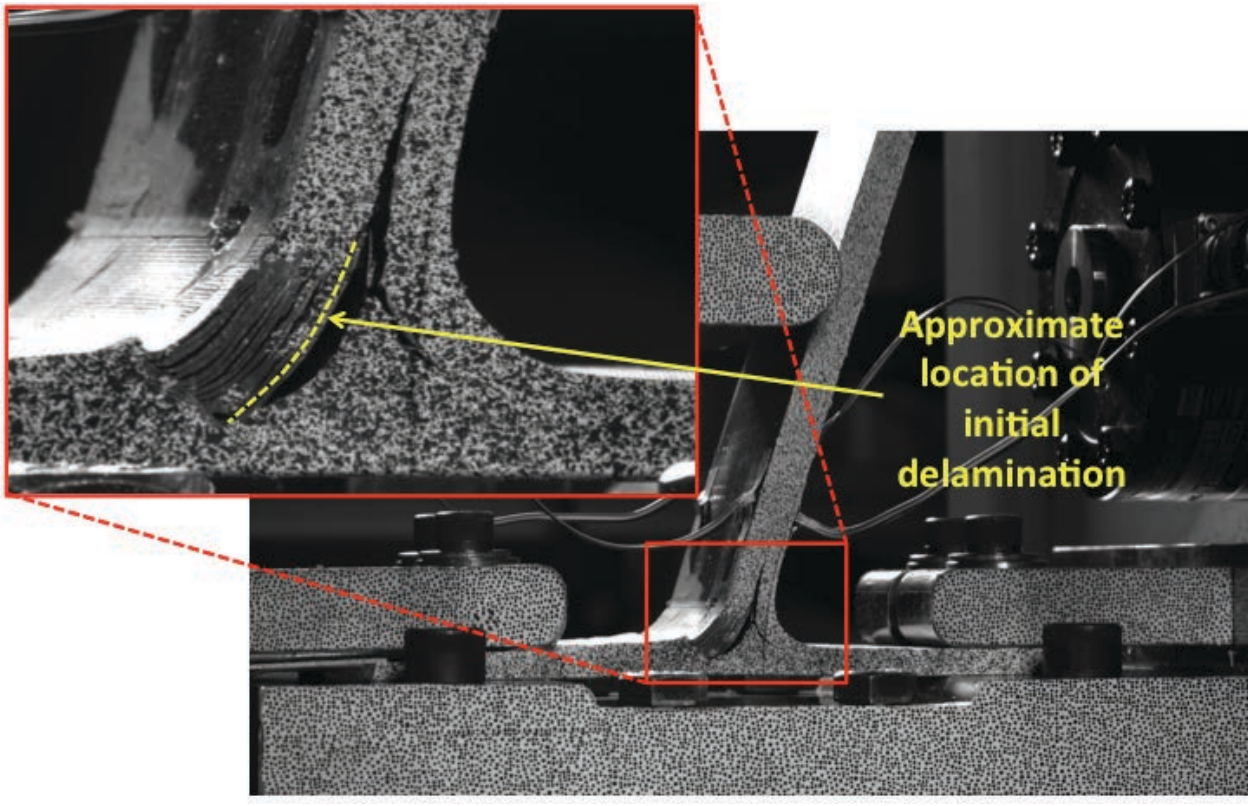

Figure C456. B5N1 image just after maximum load, back 12MP VIC data.

B5N2

This section presents the test data for the B5N2 test article.

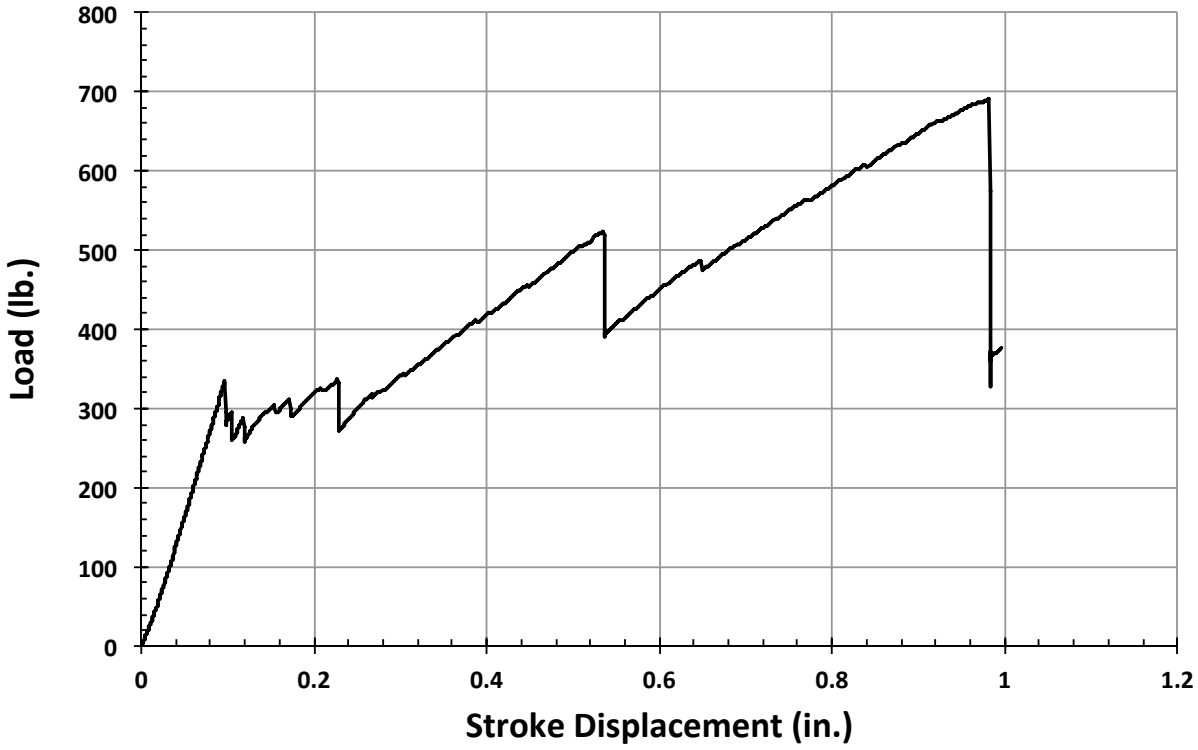

Figure C457. B5N2 load vs. stroke.

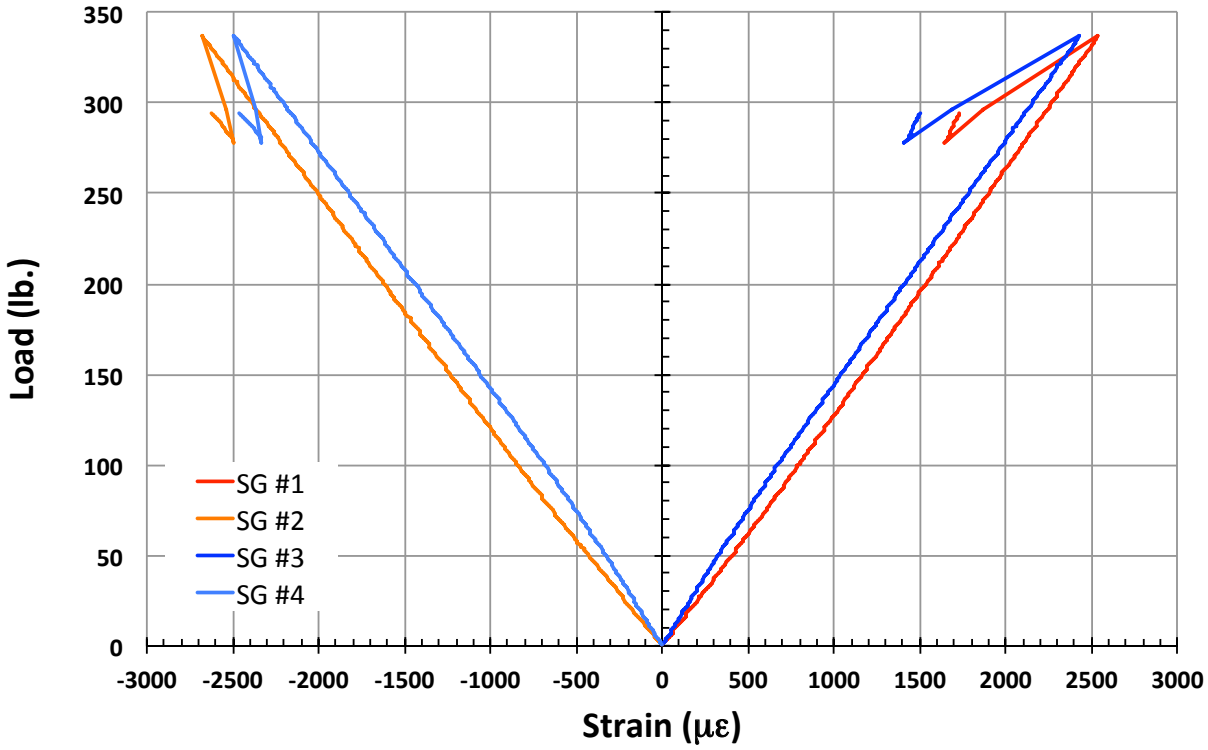

Figure C458. B5N2 load vs. strain, initial loading.

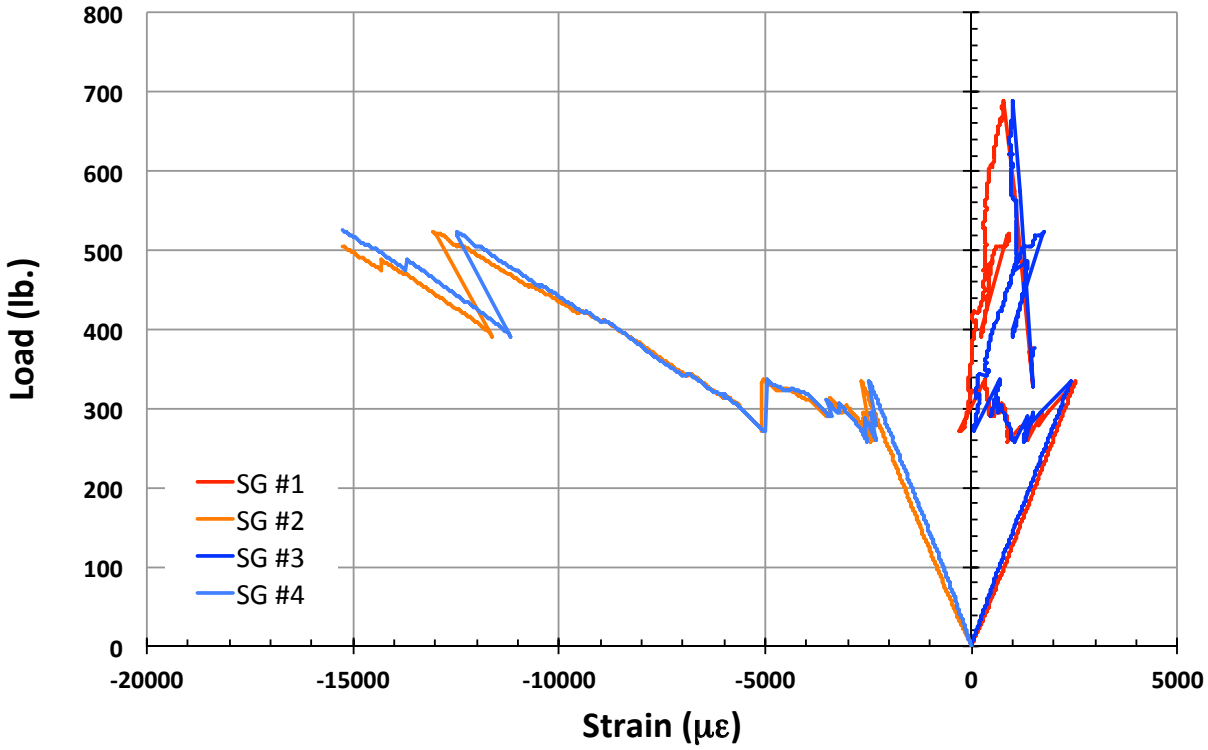

Figure C459. B5N2 load vs. strain.

B5N3

This section presents the test data for the B5N3 test article.

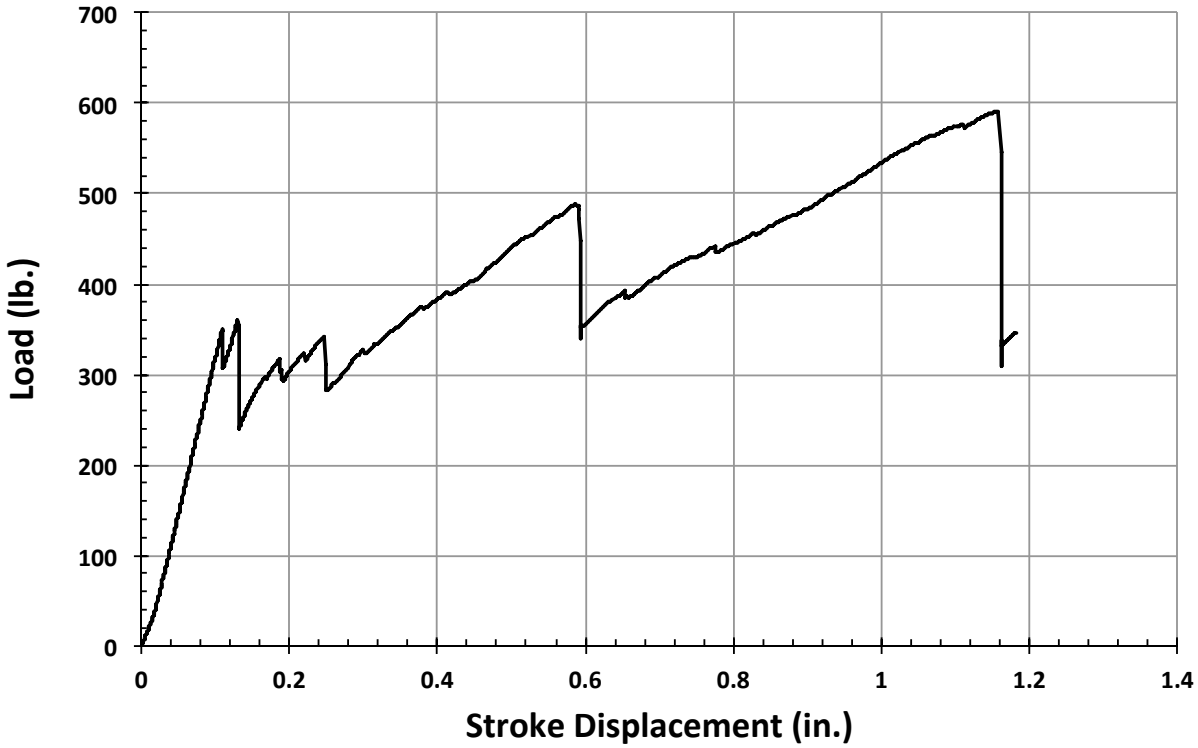

Figure C460. B5N3 load vs. stroke.

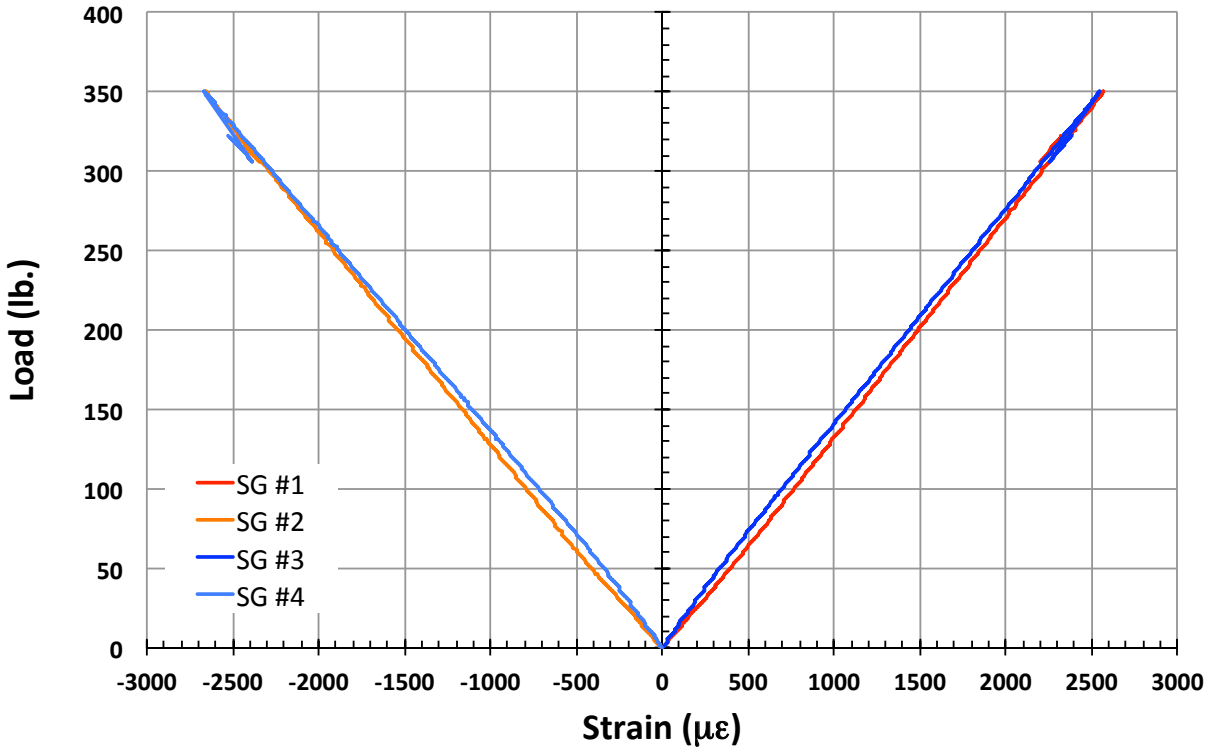

Figure C461. B5N3 load vs. strain, initial loading.

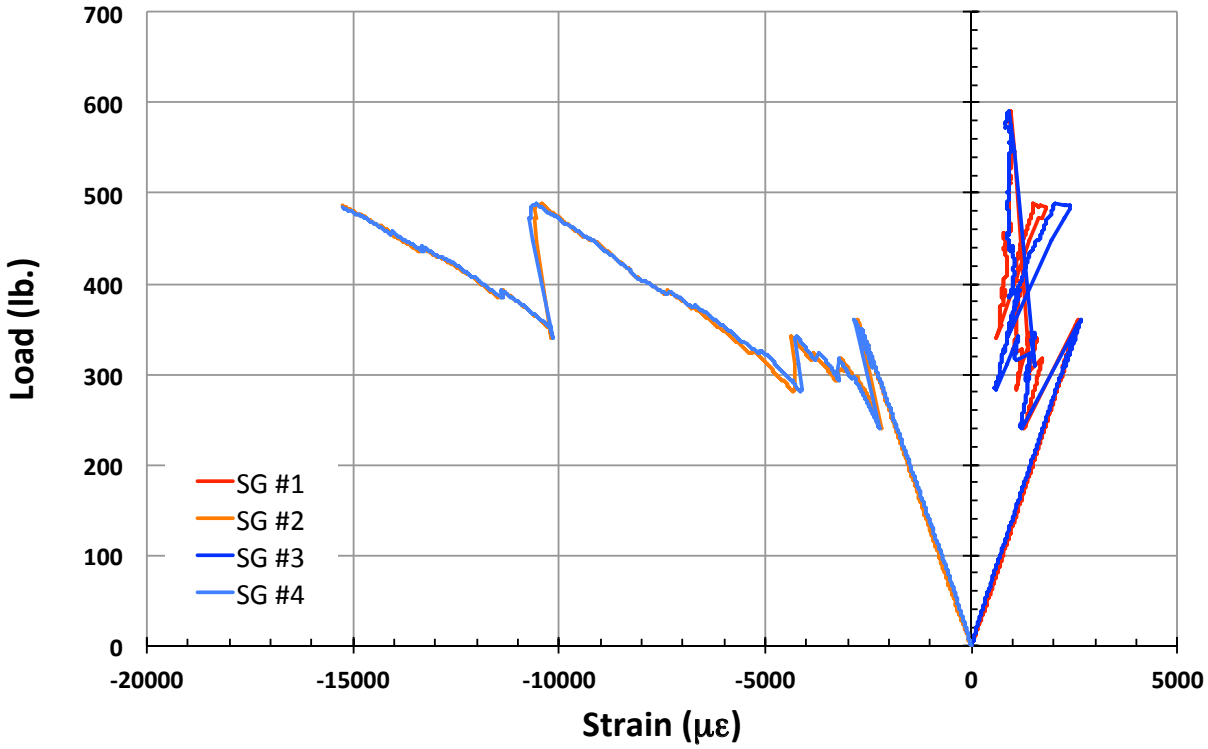

Figure C462. B5N3 load vs. strain.

REPORT DOCUMENTATION PAGE

Form Approved
OMB No. 0704-0188

The public reporting burden for this collection of information is estimated to average 1 hour per response, including the time for reviewing instructions, searching existing data sources, gathering and maintaining the data needed, and completing and reviewing the collection of information. Send comments regarding this burden estimate or any other aspect of this collection of information, including suggestions for reducing this burden, to Department of Defense, Washington Headquarters Services, Directorate for Information Operations and Reports (0704-0188), 1215 Jefferson Davis Highway, Suite 1204, Arlington, VA 22202-4302. Respondents should be aware that notwithstanding any other provision of law, no person shall be subject to any penalty for failing to comply with a collection of information if it does not display a currently valid OMB control number.
PLEASE DO NOT RETURN YOUR FORM TO THE ABOVE ADDRESS.

1. REPORT DATE *(DD-MM-YYYY)*	2. REPORT TYPE	3. DATES COVERED *(From - To)*
01- 04 - 2016	Technical Memorandum	

4. TITLE AND SUBTITLE

T-Cap Pull-Off and Bending Behavior for Stitched Structure

5a. CONTRACT NUMBER

5b. GRANT NUMBER

5c. PROGRAM ELEMENT NUMBER

6. AUTHOR(S)

Lovejoy, Andrew E.; Leone, Frank A.

5d. PROJECT NUMBER

5e. TASK NUMBER

5f. WORK UNIT NUMBER

338881.02.22.07.01.01

7. PERFORMING ORGANIZATION NAME(S) AND ADDRESS(ES)

NASA Langley Research Center
Hampton, VA 23681-2199

8. PERFORMING ORGANIZATION REPORT NUMBER

L-20628

9. SPONSORING/MONITORING AGENCY NAME(S) AND ADDRESS(ES)

National Aeronautics and Space Administration
Washington, DC 20546-0001

10. SPONSOR/MONITOR'S ACRONYM(S)

NASA

11. SPONSOR/MONITOR'S REPORT NUMBER(S)

NASA-TM-2016-218971

12. DISTRIBUTION/AVAILABILITY STATEMENT

Unclassified - Unlimited
Subject Category39
Availability: NASA STI Program (757) 864-9658

13. SUPPLEMENTARY NOTES

14. ABSTRACT

The Pultruded Rod Stitched Efficient Unitized Structure (PRSEUS) is a structural concept that was developed by The Boeing Company to address the complex structural design aspects associated with a pressurized hybrid wing body aircraft configuration. An important design feature required for assembly is the integrally stitched T-cap, which provides connectivity of the corner joint between adjacent panels. A series of tests were conducted on T-cap test articles, with and without a rod stiffener penetrating the T-cap web, under tension (pull-off) and bending loads. Three designs were tested, including the baseline design used in large-scale test articles where the only stitch row in the T-cap web is at the top of the fillet region at the web base, as well as two additional designs with stitching rows added within the T-cap web. Stitch rows in the web were added at either 0.5- or 1.0-inch spacing along the height of the web. Testing was conducted at NASA Langley Research Center to determine the behavior of the T-cap region reaulting from the applied loading. Results show that stitching arrests the initial delamination failures so that the residual strength capability exceeds the load at which the initial delaminations develop. However, it was seen that the added web stitching had very little effect on the initial delamination failure load, but actually decreased the initial delamination failure load for tension loading of test articles without a stiffener passing through the web. Additionally, the added web stitching only increased the maximum load capability by between 1% and 12.5%.

15. SUBJECT TERMS

Pultruded Rod; Stiching; Structure; T-cap

16. SECURITY CLASSIFICATION OF:			17. LIMITATION OF ABSTRACT	18. NUMBER OF PAGES	19a. NAME OF RESPONSIBLE PERSON
a. REPORT	b. ABSTRACT	c. THIS PAGE			STI Help Desk (email: help@sti.nasa.gov)
					19b. TELEPHONE NUMBER *(Include area code)*
U	U	U	UU	321	(757) 864-9658